

UNIVERSITÀ DEGLI STUDI DI BRESCIA  
DIPARTIMENTO DI INGEGNERIA MECCANICA E  
INDUSTRIALE



---

UNIVERSITÀ  
DEGLI STUDI  
DI BRESCIA

DOTTORATO DI RICERCA IN INGEGNERIA MECCANICA E  
INDUSTRIALE

---

ING/IND 22 and ING/IND 21  
Cycle XXXV

---

TECNOLOGIE E RELAZIONI DI FILIERA PER UN NUOVO  
ECOSISTEMA INDUSTRIALE: L'APPLICAZIONE DELLA  
SIMBIOSI INDUSTRIALE NEL SETTORE DEI METALLI

TECHNOLOGIES AND SUPPLY CHAIN RELATIONSHIPS FOR A  
NEW INDUSTRIAL ECOSYSTEM: THE APPLICATION OF THE  
INDUSTRIAL SYMBIOSIS IN THE METALS SECTOR

Advisor:

Ing. Giorgio Ramorino

Co-Advisor:

Dr. Marco La Monica (ENEA)

Tutor:

Prof. Giovanna Cornacchia

PhD Candidate  
Anna Gobetti

DRIMI Coordinator:

Prof. Laura E. Depero



## Acknowledgements

I would like to thank Regione Lombardia and ENEA for funding this project, and the Department of Mechanical and Industrial Engineering of University of Brescia, especially the group of Materials Science and Technology and the group of Metallurgy for the support provided in the development of this project.

In particular, a special thanks to Prof. Giorgio Ramorino and Prof. Giovanna Cornacchia for all the teachings transmitted in these 3 years, for the competences, professionalism and availability in guiding me through this challenging issue.

I wish to acknowledge the help provided by Dr Marco La Monica to deal with completely new topics outside the purely technical aspects.

I am grateful to the reviewers of this PhD thesis, Prof. Roberto Roberti and Prof. Katrin Reincke for taking the time to review the work and for constructive criticism.

A thanks goes to the DIMI members who helped me in deepening different aspects of the project: Prof. Laura Depero and Dr. Annalisa Zacco for the support in the improved slag characterization and treatment, Prof. Edoardo Piana for carrying out acoustic tests, Prof. David Vetturi for performing the vibration study and Prof. Giuseppe Tomasoni for the help in the Life Cycle Assessment.

Lastly, I would like to thank all the companies that have made their skills available, especially Asonext SPA and Novotema SPA for providing much of the material characterized during this project and for making their internal laboratories available to conduct specific tests.

## Index

Sommario.....	6
Abstract.....	10
GENERAL LITERATURE BACKGROUND.....	14
I. Circular economy, industrial ecology, and industrial symbiosis.....	14
1. Industrial symbiosis.....	18
Origins.....	19
Definitions.....	20
Industrial symbiosis models.....	20
Advantages and criticalities of industrial symbiosis.....	26
2. Industrial symbiosis as a circular economy perspective and industrial ecology perspectives.....	27
2.1 Industrial Ecology perspective on Industrial Symbiosis.....	29
Circular Economy perspective on Industrial Symbiosis.....	30
II. Steel Sector waste: metallurgical Slags.....	32
1. Blast Furnace (BF) Slag.....	33
2. Steel Slag.....	34
Basic Oxygen Furnace (BOF) Slag.....	34
Ladle Furnace (LF) Slag.....	34
Electric Arc Furnace (EAF) Slag.....	35
EAF slag characterization methods.....	39
Production process of EAF steel.....	41
3. Industrial symbiosis in the Steel Sector.....	44
Traditional slag applications.....	44
Slag reuse in cement and concrete production.....	44
Slag reuse in road construction.....	45
Other applications of slag.....	45
Case studies of implemented Industrial symbiosis in the Steel Sector worldwide.....	46
III. Polymeric sector.....	51
1. Epoxy resin.....	51
1.1 Mechanical Characterization.....	52
1.1.1 Hardness Test.....	52
1.1.2 Flexural Test.....	53
1.1.3 Compression Test.....	54
2. Rubber compounds.....	54
2.1 Nitrile Butadiene Rubber (NBR).....	54

2.1.1	Moulding processes.....	56
2.1.2	Industrial rubber scraps .....	57
2.2.	End of Life Rubber tyre.....	58
2.2.1	Management and regulation of ELT.....	59
2.3.	Rubber Characterization.....	68
2.3.1.	Vulcanization.....	68
2.3.2.	Rheometric Curve.....	68
2.3.3.	Crosslinking.....	69
2.3.4.	Static Mechanical properties.....	73
2.3.5.	Viscoelastic Behaviour.....	78
2.3.6.	Dynamic Mechanical properties.....	82
2.3.7.	Bound rubber.....	85
2.2.3.	Tribological behaviour.....	86
EXPERIMENTAL METHODOLOGIES AND RESULTS.....		88
1.	Epoxy screed filled with EAF slag as alternative filler to sand.....	88
1.1.	Materials.....	88
1.1.1.	Matrix.....	88
1.1.2.	Filler.....	88
1.1.3.	Commercial product .....	89
	Sample preparation .....	89
1.2.	Methods.....	89
1.2.1.	EAF slag Characterization .....	89
1.2.2.	Composites Characterization .....	90
1.3.	Results and discussion.....	91
1.3.1.	EAF slag characterization .....	91
1.3.2.	Composites characterization.....	93
1.4.	Conclusion.....	100
2.	Influence of EAF slag as filler for Standard NBR.....	101
2.1.	Materials.....	102
2.2.	Methods.....	103
2.2.1.	EAF slag characterization .....	103
2.2.2.	EAF slag filled NBR characterization.....	104
2.3.	Results and discussion.....	107
2.3.1.	EAF Slag characterization.....	107
2.3.2.	EAF slag filled NBR characterization.....	110
2.5.	Conclusion.....	132

3.	EAF Slag Filled recycled NBR scrap.....	134
3.1.	Materials.....	135
3.1.1.	Industrial NBR scrap.....	135
3.1.2.	EAF Slag filled recycled NBR scrap.....	136
3.2.	Methods.....	137
3.2.1.	Recycled NBR scrap Characterization.....	137
3.2.2.	EAF Slag filled recycled NBR scrap.....	139
3.3.	Results and discussion.....	140
3.3.1.	Recycled NBR scrap characterization.....	140
3.3.2.	EAF slag filled recycled NBR characterization.....	150
3.4.	Conclusion.....	156
4.	EAF slag as carbon black replacement for NBR.....	158
4.1.	Materials.....	158
4.2.	Methods.....	160
4.2.1.	EAF slag characterization.....	160
4.2.2.	Compound Characterization.....	161
4.3.	Results and discussion.....	164
4.3.1.	EAF slag characterization.....	164
4.3.2.	EAF slag and carbon black filled NBR characterization.....	166
	Conclusion.....	183
5.	Influence of EAF slag as filler for recycled end of life tyre (ELT).....	184
5.1.	Materials.....	184
	ELT powder.....	184
	EAF slag.....	184
	Compound ELT filled with EAF slag.....	185
5.2.	Methods.....	185
5.2.1.	EAF Slag Characterization.....	185
5.2.2.	Compound Characterization.....	186
5.3.	Results and discussion.....	188
5.3.1.	EAF Slag.....	188
5.3.2.	Compound characterization.....	191
5.3.	Conclusion.....	209
6.	Potential industrial Symbiosis between Steel and Rubber sector in Lombardy.....	211
6.1.	Waste and by-products.....	211
6.1.1.	By-products legislations.....	212
6.1.2.	Waste legislation.....	213

6.2	Case of black slag: management methods.....	214
6.2.1	EAF slag as by-product [341]:.....	214
6.2.2	EAF slag as Waste [341]:.....	216
6.2.3	EAF slag as End of Waste [341]:.....	218
6.3	Advantages arising from the classification of an “output” as a “by-product”.....	220
6.4	Identification of the subjects that can be involved for the use of black slag as filler in polimer matrix (“by-product”).....	220
6.5	Scenarios and economic evaluation of EAF slag management through industrial symbiosis.....	232
6.5.1	Management cost of EAF black slag as waste.....	233
6.5.2	Profit and loss of the management of EAF black slag as by-product: artificial aggregates.....	233
6.5.3	Profit and loss of the management of EAF black slag as by-product: filler for polymeric matrix 235	
6.6	Conclusion.....	243
	Conclusion.....	244
	Future developments.....	245
	References.....	246

## Sommario

Negli ultimi anni l'attenzione globale si è sempre più focalizzata verso uno sviluppo sostenibile spostandosi maggiormente verso un modello di economia circolare. Spesso questo concetto viene associato alla gestione e alla valorizzazione dei rifiuti, ma esso comprende tutto il ciclo di vita di un prodotto, dalla progettazione al fine vita, con lo scopo idealmente, di generare zero rifiuti. Nella realtà produttiva purtroppo difficilmente questo è realizzabile, perciò prendendo a modello la biosfera, la simbiosi industriale è una branca dell'ecologia industriale che coinvolge industrie tradizionalmente dissimili in un approccio collettivo che implica lo scambio fisico di materiali, energia, acqua e sottoprodotti per ottenere vantaggi economici oltre che ambientali. Le chiavi della simbiosi industriale sono la collaborazione e le possibilità sinergiche offerte dalla vicinanza geografica. Esistono diversi modelli di simbiosi industriale, quello proposto in questo progetto è il modello sviluppato dall'ENEA, cosiddetto "a rete" che tramite un'analisi del contesto territoriale e dei settori produttivi individua possibili flussi simbiotici e fa in modo di mettere in contatto tra loro anche aziende del tutto dissimili.

È in tale contesto che questo progetto di dottorato si colloca. Lo scopo del lavoro è stato quello di eseguire una caratterizzazione ingegneristica relativa ad una nuova applicazione della scoria da forno elettrico ad arco, come filler in matrici polimeriche, con particolare focus sulla gomma vulcanizzata; parallelamente è stato eseguito uno studio di questi due settori, tradizionalmente molto lontani tra loro nell'ottica implementare una simbiosi industriale basata appunto sullo scambio della scoria. Questa attività di è stata condotta con il supporto e la guida dell'ENEA.

Il motivo per cui sono stati scelti questi settori è che da una parte l'Italia è il principale produttore europeo di acciaio da forno elettrico, e più del 50% delle grandi imprese italiane di trova in Lombardia; conseguentemente in questo territorio viene prodotta una ingente quantità di scoria. Nonostante la scoria venga già riutilizzata nel settore delle costruzioni come aggregato artificiale, è stato stimato che purtroppo ancora un 30% venga smaltito in discarica (Federacciai, Rapporto Sostenibilità 2021). Per questo motivo è necessario studiare nuove applicazioni per tale materiale. Nel 2015 è stata proposta per la prima volta l'applicazione innovativa della scoria come filler in matrici di polipropilene e resina epossidica (Cornacchia et al., JOM, 2015). Nella presente ricerca ci si è focalizzati su matrici elastomeriche data la distribuzione geografica delle imprese operanti nel settore delle guarnizioni: si è stimato che, anche in questo caso, più del 50% delle grandi imprese è situata in Lombardia. Oltre a questa condizione certamente favorevole per l'implementazione di una simbiosi industriale è stato riscontrato un elevato interesse da parte di entrambi i settori, quello dell'acciaio e quello della gomma, a sviluppare lo studio di materiali elastomerici additivati con scoria nera da forno elettrico dati i potenziali vantaggi non solo ambientali ma anche economici che se ne potrebbero trarre.

Il tema della valorizzazione dei rifiuti non è un tema sensibile unicamente per i produttori di acciaio per quanto riguarda la scoria, ma anche per i produttori di articoli in gomma in quanto diversamente dai materiali termoplastici essa non è riprocessabile con il solo apporto del calore a causa dei legami chimici che vengono formati nel processo di vulcanizzazione. La produzione di pezzi in gomma porta con sé una considerevole percentuale di scarto, non dovuto a difettosità ma intrinseco nel processo. Ad oggi esistono dei processi di devulcanizzazione ma non sono comunemente attuati principalmente per i costi ancora troppo elevati. A tale proposito, in questo progetto di dottorato gli scarti industriali da articoli tecnici e anche il polverino di pneumatico fuori uso (data la sua grande rilevanza ambientale) sono stati riciclati tramite un processo

semplice di calandratura senza l'aggiunta di additivi. L'influenza della scoria come filler è stata valutata anche in questi ultimi.

Il lavoro svolto è strutturato in una prima parte di revisione della letteratura, articolato come segue:

- I) Analisi dei concetti di economia circolare, ecologia industriale e simbiosi industriale al fine di definirne caratteristiche e mutue relazioni. Particolare attenzione è stata prestata al concetto di simbiosi industriale in termini di origini, definizione e modelli. Il modello "a rete" proposto dall'ENEA sarà quello adottato nel capitolo dedicato alla simbiosi industriale potenzialmente basata sul trasferimento della scoria tra il settore dell'acciaio e della gomma in Lombardia.
- II) Analisi del settore dell'acciaio, in particolar modo della scoria d'acciaio. È stata riportata una panoramica delle varie tipologie di scorie derivanti dai diversi processi e/o fasi di processo con le relative caratteristiche. In particolar modo ci si è focalizzati sulla scoria nera da forno elettrico ad arco, oggetto di questo studio per cui è stata riportata più nel dettaglio il processo produttivo e le metodologie di caratterizzazione. Potenzialmente la scoria nera rilascia metalli pesanti pericolosi per l'ambiente e per l'uomo, per questo motivo in letteratura sono riportati metodi che rendano la scoria più stabile da un punto di vista della lisciviazione per un riutilizzo sicuro della stessa.
- III) Analisi dei metodi di caratterizzazione delle matrici polimeriche caratterizzate. Dopo una breve panoramica sulla caratterizzazione della resina epossidica (matrice polimerica termoindurente) è stata analizzata più nel dettaglio la matrice elastomerica. La gomma nitrilica utilizzata, NBR (Nitrile-butadiene rubber) è stata descritta in termini di proprietà e applicazioni prima di passare ai processi produttivi di articoli tecnici che comportano lo scarto sopra menzionato. La seconda matrice elastomerica caratterizzata è stato il polverino di pneumatico fuori uso (PFU) riciclato, per cui è stata fatta una revisione della letteratura circa la gestione e i possibili utilizzi. Infine, un paragrafo è stato dedicato alla caratterizzazione della gomma vulcanizzata in termini di:
  - cinetica di vulcanizzazione tramite curva reometrica;
  - densità di reticolazione;
  - proprietà meccaniche statiche, ovvero la durezza (con focus sulle diverse scale utilizzate nell'industria della gomma), e il comportamento a trazione e a compressione;
  - valutazione del comportamento viscoelastico (rilassamento degli sforzi, creep, deformazione permanente e effetto Mullins);
  - comportamento dinamico meccanico al variare di temperatura e frequenza, e ampiezza di deformazione. Le gomme additivate con carbon black presentano un andamento non lineare del modulo conservativo dinamico, che all'aumentare della deformazione imposta cala in modo significativo.
  - interazione tra carica e matrice tramite diverse procedure sperimentali sia sulla gomma vulcanizzata che non;
  - comportamento tribologico.

Una seconda parte relativa all'attività sperimentale svolta, suddivisa nelle diverse matrici polimeriche caratterizzate:

- I) Confronto del comportamento meccanico di una resina epossidica additivata con scoria e con sabbia di fiume al fine di proporre un materiale di scarto come alternativa a un materiale naturale

nelle cosiddette malte epossidiche. La scoria utilizzata è stata caratterizzata in termini di composizione chimica e fasi mineralogiche, inoltre è stato valutato il comportamento a lisciviazione della scoria inglobata all'interno della matrice polimerica. Si è evidenziato come la scoria rappresenti una valida alternativa alla sabbia da un punto di vista di performance meccaniche del composito e come la lisciviazione della scoria inglobata venga ridotta al di sotto dei limiti imposti per il riutilizzo sicuro della scoria.

- II) Caratterizzazione di una NBR standard additivata con una crescente percentuale di scoria. La scoria utilizzata anche in questo caso è stata caratterizzata in termini di composizione chimica, fasi mineralogiche e comportamento a lisciviazione. Come per la resina epossidica, la lisciviazione degli elementi pesanti è ridotta nel momento in cui la scoria viene inglobata nella gomma (al di sotto delle soglie imposte per lo smaltimento in discarica come inerte). Da un punto di vista del composito, è stata condotta una caratterizzazione a tutto tondo evidenziando un irrigidimento globale che in applicazioni di tenuta può comportare un vantaggio. È stata inoltre valutata l'interazione tra scoria ed NBR, e i risultati sperimentali portano ad affermare che tale interazione esista.
- III) Caratterizzazione di sfrido industriale NBR, e influenza della scoria in diverse granulometrie. È stato riscontrato che nonostante lo sfrido riprocessato tramite un processo semplice come la calandratura e il successivo stampaggio a compressione non consenta di creare geometrie complesse le sue proprietà meccaniche si mantengono globalmente buone senza alterazioni nella struttura chimica dovute a ossidazione o degradazione del materiale (spettro ATR-FTIR). Per quanto riguarda la scoria, anche in questo caso è stato evidenziato un irrigidimento e da un punto di vista di interazione carica-matrice sembra che questa aumenti per granulometrie più fini grazie a una maggiore superficie di adesione.
- IV) Il carbon black è il filler più utilizzato nell'industria della gomma grazie alla sua spiccata proprietà di rinforzo. Tuttavia, l'impatto ambientale legato alla sua produzione è enorme. Per questo motivo negli ultimi anni si stanno studiando filler alternativi. In questo capitolo la scoria è stata utilizzata in matrice NBR come filler sostitutivo e parzialmente sostitutivo del carbon black al fine poter ridurre anche solo parzialmente l'utilizzo di questo prodotto inquinante. I risultati sperimentali hanno evidenziato come per alcune proprietà meccaniche la gomma additivata con scoria possa rappresentare una alternativa a gomme standard. Sono state inoltre condotte delle prove di stampaggio a iniezione sulla base di dati di laboratorio che non evidenziavano differenza tra la cinetica di reticolazione della gomma additivata con carbon black e con scoria. Tuttavia, è emersa qualche problematica nella processabilità della gomma additivata scoria, perciò saranno necessarie ulteriori prove di processo.
- V) Caratterizzazione di polverino PFU riciclato e additivato con scoria da forno elettrico. Il processo di riciclo tramite calandratura a freddo e senza additivi ha permesso di ottenere un materiale coeso e compatto. La scoria, il cui tasso di lisciviazione di metalli pesanti è ridotto nella matrice PFU, permette variare alcune proprietà come la durezza, la conducibilità termica, e il coefficiente di attrito ampliando lo spettro delle possibili applicazioni del PFU tramite l'aggiunta di un altro materiale di scarto.

- VI) Analisi di una simbiosi industriale potenziale tra il settore dell'acciaio e quello della gomma. L'implementazione della simbiosi industriale da un punto di vista normativo prevede che i materiali scambiati non siano classificati come "rifiuti" ma bensì come "sottoprodotti". Per questo motivo è stata analizzata la normativa riguardante i sottoprodotti (con le relative criticità), quella dei rifiuti e all'interno del contesto della scoria anche la recente proposta del tavolo scorie di Regione Lombardia relativa alla cessazione della qualifica di rifiuto. In questo contesto, sono stati individuati possibili percorsi simbiotici tra il settore acciaio e il settore gomma tramite banca dati AIDA e codici ATECO 2007. La Lombardia è risultata essere la regione più densa sia di imprese operanti nei suddetti settori, perciò, la suddivisione è stata approfondita anche a livello provinciale. Questa suddivisione geografica è stata poi affiancata dalla classificazione per tipologia di impresa (micro, piccola, media e grande) in accordo con Raccomandazione dell'Unione Europea n. 2003/361/CE. Sulla base delle informazioni raccolte sono state fatte delle considerazioni anche a livello economico sui potenziali benefici dell'utilizzo della scoria come filler in matrici elastomeriche.

I risultati ottenuti in questi 3 anni di dottorato circa l'applicazione della scoria come filler in matrici polimeriche sono incoraggianti in quanto da una parte la problematica principale del riutilizzo della scoria, ovvero la lisciviazione dei metalli pesanti, può essere superata in questa applicazione, e dall'altra è possibile formulare gomme, riciclate e non, con diverse quantità e dimensioni della scoria come filler in funzione dell'applicazione finale.

## Abstract

In recent years, global attention has increasingly focused on more sustainable development, moving towards a circular economy model. Often this concept is associated to the waste management and valorisation, but it includes the entire life cycle of a product, from design to end of life, aiming to the zero-waste goal. Unfortunately, in real production processed this is hardly achievable, therefore taking the biosphere as a model, industrial symbiosis is a branch of industrial ecology that involves traditionally dissimilar industries in a collective approach that involves the physical exchange of materials, energy, water and by-products to obtain economic as well as environmental benefits. The keys to industrial symbiosis are collaboration and the synergistic possibilities offered by geographical proximity. There are different models of industrial symbiosis, the one proposed in this project is the model developed by ENEA, the so-called "network" model which, through an analysis of the territorial context and production sectors, identifies possible symbiotic flows and promotes the communication between completely dissimilar companies.

This PhD project develops in this context. The aim of the work was to perform an engineering characterization related to a new application of electric arc furnace slag, as a filler in polymeric matrices, with particular focus on vulcanized rubber. At the same time, a study was carried out on these two sectors, traditionally very distant from each other in order to implement an industrial symbiosis based on the exchange of slag. This activity was conducted with the support and guidance of ENEA.

The reason why these sectors were chosen is that on the one hand Italy is the leading European producer of electric furnace steel, and more than 50% of large-size enterprises are located in Lombardy; consequently, a large quantity of slag is produced in this area. Although the slag is already reused in the construction sector as an artificial aggregate, it has been estimated that unfortunately still 30% is disposed of in landfills (Federacciai, Sustainability Report 2021). For this reason, it is necessary to study new applications for this co-product. In 2015, the innovative application of slag as a filler in polypropylene and epoxy resin matrices was proposed for the first time (Cornacchia et al., JOM, 2015). In this research we focused on elastomeric matrices given the geographical distribution of the companies operating in the gasket sector: it is estimated that, also in this case, more than 50% of the large-size enterprises are located in Lombardy. In addition to this certainly favorable condition for the implementation of industrial symbiosis, a high interest has been found on the part of both sectors, steel and rubber, to develop the study of elastomeric materials filled with black slag from electric furnaces given the potential benefits not only environmental but also economic that could be derived. The issue of waste valorization is not a sensitive issue only for steel producers as regards slag, but also for producers of rubber articles as, unlike thermoplastics, rubber compounds cannot be reprocessed by heating due to the chemical bonds formed in the vulcanization process. The production of rubber parts implies a considerable percentage of waste, not due to defects but intrinsic in the process. To date, there are devulcanization processes, but they are not commonly implemented mainly due to the still too high costs. In this regard, in this PhD project the industrial waste from technical articles and also the end-of-life tire powder (given its great environmental relevance) were recycled through a simple calendaring process without the addition of additives. The influence of slag as a filler was also evaluated in the latter.

This thesis is structured in a first part of a review of the literature, divided as follows:

- I) Analysis of the concepts of circular economy, industrial ecology and industrial symbiosis in order to define their characteristics and mutual relationships. Particular attention was paid to the concept of industrial symbiosis in terms of origins, definition and models. The "network" model

proposed by ENEA will be the one adopted in the chapter dedicated to potential industrial symbiosis based on the transfer of slag between the steel and rubber sectors in Lombardy.

- II) Analysis of the steel sector, in particular of steel slag. An overview of the various types of slag deriving from the different processes and/or process phases with the relative characteristics has been reported. In particular, the black slag from electric arc furnaces, the subject of this study, was detailed regarding the production process and characterization methodologies. Potentially, the black slag leaches heavy metals that are dangerous to the environment and to humans, for this reason, literature reports several stabilization methods for its safe reuse.
- III) Analysis of the characterization methods of the assessed polymeric matrices. After a brief overview of the characterization of the epoxy resin (thermosetting polymer matrix), the elastomeric matrix was analyzed in more detail. The nitrile butadiene rubber was described in terms of properties and applications before moving on to the manufacturing processes of technical articles that involve the aforementioned waste. The second elastomeric matrix characterized was the recycled end-of-life tire powder (ELT), for which a review of the literature on the management and possible uses was made.

Finally, a paragraph was dedicated to the characterization of vulcanized rubber in terms of:

- kinetics of vulcanization through rheometric curve;
- crosslink density;
- static mechanical properties, namely hardness (with a focus on the different scales used in the rubber industry), the tensile and compressive behavior;
- assessment of viscoelastic behavior ( stress relaxation, creep, permanent set and Mullins effect);
- dynamic mechanical behavior as function of temperature and frequency, and strain amplitude. The carbon black filled rubber compounds show a non-linear trend of the dynamic conservative modulus, which decreases significantly with the increase in the imposed deformation.
- interaction between filler and matrix through different experimental procedures both on vulcanized and uncured rubber;
- tribological behavior.

A second part about to the performed experimental activity, divided into the different polymeric matrices characterized:

- I) Comparison of the mechanical behavior of an epoxy resin added with slag and river sand in order to propose a waste material as an alternative to a natural material in the so-called epoxy mortars. The slag used was characterized in terms of chemical composition and mineralogical phases, and the leaching behavior of the slag incorporated within the polymer matrix was also evaluated. It was highlighted that slag represents a valid alternative to sand from the point of view of mechanical performance of the composite and that the leaching of the slag incorporated into the polymer matrix is reduced below the limits imposed for the safe reuse of the slag.
- II) Characterization of a standard NBR added with an increasing percentage of slag. The slag was characterized in terms of chemical composition, mineralogical phases and leaching behavior. As for the epoxy resin, the leaching of heavy elements is reduced when the slag is incorporated into

the rubber (below the thresholds imposed for landfill disposal as inert). From a composite point of view, a complete characterization was carried out highlighting a global stiffening which in sealing applications can lead to an advantage. The interaction between slag and NBR was also evaluated, and the experimental results lead to the assertion that this interaction exists.

- III) Characterization of NBR industrial scraps, and influence of the slag in different grain sizes. It has been found that, although the scrap was reprocessed through a simple process such as calendaring and subsequent compression molding does not allow the creation of complex geometries, its mechanical properties remain generally good without alterations in the chemical structure due to oxidation or degradation of the material (ATR -FTIR spectrum). As far as the slag is concerned, also in this case a stiffening has been highlighted and regarding the filler -matrix interaction, it seems that this increases for finer granulometries due to a greater adhesion surface.
- IV) Carbon black is the most used filler in the rubber industry thanks to its unique reinforcing properties. However, the environmental impact associated with its production is enormous. For this reason, alternative fillers have been studied over the years. In this chapter, the slag was used in the NBR matrix as a substitute filler (and partially substitute) for carbon black in order to reduce the use of this polluting product. The experimental results have shown that for some mechanical properties the slag filled rubber can represent an alternative to standard rubber compounds. Injection molding tests were also conducted on the basis of laboratory data which did not show any difference between the crosslinking kinetics of the rubber with carbon black and slag. However, some problems have emerged in the processability of the rubber with slag additives, so further process tests will be required
- V) Characterization of recycled ELT powder and ELT filled with electric furnace slag. The recycling process by means of calendaring at room temperature and without additives has made it possible to obtain a cohesive and compact material. The slag, whose leaching rate of heavy metals is reduced in the PFU matrix, allows to vary some properties such as hardness, thermal conductivity, and the coefficient of friction, broadening the spectrum of possible applications of the ELT by adding another material. waste.
- VI) Analysis of a potential industrial symbiosis between the steel and rubber sectors. The implementation of industrial symbiosis from a regulatory point of view requires that the materials exchanged are not classified as "waste" but rather as "by-products". For this reason, the legislation concerning by-products (with the related criticalities), that of waste and, within the context of slag also the recent proposal of the Lombardy Region related to the "end of waste" were analyzed. In this context, possible symbiotic paths between the steel sector and the rubber sector have been identified through the AIDA database and ATECO 2007 codes, in-depth also at the provincial level. This geographical subdivision was then flanked by the classification by type of enterprise (micro, small, medium and large) in accordance with the European Union Recommendation no. 2003/361 / EC. Based on the information collected, considerations were also made at an economic level on the potential benefits of using slag as a filler in elastomeric matrices.

The results obtained in these 3 years of PhD in the application of slag as filler in polymeric matrices are encouraging as on the one hand the main problem of slag reuse, that is the leaching of heavy metals, can be

overcome in this application, and on the other hand, it is possible to formulate rubber compounds, recycled or not, with different quantities and sizes of the slag as filler depending on the final application.

## GENERAL LITERATURE BACKGROUND

### I. Circular economy, industrial ecology, and industrial symbiosis

In the last 15 years there has been a worldwide focus on the new concept and development model of Circular Economy to promote an alternative to the dominant economic development model, the so-called Linear Economy (“take, do and dispose”). The negative effects caused by the linear economy model are threatening the stability of economies and the integrity of natural ecosystems essential for the survival of humanity [1].

The circular economy is seen as a new production and consumption model for a more sustainable development model and a harmonious society. A sustainable development requires a balanced and simultaneous assessment of the economic, environmental, technological and social aspects of an economy, sector (or single industrial process), as well as the interaction between all these aspects.

The circular economy promotes a more appropriate and respectful use of resources to implement a greener economy, characterized by a new business model and innovative job opportunities [2], as well as an improvement in well-being and equity within and between generations in terms of both resource use and access because as stated in the Brundtland Report “A world where poverty is endemic will always be subject to ecological and other catastrophes[3].

The circular economy is often associated with the most appropriate approach to waste management. Such a poor definition can lead to the failure of the circular economy, as some final treatment options (recycling, reuse or recovery) may not be appropriate in a given context but prevention may be the best option. The circular economy has the potential to implement radically new models and help society achieve greater sustainability and well-being at little or no cost to materials, energy and the environment. Finally, it should be emphasized that sustainability models (such as the circular economy) require both new models of innovative economies and innovative actors. Indeed, due to the complexity of sustainable development, the implementation of the circular economy must be supported by innovation planners and intermediaries who drive radical changes in circular economies, policies and decision-making tools. [4]. The application of the circular economy must not only focus on the production process of a product but must include the environmental, social and economic impacts of the product during its entire life cycle. This can be done through life cycle thinking. Life Cycle Thinking involves all three pillars of sustainability: environmental, economic and social whose impacts can be assessed respectively by Life Cycle Assessment, Life Cycle Costing and Social Life Cycle Assessment. Through the life cycle thinking approach, it is possible to test the impacts of circular business models, validate their hypotheses and obtain feedback for improvement. Additionally, it can help define objectives and indicators to measure and promote circularity over time. To assess the impacts of the circular economy, applying a life cycle approach is extremely beneficial [5].

The circular economy as an alternative economic model offers an “approach to achieving local, national and global sustainability” [6]. Implementing an economic model to achieve a better and more sustainable future for all by 2030 [7] can be pursued through the 17 Sustainable Development Goals. Although the overall circular economy goal and the sustainable development goals appear more or less the same (social and economic prosperity within the natural capacity of our planet), the links between these two agendas are not immediately apparent. Indeed, the term “circular economy” does not appear even once in the 2030 Agenda for Sustainable Development, where the Sustainable Development Goals are set.

Waste legislation and policy of the EU Member States shall apply as a priority order the waste management hierarchy given in [8]. The framework Directive on waste 2008/98/EC, constitutes the intervention of the European legislator in the field of waste management, expressing the intention to bring the national laws of the Member States closer to the objectives identified within the Directive, guaranteeing the acceptance of the principles within national legal systems. The Waste Framework Directive pursues the objectives of environmental protection and human health by identifying first of all the need to develop a society devoted to the principle of recycling, in order to first of all avoid the excessive and superabundant production of waste (and therefore potentially polluting matrices potentially impacting on the environment) and subsequently provide for the necessary management of waste produced for recovery. Precisely with regard to these purposes, the European Directive establishes a hierarchical scale of preferential interventions in the field of waste [8]. As shown Figure 1 at the top of the scale is the aim of prevention. In order to reduce as much as possible the potentially negative impact that waste can have on the environmental good and human health, the directive pursues the fundamental preventive objective, to be understood as an attempt to avoid the production of waste materials from the outset, in such a way as to exclude the problematic issues inevitably connected to the subsequent treatment of the materials produced. At an immediately lower hierarchical step is the European purpose of reusing waste. In fact, the European legislator establishes the need, in case of impossibility to implement what has been said on prevention, to organize waste management in such a way that their reuse is pursued, in order to restore, at least as far as possible, utility, avoiding at the same time that these must be subjected to storage operations and definitive disposal, operations which, however, lead to possible harmful consequences for the two assets of constitutional rank protected by the Directive itself. The heart of the directive is the third step of the ladder, dedicated specifically to recycling. In this sense, in fact, in accordance with the purpose of developing homogeneous legislation from the point of view of pursuing the goal of developing a company dedicated and oriented to the recycling of waste materials produced, Directive 98/2008/EC expressly expresses the interest European Union for the recovery of the usefulness of waste, determining, through the processes that guarantee the realization of this purpose, the cessation of these from this qualification. This part of the Waste Framework Directive coincides perfectly with the development of a circular economy, in which the final point of the production process, consisting of waste, can at the same time constitute the origin of a new and fully functional process, in which the waste itself recovers its usefulness of use and exploitation, without posing the problems of no small importance concerning disposal. In the logic of the Directive, disposal constitutes the last resort of the waste management system. In fact, the European legislator intends to minimize (if not, as far as possible, eliminate) the use of waste disposal systems and operations, activities that have always posed the greatest doubts and the greatest criticalities in terms of environmental protection and human health.

Waste legislation and policy of the EU Member States shall apply as a priority order the waste management hierarchy given in Figure 1 [8].

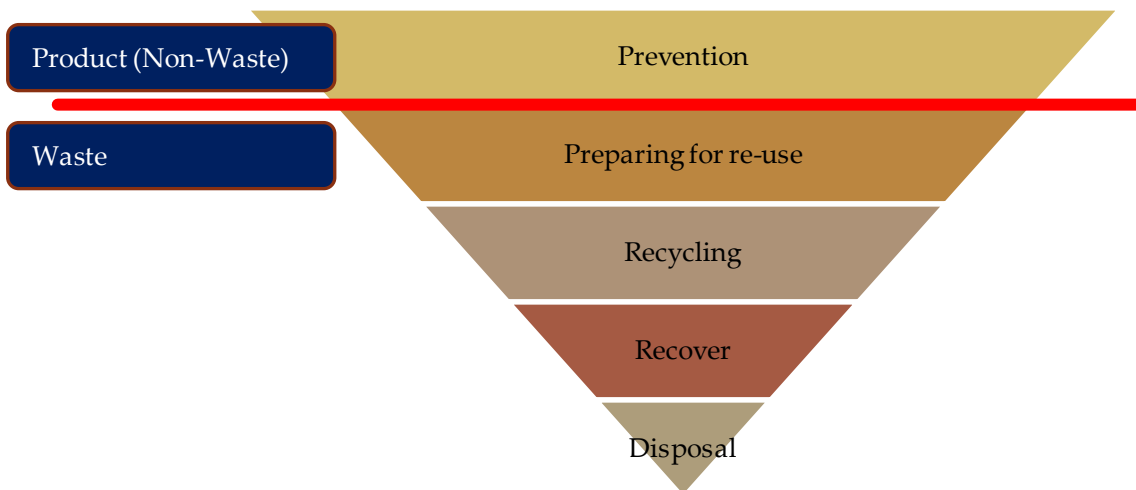


Figure 1 EU waste management hierarchy [8]

A study published in the *Journal of Industrial Ecology* [6] sheds light on the possible interconnections between the circular economy and the sustainable development goals. The study asserts that “circular economy practices can be applied as a ‘toolbox’ and specific implementation approaches to achieve a considerable number of sustainable development goals” [6] and therefore underlines the importance of the transition to the circular economy to successfully achieve the sustainable development goals [9]. Below 5 key relationships between circular economy practices and sustainable development goals are listed based on the study cited [6].

- Sustainable Development Goal 6 – Clean water and sanitation: circular economy practices such as small-scale water purification, sustainable sanitation, wastewater treatment, water reuse and recycling, recovery nutrients, biogas systems etc. they can help increase access to safe drinking water and equitable sanitation, reduce pollution and improve water quality.
- Sustainable Development Goal 7 – Clean and Affordable Energy: Renewable energy systems, energy recovery (heat) and better use in industrial systems (e.g. industrial symbiosis) all contribute to this goal.
- Sustainable Development Goal 8 – Decent work and economic growth: the new circular business models are an important potential source of greater resource effectiveness and efficiency, waste enhancement and green jobs. The implementation of the circular economy represents an opportunity for several trillion euros globally, with an annual net benefit of 1.8 trillion euros in the EU alone by 2030 [4].
- Sustainable Development Goal 12 – Sustainable Consumption and Production: Circular economy practices concern the decoupling of economic activity from the use of resources and associated environmental and social impacts. It is important to underline that this goal is an important enabling factor for the achievement of most of the other sustainable development goals [5], making the indirect impact of circular economy practices even deeper.
- Sustainable Development Goal 15 – Life on Land: at the heart of circular economy practices is the goal of restoring natural capital. This involves the adoption of sustainable and regenerative agricultural and agro-forestry practices that embrace and protect biodiversity and the return of biological material to the soil as a nutrient, fundamental practices for the restoration of terrestrial ecosystems.

The circular economy currently represents a viable option to transform linear flows of materials and energy into circular flows, obtaining benefits in terms of sustainability. In this sense, industrial ecology with its tools can help in the transition to the circular economy. The evolution of the circular economy would not be possible without the existence of concepts and tools of industrial ecology, especially with the implementation of the Industrial Symbiosis. Three levels of contribution of industrial ecology to the circular economy have been identified, such as: conceptual aspects, technicians and politicians [10].

Industrial ecology is a discipline aimed at understanding the circulation of material and energy flows [10]. Therefore industrial ecology must first understand how the industrial ecosystem works, how it is regulated and its interactions with the biosphere in order to determine how the industrial ecosystem can be restructured to resemble how natural ecosystems function [11]. The origin of industrial ecology can be traced to the work of systems ecologists in the 1950s who perceived the industrial system as part of biogeochemical cycles, although, the concept of industrial ecology was first introduced in the late 1950s [11]. The landmark article was published by Frosch and Gallopoulos in 1989, at which time it became increasingly clear that traditional and reactive approaches, such as “end-of-pipe”, were insufficient to treat industrial waste during the product manufacturing processes [12]. The concept of industrial metabolism, introduced by Robert U. Ayres in 1988 [13], is a key concept in industrial ecology, as it focuses on improving knowledge and understanding the social uses of natural resources and their total impact on the environment [14]. In addition to industrial metabolism, the concept of industrial symbiosis is fundamental for industrial ecology. This concept originates from biology and symbiotic biological relationships existing in nature, in which two or more unrelated species exchange materials, energy or information in a mutually beneficial way [15]. Therefore, the principle of industrial symbiosis is to create physical links between independent societies by exchanging energy, materials, water and by-products. Considering this, industrial symbiosis is to be considered a key strategy to close the flows of material [16]. Despite advances in sustainable development and the growing progress of industrial ecology, the evolution of the global economy has been dominated by a linear model of production, in which consumer goods are manufactured from raw materials, sold, used and then discarded as waste. The circular economy concept is based on the study of the real world and non-linear systems, in order to optimize effective flows of materials, energy, work and information (Ellen MacArthur Foundation, 2015 <https://www.ellenmacarthurfoundation.org/circular-economy/concept>). Industrial ecology can be useful for the transition to a circular economy by promoting alternatives to landfill disposal such as reuse, repair, recycling and remanufacturing of products [17]. With these alternatives, it is possible to increase component recovery with their materials and in some cases extend their life cycle.

The Conceptual contribution of industrial ecology to circular economy concerns networks of synergies, such as material energy flows to implement the circular economy through the implementation of symbiosis in industrial and/or urban environments. According to Gregson et al. [18], the integration of industrial symbiosis in the circular economy involves the exchange of by-products and waste in co-located production plants, intensifying the use of localized resources, and enhancing the initial inputs.

Its technical contribution concerns the use of industrial ecology tools to support the implementation of the circular economy. In this case, the tools most used to support the circular economy (Eco-design and Cleaner Production) are linked to the application of industrial symbiosis and implementation in eco-industrial parks. In most cases, when these tools are applied, different energy and material flows, and common infrastructure and services are shared. The study conducted by Li [19] on eco-industrial parks illustrates the feasibility and

rationality of this approach for implementing the circular economy. It can be argued that the implementation of eco-industrial parks is an important practice at an intermediate (meso) level of circular economy as it allows clusters of companies to cooperatively manage flows of materials and by-products [20]. Furthermore, the circular economy can be implemented through methods and strategies such as Cleaner Production and Eco-design. Cleaner production is important to reduce emissions, waste and risks to humans and the environment, however, when the goal is to achieve and maintain industrial symbiosis, a trade-off could occur as cleaner production can reduce or change basically the generation of waste and symbiotic exchanges [21]. Furthermore, the application of cleaner production practices mainly focuses on the efficiency of the production process, while industrial symbiosis and the circular economy are related to systemic thinking and its effectiveness (Ellen Macarthur Foundation, 2014 [https://www.werktrends.nl/app/uploads/2015/06/Rapport\\_McKinsey-Towards\\_A\\_Circular\\_Economy.pdf](https://www.werktrends.nl/app/uploads/2015/06/Rapport_McKinsey-Towards_A_Circular_Economy.pdf)). Eco-design, on the other hand, is an effective strategy to promote the eco-efficiency of businesses and can be a useful eco-innovation practice for the circular economy as it integrates costs, performance, quality and environmental attributes of a product by integrating the aspects environmental aspects in the product engineering design process.

The political and standard contribution concerns the application of industrial ecology to support the development of policies, laws and standards to implement the circular economy in local, regional and global environments. To achieve this systematic transition to a circular economy at the macro level, the collaboration of the business community, policy makers and institutions is essential. Some policy tools can be applied in this broader context of circular economy, such as regulatory tools (including laws and directives), research and education tools, technology transfer and information tools. Circular economy is often considered a broader discipline than industrial ecology due to the inclusion of economic and political issues. Despite this, the evolution of the circular economy would not have been possible without the existence of concepts and tools of industrial ecology.

### 1. Industrial symbiosis

The concept of industrial symbiosis is based on the law of conservation of mass and on the law of conservation of energy, based on which it is possible to deduce that, at least in theory, the quantity of materials and energy not used by an industrial process can be used by another industrial process. At a concrete level, industrial symbiosis involves traditionally dissimilar industries with an integrated approach aimed at promoting competitive advantages through the exchange of materials, energy, water and by-products [22]. Among the key aspects that allow the realization of industrial symbiosis are the collaboration between companies and the opportunities for synergy available in an appropriate geographical and economic environment. The main means by which symbiosis between companies is achieved are [23]:

- the use of materials traditionally intended as waste or by-products to replace commercial products or raw materials;
- sharing utilities and infrastructures for the use and management of resources, such as steam, energy, water and wastewater;
- the joint provision of services to meet ancillary needs common to businesses related to safety, hygiene, transport and waste management.

From a technical point of view, Industrial Symbiosis can take place in different ways:

- process-oriented industrial symbiosis: refers to a cooperative network around an industrial process;

- residue-oriented industrial symbiosis: refers to a cooperative network around a residual flow;
- place-oriented industrial symbiosis: refers to a cooperative network linked to a specific place [24].

Even from an organizational point of view, industrial symbiosis can occur in different ways, namely anchor manufacturer, eco-cluster development, government planning and business incubator [15], [24]–[26] defined as follow:

- anchor manufacturer means that there are one or two industries with large volumes of production, resources and by-products, seeking economic, strategic and environmental benefits through the exchange of resources [26]. These large industries provide the critical mass for the development of industrial symbiosis within an eco-industrial cluster [15];
- development of Eco cluster means that industrial symbiosis is initiated by government and/or industrial actors who elaborate a common strategic plan to create the network [27];
- government planning means that industrial symbiosis is initiated by a public/government institution with the aim of increasing the productivity and resilience of the economy by reducing the environmental impact [27];
- business incubator means that industrial symbiosis is initiated by a private project implementer who is economically interested in attracting or growing industrial or commercial tenants capable of engaging in symbiosis [25].

These are the ways in which an industrial symbiosis system is generated and structured from a technical and organizational point of view.

### Origins

In 1947, George Renner used an ecological science-based approach to describe the organic relationships between industries, describing ways in which a company can deliver its waste to another industry that can use it as raw materials. Renner has described these relationships as the industrial equivalent of the symbiosis occurring in ecosystems [28], but did not use the term “industrial symbiosis”. Ayres (1988) subsequently proposed the term “industrial metabolism”, and subsequently expanded the concept to describe the entire integrated collection of physical processes that convert raw materials, energy and labour into finished products and waste. The development of the theory of industrial symbiosis has involved both the discussion and refinement of the underlying theory, and the development of practical applications. Frosch and Gallopoulos in 1989 proposed the concept of “industrial ecosystem” and observed that the traditional model of industrial activity should be transformed into a more integrated model which is the industrial equivalent of a natural ecosystem [12]. Lowe and Evans in 1995 [29] described several ways in which an industrial ecosystem is analogous to a natural closed-loop system. In summary, these contributions provided a theoretical basis for the development of research on industrial symbiosis. However, this approach has been recognized previously, albeit without an underlying theoretical framework. In the 1970s, a group of companies from different industrial sectors in the city of Kalundborg (Denmark) began to work closely together to reduce costs, strengthen waste management and use fresh water more efficiently. During the late 1980s, some local students recognized many links between Kalundborg’s industries. Basing their description on Valdemar Christensen’s Danish terminology, researchers have begun to use the phrase “industrial symbiosis” to describe the Kalundborg system [30]–[32]. Kalundborg subsequently began to formally develop relations between the park’s industries and its success attracted worldwide attention and stimulated many subsequent studies [33].

## Definitions

The term “symbiosis” was introduced into biology from the Greek language (“living together”) by Anton de Bary in 1879 [34]. Symbiosis is a biological term that refers to “a close and prolonged coexistence of two species or types of organisms”. The prerequisite for an industrial symbiosis complex is cooperation between companies, and these companies form a network as a result of that cooperation [15], [35], [36]. The most commonly cited definition of industrial symbiosis was proposed by Chertow as follows: “The part of industrial ecology known as industrial symbiosis engages traditionally separate industries in a collective approach to competitive advantage involving physical exchange of materials, energy, water and by-products. The keys to industrial symbiosis are collaboration and the synergistic possibilities offered by geographic proximity” [15]. This definition has been accepted by many later researchers [37], [38]. Cooperation to exploit the synergistic possibilities offered by the geographical proximity of companies has been identified as a key point for the implementation of industrial symbiosis. This is because relationships between companies involve physical exchanges of materials (including water), energy, and by-products, and these exchanges occur more efficiently over short distances. Subsequently, it was noted that the reports could also include exchanges of knowledge and use of shared infrastructures [39].

In Chertow’s definition all the terms refer to the ecological metaphor which is considered the foundation of industrial symbiosis, and more generally of industrial ecology. Many have a strong (not singular) association with a particular academic discipline, such as “exchange” with economics, “competitive advantage” with business, and “physical resources” with engineering and the natural sciences. Chertow’s definition was proposed based on the knowledge of industrial symbiosis at the time, well before the establishment of the National Industrial Symbiosis Programme in the United Kingdom, the only national, facilitated industrial symbiosis program free and open to all comers. Chertow’s definition was proposed based on the knowledge of industrial symbiosis at the time, well before the establishment of the National Industrial Symbiosis Programme in the United Kingdom, the only national, facilitated industrial symbiosis program free and open to all comers. Since then, industrial symbiosis has been “uncovered” in many countries and Chertow’s definition has served to promote discussion and debate amongst the research community, in part due to varying interpretations of its terms. In 2012 Lombardi and Laybourn proposed an alternative definition that classifies industrial symbiosis as a business opportunity and tool for eco-innovation; Eco-efficiency gains are not a driver of industrial symbiosis but are generally the result of it, and geographic proximity is not mentioned because it is neither necessary nor sufficient for industrial symbiosis. This definition also carries forward various concepts introduced by Chertow and states: “Industrial symbiosis engages diverse organizations in a network to foster eco-innovation and long-term culture change. Creating and sharing knowledge through the network yields mutually profitable transactions for novel sourcing of required inputs, value-added destinations for non-product outputs, and improved business and technical processes” [40].

## Industrial symbiosis models

From an organizational point of view, industrial symbiosis can be achieved according to different approaches: development experiences of industrial symbiosis districts (bottom-up approach), eco-industrial parks (top-down approach) and networks for industrial symbiosis [22].

***Bottom-up approach: the Kalundborg case***

Kalundborg is a small town in Denmark for which the symbiosis process began spontaneously in the 1960s, due to the need for companies to find alternative solutions for water supply. Different but complementary companies have been pushed to cooperate, obtaining mutual economic benefits, with an open management style and in a climate of mutual trust. What has been generated, in fact, is an industrial, or even territorial system, which operates according to the principles of industrial symbiosis: a network of exchanges of secondary materials, production waste and residual forms of energy has been created which increase efficiency of individual production processes and which significantly reduce the environmental impact and the production costs. The entities are all connected in the same territorial area thanks to physical links with the aim of recycling and reusing waste materials/waste from some production processes. [22]. The first network consisted of cooperation between six companies: an electric power plant, an oil refinery, a biotech company, a construction products company, a waste management company and the local administration. What pushed them to cooperation were mutual economic benefits, the presence of different but complementary industries (different types of production and needs, in the absence of direct competition), an open management style in a climate of mutual trust. Over the years, the network has continued to grow, including new members and adapting industrial processes and exchanges to technological innovations and new regulations. Despite the spontaneous and autonomous initial organization, in 1996 the Kalundborg Symbiosis Center was born, a so-called “matchmaker”, to respond to the problems of management, coordination and expansion of the symbiosis network by including new participants. The Symbiosis Center Denmark was born in 2015, also in Kalundborg, demonstrating the political will to encourage such circular economy practices on an ever-wider scale. This center has in fact the task of identifying and facilitating symbiosis projects between potential partners. It searches for potential cooperation between plants, organizes meetings between the various companies and finally acts as a mediator to implement the agreements. This set of methods therefore supports the transformation of pre-existing industrial processes towards circular and sustainable business models. In 40 years this circular production approach has continued to expand, involving 12 different partners. The interactions are based on energy exchanges (steam and district heating), water recycling (sewage, cooling water, deionized water and sea water) and material recovery (e.g. gypsum, fly ash, sewage, bioethanol, sand, biomass and lignin). For example, the thermoelectric plant exchanges steam with a high enthalpy contribution with the refinery, fulfilling 40% of its requirements and receiving in exchange the exhaust gases from the refining process used by the plant to sustain the furnaces. The excess thermal energy from the electricity production processes is also redistributed between the domestic heating systems of the nearby city, greenhouses and the nearby fish farms. This has enabled the municipality of Kalundborg to do without 3,500 oil-fired domestic heating systems. The plant has also installed a fume purifier through which it obtains 85 tons of calcium sulphate a year, which it subsequently sells to Gyproc (a gypsum manufacturer). For its part, the latter installed a butane tank useful for Statoil in case of maintenance of its plants. Novonordik, a world leader in the production of insulin and enzymes, at the same time distributes sludge and other waste resulting from the production of two-component high-nutrient content to farms and agricultural enterprises as fertilizer thus avoiding having to provide for disposal costs. Finally, most of the companies share the water supply and treatment system. The ashes and combustion residues always generated by the plant in the combustion process are instead transferred to a cement factory for the production of roads and cement. The transformation of this waste into resources, the reduction of pollution and the consumption of materials

together constitute a value of 80 million euros per year, about 275,000 tons of CO<sub>2</sub> less per year, saving about three million cubic meters of water, the recovery of 150,000 tons of gypsum which replaced natural gypsum, and the production of biogas which replaced the extraction of fossil materials.

This type of approach takes the name of “bottom-up” as the system of relations between companies arises independently of a specific urban and industrial planning and has developed over the years in a “physiological” way starting from the initiative of individuals who have been able to understand the economic advantages deriving from this synergy.

### ***Top-down approach: Eco-industrial parks***

The Eco-Industrial Parks belong to US-style initiatives, initially and mainly implemented in the United States/Canada and in Asia. In this case, this is a “top-down” approach, as the eco-industrial park is planned, designed and managed on the basis of the principles of ecology and industrial symbiosis. The goal is mainly to manage the environmental services associated with industrial activities in a unique and integrated way, also in order to simplify the administrative requirements for the management of environmental aspects, rather than the actual closure of resource cycles.

One example is the Burnside Industrial Park, formally known as Dartmouth Industrial Park, one of the largest industrial parks in Canada. The park has a surface extension of about 1400 hectares. There are approximately 1,300 companies in which 17,000 people are employed. 90% of companies are small or medium-sized, and the number of employees per company generally does not exceed 20 employees. The companies present belong to different production sectors (manufacturing, electronics, transport, services): 10% of the companies belong to the manufacturing sector, 48% to trade and services, 11% to the construction industry, 9% to logistics, 8% distribution and 14% other services (professional, financial and other business). The flow of matter, energy and information in the district is complex. The park is well connected through road and railway infrastructures.

The park was initially born as an industrial park and was later gradually transformed into an ec-industrial park. The transformation process began in 1990 when the University of Dalhousie began to investigate the concept of an industrial park as an ecosystem. The aspects taken into consideration in this survey were: practices and technologies for waste reduction, symbiotic relationships, support mechanisms for the functioning of an industrial park as an ecosystem (exchange of programs, information and infrastructures). A training and technical assistance centre was thus created to serve small and medium-sized enterprises. The park has its focus on multidisciplinary research and program development. The objectives of the program concern the development of strategies and tools for the exchange of materials and energy between companies with the consequent reduction of waste and improvement of the environment and economic performance and an overall reduction of the Park's environmental impacts. The park is owned by the Halifax Regional Municipality, and the City's Burnside Park office is responsible for the management and development of the park. The eco-efficiency centre, a non-profit company, involves Dalhousie University, the school for research and environmental studies, the main electricity company (Nova Scotia Power), the Ministry of the Environment, the Regional Municipality of Eastern Canada Halifax [41].

As regards infrastructure services, the networks for water supply and sewage (white and black water) are managed by the public, while private companies provide services for energy and technological networks. An industrial network is promoted within the Park; the main initiatives and activities carried out are:

- the eco-efficiency center;

- an eco-business program that concerns the adoption of a code of environmental excellence, target for the differentiation of solid waste, the reduction of water consumption, energy efficiency, reduction of liquid waste and a reward mechanism for the best initiatives;
- the exchange of products, especially in the field of packaging materials;
- promotion of the benefits and needs of functions such as: reuse, recycling and reprocessing in companies recently established in the park. About 15% of the Park's businesses offer rental, repair, recovery, rework or recycling services;
- other networking mechanisms, including: a municipal silver recovery network, training activities on environmental aspects for employees and a recovery center for small quantities of different materials to be supplied to education centers for manual activities.

The Eco efficiency center offers the following services:

1. networking;
2. assistance to companies to improve their efficiency, reducing the consumption of energy, water, raw materials, and consequently reduce pollution;
3. training and promotion of education programs;
4. information (magazines, reports, etc.);
5. commercial assistance program that supports eco efficiency and eco design, the management of the life cycle in a timely and competent manner;
6. availability of quick information to facilitate business networks and material exchanges.

An example of technical assistance provided to companies is the "Sustainable Prosperity Program for SMEs", aimed at reducing the use of energy, water, chemicals and waste production, with a view to rationalizing operations and reducing costs; the program, at no cost to the companies that experience it, is structured in 4 steps that accompany the development of a personalized strategy:

1. the company compiles a framework of basic information (the activities carried out, current consumption, the objectives to be achieved)
2. the eco-efficiency center, based on the information provided, plans and carries out an inspection of the company (assessment of the major problems, opportunities, main sources of financing); on the occasion of the visit, a toolkit ("Greening Your Business") is delivered to start the eco-efficiency initiatives
3. the eco-efficiency center, on the basis of the results of the inspection, reviews the general picture together with the company: a list of possible interventions is drawn up, from which the company selects the most feasible and on the basis of these taxes (or updates) its environmental policy
4. Six months after the initial framework, the center conducts a follow-up visit to monitor consumption and waste production, establishing which strategies were most effective, the greatest obstacles and how the center can provide further support to strengthen long-term strategies.

At the end of the course, the center is also involved in promoting the results obtained by individual companies [42].

### *Networks for industrial symbiosis*

Networks for industrial symbiosis, on the other hand, are cognitive/relational tools aimed at allowing the meeting between supply and demand of resources (in the broad sense understood by industrial symbiosis) between interlocutors who, due to economic and social activity, otherwise have no opportunity to meeting. Unlike eco-industrial parks, networks for industrial symbiosis do not have the objective of planning and

managing the flows of material and energy between the various companies, but rather provide industries with an interconnection tool between different companies that otherwise would not they would have the opportunity to interface with each other.

An example of a network for industrial symbiosis is the ENEA methodology.

#### *ENEA Methodology for Industrial Symbiosis*

The ENEA methodology was created to support companies in the implementation of industrial symbiosis paths and consists of three phases[43][44]:

##### 1) Cognitive phase:

- analysis of the territorial context and of its productive sectors;
- creation of a company database also geo-referenced;
- networking and promotion activities through more moments of contact with the selected companies located in the area and other stakeholders (e.g. public authorities, decision makers, institutions and associations of category) to illustrate the project and invite them to the workshops organized in order to get information on company inputs-outputs;
- sending emails to the companies taking in part in the workshops where are asked to fill in ENEA input-output table before the meeting to carry out a data collection on resources that they want to put in sharing within the project (those resources could be eventually updated and improved both during and after the workshops);
- organization of workshops in which ENEA identifies together with the companies the possible symbiotic synergies using input-output tables.

In the first phase it is interesting to underline that the ENEA input-output table is a data sheet to obtain information on resources that companies want to voluntarily share with others. That one foresees a taxonomy for the inventory of inputs or requested resources and of outputs or generated resources by companies [45], taking into account as resources “materials, energy, services, skills” and using code systems officially used in Italy (according EU regulation) for different kind of inventories (e.g. Nace codes, ATECO codes, ProdCom, EWC) with which companies normally deal with. Information asked in the input-output tables for collecting data are, in fact, the more simplified available in order to allow companies to fill the tables with the less possible effort, because information asked are those already used by the companies for their normal management.

##### 2) Operational phase:

- carry out workshops with companies;
- a first moment of “data processing” during the workshops, i.e. the analysis of all the input-output data and identification of synergies with the companies;
- after the workshops, ENEA sends back an email to the companies with the list of shared resources by each company for their final control so that after information shared by companies through input-output tables are loaded on the ENEA platform;
- a second moment of “data processing” in which through the ENEA platform to identify further synergies compared to these ones found during the workshops;
- selection of the paths of IS to be proposed to companies;
- in-depth study of all issues to implement the pathway;
- first drafting of operating handbooks reporting selected industrial symbiosis paths.

Data elaboration and searching for synergies has also been realised with the help of the industrial symbiosis platform ([www.industrialsymbiosis.it](http://www.industrialsymbiosis.it)) developed by ENEA and used, with the same metrics and taxonomy in similar projects in Italy and abroad. The platform is based on the concept of industrial symbiosis which engages traditionally separate industries and other stakeholders in a network to foster eco-innovation strategies and a more sustainable use of resources [15], [40]. It works through: the interconnection (networking) among traditionally separated stakeholders (users) through matching between demand and supply of resources shared by companies; existing databases and/or created by users that can be geo-referenced through Geographic Information System; a central manager, that is ENEA.

3) Stakeholders consultation:

- discussion about the feasibility of implementing the identified industrial symbiosis paths;
- meeting between representatives of trade associations, local authorities and other institutional stakeholders who discuss the problems identified in the manuals and eventually revise their contents.
- enrichment of the handbook according to the feedback obtained during the consultation tables and drawn up in their final draft to be delivered to the companies.

In this last phase it is important to underline that the handbook offers a systemic approach and knowledge base to support companies in the implementation of industrial symbiosis patterns found during or after the workshops, providing specific and tailored information for regulations, standards, logistical aspects, technical aspects, etc related to the specific synergy analysed. The handbook is organised in a first synthetic part (summary scheme) and a second containing all the useful documentation (technical dossier), cited in the first part. This useful tool aims to verify the feasibility of the synergies identified from a technical, logistics, economic and regulatory point of view through a holistic approach that analyses every single step of the path. The handbook allows identifying the issues to deepen/solve or barriers to overcome in order to implement synergies such as characterization and qualification of materials or administrative requirements. Moreover, this document can be a solid starting point for the setting up of an handbook, valid in an average way, and that allows the replication of the described IS pathways at similar cases.

In Figure 2 a summary diagram of the ENEA methodology for the implementation of an industrial symbiosis network is shown.

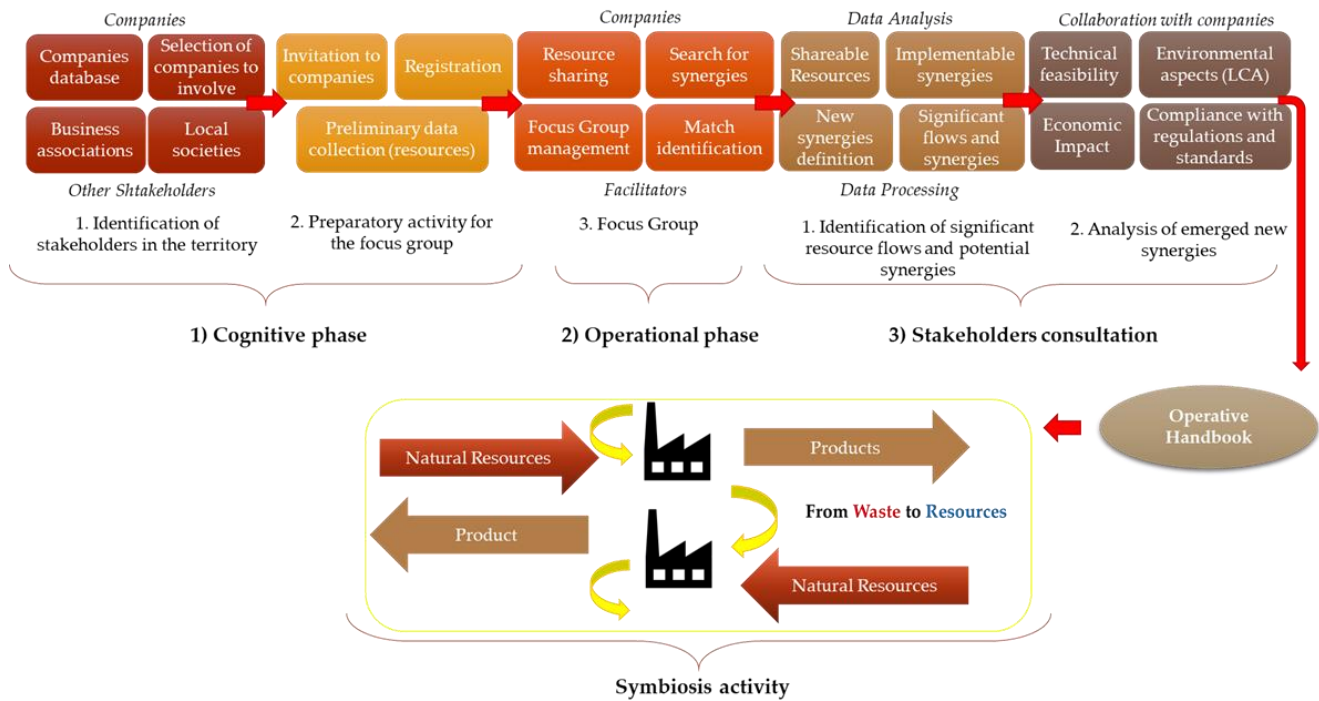


Figure 2 Summary diagram of the ENEA methodology for the implementation of an industrial symbiosis network [46]

**Advantages and criticalities of industrial symbiosis**

A circular production system is created in which, basically, the traditional concept of waste disappears, since the resources being exchanged are never waste at any moment of their existence, but always economic goods. In this way, industrial symbiosis allows a set of companies to jointly achieve profit maximization through the internalization of their externalities, so as to create important advantages for the business system and the community, both in economic and environmental terms. If, on the one hand, the costs of waste disposal are reduced, which can even turn into sources of income, on the other hand, the consumption of natural raw materials is reduced with related extraction costs and emissions harmful to the environment. Up to now the environmental and economic advantages linked to industrial symbiosis have been emphasized, but there are also positive implications from a social point of view. The different companies find themselves collaborating to achieve a common goal by bringing a cultural change within the so-called sharing economy. Therefore, the advantages of industrial symbiosis can be summarized in environmental, economic and also social advantages as schematized in Figure 3.



Figure 3 Advantages linked to the implementation of industrial symbiosis [47]

However, the implementation of industrial symbiosis presents some critical issues and can represent an obstacle to the maximum performance of this resource optimization strategy. The main criticalities are of a regulatory, technical-economic and social nature.

At a regulatory level, taking Italian legislation as an example, despite the D.M. 264/16 (by-product decree [48]), the transfer of waste from one company to another is very complex. For this reason, companies that often find themselves faced with procedural and interpretative uncertainties as a precaution prefer to implement a more restrictive interpretation of the legislation, applying the management conditions provided for waste to other industrial residues that could be exploited. In this regard, it would be desirable to clarify the legislation, harmonize it at national and European level, and streamline the procedural process.

The technical-economic criticalities are linked to various aspects. Firstly, to transport costs in different geographical areas, it goes without saying that the greater the added value of the resource, the greater the distance that makes the synergy advantageous. Secondly, productivity, volumes and quality of the waste must be continuous and give guarantees as a new raw material entering a new process. Finally, since often the waste to assume the character of raw material must be treated in special plants, the initial investment is also an important aspect.

Finally, the social criticalities are linked to the relationships of trust between the collaborating companies, since the role of supplier and customer is declined in a new way in a climate of profitable cooperation for all in a broader sense.

## 2. Industrial symbiosis as a circular economy perspective and industrial ecology perspectives

Industrial symbiosis is a collective approach that brings competitive advantages in which separate industries create a cooperative network for the exchange of materials, energy, water and/or by-product, playing an important role in the transition towards sustainable development [15], [31]. Regarding issues related to resource depletion, waste management and pollution, industrial symbiosis plays an important role in the transition to sustainable development. Two conceptual perspectives on industrial symbiosis can be identified in the literature: the industrial ecology perspective and the circular economy perspective. Despite the recognition of these two perspectives, their relationship remains unclear and no explicit attempts have yet been made to develop an integrated perspective.

The concept of industrial symbiosis has its origin in the field of industrial ecology, with the prominent example of the Kalundborg eco-industrial park [30], [31]. Within the social science-oriented industrial ecology literature, industrial symbiosis is typically studied as a dynamic collaborative process that evolves over time [49]. In line with the system perspective of industrial ecology, industrial symbiosis is defined as a process of interaction between companies bringing benefits to those who are part of it. More recently, industrial symbiosis has been studied as an example of a business model for the circular economy [50]. The circular economy is a concept that has recently gained traction in politics, business and academia to support a transition from a linear model to a circular model. The advantage of implementing a circular economy model is to reconcile environmental and economic objectives by reducing the use of resources and at the same time stimulating economic growth. Since industrial ecology can be considered as one of the main roots of the circular economy [51], a great commonality between the strands of the circular economy and industrial ecology literature is inevitable. Both industrial ecology and the circular economy are based on the idea of closing the energy and material loops in order to make a reduction in the environmental impact of industries economically attractive. The perspective of the industrial ecology process and the perspective of the circular economy business model focus on different but equally relevant aspects of industrial symbiosis. The industrial ecology perspective provides a good understanding of how industrial symbiosis is implemented but pays limited attention to the role of economic logic in symbiotic exchange; the circular economy perspective provides a good understanding of economic logic but pays no attention to the systemic behaviour of industrial ecology. Figure 4 locates visually the industrial symbiosis concept within the industrial ecology and circular economy research streams. It is immediately visible that while the field of circular economy frames industrial symbiosis as a specific type of business model archetype within a much larger context, the field of industrial ecology frames industrial symbiosis as a prominent example of how industrial ecology principles are applied, and therefore the concept has been studied significantly more in depth. . Figure 4 locates visually the industrial symbiosis concept within the industrial ecology and circular economy research streams. It is immediately visible that while the field of circular economy frames industrial symbiosis as a specific type of business model archetype within a much larger context, the field of industrial ecology frames industrial symbiosis as a prominent example of how industrial ecology principles are applied, and therefore the concept has been studied significantly more in depth.

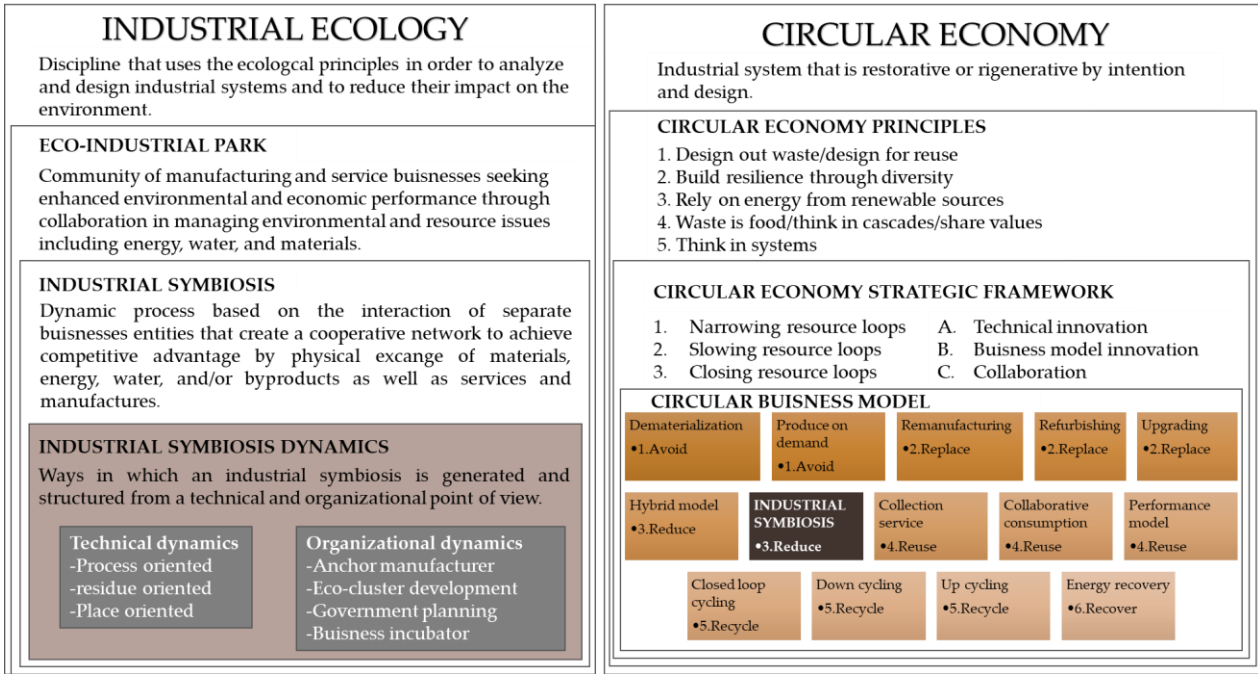


Figure 4 Locating Industrial Symbiosis in the Industrial Ecology and in the Circular Economy research streams [52]

This suggests that the integration of the two perspectives results in a more comprehensive view of industrial symbiosis and will support better design of new industrial symbiosis clusters [53]. Therefore, asked the following research question: *How can industrial ecology and circular economy perspectives on industrial symbiosis be combined in order to support the design of industrial symbiosis clusters?* To answer this question, two sequential research objectives are set. The objective is to investigate the prospects of industrial ecology and circular economy in deeper, comparing them in terms of nature, characteristics and relevance for the study of industrial symbiosis.

**2.1 Industrial Ecology perspective on Industrial Symbiosis**

From the point of view of industrial ecology, industrial symbiosis is framed as a socio-technical process based on the cooperative interaction of separate business entities that exchange materials, energy, water, by-products, services and infrastructure to obtain a competitive advantage [31], [49]. The industrial ecology perspective focuses on the quantitative assessment of the positive environmental impacts of industrial symbiosis through life cycle assessment (LCA) and/or material flow analysis (MFA) [54]. This definition can be visualized on the basis of the three pillars of the industrial symbiosis process, i.e. starting conditions, events and results. The first pillar, the starting conditions, concerns the antecedents that lead to the establishment of the organizations involved, their business profile and specific characteristics, their previous relationships and motivations for collaborating, their initial ideas regarding the technical system and selection of a potential location for the cluster. The second pillar, events, concerns the chain of technical, social and political actions that lead from the starting conditions to the implementation of industrial symbiosis [26]. The third pillar, the results, concerns the economic, environmental and social impact related to the implementation and evaluation of industrial symbiosis [54].

1.1.

### **Circular Economy perspective on Industrial Symbiosis**

From the point of view of circular economy, industrial symbiosis is framed as an archetype of the business model based on the sharing of infrastructures and by-products to improve resource efficiency and create value from waste [50], [55]. The potential of industrial symbiosis as a business model innovation for sustainability can be visualized on the basis of the three pillars of a circular business, namely technical innovation, collaboration and innovation of the sustainable business model. In the case of industrial symbiosis, the first pillar involves technical innovation based on the exchange of waste, resources and energy through multiple production processes [50], [55], [56]. The second pillar, collaboration, concerns the identification of stakeholders who need to collaborate in order for industrial symbiosis to be successfully implemented. The third pillar, the innovation of the sustainable business model, concerns the definition of a specific value proposition around the elimination of the concept of waste, specific value creation/supply activities and cross-sector partnerships to eliminate life cycle waste, specific value acquisition mechanisms to transform waste into value and save virgin material and energy.

The model of linear economy traditionally adopted is no longer implementable because it is threatening the stability of economies and the integrity of natural ecosystems essential for the survival of humanity. The circular economy is the new business model for a more sustainable development model and a harmonious society. Circular economy describes an economic system that is based on business models which replace the 'end-of-life' concept with reducing, alternatively reusing, recycling and recovering materials in production/distribution and consumption processes, thus operating at the micro level (products, companies, consumers), meso level (industrial symbiosis) and macro level (city, region, nation and beyond), with the aim to accomplish sustainable development, which implies creating environmental quality, economic prosperity and social equity, to the benefit of current and future generations. The concept of circular economy is intrinsically linked to that of industrial ecology due to the circular economy goal to maintain the value of products, materials and resources for as long as possible, minimizing the production of waste can be achieved by implementing the circulation of material and energy flows in the industrial system taking the biosphere as a model, thus creating an industrial metabolism. While in the original concept of circular economy proposed by Pearce and Turner in 1989 the environment acts as resource supplier, life supporter system and waste and emission sink, the concept of industrial ecology introduced a different perspective that studies the industrial system and its environment in a unique ecosystem. Therefore, the goal of imitating a natural system cannot be taken literally: it constitutes a vast metaphor with significant differences between industry and nature. The most important is related to the question of "intended purpose" and "natural purpose". The first characterizes the economy, while the second is typical of nature. The economy is "willed", this means it is driven by human will while there is no final goal in nature. Moreover, in the economic system there are no primary producers in the sense in which they operate in nature, the outputs of economic processes are more diversified and the notions economics of the medium of exchange (such as money) and labour have no counterparts in nature. However, it can be assumed the companies as organisms and economies as ecosystems. Both industrial ecology and the circular economy are based on the idea of closing the energy and material loops to make a reduction in the environmental impact of industries economically attractive. The evolution of the circular economy would not be possible without the existence of concepts and tools of industrial ecology, especially with the implementation of the Industrial Symbiosis. Three levels of contribution of industrial ecology to the circular economy have been identified, such as: conceptual aspects, technicians and politicians. Conceptual

aspects contribution concerns networks of synergies, such as material energy flows to implement the circular economy through the implementation of symbiosis in industrial and/or urban environments. Technical contribution concerns the use of industrial ecology tools (linked to the application of industrial symbiosis and implementation in eco-industrial parks-practices of circular economy at meso level) to support the implementation of the circular economy. Political contribution concerns the application of industrial ecology to support the development of policies, laws and standards to implement the circular economy at macro level. The perspective of the industrial ecology process and the perspective of the circular economy business model focus on different but equally relevant aspects of industrial symbiosis. The industrial ecology perspective provides a good understanding of how industrial symbiosis is implemented but pays limited attention to the role of economic logic in symbiotic exchange; the circular economy perspective provides a good understanding of economic logic but pays no attention to the systemic behaviour of industrial ecology. The concept of industrial symbiosis is based on the law of conservation of mass and on the law of conservation of energy, based on which it is possible to deduce that, at least in theory, the quantity of materials and energy not used by an industrial process can be used by another industrial process. At a concrete level, industrial symbiosis involves traditionally dissimilar industries with an integrated approach aimed at promoting competitive advantages through the exchange of materials, energy, water and by-products. Among the key aspects that allow the realization of industrial symbiosis are the collaboration between companies and the opportunities for synergy available in an appropriate geographical and economic environment. The concept of industrial symbiosis is part of the research fields of industrial ecology and the circular economy. The circular economy frames industrial symbiosis as a specific type of business model archetype (at meso level) within a much broader context; industrial ecology frames industrial symbiosis as an important example of how the principles of industrial ecology are applied, and therefore the concept within this line of research has been studied in much more depth. While industrial ecology focuses on all levels of analysis (facility level, intercompany level, regional and global level), industrial symbiosis refers to the intercompany level because it involves physical exchanges between different organizations.

## II. Steel Sector waste: metallurgical Slags

The attention of manufacturing industries in recent years has increasingly focused on the implementation of systems aimed at improving the recycling rate of by-products and the valorisation of waste as an environmentally and economically advantageous alternative to the ever-increasing disposal costs. This is due to the increasing sensitivity towards the preservation of natural resources and the big problem of waste disposal that led the EU commission to issue Directive 2008/98 [57] and the ambitious goal of “zero waste” [58].

Modern steelmaking is an integrated process consisting of blast furnace (BF) ironmaking and basic oxygen furnace (BOF) or electric arc furnace (EAF) steelmaking. Molten steel from BOF or EAF process can undergo a secondary refining process in a ladle furnace, or be sent directly to the continuous caster [59].

About 60% of the world’s steel is produced using the integral cycle, based on the blast furnace (BF), where iron ore is reduced to cast iron, which is subsequently converted to steel in the basic oxygen furnace (BOF). The inputs to this route are mainly iron ore, coal, limestone and steel scrap. The remaining 40% follows the second route, where the ferrous scrap is melted by the electric arc furnace (EAF) [60].

Depending on the steel production process, different type of slags are produced. Mainly they are blast furnace slag (BF), basic oxygen furnace slag (BOF), electric arc furnace acid slag (EAF) and ladle furnace slag (LF) also called refining slag. Parallel to this classification, smelting furnace slag is called “black slag” while ladle slag is called “white slag” as shown in Figure 5. Finally, it is often possible to find a classification that separates the slag from blast furnace (BF), from all the others that take the name of “steel slags” due to the production of “Iron” or “steel”.

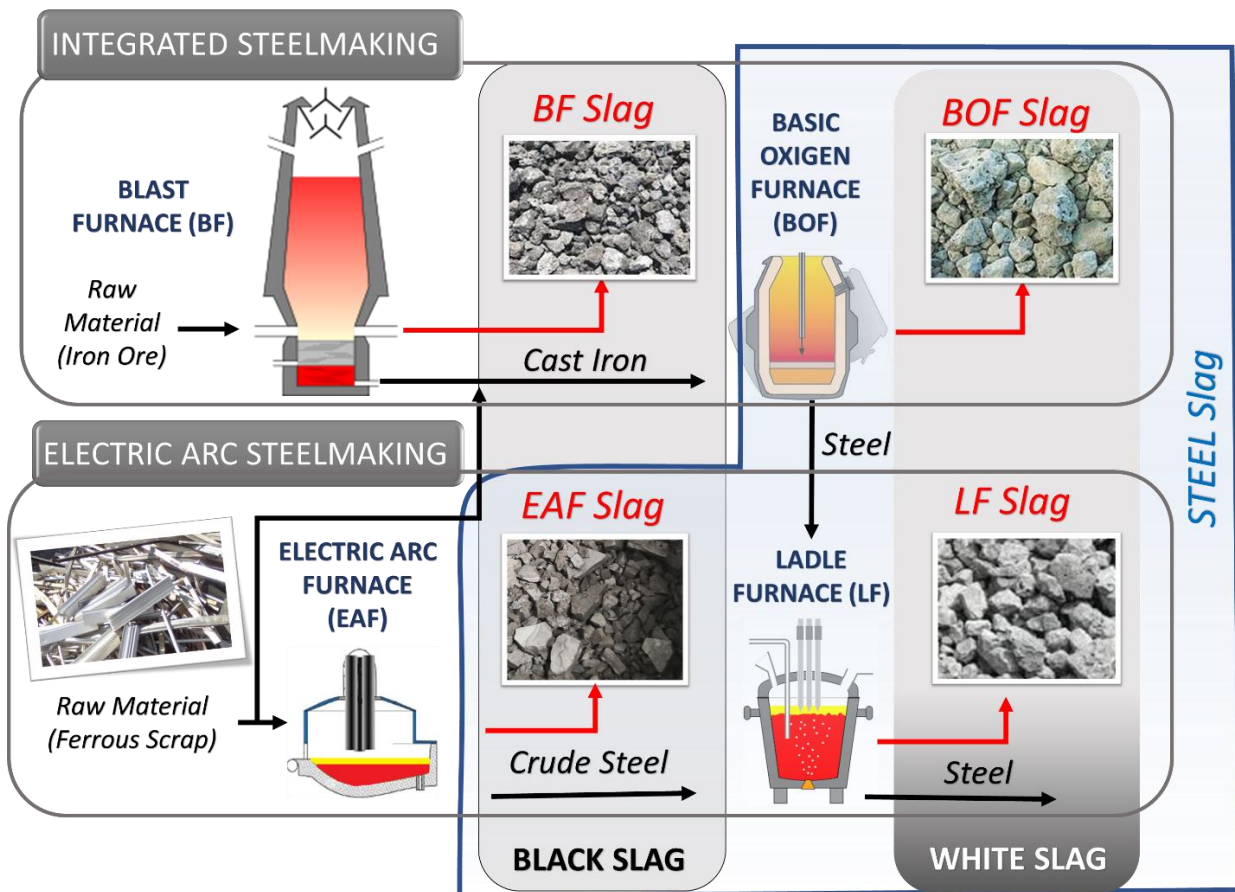


*Figure 5 Principal steelmaking processes and relative slag types.*

This in combination with their integrated and complicated production processes, huge material and energy consumption (13–14 GJ/ton versus 4–6 GJ/ton of steel at EAF [61]), and potentially abundant connections with other actors, makes integrated steel mills hubs for the industrial symbiosis concept. For this reason, the emphasis is mainly placed on case studies involving integrated steel mills [62].

Slag is the by-product produced in greater quantity (90% by mass of all by-products) by iron and steel production.

In 2020, 1828 million tons of crude steel were produced worldwide. Of this amount, 57.7% comes from China. Since slag constitutes about 15% by weight of the steel produced, the amount of slag produced in 2020 is approximately 275 million tons [60].

The slags derived from different processes differ each other in structure, composition, chemical-physical and mechanical properties, due to the characteristics of the raw materials and the adopted technologies.

## 1. Blast Furnace (BF) Slag

In the blast furnace, the cast iron production process is carried out by reducing the metal oxides contained in the iron ore loaded into the blast furnace together with the coke and calcareous fluxes, consisting mainly of calcium and silicon oxides. The slag from blast furnaces originates from physical separation, due to the difference in density between the cast iron and all the other oxides that have not undergone reduction to the metallic state. The composition of the BF slag depends on the characteristics of the feed, but consists mainly of calcium oxide (CaO), magnesium oxide (MgO) and silicon dioxide (SiO<sub>2</sub>), and partly of aluminum oxide (Al<sub>2</sub>O<sub>3</sub>) and modest quantities of other compound minerals.

BF slag is defined by the American Society for Testing and Materials (ASTM) as the non-metallic product, consisting essentially of silicates and aluminosilicates of calcium and other bases that is developed in a molten condition simultaneously with iron in a BF [63]. Air-cooled BF slag solidifies under atmospheric conditions, either in a pit adjacent to the furnace or in one some distance away to which it is transported in large ladles. After solidification, the cooling may be accelerated by water sprays that produce cracking and facilitate digging of the slag.

The average chemical composition of the BF slag (on a sample of more than 100 slag [64]) is reported in Table 1. It is influenced by various factors, including the nature of the mineral, the chemical composition of the streams fed into the kiln, the coke and the type of iron used.

The chemical composition can also change over the years with alterations in the primary sources and the types of mineral to be melted. These variations affect the relative content of the four main constituents (lime, silica, alumina and magnesia) and also the quantities of the minor constituents (sulphur in the form of sulphide and ferrous oxides and manganese).

Table 1 BF slag chemical composition [64].

Component	Component range (%)
Lime (CaO)	31–50
Iron (FeO or Fe <sub>2</sub> O <sub>3</sub> )	0.3–2
Silica (SiO <sub>2</sub> )	27–45
Manganese (MnO)	0.1–2.3
Alumina (Al <sub>2</sub> O <sub>3</sub> )	7–24
Sulfur (S)	0.6–3
Magnesia (MgO)	1–18
P <sub>2</sub> O <sub>5</sub>	<0.1

The minerals constituting BF slag cannot be predicted with certainty from phase equilibrium diagrams, however the most common are melilite  $2\text{CaO}\cdot\text{MgO}\cdot 2\text{SiO}_2$  ( $\text{C}_2\text{MS}_2$ ), and gehlenite  $2\text{CaO}\cdot\text{Al}_2\text{O}_3\cdot\text{SiO}_2$  ( $\text{C}_2\text{AS}$ ). In slags of low lime and high alumina content, the mineral anorthite  $\text{CaO}\cdot\text{Al}_2\text{O}_3\cdot 2\text{SiO}_2$  ( $\text{CAS}_2$ ) may appear. In slag having a high lime content, the dicalcium silicate (or orthosilicate)  $2\text{CaO}\cdot\text{SiO}_2$  ( $\text{C}_2\text{S}$ ) may be formed. This last is one that can cause falling, or spontaneous disintegration, when it changes its crystalline structure from  $\beta$  to  $\gamma$  form [65].

## 2. Steel Slag

### Basic Oxygen Furnace (BOF) Slag

The primary raw materials for the BOF include approximately 70–80% liquid hot metal from the BF, balanced with recycled steel scrap and flux materials, which are mainly limestone, dolomite, and fluorspar ( $\text{CaF}_2$ ) [64]. The oxygen converter allows to produce steel through the oxidation of the excess carbon, silicon and manganese contained in the liquid cast iron. At the end of the conversion process the slag is formed on the surface of the bath, it mainly consists of oxides of lime, silica, iron and manganese, from traces of other metals both oxidized and in the metallic state. The average chemical composition is reported in Table 2.

The main critical aspect limiting the use of BOF slag is the insufficient volumetric stability in the short term, even if it has good properties and environmental compatibility.

Table 2 BOF slag chemical composition [64].

Component	Component range (%)
CaO	35–40
SiO <sub>2</sub>	12–17
Al <sub>2</sub> O <sub>3</sub>	0.98–3.4
FeO	10–25
MgO	3–15
MnO	5–15
SO <sub>3</sub>	0–0.3
P <sub>2</sub> O <sub>5</sub>	0.2–4

### Ladle Furnace (LF) Slag

Following tapping from the BOF or EAF, the molten steel produced by the primary processes can be refined to remove impurities or to add elements to obtain the required chemical composition and grade of product. This refining process is called a secondary steelmaking operation, secondary refining or ladle refining because it is completed within the transfer ladle.

The main characteristic that differentiates ladle slag from EAF slag is the content in iron and calcium oxides: in the LF slag, the FeO content is very low (0-15%), while the calcium oxide CaO is very high (40-60%). Other elements present, Al<sub>2</sub>O<sub>3</sub>, SiO<sub>2</sub>, derive from slag formers, from the deoxidation of steel and from MgO refractories. The LF slag chemical composition range is reported in Table 3.

The LF slag deriving from the production of high-alloy steels may differ from those deriving from the production of carbon steels due to a different quantity of metal oxides present. Given the preponderant presence of calcium and magnesium oxides, these slags after cooling undergo a transformation of the crystalline lattice which leads to the formation of a fine product.

Their main use derives from their chemical composition, so they represent an alternative to lime.

Table 3 LF slag chemical composition [64].

Component	Component range (%)
CaO	30–60
SiO <sub>2</sub>	2–35
Al <sub>2</sub> O <sub>3</sub>	5–35
FeO	0–15
MgO	1–12.6
MnO	0–5
SO <sub>3</sub>	0.1–1
P <sub>2</sub> O <sub>5</sub>	0–0.4

### Electric Arc Furnace (EAF) Slag

The electric arc furnace, used in the steel industry to produce steel starting from ferrous scrap, generates the black EAF slag, or steel slag. Steel slag features vary according to the type of steel being produced (EAF-C slag from carbon steel production and EAF-S slag from stainless/high-alloy steel production) and its chemical composition may present differences related to the type of scrap used, the amount of oxygen blown into the bath and the kiln management practice. In general, the slag can still be assimilated to natural effusive rocks of volcanic origin and consists mainly of a ternary mixture of calcium oxide (CaO), silicon dioxide (SiO<sub>2</sub>) and iron oxides (FeO), to which are added, in smaller percentages, other components. The average chemical composition is reported in Table 4.

The oxides forming the slag can be divided into two main groups, basic oxides, and acid oxides. Amphoteric oxides are also present, i.e. Al<sub>2</sub>O<sub>3</sub> and Fe<sub>2</sub>O<sub>3</sub>, which, depending on the conditions, can be acid or basic [66]. The ratio between the percentage of basic and acidic components (basicity index IB) allows to express and to interpret important metal-slag balances, such as oxidizing power of slag, the balance of desulphurization, and dephosphorization, metal-slag distribution of manganese. The simplest expression of the basicity index, by means of the ratio between the weight percentages of CaO and SiO<sub>2</sub>, does not consider the presence of other components with acidic or basic behaviour, so it is possible to define the complete basicity factor with parameter, calculated as ratio between principal basic oxides (CaO+MgO) and main acid oxides (SiO<sub>2</sub>+Al<sub>2</sub>O<sub>3</sub>). The basicity of the slag is required in steelmaking process in order to preserve the integrity of the refractories, which are also basic, for as long as possible.

The exploitation of steel slag originates from its assimilation to natural hard rocks and therefore from the possibility of replacing inert material in various sectors including construction.

The production process of origin and the transformation of the slag influence the final product and the possibility of being effectively used, so all the necessary checks are carried out on them.

Table 4 EAF slag chemical composition [64].

Component	Component range (%)
CaO	40–60
SiO <sub>2</sub>	10–30
Al <sub>2</sub> O <sub>3</sub>	2–9
FeO	10–30
MgO	3–8
MnO	2–5
SO <sub>3</sub>	0.1–0.6
P <sub>2</sub> O <sub>5</sub>	0–1.2

The RFSC (REACH Ferrous Slag Consortium) for the slag chemical composition, adopts the ternary diagrams for which three specific phases have been taken as a reference, i.e. for the slag EAF-C CaO + MgO, SiO<sub>2</sub> + Al<sub>2</sub>O<sub>3</sub>, FeO<sub>n</sub> + MnO.

On the ternary diagram relating to the EAF-C slag, and similarly for the other families of slag, it was identified, through the analysis of all representative samples of that type of slag subjected to REACH registration, an area indicative of the average of the values and within it the target composition was chosen on which the ecotoxicological and toxicological tests required by the REACH protocol (Figure 6).

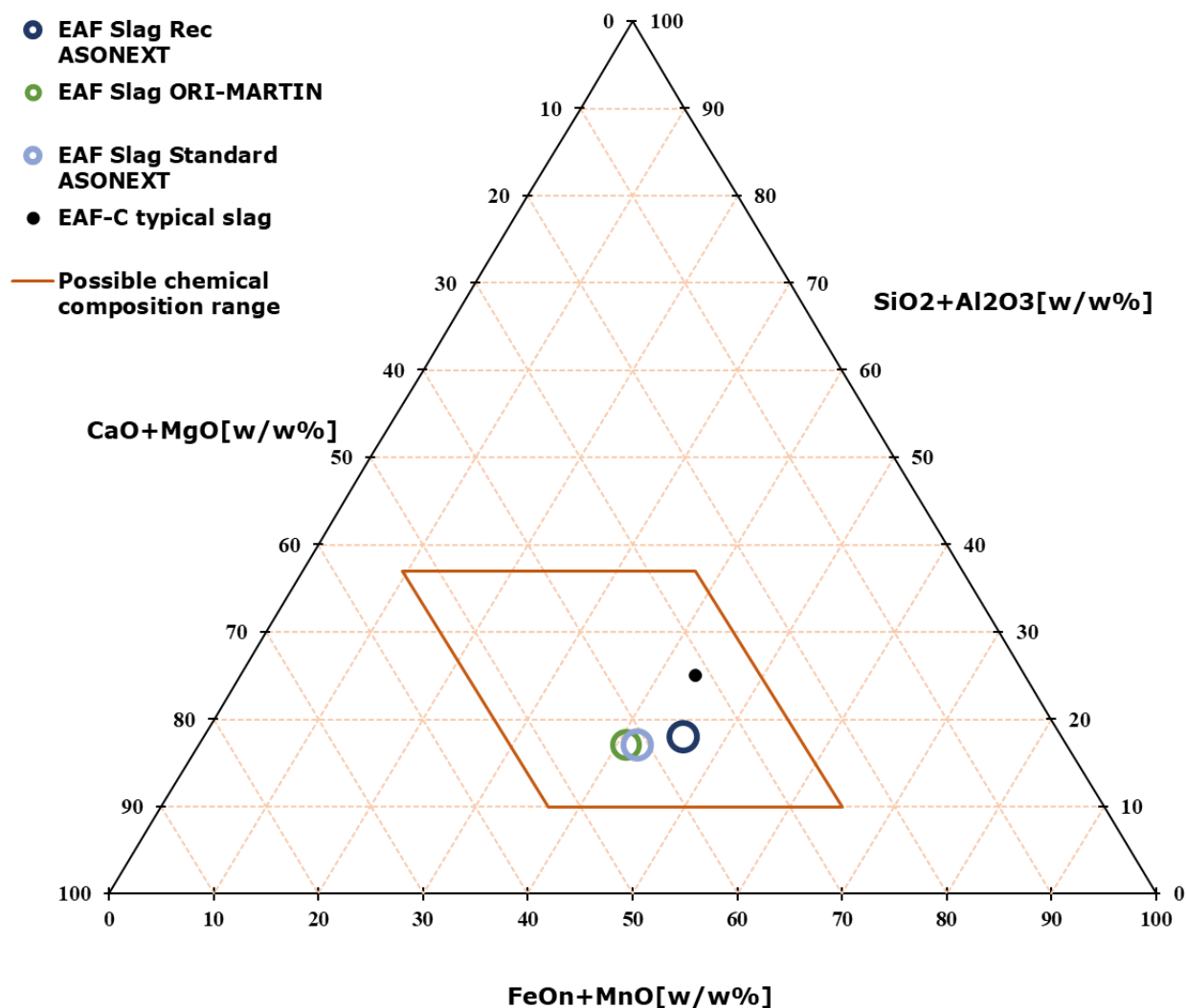


Figure 6 Ternary diagram of EAF slag chemical composition according to REACH Ferrous Slag Consortium. Typical chemical composition, indicative of the average range and chemical composition of 3 EAF slags tested by the author.

The formation of all types of minerals in the slag is influenced by the rapid cooling method that determines its crystalline structure and its chemical composition. The mineralogical components more frequently found in EAF slag from carbon steel production are reported in Table 5.

Table 5 Mineralogical components frequently present in EAF slag.

Primary mineral components	Molecular formula
Larnite	$\text{Ca}_2\text{SiO}_4$
Srebrodolschite	$\text{Ca}_2\text{Fe}_2\text{O}_5$
Brownmillerite	$\text{Ca}_2\text{AlFeO}_5$
Spinel	$\text{CaMgSiO}_4$
Wuestite	$(\text{F}_{11-x-y}\text{Mg}_x\text{Mn}_y)\text{O}_z$
Ghelenite	$\text{Ca}_2\text{Al}_2\text{SiO}_7$
Bredigite	$\text{Ca}_{14}\text{Mg}_2\text{SiO}_{32}$
Chromite	$\text{Cr}_2\text{FeO}_4$

Physical-mechanical properties of steel slag are represented by its high angular shape and rough surface texture. Steel slag has high bulk specific gravity and moderate water absorption. Low impact value, high compressive strength, good polishing, and freeze/thaw resistance [67] are also very favourable steel slag characteristics that permit its main application as a substitute for natural rock or gravel materials.

The EAF slag typically contains heavy metals whose leaching is regulated by the UNI EN 12457-2 standard. In order to increase the eco-compatibility of the black slag and improve its technical characteristics, the following methodologies have been developed: addition of compounds (iron, magnesia and silica flakes) and action on cooling to generate a chemically inert product.

- Fast cooling

Rapid cooling by granulation in water is an effective method for reducing the environmental release of harmful elements present in them. This produces amorphous glass slag, and, by isolating metals and oxides, creates a lowering of the solubility of heavy metals. Considering the microstructure strictly linked to the chemical composition and cooling methods, a hypothesis was formulated about the release behaviour by defining some compositional ranges on the main ternary diagrams ( $\text{CaO-SiO}_2\text{-FeO}_x$  and  $\text{CaO-SiO}_2\text{-Al}_2\text{O}_3$ ) which distinguish the EAF steel slags. Cooling control conditions can represent a strategy to influence the mineral transformation and the solubility of elements such as Cr, which is crucial for problems involving human health and environmental protection. In fact, the rapid cooling should cause the prevention of the leaching of the Cr. The cooling rate is an important parameter in the formation of hexavalent Cr ( $\text{Cr}^{6+}$ ) because this cation is formed at lower temperatures (below  $1228^\circ\text{C}$ ) than those of the EAF process. Chemical compounds that contain  $\text{Cr}^{6+}$  are much more toxic than those that contain  $\text{Cr}^{3+}$  [68].

The rapid cooling in the EAF slag, from the point of view of volumetric stability, generates a reduction in dusting, as the  $\gamma\text{-C}_2\text{S}$  form is prevented in the larnite, a reaction that involves a volumetric expansion and leads to the disintegration of the slag. If the slag is cooled slowly, the presence of a crystalline microstructure is highlighted [68].

- Re-melting and annealing

The remelting process of the EAF slag allows to increase the formation of glassy phases through the addition of vitrifying elements; it can be performed by another electric arc furnace or a plasma torch since these plants allow to reach high temperatures and to remelt the slag. To the detriment of this process, there are high initial investments for the installation of new machines, conspicuous energy consumption and frequent maintenance. Annealing consists of heating to a temperature usually lower than that of melting, followed by a stay of a suitable duration and slow cooling, usually in an oven. The optimal condition for reducing the dissolution of  $\text{Cr}^{6+}$  seems to be annealing at high temperatures above 1273 K and at low partial pressure of oxygen [68]. Some studies [68]. Have highlighted the importance of slow cooling and a reduced basicity of the slag in order to increase the spinel phase very rich in Cr, thus reducing the concentration of Cr in the other phases of the soluble matrix.

- Addition of magnesia and/or silica

The concentration of Magnesium Oxide  $\text{MgO}$  in EAF steel slags seems to favour the immobilization of elements such as Cr, but increases the leaching of other harmful elements such as barium, vanadium, selenium, which have a parabolic dependence as a function of the concentration of  $\text{CaO}$  and  $\text{MgO}$ , while only linear as a function of the silica concentration. A not excessive reduction of the alkalinity of the slag guarantees a good

quality of the product and allows to increase the ability to retain harmful elements such as barium and vanadium.

The correct balance of acidic and basic species in the slag (MgO, CaO, FeO and SiO<sub>2</sub>) is essential for having the favorable microstructure and avoiding chemical leaching. The addition of acidic species to the slag, such as silica, causes a lowering of the melting temperature of the ionic solution which allows the diffusion of oxidized species and their redistribution, leading to the formation of more stable structural constituents at room temperature. In addition to modifying the microstructure to reduce the risk of releasing harmful metals into the environment, this treatment has the advantage of reducing the formation of larnite avoiding the risk of pulverization of the slag.

The combined use of several elements can also be considered, which allows the benefits of each individual chemical species to be exploited [69].

### **EAF slag characterization methods**

The knowledge of chemical, mineralogical and physical characteristics is of fundamental importance for the environmental safety and reuse of slags.

The main analytical techniques used for the slags characterization are listed below.

#### *1. X-Ray Fluorescence Spectroscopy (XRF)*

X-ray fluorescence (XRF) allows the determination of elementary constituents within a material using a simple methodology. This test technique is based on the principle that individual atoms can emit X-ray photons of a characteristic energy or wavelength. The energy or wavelengths correspond to a specific element within the sample and allow for its identification. In other words, using an X radiation of appropriate energy and intensity it is possible to create, by photoelectric effect, a vacancy in an inner shell of the atom of an element. This position is subsequently reoccupied by an electron belonging to one of the outermost shells, which in de-excitation produces a photon that has an energy equal to the difference between the energies of the electron in the two initial and final positions.

XRF can be both a qualitative and a quantitative measurement technique, so based on the total energy counts or characteristic wavelength, it is also possible to determine the quantification of the element.

X-ray fluorescence can detect and measure most elements in the periodic table running from Uranium, the heaviest element, all the way to lighter elements such as magnesium and beryllium. This means XRF can determine the elemental composition of any material.

For qualitative analysis, XRF can be used without any sample preparation, regardless of the shape or size of the sample. However, for meaningful quantitative analysis, slag samples are typically crushed and ground in a mill to produce a particle size of less than 50 microns, which helps minimize the effects on particle size. Although the powder can be analyzed directly, sample-to-sample accuracy and repeatability improve if the powder is pressed [70].

#### *2. X-Ray Diffraction (XRD)*

The XRD technique (X-ray diffractometry or X-ray diffraction) is one of the most used diagnostic tools to identify the structure of unknown materials. While not providing direct information on the elemental composition, it allows to define the crystalline phases present in an unknown sample and their three-dimensional structure.

It is also applicable to any type of material, as long as it is crystalline, which includes about 95% of all solid materials. By means of this analytical technique, the X radiations diffracted by crystalline materials, that is having an ordered structure, are recorded.

Each material produces a characteristic diffraction spectrum that makes it possible to identify an unknown material by comparison with a library of spectra of known substances.

This technique is based on the coherent scattering of the X radiation by diffuser centers distributed spatially in a regular way (as occurs in a crystalline material) with distances of the same order of magnitude as the wavelength ( $\lambda$ ) of the radiation used.

The condition of constructive interference between the X-rays scattered by the atomic planes of a crystal is described by Bragg's law:

$$2 d \sin\theta = n \lambda$$

*Equation 1*

Where  $n$  is the order of diffraction;  $\lambda$  the wavelength of the incident radiation;  $d$  the interplanar distance between two reticular planes and  $\theta$  the angle of incidence formed by the direction of the X-rays and the family of planes. A typical diffraction spectrum consists of a series of reflections, each characterized by its own intensity, amplitude and position (the latter expressed as  $2\theta$ , i.e. the sum of the incidence and collection angles formed by the incident beam with the sample surface). By determining the position and intensity of the reflections and comparing them with those of the reference spectra, it is possible to identify the type of material, the various crystalline phases that make it up and its possible preferential orientation.

In the case of steel slag, XRD analysis allows to determine the mineralogy reported in Table 5.

### 3. Scanning Electron Microscope (SEM-EDS) Analysis

The scanning electron microscope (SEM) connected to an energy dispersion microanalytical system (EDS) is a versatile and reliable system for the analysis of the minerals and glasses that make up the rock. The electron microscope is a type of microscope that uses electrons as a source of radiation. Electrons have a much shorter wavelength than photons and since the resolving power of a microscope is inversely proportional to the wavelength of the radiation it uses, using electrons a resolution several orders of magnitude is reached superior. In the scanning electron microscope, the electron beam is not fixed but is made to scan: that is, it is passed over the sample in a rectangular area, line by line, in sequence. Numerous particles are emitted from the sample surface, including secondary electrons, which are captured by a special detector and converted into electrical impulses. The chemical analysis (microanalysis) at the scanning electron microscope (SEM) is carried out by measuring the energy and intensity distribution of the X-rays generated by the electron beam on the sample using an energy dispersion detector EDS (energy dispersion spectrometry).

The high-energy electron beam (up to 30 eV) that interacts with the sample surface generates a series of signals that are detected by the appropriate detector. In particular, for each scanned point, the following are produced [71]:

- secondary electrons (SE), are the electrons originally linked to the outermost atomic levels, which receive enough additional energy from the incident beam to remove them. They have energy included between 0 and 50 eV and are emitted by sample surface thicknesses ( $\sim 10\text{nm}$ ). They are frequently used for the study of surface morphology.

- backscattered electrons (BSE), represent that portion of electrons of the beam that is reflected with energy ranging from 50 eV up to that of incidence. They carry mainly compositional and morphological (topographical) signals and come from maximum depths of a few  $\mu\text{m}$ . The quantity of BSE depends both on the morphology of the surface and on the average atomic number of the material present in the small volume radiated by the beam. The BSE image reflects the variation of the average atomic number within the sample and allows to identify the constituent minerals of the sample.

Microanalysis is an analysis of a sample on a microscopic scale, which allows for structural, compositional and chemical information on the sample under study.

Among the different signal analysis techniques, the X-rays characteristic of the elements that make up the sample under examination, can be recorded and discriminated on the basis of energy (EDS). The intensity of these characteristic radiations is proportional to the concentration of the element in the sample. Therefore the X-ray microanalysis gives specific information about the composition of the elements of the sample, in terms of quantity and distribution.

#### 4. Leaching Test CEN EN 12457-2

The leaching test allows to quantify the concentration of heavy metals which can be dissolved when the slag meets a solvent (water). According to the standard EN 12457-2 [72] a slag sample of 90g (grain size <4mm at 95%) is immersed in 900ml of  $\text{H}_2\text{O}$  (HDPE bottle) for 24h in agitation. Then the solution is filtered by a  $45\mu\text{m}$  filter and analysed by ICP-OES.

The acronym ICP-OES stands for “Inductively Coupled Plasma – Optical Emission Spectroscopy”. This definition identifies an analytical instrument capable of measuring the light (optical emission) produced by a liquid sample when introduced into an inductively coupled argon gas plasma. Through this mechanism it is possible to quantify the metals contained in the sample by measuring, for each, the intensity of the light emitted with a specific optical bench (system of mirrors, lenses and gratings). For the determination in ICP-OES it is necessary to have samples in liquid form.

The operating principle provides that an argon flow transports the vaporized sample into an ICP torch, where it reaches a temperature of 6000-8000 °C and ionization and atomization take place.

In an ICP-OES (Optical Emission Spectroscopy) the spectral composition of the light emitted by the source is analyzed through a monochromator (diffraction grating) which splits the incoming light into spectra that are intercepted by a photomultiplier. The ICP-OES allows you to determine metals in highly variable concentrations and in multiple matrices, which is why it is today the most versatile technique for determining metals in water, soils, sediments or even in food and petroleum products.

#### **Production process of EAF steel**

The electric arc furnace is used for melting steel scrap in steelmaking: an electric arc is formed between the ferrous scrap and the electrodes, the heat of which causes the steel scrap to melt.

The EAF comprises three water-cooled parts, namely (i) the roof, (ii) panels and (iii) the sole lined with a refractory material.

Fusion is the main task of the EAF process and is accomplished by the energy supply which includes both electrical energy and chemical energy. Electricity is supplied by the graphite electrodes which are the main energy supplier. Chemical energy is supplied through several sources which mainly include oxy-fuel burners and  $\text{O}_2$  injection.

The electrical energy is distributed between the three electrodes, which melt the scrap creating an arc between them and the scrap. The electrodes are consumed during the process with progressive wear according to the individual frequency during ignition. Some adjustments to the electrode positions need to be made to ensure that all three electrodes are in contact with the material so that energy is transferred efficiently.

Electrodes have brittle properties (limited mechanical toughness) and are consumables with a high cost. Therefore, they must be handled with care. If the oven is filled with an excessive amount of coarse scrap, the electrodes must be lowered very carefully to avoid costly breakage.

A Schematic illustration of an EAF is shown in Figure 7.

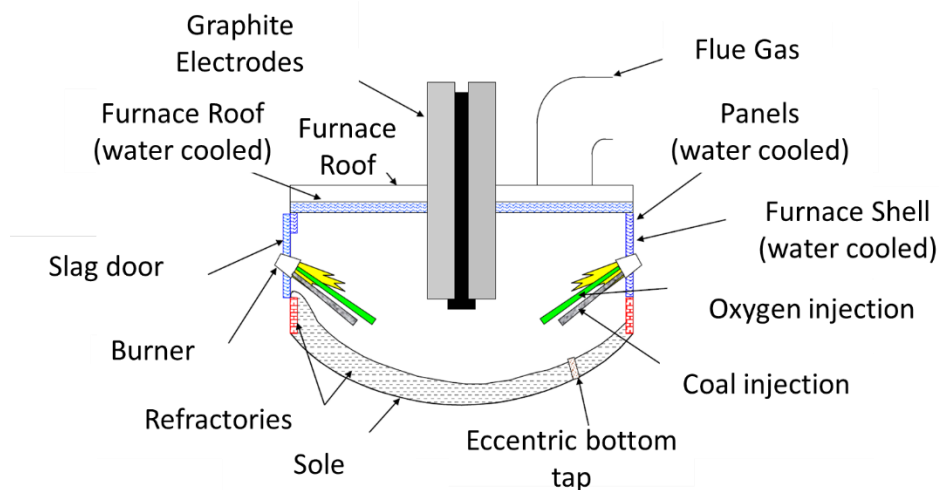


Figure 7 Schematic illustration of an EAF.

The operating cycle of the electric oven is defined as the “tap-to-tap” cycle and in modern ovens it lasts about 60 minutes. The cycle can be divided into 7 phases:

1. Scrap charging: The roof and electrodes are raised and are swung to the side of the furnace to allow the scrap charging crane to move a full bucket of scrap into place over the furnace. The bucket bottom is normally of a clam shell design, i.e. the bucket opens up by retracting two segments on the bottom of the bucket. The scrap falls into the furnace and the scrap crane removes the scrap bucket. The roof and electrodes swing back into place over the furnace. The roof is lowered and then the electrodes are lowered to strike an arc on the scrap. This commences the melting portion of the cycle. The number of charge buckets of scrap needed to produce a heat of steel is dependent primarily on the volume of the furnace and the scrap density.
2. Scrap melting: The heat needed to melt the steel scrap is provided by electric arcs, created between the electrodes and the scrap in the furnace. The electrical power of normal EAFs is between 50 MW and 120 MW, depending on the size of the furnace. The melting of the scrap takes place at a temperature range from 1500 °C to 1550 °C, depending on the composition of the steel scrap. Melting is achieved by supplying energy inside the furnace. This energy can be electrical or chemical. Electrical energy is supplied through the graphite electrodes and is normally the largest contributor to smelting operations. Chemical energy must be supplied through various sources, including oxy-fuel burners and O<sub>2</sub> lances. In oxyfuel burners the combustible gas is burned using O<sub>2</sub> or a mixture of O<sub>2</sub> and air. The heat is transferred to the scrap by radiation of the flame and by convection from the hot products of combustion. The heat is transferred into the scrap by conduction. Once a liquid steel pool has

generated in the furnace, the  $O_2$  can be thrown directly into the bath. This  $O_2$  reacts with different components in the bath which include C, Fe, Al (aluminum), Si (silicon), Mn (manganese) and P (phosphorus). All of these reactions are exothermic (i.e. they generate heat) and provide additional energy to help melt the scrap. The metal oxides that are formed end up in the slag. The reaction of  $O_2$  with C in the bath produces CO, which burns in the furnace if there is sufficient  $O_2$ , and/or is exhausted through the direct evacuation system where it is burned and conveyed to the pollution control system. Once the “flat bath” condition is added, a metal sample can be taken to determine the chemical composition and temperature of the bath. Bath chemistry analysis allows the operator to determine the amount of  $O_2$  to blow during refining. At this point the operator can also start preparing the additions of loose ferroalloys to the tap. These quantities are finalized after the refinement period.

3. Refining: the refining process aims to eliminate some elements such as P, S, Al, Si, Mn and C. Refining operations are carried out once a flat bath is achieved.  $O_2$  is lanced at the end of meltdown to lower the C content to the desired level for tapping. Majority of the compounds which are to be removed during refining have a higher affinity for  $O_2$  than that the C. Hence these elements preferentially react with  $O_2$  to form oxides which float into the slag.
4. then the oxygen blown into the bath reacts with these impurities forming insoluble compounds that float in the slag as well as favoring the removal of nitrogen and hydrogen.
5. Slagging operation: the oven is tilted to remove the slag from the slag door.
6. Tapping: the metal is poured and tapped into a crucible to be transported to the next station. The alloying elements and deoxidizers (Al, Fe-Si, Fe-Mn) are added.
7. Restart: In this phase any potential damage is immediately checked and repaired.

### 3. Industrial symbiosis in the Steel Sector

#### Traditional slag applications

As anticipated, slag represents the main by-product (90% by mass of all by-products) of iron and steel production. The most common application of slag sees it used as a substitute aggregate for sand in cement, often in combination with its CO<sub>2</sub> sequestration properties. However, the composition of the slag is highly variable, and this can affect the characteristics of the final product. For this reason, a general monitoring tool has been developed for simulating and evaluating the feasibility of replacing lime and dolime with LF slag with or without partial recovery of EAF slag for the production of two steel families [73]. A small 3-4% increase in electricity calendering was detected but offset by a reduction of approximately 14-16% in non-metallic raw materials.

Alongside the steel industry, the construction and infrastructure industry also act to address their environmental impact. The latter aim to reduce overall emissions of 50% by 2050, compared to 1990 levels [74]. As for the steel industry, the amount of steel slag produced in 2010 amounts to approximately 21.8 Mt [75]. Of this amount, only 6% was used in cement production, 48% for road construction and the rest was deposited or used for other purposes. The challenge is to develop integrated, "zero waste" flow streams that recover both metals and use the various residues in construction applications [76]. Due to this the main fields of application of steel slag are the cement production and the road construction. However, other steel slag can be used in other areas in minor quantity and new applications are continuously under study.

#### Slag reuse in cement and concrete production

The reuse of slag and other by-products in the production of cement on the one hand reduces the amount of waste to be disposed of and on the other hand reduces the exploitation of new resources. In particular [62]:

- the BF slag in vitreous and granular form obtained after rapid cooling by quenching in water, has the suitable chemical-physical characteristics for the production of Portland cement [76];
- ground granulated blast furnace slag (GGBS) has characteristics that make it suitable for cementing concrete, for the production of which the replacement of cement with GGBS is between 40% and 45% by weight [77];
- granulated blast furnace slag (GBFS) is suitable as a substitute material for calcareous aggregate from 0% to 60% in self-compacting concrete (SCC)[78].

Due to their relatively low hydraulicity and problems related to their volumetric expansion, steel slag is mainly used as a backfill material in dam construction. However, thanks to recent advances in slag treatment (primarily rapid cooling) the properties of steel slag have been greatly improved. In particular, BOF, EAF and LF slag, currently used in road construction, asphalt concrete, agricultural fertilizers and soil improvement, can be valuable materials for the production of cement clinker. This potential use can have environmental and economic benefits, for this reason recent studies have focused on the use of steel slag as a substitute for cement and aggregate in cementitious concrete. For this purpose, due to the low cementitious capacity of the steel slags in the concrete and the need for their activation, suitable aging/atmospheric agents and treatments were carried out to improve the hydrolysis of free CaO and MgO, aiming to mitigate their instability [79].

According to [80] (area of Brazil) the use in the cement industry implies high logistics cost because the material requires previous handling, mainly an additional comminution process and a transportation operation as well as safety concerns all over the entire process.

### Slag reuse in road construction

The by-products of the steel industry can also be used in road construction with the advantage of reducing their disposal in landfills and without compromising the quality and performance of the road. Steel slag is a material of choice, and this is evidenced by special specifications, a sufficient record of its uses and performance in major projects around the world. Khan et al. [81] in their work argue that one of the advantages of using bituminous concrete with steel slag is the high slip resistance (in wet or dry conditions) provided throughout the useful life of the pavements [81]–[83]. Asphalt pavement mixes using steel slag aggregates have shown exceptionally high stability, which can improve roadway resistance when used in the surface layers of pavement. The mixture produced using aggregates of steel slag and natural sand showed exceptionally high stiffness modulus values, which implies that a reduced pavement thickness can be used [84]. It has been observed that the use of EAF steel slag for low volume roads is economical compared to natural aggregates. Properly seasoned EAF steel slag was investigated for low-volume road construction as a base material. Satisfactory results of the elastic modulus have been obtained from EAF steel slag compared to natural aggregates [85].

### Other applications of slag

#### *Slag as Fertilizer*

Since the 1950s, BOF slags have been used in Germany as fertilizer crops. The slag promoted crop growth in larger quantities, without causing short-term negative soil effects, although long-term studies have recorded increased levels of vanadium and chromium. BOF slags have also shown good use as a calciner material when spread over acidic soils to help raise the pH to a more neutral level [86]. According to [80] (area of Brazil) the main obstacles for this slag application are the environmental licensing and the logistics costs. Due to this, agricultural applications are still unattractive, requiring further research and environmental licenses, usually expensive and time-consuming.

#### *3.1.3.2 Water and Wastewater Treatment*

Since slag has good characteristics and is low cost, it is widely used in wastewater and water treatment and can be the alternative to using granular activated carbon. Various researches such as adsorption of dyes, heavy metals and organic substances have been conducted using steel slag. However, the slag absorption capacity depends on the pH solution. Hydration of the slag composition in aqueous solutions provides a high pH. The wastewater from the steel plant contains a high concentration of heavy metals due to the accumulation of particles filtered by the wastewater filtration process. A direct release of backwash water into the environment can cause severe effects on both land and aquatic life. Based on toxicological studies, metals are toxic and non-biodegradable and can continue to exist in these water bodies. Furthermore, heavy metals also have a tendency to accumulate in the food chain. Therefore, strict environmental regulation has been established in an effort to mitigate heavy metal contamination of the industrial effluent discharge [87].

#### *3.1.3.3 Phosphorus removal*

Phosphorus is an essential nutrient for biomass growth. However, excessive P intake in water bodies, such as rivers, lakes or lagoons, results in abnormal growth of algae and aquatic plants, resulting in degradation of water quality. The regulatory limits on the presence of this element in water bodies have become increasingly restrictive, even for small purification plants. An appropriate technology to improve P removal in small

treatment plants is to filter through materials with high affinity for P binding. Several studies have shown that slag from steelmaking is a suitable and effective substrate for the removal of P from waste water [88][89].

### **Case studies of implemented Industrial symbiosis in the Steel Sector worldwide**

It was from the literature by initially selecting several key words such as “industrial symbiosis in the steel sector”, “slag reuse”, “steel sector by-product reuse”, “steel sector waste reuse” and “circular economy in the steel sector”. The search was limited to papers published in the past twenty years. No geographical restrictions have been applied. The search engines used included databases such as Web of Science and Scopus, and freely accessible search engines, such as ResearchGate and Google Scholar. The main findings are summarized in Table 6.

Table 6 State of art of Industrial Symbiosis in the metal sector worldwide.

Case Study	I.S. Model	Production	Type of symbiotic sharing	Stakeholders	Economic and environmental impacts	Barriers and criticalities
			Steelmaking waste	Receiver		
Taranto, Italy [90]–[92]	Bottom-Up	BF-BOF	BF slag mill scales	Concrete industry	Reduction of waste in landfills exploitation of natural resources (15% BF slag)	Long-term economic return Poor trust in partners Little regulatory clarity Need for a mediator Corporate core business focused exclusively on the product
Styria, Austria [33], [93], [94]	Top-Down	BF-BOF	BF slag and sand  BOF dust	Cement and construction industry Paint Industry	Scrap materials cheaper than virgin materials Reduction of costs and taxes for waste disposal Reuse of 120Mt of BOF waste and 8.Mt of BF slag	Poor trust in partners Slow bureaucracy
Kwinana, Australia [33], [95]–[97]	Top-Down	BF	BF slag	Cement industry and road construction	Creation of new jobs and a broader and more diverse employment base.	Relatively low costs for waste disposal Confidentiality Regarding Commercial Matters Intensive regulatory approval procedure for the reuse of by-products Core business focus on the product
Jinan, China [98], [99]	Top-Down	BF-BOF	BF and BOF slag	Cement industry and road construction	Revenues from sales to the cement industry 10.37 M USD/year Eliminated disposal cost of 5.19 M USD/year Reuse of waste of 180 Mt/year	
Liuzhou, China [99]–[101]	Top-Down	BF-BOF	BF and BOF slag	Cement industry and road construction	Savings of approximately 2.4 million tons of raw materials. Reduction of approximately 3.4 million tons of solid waste.	Absence of specific waste treatment sites
Lin-Hai, Taiwan [102]–[104]	Top-Down	BF-BOF	BF and BOF slag  Sludge  Desulfurization slag	Cement industry and road construction Agricultural sector	Reduction of energy costs and waste disposal Sharing of resources	High costs of sustainable technologies Knowledge of technologies is not shared The laws governing intellectual property rights make it difficult to share information. Slow and unclear bureaucracy
Kawasaki, Japan [98], [104], [105]	Bottom-Up	BF-BOF	BF slag	Cement industry	About 130 million dollars/year saved (on all symbiotic exchanges) Reduction of emissions and energy required in cement production	Wet granulation of slag requires large amounts of water Lack of a standardized system for waste management

Puhang, South Korea, [106]–[108]	Bottom-Up	BF-BOF	BF slag Mill scale	Cement industry and road construction Metal recovery plant	-40% emissions into the atmosphere 98.3% of by-product recycling	The global standard for the circular economy is immature. If the circular economy were certified by internationally recognized institutions, many small and medium-sized enterprises will participate in the circular economy movement. Low demand for recycled products
Texas, USA [109], [110]	Top-Down	EAF	EAF slag Mill scale	Cement industry and road construction (+ recycling plant)	Increase in productivity of cement Reuse of 130,000 tons of steel slag	
Avesta Sweden [104], [111]	Network	EAF (inox)	Sludge and dust EAF slag OKTO product	Metal recovery plant Infrastructure	Lower cost of secondary raw materials compared to traditional aggregates Lack of cost of disposal 77% of EAF slag is avoided landfilling	
Unknown, Brasil [80], [112]	Bottom-Up	EAF	EAF slag EAF dust Mill scale Sludge	Infrastructure ( <i>Outsourcing slag treatment</i> ) Zamak alloy producers Cement industry Zinc alloy producers	The steel mill saves the costs of landfill disposal 144,000 tons/year of waste stolen from landfills	Need for environmental licenses High transport costs Lack of research
Ferriere Nord, Udine, Italy [113]	Network	EAF	EAF slag “GRANELLA” EAF dust slag Furnace refractories Mill scale	Infrastructure ( <i>Outsourcing slag treatment</i> ) Zinc producers Steel Mill (Treatment for the recovery of lime substitutes) Cement industry Chemical Industry Steel mill BF	Saving of raw materials 200 tons/year Basalt and phosphorus 25k tons/year ore Zn 30k tons/year lime 30k tons/year ore Fe	The zinc recovery project through an internal process has not proved to be economically advantageous (problem linked to technological limitations)
Alfa Acciai Brescia, Italy [114]		EAF (SiO)	EAF Slag “ALFA SINSTONE”	Cement industry and road construction	Reduction of waste in landfills Less exploitation of natural resources	Prejudice by public opinion
Global Blue ABS Udine, Italy [115], [116]		EAF-S	EAF and LF slag “ECOGRAVEL”	Cement industry and road construction	Reduction of waste in landfills Less exploitation of natural resources	
Acciaierie Arvedi, Cremona, Italy [117]		EAF-C	EAF Slag and LF slag “INERTEX,” “CALCETEK”	Cement industry and road construction	Over 95% of waste and processing waste are recycled and recovered. 98% of the black slag is recovered and destined for the construction sector. 40% of the white processing slag is recovered and used in the stabilization of clayey soils and as a substitute for lime	

In this analysis, 12 (+3) cases of industrial symbiosis in the steel industry in Asia, America, Australia and Europe are analysed. The steel mills surveyed range from 0.8 to 16.5 million tons of annual steel production and 5 of the analysed cases are located in Asia as China is the world leader in steel production.

Most of the cases analysed consist in the production of integral cycle steel (8) while the implemented cases of industrial symbiosis involving electric arc furnace slag are 4 (Avesta (Sweden), Texas (US), Brazil and Osoppo (Italy)). In order to investigate the reuse of EAF waste, especially in the Italian territory, three cases (indicated as +3) were analysed that do not consist of real cases of symbiosis. The cases of Brescia, Udine and Cremona provide for the treatment of EAF and LF slag for the production of aggregates with their own CE marking which bring economic and environmental advantages but which are nevertheless more a valorisation of the waste transformed into a finished product to be marketed (Ecogravel, Alfa Sinstone and Inertex) than a symbiotic activity. Also in the case of Avesta and Osoppo the slag is transformed into finished products (OKTO-products and Granella respectively) but in these cases the marketing is carried out by infrastructure companies which, by combining traditional products, offers a sustainable alternative. In addition, other symbiotic exchanges were also highlighted.

While all industrial symbiosis activities at Asian sites (except Lin-Hai) have been induced by government initiatives via China's Five-Year Development Plan, Japan's Eco-Town Program, or South Korean EIP Initiative, the symbiotic connections documented in the rest of the world (EU, USA, AUS) have spontaneously formed from the motivation of cost reduction.

In most of the industrial symbiosis activities defined in the analysed case studies, the cement and building materials industry is involved as a receiving symbiotic partner. The most frequent synergistic exchange is the use of BF slag and steel slag as a substitute for clinker for the production of cement.

Other flow exchanges between the steel and cement industry also include fly ash, mill scale and sludge, whereby the latter must be mixed with coal ash to be used in the cement manufacturing process (Lin-Hai).

The local community is the second most common symbiont of the steel mills considered. In this case, the recycling of steel scrap is the most common symbiotic activity. In Kawasaki, community-collected mixed waste plastics are used as an alternative BF reducing agent. Water is also an important resource that is relatively easily shared, specifically in Jinan urban wastewater is reused as industrial water. As regards the recovery of waste heat for district heating, this is implemented only in the case of Avesta where the resident EAF plant is both a producer and a consumer of district heating.

Around the treatment and processing of by-products of steel production, an important industrial sector has developed for the processing of by-products of steel production. The most frequent activities are aimed at recovering metals from the following by-products: BF slag, steel slag, mill scale, BOF scrap, sludge and dust. At the Lin-Hai site the contaminated pickling acid is sent to a regeneration plant to obtain regenerated hydrochloric acid and iron oxide powder in exchange. The main flue gases of integrated distillation plants, i.e. COG, BFG, BOFG, are usually used as alternative fuels for electricity generation in power plants, with only one case cited of COG valorisation for hydrogen production in Jinan. Steam is most commonly supplied to the chemical industry as an alternative energy source for gas production. Further symbiotic activities with the chemical industry are the supply of coal tar as raw material for the production of chemicals (Lin-Hai) and the production of fertilizers from ammonium sulphate obtained from the desulfurization of desulphurized sintered flue gases (Liuzhou).

The most substantial economic benefit deriving from symbiotic activities in the analysed case studies is the annual benefit of € 40.82 million from the sale of slag powder produced from 1.2 Mt of BF slag to the cement and construction industry in Liuzhou.

The European steel industry to preserve competitiveness and maintain the current number of jobs, as well as to meet stricter emission standards (eg the Paris Agreement), is an inevitable measure. Currently the Chinese steel industry is at the forefront of adopting the industrial ecology paradigm following various government initiatives and circular economy practices that enforce regulations. Five direct synergistic solutions have been identified between the symbiotic flows analysed: the use of BF and steel slag as raw material for the cement and construction industry, the valorisation of steel mill exhaust gases for electricity generation, regeneration of pickling acid and the use of waste plastic as an alternative BF reducing agent.

### III. Polymeric sector

#### 1. Epoxy resin

Epoxy resins are thermosetting polymers with cold reaction. The formulation is normally made up of a base resin (component A) and a hardener (component B), which, carefully mixed in the ratio of use indicated by the manufacturer, will solidify, giving rise to a glossy vitrified layer.

Its use in the construction world is very wide. In fact, it is used in every area of production, from the mechanical sector to the hospital, up to the food and construction sectors. The resin is suitable for the construction of floors, coverings, consolidation of structures and furnishing components.

Since the 1950s, resins find great space in the building and construction sector, first as an adhesive, then for the construction of pipes and panels. Only in the nineties were the potential of resins explored for the construction of industrial and commercial floors, in the flooring of hospitals or sports facilities. In fact, it is a material that resists mechanical stresses and impacts very well; in addition, it guarantees a high level of hygiene and ease of cleaning.

Epoxy resins are among the most common types for building resin floors, whether it is a protective layer of just a few millimetres on an existing floor or whether an entire screed has to be created from scratch, all in resin. In this second case, the screed is enriched with quartz sands, to increase the mechanical resistance of the floor. The laying of the epoxy resins is quite long and requires about a week of settling to be walkable. However, the results that can be obtained with this type of resin are excellent.

The screed in building is that horizontal constructive element that is adopted to level a surface making it perfectly flat, to distribute the load of the elements above and to receive the final flooring.

The thickness of the screed varies according to the type of environment; its purpose is to make the underlying substrate flat (substrate or collaborating slab) and secondly, it serves to reach the necessary height to connect the various environments correctly.

The screed is generally composed of three materials used in suitable proportions: binder (cement, or anhydride, or special binders such as epoxy resins), inert (sand and/or poly-foam, for example) and water. The dosage of the various elements varies according to the external environment and the location it will have (internal or external, for civil or industrial purposes). Very often additives or other materials are used in addition to those.

In some production contexts, such as the heavy mechanics or intensive logistics sector, industrial floors are subject to particularly heavy use, due to the loads, abrasions and all the chemical and physical aggressions they are required to endure.

An industrial floor in trowelled resin mortar (epoxy screed) may be the ideal solution.

The epoxy screed is nothing more than a surface coating (on concrete or clinker supports), generally having a thickness between 6 and 12 mm, made with epoxy resin and quartz sands in a suitable granulometric curve, carefully smoothed, compacted and finished with resins non-slip pigmented.

Due to its technical characteristics, the epoxy screed can be the ideal choice for:

- New industrial floors subject to heavy use.
- Restoration of old industrial floors in an advanced stage of deterioration.
- Floors of mechanical industries, logistics, intensive warehouses, etc.
- AGV high traffic lane floors in logistics.

- Food industry floors.

### 1.1 Mechanical Characterization

In order to evaluate the performance of these materials to verify their suitability in service life, it is necessary to characterize their intrinsic properties. Following the theoretical background of the tests conducted in the experimental part is reported.

#### 1.1.1 Hardness Test

Hardness tests are certainly among the most widespread mechanical tests because:

- often they can be performed directly on the final product;
- they are not destructive;
- allow to provide useful information for the qualification of some production processes;
- they are generally quick and easy.

There are different hardness scales, however the basic principle is the same: an indenter with an applied load penetrates the material under test, remains for a certain time and subsequently by evaluating the permanent deformation (plastic or elasto-plastic) that the material has suffered, a hardness number is given.

The different scales differ in the methods of execution, in the test parameters, in the shape and size of the indenter, in the load force applied and in the methods of measuring the deformation undergone by the material. The hardness scale used for epoxy resin was micro Vickers (mHV) which means the Vickers procedure and test equipment is adopted with an applied force lower than 0.5N.

The operative procedure for the test consists in compressing a pyramidal-shaped diamond indenter (angle at the vertex of the indenter 136 °) with a known force against the surface of the material under test for a fixed time, and subsequently measure the two diagonals of the footprint due to the plastic deformation of the material (see Figure 8) and calculate the Vickers HV hardness as shown in Equation 2:

$$HV = \frac{F}{9,80665 S} = \frac{F \operatorname{sen} \frac{136^\circ}{2}}{9,80665 \frac{d^2}{2}} = 0,189 \frac{F}{d^2}$$

*Equation 2*

F = force normal to the indenter surface in newtons;

S = area of the surface of the footprint in millimetres ( $d^2/2$ );

d = average diagonal of the footprint in millimetres  $(d_1 + d_2)/2$ .

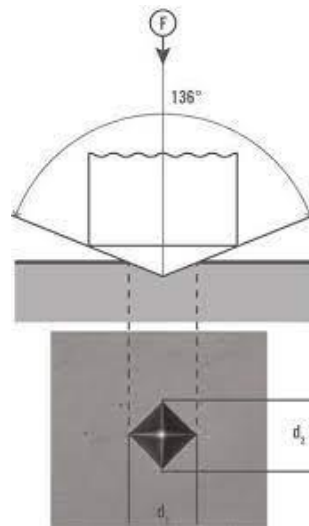


Figure 8 Principle of hardness measurement according to Vickers scale.

The main factors affecting the epoxy resin hardness are: reinforcing content, particle size and shape, the degree of bond between the filler and the polymer matrix, and the distribution of the filler in the matrix [118].

### 1.1.2 Flexural Test

Flexural strength can be defined as the normal stress generated in the material due to bending or flexing of the member in a bending test. It is evaluated using a three-point bending method where a circular or rectangular cross-section specimen is yielding to fracture. It is the maximum stress experienced at the yield point by that material. The lower surface of the specimen is subjected to a tensile load, the upper surface to a compression load. In the central part there is no traction or compression effort. In addition, in this test setup, flat shear stresses occur, which can be reduced by selecting a large span proportional to the thickness of the specimen.

In the 3-point bending test, the specimen is placed on two supports and loaded centrally via a test punch, test method is detailed in the standard ISO 178 [119].

The flexural stress at maximum deflection point is calculated according to Equation 3:

$$\sigma_f = \frac{3FL}{2bd^2}$$

Equation 3

Where:

$\sigma_f$  is the flexural stress for a rectangular shape specimen;

F is the applied load in newtons;

L is the support span in millimetres;

b is the specimen width;

d is the specimen thickness.

The flexural strain at maximum deflection point is calculated according to Equation 4:

$$\varepsilon_f = \frac{6Dd}{L^2}$$

Equation 4

Where:

$\varepsilon_f$  is the flexural stress;

D is the maximum deflection.

The flexural elastic modulus is calculated according to Equation 5.

$$E_f = \frac{L^3 m}{4bd^3}$$

Equation 5

Where m is the slope of the initial straight-line portion of the load deflection curve (N/mm).

### 1.1.3 Compression Test

In the compression test the specimen is cylindrical and bulk so that the buckling phenomenon does not occur. It is essential that the bases are perfectly parallel to ensure that the stresses are as constant as possible on the circular section and equal to the stress applied and it does not occur in the case of bending where the force concentrated in a point other than the center of gravity generates a bending moment that in turn, it causes a butterfly distribution of tension-compression stresses.

Despite these precautions, it remains difficult to subject the specimen to a uniaxial compressive stress, in fact, having to test the specimen up to high levels of deformation, the height of the cylinder greatly decreases during the test; given the nature almost incompressible rubber, the volume lost due to the decrease in height is recovered on the side walls, this greatly changes the initial section of the specimen; but this is not the only problem, in fact the volume is recovered in an uneven way, on the side walls giving rise to the "barrel" phenomenon.

The compression test method is detailed in the standard ISO 14544 [120] for rigid plastics, and in standard ISO 7743 [121] for vulcanized rubber and thermoplastics.

## 2. Rubber compound

### 2.1 Nitrile Butadiene Rubber (NBR)

Acrylonitrile Butadiene Rubber (NBR) or Nitrile rubber is one of the most popular compounds for automotive applications. Nitrile rubber compounds according to ISO 1629 are identified by the initials NBR. This rubber belongs to the family of unsaturated copolymers of acrylonitrile and butadiene. NBR is the polymerization of Acrylonitrile ( $\text{CH}_2=\text{CHCN}$ ) and Butadiene ( $\text{CH}_2\text{CH}=\text{CH}_2$ ) into one large multiple-unit chains (Figure 9) [122].

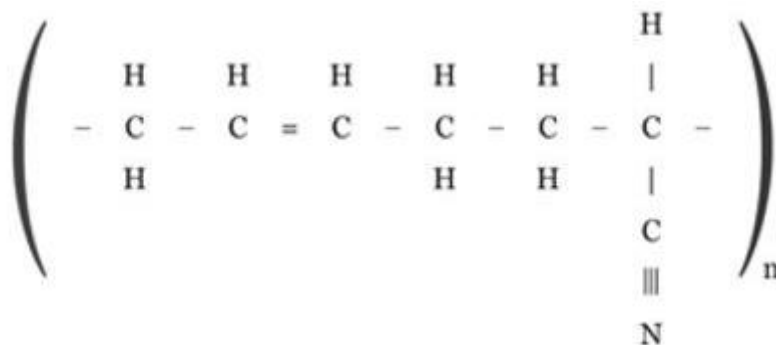


Figure 9 Acrylonitrile Butadiene rubber (NBR) chemical structure.

The typical features of NBR are:

- Hardness 20 ÷ 95 ShA
- Density 1.20 ÷ 1.40 gr/cm<sup>3</sup>
- Excellent abrasion resistance.
- Excellent adhesion to metal.
- Good/very good compression set
- Good tear and abrasion resistance
- Poor vibration damping
- Excellent oil resistance
- Excellent mechanical properties
- Excellent resistance to solvents
- Excellent adhesion to metals
- Compression set: good
- Resilience/rebound: good
- Aging climate/sunlight: poor
- Adhesion to metals: good to excellent
- Working temperature -40 – 130 ° C (depends on the nitrile content)
- It has lower strength and flexibility than natural rubber.
- Nitrile rubber is also resistant to aliphatic hydrocarbons
- It is less resistant to ozone, aromatic hydrocarbons, ketones, esters and aldehydes

#### Physical-mechanical properties

Oil and abrasion resistance are better for high acrylonitrile content, while low acrylonitrile content improves flexibility and resistance to low temperatures.

In general, nitrile rubber compounds have only moderate physical properties but good abrasion and excellent resistance to oil and hydrocarbons, however, they are not suitable for use with polar solvents.

Nitrile rubber compounds can therefore be classified according to the nitrile content:

- High Nitrile > 45%
- Medium Nitrile 30 – 45%
- Low Nitrile < 30%

The best overall balance for most applications is an average nitrile content.

#### Thermal properties

The main problem with this rubber is the search for the most favorable compromise between resistance to oils and fuels, on the one hand, and elasticity and resistance to cold, on the other. NBR has excellent heat resistance, up to a maximum of 120 ° C, depending on the nitrile content. The typical temperature range of NBR elastomeric rubber is 120 ° C (upper limits) and -55 ° C (lower limits).

#### Electrical properties

It has poor dielectric properties, it is a semiconductor, its vulcanizates are not very suitable for electrical insulation. NBR elements are not recommended for electrical insulation.

#### Chemical properties

Typical working temperature range of an NBR is -40 ° C to + 120 ° C. Some low acrylonitrile materials are suitable for applications down to -55 ° C and some peroxide cured grades increase to + 150 ° C .

It has excellent resistance in the presence of gas (methane, LPG, butane, propane), good resistance to mineral oils and fats, animals, vegetables, silicones, hydraulics, aliphatic hydrocarbons, non-polar solvents, non-flammable liquids HFA, HFB, HFC, resistance to mineral oils and greases even at low temperatures.

It is not compatible with aromatic and chlorinated hydrocarbons, ketones, esters, phenols, polar solvents and concentrated acids, high-aromatic fuels, polar solvents, glycol-based brake fluids and non-flammable HDF hydraulic fluids.

#### Fillers

The most used filler is certainly carbon black. Carbon Black is produced from the combustion of petroleum or natural gas and can have various particle sizes which give varying levels of reinforcing properties in a rubber compound. Lower particles (N110, N330) give the polymer a higher level of reinforcement, thus providing higher physical properties. The trade-off is typically to provide a higher compression set for seal application. The larger particle (N990) provides lower physical properties, but a better compression set. Typical NBR compounds use a combination of N550 and N774. A different amount of carbon black will change the Shore hardness of the final compound.

White fillers can be used for compounds that need to be colored or in some cases improve the abrasion resistance of a compound such as silica. Some non-black fillers are calcium carbonate, clay, silica, talc, and mica. Each of these fillers has different levels of reinforcement and, like carbon black, has different particle size and structure.

### 2.1.1 Moulding processes

Moulding is the phase in which the uncured rubber is processed so that it takes on its final shape. Due to the rise in the temperature of the compound during the process, it can totally or partially coincide with the vulcanization phase. In the latter case, post-vulcanization ovens are provided following moulding.

#### 2.1.1.1 Injection moulding

The injection moulding equipment consists of an injection unit and a closure unit. The injection unit includes a temperature-controlled plasticization chamber, inside which resides a rotating screw with a diameter increasing towards the injection nozzle.

In the first phase of injection moulding, the screw moves back to accumulate the mixture near the injection nozzle, then advances with controlled speed and pressure to push the material through the nozzle into the mould.

Inside the mould, the primary and secondary channels have the task of making the material flow up to the cavities, where the rubber will take its final shape by vulcanizing thanks to the increase in temperature. The dimension of the channels depends on the material and the geometry of the articles.

The great advantage of injection moulding is the high degree of automation, which allows greater productivity compared to other processes and makes it the ideal choice for large production volumes, so as to make the high initial investment for the purchase economically advantageous for the equipment.

However, there are two main problems, one deriving from the high heating of the compound, both in the mixing phase and in the passage of the channels. It is therefore necessary to carefully fine-tune the process to avoid burning the rubber. On the other hand, the passage inside the channels makes injection moulding unsuitable for high viscosity rubber compounds, due to their difficulty in flowing.

### 2.1.1.2 Compression Moulding

In compression moulding the uncured rubber preforms are positioned on the cavities of the lower mould, the upper mould descends pushed by a press and guided by pins which correspond to guides in the lower mould. The volume of the preforms is greater than that of the cavities, so there is a quantity of excess rubber (burr). Unlike injection moulding, this process requires the intervention of an operator for the preparation and positioning of the incoming material.

### 2.1.2 Industrial rubber scraps

The moulding of rubber parts generates a high amount of waste given not only by the moulding channels (in the case of injection moulding) but also by the burr, that is material deliberately in excess that comes out of the cavities so as to create a thin film as large as the whole width of the mould from which the pieces will be punched (Figure 10). This difference is quantified to be approximately 20-30% of the rubber entering the process.



Figure 10 Example of compression moulded parts with thin film of burr to be removed.

The recycling and re-processing of crosslinked elastomers are difficult due to their three-dimensional chemical network. This network makes the material insoluble and non-melting after the vulcanization takes place. Vulcanization is required to give rubber its characteristics such as high elasticity and strength. Unfortunately, once rubber compounds are crosslinked, they become a serious recycling problem.

The global consumption of both natural and synthetic rubber has grown from a yearly production of about 5 and 9.6 million tons respectively in 1990 to a yearly production of about 12.7 and 14.2 million tons in 2020 [123].

While the reuse techniques and possible applications of end-of-life tire rubber compounds have been extensively studied and implemented in recent years [124]–[128], the same has not been done for synthetic rubber compounds used for the production of general rubber goods (seals, dampers, etc.). As evidence of this, in Italy, recycled rubber from End-of-Life rubber Tires is classified as a “material” since July 2020 by the “End of Waste” Decree [129], which details the correct ELT recycling procedures and the applications of recycled rubber as a raw material second, while the recycled rubber derived from general rubber goods production is not counted. In the current scenario, the circular economy for recycled rubber goods is lacking [130].

Besides rubber tires, about 50% of the world’s rubber production is used for the production and consumption of general rubber goods. Reliable industrial technology and processes are needed to reuse and recycle the waste produced from general rubber goods on one side due to the increasing rubber demands and on the other side due to the more and more relevant problem of waste disposal.

Rubber waste can be classified as industrial scraps and consumer scraps [130]. Successful waste management mainly depends on cleaning and segregating the generated waste (to avoid compounding potentially incompatible material). For this reason, industrial waste (the object of the present research), is more suitable to be recycled.

However, independent of the type of rubber waste generated, the most commonly used disposal methods are open dumping, landfilling, burning, and grinding the rubber waste into powder [130], [131]. The processed waste can be transformed into cheaper and more sustainable products, nevertheless it is necessary to develop some specific processes for cured rubber.

The management of rubber scraps derived from rubber goods production is becoming an increasingly critical problem in the sector and unfortunately, the recycling and reuse of general rubber goods amount to only 1.5% of the total waste generated [130]. The amount of industrial rubber scraps consists of about 20-30% by weight of the processed material, due to the presence of filling channels (in the injection moulding process) and infiltrated material between the two half-moulds which creates a thin rubber film (rubber flash) from which the pieces will be removed by subsequent processing (deburring).

The re-processing of crosslinked elastomers is possible when the crosslinks formed during the vulcanization (C-S and S-S for sulfur curing) are cleaved without damaging the C-C bonds of the macromolecular chain [130], [132], [133]. When the cleavage of C-C bonds occurs, and it is predominant to that of C-S and S-S bonds, the degradation process takes place with consequent deterioration of the mechanical properties of the rubber [130].

The phenomena of vulcanization and degradation are both interconnected with each other. It is not possible to only cleave crosslinks or to only cleave the main polymer chain during a process, to that both of them take place during the rubber re-processing. Because of this, the importance to limit the degradation and increase the devulcanization enhancing the chances of rubber recycling is therefore evident.

Rubber waste management processes can be classified into thermal, mechanical, physical, chemical, and biological [130]. Each method involves different processes that in turn involved different parameters and chemicals to make the rubber re-processable via devulcanization and unavoidable degradation.

## 2.2. End of Life Rubber tyre

When a tire loses the essential characteristics for a safe and efficient performance on the vehicle, without the possibility of retreading, it becomes a special non-hazardous waste and must be collected for recovery and recycling in special plants.

Every year in Italy there are about 435,000 tons of used tires, of which about 20% are sent for retreading because they are still usable. On the other hand, there are approximately 350,000 end-of-life or end-of-life tires: half are destined for energy recovery; about 25% is recovered as material and the remainder is dispersed.

The rubber of which the tire is made is in fact a mixture of high quality polymers with exceptional chemical-physical characteristics that remain unchanged even in the recycled rubber obtained from them. This is a problem if the tire is dispersed in the environment, in fact the average decomposition times exceed one hundred years, in addition to the fact that it takes up a lot of space, pollutes and represents a potential fire risk; on the other hand it is an advantage if it is recycled.

### 2.2.1 Management and regulation of ELT

Due to the bio persistence and chemical inertia of waste rubber, ELTs management is shifting from landfilling towards recycling and recovery. Although these operations are rising issues in the sustainable waste management field, they provide an opportunity to produce new products with recovery materials. Latest data from the European Tire and Rubber Manufacturers' Association (ETRMA) confirm tire recovery rates of 92% in Japan, 82% in South Korea, around 80% in the USA, and Europe continues to lead the way with 93% (data obtained from Annual Report 2018 – BIR Bureau of International Recycling)[134].

The European Directive, 2000/53/EC is aimed primarily at preventing the production of waste resulting from vehicles, including tires (classified as CER 160103), and to promote the reuse, recycling and other forms of recovery. Before a product becomes waste must take all the necessary measures that will reduce the amount of waste generated, prolong its life, reduce the detrimental environmental effects and risks to human health. Waste tire management should be viewed in the context of the waste hierarchy, as shown in Figure 11 and detailed below:

- this hierarchy accords priority to waste prevention, that is an appropriate tire maintenance to take full advantage of the service life of the tires;
- secondly, the reuse of partly worn tires through the retreading is highly recommended to avoid premature disposal. The retreading processing cycle consists of the following steps: verifying compliance of the carcass by visual inspection, possible repair, possible drying, removal by rasping of the residual layer and retreading of the new tread that can be carried out by hot vulcanisation, mould or cold process using pre-vulcanised bands;
- when tires can no longer be restored for their original purpose as they could compromise safety, they can take the path of material recovery. With this action, product goes through a mechanical process to change its form into particles, which are then used in different application. Depending on the field of application, different particle sizes can be needed and specific tests must be carried out on the samples to assess their suitability for the new specific use. This waste management route is the topic of the present review. The main waste tire recovery sectors are: building materials, structural elements, plastic compounds fillers, infill or sports flooring, energy recoveries, pyrolysis, gasification, special reuses of devulcanized rubber or experimental applications such as the removal of some organic pollutants from the water or protective layers of guard rails to prevent more traumatic consequences for motorcyclists in the event of an impact;
- if there are no suitable conditions for the previous type of recovery, the other option other than landfilling is energy recovery. This means that ELTs are used as fuel substitutes due to their high calorific value. Fuel derived from tires (TDF) has a higher calorific power than coal and is also less harmful to the environment due to lower emissions into the atmosphere because of thermal treatment. Among the most important applications regarding energy recovery are cement kilns or incinerators to produce electricity or steam. Both material recycling and energy recovery offer a complementary solution to obtain the best sustainable development benefits from natural resources and their waste, allowing reduction of natural resources consumption and minimizing waste and environmental impacts. However, energy recovery must be considered a second-order form of recovery, and material recovery must always be privileged;

- ELTs disposal in the landfills is the last option but it is not recommended. ELTs occupy a large portion of valuable space in the landfills, store water and create a breeding habitat for rodents and insects, and are exposed to a considerable risk of fire and combustion [135]. The legal prohibition of tire stockpiling in landfills in European Union countries was introduced by a Waste Landfill Directive in 1999 (Council directive 1999/31/EC on the landfill). Effects are impressive. In 1996, about 50% of waste tires were stored at landfill sites, and in 2010 only 4% [136]

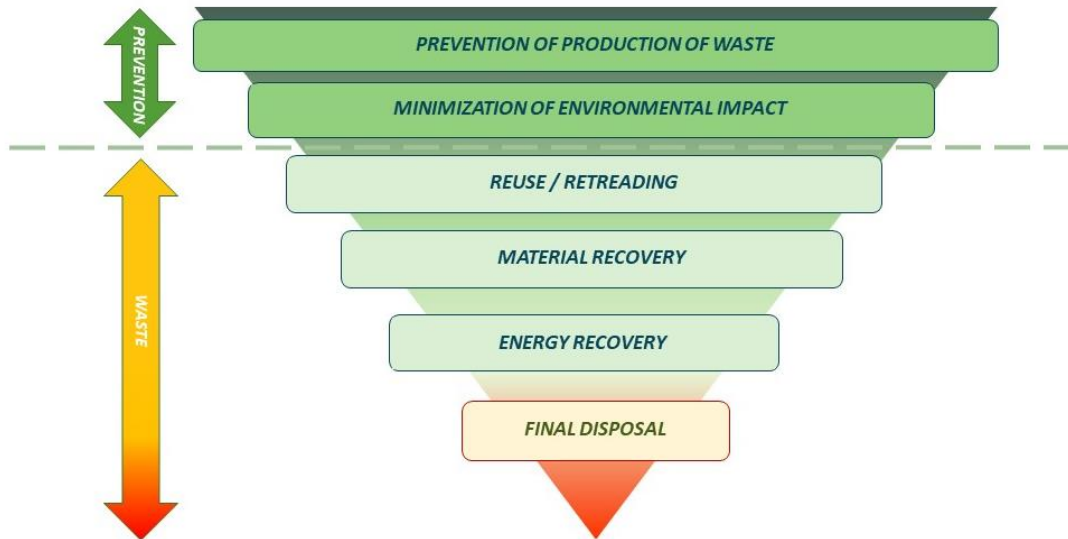


Figure 11 Waste tire management diagram [124].

In summary, it is possible to state that the main forms of post-consumer tire recovery are focused on obtaining:

- reconstructed tires;
- materials that can be used in different production and/or consumption cycles;
- energy (by pyrolysis and gasification processes).

### 2.2.1.1 Material recovery

The treatment of waste tires largely depends on the type and quality of the tires. After being removed from the vehicle, the ELTs are collected and deposited at the sorting centers. Here they are weighed and checked, then stored as the first step in the treatment process (Figure 12). The second phase is the “bead breaking”, i.e. the removal, by means of special machinery, of the steel ring, called the rim [126]. Once removed, the bead is recovered, for example in steel mills and foundries. The tire is crushed through three processing steps: primary, secondary and tertiary, to obtain the fine grade of the crumbled rubber, for example the formation of rubber dust. The primary processing phase reduces the entire tire to homogeneous granulometries between 5 and 40 cm called “slippers” which can be sent directly to energy recovery or be further crushed (volumetric reduction) to separate rubber, steel and textile fibers.

The secondary grinding step converts the coarse waste rubber chips into granular rubber material.

Tertiary grinding is the ultimate breakdown of crumbled rubber to a fine powder, as these 100% conversions in a single unit can be achieved by wet grinding techniques [133].

1. ELTs Storage	<ul style="list-style-type: none"> <li>• Visual check</li> <li>• Weighting</li> </ul>
2. Bead Breaking	<ul style="list-style-type: none"> <li>• Steel circle removal--&gt; Foundries</li> </ul>
3. First grinding	<ul style="list-style-type: none"> <li>• "Slippers": grain size 5-40 mm (contain textile and metal fragments)</li> </ul>
4. Second grinding	<ul style="list-style-type: none"> <li>• "Granulate": grain size 0.8-20mm (divided in rubber, metal and fibres)</li> </ul>
5. Third grinding	<ul style="list-style-type: none"> <li>• "Powder": grain size &lt;0.8mm</li> </ul>

Figure 12 ELTs treatment process [124].

The specification EN 14243:2019 (Materials obtained from End of Life Tires – Part 1: General definitions related to the methods for determining their dimension(s) and impurities) [137] prepared by Technical Committee CEN/TC 366 defines the materials obtained from ELTs including the definition, dimensions and methods for determining the particle size. Table 7 reports the classifications of materials according to their dimension.

Table 7 Types and dimensions of materials obtained from ELTs

**European Committee for Standardization (CEN) Technical Specification 14243-1:2019**

TYPE OF COMPONENT	DIMENSIONS
primary cut	> 300 mm
shreds	20 – 400 mm
chips	10 – 50 mm
granulates	0,8 – 20 mm
powders	< 0,8 mm
steel	n.d.
textile	n.d.

Part 2 of the same specification (Granulates and powders – Methods for determining the particle size distribution and impurities, including free steel and free textile content) [137] defines the test methods for determining the distribution of the particle size of the particles in the various process phases and for the determination of impurities. The determination methods are based on a proper sampling process so that the analysed sample is representative of the whole lot of material from which a characteristic is to be determined (probabilistic sampling). At first, a sampling plan should be prepared, as a function of lot size and particle size and the number of increments to be taken, then the sample division is made. Sample division consists of homogenization and reduction of the mass of the laboratory sample, to obtain several duplicate test samples to be then analysed. Finally, the complete test procedure for the determination of particle size distribution and impurities is described in the standard EN 14243:2019 part 2: the reader is invited to read the document for further details.

### 2.2.1.2 ELT applications

As regards the reuse of ELTs, a review of the literature has been carried out and the possible reuses have been divided by field of application: building materials, structural elements, fillers in plastic compounds, infill or sports flooring, recovery by pyrolysis or gasification, reuses special devulcanized rubber and experimental

applications, such as absorbents for the removal of organic pollutants from water or protective layers of guard rails for motorcyclists.

The detailed description of such applications, along with their advantages and disadvantages, is detailed in [124]. Table 8 gives an overview of the information obtained and, in particular: size of rubber waste used, brief description of the application, type of parameters tested experimentally, characteristics of the final products obtained and quantity of rubber waste to optimize their properties. This review focuses on the most recent findings from each field of application.

Table 8 Possible recovery of post-consumer tires by type of product, size, parameters evaluated, final application and optimal values.

FIELD OF APPLICATION	REF	ELTs material	SIZE (mm)	APPLICATION	PARAMETERS EVALUATED	FINAL PROPERTIES	OPTIMAL VALUES
BUILDING MATERIAL	[138]	fibre	fibre	Reused tire polymer fibre for fire spalling mitigation	Fire-induced spalling	Lower vulnerability to spalling	Reused tire polymer fibre: 2kg/m <sup>3</sup>
	[139]	crumb	2-5	Fibre-reinforced lightweight self-compacting concrete	Performance of the concrete after exposure to elevated temperatures	Improvement of strength parameters sacrificing workability	20% replacement of fine aggregate with crumb
	[140]	powder	0,16	Concrete obtained by replacing fine and coarse aggregates with waste tire rubber	Compressive strength, water absorption and carbonation	high compressive strength of 50.8MPa	3wt% replacement of fine aggregate
	[141]	crumb	0-4	Lightweight geopolymer mortar incorporating crumb rubber	Workability, compressive and flexural strengths, porosity, water absorption and thermal conductivity	Compressive and flexural strengths reduction of the geopolymer mortar	100% replacement of river sand
	[142]	crumb/powder	0,5-10	Composites with recycled rubber aggregates	Durability, outstanding abrasive resistance	Improvement of insulation and acoustic properties	Limited since fire protection measures
	[143]	granule	0,5-2	Environmentally sustainable cement composites based on ELT and recycled waste porous glass	Rheological, mechanical, thermal, microstructural and wettability tests	Thermal conductivity reduction of the lightweight porous granule and glass composites	50% replacement of the sand volume with granules
	[144]	crumb	0-7	Hollow blocks and bricks made of concrete doped with waste tire rubber	Thermal insulation capacity	The addition of the crumb rubber increases the insulating power	63alenda 20wt% crumb rubber
	[145]	powder	0,105 0,125	Reinforced plywood using carbon fibre and waste rubber powder	Modulus of rupture, modulus of elasticity, impact strength, water absorption and thickness swelling	Improvement of the impact resistance of the plywood	Addition of 30wt% of the waste rubber
[146]	scrap	1-20	Sub ballast layers under railway tracks	Resilient modulus and permanent deformations under cyclic loads	Resilient modulus tends to decrease as the rubber content increases	2,5-5weight %	
[147]	tread layer	4-11,5 5-20 11-44 (layer thickness)	Elastic elements in railway tracks	Influence of thickness, resistance to mechanical fatigue and climatic deterioration	Viability of developing elastic elements to be used in railway infrastructures	Depend on the specific reuse (e.g. 7,5-9mm thickness of soft pads)	

	[148]	chip	14-20	Elastic layer under the sleeper	Stiffness of track section, evolution of settlement and stress under ballast layer.	Increase of section resilience	Inclusion of 35% rubber calculated by volume of stones
	[149]	shred	8-18	Railways sub ballast	Response to dynamic excitation	Capacity to attenuate vibrations	Contents of between 1-10wt%
	[150]	crumb	1-7	Alternative sub ballast material to replace traditional capping materials	Deformation behaviour, resilient modulus, damping ratio and shear modulus under cyclic loading	High energy-absorbing capacity, adequate damping ratio and acceptable magnitude of resilient modulus	Inclusion of 10wt% of rubber
	[151]	chip	0,6-4,75	Stabilization of sandy soil	Shear strength of sand	Improvement of load bearing capacity of treated sand	Adding tire chips up to 8wt%
	[152]	crumb		Soil reinforcement	Soil stability, soil reinforcement, drainage, energy absorber, dispatcher stress	Improvement of the thermal stability and mechanical properties of soil	18% of recycled rubber powder in modified asphalt
	[135]	textile fibre		Reinforced soil, road pavements, foundation	Compaction, direct shear, Unconfined Compressive Strength, California Bearing Ratio and Split Tensile Strength	WTTF (waste tire textile fibres) may be used as highly efficient reinforcement materials	Addition of up to 4% fibres
	[153]	scrap	2-5	Stabilization of retaining walls	Bearing capacity and horizontal displacement	Improvement of bearing capacity of the wall	Addition of 15wt% rubber
	[154]	scrap	12-305	Geoengineering applications	Shear strength and deformability properties	Significant reduction of earth pressures and displacements	Addition of 30–40wt% rubber
PLASTIC COMPOUND	[155]	textile fibre		Textile fibres as second-life material for the preparation of plastic compounds	Environmental impacts	Reinforcement in plastic compounds	Plastic loaded with 50wt% of fibre
SYNTHETIC TURF	[156]	granulate	0,8-2	Synthetic turf areas and athletic track surfaces	Leaching behaviour	Release of contaminants due to matrix degradation after ageing	there are no specific values for sports grounds

PAVEMENTS	[157]	crumb	2-5	Recycled tire crumbs for road applications	Leaching test for 100 potential contaminants	Using tire crumbs for road applications allows to save carbon footprint and not release pollutants	Using tire crumbs at 2-3%
	[158]	crumb	0,5	Recycled concrete aggregate (RCA) as base/subbase applications	Effect of high temperature and rubber contents on the mechanical behaviours	By increasing the rubber content deformability index increases (more ductile behaviour)	Recycled concrete aggregate with 1% rubber
	[159]	crumb	2-4	Road paving asphaltic materials	Performance of road-paving (Marshall stability, flow and compression) and durability (weathering)	Improvement of weathering resistance (higher durability) and compressive strengths	Using crumb rubber at 5% and PET at 1%
	[160]	granule	5-10	Permeable pavements	Mechanical behaviour and load bearing mechanism	Improvement of drainage performance, long-term durability, flexibility and resilience	0,3<Volume fraction of Tire Derived Aggregates<0,5
	[128]	crumb	0,0075-4,75	Porous concrete pavements	Drainage, noise absorption, abrasion resistance and durability	Improvement of abrasion resistance and freeze thaw. Reduction of permeability coefficient	The ratio of recycled aggregates should not exceed 30 percent of total aggregates.
	[127]	crumb	1	Waste materials (Tires and others) used in the pavement porous concretes	Durability, permeability, compressive and flexural strength	Improvement of abrasion resistance with regards to the depth of wear	Content of rubber up to 20%
	[161]	granule	type A 1,18-4,75 type B 0,6-2,36	Polymer, silica fume and rubber aggregates from rubber tire particles in porous concrete	Mechanical strength, permeability and abrasion resistance	Improvement of flexural, compressive strength, impact resistance and abrasion resistance	Type A 18% and type B 14%
SPECIFIC REUSE	[162]	scrap		Motorcyclists protection system	Impact speeds, the impact point on the barrier and the admissible biomechanical values	Reducing the severity of the injury of the motorcyclists	Depends on the size of the barrier
	[163]	fibre		Removal BTEX compounds in soil treated with cement	Mechanical properties of soil-cement composites	Effectiveness of RTPF (Recycled Tires Polymer Fibres) as a BTEX removal material	The addition of fibres was at 5wt% of raw soil
DEVULCANIZATION	[132]			Devulcanized material can be mixed with virgin rubber or used as filler in compounds	Different devulcanization techniques	Devulcanized material can be mixed with virgin rubber or with other kinds of matrices	Depend on the different devulcanization techniques

	[164]			The obtained product could then be introduced in part or completely in new materials	Mechanical properties and re Vulcanisation abilities of material produced by devulcanization	The obtained product could then be introduced in part or entirely in new materials	Sustainable and efficient recycling process
GASIFICATION	[165]	chips	15	Co-gasification of waste tire and pine bark (PB) in CO <sub>2</sub> atmosphere	Gas yield efficiency and energy recovered	Higher energy density syngas using CO <sub>2</sub> as gasifying agent	Content of waste tire 75%
	[166]	crumb	0,42	Pyrolysis process of crumb tire rubber in waste cooking oil	Gel content, molecular weight, dynamic shear and segregation test	improvement in the safety and controllability of the process	Compatibility of rubber with virgin asphalt is improved using waste cooking oil
PYROLYSIS	[167]	scrap		Pyrolytic gas from waste tire as a fuel	Properties of gas phase: heating value and concentration of sulphur compounds	Depending on the technology used and the process conditions	Compared with natural gas pyrolytic gas seems to be a promising fuel
	[168]	scrap	0,31	From pyrolytic residues to commercial carbon black	Removal efficiency for the ash and sulphur	Pyrolytic carbon black will be a potential alternative of commercial carbon black	Carbon content of pyrolytic carbon black is associated with pyrolysis temperature
	[169]	scrap	0,2	Improve the reinforcing performance of pyrolytic carbon black on rubber	Reinforcing performance of pyrolytic carbon black	Specific surface area of pyrolytic carbon black increases after electron bombardment	Thermal treatment at 1000°C reduces the volatile content of pyrolytic carbon black
	[170]	scrap		Reuse of carbon black from ELT in new pneumatic formulations	Environmental benefits of recovering carbon black	All impacts associated with thermolysis process are lower than those of tire production.	Replace the most expensive virgin carbon black with recycled contributes to obtain green tires
	[171]	granule	2	Co-pyrolysis of waste tire and cotton stalk	Liquid co-pyrolysis yield quantity and quality	Potential feedstock for preparation of commercial fuel after desulphurization	Blend ratio cotton stalk/waste tire (2:3) showed maximum oil yield (48wt%).
	[172]	whole		Energy recovery	Determination of ash content, flame propagation test and thermal analysis	Duration and temperature range of the burning process are not influenced by the type of tire	Heat the furnaces up to about 900°C: the mass loss is almost 100% and there is no ash residue
	[173]	granule	2-4	Co-pyrolysis of grape seeds (GS) and waste tires	Thermal behaviour of both feedstocks (grape seeds+waste tire) under pyrolysis conditions	Oxygen content reduced to 4,2wt%, minimizing any problems related to corrosivity and instability	Adding 40wt% waste tire and calcined calcite as a catalyst the organic phase yield is improved
	[174]	scrap	0,6-1,8	Co-pyrolysis of sugarcane bagasse (SB) and scrap tire	Co-pyrolysis liquid yields	Co-pyrolysis oil showed high potential to be used as feedstock for fuel	Sugarcane bagasse:scrap tire 1:3 produced highest liquid yield and calorific value of 41MJ/kg

	[175]	scrap		ELT as carbon source in synthesis of nanocomposite	Crystallinity, amorphous content and porosity of carbon source	Waste tire char can be used as supplementary carbon source for synthesising SiC/Si <sub>3</sub> N <sub>4</sub> nanocomposite	SiO <sub>2</sub> and char (%C) were used in 1:2,5 ratio	
	[176]	granule	<5 20	10- 50-100	additive in coal blends for metallurgical coke production	Coke chemical composition, morphology and compressive strength	Tire addition (grain size <5mm) decreases drum index and mechanical strength; greater grain size shows opposite trend reducing crack propagation	Waste tire up to 3% in average particle size (20-30 mm)
WATER REMEDIATION	[177]	activated carbon			Removal of organic dyes and antibiotics from water	Absorption capacity with different variables such as pH, temperature, concentration of pollutants	high capacity regenerable adsorbent	Depend on the pH of the solution
	[178]	activated carbon			Pyrolysis followed by chemical activation process to produce porous activated carbons	Surface activation, active sites, porosity and pH of the solution	Activated carbons are effective adsorbents for organic and inorganic removals from wastewaters	pH for pollutant adsorption: high for cationic and low for anionic
	[179]	activated carbon			Anthracene removal from water	Anthracene adsorption, pH solution and dose of adsorbent	Anthracene adsorption enhances by increasing the amount of adsorbent	Adsorption maximum at pH=2 (99% adsorbed on 14mg of rubber)
	[180]	activated carbon			Chloromethane removal using cost-effective activated carbon	Adsorption interaction of the synthesized carbon with halogenated organic compounds	Chloromethane Removal using cost-effective activated carbon	Activated carbon dosage of 5g/L and contact time of 60min
	[181]	activated carbon			Removal of Mn from aqueous solutions	Porosity analysis, SEM analysis, adsorption kinetics and isotherm models	Good efficacy for removing Mn ions	Maximum specific surface area of carbon is 550m <sup>2</sup> /g. Maximum adsorption 120mg/g.
	[182]	fibre			Remediation of water from crude oil	Rate of adsorption, adsorption capacity, oil retention, water uptake	Reusability of sorbents showed that this sorbent can have 75,7% of adsorption capacity after 10 cycles	Total amount of adsorbed oil was 107.66 g oil/g of waste tire cord fibre for 10 cycles
	[183]	scrap	0,125-1			Removal of boron from water	pH values, initial boron concentration, adsorbent dosage and particle size	Waste tire rubber is excellent and cost-effective material available for removal of boron from water

## 2.3. Rubber Characterization

### 2.3.1. Vulcanization

In 1839 Charles Goodyear found out that heating a mixture of rubber and sulfur produced an elastic material neither sticky nor brittle with change of temperature. Thomas Hancock got at the same results in the same period. This process was called vulcanization (the name come from Vulcan, the roman god of fire) and was the beginning of the development of the rubber industry as know nowadays. Vulcanization (or curing) is a process where a soft compound is converted into a hard-elastic engineering product. It is a chemical process designed to reduce the effects of heat, cold, or solvents on the properties of a rubber compound and to create useful mechanical properties. This is most often accomplished by heating with vulcanizing agents, such as elemental Sulphur, organic peroxides, organic resins, metal oxides, or urethanes. In this process long chain rubber macromolecules are bound together to form a three-dimensional elastic network.

### 2.3.2. Rheometric Curve

The characteristics of vulcanization can be determinate by an Oscillating Rheometer in which the disc is oscillated through constant angular displacement and the torque required monitored. The chemical reactions of vulcanization are graphically expressed by kinetic curve. As showed in Figure 13 the kinetic curve is expressed as torque in function of time. A typical cure curve consists of three regions: the first region is the scorch delay or induction period, during which the most of the accelerator reactions occur; the second period is due to the curing reaction, during which the network structure is formed; the last region, the network matures by overcuring reversion, equilibrium or additional but slower crosslinking, depending on the nature of the compound[184].

From the kinetic curve is possible to determine some parameters. When the rubber compound is practically cold (several seconds after inserting the specimen in the measuring chamber) the torque is called  $M_0$ . After this, the compound absorbs heat from the instrument and it softens until the lowest level of torque that is called  $M_{min}$ ; this decrease is because the viscosity decreases while the temperature increases. In correspondence of the lowest level of torque is possible to determine the viscosity at the vulcanization temperature, and this torque value characterizes the compound hardness. Running the time, the viscosity keeps constant for a longer or less long time before it rises. The time before the vulcanization begins is the scorch time. When the rubber compound ends the vulcanization, the torque achieves the maximum value that is called  $M_{max}$ . Once known  $M_{min}$  and  $M_{max}$  it is possible to calculate the optimum time of vulcanization ( $t_{90}$ ) defined as the time required for reaching 90% of the maximum achievable torque at set temperature as in the Equation 6:

$$M_{90} = M_{min} + 0.9(M_{max} - M_{min})$$

Equation 6

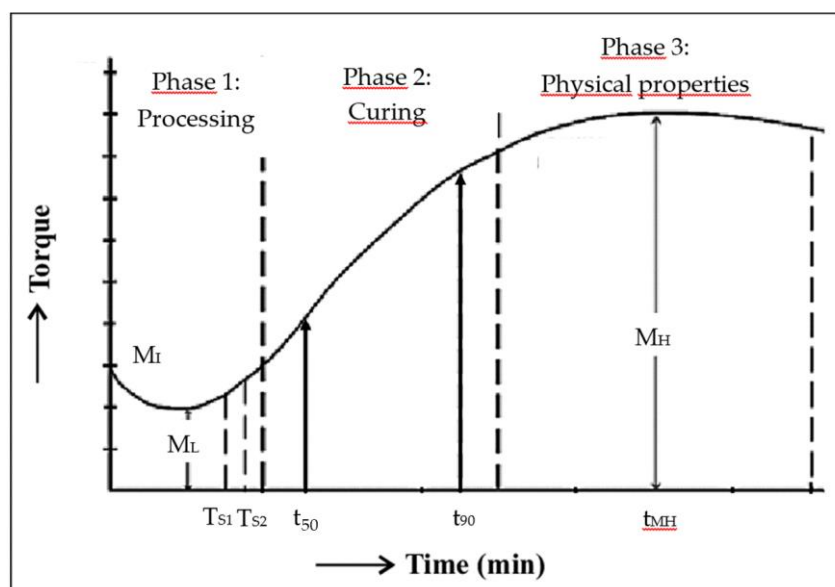


Figure 13 – typical cure curve.

Ingredients that have become part of the common recipe to optimize the vulcanization process are Vulcanizing Agents and Activators.

Vulcanizing agents are directly responsible for the formation of crosslinks during the rubber curing process. Examples of these agents are sulphur, organic sulphur donors, and certain organic peroxides. Activators are chemical additives which activate the accelerator in a cure and improve its efficiency. Stearic acid and zinc oxide together are the most widely used activators. Some vulcanizing agents and activators may be the same in this broad group because certain agents, such as zinc oxide, can be an activator for the cure of most general purpose rubber compounds, but functions as the vulcanizing agent in specific halogenated elastomers.

### 2.3.3. Crosslinking

A polymer network can be defined as a highly crosslinked macromolecule in which all units are connected to each other via chemical bonds or physical associations. The structure of a polymer network is a three-dimensional “mesh” formed by polymer chains interconnected by crosslink points. However, the actual structure of this “mesh” is not regular and the distribution of polymer chain length between joining points is unequal throughout the whole network. Due to this, the network consists in numerous regions of different structures with different crosslink densities, resulting in a heterogeneous structure. Four main types of inhomogeneities are commonly recognized in a polymer network structure: (i) chains bounded to the network by only one end; (ii) chain joined by its two ends to the same crosslink point; (iii) permanent chain entanglements between two adjacent crosslinks; and (iv) multiple connection between two crosslink points, as shown in Figure 14 [185].

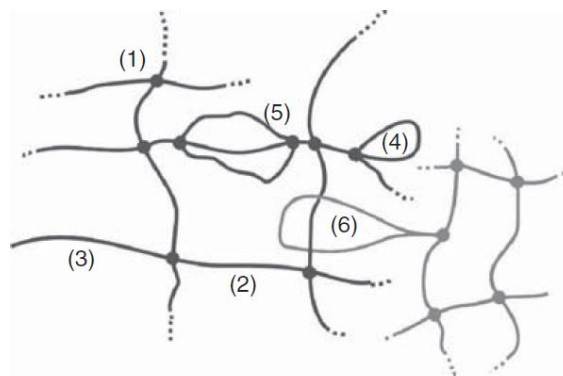


Figure 14 Main elements constituting the structure of a polymer network: (1) crosslink point, (2) elastically active chain, (3) dangling chain, (4) loop or cycle, (5) multiple connection between two crosslink points, and (6) permanent chain entanglements between two adjacent crosslinks.

Inhomogeneities can be formed during both physical and chemical crosslinking. According to the topology and structural level of perfection, several types of polymer network can be identified: ideal (or perfect), model, and imperfect networks. The ideal network consists in chains all of which are connected at both of their ends to different junction points; the imperfect network is characterized by high presence of loose, dangling (singly attached) chains, and inactive rings or loops (cycles) affecting the network elasticity; a model network is half way between the previous two. It should, satisfy the following conditions: (i) each elastic chain should be connected by its two ends to two different crosslink points; (ii) crosslinking density should be constant throughout the gel; and (iii) a model network should exhibit a known and constant functionality of crosslink points.

According to the IUPAC Commission on macromolecular nomenclature, crosslink density is defined as the number of crosslinks per unit volume in a polymer network. The degree of crosslinking is a fundamental property for polymer networks. A change in the level of crosslinking causes remarkable changes in the properties of the polymeric material. Crosslinking improves resistance to thermal degradation and resistance to cracking effects by liquids and other harsh environments, as well as resistance to creep, among other effects. Slight crosslink densities impart good recovery properties to polymers used as elastomers. On the other hand, high crosslink densities impart high rigidity and stability under heat and stress to polymers such as phenol–formaldehyde and urea–formaldehyde polymers.

Elastomers are generally crosslinked in a random manner and therefore, it is difficult to identify the principal effects of modification through mixing of certain components on the mechanical properties. The classical kinetic theory of rubber elasticity ascribes the high elasticity of a crosslinked rubber to the change of the conformational entropy of long flexible molecular chains. The classical kinetic theory of rubber elasticity predicts the following relation in simple extension [186].

$$\Sigma = \nu KT \left( \lambda - \frac{1}{\lambda^2} \right)$$

Equation 7

Where:

$\sigma$  is the nominal stress;

$\nu$  is the number of effective crosslink per unit volume;

K is Boltzman`s constant;

T the absolute temperature;

$\lambda$  is the extension ratio;

Crosslinking in soft or flexible materials (rubber like) gives a considerable increase in elastic modulus, a marked increase in hardness, and usually a reduction in the ultimate elongation and permanent set. The nature of crosslinks plays a big role in determining the physical properties [187]. In other words, crosslink density is an extremely important factor in determining physical properties of a vulcanizate.

### Flory-Rehener equation

Linear polymers often will completely dissolve in their own monomers or in another good solvent. A good solvent for a polymer is one that is either similar in chemical structure to the polymer or one, which can interact with the polymer main-chain or side groups.

One way for determining the solubility of polymers in solvent is through the estimation of solubility parameter ( $\delta$ ). The following relationship can often be used to estimate the solubility of a polymer in a solvent [188].

$$(\delta_1 - \delta_2)^{1/2} < 1$$

Equation 8

where:

$\delta_1$  is the rubber solubility;

$\delta_2$  is the solvent solubility.

If Equation 8 is verified, then the polymer will dissolve in the solvent. Using a group contribution analysis approach, the solubility parameter of a material can be estimated by:

$$\delta = (\rho \Sigma F_i) / M$$

Equation 9

where

$\delta$  is the solubility parameter;

$\rho$  is the density of the material;

$F_i$  is the group molar attraction constant;

M is the molecular weight of the material.

Using Equation 8, we find the square-root of the difference between rubber and solvent (Toluene) as shown in Table 9:

Table 9 Values of solubility parameter of the rubber under investigation [188]

$(\delta_1) (\text{cal/cc})^{1/2}$ for rubber	$(\delta_2) (\text{cal/cc})^{1/2}$ for solvent (Toluene)	$(\delta_1 - \delta_2)^{1/2} (\text{cal/cc})^{1/2}$
NR 8.1	8.9	0.89
SBR 8.04	8.9	0.927
NBR 9.25	8.9	0.59

From the previous results, it can be concluded that toluene is a good solvent for the three rubber compounds (NR, SBR & NBR). Therefore; toluene is the most suitable solvent.

The swelling of a rubber by a liquid is a mixing process; two substances mix when the free energy of mixing ( $\Delta G$ ) is negative, if the change in enthalpy ( $\Delta H$ ) is less than the product of absolute temperature ( $T$ ) and the change in entropy  $\Delta S$  as given by the Gibbs equation:

$$\Delta G = \Delta H - T \Delta S$$

Equation 10

In simple terms, mixing is favoured by minimum or negative enthalpy change and mixing entropy change. Swelling is defined as the increase in volume of a gel or solid associated with the uptake of a liquid or gas. The swelling is the first stage in every polymer solution process, in which the solvent molecules diffuse through the polymer matrix to form a swollen, solvated mass, known as polymer gel. However, the gel formed after swelling polymer networks does not break up and the polymer molecules do not diffuse out of the swollen mass, and therefore, no real solution can be formed. The swelling coefficient,  $Q$ , is defined by:

$$Q = \frac{m - m_0}{m} \frac{1}{\rho_s}$$

Equation 11

Where:

$m$  is the weight of the swollen sample;

$m_0$  is the dry weight;

$\rho_s$  is the density of the swelling agent.

Equilibrium swelling index is determined by crosslink density and the attractive forces between solvent and polymer. The theoretical extent of swelling is predicted by the Flory–Rehner equation [185], [189], [190]:

$$\frac{1}{M_c} = \frac{\ln(1 - v_{Rf}) + v_R + \chi v_{Rf}}{v_{Rf}^{1/3} - \frac{2v_{Rf}}{f}} \frac{1}{V_s \rho_R}$$

Equation 12

Where:

$M_c$  is the average molecular weight of rubber segment between crosslinks;

$v_{Rf}$  is the volume fraction of polymer in the swollen mass, equal on the inverse of  $Q$ ;

$\chi$  is the Flory–Huggins solvent–polymer interaction parameter;

$V_s$  is the solvent molar volume;

$f = 3, 4$  for tri- & tetra-functional network junctions, respectively

$\rho_R$  is the rubber density.

The Flory–Huggins solvent–polymer interaction parameter can be determined from the Bristow and Watson semi-empirical equation [191]–[193]:

$$\chi = \beta_1 + \frac{V_s}{RT} (\delta_2 - \delta_1)^2$$

Equation 13

Where:

$\beta_1$  is the lattice constant approximately 0.34;

$R$  is the universal gas constant ;

$T$  is the absolute temperature.

$v_{Rf}$  is the volume fraction of elastomer in the swollen mass, determined according to Ellis and Welding equation [194] Equation 14.

$$v_{Rf} = \frac{\frac{w_2}{\rho_c}}{\frac{w_2}{\rho_c} - \frac{w_1}{\rho_s}}$$

Equation 14

Where:

$w_2$  is the weight fraction of the compound in the swollen specimen;

$w_1$  is the weight fraction of the solvent in the swollen specimen;

$\rho_s$  is the density of the swelling agent;

$\rho_c$  is the compound density.

The Flory–Huggins solvent–polymer interaction parameter is equal to 0.36 for NBR and toluene and it has been determined from the Bristow and Watson semi-empirical equation [191]–[193].

The properties of filled elastomers are linked to the interaction between filler and matrix which can be theoretically estimated by Kraus equation [195]:

$$\frac{v_{R0}}{v_{Rf}} = 1 - K \left( \frac{\phi}{1 - \phi} \right)$$

Equation 15

Where:

$\phi$  is the filler volume fraction;

$K$  is the polymer–filler interaction parameter;

$v_{Rf}$  is the elastomer volume fraction;

$v_{R0}$  is the rubber gum vulcanizate volume fraction.

The relation between  $M_c$  and the crosslink density ( $\nu$ ) is given by Equation 16 [189]:

$$\nu = \frac{2\rho_R}{fM_c}$$

Equation 16

### 2.3.4. Static Mechanical properties

#### 2.2.2.1. Hardness Test

Hardness is defined as material resistance to penetration in specific conditions, in particular the hardness of an elastomer is more accurately thought of as two relative properties: Intrinsic hardness and processed hardness.

As a result of chemical structure, each elastomer has its own intrinsic hardness. This inherent hardness can be modified (and is typically supplemented) via compounding and vulcanization. The hardness of the rubber articles obtained via injection or compression moulding process (processed hardness) is mainly influenced by crosslinking density and the amount of fillers. The more crosslinking a given material undergoes during vulcanization, the harder the mould material will be. When evaluating the potential effectiveness of a moulded article, processed hardness is one of the most common evaluation criteria in the rubber industry.

Unfortunately, hardness is also one of the less consistent concepts as the most used measuring scales have only limited comparability. There is no single “universal hardness” unit, so it is often impossible to trace a

clear and simple relationship between the readings on two different scales, even when the samples to be measured are absolutely identical. There are currently two hardness tests that predominate in the rubber industry: Shore hardness and International Rubber Hardness Grade (IRHD).

Shore durometer device consists of a calibrated spring applying a specific pressure to an indenter foot, which can be either cone (Shore D), truncated cone (Shore A) sphere shaped (Shore 00) as shown in Figure 15. An indicating needle in a dial measures the depth of indentation in a scale from 0 (for full penetration of the indenter) to 100 (corresponding to no penetration of the indenter). The method measures, in fact, the maximum penetration at the applied load and not the deformation of the material. As this method is used to measure viscoelastic materials, it requires to measure also the movement of the indenter during a specific time [196]. There are different Shore Hardness scales for measuring the hardness of different materials. For each scale there is either a different probe/indenter shape as well as a specific spring force. The Shore 00 Scale measures extremely soft materials like gels (think of gel insoles). The Shore A Scale measures a wide range of material types; from very soft and flexible to semi-rigid plastics with almost no flexibility at all. The Shore D Scale measures very hard rubber compounds, semi-rigid and rigid plastics (PVC pipe, for example). Hardness Shore A is the used scale in this work.

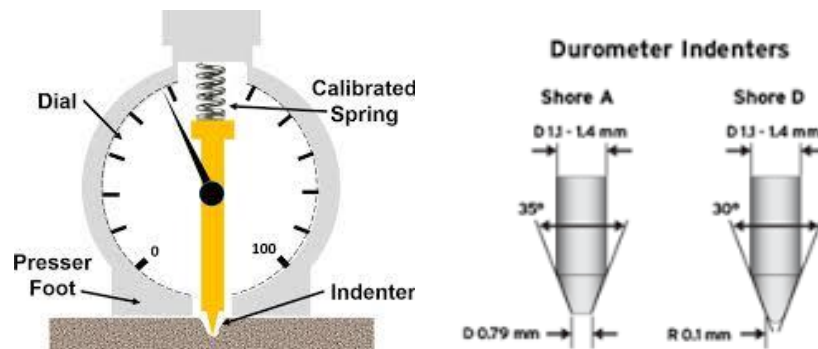


Figure 15 Basic scheme of Shore tester [196]

In the IRHD measurement a ball fitting inside an annular foot to hold the sample in place under the action of a contact force  $L_0 = 0.3 \text{ N}$  with a duration time of 5 s, and the depth-measuring system is reset to zero. Then, an additional constant indenting force of  $L_1 = 5.4 \text{ N}$  is applied during 30 s and the penetration depth  $D$  is measured (Figure 16). The relation between the difference of penetration  $D$  and the IRHD hardness is based on the empirical equation of contact mechanics for a fully elastic isotropic material [196]:

$$\frac{F}{E} = 0,0038r^{0,65}D^{1,35}$$

Equation 17

Where  $F$  is the indenting force in Newtons,  $r$  is the radius of the ball in mm, and  $D$  is the indentation depth in mm. The measured penetration  $D$  is converted into IRHD using the value of  $E$  obtained from Equation 17 into the Equation 18 :

$$IRHD f(E) = \frac{100}{\sigma \sqrt{2\pi}} \int_{-\infty}^{\log_{10} E} e^{-\frac{(t-a)^2}{2\sigma^2}} dt$$

Equation 18

with  $a = 0.34$  and  $\sigma = 0.7$ . This relation is chosen in a way that IHRD = 0 represents a material having an elastic modulus  $E = 0$  and IHRD = 100 represents a material of infinite elastic modulus.

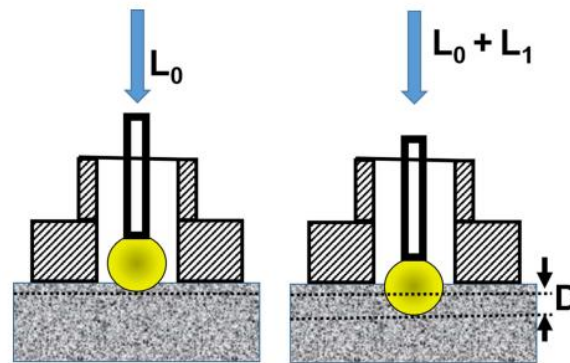


Figure 16 Scheme of IRHD test

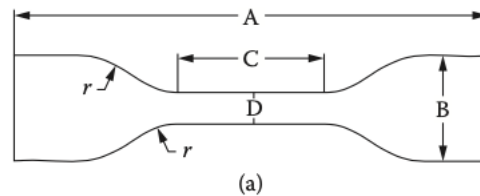
The micro-indentation IHRD test is similar to the macro indentation test IRHD. The difference is the use of a lower load and smaller ball. The method at the microscale uses a ball diameter of 0.395 mm, a contact load,  $L_0 = 0.0083$  N, and a total force  $L_0 + L_1 = 0.1533$  N. The test can be used in rubber sheets from 1 to 5 mm thick. This test at microscale is very useful because it avoids the trouble and cost of making an extra moulding to make a macro sized sample, which might also have a different degree of cure. The method is also useful when the change of hardness is used to measure the effect of aging or weathering, as the restriction on oxygen diffusion would be much less than in a macro test piece.

#### 2.2.2.2. Tensile Test

These tests are used to determine the modulus, tensile strength, elongation at break and stress at a given elongation (tensile stress).

These properties being dependent on the material and the conditions of test (like for example specimen geometry and displacement rate) and therefore should be compared only when tested under the same conditions, i.e. standard.

The tensile test is conducted by tensile dynamometer, using dumbbell specimens. Dumbbell specimens (the dumbbell specimen adopted by the standard ISO 37 [197] is shown in Figure 17) are 10 or 13 centimeters long, die cut from flat sheet, with the length of narrow portion of about 25 mm.



Dimension in mm	Type 1	Type 1A	Type 2	Type 3	Type 4
A Overall length	115	100	75	50	35
B Width of ends	$25 \pm 1.0$	$25 \pm 0.5$	$12.5 \pm 1$	$8.5 \pm 0.5$	$6 \pm 0.5$
C Length of narrow portion	$33 \pm 2$	$20 + 2/-0$	$25 \pm 1$	$16 \pm 1$	$12 \pm 0.5$
D Width of narrow portion	$6 + 0.4/-0$	$5 \pm 0.1$	$4 \pm 0.1$	$4 \pm 0.1$	$2 \pm 0.1$
E Transition radius outside	$14 \pm 1$	$11 \pm 1$	$8 \pm 0.5$	$7.5 \pm 0.5$	$3 \pm 0.1$
F Transition radius inside	$25 \pm 2$	$25 \pm 2$	$12.5 \pm 1$	$10 \pm 0.5$	$3 \pm 0.1$
Gauge length	$25 \pm 0.5$	$20 \pm 0.5$	$20 \pm 0.5$	$10 \pm 0.5$	$10 \pm 0.5$

Figure 17: Dumbbell specimen for tensile test [198]

Tensile tests are carried out on a tensile machine with two grips at the extremities to hold the test piece, a load cell to measure force applied and an extensometer to measure elongation. Nowadays is very often used video and laser extensometer to make non-contact with the measure of the elongation, using benchmarks on the extremities. The measure of elongation is taken as the distance between the benchmarks widens during the test.

Measurements of stress and strain are taken continuously from the zero-strain point to the breaking point and recorded graphically.

The standard temperature in which the test is accomplished is room temperature, around 23°C.

The results of the test can be resumed in a typical tensile stress/ strain (or elongation) curve for rubber compounds and analyzed. A typical stress/strain curve is illustrated in Figure 18.

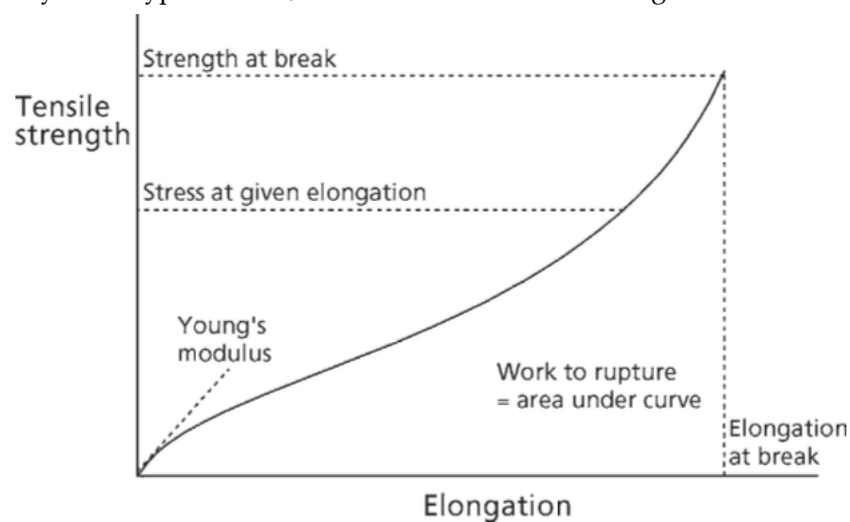


Figure 18: Typical tensile stress strain curve [199]

As it is pointed out from the curve, the stress-strain curve linear section (where the stress increases linearly with deformation) of the curve has a very short length: in this part is it possible to define the Young Modulus ( $E$ ) as the ratio between stress and deformation, as constant.

Tensile strength is the maximum tensile stress reached in a stretching piece, to its breaking point. As convention the force required is expressed as force per unit area of the original cross section.

Tensile stress, or modulus, is the stress required to produce a certain elongation.

Elongation, or strain, is the extension between benchmarks produced by a tensile force applied to the specimen. Is expressed as a percentage of the original distance between the marks.

Elongation at break, is the elongation at the moment of rupture, or maximum elongation.

After a short length, stress is not directly proportional to strain, so, after in the non-linear part of the curve the modulus represents the stress at a certain strain. It is just the coordinates of the stress/strain curve. This is the reason why often the also the secant modulus at 100% is assessed.

### 2.3.2.3 Compression Test

In rubber compounds, the compression behaviour is similar to tensile behaviour, but the Young Modulus in compression conditions is higher than the tensile one.

The specimen used for the compression test is cylindrical: this shape is fundamental in order to avoid the *buckling* phenomenon. The two surfaces must be parallel in order to guarantee a constant distribution of the stresses. It is difficult to submit the specimen to a uniaxial compressive stress, because the test reaches high levels of deformation.

The height of the cylinder specimen highly decreases during the test, and this greatly changes the thickness of the specimen. This type of problem is called *barrel* and it is shown *Figure 19*.

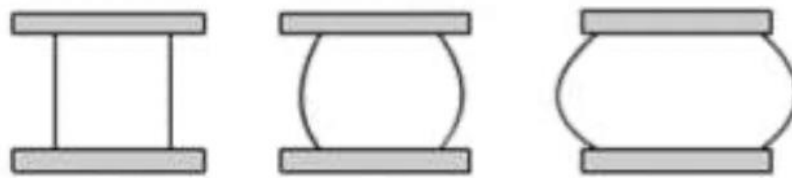


Figure 19: Compression specimen during compression test, barrel problem.

The compression test conditions on rubber specimen are determined by the standard ISO 7743 [121] which classifies 4 methods:

- Method A: Standard specimen A (diameter  $29 \pm 0.5$  mm thickness  $12 \pm 0.5$  mm) with lubricated metal plates;
- Method B: Standard specimen A (diameter  $29 \pm 0.5$  mm thickness  $12 \pm 0.5$  mm) with metal plates bounded to the specimen;
- Method C: Standard specimen B (diameter  $17.8 \pm 0.15$  mm thickness  $25 \pm 0.25$  mm)
- Method D: product or part of the product with lubricated metal plates.

### 2.3.5. Viscoelastic Behaviour

All polymers exhibit viscoelastic properties, due to the internal structure produced by interlinking monomers. Polymers consists in many polymer chains also called macromolecules, the arrangement and conformation of which affect properties. In the unstressed state, macromolecules tend to wrap and tangle around each other, however, when stress is applied, the conformation changes and the chains unwind and extend in the direction of the line of action of the force. *Figure 20*.

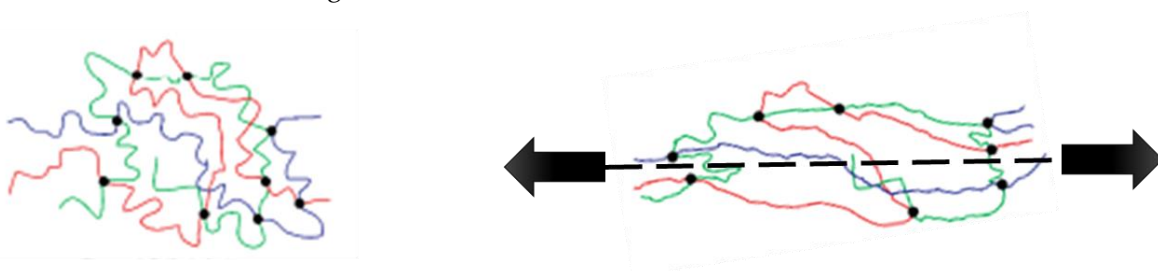


Figure 20 Coiled chains (left); uncoiled chains under tension (right).

Although these chains exhibit elastic properties (i.e. they store the energy used to move them), the friction between the chains causes an observable loss of energy (hysteresis) returning to the unstressed state. For this

reason, the force required to generate a specific displacement is proportional to the applied displacement rate. Therefore rubber is said to have viscoelastic properties [200].

Specifically, in the case of vulcanized rubber, in addition to the physical nodes, i.e. the entanglements, covalent bonds are formed between atoms in separate chains through vulcanization, increasing the rigidity of the rubber.

### **2.2.2.3. Stress Relaxation**

Stress relaxation is defined as a decrease in stress with time at constant deformation. In rubber, stress relaxation occurs due to the slipping of entanglements loosening the network of molecular chains so they apply less force. This action can occur under both constant and cyclic deformation. The magnitude of stress relaxation effects, particularly in the first few deformation cycles, must be taken into account in engineering calculations [201].

### **2.2.2.4. Creep**

Creep is defined as the time dependent deformation of material under stress. The effect of the creep is clearly visible when a specimen maintained at a certain deformation for a certain time is discharged, zero stress occurs in correspondence with a positive deformation. Most rubber components are designed to prevent sliding under tension or cutting. In these modes, creep can easily lead to failure by breakage.

### **2.2.2.1. Permanent Set**

A unique feature of elastomer behaviour is set. It consists in a permanent residual deformation after the applied force or deformation has returned to zero. It is often difficult to measure, because the duration of the force or deformation also produces stress relaxation and/or creep.

In rubber industry it is usually measured in compression as compression set.

The compression set is permanent deformation remaining after removal of a compression force that was applied on the elastomer for a period.

For good performance in many applications, compression set should be low. A low compression set value indicates that a material recovers much of its original height after compression and release of compression force. A less than 20% compression set is a good result and give satisfactory compression results, and a good sealing capacity.

The compression set test is used to determine the ability of elastomeric materials to maintain elastic properties after a long compression stress. This kind of test is also used to determine the degree of vulcanization.

The test is conducted on small cylindrical samples of known thickness. The samples are compressed to a fixed height in a spacer. The spacer consists of two flat, parallel metal plates, that are sufficiently rigid to stand the compression imposed without deforming. These two plates are clamped together, in order to give on the samples a fixed compression typically of 25% of their original height. It must be used three test pieces. They could be placed in the same spacer.

Once the apparatus is fixed together, it is putted into an oven and it is maintained at a test temperature. The duration of the test is 24 hours at elevated temperatures (typically 100°C), or 72 hours at 23°C.

After this period of time, the compressive force is eliminated, and the samples are allowed to recover at room temperature for about 30 minutes. After that the final thick of the specimens is measured.

There are two methods to evaluate the compression set.

In method A, the compression set is the difference between the original thickness and the final thickness of the sample, expressed as a percentage of the original thickness.

$$\frac{b_0 - b_f}{b_0 - b_c} \times 100$$

Equation 19

Where:

$b_0$  = initial thickness of the sample;

$b_f$  = final thickness of the sample after recovery;

$b_c$  = device clamping thickness.

If there is no recovery, compression set is 100%. If there is a full recovery compression set is 0%.

In method B, the compression set is expressed as the difference between the original thickness and the final thickness of the sample as a percentage of the deflection to which the sample was subjected. [8]

#### 2.2.2.2. Mullins Effect

The Mullins effect is perhaps the most dramatic of the effects occurring in cyclic deformation consisting in an appreciable change in their mechanical properties resulting from the first extension. Figure 21 shows three loading-unloading cycles at successively higher maximum stress. In the first cycle the material has not undergone previous deformations and the loading and unloading of the first cycle reaches a maximum of 100% of deformation (point A). In the second loading, the stress is noticeably reduced and only increases to meet the first corner at the maximum of the first cycle. The loading cycle is stopped and reversed at 150% of deformation (point B). The hysteretic effect is observable by the loading curve which is higher than the unloading one. The unloading curve almost coincides with that of the first cycle at some deformation of less than 100%. The third loading curve, like the second one, is well below the first. Like the second, the third loading curve shows up only to meet the second at a maximum of 150%. Similarly, the third loading appears to be a continuation of the second cycle after 150%. At 200% extension (point C) the third cycle is reversed, and the unloading intercepts the retraction of the second cycle as the second cycle intercepted the first.

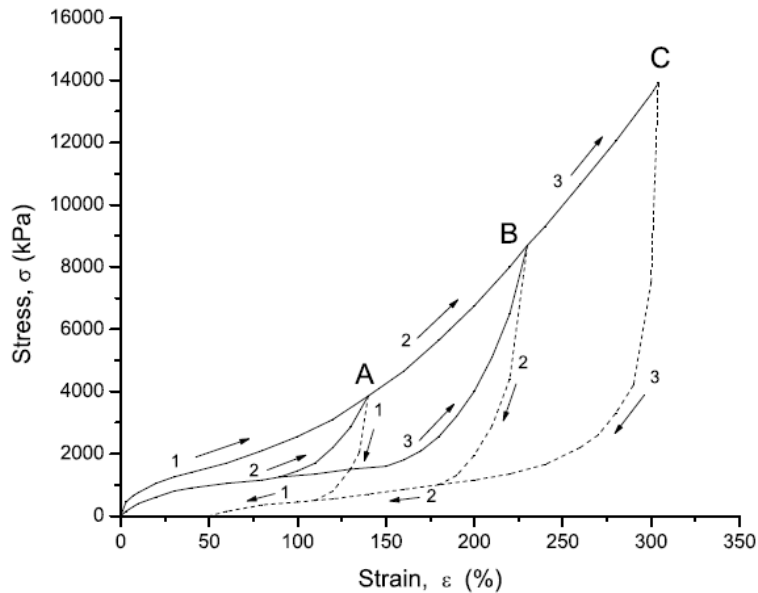


Figure 21 Mullins effect [201]

According to the literature [202], the physical explanation of the Mullins effect is related to several factors such as: Bound rupture, molecules slipping on the filler surface (weak filler-matrix interaction due to low adsorption), filler aggregates rupture, and disentanglements and double layer model (double-layer structure of bound rubber embedded in a crosslinked rubbery matrix).

Some researchers [203], [204] attributed the Mullins effect to bond ruptures; particular attention was paid to the chain linking different filler particles that when completely extended breaks in correspondence of the particle surface.

Other authors [204] confuted this model as it does not fit with the recovery of the imposed deformation at room temperature, because a bound rupture would involve a permanent set.

Therefore, Houwink [204], [205] proposed the slipping of polymer chains over the filler surface in the first loading cycle resulting on a change of the material entropy, which however could be restored apportioning heat. Hamed et al. [206] proposed the disentanglement model as responsible for the Mullins effect. The disentanglements caused by the imposed strain causes the stress-softening. In this configuration the number of active chains is unaffected so that the recovery is possible by apportioning heat due to the genesis of new entanglements.

For carbon black filled elastomers, Fukahori [207] proposed an interface model where the filler particles are surrounded by a immobilized polymer fraction in a glassy state which in turn is surrounded by a polymer layer constrained compared with bulk polymer. In the first loading cycle this creates a network as it comes into contact with that of the adjacent particles. During the first discharge this mesh persists and the bulk polymer compensates for the deformation. When the imposed strain exceeds that of the previous load cycle, the network structure returns to the previously extended state and supports the stress. Entropic forces in the network structure are believed to be the source of the recovery of the Mullins effect.

### 2.3.6. Dynamic Mechanical properties

The initial studies of viscoelasticity focused on the polymer response with respect to a non-cyclic deformation imposed at either a constant strain (creep or stress relaxation) or a constant strain rate (static tests). It was found that the elastic response is proportional to the strain level and the viscous response is proportional to the strain rate. However, rubber products often work under conditions of cyclically varying stress or strain rates and amplitudes. To correlate the viscoelastic properties of a rubber to its performance in a product, these properties must be measured under dynamic conditions: elastic stress in phase with the strain, and viscous stress in phase with the strain rate (90° out of phase with the strain). Under dynamic conditions, a rubber absorbs energy which is partially stored, as in an ideal solid (usually modelled as a spring); and partially it is dissipated in overcoming internal friction, as in an ideal fluid (usually modelled as a dashpot) [208].

This separation of the stress components vectorially allows the material's dependence on strain amplitude and strain rate to be measured simultaneously. The elastic and viscous stresses are related to material properties through the ratio of stress to strain, the modulus. The ratio of the elastic stress to strain is the elastic (or storage) modulus  $G'$ ; the ratio of the viscous stress to strain is the viscous (or loss) Modulus  $E''$ . The complex modulus  $E^* = E' + E''$  reflects the contribution of both elastic and viscous components to the material's stiffness. The ratio of the viscous modulus to the elastic modulus is the tangent of the phase angle  $\delta$  between the stress and strain vectors. Thus,  $E''/E' = \tan \delta$  (loss factor).

The addition of reinforcing fillers to elastomeric materials increases, stiffness as well as tensile and tearing resistance which, on the other side, is often associated to an strain at break reduction [209]. The presence of filler strongly influence also the low amplitude dynamic properties [209]–[218], providing an increase of the storage modulus with increasing the filler content. The dynamic moduli behaviour of unfilled rubber follows the classical theory of linear viscoelasticity, in other words they are not influenced by the strain amplitude [217], [218] and the classical time/temperature superposition principle can be used [208].

#### 2.2.2.3. Influence of strain amplitude: Payne effect and Kraus Model

The filled rubber dynamic modulus dependence to the strain amplitude is known as the “Payne effect” [219]–[222]. The storage modulus shows a plateau at low strain amplitude and then it decreases with increasing the strain amplitude up to a high strain amplitude plateau. In the meantime, the loss factor shows a single peak with increasing strain amplitude over a certain range of amplitude.

In the engineering design, often the materials' constitutive models are needed to understand the behaviour of filler-reinforced rubber and properly design parts [223]. The Payne effect has been the subject matter of several theories which can be classed in two main types: filler structure models and matrix–filler bonding and debonding models [224]. However there are two other factors that govern the conservative modulus but unlike the previous ones they are independent of the amplitude of the shear stress: the hydrodynamic effect and the rubber network [225] (Figure 22).

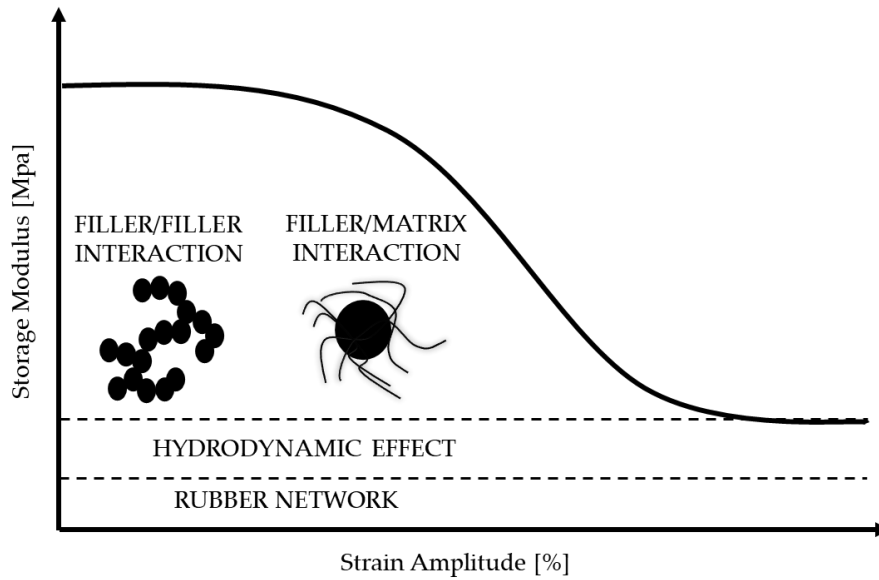


Figure 22 Schematic representation of Payne effect according to different interpretations.

Payne [226] stated that the strain amplitude influence on dynamic moduli is related to the agglomeration and de-agglomeration of the filler network, and for carbon black filled elastomers, the rigidity of the structure depends on the rigidity of the filler–filler bonds. It is assumed that the application of a strain of sufficient magnitude results in a rigidity loss due to damaging of filler network. The dissipative phenomenon of filler network agglomeration and de-agglomeration is assumed to be the cause of the peak of the loss modulus. Under these assumptions, both the storage and loss moduli dependencies on the strain amplitude, have been modelled by Kraus [227] (Equation 20 and Equation 21).

$$G'(\gamma) = G'_{\infty} + \frac{G'_0 - G'_{\infty}}{1 + \left(\frac{\gamma}{\gamma_c}\right)^{2m}}$$

Equation 20

$$G''(\gamma) = G''_{\infty} + \frac{2(G''_m - G''_{\infty}) \left(\frac{\gamma}{\gamma_c}\right)^m}{1 + \left(\frac{\gamma}{\gamma_c}\right)^{2m}}$$

Equation 21

where  $\gamma_c$  is the the strain amplitude in correspondence of which the loss modulus achieves its maximum  $G''_m$ .  $G'_0$  is the storage modulus low strain amplitudes (lower than 0.01%);  $G'_{\infty}$  and  $G''_{\infty}$  are the asymptotic plateau values of the storage and loss modulus at high strain amplitudes, respectively;  $m$  is a non-negative phenomenological exponent to fit the experimental data[216]. Within the filler aggregation models, the concept of occluded rubber (rubber trapped inside an aggregate and shielded from external forces) is often introduced [228], [229]. Under increased applied strain, the trapped matrix is less and less shielded so that the dynamic properties are affected by the immobilized rubber fraction.

The second theory states that the Payne effect is related to the matrix–filler interaction [230]. This theory bases on the idea of bound rubber (polymer adsorbed at the filler surface) that present a reduced molecular mobility

acts as supplementary crosslinks. With the strain amplitude increasing, a mechanism of adhesion and de-adhesion of polymer chains at the filler interface is proposed.

From swelling experiment, Gauthier et al [224] established that fillers immobilize nonvulcanized rubber since they avoid the migration of the bound rubber into the solvent. However, it is worth pointing out that although the models of the first type (infill structure models) can explain several aspects of the non-linear behaviour of the filled rubber, they can barely explain the Payne effect. Meanwhile, it would reasonably not be correct to neglect the filler-filler interaction but neither the filler-polymer interaction. Indeed, the viscoelastic nature of the mechanical connection of the filler to the matrix, highlighted by recovery experiments, suggests that the filler-filler bonds are made through a layer of polymer adsorbed on the surface of the charge [209].

#### 2.2.2.4. Influence of temperature and frequency

The storage modulus as a function of temperature gives the idea about the interaction between the rubber matrix and the EAF slag as filler [231]. The storage modulus as a function of temperature shows three distinct regions, such as glassy, transition, and rubbery regions (Figure 23). The sharp fall of storage modulus in the transition region is associated to the mobility of polymer chains which increases with temperature.

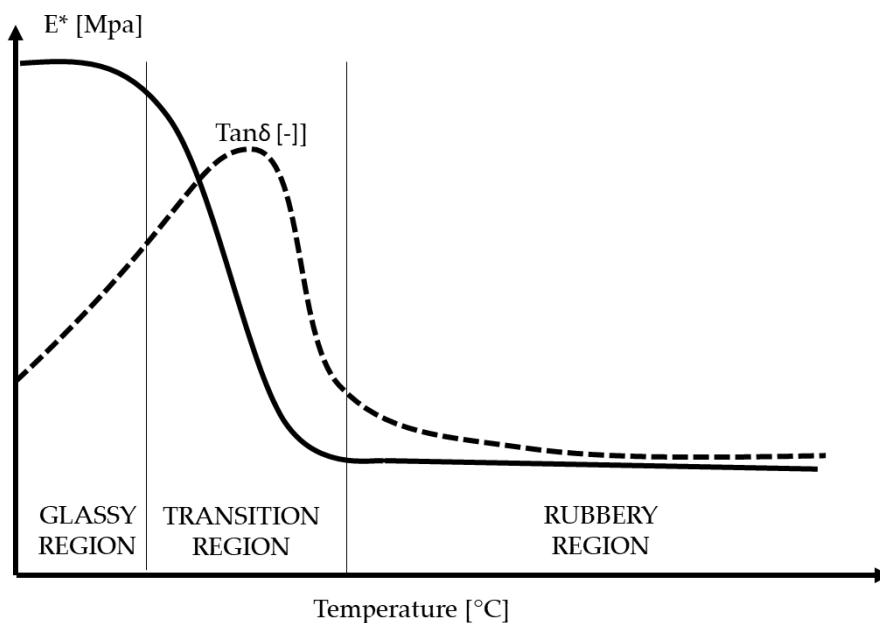


Figure 23 Effect of temperature on dynamic properties

Due to the increase of mobility of polymer chains which increases with temperature it is possible to determine the glass transition temperature  $T_g$ . It can be determined as the onset of the storage modulus drop which is associated to the maximum reduction of mechanical properties. A The loss modulus peak is associated to the increase of the polymer chains mobility and represents the point of maximum damping.

Dynamic properties are dependent on both frequency and temperature, and it is possible to approximately relate the two effects quantitatively. Since not always it is possible to conduct experimental tests in the frequency range of interest, it is possible thanks to the time-temperature principle of equivalence, to predict the required data. The individual isothermal curves, measured at different frequencies, are related to a reference temperature and shifted to the best overlap to create a so-called master curve as shown in Figure 24. This allows the complete relaxation behaviour of a polymer to be described.

The general form of the effect of temperature on complex modulus and  $\tan\delta$  is shown in Figure 23 . The effect of increasing or decreasing frequency is to shift the curves to the right or left respectively along the temperature axis. At room temperature the order of magnitude of the effect of temperature on modulus for a typical rubber is 1% per °C and the effect of frequency of the order of 10% per decade[232].

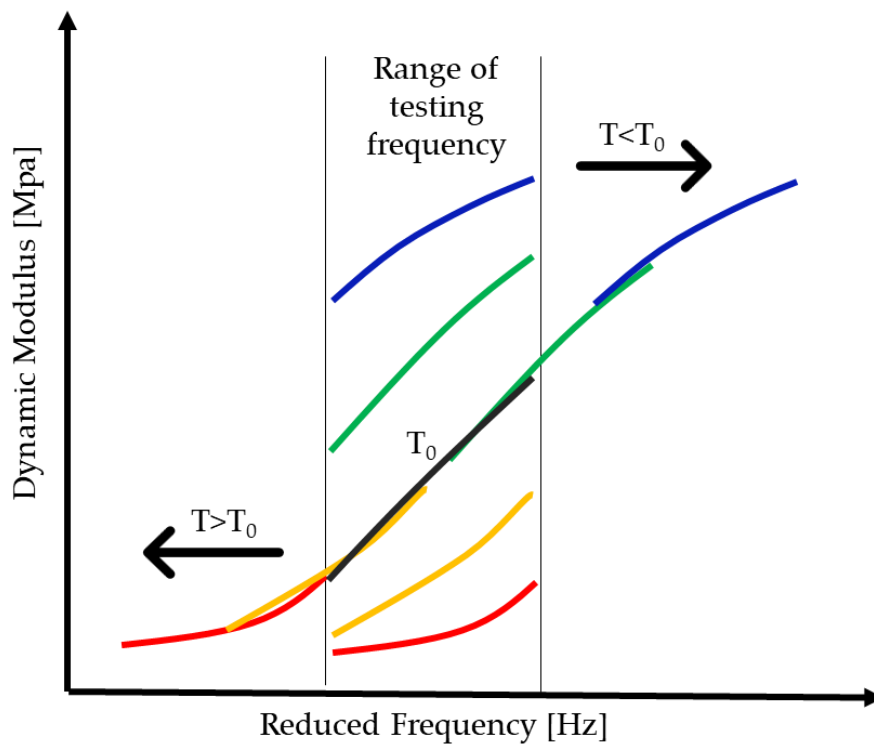


Figure 24 Master curve obtained by the time-temperature principle of equivalence.

### 2.3.7. Bound rubber

#### 2.3.7.1. Bound rubber content

The measurement of the bound rubber content in rubber compounds is considered a feature of filler-matrix interaction. It is defined as the rubber portion in an uncured rubber compound, which cannot be extracted by a good solvent due to the adsorption of rubber macromolecules onto the filler surface.

The bound rubber content (BRC %) was determined as:

$$BRC[\%] = \frac{m_d - m_0 \left( \frac{m_f}{m_f + m_r} \right)}{m_0 \left( \frac{m_r}{m_f + m_r} \right)}$$

Equation 22

Where  $m_0$  is the initial sample mass,  $m_d$  is the mass of dry sample after extraction,  $m_f$  is the mass of the filler and  $m_r$  is the mass of the rubber.

#### 2.3.7.2. Immobilized rubber fraction (IRF)

The bound rubber is sometimes named “immobilized rubber fraction” and it can be quantified by DSC analysis, in particular by the variation of heat capacity scan at neat of filler ( $C_p^*$ ) in correspondence to the glass transition temperature as shown in Equation 23:

$$Cp^* = \frac{Cp}{1 - \text{filler (\%wt)}}$$

Equation 23

The heat capacity increment,  $\Delta Cp^*$  is a measure of the amount of polymer which participates in the glass transition and it is dependent on the intermolecular rigidity, that is, the polymer–filler interaction in the filled rubber [231]. The dependency of  $\Delta Cp^*$  on intermolecular rigidity is often evaluated in terms of immobilized polymer chains in the composites. The fraction of immobilized polymer is calculated by [233]:

$$\text{Immobilized rubber fraction [\%]} = 1 - \frac{\Delta Cp^*}{\Delta Cp^0}$$

Equation 24

Where  $\Delta Cp^0$  is the heat capacity variation of neat rubber.

### 2.2.3. Tribological behaviour

#### 2.2.3.1. Friction

The coefficient of friction of a rubber surface against a hard surface can be expressed in terms of the contribution of adhesion, deformation (hysteresis), viscous and cohesion (tear)[234], [235]. It is generally recognized that adhesion consists of the formation and rupture of joints at the molecular level. Hysteretic friction is a consequence of the energy loss associated with internal damping within the viscoelastic body.

Contribution of adhesion and hysteretic friction depends on the temperature, sliding velocity, geometry and cleanliness of the mating surfaces. The adhesion component is more significant on very clean and smooth rubber surfaces. It can also be significant at low loads, even in lubricated conditions, because of the significance of the attractive Van der Waals' forces in temporary bonds between the surfaces in comparison to the normal load.

When a soft rubber slides against a hard track, or a hard slider slide against a soft rubber track, the relative motion between the two frictional members is often due to 'waves of detachment' crossing the contact area at high speed from front to rear. These waves, which move much faster than the two bodies in sliding, are known as 'Schallamach waves'. The Schallamach waves appear at a critical sliding speed whose value depends on the adhesive properties of the interface, the geometrical characteristics of the contact, elastic properties of the rubber-like material, load and the temperature.

#### 2.2.3.2. Wear

Three different mechanisms of wear can be identified when an elastomer slides against a hard substrate. During sliding against a hard countersurface with a sharp texture, abrasive wear takes place as a result of tearing of the sliding surface of the elastomer. Fatigue wear is another mechanism of wear which occurs on the surface of an elastomer sliding against blunt projections on the hard substrates. When a highly elastic elastomer slides against a smooth surface, roll formation occurs. In this type of wear the high frictional force shears a projection on the rubber surface, tears and then rolls the tongue along the direction of sliding [235]. A critical value of shear stress can be defined for each rubber such that if the shear stress is higher than the critical shear stress, roll formation occurs and for shear stresses lower than the critical value, wear is mainly due to fatigue. Thus the friction coefficient is one of the most important properties of rubber governing the type of wear. Figure 25 shows the schematic diagram of the friction and wear mechanisms in elastomers.

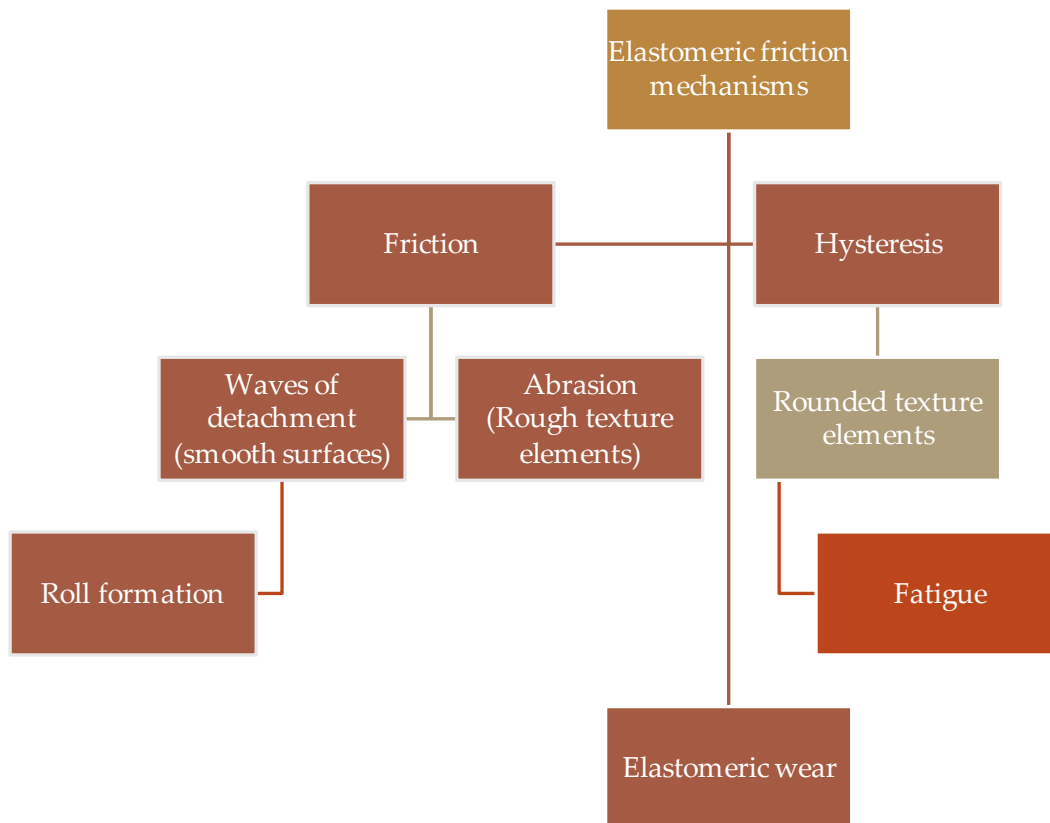


Figure 25 Schematic diagram of the friction and wear mechanisms in rubber-like materials [235].

The specific wear rate ( $W_s$ ) can be calculated as the mass loss divided by the product of the normal load and the sliding distance as reported in Equation 25.

$$W_s = \frac{(\Delta m)}{Pl}$$

Equation 25

## EXPERIMENTAL METHODOLOGIES AND RESULTS

### 1. Epoxy screed filled with EAF slag as alternative filler to sand

This characterization aims to propose the EAF slag as alternative reinforcing filler in epoxy resin composite for epoxy screed floor. The epoxy screed is a resin flooring characterised by a thickness between 6 and 15 mm, which guarantees excellent mechanical resistance, foot load resistance, and chemical agents resistance [236]–[238]. The replacement of a traditional filler such as river sand with a waste material such as EAF slag would lead to multiples benefits, not only from the environmental point of view (reduction of activities impacting on the territory (i.e., extraction and drilling), energy-saving, and the related decrease of CO<sub>2</sub> emissions) but also from the economical point of view. The replacement of sand with slag would lead to reduce the exhaustion of natural resources with the relative cost of extraction, and on the other hand to reduce the waste disposal in landfills with the related disposal costs by steel producers.

EAF slag phases have been determined by X-ray Diffraction (XRD) and Scanning Electron Microscopy (SEM) integrated with Energy Dispersive X-ray Spectrometry (EDXS) for the morphological and elemental analysis of the phases; the chemical composition has been determined by X-ray fluorescence (XRF) spectroscopy. The leaching test has been performed on the slag and on the composite material demonstrating the polymeric matrix's ability to immobilize the heavy metals. Epoxy composites filled with EAF slag have been mechanically characterized by three points flexural, compression and hardness test; epoxy composites filled with equivalent volume fraction of river sand have been also tested in order to compare the mechanical behaviour of a traditional filler such as river sand and a more sustainable filler such as EAF slag. Moreover, the fracture surfaces have been observed by scanning electron microscope (SEM). Three-point flexural and compression tests show the new composite's excellent behaviour compared to commercially available materials used for epoxy screeds demonstrating that EAF slag could be a valuable resource.

#### 1.1. Materials

##### 1.1.1. Matrix

The thermosetting matrix consists of epoxy resin E-227 provided by Prochima Srl (Colli al Metauro PU, Italy), also known as polyepoxides, a class of reactive pre-polymers and polymers characterized by the presence of epoxide groups. The bi-component product is formed by polymer and catalyst that must be mixed to obtain the final product.

##### 1.1.2. Filler

The slag used as filler was supplied by ASONEXT Spa (Ospitaletto BS, Italy) steelmaking plant, which produces special-grade steels. The slag employed in this research has been produced by a specific system named Slag-Rec [239] for dry granulating EAF molten slag. The slag has been ground by the manual pulverizing mill HSM100 provided by Herzog (Osnabrück, Germany) for 25 seconds and then sieved to obtain a grain size <106 µm.

For comparison, river sand (grain size <106 µm) was also used as a filler in the same epoxy matrix.

### 1.1.3. Commercial product

As a reference, a three-component epoxy mortar was also characterised, a commercial material specifically formulated for laying epoxy screeds. This material consists of a fluid epoxy resin (7,5% by weight), a hardener (2,5% by weight), and a mineral filler based on silica sand (90% by weight) with a suitable particle size to obtain a high degree of compactness of the mortar (<0.25 mm).

### Sample preparation

The preparation of the composite material samples with an epoxy resin matrix included the following steps: manual mixing the filler with the epoxy resin (100:50) before pouring the mixture into a silicone mould. The material so obtained has been maintained for 24 hours at room temperature to allow the polymerization, then the samples have been manually demoulded.

Known the slag (3,87 g/cm<sup>3</sup>) and epoxy resin (1,12 g/cm<sup>3</sup>) densities, the quantity of slag as a filler and epoxy resin as the matrix were calculated to obtain a composite with a percentage by weight of 60, 70, 80, 90%. Known the density of sand (1,5g/cm<sup>3</sup>), its quantity was calculated to have in the composites the same percentage by volume of the EAF composites (see *Table 10*). The comparison between composite filled with EAF slag and composite filled with river sand was made with the same volumetric fraction of filler in order to keep the same adhesion surface between filler and matrix since it plays a fundamental role in load transmission.

The commercial product uses 90%wt of sand, corresponding to 87% v/v. The mechanical properties of the EAF composites and the sand composites were tested.

*Table 10 EAF slag and river sand percentage by weight with the equivalent percentage by volume.*

EAF slag %wt	% v/v	Sand %wt
60	30,3	36,8
70	40,3	47,5
80	53,7	60,8
90	72,3	77,7
Commercial product	87,0	90

Specimens with two different geometries were produced for flexural (according to the standard ISO 178:2010 [119]) and compression (according to the standard ISO 14544:2016 [120]) mechanical characterization.

## 1.2. Methods

### 1.2.1. EAF slag Characterization

The principal techniques adopted to characterize the chemical composition and the phases of the slags are X-ray Diffraction (XRD) and Scanning Electron Microscopy (SEM) integrated with Energy Dispersive X-ray Spectrometry (EDXS) for the morphological and elemental analysis of the phases [240]. Black slag samples were prepared for these 2 techniques. In particular, for the identification of the phases and structure of the slag with SEM-EDXS (SEM Leo Evo 40, Carl Zeiss, Oberkochen, Germany; EDXS microprobe Link Pentafet Oxford mod 7060; Oxford Instruments, Oxfordshire, U.K.) a standard metallographic polishing procedure was used. XRD analysis is performed with a Panalytical X'Pert Pro diffractometer equipped with an X'Celerator detector and Cu anode (CuK $\alpha$  = 0.15406 nm), operating at 40 KV and 40 mA, on pulverised and sifted slag.

The X-Ray Fluorescence Spectroscopy has been carried out by the Thermo Scientific™ ARL™ PERFORM'X provided by Thermo Fisher Scientific (Rodano MI, Italy). The sample consists of 9g of fine slag and 1 g of

methylcellulose Alfa Aesar mixed for 30 seconds in the pulverising mill. The button is then prepared by pressing the mixed slag and methylcellulose on a primer of boric acid at 200kN for a pressure time of 30 seconds. EAF slag chemical composition is given in *Table 11*.

According to the standard CEN EN 12457-2 [72], the leaching of heavy metals has been determined. The slag has been ground by a mortar then it has been sieved to obtain a grain size <4mm. To evaluate the influence of the grain size on the leaching, the test has been performed on slag grain size sieved between 4 and 3 mm and between 1 and 2 mm. Each test has been performed twice. After it has been properly mixed to optimise the representativeness of the sample and then the ferromagnetic materials (i.e. iron, nickel, and steel) have been removed by a magnet. A 90 g of slag was mixed with 900g of water in HDPE bottles and stirred for 24 hours at 8rev/min.

After 24 hours of stirring, the solutions have been settled for 15 minutes and then filtered through a filter of 45  $\mu\text{m}$  into a flask under suction at 70 kPa. To obtain a better reading of the ICP Optical Emission Spectrometer, the solution has been acidified by acid nitric 1/20 V/V.

The solution has been analysed by a Avio 200 ICP Optical Emission Spectrometer provided by Perkin Elmer (Milano, Italy) to measure the concentration in the solution of Cr, Mo, and V.

## 1.2.2. Composites Characterization

### 1.2.2.1. Mechanical tests

The three-point flexural test has been carried out according to the standard ISO 178:2010 [119]. The purpose of this test is to measure flexural strength and flexural modulus. Flexural strength is defined as the maximum stress at the outermost fiber on either the specimen's compression or tension side. Flexural modulus is calculated as the slope of the linear section of the stress-strain deflection curve. These two values can be used to evaluate the sample materials' ability to withstand flexure or bending forces. Tests are carried out at room temperature (23 °C) by a dynamometer Series 3366 provided by Instron (Pianezza TO, Italy), equipped with a 10 kN load cell with a crosshead rate of 10 mm/min and support span 64 mm. Five 80x4x10mm<sup>3</sup> specimens for each composite are measured.

Compression test has been carried out according to the standard ISO 14544:2016 [120]. In the compression test, the test sample is cylindrical (diameter 10mm and height 20mm) and is positioned between two plates which distribute the applied load over the entire surface area of two opposite faces of the test sample. The plates are pushed together with a crosshead rate of 1mm/min by an electromechanical dynamometer (Instron Series 3366) equipped with a 10 kN load cell. The compression test evaluates the material's response to a compressive load measuring the yield stress and compressive elastic modulus.

By a digital microhardness tester (Hardness testing machine HM-200 provided by Mitutoyo (Kawasaki, Japan)), a 300g load was applied through the Vickers indenter for 15 seconds. Five indentations were made at different points on each specimen and the mean Vickers Hardness (HV) was calculated.

### 1.2.2.2. Composite leaching test

As for the EAF slag, the leaching test on the composite material (epoxy resin filled with EAF slag) was conducted, according to the CEN EN 12457-2 standard [72]. The composite material (slag with particle size less than 106  $\mu\text{m}$  incorporated in the epoxy resin matrix) was crushed to a particle size of less than 4mm. In the test, the composite's amount was calculated to maintain the ratio of 1: 10 with the solution. The leaching

test was conducted on two groups of materials with an average filler percentage of 65% wt and 85% wt, respectively. Three measurements were made on each eluate, and the most severe value is shown in Table 12.

### 1.2.2.3. Scanning electron microscopy (SEM) analysis

The fracture surface of cross-sections of specimens broken by flexural tests has been analyzed by SEM. Observations have been performed by a LEO EVO 40 SEM (Carl Zeiss, Oberkochen, Germany).

## 1.3. Results and discussion

### 1.3.1. EAF slag characterization

Table 11 shows the chemical composition of the EAF slag determined by XRF. The basicity index  $IB2 = CaO/SiO_2$  is 3,15. It should be noted that among the most important aspects in reducing leaching of heavy metals from the slags is controlling its chemical composition with a rapid cooling with the formation of glass phases [241] and the basicity factor calculated as  $(CaO + MgO)/(SiO_2 + Al_2O_3)$ ; if this parameter is greater than 1, then glass may form when cooled rapidly, so to shelve the heavy metals and prevent them from leaching [242]. ). In Figure 26 it is possible to observe the X-ray diffraction pattern obtained thanks to the high crystalline nature of the slag phases used for this [243] and in Figure 27 SEM-EDXS analysis carried out on a metallographically polished sample utilizing back-scattered electron (BSE) mode. It is important to highlight that it is difficult to identify the exact mineralogy because the slag appears very complex and some phases have varying contents of substituted ions. Thanks to the comparison with the two analytical techniques used, it was possible to classify the main phases present, namely iron oxides (principally wüstite FeO with the presence of hematite  $Fe_2O_3$  and magnetite  $Fe_3O_4$ ) also containing a small quantity of Cr and Ca, larnite ( $Ca_2SiO_4$ ) with the presence of a minor amount of brownmillerite ( $Ca_2(Al, Fe)_2O_5$ ) with traces of Ti and V. Some large clusters with a composition that is very similar to that of chromite ( $FeCr_2O_4$ ) or magnesio-chromite are identified only with SEM/EDXS analysis; this phase has a small volume fraction and this would explain why it is possible that it was not detected by XRD.

Table 11 EAF slag chemical composition determined by X-ray fluorescence spectroscopy (XRF) and basicity indexes. All amounts are reported in [%wt]

SiO <sub>2</sub>	Al <sub>2</sub> O <sub>3</sub>	Fe <sub>2</sub> O <sub>3</sub>	MnO	CaO	MgO	P <sub>2</sub> O <sub>5</sub>	TiO <sub>2</sub>	Cr <sub>2</sub> O <sub>3</sub>	S	Na <sub>2</sub> O	K <sub>2</sub> O	F
9.45	7.61	40.19	5.58	29.83	3.64	0.48	0.38	2.30	0.09	0.44	0.01	0.00
Sum [%]			Basicity [-]		CaO/Al <sub>2</sub> O <sub>3</sub> [-]		Al <sub>2</sub> O <sub>3</sub> /SiO <sub>2</sub> [-]		IB2 [-]		IB4 [-]	
100			0.62		3.92		0.81		3.15		1.96	

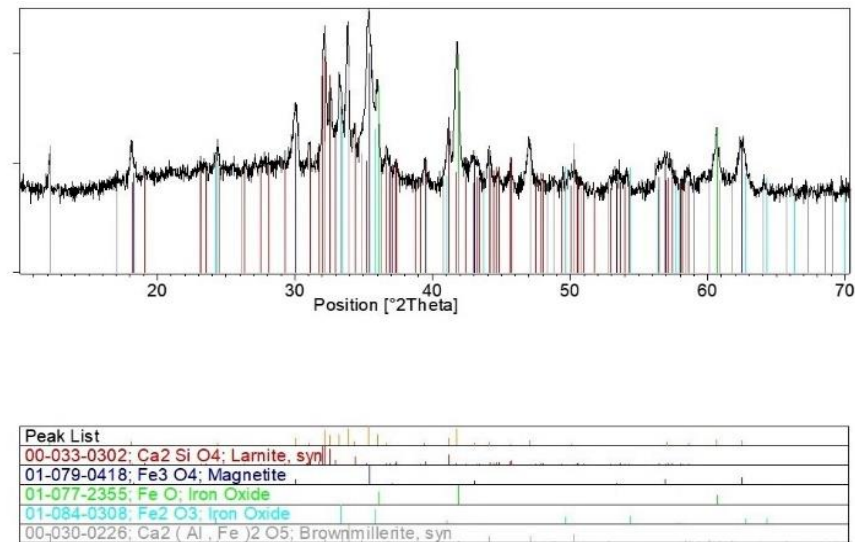
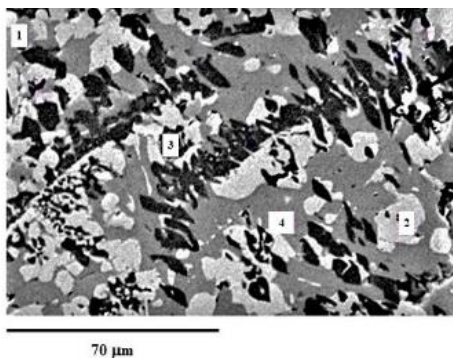


Figure 26 X-ray diffraction pattern collected from slag sample and crystalline phase identification.



Analysis	O	Mg	Al	Si	Ca	Ti	V	Cr	Mo	Fe	Phases identification
1	18.17	8.59	1.63		1.13			50.37	3.31	16.80	Chromite
2	14.29	3.34	0.53		2.67			2.54	5.09	71.55	Iron Oxide
3	28.13			19.37	50.47					2.03	Larnite
4	21.35		4.18	2.37	35.07	1.16	0.57	0.80		34.50	Brownmillerite

Figure 27 SEM back-scattered electron (BSE) image of slag microstructure [%wt] with its EDXS analysis on metallographically polished sample.

### 2.3.7.2. Free slag and composite material leaching

Italian legislation imposes different threshold limits of leaching of several elements (measured according to the standard CEN EN 12457-2 [72]) function of slag destination. For material reuse, the Italian Ministerial Decree 5/2/98 [244] (updated 5/4/06 [245]) limits the V and Cr leaching at 0.25mg/l and 0.050mg/l, respectively. For landfill disposal as inert waste, according to Ministerial Decree 30/8/05 [246], the Cr and Mo maximum values allowed are 0.05mg/l and 1 mg/l, respectively. Thus, in Italy, the EAF slag can be landfilled as non-hazardous waste. Italian legislation imposed the most stringent CEN EN 12457 standard (i.e. CEN EN 12457-2) requiring a slag grain size lower than 4mm. Other European countries, like France and Spain, adopted the CEN EN 12457-4 standard, which requires a particle size smaller than 10mm for the leaching test. Riboldi et al. [247] showed that this can significantly influence the final results, since when the grain size decreases the release rate increases.

In this work, these results are confirmed, as shown in Table 12, for Mo, while the release of Cr and V does not change significantly. It is worthwhile to notice that for a grain size less than 4mm (standard test conditions), Mo release is lower than that of grain size range 1-2mm and higher than that of grain size range 3-4mm due to the presence of both grain size of 3-4mm and very fine powder (lower than 1mm). The Cr release of a grain size less than 4mm is about the same as the other grain size ranges, and the V release for a grain size less than

4mm is higher than that of both grain size range 1-2mm and grain size range 3-4mm. Similar results were found by Riboldi et al. [247], who concluded that this behaviour is probably due to the grinding, which causes a higher percentage of hard phases in the large grains.

The leaching of Mo, Cr, and V of EAF slag in the composites is reported in Table 12. The leaching of Mo, Cr, and V is reduced and, consequently, both composite materials are compliant for material reuse according to the Italian Ministerial Decree 5/2/98 [244]. As expected, the reduction of metal leaching is higher for lower EAF slag content, except for V. This behaviour is probably due to the slag's heterogeneity and the fact that different samples can give different leaching results, even if they come from the same casting.

Table 12 Leaching test UNI EN 12457-2 results.

	Free EAF Slag Grain size			Composite EAF slag (<106 $\mu$ m) [%wt]	
	x<4 [mm <sup>2</sup> ]	1<x<2 [mm <sup>2</sup> ]	3<x<4 [mm <sup>2</sup> ]	65%	85%
Electrical Conductivity [ $\mu$ s]	816 $\pm$ 231	746 $\pm$ 115	797 $\pm$ 28	928	1343
PH [-]	11,8 $\pm$ 0,2	11,4 $\pm$ 0,1	11,5 $\pm$ 0,01	11,5	12
Mo [mg/l]	0,15 $\pm$ 0,07	0,23 $\pm$ 0,06	0,136 $\pm$ 0,003	0,119	0,172
Cr [mg/l]	0,073 $\pm$ 0,01	0,076 $\pm$ 0,004	0,074 $\pm$ 0,001	0,026	0,036
V [mg/l]	0,1 $\pm$ 0,1	0,14 $\pm$ 0,06	0,1 $\pm$ 0,01	0,051	0,007

### 1.3.2. Composites characterization

#### 1.3.2.1. Flexural properties

Flexural stress-strain curves of EAF and sand composites are shown in Figure 28 as solid and dashed lines, respectively. For comparison, the epoxy matrix and the commercial product flexural stress-strain curves are shown as solid grey and dark blue dashed lines, respectively. The three-point flexural test's parameters were obtained: flexural strength, flexural strain (Figure 29), and flexural modulus (Figure 30). As expected, the epoxy matrix shows an elongation at break higher than the composites, and it did not break brittle, but it yields above the peak. At the same filler volume percentage, the sand composites are more brittle than the EAF ones, especially for 30,3% and 40,3%, likely because the sand has a better adhesion with the matrix. The commercial product does not brittle fracture, while it exhibits slight yield strength at break.

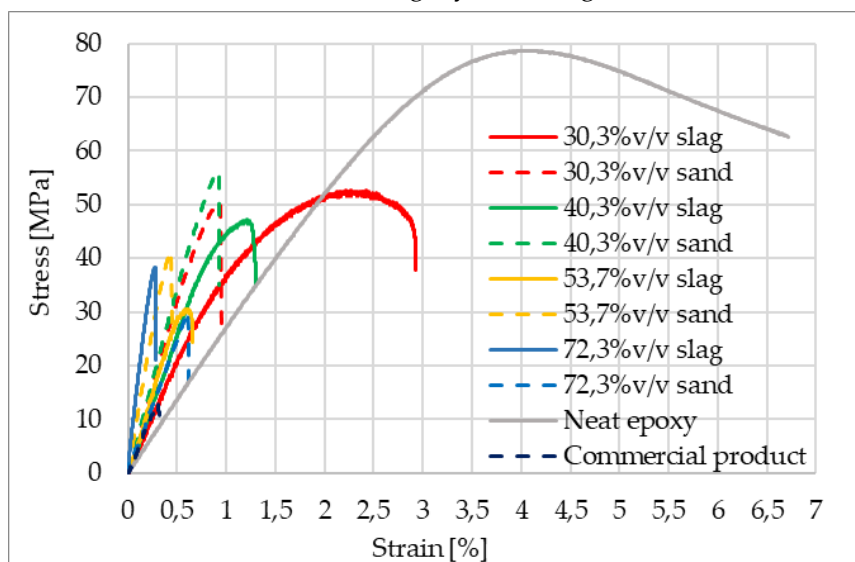


*Figure 28 Flexural stress-strain curves of neat epoxy, epoxy resin filled EAF slag (solid lines) and filled sand river (dashed lines) and a commercial product.*

In Figure 29, flexural strength and flexural strain of different composites function of percentage by volume of filler are shown. EAF slag and river sand have the common effect of reducing the flexural strength of the composites. Increasing the filler amount, flexural strength decreases from about 75MPa for the epoxy matrix to about 55MPa for 30,3%v/v composite materials. The lowest value of 10 MPa has been obtained for the commercial product filled at 87%v/v. The reduction of the flexural strength is about the same for EAF slag and sand composites; in fact, the 30,3%v/v and 72,3%v/v sand composites have flexural strength of about 10MPa lower compared to the slag composites. For filler equal to 40,3%v/v and 53,7%v/v, the composite materials filled with EAF slag have a lower flexural strength of about 10MPa than that filled with the sand river. The commercial product shows the lowest flexural strength, probably because of two factors: the highest filler presence (87%v/v) and the larger filler grain size, which reduces the filler-matrix contact surface/filler volume ratio.

According to literature [248], the reduction of flexural strength with increasing the filler content can be attributed to Insufficient particles embedding. While for small fractions in volume the flexural strength of the composite increases because the amount of resin between filler particles allows the filler to bear most of the load, beyond a certain filler volume fraction it is reduced due to the poor embedding of the filler particles. In the case of the composites studied in this work, it is possible to state that this threshold is lower than 30.3% v/v of filler (grain size lower than 106 $\mu$ m).

As a general trend, increasing the filler percentage, the flexural strain decreases. However, while sand composites materials show a slight flexural strain reduction, for EAF composites, the reduction is significant, beginning from a much higher flexural strain value. This trend correlates with the flexural stress-strain curves (Figure 28), where EAF composite materials show a slight yield at the break, especially at low percentages of filler.

As the percentage of filler increases, the difference in the strain at the break value is lower until being approximately the same for 72,3%v/v, showing that, up to 53,7%v/v, the slag reduces the composites strain at break less than the sand river. The commercial product flexural strain is found similar to that of the 73,2%v/v slag composite.

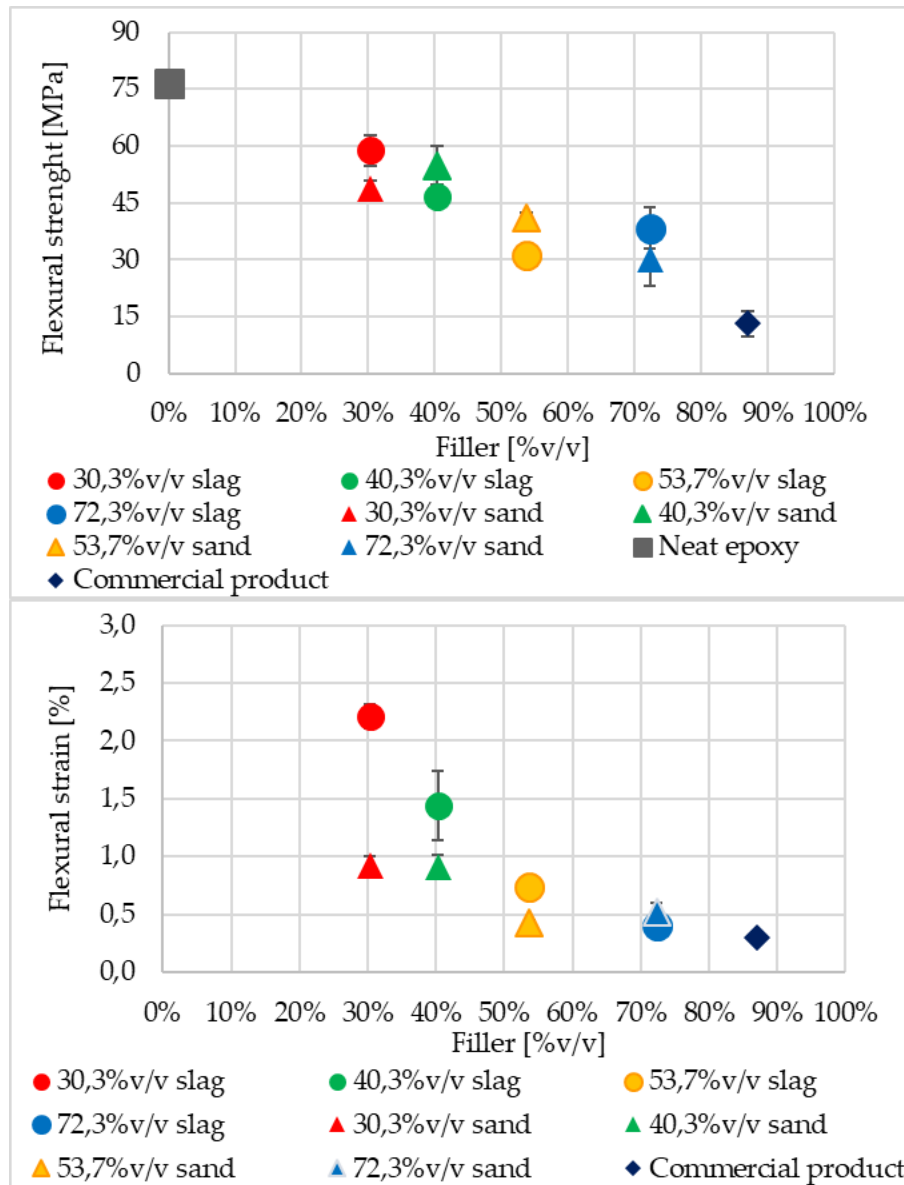


Figure 29 Flexural strength and flexural strain of neat epoxy, epoxy resin filled EAF slag and sand river and a commercial product.

Figure 30 shows the flexural modulus of the epoxy matrix, EAF, and sand composites, and the commercial product.

The slag composites' flexural modulus increases with the EAF content up to about 13000 MPa for the sample filled at 72,3%v/v. Similar behaviour is observed for the sand composites' flexural modulus until the 53,7% v/v sand composite, then the value decreases. This difference can be explained by a not sufficient wettability of the sand in the sample with the highest percentage, leading to a composite material with a minor stiff. Probably, the EAF composites do not exhibit this effect because the high percentage of fine dust ( $<50\mu\text{m}$ ) guarantees a good sample's wettability.

For filler contents up to 53,7% v/v, sand composites are stiffer than EAF ones because of the better sand adhesion to the matrix than that of the EAF slag. As a consequence, the slag composites are less rigid but tougher.

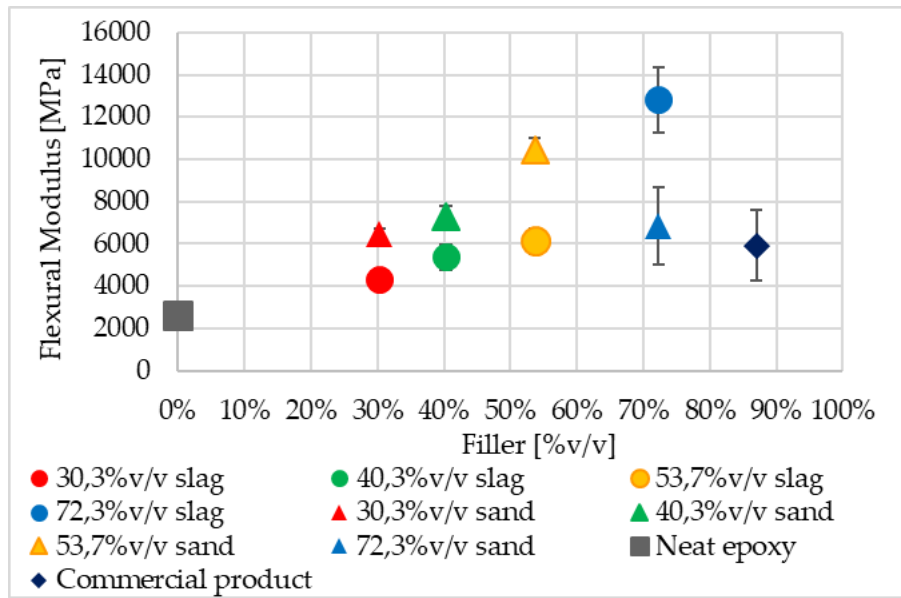


Figure 30 Flexural elastic modulus of neat epoxy, epoxy resin filled EAF slag and sand river and a commercial product.

The flexural modulus of elasticity increases with filler volume fraction until the capacity of the matrix to coat the filler particles is exceeded; in other words, a fundamental role is played by the filler particles embedding. As long as the matrix volume fraction is sufficient to embed filler particles in order to make it to the load-bearing phase, the modulus increases.

The increase in modulus with the volumetric fraction of the filler has been found in many other types of research [248]–[251].

#### Fracture surface

Epoxy resin is a highly resistant material to plastic deformation. However, when it is filled with a second phase, the filler particles can induce shear yielding in the matrix by promoting a change in the stress state. This may result from the formation of voids with debonding effects [252], [253]. In the present work, it was found a reduction in the mechanical strength of filled epoxy (both sand and EAF slag) compared to neat epoxy; in particular, the reduction is more pronounced for high filled composites. This behaviour has been observed in some scientific works in which is reported that an interfacial particle-matrix layer is formed by immobilized polymer chains, and it is characterized by physicochemical properties quite distinct from those of the bulk polymer matrix. As consequence, with the increase of the filler volume fraction, the inter-particle distance is reduced. Once that the inter-particle distance reduces to a critical value, the interfacial layers may overlap, creating a tridimensional network that affects greatly the material properties [253], [254]

SEM micrographs of fracture surfaces of flexural broken epoxy filled with river sand and EAF slag at different filler volume fractions are shown in Figure 31.

It is possible to notice that in all specimens cracks propagate directly showing no retardation in crack growth. This indicates the brittle behaviour of the composites, and there is no evident plasticity observed before final failure. All the composites' fracture surfaces are brittle and composites filled with EAF slag and river sand exhibit similar fracture surfaces.

It is important to highlight that in a typical brittle material, catastrophic failure occurs with no crack deflection when energy is sufficient to initiate crack growth. For composites, when the crack reaches the particulate-matrix interface, can propagate in two ways: it can break up the particulate or it can be deflected along with the interface, causing debonding. The mechanism of crack growth strongly depends on the adhesion between the filler particles and the matrix. If the particulate resistance is greater than the interfacial shear resistance, the particulate is pulled out before it breaks down and vice versa [255], [256].

From the observation of the fracture surfaces of composites with a volumetric fraction of sand from 30,3 to 57,3%, it is possible to see smooth surfaces parallel to the fracture surface of the filler particles. Linking the fracture surface and the results of flexural properties, it is possible to confirm that the sand composites have a more brittle behaviour. This phenomenon is probably due to better adhesion between matrix and sand, it is possible to assume that the fracture has broken up in a brittle way through the sand particles fracture. This behaviour is less visible in samples filled to 72,3% v/v probably due to the poor resin volume fraction and consequently, the particles are not well embedded resulting in a sharp drop in modulus. Similar results were found by Tahir et al. [257].

Regarding EAF slag composites, the filler surface is less smooth, although the brittle fracture mode. The composite filled with EAF slag at 30,3% v/v shows small areas of ductility, according to the results of the flexural test where the composite yields before breaking. In the case of epoxy filled up to 57,3%v/v, the slag particles are well embedded in the epoxy matrix. When the filler reaches the volume fraction of 72,3% the fracture surface becomes rougher and a large amount of slag particles are exposed outside with few epoxy resin coating, which indicates a minor adhesion between slag and the matrix. Similar results were found by Li et al. in their research [258], although the different particles size.

This attests the minor brittleness of EAF slag composite which will be less prone to a catastrophic failure without the debonding reduces the modulus.

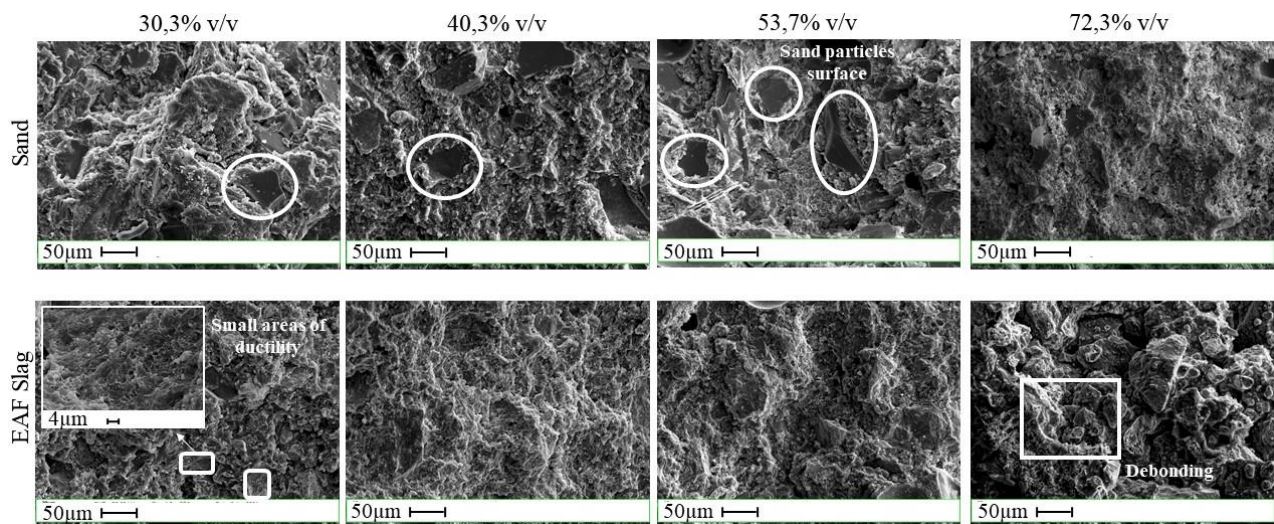


Figure 31 SEM images of fracture surfaces of epoxy filled with river sand and EAF slag at different filler volume fractions.

### 1.3.2.2. Compressive properties

The compressive strength of the samples is shown in Figure 32. As a general trend, the compressive strength is about 60MPa and is independent of the filler percentage. Only the commercial product shows a lower compressive strength of about 30MPa. This behaviour is probably due to the larger grain size of the fillers in

the composites. At the same percentage by volume of filler, the EAF composites have the compressive strength not different from that of sand composites, but for the samples with 30,3%v/v where the compressive strength of EAF composite is higher (about 65 MPa and 50 MPa, respectively). The compressive strength of the epoxy matrix is not significantly different from that of the composites.

This is a good result because the reduction of compressive strength with increasing the filler fraction would mean that the intercalated structure of fillers creates high-localised stresses in the matrix during compression. It is important to highlight that if the filler-matrix interfaces, the ability to transfer load and plastic deformation would be reduced. Filled epoxy resins that have lower yield strength compared to the pure system evidence a weak interfacial adhesion between the particles and the matrix [259], [260].

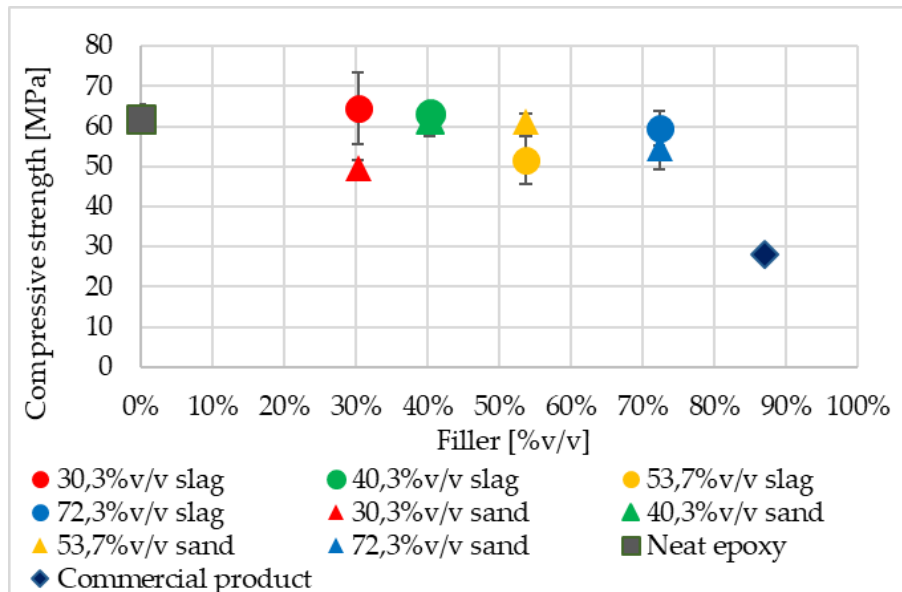


Figure 32 Compressive strength of neat epoxy, epoxy resin filled EAF slag and sand river and a commercial product.

Figure 33 shows the compression elastic modulus of samples. As a general trend, the elastic modulus of sand composites is not different from those of the epoxy matrix and commercial product. For EAF composites, all the samples' compression modulus is higher than those of the sand composites, being about twice for 30,3%v/v and 40,3%v/v samples. We can conclude that the percentage of sand in the composites does not significantly affect the compressive strength and the compression elastic modulus values, while the EAF slag makes the composites stiffer.

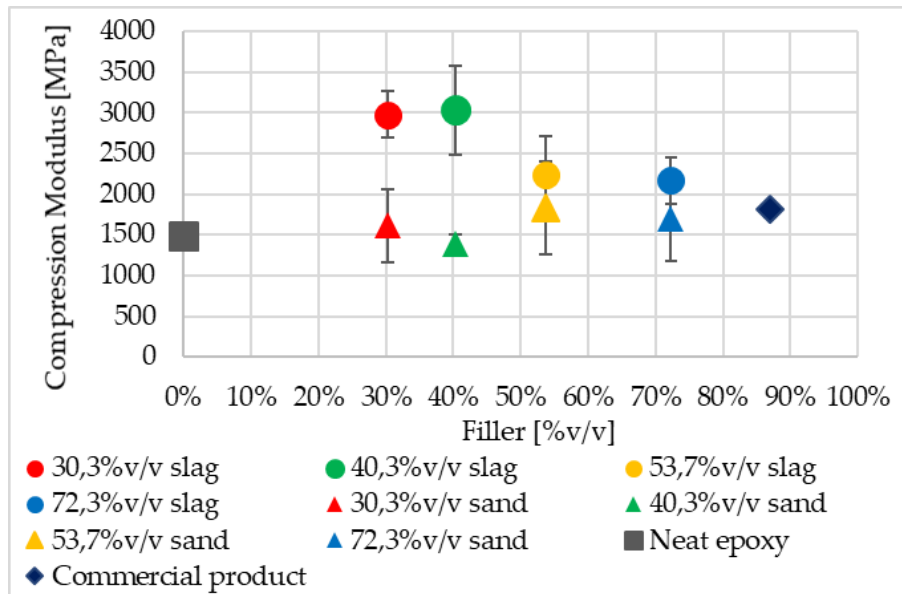


Figure 33 Compression elastic modulus of neat epoxy, epoxy resin filled EAF slag and sand river and a commercial product.

### 1.3.2.3. Hardness

Figure 34 shows the Vickers microhardness values for all the samples. The Vickers microhardness increases with the filler content from about 20 HV for the epoxy matrix up to about 60 HV for composites with the content of a 72,3%v/v filler. Instead, the commercial product microhardness is not different from that of the 40,3%v/v EAF composite. The Vickers microhardness of the EAF composite is slightly higher with respect to the sand composite with the same percentage of filler. We highlight that the hardness of the commercial product filled at 87% v/v is already reached with an EAF slag content of 40,3%, and this value increases in EAF composites proportionally to the filler percentage.

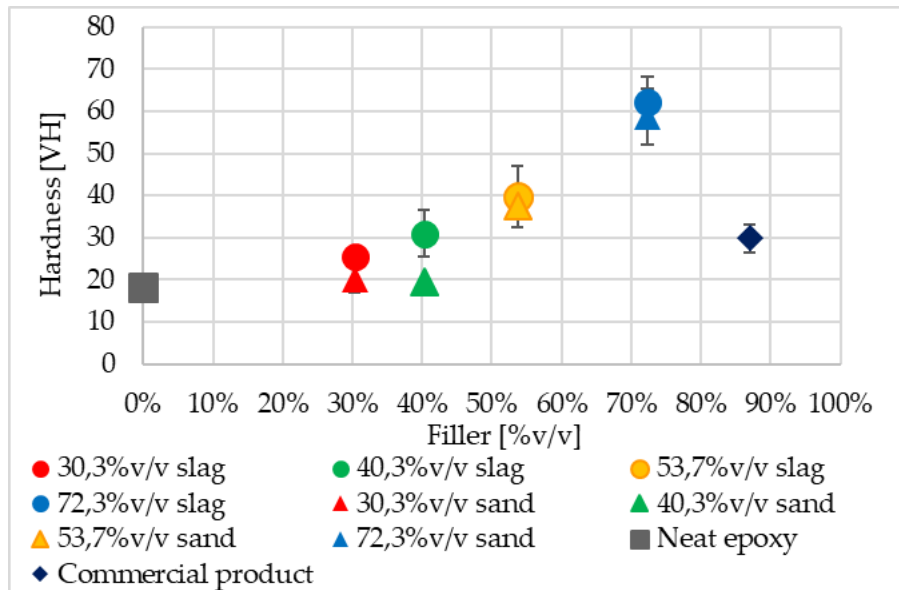


Figure 34 Vickers microhardness of neat epoxy, epoxy resin filled EAF slag and sand river and a commercial product.

The increase in microhardness with the volumetric fraction of the filler is due to a growing presence of rigid particles; this implies a greater resistance to penetration which therefore results in an increase in the hardness of the composite material. Analogous results have been found by D'Almeida and Manfredini in [261].

#### 1.4. Conclusion

To assess its potentiality in construction applications such as the epoxy screeds, the EAF slag influence in a thermosetting matrix is investigated. The slag has been characterized and the release of heavy elements tested in accordance with the CEN EN 12457-2 standard. Based on the results and according to the Italian legislation (Ministerial Decree 5/2/98 and 5/4/06), the EAF slag should be landfilled as "non-hazardous waste" (DM 03/08/05). The influence of the slag particle size on the release of the heavy elements Mo, Cr, and V was confirmed. Mo, Cr, and V leaching are significantly reduced in the EAF composites and, according to the Italian Ministerial Decree 5/2/98, those filled with more than 65% v/v are compliant for material reuse. EAF composites were mechanically characterized by flexural test, compression test, and Vickers microhardness.

The results of the flexural test show that:

- the filler reduces the flexural strength and both, EAF slag and sand composites have a similar flexural strength;

- the sand composites are more rigid and brittle than the EAF slag composites with the same v/v percentage. This was confirmed by fracture surfaces observations. While sand composites materials show a slight flexural strain reduction, for EAF slag composites, the reduction is significant, beginning from a much higher flexural strain value at low slag content. Similarly, in the flexural stress-strain curves, slag composites show a slight yield at the break, especially at low filler percentages.

The flexural modulus increases as the percentage of filler increases. For slag composites, the flexural modulus reaches the maximum value at 72,3% v/v, while for sand composites, probably because of poor wettability, the maximum is reached at 53,7% v/v. At this percentage, the slag composite is more rigid than the corresponding sand composite. This different behaviour can be related to the unlike granulometric curves.

The results of the compression test show that the sand does not affect the compressive strength and the compression elastic modulus significantly, while an equivalent percentage by volume of EAF slag makes the composite material stiffer, especially at 30,3%v/v and 40,3% v/v.

Finally, the Vickers microhardness increases with the filler percentage, the values of slag composites being slightly higher than those of sand composites.

The commercial product's mechanical properties are equal or worse than those of the composites, probably due to three factors: (i) the highest filler presence (87%v/v), (ii) the larger filler grain size which reduces the filler-matrix contact surface/filler volume ratio, and (iii) a different neat epoxy. However, to better understand the differences found for the commercial product, the tests should be performed with composites samples with the same matrix and particle size distribution.

In conclusion, we demonstrate that EAF slag can properly substitute the sand in the epoxy screeds, thus making it possible to use this by-product material since the matrix inhibits the release of the heavy elements. This finding is relevant since, by saving natural resources, we obtain a composite material with mechanical properties equal or greater to those of commercial products.

## 2. Influence of EAF slag as filler for Standard NBR

Elastomers are important polymeric materials because of their unique elastic properties. However, for the many different practical applications, it is essential to improve the mechanical properties of these soft matrices by the addition of a reinforcement [194], [224], [262], [263]. Fillers are extensively used in the rubber industry, not only to reinforce the polymer matrix but also to improve the rubber processing and, in some cases, to reduce the price of the final material [262]. Due to this, in rubber science and technology, the topic of rubber reinforcement can be considered as one of the most important.

Reinforcement of polymers, by the addition of particles filler, is a complex phenomenon that depends on several factors including the hydrodynamic effect and a complex interplay between the properties of the individual constituent phases: the polymer, the filler, and the interfacial region [264][265]. The hydrodynamic effect refers to the addition of fillers to an elastomer resulting in a composite material whose macroscopic mechanical properties are, by construction, a weighted average of the properties of the soft elastomer and the rigid fillers [265]. The actual reinforcement is strongly influenced by the arrangement of the particles which in the case of carbon black are dispersed as fractal aggregates because of the surface activity of the particles that results in a filler-filler interaction. Another factor that causes the variation of bulk properties in filled polymers is related to the filler-polymer interface. The polymer chains that interact with the surface of the particles undergo a substantial modification of their chain dynamics, leading for example to shifts in the glass transition temperature ( $T_g$ ) [231], [266]. The existence of a rigid layer at the polymer-filler interface has been established by several authors [267]–[269]. Assuming a glass transition temperature gradient away from the particle interface, a mesoscale model to explain the reinforcement of elastomers in both linear and non-linear regimes (Payne effect) has been developed by Merabia et al [270]. According to this model, the glassy layer around the particles (or aggregates) is responsible for the reinforcement because it acts as a “glue” between the particles, making its effect particularly strong when combined with the percolation of the filling network [270].

The fillers often used to modify the properties of NBR are mainly carbon black, silica, and fibers [271]. However, these traditional fillers are required in large quantities to get optimum properties for the final applications [194].

According to the reinforcing performance, the rubber fillers can be divided into reinforcing filler and non-reinforcing filler. Among them, a typical non-reinforcing rubber filler is calcium carbonate, which can reduce the amount of needed rubber and achieve the purpose of reducing cost because the market price of calcium carbonate is much lower than that of natural rubber, its addition can reduce the cost of raw materials.

Calcium carbonate is widely used as an additive or modifier in paper, paints, plastics, inks, adhesives and pharmaceuticals [272]; kaoline clay improve electrical resistivity when applied as plastic filler, and also offers better colors, higher physical properties, and abrasion resistance, and zinc oxide was the first manufacturing by-product used as reinforcing filler for rubber. Since mineral fillers are cheaper than polymer, they serve as a low-cost extender, while also increasing the modulus. However, they do not provide high degrees of compound reinforcement, so the failure properties of mineral-filled compounds are poorer than rubber containing carbon black [273].

In this context, the present research evaluates the influence of a waste material such as an electric arc furnace (EAF) steel slag as a filler in a Nitrile-Butadiene Rubber (NBR).

In this study, a commercial NBR has been filled with an increasing volume fraction of EAF slag in order to propose an alternative use of the main steel industry scrap as a low-cost filler for vulcanized rubber.

The reinforcing effect of this new filler was evaluated following the same experimental procedures and analytical calculations adopted in evaluating the reinforcing effect of traditional fillers.

In particular, static and dynamic tests have been performed with the aim to assess the influence of the EAF slag as filler on tensile properties and dynamic behaviour. The results showed that with increasing the filler presence the NBR composite stiffens; the increase of static tensile and dynamic shear storage moduli was found to be consistent with the Halpin-Tsai and Guth-Gold prevision models respectively. Moreover, the non-linear dynamic behaviour was found to be well fitted by the Kraus equation models [227].

The reinforcing ability of the slag particles as filler was evaluated by the swelling test, in particular, the crosslink density determined by the Flory-Rehner equation increased with the filler volume fraction and the Kraus equation [195] showed a reinforcing effect of EAF slag as filler.

The immobilized rubber fraction around the filler particles (bound rubber), identified as one of the key factors to explain the mechanical dynamic behaviour of compounds (filler-rubber interaction), has been quantified by differential scanning calorimetry (DSC) analysis [231].

A homogeneous dispersion and distribution of EAF slag particles have been observed by SEM images.

## 2.1. Materials

EAF slag was supplied by the ASONEXT Spa (Ospitaletto BS, Italy) steelmaking plant. The slag has been produced by a specific system named Slag-Rec [274] for dry granulating EAF molten slag.

EAF slag has been ground and the pulverized EAF slag has been sieved to obtain a grain size lower than 106  $\mu\text{m}$ .

The vulcanized rubber used as a composite matrix is a Nitrile Butadiene Rubber (NBR) with nominal hardness 70 Shore A (carbon black 40 phr, vulcanized with sulphur) provided by Novotema Spa (Villongo BG, Italy).

The influence of EAF slag as reinforcing filler for NBR has been evaluated on four different compounds with different amounts of filler and the results have been compared to that of standard NBR.

The tested compounds are:

- Standard NBR as a reference which is only compression-moulded;
- NBR 0% which is a standard NBR calendered and compression-moulded;
- compounds filled with EAF slag at 5, 10, 20, 30% v/v calendered and compression-moulded.

The compounding process has been performed to disperse the filler particles in the NBR matrix by calendering process. The calendering process consists of forcing rubber and slag between two rotating cylinders (diameter of 150 mm) 0.1 mm apart at room temperature. The calender machine has been provided by Meccaniche Moderne srl (Busto Arsizio VA, Italy). In the calendering process, the uncured rubber is worked in several steps during which the temperature increases (70-80°C) due to the high shear stresses generated by the cylinder in the material that gets soft. The compounds are then compression moulded for 15 minutes at 180°C at 40 MPa to obtain test plates with a dimension of 200x200x2 mm and 100x60x6 mm from which samples for mechanical tests are obtained by mechanical punching.

## 2.2. Methods

### 2.2.1. EAF slag characterization

#### 2.2.1.1. X-ray fluorescence spectroscopy

EAF slag chemical composition was determined by X-ray fluorescence spectroscopy carried out by the Thermo Scientific™ ARL™ PERFORM'X provided by Thermo Fisher Scientific™ (Waltham, Massachusetts, United States). EAF slag chemical composition is reported in Table 14.

#### 2.2.1.2. X-ray Diffraction (XRD)

Crystalline phases identification of the slag was carried out by XRD analysis performed by PANalytical X'Pert Pro diffractometer (PANalytical, Almelo, The Netherlands) equipped with an X'Celerator detector and Cu anode ( $\text{CuK}\alpha = 0.15406 \text{ nm}$ ), operating at 40 kV and 40 mA, on pulverized and sifted slag. In Figure 36 the X-ray diffraction pattern of the slag sample [243] is shown.

#### 2.2.1.3. Scanning Electron Microscope (SEM-EDXS) analysis

An other useful technique useful for the morphological and elemental analysis of the phases is the analysis performed by the Scanning Electron Microscopy (SEM) integrated with Energy Dispersive X-ray Spectrometry (EDXS) [240]. A standard metallographic polishing procedure was performed on the EAF slag sample which was analyzed by a SEM-EDXS (SEM Leo Evo 40, Carl Zeiss, Oberkochen, Germany; EDXS microprobe Link Pentafet Oxford mod 7060; Oxford Instruments, Oxfordshire, U.K.). In Figure 37 the SEM-EDXS analysis carried out on a metallographically polished sample utilizing back-scattered electron (BSE) mode is reported.

#### 2.2.1.4. Leaching behaviour

The leaching test was conducted both on the composite material with the highest filler content (i.e. 30%v/v) and on the free slag, following the CEN – EN 12457-2 standard [72]. The results are reported in Figure 38. The composite material plate was cut to a particle size of less than 4 mm and the slag dust lost from the cutting surface was removed to evaluate only the inertizing effect of the polymer matrix. As for the characterization of free slag, the amount of tested composite was calculated to maintain the 90 g of slag in a ratio of 1:10 with the liquid, according to the standard [72].

Since it was found that the slag grain size affects its leaching behaviour [247], the leaching test was performed also on free EAF slag of a grain size lower than 106  $\mu\text{m}$  in order to evaluate the shielding capability of the rubber matrix that incorporates the filler. The leaching of standard NBR and an EAF slag block completely incorporated in NBR were also performed. The picture of each sample subjected to leaching test is shown in Figure 35). The results of the leaching test are given in Figure 38.

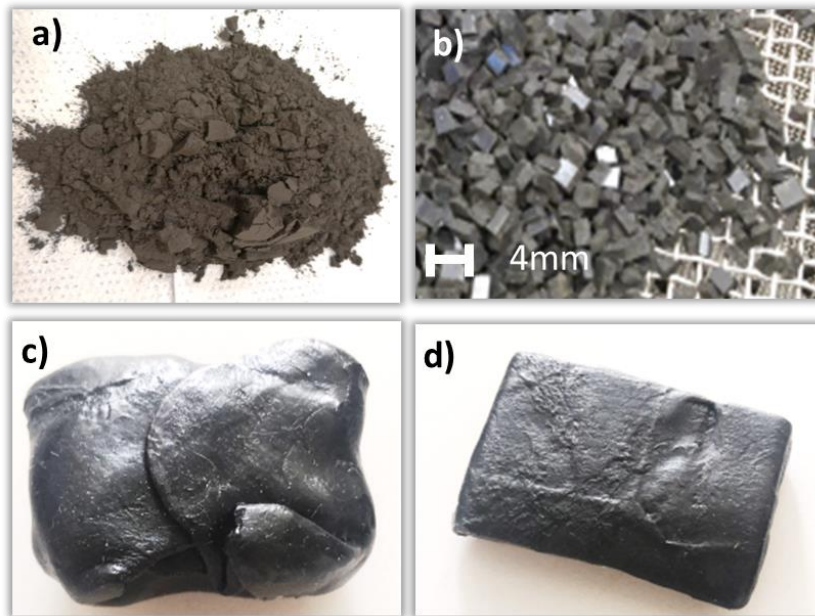


Figure 35 Samples subjected to the leaching test. a) free EAF slag (grain size lower than  $106\ \mu\text{m}$ ); b) EAF slag filled NBR (30%v/v) cut in particle size of less than 4 mm; c) EAF slag block completely incorporated in NBR; d) standard NBR.

### 2.2.2. EAF slag filled NBR characterization

The correctness of the slag and rubber amount in the different compounds were verified retrospectively by density measurements and by thermogravimetric analysis (TGA) analysis (see Table 13), which were carried out on specimens with a weigh between 7 and 15 mg and heating rate of  $10^\circ\text{C}/\text{min}$ . The samples were heated from room temperature up to  $700^\circ\text{C}$  to determine the complete thermal degradation of the NBR matrix. The TGA curves were obtained in air. The residue measured by the TGA is slightly higher than the nominal one because in the standard NBR there are other fillers in addition to EAF slags such as accelerators, activators, antioxidants, and anti-aging. Nevertheless, by subtracting the standard NBR residue, the percentage by weight of EAF slag in the various compounds is lower than the nominal one. This is probably due to the loss of a certain amount of slag dust during the calendaring process. Even the density measured on the different compounds is slightly lower than the theoretical one, as shown in Table 13.

Table 13 Nominal percentage of EAF slag as filler and real percentage of all fillers measured by TGA. Nominal and measured densities of compounds filled with different amounts of EAF slag.

EAF slag		Residue measured by TGA [%wt]	Nominal density [ $\text{g}/\text{cm}^3$ ]	Measured Density [ $\text{g}/\text{cm}^3$ ]
[%v/v]	[%wt]			
0	0	3.40	1.240	$1.240 \pm 0.010$
5	14	16.46	1.366	$1.349 \pm 0.001$
10	26	26.59	1.496	$1.469 \pm 0.009$
20	44	46.68	1.752	$1.722 \pm 0.001$
30	57	59.77	2.013	$2.005 \pm 0.004$

### **2.2.2.1. Rheometric parameters**

The influence of EAF slag on the processability characteristic is assessed by the parameters extrapolated by the rheometric curves, determined by the rheometer machine provided by Gibitre Instruments (Bergamo, Italy). The temperature of the rheometer plates is 177°C and an oscillating force is applied to the sample with an oscillating amplitude of 0.5 deg. Testing time is about 3 minutes. One sample for each compound is tested. The rheometric curves were defined according to the standard ASTM D5289 [275].

### **2.2.2.2. Hardness test**

The compounds' hardness was measured according to the most widely used scales in the rubber industry: Shore A hardness and micro International Rubber Hardness Grade (mIRHD). The Shore A measurements were carried out by an automatic hardness tester Shore PC type A provided by Gibitre Instruments (Bergamo, Italy). The mIRHD measurements were carried out by an automatic hardness tester Micro IRHD-PC provided by Gibitre Instruments (Bergamo, Italy).

Shore A measurements were carried out according to the standard ISO7619-1 [276], The mIRHD measurements were carried out according to the standard ISO 48 [277].

### **2.2.2.3. Compression test**

Compression tests were performed on three samples for each material by a dynamometer (mod. 3366) provided by Instron (Pianezza, TO, Italy) at room temperature and a strain rate of 10 mm/min. Cylindrical specimens with a nominal diameter of 12mm and a height of 6 mm were produced for this test. The compression test was performed according to the standard ISO 7743 [121].

### **2.2.2.4. Stress relaxation**

Stress relaxation is assessed in compression by a dynamometer (mod. 3366) provided by Instron (Pianezza, TO, Italy) at room temperature on cylindrical specimens with a nominal diameter of 12mm and a height of 6 mm. The stress relaxation is assessed as the stress loss [%] after 600 second at 15, 30 and 40% imposed strain.

### **2.2.2.5. Permanent set**

The permanent set is determined in compression (compression set). It was determined by imposing a compression deformation of 25% on cylindrical samples (nominal diameter 12mm and a height of 6 mm) for 24h at 100°C. The compression set was determined according to the standard ASTM D395 (test method B) [278].

### **2.2.2.6. Tensile test**

Mechanical tensile tests were performed by an Instron dynamometer (mod. 3366) at room temperature and a cross-head rate of 100 mm/min on test pieces of 50 mm length (distance between the grips of about 30 mm) and 4 mm width according to the standard ISO 37:2017 type 2 [197]. The considered strain is the optical one in order to exclude the influence of the sample edges. The measurement is performed three times for each compound. Young's modulus has been determined as the slope of the stress-strain curve in correspondence with the initial linear section.

### **2.2.2.7. Scanning Electron Microscope (SEM) analysis**

The morphology and distribution of slag particles in the NBR composites were assessed by SEM observations of cross-sections of specimens broken in liquid nitrogen after coating the surface with sputtered gold.

### 2.2.2.8. *Dynamic Mechanical Analysis (DMA)*

Rectangular specimens were cut from the rubber sheets (obtained by compression moulding process for 15 min at 180 °C with 40 MPa pressure) and had the following nominal dimensions: height (h) = 8 mm, width (w) = 4mm, and thickness (t) = 2 mm. The actual dimensions of each specimen were measured before testing by a micrometer.

Dynamic mechanical tests were performed by a Dynamic Mechanical Thermal Analyser Q800 by TA instruments (New Castle, United States). Dynamic mechanical tests in the shear mode were performed at room temperature and a frequency of 1 Hz with varying shear strain amplitude in the range between 0.02 up to the maximum applicable strain level, according to the machine bearing capabilities (maximum load: 18 N). Therefore, the actual maximum strain value experimentally achieved was dependent on the specimen stiffness and geometry. The measurement of dynamic properties was carried out under a shear sandwich configuration. In this configuration, the two outer clamps were fixed and the inner was moving. Two specimens were compressed between the moving and the fixed clamps, and a compressive strain of about 10% was employed in order to maintain the specimen surfaces fixed to the clamp faces by friction forces. The storage shear modulus was recorded as a function of strain amplitude. Before each test, the specimen was mechanically conditioned by means of the first sweep of shear amplitude so that the following phases preceded each test: (1) mounting of the sample; (2) equilibration of the sample by keeping it for 15 min at the minimum strain (0.02% shear strain amplitude, 1 Hz); (3) strain sweep (0.02% maximum shear strain amplitude, 1 Hz); (4) further equilibration (0.02% shear strain amplitude, 1 Hz). For each test, at least three repetitions were performed.

Recovery tests of low strain amplitude dynamic modulus after the application of a high amplitude dynamic strain were performed using the same fixture for a recovery time of 15 minutes.

Dynamic mechanical analysis has been employed to assess the influence of EAF slag as filler for NBR on dynamic properties function of temperature. This test has been performed by a Dynamic Mechanical Thermal Analyser Q800 by TA instruments (New Castle, United States) Dynamic mechanical tests in the tensile mode were performed at room temperature and a frequency of 1 Hz with the varying temperature at 1°C/min in the range between -50°C +70°C on nominal dimensions specimens of 2x5x30mm.

### 2.2.2.9. *Swelling test*

For the swelling test rectangular samples of about 500mg were cut and immersed in toluene in sealed glass tubes for 48 hours at room temperature. The swelling coefficient is determined according to Equation 11.

The equilibrium swelling index is determined by crosslink density and the attractive forces between solvent and polymer. The theoretical extent of swelling is predicted by the Flory–Rehner equation [185], [189], [190] (Equation 12 and Equation 16).

The properties of filled elastomers are linked to the interaction between filler and matrix which can be theoretically estimated by Kraus equation [195] (Equation 15).

### 2.2.2.10. *Differential scanning calorimetry*

The calorimetric glass transition was determined using differential scanning calorimetry (DSC). Measurements were carried out in the temperature range -90°C to 80°C, in nitrogen atmosphere (purge) using DSC (Model: Q100 provided by TA instruments (New Castle, United States)). The samples were then cooled from room temperature to -90°C at 10°C/min and held at this temperature for 60 min at the end of each cooling

cycle and the measurement was carried out during subsequent heating at 10°C/min. The difference of heat flow between the sample pan filled in by sample and the empty reference pan was recorded with increasing temperature at the heating rate of 10°C/min. DSC analysis is performed twice.

The heat flow [mW] is converted to heat capacity ( $C_p$  [J/(g\*°C)]). NBR composites samples consist of a weight fraction of filler and a weight fraction of polymer; since only the latter is responsible for the variations associated to the glass transition, the heat capacity has been normalized to the polymer fraction as shown in Equation 23.

$\Delta C_p^*$  is determined in a temperature range of  $\pm 4^\circ\text{C}$  with respect to the glass transition temperature ( $T_g$ ). The fraction of immobilized polymer is calculated according to Equation 24, Where  $\Delta C_p^0$  is assumed to be the heat capacity variation of standard NBR.

**2.2.2.11. Magnetic properties**

The presence of iron/iron oxides in the slag gives the composite magnetic properties. The magnetic attraction force was evaluated by quantifying the force required to detach a magnet from the NBR filled with different amounts of EAF slag. A magnet was fixed to the beam of the dynamometer in contact with the material, moving the beam at a speed of 10 mm /min a 500N load cell detected the load every 0.01 seconds, the peak of the curve obtained is identified as the detachment load.

**2.2.2.12. Friction test**

The coefficient of friction is an important parameter for rubber parts. In fact, usually rubber parts are subjected to surface treatments to reduce the coefficient of friction. The influence of EAF slag as filler on the coefficient is assessed by a comparative analysis. A load of 197g is placed on a rubber disk of diameter 17 mm and thickness 2mm. The weight is dragged horizontally by a wire that passes through a pulley and is then connected to the 10N load cell. The Instron 3365 gauge crosshead moves with a set speed of 100mm/min with a preload of 0.2N.

The coefficient of friction is calculated as the ratio between the frictional force and the perpendicular force which in this case is 1,9325N. The frictional force is defined as the peak of the frictional force curve and it is defined as the plateau of the frictional force curve in case of dynamic frictional force.

**2.3. Results and discussion**

**2.3.1. EAF Slag characterization**

**2.3.1.1. X-ray fluorescence spectroscopy results**

The chemical composition of the EAF slag determined by X-ray fluorescence spectroscopy is reported in Table 14.

*Table 14 EAF slag chemical composition determined by X-ray fluorescence spectroscopy (XRF) and basicity indexes. All amounts are reported in [%wt]*

SiO <sub>2</sub>	Al <sub>2</sub> O <sub>3</sub>	Fe <sub>2</sub> O <sub>3</sub>	MnO	CaO	MgO	P <sub>2</sub> O <sub>5</sub>	TiO <sub>2</sub>	Cr <sub>2</sub> O <sub>3</sub>	S	Na <sub>2</sub> O	K <sub>2</sub> O	F
9.5	7.6	40.2	5.6	29.8	3.6	0.5	0.4	2.3	0.1	0.4	[/]	[/]
Basicity		CaO/Al <sub>2</sub> O <sub>3</sub>		Al <sub>2</sub> O <sub>3</sub> /SiO <sub>2</sub>		IB2 CaO/ SiO <sub>2</sub>		IB4 (CaO+MgO)/(SiO <sub>2</sub> +Al <sub>2</sub> O <sub>3</sub> )				
0.6		3.9		0.8		3.2		2.0				

The ratio between the percentage of basic and acidic components (basicity index IB) allows to express and to interpret important metal-slag balances, such as oxidizing power of slag, the balance of desulphurization, and dephosphorization, metal-slag distribution of manganese. The simplest expression of the basicity index, by means of the ratio between the weight percentages of CaO and SiO<sub>2</sub>, is IB<sub>2</sub>, here equal to 3.2. IB<sub>2</sub> does not consider the presence of other components with acidic or basic behaviour, so it is possible to define the complete basicity factor with IB<sub>4</sub> parameter, calculated as ratio between principal basic oxides (CaO+MgO) and main acid oxides (SiO<sub>2</sub>+Al<sub>2</sub>O<sub>3</sub>). The basicity of the slag is required in steelmaking process in order to preserve the integrity of the refractories, which are also basic, for as long as possible. Moreover, the slag chemical composition is related also to the leaching of heavy metals; in turn, it is affected by the cooling conditions adopted in the slagging phase. A rapidly cooled slag is prone to form a glassy phase which shields the heavy metals and prevents them from leaching [241], [242]. It was observed by Tossavainen et al. [242] that if the basicity factor IB<sub>4</sub> is greater than 1, as in the EAF slag object of this study (see Table 14), it is possible to affirm that the glassy phase formation occurred leading a heavy metal leaching prevention.

### 2.3.1.2. X-ray diffraction results

The Figure 36 shows the X-ray diffraction (XRD) pattern and the crystalline phases identification of slag sample. From these results it was possible to notice that the main detected crystalline phases are larnite (Ca<sub>2</sub>SiO<sub>4</sub>), brownmillerite (Ca<sub>2</sub>(Al, Fe)<sub>2</sub>O<sub>5</sub>) and iron oxides in the mineralogical forms of hematite (Fe<sub>2</sub>O<sub>3</sub>), magnetite (Fe<sub>3</sub>O<sub>4</sub>) and wüstite (FeO). These results are in accordance with the chemical composition reported in Table 14 that show a massive presence of iron and calcium.

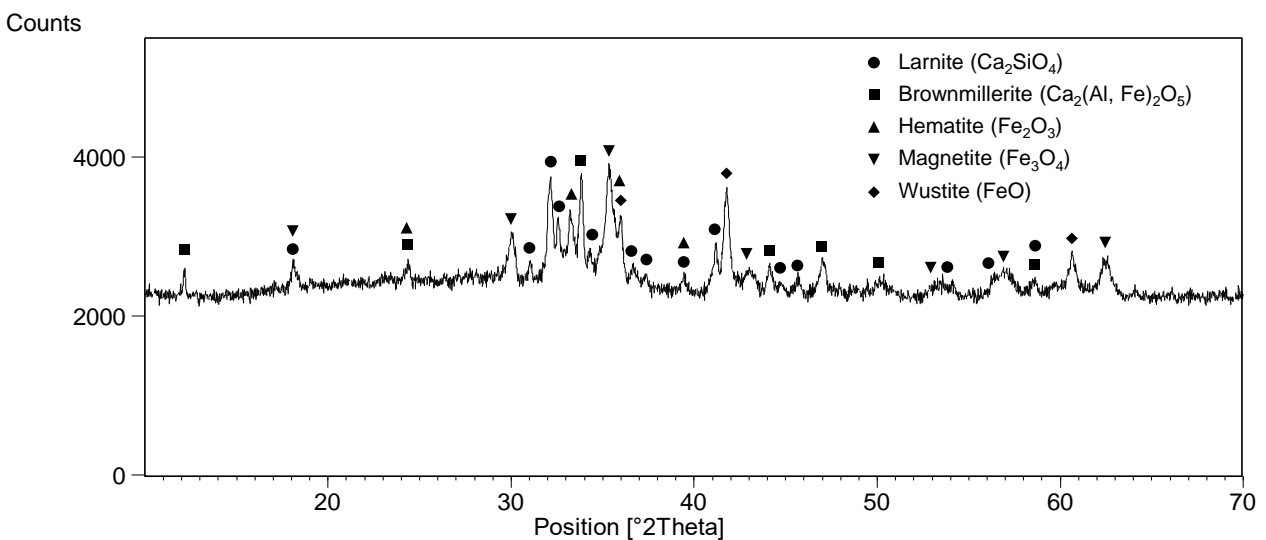


Figure 36 X-ray diffraction pattern collected from EAF slag sample and crystalline phases identification.

### 2.3.1.3. SEM/EDS analyses

In Figure 37 is shown the SEM-EDXS analysis of a metallographically polished sample using back-scattered electron (BSE) mode. The exact mineralogy identification is difficult because some slag phases have varying contents of substituted ions. Moreover, the slag studied in the present work was obtained by a rapid cooling process, that allows to obtain a very fine phase distribution to reduce the intrinsic heterogeneity of the slag but on the other side makes the identification of the phases more difficult by SEM/EDXS analysis due to the fine available areas. Nevertheless, thanks to the comparison with the two analytical techniques used, it was

possible to classify the main phases present, namely Iron Oxides identified by the XRD as wuestite (FeO), hematite (Fe<sub>2</sub>O<sub>3</sub>), and magnetite (Fe<sub>3</sub>O<sub>4</sub>) containing a small quantity of Cr, Ca, Si, Mg, Mn, and Al. Both analyses detected the presence of larnite (Ca<sub>2</sub>SiO<sub>4</sub>) and brownmillerite (Ca<sub>2</sub>(Al Fe)<sub>2</sub>O<sub>5</sub>) with the presence of other elements in small quantities.

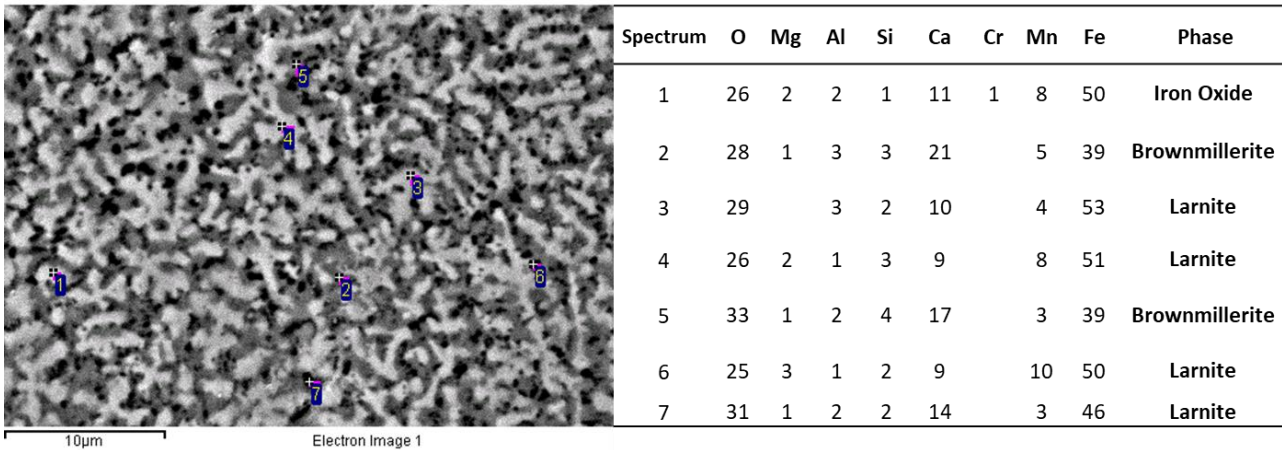


Figure 37 SEM back-scattered electron (BSE) image of slag microstructure [%wt] with its EDXS analysis on metallographically polished sample.

**2.3.1.4. Free slag and composite material leaching behaviour**

Figure 38 and Table 15 show the concentration of Molybdenum, Chromium and Vanadium in the leachates detected by ICP of EAF slag (grain size <4mm in accordance with the standard CEN EN 12457-2[72]) and EAF slag (grain size <106 microns) both free and incorporated into the NBR matrix at 30%v/v.

From the comparison between slag and composite at equal grain size, it can be noted that the concentration of Mo, Cr, and V in the eluate is lower when the slag particles are incorporated into the rubber matrix (especially Mo and Cr). The shielding effect of the rubber is evident in the leaching of the monolithic slag completely embedded in the rubber which shows virtually no release just like NBR alone.

For the sake of clarity, it is important to underline that the slag incorporated in the rubber is not the same tested as the free slag, however, the inertizing effect of the polymer matrix is attributable to the hydrophobicity of NBR. As last, it was found that the leaching behaviour is affected by the slag grain size, especially for Mo leaching which for fine slag is almost twice than for coarse slag. The correlation between the slag grain size and its leaching behaviour was confirmed by several literature researches [247], [279]–[281].

The mechanism at the basis of the reduction of heavy metals leaching is based on NBR’s characteristic of being a hydrophobic material. In accordance with [282] the absorption of water by the NBR matrix is very low therefore the contact between the slag particles and the water is limited only to the particles not completely incorporated (at the edges of the surfaces). For this reason, it is possible to state that as the volume/surface ratio of a generic component increases, leaching will be reduced.

Finally, it should be noted that according to the Italian legislation and concerning the leaching of Mo, Cr, and V, the free slag tested in accordance to the CEN EN 12457-2 [72] (grain size lower than 4mm) is compliant to be disposed of as non-hazardous waste (Cr, Mo <1mg/l)[246], while the slag incorporated in rubber matrix is compliant for the recovery of material (Cr<0.05 and V<0.25mg/l)[244] and can be disposed of in landfills as inert waste Cr, Mo <0.05mg/l[246].

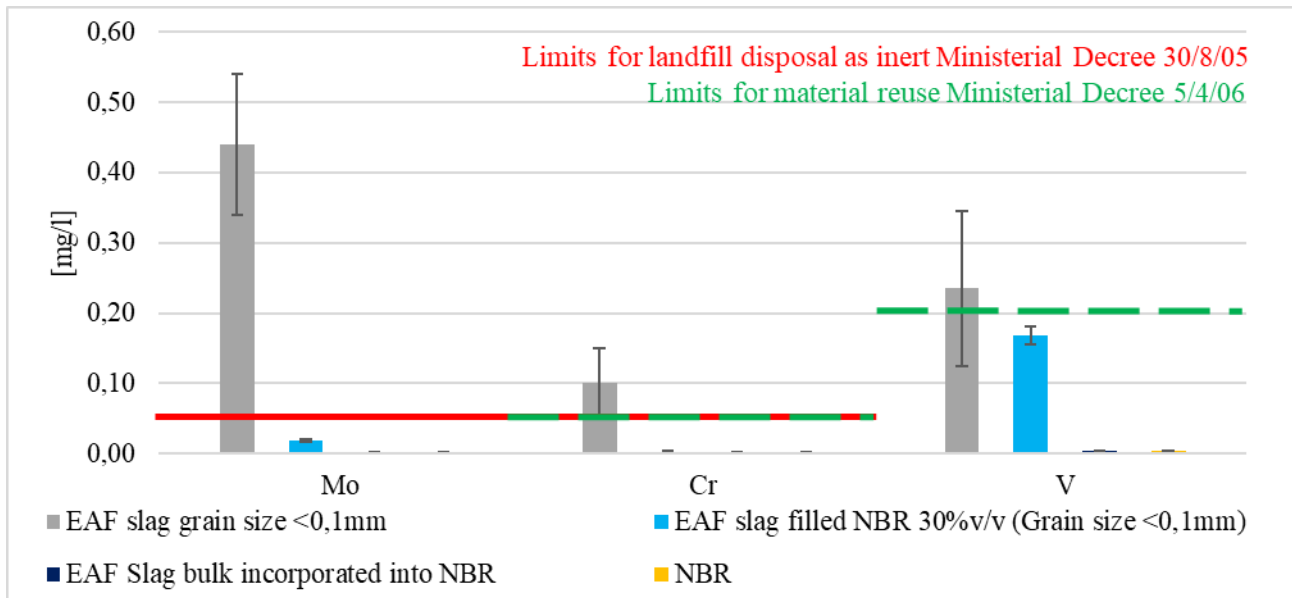


Figure 38 Leaching test CEN EN 12457-2 results of EAF slag (grain size lower than  $106\mu\text{m}$ ), NBR filled with EAF slag at 30%v/v (grain size  $<106\mu\text{m}$ ), EAF slag block incorporated into NBR and standard NBR.

Table 15 Leaching test CEN EN 12457-2 results of EAF slag (grain size  $<4\text{mm}$ ), free EAF slag, NBR filled with EAF slag at 30%v/v (grain size  $<106\mu\text{m}$ ), EAF slag block incorporated into NBR and standard NBR.

	EAF slag grain size $<106\mu\text{m}$			EAF slag filled NBR 30%v/v (Grain size $<106\mu\text{m}$ )			EAF Slag bulk incorporated into NBR			NBR		
		$\pm$			$\pm$			$\pm$			$\pm$	
Conductivity [ $\mu\text{m}$ ]	1397	$\pm$	34	253	$\pm$	18	90	$\pm$	5	91,5	$\pm$	3
pH [-]	12,3	$\pm$	0,11	11,4	$\pm$	0,01	8,5	$\pm$	0,01	8,28	$\pm$	0,01
Mo [mg/l]	0,440	$\pm$	0,10	0,019	$\pm$	0,002	Under detection limit			Under detection limit		
Cr [mg/l]	0,100	$\pm$	0,05	0,002	$\pm$	0,001	Under detection limit			Under detection limit		
V [mg/l]	0,235	$\pm$	0,11	0,169	$\pm$	0,012	Under detection limit			Under detection limit		

## 2.3.2. EAF slag filled NBR characterization

### 2.3.2.1. Rheometric parameters

The rheometric parameters data are given in Table 16. The rheometric curve provides indications regarding the processability characteristics (phase 1), the curing kinetics (phase 2), and the physical properties (phase 3) of the tested materials.

In phase 1 it is possible to note that as a general trend initial torque (IT) and minimum torque (MinT) increase with increasing the filler amount in the compound. The IT behaviour allows to observe that the high-filled compound just placed in the chamber offers more resistance to torque than the low-filled one. MinT is the parameter related to the material viscosity; in this case, its trend indicates that by increasing the amount of slag in NBR the viscosity slightly increases. This phenomenon is probably due to the presence of rigid filler that limits the mobility of the polymer chains even before the starting point of the vulcanization process. The time during which this first phase occurs is called scorch time, specifically the time at which the curing starts. It is related to the parameters Ts1 and Ts2 (the time at which the minimum moment increases by  $1[\text{dN}\cdot\text{m}]$  and

2[dN\*m] respectively). The scorch time is shortened by increasing the amount of filler and this means that the material can stay in the injection chamber without vulcanizing for a shorter time.

In phase 2,  $t_{50}$  and  $t_{90}$  (time at which 50% and 90% of the vulcanization is reached) get shorter by increasing the amount of filler. The presence of slag as filler accelerates crosslinking kinetics due to two different mechanisms. In the first mechanism, the reduction of scorch and curing time is associated with the increase of the compound viscosity and the shear heating effect. The second mechanism is related to the NBR volume fraction that is reduced by increasing the amount of filler so that the crosslinking reaches 100% faster. From the injection moulding production process point of view, this is a great advantage because it allows reducing the production cycle time saving on production costs.

In phase 3 the maximum torque (MaxT) is determined. It is noticeable that by increasing the amount of filler in the compound the torque needed to maintain the imposed rotation at complete vulcanization increases. This means the high-filled compound gets harder.

The influence of the calendaring process on standard NBR slightly accelerates the vulcanization kinetics and softens the material. On the other hand, the presence of EAF slag as filler in the rubber matrix hardens the compound and accelerates the vulcanization kinetics. The same trend was found in the literature for several fillers: silica and multiwall carbon nanotubes as found by Salehi et al. [283], iron oxide obtained by El-Tantawy et al. [284] and nano calcium carbonate as observed by Kumarjyoti et al. [285].

Table 16 Rheometric curve data for standard NBR and NBR filled with EAF slag at 0,5,10,20,30%v/v.

Compound	Phase 1				Phase 2		Phase 3
	IT	MinT	Ts1	Ts2	t50	t90	MaxT
	[dN*m]	[dN*m]	[s]	[s]	[s]	[s]	[dN*m]
Standard NBR	3	1,06	46	54	81	123	18,04
0 [%v/v] EAF slag	1,84	0,84	45	52	78	121	16,91
5% [%v/v] EAF slag	2,76	0,89	45	52	79	125	18,44
10% [%v/v] EAF slag	3,1	0,95	43	51	78	122	20,28
20% [%v/v] EAF slag	4,1	1,16	43	50	79	120	24,47
30% [%v/v] EAF slag	5,93	1,54	37	44	75	113	31,48

### 2.3.2.2. Hardness

Figure 39 shows the hardness results obtained for NBR compounds filled with different amounts of EAF slag in mIRHD and Shore A measurement scales. It is possible to notice that with increasing the amount of EAF slag the hardness in both measurement scales increases from a value of about 63 up to a value of 75. According to Wang et al. [286], the reason for this increase is due to the hardness of the EAF slag that is bigger with respect to the NBR one. This property of slag allowed an increase of the hardness of the composites proportionally to the quantity added. Regarding the influence of the calendaring process, it does not affect the hardness of standard NBR.

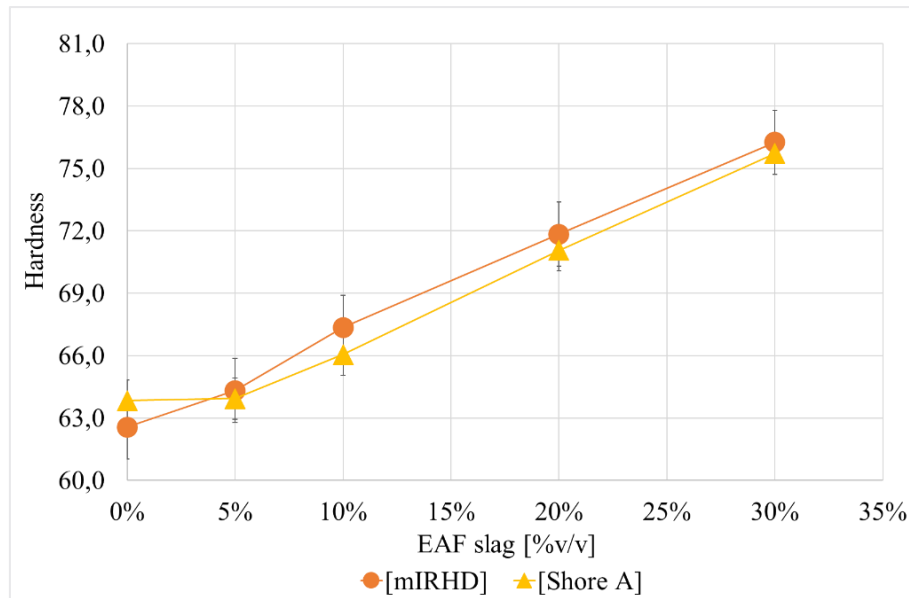


Figure 39 Hardness results in Shore A and IRHD for NBR compounds filled with EAF slag.

### 2.3.2.3. Compressive properties

Compression test has been performed and compression Young's modulus value and the stress at 50% compression strain acquired from the stress strain curves are reported in Figure 40 and the numerical values are given in

Table 17. The compression test results show that the material offers a greater deformation resistance with increasing the slag content. The calendaring process in the compression test results allows to observe in Figure 40 a softening of the calendared compound compared to the standard NBR.

It is possible to observe how the compression Young's modulus increases remarkably with the increments of slag filler up to an increase of 50% for NBR with slag at 30%v/v respect to standard NBR (Figure 40).

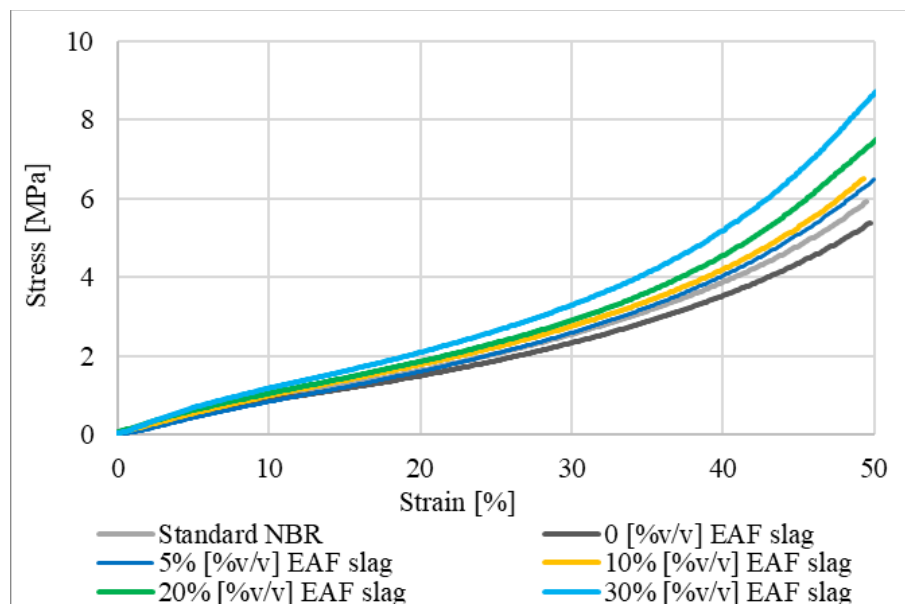


Figure 40 Compression stress strain curve of Standard NBR and EAF slag filled NBR 0, 5, 10, 20, 30% v/v.

Table 17 Compression test results.

	Ec [MPa]			$\sigma(\epsilon=50\%)[MPa]$		
		$\pm$			$\pm$	
Standard NBR	10,1	$\pm$	0,50	5,9	$\pm$	0,01
0 [%v/v] EAF slag	9,7	$\pm$	0,08	5,4	$\pm$	0,05
5% [%v/v] EAF slag	10,0	$\pm$	0,25	6,4	$\pm$	0,18
10% [%v/v] EAF slag	10,8	$\pm$	0,29	6,5	$\pm$	0,07
20% [%v/v] EAF slag	12,3	$\pm$	0,19	7,5	$\pm$	0,32
30% [%v/v] EAF slag	15,0	$\pm$	0,09	8,7	$\pm$	0,40

2.3.2.4. Stress relaxation

Figure 41 shows the stress relaxation as function of time of Standard NBR and EAF slag filled NBR 0, 5, 10, 20, 30% v/v at imposed strain 15, 20, 30%. As expected the stress is proportional to the imposed strain, i.e. higher strain implies higher stress as evidenced also by the compression stress-strain curves in Figure 40. In particular it is possible to observe that under the same imposed strain, the stress curves appear to be rigidly translated upwards in proportion to the slag content and after a sharp stress reduction it assesses in a plateau. Standard NBR deviates from this trend and especially at 40% strain exhibits the lowest stress relaxation. This is probably attributable to the different production process (it is not calendered but just compression moulded) that affects the carbon black distribution and dispersion and the macromolecular network resulting in improved elastic properties.

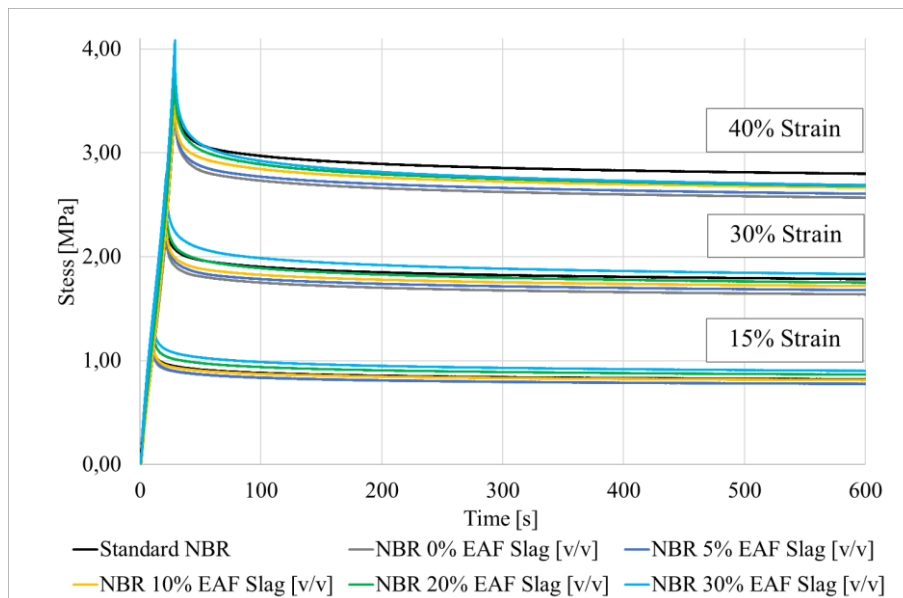


Figure 41 Stress relaxation curves of Standard NBR and EAF slag filled NBR 0, 5, 10, 20, 30% v/v at 15, 20, 30% strain.

Figure 42 shows the stress relaxation expressed as stress percentage loss imposed of EAF slag filled NBR 0, 5, 10, 20, 30% v/v at 15, 20, 30% strain. It is possible to observe that with increasing the slag content, the stress relaxation remains about constant up to a slag content of 10%v/v, then it increases.

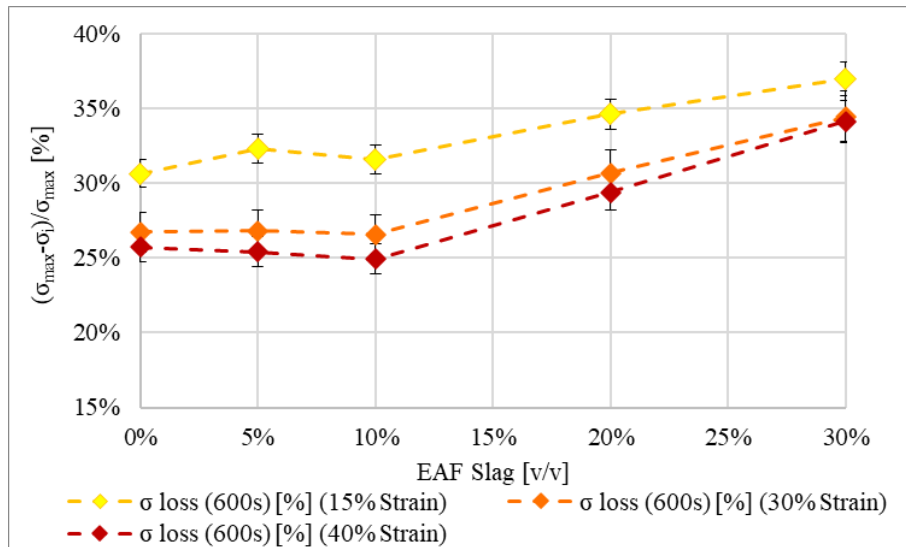


Figure 42 stress relaxation expressed as stress percentage loss imposed of EAF slag filled NBR 0, 5, 10, 20, 30% v/v at 15, 20, 30% strain

### 2.3.2.5. Permanent set

The compression set results are reported in Figure 43. In this case, the presence of EAF slag as filler reduces the material's ability to recover an imposed deformation proportionally to the amount of filler added. It is worthwhile to note that up to a filler content of 10%v/v the compression set is above 15% which is a good value for real applications. Nevertheless, a compression set value of 20% is still acceptable for real applications.

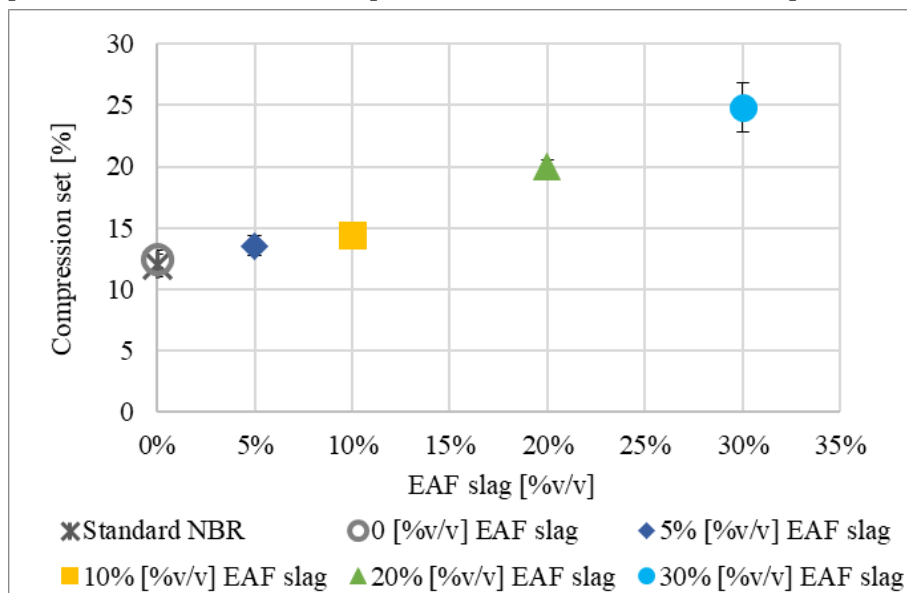


Figure 43 Compression set function of the percentage of EAF slag in NBR matrix.

Analyzing the results of the compression test and compression set, the increase of stiffness could be a positive aspect for new compounds. In a real application, rubber gaskets could be assembled in displacement control or load control as shown in Figure 44 (b) and (c) respectively. It should be noted that the correct assembly of a gasket in a sealing system does not provide their presence in the center of the slot, but rather leans it against the wall of the housing on the opposite side to the direction of the operating pressure, as shown in Figure 44 (a).

In both configurations (Figure 44 (b) and (c)) the O-rings fit in the groove and the housing, with overlap, provides initial preload after assembly Figure 44 (a). This preload ( $P_c$ ) with the operating pressure ( $P_f$ ) allows to obtain the sealing effect. When the O-ring is pressed to the side of the groove it deforms and the pressure is transferred to the surrounding surfaces Figure 44 (b) and (c). The operating pressure ( $P_f$ ) is superimposed on the initial pressure because the pressure propagates the material without weakening as the vulcanized rubber is nearly incompressible. Despite this, as the material shows viscoelastic behaviour and relaxes, the maximal contact pressure will be slightly less (about 80%) than the sum of the two pressures [287]. According to Szabò et al. [287], the overall contact area increases as the O-ring deforms and the maximum value of the contact pressure is at the side of the O-ring where it touches the shaft.

If a gasket is assembled in a displacement-controlled sealing system as shown in Figure 44 (b), the high filled rubber (grey) requires higher clamping force due to its higher stiffness and this results in higher contact pressure compared to standard NBR (black) ( $P_{c2} > P_{c1}$ ). This is a great advantage since the necessary condition for a sealing system to function properly is that the contact pressure is greater than the fluid pressure ( $P_c + \approx 0.8P_f > P_f$ ).

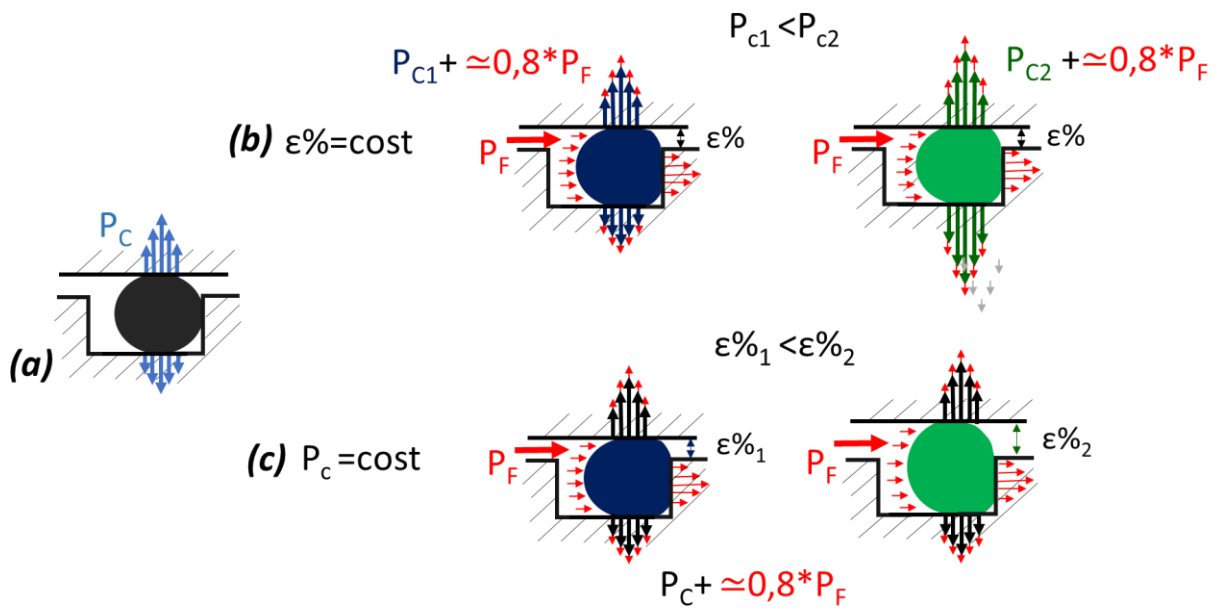


Figure 44 Schematic of a sealing system without operating pressure ( $P_f$ ) (a) and with operating pressure ( $P_f$ ) assembled in displacement control (b) and load control (c) for NBR standard (black) and a standard NBR filled with EAF slag (grey).

Regarding the contact pressure trend over time, the NBR filled with EAF slag has a higher compression set so, according to the relationship between compression set and compression stress relaxation (and stress relaxation results), it drops faster with respect to standard NBR. In literature the direct relationship between compression stress relaxation and compression set is observed [288], [289]; in particular, an increase of compression set corresponds to a decrease of the contact pressure due to the compression stress relaxation. On the one hand, the initial contact pressure of the NBR filled with EAF slag, known from the compression test, is higher than that of the standard NBR (in proportion to the amount of filler added); and on the other hand, the compression set of the NBR filled with EAF slag is slightly higher than that of the standard NBR. From these results, it is possible to assume that the filled NBR contact pressure at a sufficiently long time for the stress relaxation to settle at a constant value is in any case greater than that of standard NBR.

If a gasket is assembled in a load-controlled sealing system ( Figure 44 €) with equal contact pressure, the high-filled NBR is less deformed than the standard NBR. As a result of the different initial deformation, the filled NBR contact pressure falls less steeply over time compared to standard NBR due to its lower initial deformation [290].

It is important to highlight that, in both sealing system configurations, the EAF slag as filler positively affects the compound properties.

### 2.3.2.6. Tensile Properties

Figure 45 shows a representative tensile test stress-strain curve for each compound. From these curves the main tensile properties such as stress at break, strain at break, and Young's modulus are determined.

Tensile test results show a reduction of the stress at break of about 65% between standard NBR and NBR filled with EAF slag 30%v/v, while the reduction of the strain at break is about 30%. It is possible to state that the elongation at break and the stress at break are significantly reduced for filler quantities exceeding 10% v/v. The calendering process has the effect of increasing both elongation at break (by about 15%) and stress at break (by about 5%). This is due to a better dispersion and distribution of the carbon black in the compound as evidenced by SEM observations (see 2.3.2.7 Morphology and distribution filler particles) that likely reduces the fraction of occluded rubber. Similar results were found in [291], [292]. Furthermore, it is possible to note that standard NBR at large deformations (>100%) and up to failure presents a greater stress than the same compound subjected to calendering process (named 0%v/v EAF slag) at the same deformation. This results in a higher secant elastic modulus at large strain. The calendering process implies a double effect on the material: on one side it improves the ultimate tensile properties by a better dispersion and distribution of the carbon black, on the other hand it softens the compound as it dissolves the macromolecular structure. The compounds stiffening due to the presence of EAF slag as filler is clearly appreciable in the Young's modulus value as shown in Figure 46.

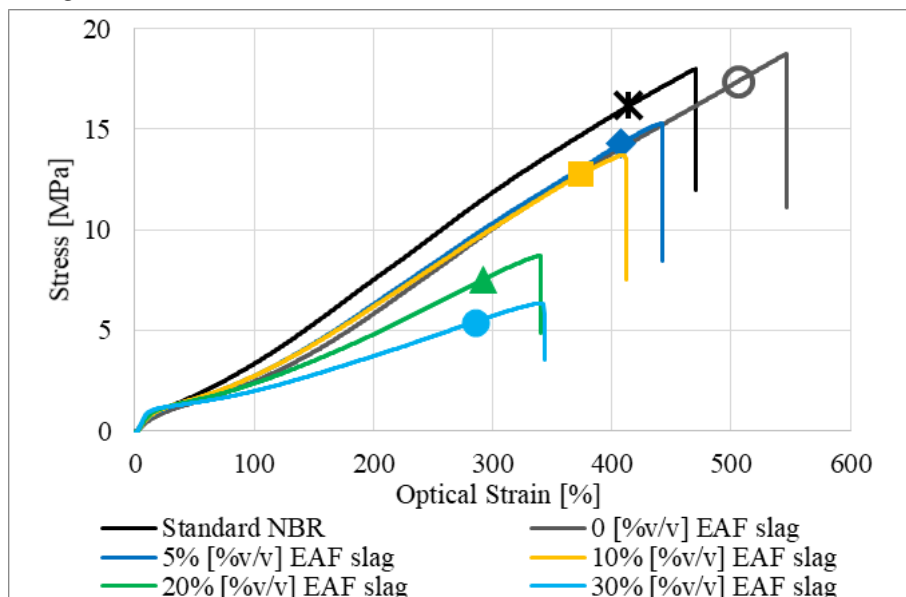


Figure 45 Stress-optical strain curves of a representative sample for standard NBR and compound filled with 0,5,10,20,30% of EAF slag.

The effect of particle reinforcement was also evaluated using analytical models. Guth-Gold and Halpin-Tsai equations have been used to predict the tensile modulus of NBR composites (see Figure 46) under the

approximation of spherical particles. In the following calculation the considered filler is only the EAF due to its greater size and content with respect to fillers present in standard NBR. Guth and Gold [293] proposed a quadratic term to explain the reinforcement effect of spherical fillers on elastomers, as shown in Equation 26:

$$E = E_m(1 + 2.5\varphi + 14\varphi^2)$$

*Equation 26*

Where  $E$  and  $E_m$  are the Young's modulus of NBR filled with different EAF slag volume fraction ( $\varphi$ ) and calandered NBR with no EAF slag added respectively.

Halpin-Tsai equation has been also used to study the reinforcement effects of filler in composites. Normally this model is used to predict the modulus for aligned fiber composites, but it has been used before to predict the modulus of nanocomposites [294]. The studied NBR composites filled with EAF slag are not nanocomposites due to the greater size of filler particles, nevertheless it was found a good experimental data prevision. Halpin-Tsai equation is reported in

$$E = \frac{E_m(1 + \zeta\eta\varphi)}{1 - \eta\varphi}$$

*Equation 27*

Where  $\zeta$  is a filler shape factor which is 2 for spherical particles and  $\eta$  is given by Equation 28

$$\eta = \frac{E_f/E_m - 1}{E_f/E_m - \zeta}$$

*Equation 28*

Where  $E_f$  and  $E_m$  are the Young's modulus of rubber and filler respectively. Since the modulus of EAF slag is much higher than that of NBR the constant  $\eta$  is taken as unity.

In Figure 46 the experimental and the theoretical Young's modulus is reported as a function of EAF slag volume fraction. Experimental data show that the modulus increases with slag volume fraction up to double for a filler presence of 30% v/v. The NBR composites stiffening could be attributed to two factors: the bound rubber content and the hydrodynamic effect. The bound rubber may be defined as the polymer layer adherent to the filler particles which is stiffer than the bulk polymer. With increasing the filler volume fraction the immobilized rubber fraction around the filler particles (bound rubber) increases (see 2.3.2.10 Differential scanning calorimetry analysis) causing also an increment of the crosslink density [224] (see 2.3.2.9).

It was found that for EAF slag volume fraction up to 20% both theoretical models well predict the experimental data, while for NBR filled with 30%v/v the Halpin-Tsai model reveals to better fit experimental data.

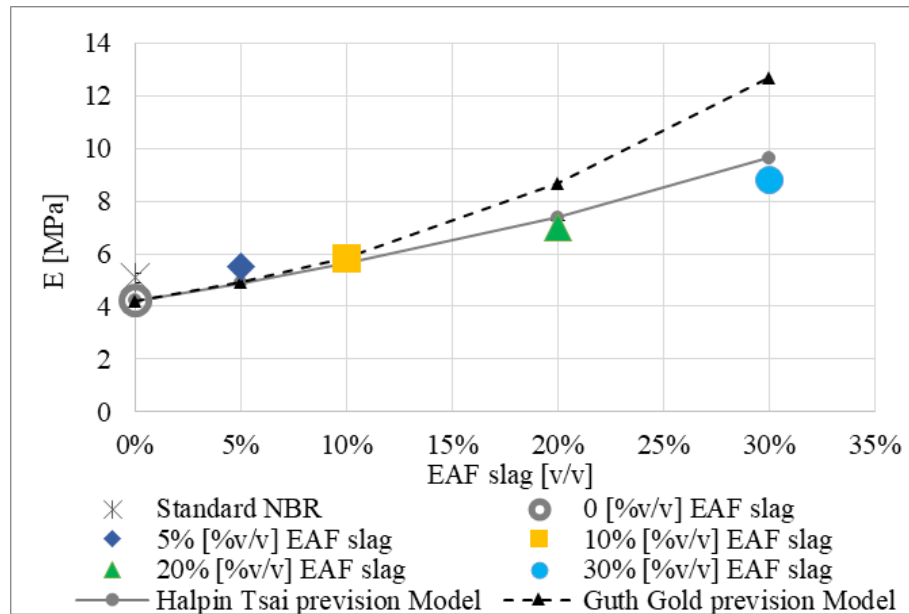


Figure 46 Experimental and theoretical Young's modulus as function of EAF slag as filler [%v/v]

The presence of rigid filler in the elastomeric matrix limits the polymer mobility increasing the compound stiffness much more than it reduces the elongation at break. For what concern the reduction of the stress at break it is probably due to the inability of the polymer to orient itself completely in the direction of the effort due to the decreasing of rubber-filler interaction, creating localized overstress. The stress at break reduction with increasing the amount of filler above a small filler percentage by weight (less than 5%) was found also by Kumarjyoti et al. [285] and Wang et al. in their study on mechanical properties of nano- $\text{Fe}_3\text{O}_4$  or nano- $\text{SrO} \cdot 6\text{Fe}_2\text{O}_3$  reinforced NBR [286] [295].

### 2.3.2.7. Morphology and distribution filler particles

Figure 47 shows SEM images of the fracture surface of all material investigated broken in nitrogen. Figure 47 a) and b) show the micrograph of standard NBR and calandered NBR without EAF slag (0% [v/v] EAF slag) in order to assess the influence of the calendering process on the distribution and dispersion of carbon black in NBR. It is possible to note that some carbon black agglomerates are observable in standard NBR (Figure 47 a)), while the filler dispersion is noticeably improved in calandered NBR. Regarding the EAF slag filled NBR composites (Figure 47 b-f)) in the backscattering SEM images a good filler distribution and dispersion are evident. In particular, it is possible to observe a better filler particles incorporation for slag particles of a size lower than  $50 \mu\text{m}$ . In fact, in the micrographs, at the edges of the larger particles there seems to be a small gap given by a lower cohesion between the filler and the matrix. This means that a smaller particle size of the filler leads to a better incorporation into the matrix, but on the other hand in the case of the slag, it also involves high grinding costs, so it is necessary to find a compromise. Among the size of EAF slag particles, another important aspect is the particle shape: generally the larger particles show acute angles which in an elastomeric matrix lead more easily to the initiation of a crack by decohesion due to by a triaxiality of the stresses. The reinforcing effect of EAF slag particles smaller than  $106 \mu\text{m}$  was evaluated by the Kraus plot (see 2.3.2.9) and it was found to be good due to the negative slope of the obtained curve.

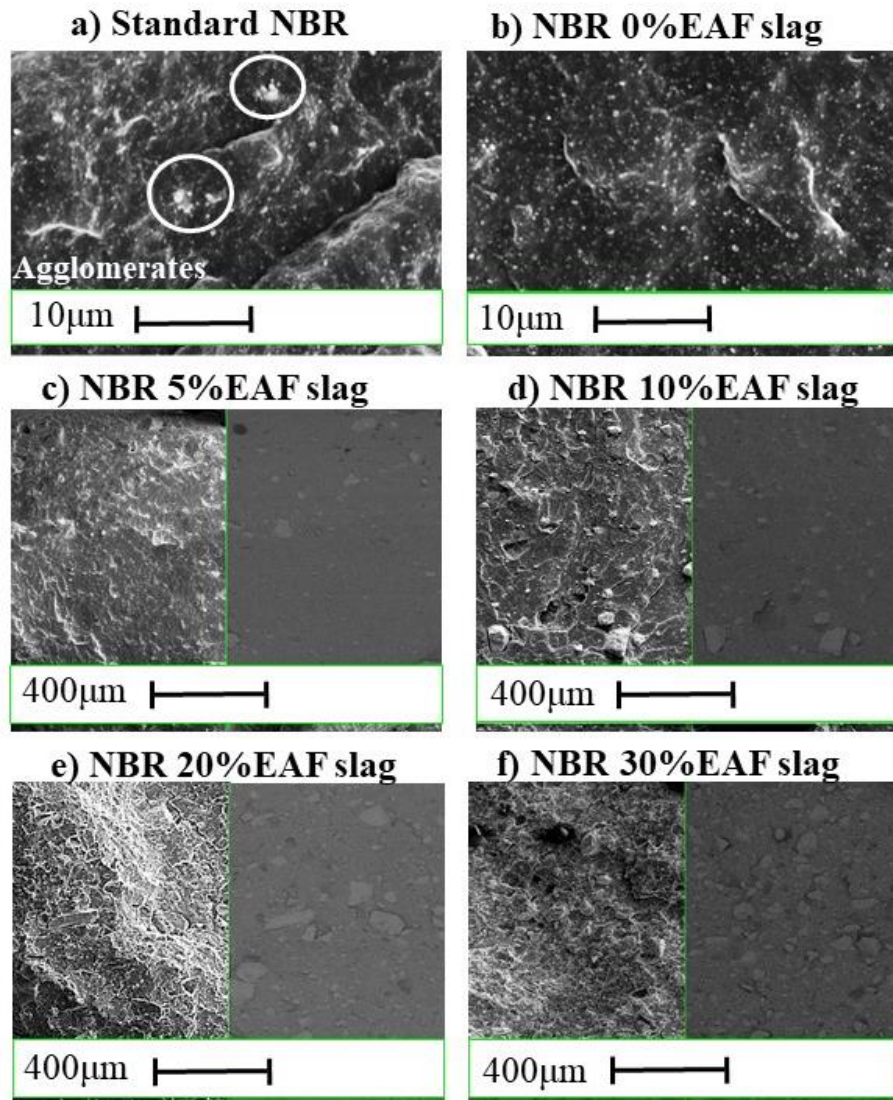


Figure 47 SEM micrograph and backscattering images of cross sections of specimens broken in liquid nitrogen. A) micrograph of standard NBR; b) micrograph of calandered NBR filled with 0% EAF slag; c) micrograph and backscattering images of calandered NBR filled with EAF slag at 5%v/v; d) micrograph and backscattering images of calandered NBR filled with EAF slag at 10%v/v; e) micrograph and backscattering images of calandered NBR filled with EAF slag at 20%v/v; e) micrograph and backscattering images of calandered NBR filled with EAF slag at 30%v/v.

#### 2.3.2.8. Dynamic properties

Under dynamic conditions, a rubber absorbs energy which is partially stored, as in an ideal solid (usually modelled as a spring); and partially it is dissipated in overcoming internal friction, as in an ideal fluid (usually modelled as a dashpot)[208]. This separation of the stress components vectorially allows the material's dependence on strain amplitude and strain rate to be measured simultaneously. The ratio of the elastic stress to strain is the elastic (or storage) modulus  $G'$ ; the ratio of the viscous stress to strain is the viscous (or loss) Modulus  $G''$ . The complex modulus  $G^* = G' + G''$  reflects the contribution of both elastic and viscous components to the material's stiffness.

*Shear dynamic properties: Strain sweep*

The addition of reinforcing fillers to elastomeric materials leads to an improvement of stiffness as well as tensile and tearing resistance; this last sometimes is associated to an elongation at break reduction [209]. The presence of clay strongly affects also the low amplitude dynamic properties [209]–[218], providing with increasing the clay content an increase of the storage modulus, which is particularly marked in the region of the rubbery plateau, associated to a growth of the loss peak. In the case of unfilled rubber or natural gum, the dynamic moduli behaviour can be predicted by the classical theory of linear viscoelasticity, i.e. they are independent of the strain amplitude [217], [218] and the classical frequency/temperature shift principle can be applied successfully [208].

The dynamic shear storage and loss modulus of all tested materials are reported in Figure 48 and Figure 52 respectively. Experimental data are represented by the curves in the shear strain amplitude range of about 0.02-10%, and they are interpolated by Kraus's model (Equation 20 and Equation 21) in order to figure out the high strain amplitude plateau which was not reached experimentally due to the strain limitation of the device configuration. As found by different authors for filled rubber compounds [296]–[298], at very low strain amplitudes (<0.1%) the storage modulus of filled rubber compounds is expected to reach a plateau level  $G'_0$ , whereas at sufficiently high strain amplitudes (>20%) it reaches a lower plateau value  $G'_\infty$  [209]. Kraus's model storage and loss modulus curves are reported in Figure 48 and Figure 52 respectively up to shear strain amplitude of 100%. It was found that the Kraus's model well represents the experimental data for the phenomenological exponent  $m$  fixed at 0.55.

As expected, the EAF slag content within the material is found to promote a nonlinear dynamic behaviour consisting in a decrease of the storage modulus,  $G'$ , and a genesis of a maximum in the loss modulus,  $G''$ , by increasing the shear strain amplitude (Payne effect). This result was found to be in accordance to Ramorino et al [209]. In particular this behaviour is more marked for a slag content higher than 20%v/v, while Standard NBR dynamic behaviour was found to be very similar to that of NBR filled with EAF slag at 10%v/v. This is probably because in Standard NBR carbon black is more agglomerate and the calendaring process reduce the occluded rubber improving the distribution and the dispersion of carbon black. The better carbon black distribution for calendered NBR is observed by SEM images.

It was found that by increasing the amount of EAF slag incorporated within the NBR matrix the Payne effect become more pronounced as shown in Figure 49. The drop of the storage modulus with shear strain amplitude (Figure 48) can be considered a measure of the Payne effect and it was found an increasing of this effect with filler volume fraction according to many literature works [209], [216], [296], [297], [299], [300]. NBR composite filled with EAF slag at 30%v/v shows a drop of about 6.6 MPa, while calendered NBR with no added slag about 0.7 MPa. Figure 49 shows the influence of EAF slag volume fraction on the percentage change of the storage modulus from the low amplitude strain  $G'(\gamma_0)$  to the high amplitude strain plateaus  $G'_\infty$ .

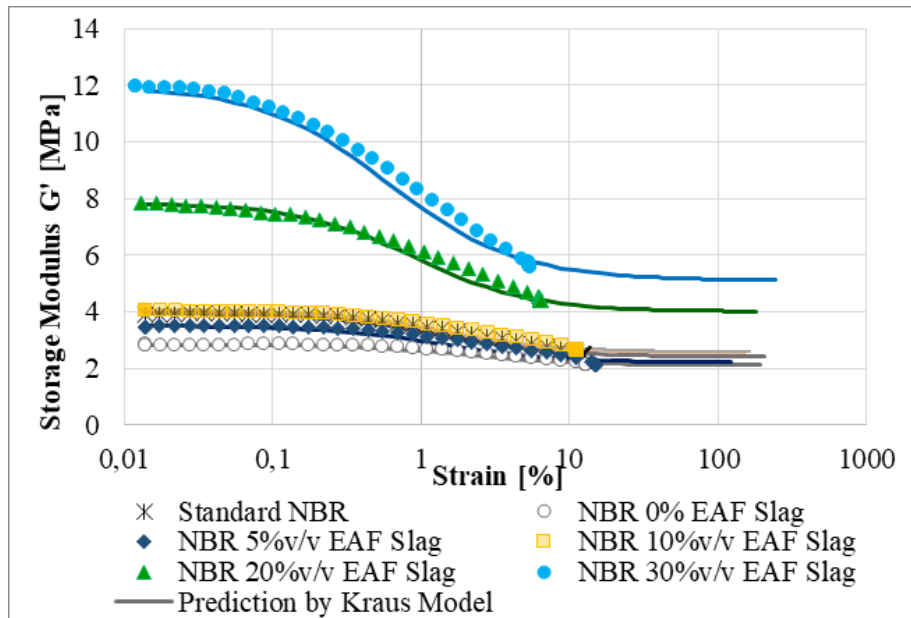


Figure 48 Dynamic storage modulus in shear mode at 1 Hz, 23°C plotted against strain amplitude (0.02-10%) for Standard NBR and NBR filled with 0, 5 10 20 and 30% with EAF slag and application of Kraus model ( $G'(\gamma)$ ).

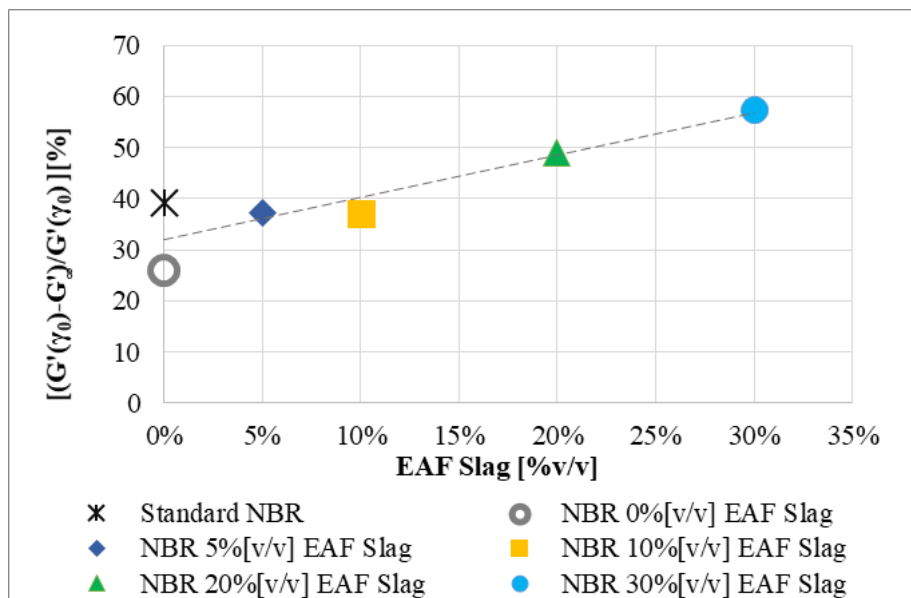


Figure 49 Payne effect as Storage modulus variation [%] from low amplitude to high amplitude plateaus ( $G'(\gamma_0)$  and  $G'_\infty$ ) function of EAF slag volume fraction.

Regarding the theoretical factors governing the storage modulus  $G'$  it is possible to assume that at low strain amplitude the predominant mechanism is filler-filler interaction, and with increasing the strain amplitude it turn out to be the rubber-filler interaction (bound rubber).

Nevertheless, at sufficient high strain (about 10%), where the filler network is believed to be fully destroyed,  $G'$  is proportional to the filler content showing the highest value for the highest EAF slag volume fraction. To explain this behaviour, it is necessary to consider the hydrodynamic effect and the occluded rubber [273][301]. According to Medalia [301] the principal line of theoretical development has involved the treatment of the elastic modulus on a hydrodynamic basis, modified by the occluded rubber concept according to the Guth-Gold prevision model [293] that find a good agreement with the experimental storage modulus at low strain

amplitude as shown in Figure 50. The rubber network contribute can be neglected for the purpose of evaluating the influence of filler particles in NBR matrix because it can be assumed constant for all tested materials.

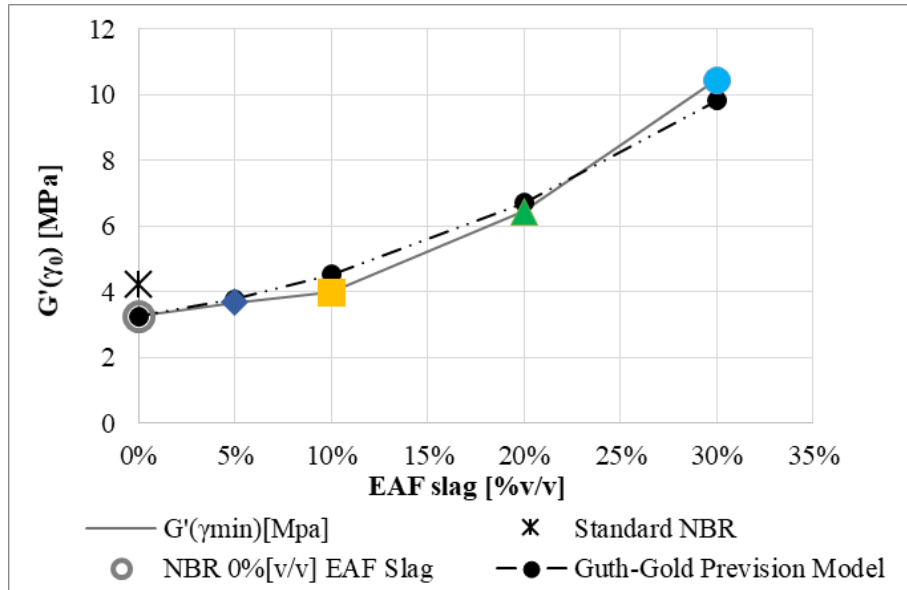


Figure 50 Experimental and theoretical storage modulus at low strain amplitude  $G'(\gamma_0)$  function of EAF slag volume fraction.

Payne and Whittaker in their research [296] showed that the maximum of the loss modulus  $G''_{max}$  is linearly related with  $(G'(\gamma_0) - G'_{\infty})$ . Considering  $G'(\gamma_0)$  and  $G'_{\infty}$  employed for fitting experimental data with the Kraus's model, it was found that the expected linear dependence is anyway satisfactorily displayed as shown in Figure 51.

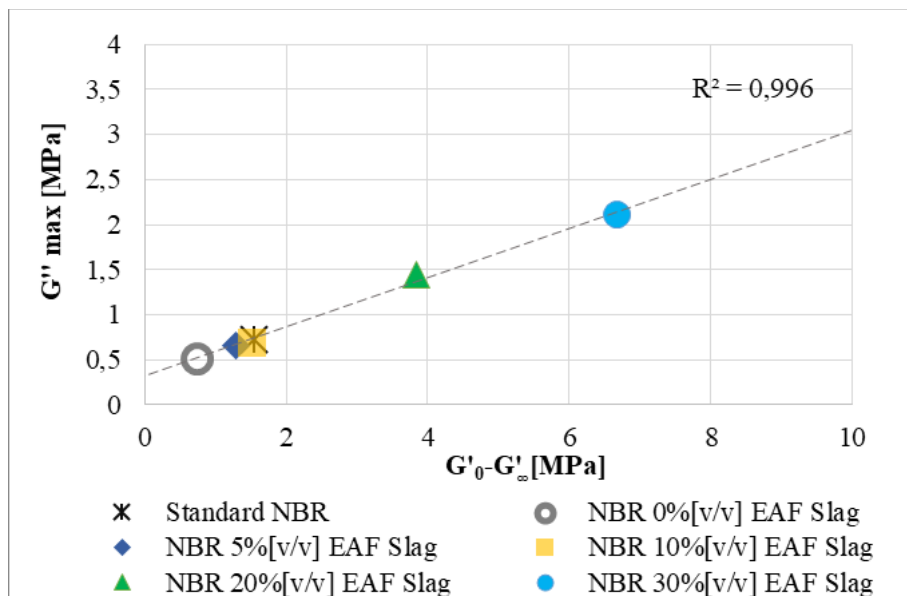


Figure 51 Payne plot ( $G''_{max}$  versus  $(G'(\gamma_0) - G'_{\infty})$ ) for Standard NBR and calandered NBR filled with EAF slag at 0,5,10,20,30%v/v.

The loss modulus (Figure 52) shows a typical loss peak, which occurs at approximately the same dynamic amplitude range where the storage modulus is most rapidly decreasing. It is interesting to note that the peak

of the loss modulus is much higher and occurs at lower strains as the filler volume fraction increases especially for NBR filled with EAF slag at 20 and 30%v/v (see Figure 53). This could be explained by the presence of a layer of rigid rubber adherent to the filler particles that makes the compound stiffer (increase of storage modulus at low amplitude  $G'(\gamma_0)$  and Young's modulus with filler volume fraction) and leads an increase in the dissipation because the compound behaviour will be more viscous. On the other hand, the dissipative phenomenon at the origin of the loss modulus peak is assumed to the agglomeration and de-agglomeration of the filler network which is consequently more marked and occurs at lower strain amplitude for higher filler volume fraction.

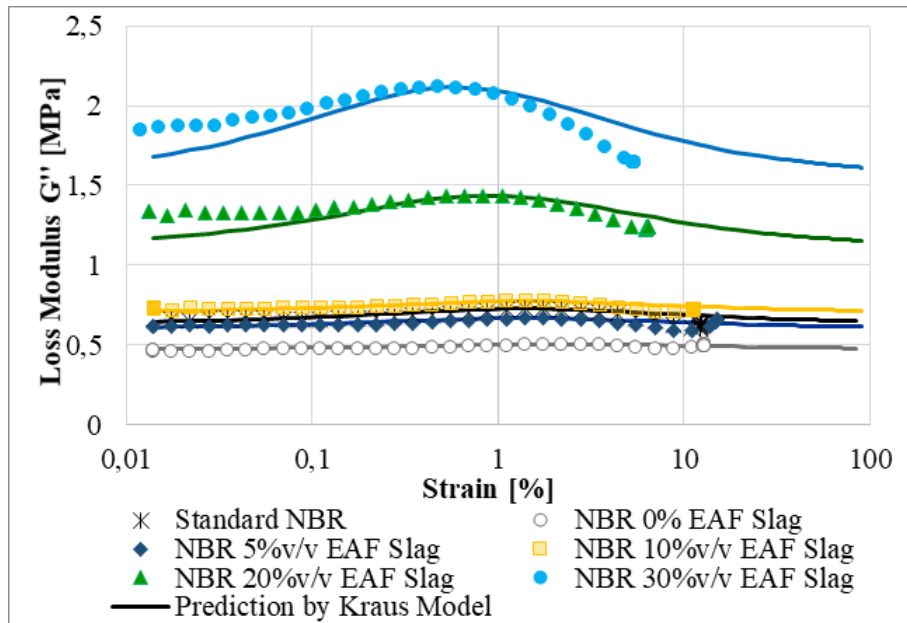


Figure 52 Dynamic loss modulus in shear mode at 1 Hz, 23°C plotted against strain amplitude (0.02-10%) for Standard NBR and NBR filled with 0, 5 10 20 and 30% with EAF slag and application of Kraus model ( $G''(\gamma)$ ).

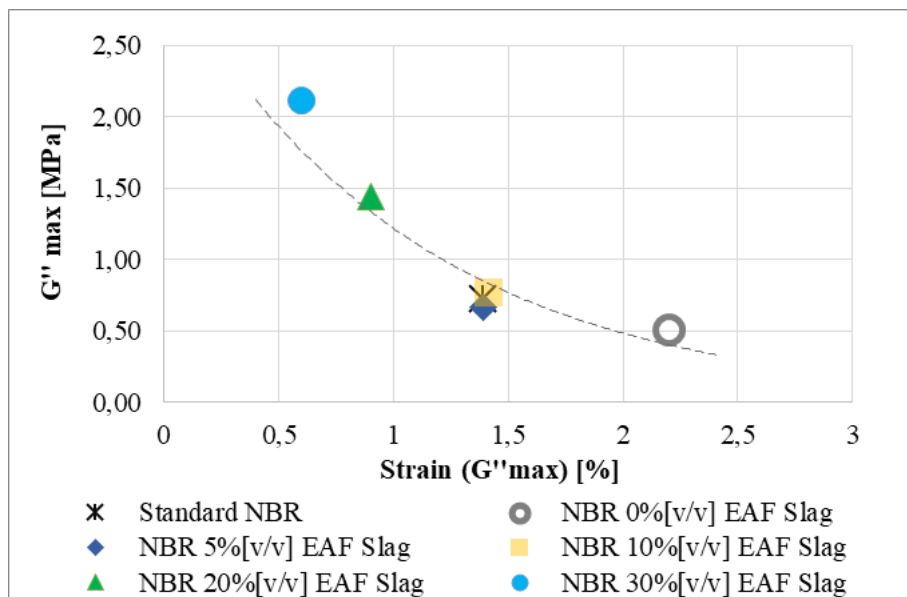


Figure 53 Loss modulus peak ( $G'' \max$ ) function of shear strain amplitude.

Experiments of low amplitude storage modulus recovery after the application of a large amplitude dynamic strain were performed for all the material investigated. The results are shown in Figure 54, where the low amplitude storage modulus, measured after the application of the large strain perturbation, is plotted against logarithmic time. Experimental results show that the presence of EAF slag does not affect the recovery of the material and the storage modulus at low amplitude strain after a large strain perturbation is only slightly lower than the initial one (represented by dotted lines). This behaviour may be attributed to a small modification of the structure, which is restored after about 10 minutes.

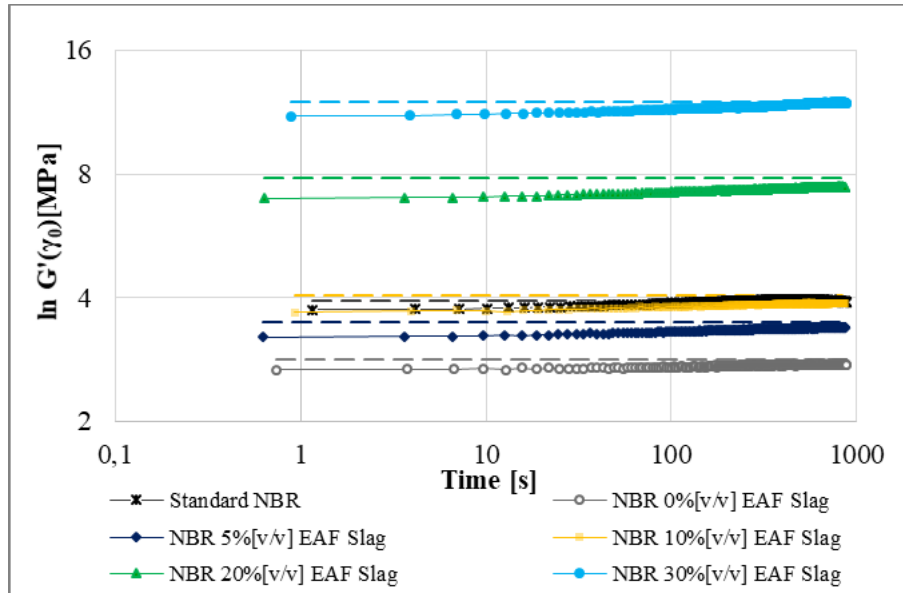


Figure 54 Recovery of low strain amplitude storage modulus  $G'(\gamma_0)$  with time after the application of a high amplitude dynamic strain (about 10%) for Standard NBR and NBR filled with EAF slag at 0,5,10,20,30% [v/v]. Test frequency of 1 Hz. Dotted lines represent the storage modulus  $G'(\gamma_0)$ .

*Tensile dynamic properties: temperature sweep*

The storage modulus as a function of temperature gives the idea about the interaction between the rubber matrix and the EAF slag as filler [231]. Figure 53 shows the dynamic moduli as a function of temperature: the storage modulus graphs show three distinct regions, such as glassy, transition, and rubbery regions. The sharp fall of storage modulus in the transition region is associated to the mobility of polymer chains which increases with temperature.

The EAF slag as filler in NBR matrix increases the storage modulus  $E'$  proportionally to the filler content: the  $E'$  curves are shifted up of about 100% for slag amount of 30%v/v with respect to standard NBR.

This behaviour could be attributed to the interfacial interaction between NBR matrix and slag particles improving the efficiency of transfer the load from the rubbery matrix to the rigid filler trough the rigid layer of polymer around the slag particles. It is important to highlight that the fraction of rigid rubber increases with the slag content. It was found that the calendaring process increases the storage modulus of calendered NBR compared to standard NBR over the investigated temperature range of about 10% due to the better dispersion of carbon black (evinced also by SEM observations).

Similar considerations can be done regarding the loss modulus  $E''$ . The loss modulus highlights the viscous properties of the materials and represents energy lost as heat or dissipated during one cyclic load. It is shown in Figure 55 as dotted curve for each tested NBR composite.  $E''$  maximum value (and related temperature) is

reported in Table 18. It was observed that the loss modulus  $E''$  increases with EAF slag content: the  $E''$  curves are shifted up of about 100% for slag amount of 30%v/v with respect to standard NBR.

The presence of EAF slag as filler in NBR matrix increases both the material capability to store and dissipate energy due to the presence of rigid layer around the slag particles (bound rubber).

Due to the increase of mobility of polymer chains which increases with temperature it is possible to determine the glass transition temperature  $T_g$ . It can be determined as the onset of the storage modulus drop which is associated to the maximum reduction of mechanical properties. A The loss modulus peak is associated to the increase of the polymer chains mobility and represents the point of maximum damping. The glass transition temperature is not affected by the slag content, and it remains constant in all the tested materials for both determining methods. This behaviour suggests that although the fraction of bound rubber increases with increasing the EAF slag content, the temperature necessary to activate the mobility of polymer chains does not vary. This means the interaction force between filler and matrix remains constant.

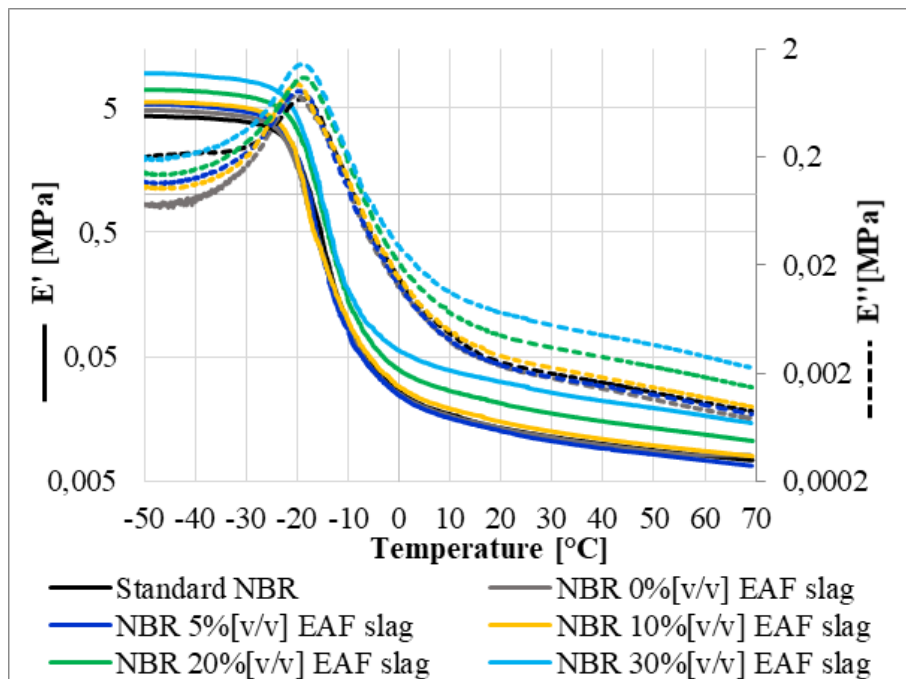


Figure 55 Tensile storage and loss modulus of Standard NBR and NBR filled with EAF slag at 0,5,10,20,30% [v/v]. Test frequency of 1 Hz.

Table 18 Dynamic mechanical properties and glass transition temperature of Standard NBR and NBR filled with EAF slag at 0,5,10,20,30% [v/v].

Material	Maximum storage modulus ( $E'$ [MPa])	Maximum loss modulus ( $E''$ [MPa])	Glass transition temperature ( $T_g$ [°C])	
			$E'$ drop	$E''$ peak
Standard NBR	4,31	0,69	-25,5	-19,1
NBR 0%[v/v] EAF slag	4,79	0,74	-26,0	-19,7
NBR 5%[v/v] EAF slag	5,36	0,82	-26,2	-19,7
NBR 10%[v/v] EAF slag	5,59	0,95	-26,0	-19,9
NBR 20%[v/v] EAF slag	7,02	1,09	-25,0	-18,9
NBR 30%[v/v] EAF slag	9,52	1,45	-25,3	-19,0

It is important to highlight how the influence of the slag as a filler for the NBR matrix on the dynamic properties leads to the same considerations on the viscoelastic behaviour, both with the variation of the strain amplitude and with the variation of the temperature.

The ability of NBR composites to store energy is evidenced by the storage modulus curves shift at higher modulus values proportionally to the amount of slag content. This is associated to the stiffening of the rubber matrix by the presence of rigid fillers through the hydrodynamic effect and the filler-matrix interaction which creates a rigid layer of rubber around the filler particles (bound rubber).

The ability of NBR composites to dissipate energy is evidenced by the loss modulus curves shifted at higher modulus values proportionally to the amount of slag content, as well as the storage modulus.

The loss modulus curves as function of strain amplitude show a peak which is ever more marked and occurs at ever smaller amplitude strain with increasing the EAF slag content. As the slag content increases, the fraction of rigid rubber around the filler particles, responsible for energy dissipation, also increases. The loss modulus peak is more marked and shifts towards smaller deformation amplitudes for high slag contents as the fraction of rigid rubber is greater, and the rigid layers of different particles come into contact with each other already at small deformations. The loss modulus peak increase with EAF slag content is evidenced also as function of temperature. In correspondence of the glass transition temperature the energy dissipation is more marked for high filled compounds, due to higher rigid rubber fraction.

#### 2.3.2.9. *Swelling behaviour and crosslink density*

The crosslink density is an important structural parameter for cured rubber. Mechanical properties such as hardness, tensile strength and modulus at a certain deformation are usually the first consideration when designing a rubber formulation for a specific purpose. These properties strongly depend on the structure of the network, such as its density and the type of crosslinking [302]. Due to this is crucial to evaluate the influence of EAF slag as filler for NBR matrix not only on the mechanical properties but also on the crosslink density.

Figure 56 shows the swelling coefficient [%] and the crosslink density ( $\nu$  [mol/cm<sup>3</sup>]) determined by the Flory-Rehner equation (Equation 11 and Equation 12 respectively) for standard NBR and NBR composites filled with EAF slag in different amount.

It is observable that with increasing the EAF slag content in NBR matrix the swelling coefficient decreases because the average molecular weight of rubber segment between crosslinks  $M_c$  is reduced and consequently the crosslink density increases. This trend is in line with what expected because it is reasonable to state that the immobilized rubber fraction around the slag particles is subjected to a lower swelling, and with increasing this immobilized rubber fraction the average rubber crosslink density increases [263].

No differences are detected on the crosslink density of standard NBR and calendered NBR without EAF slag. This means the calendaring process does not affect the polymer capability to vulcanize. This is probably due to two opposite phenomena: the better filler dispersion increases the carbon black surface area for the bound rubber formation, but on the other side the occluded rubber is reduced.

The increase of crosslink density with EAF slag volume fraction due to the increase of bound rubber fraction [263] could be related the general stiffening and strain at break reduction of NBR composites filled with slag. The improvement in crosslink density as function of filler dosage can be further explained by considering the bound rubber around the filler surface [263], [303]–[305]. The rigid and immobilized NBR layer around the filler particles surface is a consequence of the interaction between slag and NBR. The slag particles can be

covered by rubber layer of high modulus and this in turn gets covered by clay layer of low modulus. The resultant rigid amorphous phase contributes to the high crosslink density and tensile modulus of the NBR composite [263].

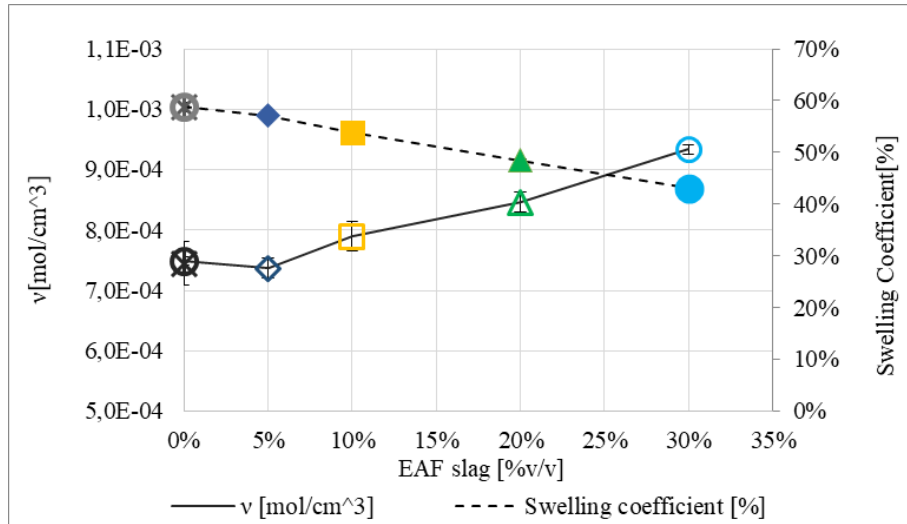


Figure 56 Crosslink density determined by Flory-Rehner equation and swelling coefficient of Standard NBR and calendered NBR willed with 5, 10, 20, 30%v/v of EAF slag.

Figure 57 shows the plot of  $(V_{r0}/V_{rf})$  against  $(\phi/1-\phi)$  gives the extent of reinforcement (K) versus the filler volume fraction. The slope of the Kraus plot (K) is a measure of the polymer-filler interaction in the composite material. According to Kraus theory, the higher the negative value of the slope, the greater is the reinforcement of the polymer matrix with the filler.  $V_{rf}$  is assumed equal to  $V_{r0}$  in order to evaluate the EAF slag influence neglecting that of carbon black which is constant for all the compounds. The ratio  $V_{r0}/V_{rf}$  is less than unity and the magnitude of the ratio decreases with filler loading, from a value of 1 for NBR without EAF slag to a value of 0.92 for EAF slag volume fraction of 30%, showing a reinforcement effect. As the reinforcement increases, the degree of transfer of stress from the polymer matrix to the filler will increase, which in turn increases the constraint zone of polymer chains. Thanks to the strong physisorption of NBR chains on to the filler particles surface, the latter are well adherent to the NBR matrix leading to reinforcement [263].

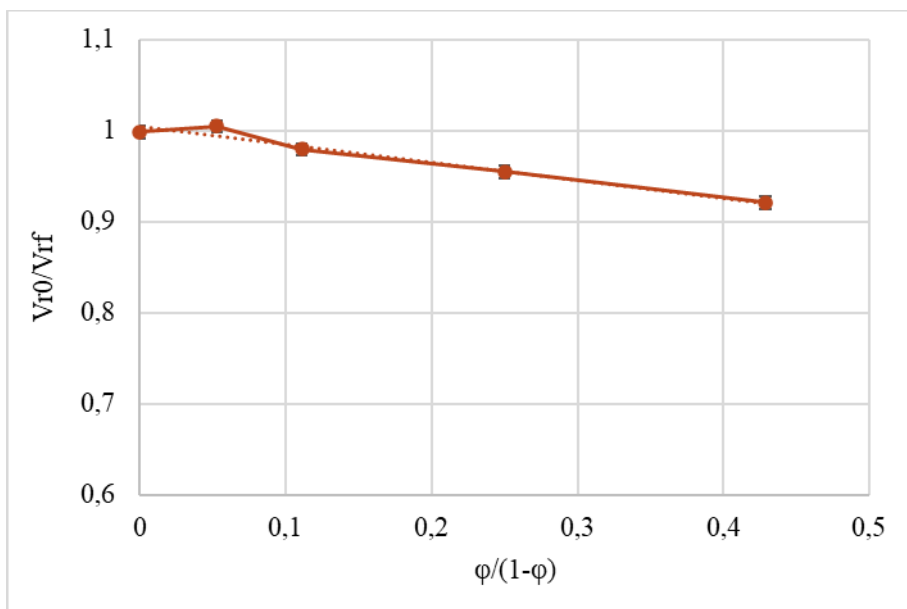


Figure 57 Kraus plot of EAF slag filled NBR.

### 2.3.2.10. Differential scanning calorimetry analysis

The heat capacity  $C_p^*$  [J/(g °C)] of the rubber fraction of NBR composites is shown in Figure 58. It is evident that the glass transition temperature almost remains constant on a value of  $-24$  [°C] with increasing EAF slag content in rubber composites. This is consistent with the trend observed in the DMA results.

The glass transition temperature, the heat capacity increment  $\Delta C_p^*$  and the immobilized rubber fraction of each tested material are reported in Table 19.

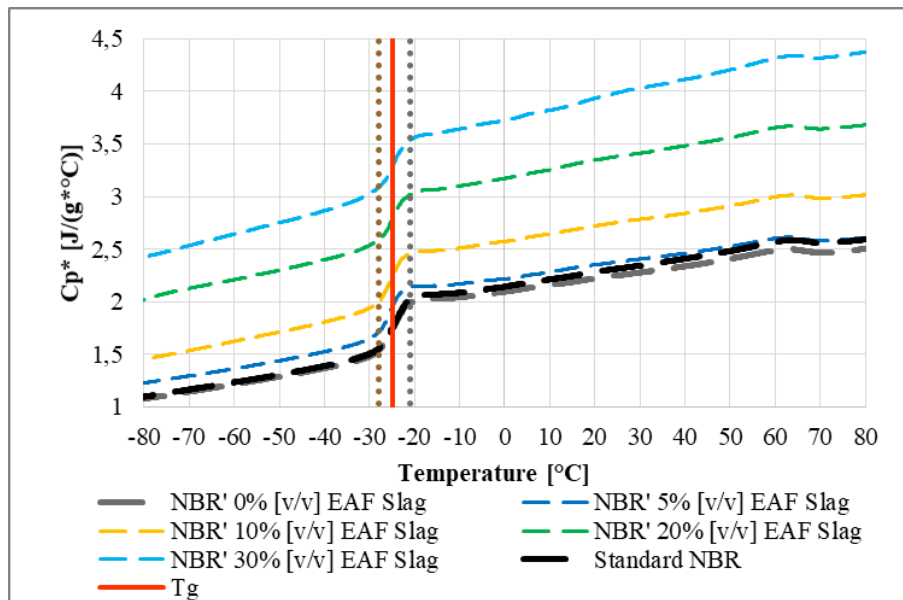


Figure 58 Heat capacity of the NBR composites' polymer fraction  $C_p^*$  determined by DSC thermograms; glass transition temperature as  $C_p^*$  deflection point and temperature range of  $\Delta C_p^*$  ( $-2.5^\circ\text{C} < T_g < 2.5^\circ\text{C}$ ) for the immobilized rubber fraction calculation.

The heat capacity increment,  $\Delta C_p^*$  as a measure of the amount of polymer which participates in the glass transition is dependent on the intermolecular rigidity, that is, the polymer–filler interaction in the filled rubber composites. The dependency  $\Delta C_p^*$  on intermolecular rigidity is evaluated in terms of an immobilized polymer chains in the composites. The immobilized rubber fraction was quantified according to Equation 24, the results are shown in Figure 59. It is observable that with increasing the EAF slag content the heat capacity increment required by the rubber fraction in correspondence of the glass transition temperature decreases due to the presence of a rigid rubber fraction which remains in a glassy phase also above  $T_g$ .

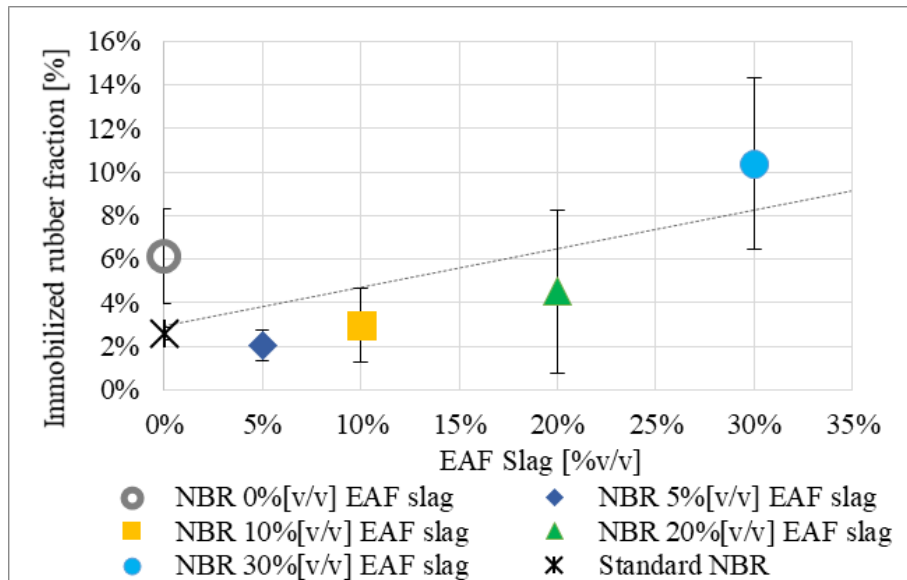


Figure 59 immobilized rubber fraction [%] of Standard NBR and of Standard NBR and calendered NBR filled with 5, 10, 20, 30%v/v of EAF slag.

Table 19 Parameters of calorimetric glass transition: glass transition temperature, heat capacity increment and immobilized rubber fraction.

Material	Glass transition temperature (Tg [°C])		Heat capacity increment $\Delta C_p^*$ [-]		Immobilized rubber fraction [%]	
Standard NBR	-23,90	± 0,42	0,38	± 0,003	3%	± 1%
NBR 0%[v/v] EAF slag	-24,24	± 0,01	0,36	± 0,008	6%	± 2%
NBR 5%[v/v] EAF slag	-25,22	± 0,07	0,38	± 0,003	2%	± 1%
NBR 10%[v/v] EAF slag	-25,23	± 0,10	0,38	± 0,007	3%	± 2%
NBR 20%[v/v] EAF slag	-25,18	± 0,06	0,37	± 0,015	5%	± 4%
NBR 30%[v/v] EAF slag	-24,70	± 0,22	0,35	± 0,015	10%	± 4%

2.3.2.11. Magnetic properties

Figure 60 show the force required to detach a magnet from the NBR filled with different amounts of EAF slag. As expected, the standard NBR does not require any detachment load but, by adding an increasing amount of EAF slag as filler the detachment load grows. This force is still low compared to a metallic material but may be sufficient for mounting applications where the magnetic force helps the rubber part to seat. For example, in automatic assembly systems to handle a rubber part it will be sufficient to apply a magnet to the end of the robotic arm. This solution, in addition to being economical in terms of equipment required, also minimizes the risk of damage to the rubber compared to a mechanical handling system by clamps that could generate micro cracks causing malfunctions in operation. From an application point of view, EAF slag gives NBR ferromagnetic properties so it could potentially be used as a shield for magnetic fields. Ferromagnetic materials, having a higher permeability than that of air, offer a preferential path to the magnetic field. In this way they absorb the flux lines of the magnetic field from the area around the source to be shielded. Obviously for this application a specific characterization of the material will be required which is not the purpose of this study.

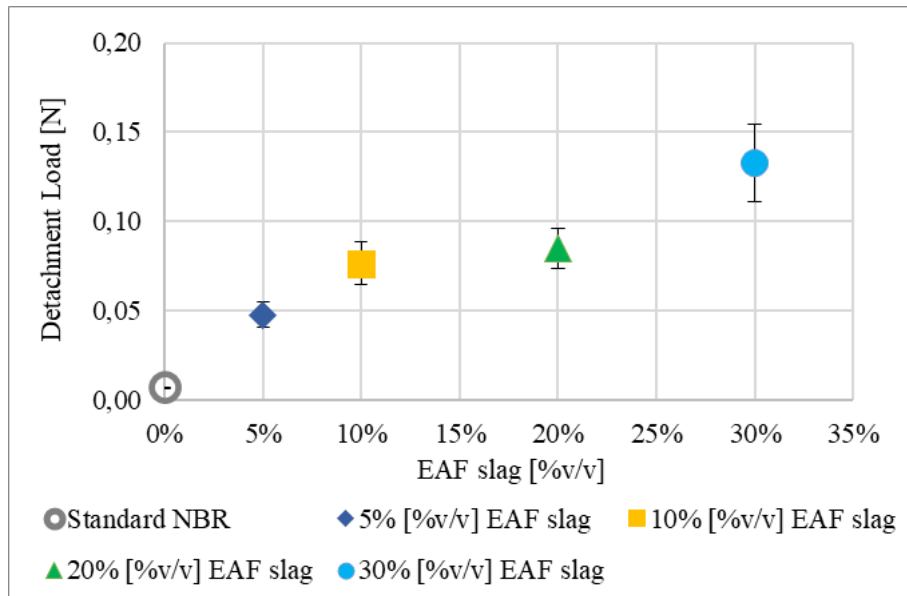


Figure 60 Detachment force between a magnet and the compound filled with EAF slag in different quantities.

2.3.2.12. Friction

Figure 61 shows the friction force curve during the friction test. The peak of the force detected is the static frictional force, while the force necessary to keep the system in motion is the dynamic frictional force.

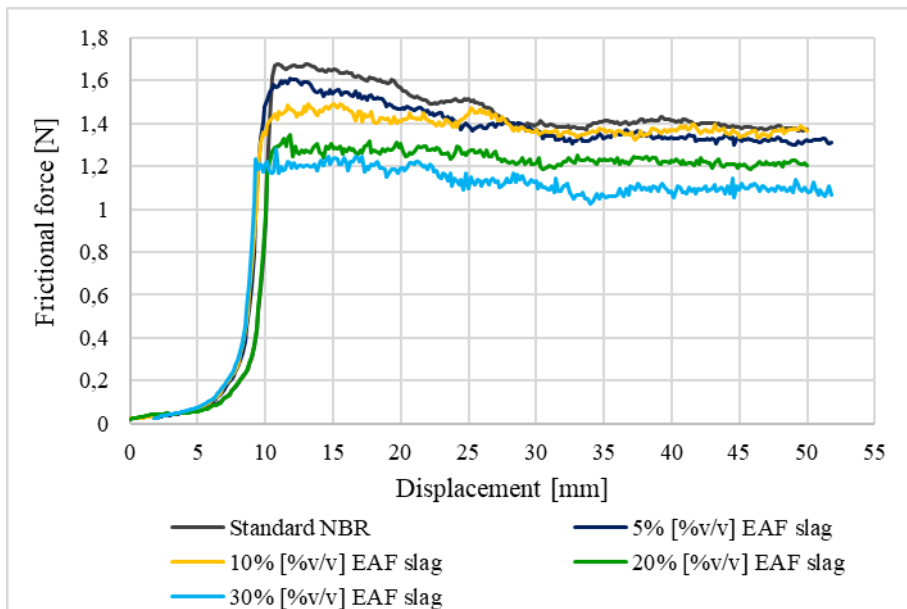


Figure 61 Friction force for standard NBR filled with EAF slag

The influence of EAF slag on standard NBR coefficient of friction is shown in Figure 62, while Table 20 shows the static and dynamic coefficient of friction average and standard deviation values. It is possible to notice that with increasing the amount of EAF slag as filler both the static and the dynamic coefficient of friction decrease. The static coefficient of friction decreases linearly of about 20% from the standard NBR to NBR filled with EAF slag at 30%v/v. The dynamic coefficient of friction remains constant up to a value of EAF slag of 10%v/v than it decreases of about 20%. This is a good result because the addition of EAF slag as filler in rubber matrix could

give the possibility to avoid a further anti-sticking treatment in the industrial process with the consequent economic saving.

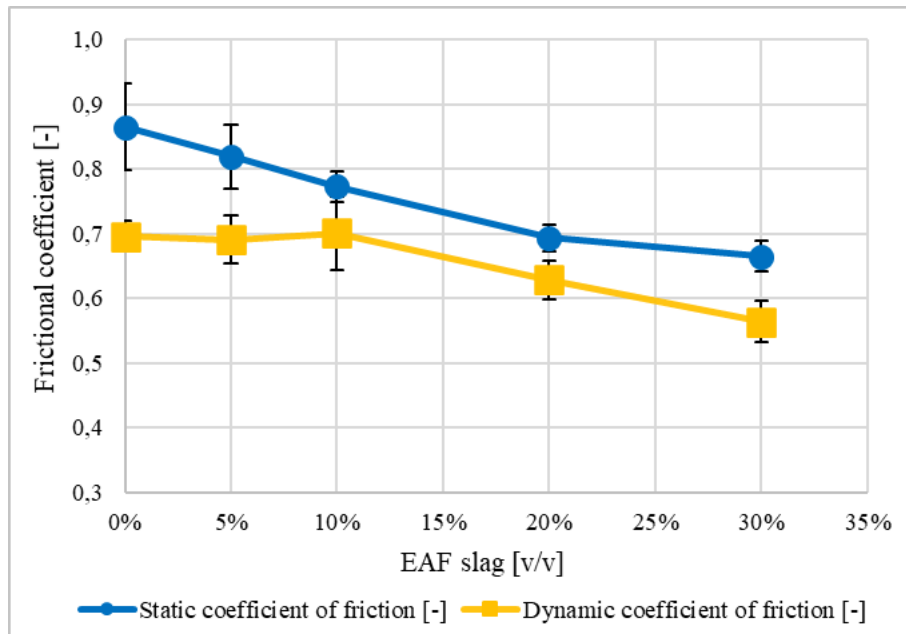


Figure 62 Static dynamic coefficient of friction function of EAF slag percentage by volume added in standard NBR

Table 20 Static dynamic coefficient of friction.

Compound	Static coefficient of friction [-]		Dynamic coefficient of friction [-]	
Standard NBR	0,86	± 0,034	0,70	± 0,012
5% [%v/v] EAF slag	0,82	± 0,026	0,69	± 0,019
10% [%v/v] EAF slag	0,77	± 0,012	0,70	± 0,029
20% [%v/v] EAF slag	0,69	± 0,011	0,63	± 0,016
30% [%v/v] EAF slag	0,67	± 0,012	0,56	± 0,017

## 2.5. Conclusion

This paragraph aims to characterize an innovative compound consisting of vulcanized rubber NBR filled with EAF slag, in order to pave the way to a new EAF slag application economically and environmentally convenient. The influence of four different amounts of EAF slag (5, 10, 20, and 30% v/v) has been evaluated in comparison with standard NBR and its influence has been assessed according to experimental procedures and analytical calculations commonly adopted in evaluating the reinforcing effect of traditional fillers.

The main results can be summarized as follow:

- Still today a large amount of EAF slag is disposed of as special waste. For safe reuse of slag, the leaching of heavy metals must remain under specific values. The leaching of Cr, Mo, and V of EAF slag incorporated in the rubber matrix is significantly reduced compared to that of free slag.
- The processability characteristics of the analysed compound have been evaluated by the rheometric curve. The results show that a higher amount of slag in NBR slightly increases the compound viscosity and accelerates the crosslinking kinetics. From the production point of view, this is a great advantage because it allows to reduce the production cycle time saving on production costs. On the other hand, this phenomenon reduces the scorch time, so that the time during which the material can stay in the injection chamber without vulcanizing is less. The risk of producing not compliant rubber parts is higher. As last, the rheometric curve data shows an increase in the torque needed to maintain the imposed rotation at complete vulcanization, indicating an increase in stiffness.
- Compression modulus increases with growing the filler amount by 50% from standard NBR to NBR filled with EAF slag at 30%v/v. The compression test results demonstrate that by increasing the amount of slag the material offers an ever-increasing resistance to deformation.
- Hardness value (both Shore A and mIRHD) increases with increasing the amount of added filler.
- Compression set results show that the presence of filler reduces the material's ability to recover an imposed deformation; up to a filler content of 10%v/v the compression set is below 15% which is a good value for real applications, while for a filler content of 20%v/v it is below 20% which is still acceptable.
- In the real case of gasket assembled in load control or displacement control, comparing the performance of a standard NBR and an NBR filled with EAF slag it is possible to observe that in both assembly configurations EAF slag affects the compound properties positively.
- The addition of metal slag in an elastomeric matrix gives the final compound magnetic properties that the elastomer alone does not possess. These properties can be exploited both in the application field or simply for the optimization of assembly. The force required to detach a magnet from the compound increases as the added EAF slag amount increases.
- The static and dynamic coefficient of friction are reduced with increasing of EAF slag content.
- Static and the dynamic properties of EAF slag filled NBR composites are affected by the slag content, in particular, in addition to an important contribution of the hydrodynamic effect, by the presence of a layer of rigid rubber around the filler particles (bound rubber) related to the filler-rubber interaction. With increasing the filler content the immobilized rubber fraction quantified by DSC analysis increases as well as the crosslink density determined by the Flory-Rehner equation.
- The hydrodynamic effect was evaluated on the Young's modulus (E) determined by the tensile test and on the shear storage modulus (G') by DMA. It was found that the experimental data of E are well predicted by the Halpin-Tsai prevision model, while  $G'(\gamma_0)$  by that proposed by Guth and Gold.

- The presence of the EAF slag on the dynamic properties of NBR composites can be summarized as follow:
  - The ability of NBR composites to storage and to dissipate energy is evidenced by the storage and loss moduli curves shifted at higher modulus values proportionally to the amount of slag content.
  - EAF slag volume fraction increases the non-linear behaviour (Payne effect): the immobilized rubber fraction increases so that the filler-matrix interaction contribute rises. The loss modulus peak occurs at approximately the same dynamic amplitude value where the storage modulus is most rapidly decreasing. The loss modulus peak is more marked and shifts towards smaller deformation amplitudes for high slag contents because the immobilized rubber fraction is greater, and the rigid layers of different particles come into contact with each other at lower strain amplitude.
  - The increase of the loss modulus peak with EAF slag content is evidenced also as function of temperature. In correspondence of the glass transition temperature the high filled compounds show a more marked loss modulus peak because of the immobilized rubber fraction which does not participate in the glass transition (lower heat capacity increment is required). A good incorporation of the particles into the matrix was also evident from the SEM observations.
  - The glass transition temperature is not affected by the EAF slag content, this suggests the rubber-filler interaction force is not modified.
  - The presence of EAF slag as filler does not affect the storage modulus recovery after a large strain perturbation.

The addition of EAF slag up to 10% v / v can bring economic and environmental benefits thanks to the saving of raw material without dramatically altering the properties of the standard material.

### 3. EAF Slag Filled recycled NBR scrap

The management of rubber scraps derived from rubber goods production is becoming an increasingly critical problem in the sector and unfortunately, the recycling and reuse of general rubber goods amount to only 1.5% of the total waste generated [130]. The amount of industrial rubber scraps consists of about 20-30% by weight of the processed material, due to the presence of filling channels (in the injection moulding process) and infiltrated material between the two half-moulds which creates a thin rubber film (rubber flash) from which the pieces will be removed by subsequent processing (deburring). The re-processing of crosslinked elastomers is possible when the crosslinks formed during the vulcanization (C-S and S-S for sulphur curing) are cleaved without damaging the C-C bonds of the macromolecular chain [130], [132], [133]. When the cleavage of C-C bonds occurs, and it is predominant to that of C-S and S-S bonds, the degradation process takes place with consequent deterioration of the mechanical properties of the rubber [130].

The phenomena of vulcanization and degradation are both interconnected with each other. It is not possible to only cleave crosslinks or to only cleave the main polymer chain during a process, to that both of them take place during the rubber re-processing. Because of this, the importance to limit the degradation and increase the devulcanization enhancing the chances of rubber recycling is therefore evident.

In this section, the NBR scraps are recycled via calendering process at room temperature with no additives. The calendering process consists in forcing the rubber between two rotating cylinders which generate high shear stresses and extensional stressing levels on the material leading to the obtaining of a rubber sheet that can be further processed via compression moulding. Obviously, as the fraction of recycled rubber increases, the possibility of creating complex geometries decreases due to an ever-greater degree of crosslinking, however for simple geometries and for specific applications it is possible to replace even only partially virgin rubber with recycled industrial waste.

This rubber recycling method, according to the best knowledge of the authors, is not reported in any literature work and it doesn't require any specific tool since the calender (or open mixer) is a machine of common use in the rubber industry.

Different amounts of recycled NBR (20, 80 100% wt) were characterized by swelling test, tensile and compression test, hardness test, and compression set. Also, the influence of recycling methods was assessed: compression moulding, calendering process, and calendering process followed by compression moulding. Furthermore, the characterization was also performed via Attenuated Total Reflection – Fourier Transform-Infrared Spectroscopy (ATR-FTIR) coupled with chemometrics to detect if any changes due to oxidation related to the recycling process had occurred. FT-IR spectroscopy technique has been extensively applied in the analysis of polymers and rubber-based compounds [306]–[308]. Furthermore, in this field, IR spectroscopy has been applied to vulcanized rubber for detecting changes in chemical structure due to oxidative aging of NBR [309], developing methods for supervising the vulcanization and recovery processes of EPDM rubber [310], and for characterization of NBR surface alterations caused by chemical oxidation [311].

It has been found that in general the increase in the recycled rubber fraction does not have a marked detrimental effect on some original properties, in fact, the hardness remains within the tolerance allowed for virgin NBR, up to 80% of recycled NBR compression set does not vary, while the tensile modulus increases at the expense of stress and strain at break and under compression stress the recycled materials shows a stiffer behaviour. On the other hand, no differences were found in the multivariate analysis of the FT-IR spectra. This means that no changes regarding the chemical structure of the polymer were detected.

Once the recycled NBR study was completed, another test campaign was carried out on 100% recycled NBR with EAF slag additives. In particular, the influence of 10% by volume of EAF slag as filler was investigated but also with the same amount of filler the influence of different granulometric ranges 0-50 $\mu\text{m}$  and 50-100 $\mu\text{m}$ . As first the EAF slag was characterized in terms of chemical composition by XRF and mineralogical phases by SEM-EDXS analysis, then the leaching behaviour of different slag grain size ranges has been investigated. It was found that the EAF slag chemical composition consists mainly in Iron oxide, Silicon oxide, Calcium Oxide and other oxides in minor quantities. The identified mineralogical phases were larnite, brownmillerite and chromite. The leaching test results confirmed that as general trend the fine slag releases more than coarse slag, but due to the heterogeneity of the slag cannot be stated, without further investigations, that a finer pulverized slag presents higher leaching than another less fine slag.

As regard the characterization of 100% recycled, 100% recycled NBR filled with EAF slag 10%[v/v] in a grain size 0-50 $\mu\text{m}$  and 50-100  $\mu\text{m}$  respectively, the crosslink density was assessed by the Flory-Rehner equation based on swelling test data; a mechanical characterization was carried out in terms of hardness, tensile properties and dynamic mechanical analysis (Payne effect) and low strain amplitude recovery after a large strain amplitude perturbation. The results show an increase of crosslink density, hardness, and static and dynamic modulus of EAF slag filled recycle NBR, and in particular that filled with the finest EAF slag (lower than 50 $\mu\text{m}$ ).

On the basis of the results obtained, it is possible to state that both industrial rubber wastes, EAF slag and rubber scraps, have a potential that can be exploited bringing advantages not only in environmental terms for non-disposal but also in economic terms.

### **3.1. Materials**

#### **3.1.1. Industrial NBR scrap**

The tested material is an industrial NBR hardness 60SH A, carbon black 40 phr vulcanized with Sulphur provided by Novotema Spa (Villongo BG, Italy).

The industrial scraps are recycled by calendaring process on an open mixer and it is tested as 100% recycled NBR or compounded with different amounts of virgin NBR. Moreover, the influence of further compression moulding is assessed in order to produce rubber sheets thicker than 2mm for compression tests.

Tested materials and production process are listed below:

##### **3.1.1.1. Virgin NBR compression moulded**

Virgin NBR samples have been obtained by compression moulding. About 18 g of unvulcanised NBR is placed between pre-heated plates and kept under a pressure of 40 MPa for 15 minutes at 180°C. The test plates so obtained are then cut in the required shape for the mechanical characterization.

##### **3.1.1.2. Virgin NBR Calendered and compression moulding**

In order to evaluate different materials subjected to the same production process a virgin NBR has been produced by calendaring process followed by compression moulding under a pressure of 40 MPa for 15 minutes at 180°C to obtain test plates. This is the same process adopted for the production of recycled materials as explained following.

### 3.1.1.3. 100% recycled NBR: Calandered

100% recycled NBR samples have been obtained by calendering the industrial scraps previously produced by injection moulding at temperature of 170°C. The used calender machines has been provided by Meccaniche Moderne srl (Busto Arsizio VA, Italy). In the calendering process the rubber is worked in several steps during which the temperature increases (70-80°C) due to the high shear stresses generated by the cylinder in the material that gets soft and plasticized as shown in Figure 63. The material obtained at the end of the calendering process is a sheet of about 1-2 mm.



Figure 63 Plasticized rubber during calendering process

### 3.1.1.4. 100% recycled NBR: Calendered and compression moulded

In order to produce thicker sheets, the rubber scraps is also compression moulded after the calendering process with the same process parameters as virgin NBR (15 minutes at 180°C at 40MPa).

### 3.1.1.5. 80% recycled and 20% virgin NBR: Calendered

A calendered sample has been obtained by adding 20%wt of unvulcanised virgin material in the industrial scraps and the mix has been thus calendered as described above.

### 3.1.1.6. 80% recycled and 20% virgin NBR: Calendered and compression moulded

Calendered and mix 20%virgin and 80%recycled NBR also compression moulded with the process parameters equal to 15 minutes at 180°C at 40MPa.

### 3.1.1.7. 20% recycled and 80% virgin NBR: Calendered and compression moulded

As last, a calendered sample has been obtained by adding 80%wt of unvulcanised virgin material in the industrial scraps and the mix has been thus calendered as described above. This mix due to the high presence unvulcanized rubber cannot be tested without a further compression moulding process which is performed with the usual parameters (15 minutes at 180°C at 40MPa).

## 3.1.2. EAF Slag filled recycled NBR scrap

EAF slag was supplied by Ori-Martin (Brescia, Italy) steelmaking plant. The slag used as filler was grinded and sieved in 4 grain size range: 0-50µm, 50-100µm, 100-150µm, 150-300µm.

The used rubber scrap is an industrial NBR hardness 60SH A, carbon black 40 phr vulcanized with Sulphur provided by Novotema Spa (Villongo BG, Italy). For safe of clarities it is important to highlight that this characterization has been carried out on the same NBR scrap as 3.1.1 Industrial NBR scrap but on different industrial batch and the used calender machine has been provided by Gaoge-tech instrument (Dongguan, China). The industrial rubber scrap was recycled following the same procedure detailed in 3.1.1.4 100%

recycled NBR: Calendered and compression moulded with the addition of 10% by volume of EAF slag in a grain size lower than  $50\mu\text{m}$ , and between 50 and  $100\mu\text{m}$  in order to investigate the influence of different filler grain size with no changes in the filler content. In summary the characterized materials are:

- 100% recycled NBR
- 100% recycled NBR filled with 10% EAF slag [v/v] grain size 0-50  $\mu\text{m}$
- 100% recycled NBR filled with 10% EAF slag [v/v] grain size 50-100  $\mu\text{m}$

## 3.2. Methods

### 3.2.1. Recycled NBR scrap Characterization

#### 3.2.1.1. Swelling test

For the swelling test rectangular samples of about 500mg were cut and immersed in toluene in sealed glass tubes for 48 hours at room temperature. The swelling coefficient is determined according to Equation 11. The equilibrium swelling index is determined by crosslink density and the attractive forces between solvent and polymer. The theoretical extent of swelling is predicted by the Flory–Rehner equation [185], [189], [190] (Equation 12 and Equation 16).

#### 3.2.1.2. Tensile test

Mechanical tensile tests were performed by an Instron dynamometer (mod. 3366) at room temperature and at a cross-head rate of 100 mm/min on test pieces of 50 mm length (distance between the grips of about 30 mm) and 4 mm width according to the standard ISO 37:2017 type 2 [197]. The considered strain is the optical one in order to exclude the influence of the sample edges. The measurement is performed three times for each compound. The Young's modulus has been determined as the slope of the stress strain curve in correspondence to the initial linear section.

#### 3.2.1.3. Compression Test

Compression tests were performed on three samples for each material by a dynamometer (mod. 3366) provided by Instron (Pianezza, TO, Italy) at room temperature and a strain rate of 10 mm/min. Cylindrical specimens with a nominal diameter of 12mm and a thickness of 6 mm were produced for this test. The compression test was performed according to the standard ISO 7743 [121].

#### 3.2.1.4. Compression Set

The compression set is determined by imposing a compression deformation of 25% on cylindrical samples (nominal diameter 12mm and a height of 6 mm) for 24h at  $100^\circ\text{C}$ .

The compression set was determined according to standard ASTM D395 (test method B) [278].

#### 3.2.1.5. Hardness Test

The compounds' hardness was measured according to the most widely used scales in the rubber industry: Shore A hardness and micro International Rubber Hardness Grade (mIRHD). The Shore A measurements were carried out for 3 seconds according to the standard ISO 7619-1 [276] by an automatic hardness tester Shore PC type A provided by Gibitre Instruments (Bergamo, Italy). The mIRHD measurements were carried out for 30 seconds according to the standard ISO 48 [277] by an automatic hardness tester Micro IRHD-PC provided by Gibitre Instruments (Bergamo, Italy).

### 3.2.1.6. FT-IR Measurements

Attenuated total reflection Fourier transform infrared (ATR-FTIR) spectroscopy was performed with a Nicolet iN10MX (Thermo Scientific, Milan, Italy) Microscope equipped with a cooled MCT detector. Each spectrum was recorded in a triplicate, at 16 scans with a resolution of  $8\text{cm}^{-1}$ , in the range of  $4000\text{-}675\text{ cm}^{-1}$ . For all spectra manipulations OMNIC™ Specta™ (Thermo Scientific, Milan, Italy) software was used.

#### Principal Component Analysis

Among the most significant and powerful approaches in chemometrics, principal component analysis (PCA) is used in a wide variety of different fields [312]. PCA aims to extract the information encoded into a certain number of variables, into a smaller set of new orthogonal, named principal components. The key issue of the PCA method consists in the rotation of the data matrix in a way that the first new axis is oriented in the maximum variance of the data, while the second one is perpendicular to the first and oriented in the direction of the next maximum variance of the data and so on, for the other PCs.

The computational procedure of PCA is the following[313]:

1. Starting from the data matrix  $\mathbf{X}$ , the correlations between the variables are evaluated with the covariance matrix  $\mathbf{S}$ . Then  $\mathbf{S}$  is diagonalized according to Equation 29.

$$\text{diag}(\mathbf{S}) = \text{diag}\left[\frac{\mathbf{X}_c^T \mathbf{X}_c}{n-1}\right]$$

Equation 29

Where  $\mathbf{X}_c$  is the centered data matrix and  $\mathbf{X}_c^T$  represents its transposition. The diagonalization of the matrix leads to obtain the eigenvalues matrix  $\mathbf{\Lambda}(p, p)$ , where on the diagonal there are the eigenvalues ordered in a decreasing way and the loadings matrix  $\mathbf{L}(p, M)$  where the columns represent the eigenvectors of the covariance matrix. It is worth noting that the eigenvectors are the vectors of a new space and they are directed in the directions of maximum variance, ordered in a decreasing way.

2. The two matrices  $\mathbf{L}$  and  $\mathbf{\Lambda}$  can be obtained by applying the single value decomposition technique (SVD) on the covariance matrix according to Equation 30:

$$\mathbf{S} = \mathbf{L} \times \mathbf{\Lambda} \times \mathbf{L}^T = \sum_j \lambda_j l_j l_j^T$$

Equation 30

3. By the operation reported in Equation 31, it is possible to represent the new objects in a new space defined by the PCs:

$$\mathbf{T} = \mathbf{X} \times \mathbf{L}$$

Equation 31

Where  $\mathbf{L}$  is a rotation matrix and  $\mathbf{T}$  represents the object coordinates in the new PC space. Each component is a linear combination of the original variables. The coefficients of the corresponding variable for each principal component, are collected in each column of  $\mathbf{L}$ . Furthermore, loadings are standardized linear coefficients and the sum of squares of loadings for each  $m$ -th eigenvector  $l_m$  is equal to 1, according to Equation 32:

$$-1 \leq l_m \leq 1 \quad \sum_j l_m^2 = 1$$

Equation 32

This means that a value of  $l_{jm}$  close to 1, in absolute value, indicates that the  $j$ -th variable is important in defining the  $m$ -th principal component, while  $l_{jm}$  close to 0 indicates that the  $j$ -th variable is not relevant for the  $m$ -th component. The scores  $t_{im}$  represents the coordinates of the samples in the new orthogonal space defined by the  $M$  principal components and they are obtained by a linear combination of the original variable values through the loadings according to Equation 33:

$$t_{im} = \sum_j x_{ij} \cdot l_{im}$$

Equation 33

The reductant information can be excluded from the original data because the lowest eigenvalues are coupled with the principal components that contain only noise or not relevant information. Therefore, only a subset  $M < p$  of principal components may be considered.

#### Software

Multivariate processing and statistical tools were carried out with MATLAB 2020b (The MathWorks, Inc, Natick, MA USA.). To normalize ATR/IR spectra, spectral pre-processing based on Standard Normal Variate and mean centering was applied [314]. All the calculations were carried out by means of PLS-Toolbox (Eigenvektor Research, Inc. Manson, Washington).

### 3.2.2. EAF Slag filled recycled NBR scrap

#### 3.2.2.1. X-ray fluorescence spectroscopy

The EAF slag chemical composition has determined by X-ray fluorescence spectroscopy carried out by the Thermo Scientific™ ARL™ PERFORM'X provided by Thermo Fisher Scientific™ (Waltham, Massachusetts, United States). EAF slag chemical composition is reported in Table 21.

#### 3.2.2.2. SEM-EDXS analysis

The identification of the mineralogic phases which constitutes the slag has been carried out by SEM-EDXS analysis. A standard metallographic polishing procedure was performed on the EAF slag sample which was analyzed by a SEM-EDXS (SEM Leo Evo 40, Carl Zeiss, Oberkochen, Germany; EDXS microprobe Link Pentafet Oxford mod 7060; Oxford Instruments, Oxfordshire, U.K.).

In Figure 73 the SEM-EDXS analysis carried out on a metallographically polished sample utilizing back-scattered electron (BSE) mode is reported.

#### 3.2.2.3. Leaching behaviour

The leaching test was conducted of slag grain size lower than 4mm (according to the standard CEN EN 12457-2 [72]) and also on slag in different grain size range: 0-50 μm, 50-100 μm, 100-150 μm, 150-300 μm. The test conditions were maintained at mixing time 24h, liquid/solid ratio 10:1.

The eluates were then analyzed by by an Avio 200 ICP Optical Emission Spectrometer Perkin Elmer (Milano, Italy) to measure the concentration in the solution Cr, Mo, and V (3 measurements).

#### 3.2.2.4. Swelling test

See procedure detailed in 3.2.1.1 Swelling test

### 3.2.2.5. *Hardness test*

Hardness test in mIRHD scale was performed according to the standard ISO 48 [277] as detailed in 3.3.1.5  
Hardness test

### 3.2.2.6. *Tensile test*

See procedure detailed in 3.2.1.2 Tensile test.

### 3.2.2.7. *Dynamic mechanical analysis*

Dynamic mechanical analysis performed by a Dynamic Mechanical Thermal Analyser Q800 by TA instruments (New Castle, United States) in the tensile mode at room temperature and a frequency of 1 Hz by varying the applied strain amplitude between 0,001% and 50% to observe the low and high amplitude plateau of the storage modulus. This test was performed twice on specimens of nominal dimension 1x5x30mm. Recovery tests of low strain amplitude dynamic modulus after the application of a high amplitude dynamic strain were performed using the same fixture for a recovery time of 5 minutes.

## 3.3. Results and discussion

### 3.3.1. Recycled NBR scrap characterization

#### 3.3.1.1. *Swelling test*

The swelling behaviour of cured rubber provides indications on the crosslink density of the material. This property is particularly relevant in the rubber recycling because on one side the crosslink density affects the mechanical behaviour of the material and on the other side the crosslinks are the responsible of the rubber curing or else of the impossibility to re-process the rubber compound by heating the material as for thermoplastic polymers.

The crosslink density is an important structural parameter for cured rubber. Mechanical properties such as hardness, tensile strength and modulus at a certain deformation are usually the first consideration when designing a rubber formulation for a specific purpose. These properties strongly depend on the structure of the network, such as its density and the type of crosslinking [302]. Due to this, it is crucial to assess the swelling behaviour which is related to the crosslink density, of recycled NBR in different amounts compounded to virgin NBR.

The swelling coefficient indicates how much solvent has penetrated the material: the lower the swelling coefficient, the greater the resistance of the macromolecular structure to solvent absorption.

Nitrile-butadiene rubber has a loose collection, large molecular clearance and weak intermolecular interaction, for which Toluene can easily penetrate the polymer. Due to the affinity between Toluene and NBR, solvation with surface macromolecules will take place and solvents permeate into the inside gaps of the macromolecules. The solvent molecules that penetrate can also cause the solvation of the macromolecular chains, weakening the force between segments of the macromolecular chains and increasing the spaces, which is called swelling. The swelling of polymer materials is characterized by significant volume expansion and mass increase from the macroscopic perspective [315].

Figure 64 shows the crosslink density determined by the Flory-Rehner equation of virgin NBR and different compounds (virgin and recycled NBR mixed in different amounts up to 100% recycled NBR) processed by compression moulding ( $\Delta$ ), calendaring process ( $\square$ ) and calendaring process followed by compression moulding ( $\bullet$ ).

By observing calendered and compression moulded materials, virgin NBR has a crosslink density, higher than that of 20% recycled NBR and lower than that of 80% and 100% recycled NBR.

In general, with increasing the amount of recycled rubber from 20 to 100% the crosslink density increases because the amount of material subjected to 2 curing processes (injection moulding and compression moulding) is larger.

It is also important to consider that the calendaring process on cured rubber acts damaging the macromolecular network of cured rubber via a mechanical devulcanization that breaks not only the crosslinks but also the covalent bonds of the principal macromolecular chains causing a material degradation.

If on the one hand devulcanization reduces the crosslinking density, on the other hand the aging phenomenon linked to oxidation and thermal oxidation must be investigated because the oxidative crosslinking, may occur in calendaring process of rubber scraps caused by the temperature increase by friction, resulting in an opposite effect on the swelling behaviour.

Because of the presence of unsaturated double bonds in butadiene units, NBR generally becomes hard and brittle, and cracks often occur during the thermal oxidation process due to the predominant oxidation and cross-linking reactions. The carbon atoms adjacent to double bonds are easily attacked due to electron shifts, and they form radicals to initiate thermal oxidation and crosslinking reactions during aging [316], [317].

Nevertheless it was found by the FT-IR analysis that the calendaring process does not affect the NBR chemical structure (see 3.2.1.6 FT-IR Measurements).

Compared to standard NBR, that is virgin, the addition of 20% of recycled NBR leads the devulcanization mechanism to be preponderant. As the quantity of recycled NBR increases, the crosslink density increases both due to the increase of cured rubber fraction.

As last it is interesting to notice that the crosslink density of compression moulded virgin NBR is slightly higher than that of calendered and compression moulded one. This means that the macromolecular network of compression moulded NBR is less prone to absorb the solvent due to a lower macromolecular mobility which is found also in

This suggests that the improved distribution and dispersion of carbon black promote the crosslinking due to greater surface to which the polymer can adhere, forming the so-called "bond rubber" [227], [231], [318].

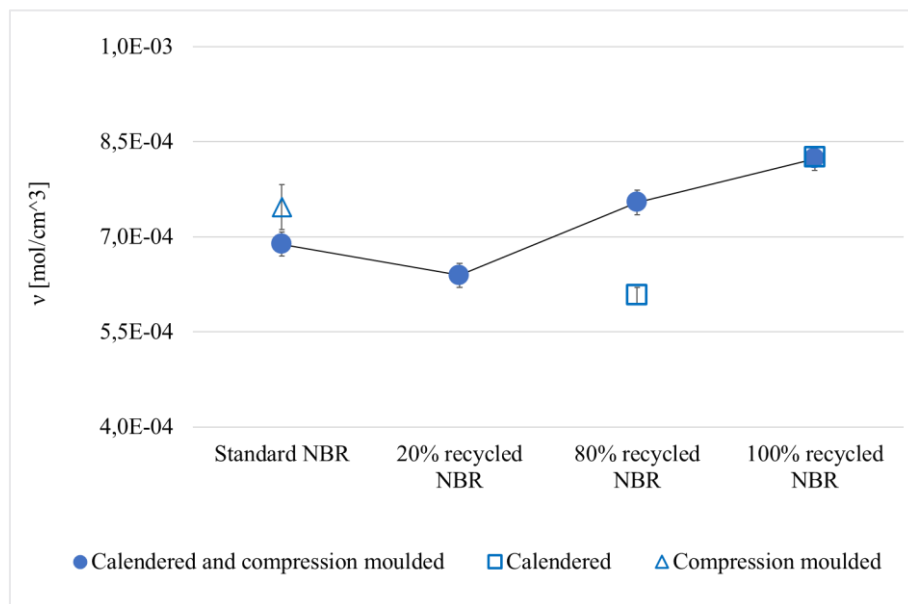


Figure 64 Crosslink density determined by Flory-Rehner equation (swelling in Toluene for 48h at room temperature).

### 3.3.1.2. Tensile test

Figure 65 shows the mean the stress-optical strain curve for the tested materials.

As first it is possible to notice that the calendaring process affects the tensile behaviour of virgin NBR. Virgin NBR calendered and compression moulded show the highest stress and strain at break (19MPa and 530% respectively); the same material processed only by compression moulding process shows higher stress at equal strain up to break which occurs at 17 MPa and 380% optical strain. This behaviour results in a higher tensile modulus (Figure 66).  $E$  (as the slope of the first linear section of the stress strain curve) is equal to 7 MPa for the virgin NBR compression moulded and 5.8 MPa for virgin NBR calendered and compression moulded.  $E(100\%)$  (as the slope of the secant at 100% strain) is equal to 4MPa for the virgin NBR compression moulded and 2.5MPa for virgin NBR calendered and compression moulded (see Figure 66). According to Boonstra et al. [319] this could be attributable to the carbon black dispersion. A better dispersion of the carbon black leads to a smaller quantity of occluded rubber which can contribute to deformation and to a greater surface area of the filler to which the polymer can adhere, leading to an increase in the stress at break. As the carbon black dispersion in the elastomeric matrix increases, the ultimate properties and the elastic modulus increase [318]. As regarding the reduction of the elastic moduli for the virgin NBR calendered and compression moulded which respect to that compression moulded, it could be attributable to a higher fraction of occluded rubber due to the lack of calendaring process. In other words, the calendaring process implies a double effect on the material: on one side it improves the ultimate tensile properties and the Young's modulus by a better dispersion of the carbon black, on the other hand it softens the compound as it dissolves the macromolecular structure and reduced the occluded rubber fraction.

The 20% recycled NBR compound processed by calendaring and compression moulding process shows a stress strain curve similar to that of virgin NBR processed likewise with slightly lower ultimate properties, and equal tensile moduli ( $E$  and  $E(100\%)$ ) as shown in Figure 66.

Stress and strain at break are significantly reduced for a presence of 80% of recycled NBR. The material obtained by mixing in the calendaring process recycled NBR and virgin unvulcanised NBR 20% shows the lowest stress at break and secant elastic modulus at 100% strain, and strain at break equal to compression moulded Virgin NBR. This material is the one with the lowest crosslink density (as shown in Figure 64) due to the presence of 20%wt of uncured NBR that promote the macromolecules alignment achieving high elongation at break. For the same reason, 80% recycled NBR processed by calender shows the lowest moduli and the lowest stress at break.

When the same material (80% recycled NBR) is processed also by compression moulding, its mechanical properties are markedly improved due to the cure of the unvulcanized rubber fraction according to the swelling behaviour (Figure 64).

As regards the 100% recycled NBR, the industrial scraps processed only by calendaring process show a tensile behaviour similar to that of 80% recycled NBR calendered and compression moulded with a slight stress and strain at break reduction and equal elastic moduli (Figure 66).

The same material processed by calendaring process followed by compression moulding shows a stiffer behaviour (highest secant elastic modulus at 100% strain as shown in Figure 66) and marked strain hardening. This could be attributed to a lower macromolecular mobility, which however has not been detected in terms of crosslink density increase by the swelling test nor in terms of alteration of chemical structure due to aging

by the FT-IR spectrum. It is then possible to relate this macromolecular mobility reduction to a higher entanglements' presence.

The 100% recycled NBR calendered shows lower stress at break and secant elastic modulus at 100% strain but higher strain at break than the same material calendered and compression moulded because its macromolecular network mobility is not reduced by the compression moulding.

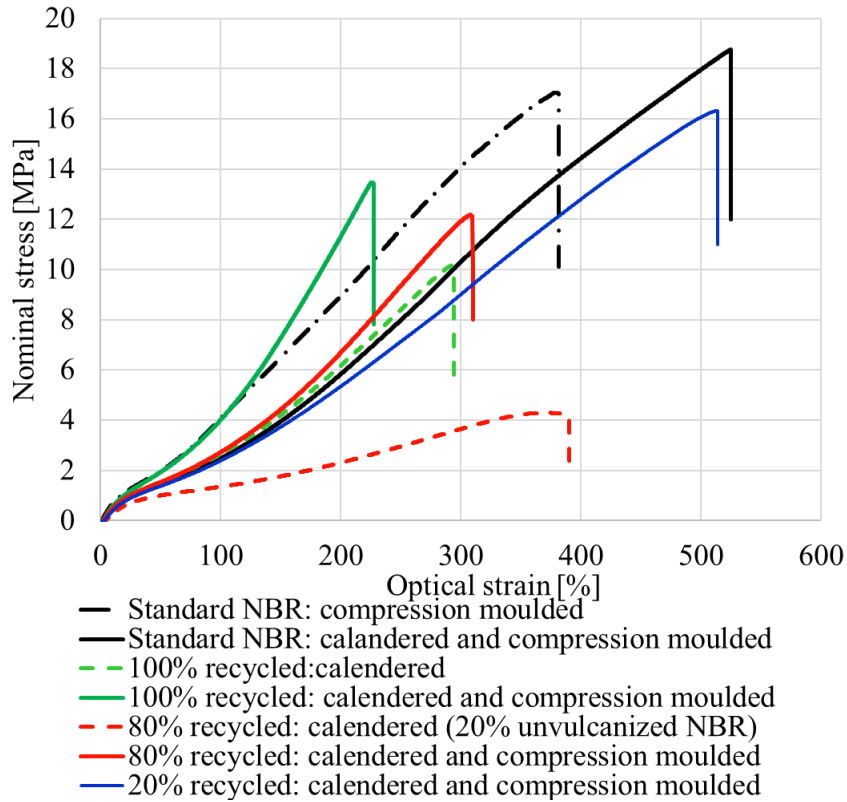


Figure 65 Tensile stress optical strain mean curve for each material (100/mm/min, ISO 37 type 2).

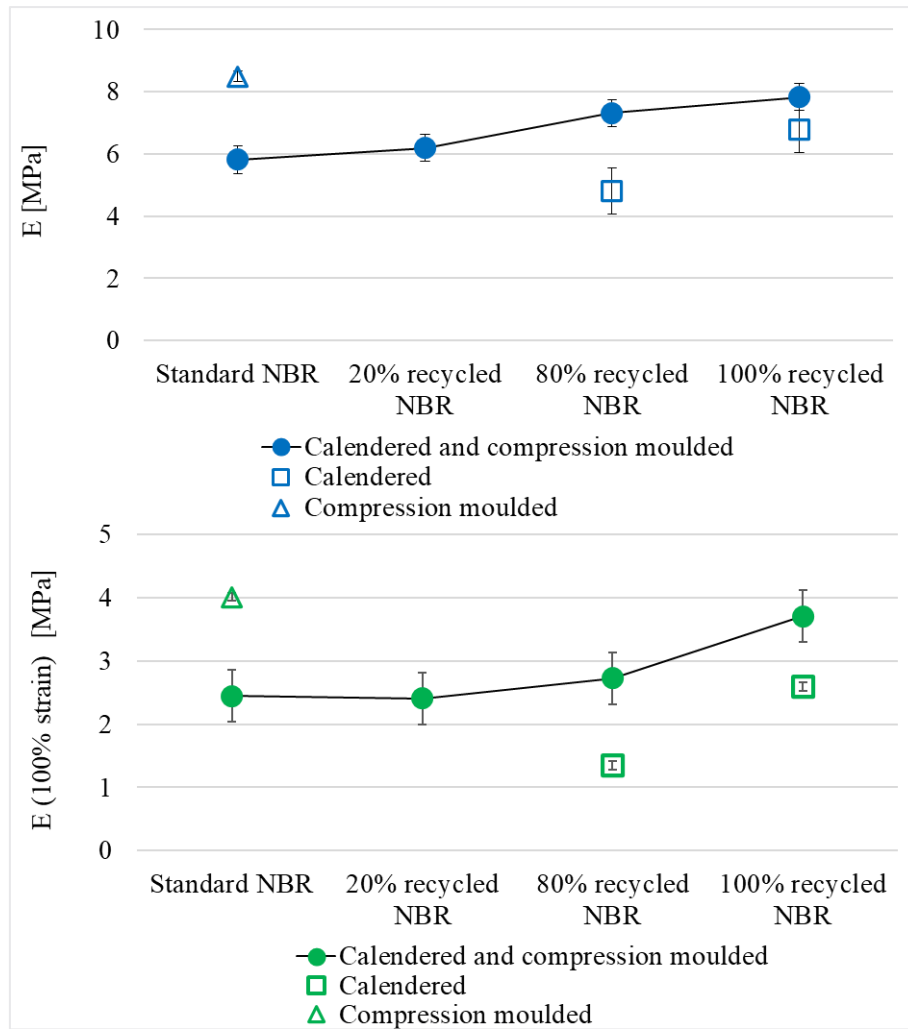


Figure 66 Tensile tangent modulus ( $E$  [MPa]) and tensile secant modulus at 100% optical strain ( $E(100\% \text{ strain})$  [MPa]).

### 3.3.1.3. Compression Test

Figure 67 shows the compression stress strain curves of the materials subject to compression moulding that allowed to obtain specimens of the required thickness. It is possible to notice that the calendered and compression moulded NBR 100% recycled requires the highest compressive stress to achieve a strain value of 50%. This could be due to its highest crosslink (see Figure 64) and entanglement density. As general trend is it possible to state that with increasing the amount of recycled NBR, the compression resistance at 50% strain increases. Standard NBR deviates from this trend. Calendered and compression moulded standard NBR require a compression stress lower than that of 100% recycled NBR and higher than that of 80% recycled NBR, while compression moulded standard NBR shows a compression stress strain curve similar to that of 80% recycled NBR.

The calendering process on standard NBR makes the compound softer at high strain but with higher compression elastic modulus  $E$  [MPa] (defined as the slope of the first linear section of the stress-strain curve) as shown in Figure 68.

At large deformations the addition of recycled NBR initially makes the material softer (drop from standard NBR to 20% recycled NBR) after which as the amount of recycled NBR increases the material becomes more

rigid until it exceeds the Standard NBR. This trend is compliant to that of crosslink density shown in Figure 64.

The effect of the calendering process carried out on the not yet vulcanized material (virgin) and on the vulcanized material (recycled) is different: in the first case the macromolecular structure has a clearly more viscous than elastic behaviour, while after the curing the material has a more elastic than viscous behaviour. For this reason, calendering process initially crumbles the cured material into small pieces with consequent reduction in the macromolecular weight. After several passages in the calender, the crumbles of cured rubber are able to return to being a cohesive material. As regards the compounding a fraction of vulcanized rubber to an uncured virgin rubber fraction, during the calendering process the uncured rubber fraction acts as a viscous matrix within which the vulcanized NBR fraction is dispersed.

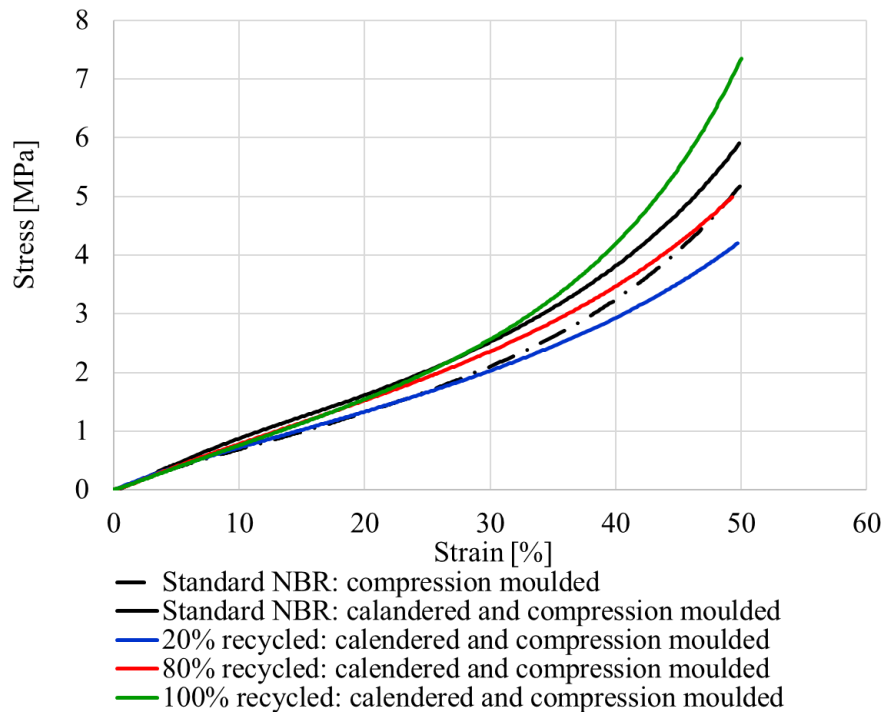


Figure 67 Compression stress-strain curves mean curve for each material ( 10mm/min, ISO 7743 [121])

Unlike what is shown in the tensile modulus of elasticity, the compressive modulus of elasticity of recycled and calendered materials slightly decreases for a recycled rubber fraction of 20% and then it remains about constant as shown in Figure 68. It is interesting to highlight that the compression elastic modulus of the recycled NBR in different amounts is equal to that of virgin NBR compression moulded.

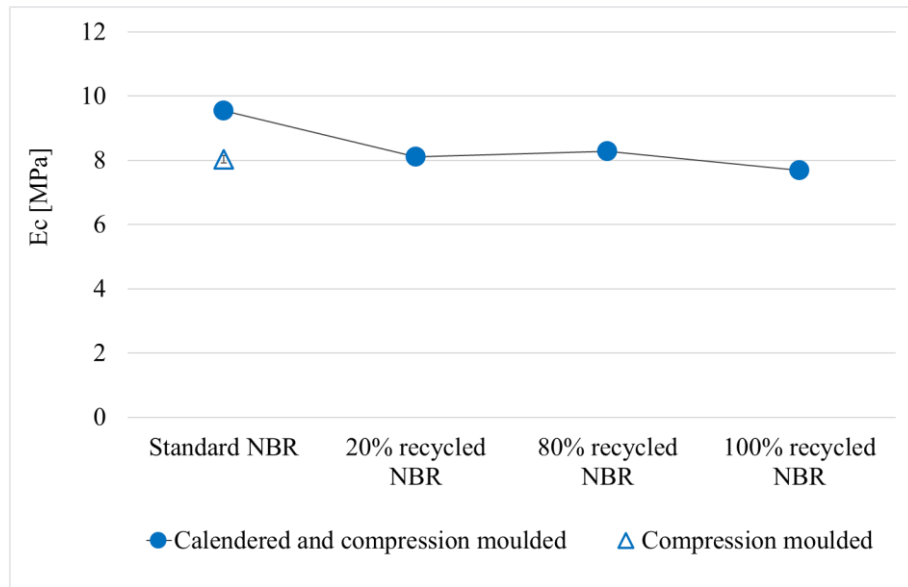


Figure 68 Elastic compression modulus.

### 3.3.1.4. Compression Set

To determine the effect of recycled NBR on the capability of the material to recover an imposed deformation, the compression set test was carried out. The experimental results are shown in Figure 69. It was found that the presence of recycled rubber up to a value of 80% does not affect significantly the compression set (whose value remains about 20%), but a slight peyorative effect was evidenced for 100% recycled NBR whose compression set is 24%.

This could be attributable to the highest crosslink and entanglement density that reduces the mobility of rubber chains in recovering the imposed deformation. The same correlation between crosslink density and compression set was found also by Mostafa et al. [320], Van Der Schuur et al. [321] and Zhao et al. [317].

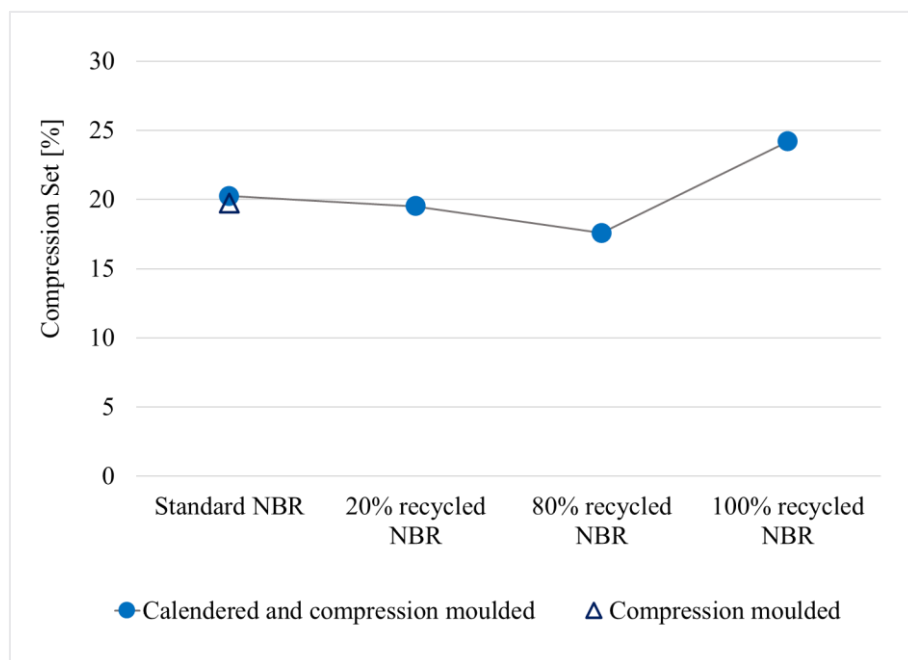


Figure 69 Compression set (100°C, 24h, compression strain 25%)

### 3.3.1.5. *Hardness test*

Hardness is defined as material resistance to penetration in specific conditions, the hardness of an elastomer is more accurately thought of as two relative properties: Intrinsic hardness and processed hardness.

As a result of chemical structure, each elastomer has its own intrinsic hardness. This inherent hardness can be modified via compounding and vulcanization. The hardness of the rubber articles obtained via injection or compression moulding process (processed hardness) is mainly influenced by crosslinking density. The more crosslinking a given material undergoes during vulcanization, the harder the mould material will be [321], [322]. When evaluating the potential effectiveness of a moulded article, processed hardness is one of the most common evaluation criteria in the rubber industry.

Unfortunately, hardness is also one of the less consistent concepts as the most used measuring scales have only limited comparability. There is no single “universal hardness” unit, so it is often impossible to trace a clear and simple relationship between the readings on two different scales, even when the samples to be measured are identical. The most used rubber test are: Shore hardness and International Rubber Hardness Grade (IRHD).

Experimental results of hardness measured in Shore A and micro IRHD are reported in Figure 70.

The used virgin NBR is commercialized with a nominal hardness 65+/-5 SH A, it is possible to notice that the hardness Shore A of all tested compound is in the tolerance admitted range. It is worth wide to highlight that one of the most important properties, i.e. the hardness is not affected by the presence of different amounts of recycled NBR. As expected, the calendered 80% recycled NBR (with 20% of unvulcanized NBR) shows a hardness value clearly lower than the nominal value and is out of tolerance. This is due to the relationship between hardness and crosslinking density for which a lower degree of crosslinking given by the presence of 20% of uncured NBR also leads to a decrease in hardness.

The microhardness IRHD is slightly lower than the hardness SH A for all tested compounds except for the 20% recycled NBR compound which shows a microhardness value markedly lower. This could be related to the different test configurations: hardness in SH A is measured after a load application for 3 seconds while micro hardness in mIRHD is measured after a preload application (5 seconds) and a load application (30 seconds). Due to the viscoelastic nature of rubber, a longer time of application of a constant load allows the material to relax. The material with a lower crosslink density relaxes more showing resulting in a lower hardness.

Regarding the compounds subjected only to calendering process, the 100% recycled NBR does not seem to be affected by the compression moulding because it is already fully vulcanized during the injection moulding process that generated the rubber scraps. The calendered 80% recycled NBR shows a microhardness mIRHD just below that of the same material processed also by compression moulding.

The influence of calendering process on virgin NBR before compression moulding leads a slight reduction of hardness [mIRHD] due to a better distribution and dispersion of carbon black particles (decrease of occluded rubber and increase of bound rubber). This finding is in agreement with the crosslink density and tensile modulus results.

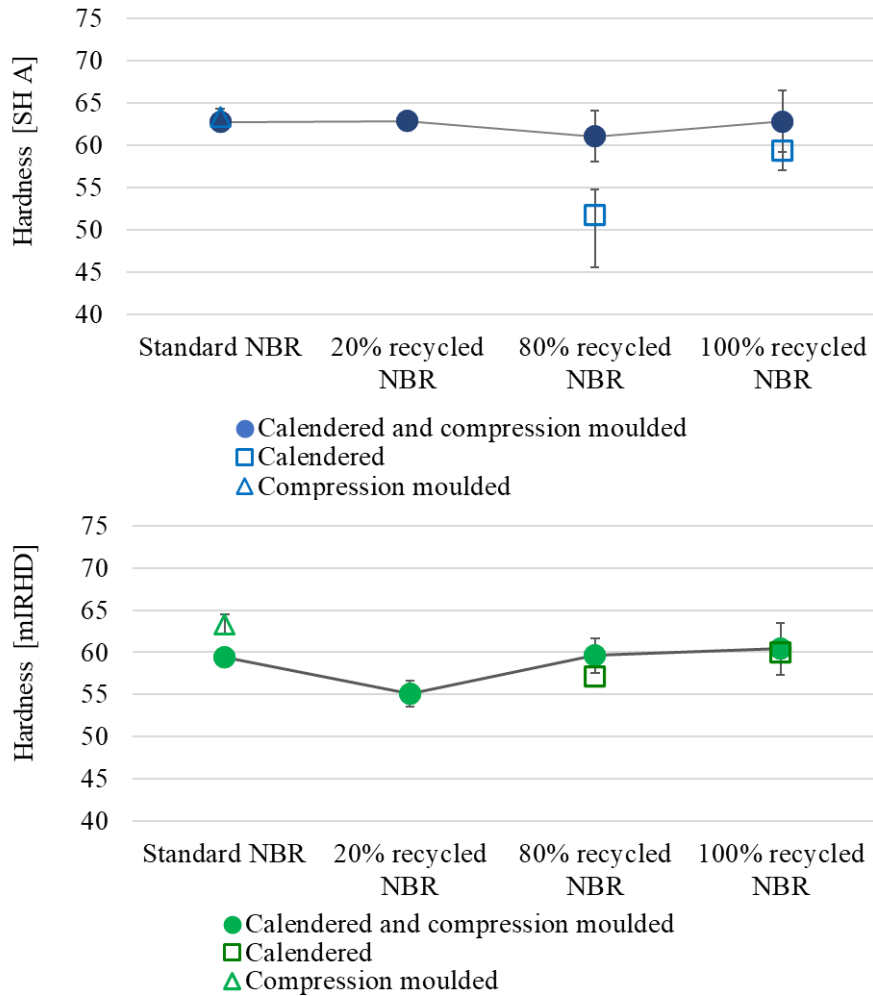


Figure 70 Hardness values in Shore A and microhardness values in mIRHD.

### 3.3.1.6. ATR-FT-IR Results

Original spectrum of the NBR compound is shown in Figure 71. By way of example, Virgin NBR is presented. The spectrum is dominated by the following main peaks:

- 990-960  $\text{cm}^{-1}$  attributable to C-H stretching and Deformation Vibrations of trans olefin (-CH=CH-).
- 1000-1050  $\text{cm}^{-1}$  is from silica. NBR has silica as one of its reinforcing fillers [309].
- 1390-1370  $\text{cm}^{-1}$  related to symmetric  $\text{CH}_3$  vibration.
- 1440-1410  $\text{cm}^{-1}$  which represents the  $\text{CH}_3$  deformation vibration overlapped with  $\text{CH}_2$  scissor vibration.
- 1550-1600  $\text{cm}^{-1}$  related to something not attributable to the structure of NBR. It is probably related to additives or accelerators of vulcanization process.
- 2260-2220  $\text{cm}^{-1}$  in which C=N stretching is occurring.
- 2800-3000  $\text{cm}^{-1}$  which are the absorptions associated with C-H symmetric and asymmetric stretching of  $\text{CH}_3$  and  $\text{CH}_2$  groups, respectively.

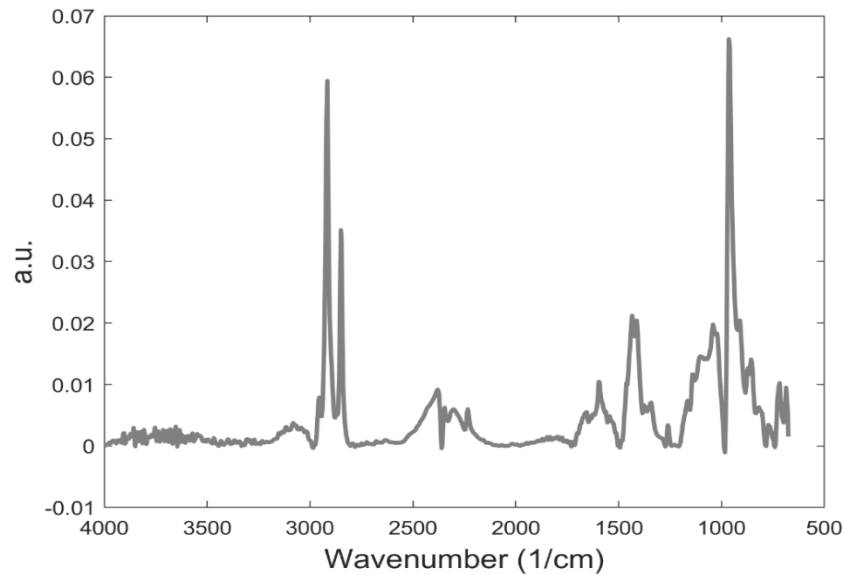


Figure 71 Typical FT-IR spectrum obtained by NBR is used in this study.

#### PCA Results

The 24 collected spectra have been retrieved in a single matrix,  $24 \times 863$  (Samples  $\times$  Wavenumber), and imported in Matlab environment for the application of multivariate analysis. PCA was applied overall spectral region after the pre-processing previously described. Figure 72 shows the score plot of PC1 vs PC2 (a), and PC1 vs PC3 (b). The three first components explain the 82% of the total variability, and we can note immediately that there is no separation between the several types of samples. In fact, the different sample categories overlap with each other, in the score plot of PC1 vs PC2 as well as for PC1 vs PC3. This means that there are no differences between the recycled rubber fraction, with the virgin one. Moreover, the type of process does not affect the spectra. Samples are distributed randomly without the formation of clear and tight clusters; the variability is not attributable neither to the type of the process, neither to percentage of the recycled fraction. Therefore, in the course of the recycling process, no chemical changes were observed as a result of oxidation.

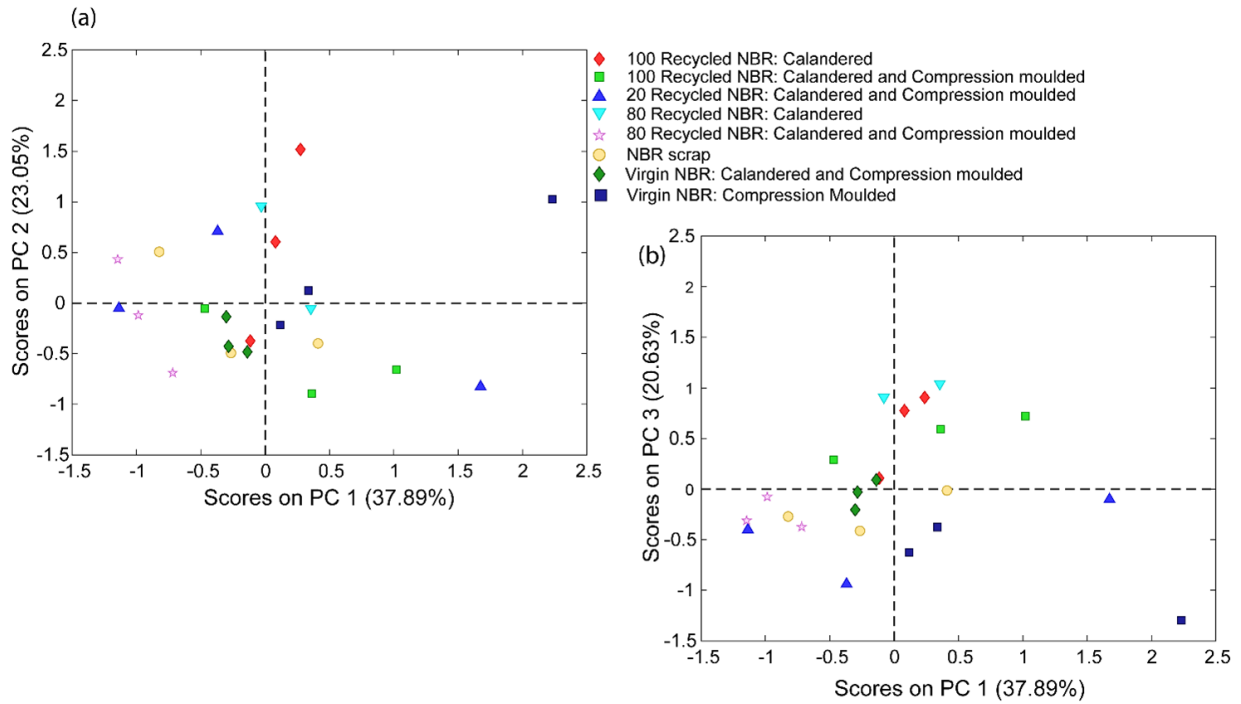


Figure 72 Score plot of PCA was carried out on 24 FT-IR spectra collected in this study. PC1 vs PC2 (a) is presented, as well as PC1 vs PC3 (b).

### 3.3.2. EAF slag filled recycled NBR characterization

#### 3.3.2.1. X-ray fluorescence spectroscopy results

The EAF slag chemical composition determined by XRF is reported in Table 21. As expected, the main oxides composing the slag are iron oxide, calcium oxide, silicon oxide.

Also in this slag the basicity index IB4 is greater than 1, so according to Tossavainen et al. [242] a glassy phase preventing the heavy metals leaching would have been formed in the cooling phase.

Table 21 EAF slag chemical composition determined by X-ray fluorescence spectroscopy (XRF) and basicity indexes. All amounts are reported in [%wt]

SiO <sub>2</sub>	Al <sub>2</sub> O <sub>3</sub>	Fe <sub>2</sub> O <sub>3</sub>	MnO	CaO	MgO	P <sub>2</sub> O <sub>5</sub>	TiO <sub>2</sub>	Cr <sub>2</sub> O <sub>3</sub>	S	Na <sub>2</sub> O	K <sub>2</sub> O	F
13,8	2,5	35,5	6,2	29,0	9,6	0,5	0,4	2,0	0,0	0,5	0,0	0,1
Basicity [-]		CaO/Al <sub>2</sub> O <sub>3</sub> [-]		Al <sub>2</sub> O <sub>3</sub> /SiO <sub>2</sub> [-]		IB2 CaO/ SiO <sub>2</sub> [-]			IB4 CaO+MgO)/(SiO <sub>2</sub> +Al <sub>2</sub> O <sub>3</sub> ) [-]			
0,7		11,7		0,2		2,1			2,4			

#### 3.3.2.2. SEM/EDS analyses

Figure 73 shows the SEM-EDXS analysis of a metallographically polished EAF slag sample using back-scattered electron (BSE) mode. The phases morphology of the analysed slag shows fine phases and a coarser phase with an angular geometry. The presence of fine phases indicates that the slag has undergone a rapid cooling, a practice commonly used as it allows the formation of a glassy phase which reduces the leaching of heavy elements. From the SEM analysis with EDXS probe, 3 mineralogical phases have been identified. The fine ones have been identified as larnite (Ca<sub>2</sub>SiO<sub>4</sub>) and brownmillerite (Ca<sub>2</sub>(Al Fe)<sub>2</sub>O<sub>5</sub>), while the larger phases has been identified as chromite (Fe<sup>2+</sup>Cr<sub>2</sub>O<sub>4</sub>).

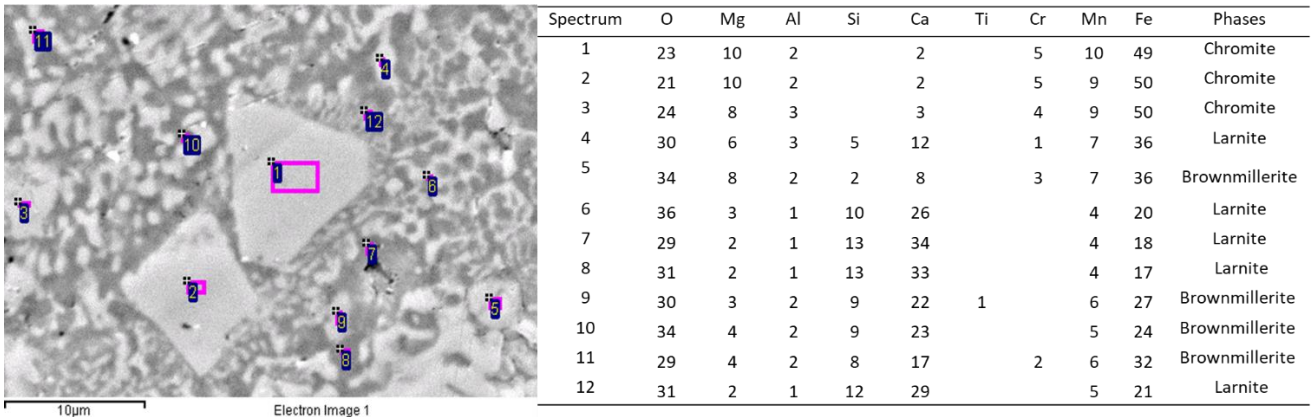


Figure 73 SEM back-scattered electron (BSE) image of slag microstructure [%wt] with its EDXS analysis on metallographically polished sample.

3.3.2.3. Leaching behaviour

The leaching test was performed on EAF slag in different grain size, lower than 4mm according to the standard CEN EN 12457-2 [72] and also on different fine grain size ranges (0-50µm, 50-100µm, 100-150µm and 150-300 µm). The leaching test results are shown in Figure 74. Is it possible to note that as general trend the smallest the slag grain size the higher the leaching of Mo and Cr and the eluate electrical conductivity; the leaching of V and pH values don't seem to be affected by the slag grain size.

In particular it is interesting to note that the leaching of Cr is very low (below 0,05mg/l) for the slag grain size lower than 4mm, it increases at about 0.2mg/l for a grain size 50-100µm, 100-150µm and 150-300 µm and it reach a value of 0.35mg/l for grain size 0-50µm. The Cr leaching is probably related to the Chromite phase.

It is important to highlight the slag is a very heterogenous material, so that it is possible to affirm that pulverized slag shows higher leaching that coarse slag, but it is not possible to certainly affirm that in general a slag in grain size 0-50µm releases greater amount of heavy metals than a slag in a grain size 150-300µm; further investigations have to be carried out.

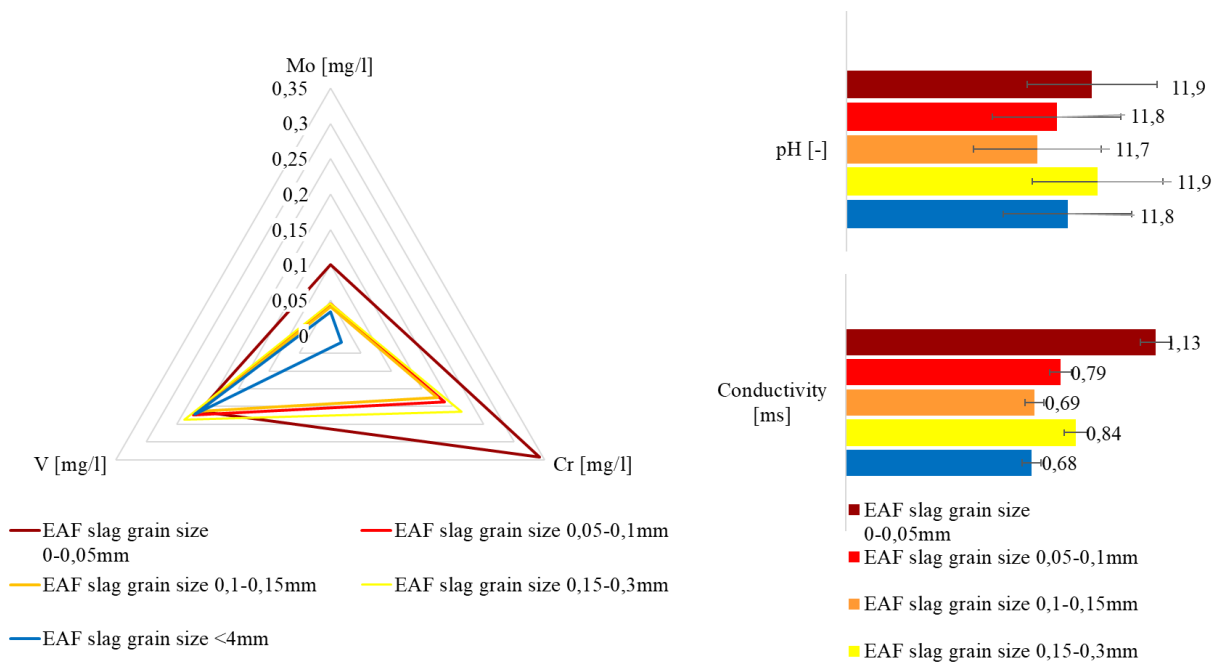


Figure 74 Leaching test CEN EN 12457-2 results of EAF slag in different grain size ranges. The maximum detected leaching value for each material is reported.

#### 3.3.2.4. Crosslink density

The crosslink density of 100% recycled NBR, 100% recycled NBR filled with EAF slag 10%[v/v] in a grain size 0-50 $\mu$ m and 50-100  $\mu$ m was determined by the Flory-Rehner equation [189], [323]. In order to assess the influence of the recycling process by calendering and the further compression moulding also the crosslink density of initial NBR scrap was determined.

It was found that the crosslink density of recycled NBR unchanged after the calendering process, and it slightly increases just for a slag content of 10% [v/v] in grain size between 50 and 100  $\mu$ m.

As expected the compression moulding leads an increase in the crosslink density for each material, but in this case that showing the highest crosslink density is that with slag grain size lower than 50 $\mu$ m.

The crosslink density of filled rubber can give an indication on the rubber-filler interaction due to the increase of bound rubber fraction [263]. The rigid and immobilized NBR layer around the filler particles surface is a consequence of the interaction between slag and NBR. The slag particles can be covered by rubber layer of high modulus and this in turn gets covered by clay layer of low modulus. The resultant rigid amorphous phase contributes to the high crosslink density and tensile modulus of the NBR composite [263]. Since the tested composited differ not for the filler amount but for the filler grain size, the finer grain size filler will have a greater surface area to which the rubber can adhere, so these results indicate that there is an interaction between slag and NBR.

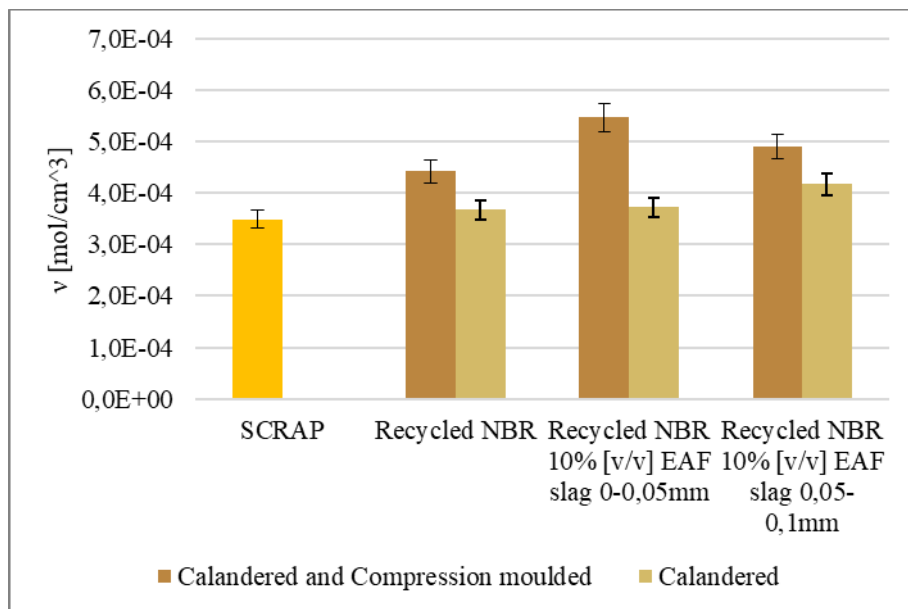


Figure 75 Crosslink density determined by Flory-Rehner equation (swelling in Toluene for 48h at room temperature).

#### 3.3.2.5. Hardness

Hardness test results are shown in Figure 76. The hardness of the recycled NBR is within the tolerance range of 60 $\pm$ 5 mIRHD, while the addition of rigid filler particles increases the composites hardness. In particular, at equal EAF slag content (10%v/v), the filler grain size affects the hardness value. The recycled NBR filled with slag grain lower than 50 $\mu$ m shows a hardness value of about 72 mIRHD, while that filled with the same amount of slag but in a grain size between 50 and 100  $\mu$ m is about 67mIRHD. This result can be attributed to

the different filler surface area to which the rubber can adhere resulting in greater constrained polymer fraction. Also this test leads to assume a good NBR-EAF slag interaction.

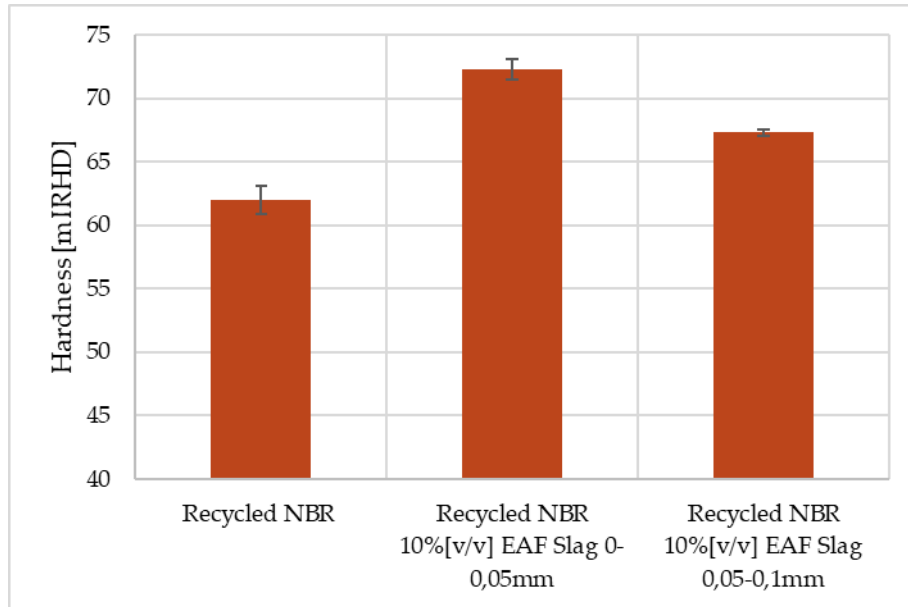


Figure 76 Hardness values in mIRHD.

### 3.3.2.6. Tensile properties

Tensile stress-optical strain curves of recycled NBR and recycled NBR filled with EAF slag 10%[v/v] in a grain size 0-50 $\mu$ m and 50-100 $\mu$ m is shown in Figure 77. As expected, it was found that the presence of 10%v/v of EAF slag as filler reduces the stress and the strain at break. In particular the material filled with EAF slag in a grain size 0-50 $\mu$ m shows a greater reduction in the tensile properties. This could be attributable to the EAF slag particles shape which is sharp (according to SEM observations) and for smaller granulometries precisely because the surface area is greater, the possibility of having edges that trigger a crack is also greater.

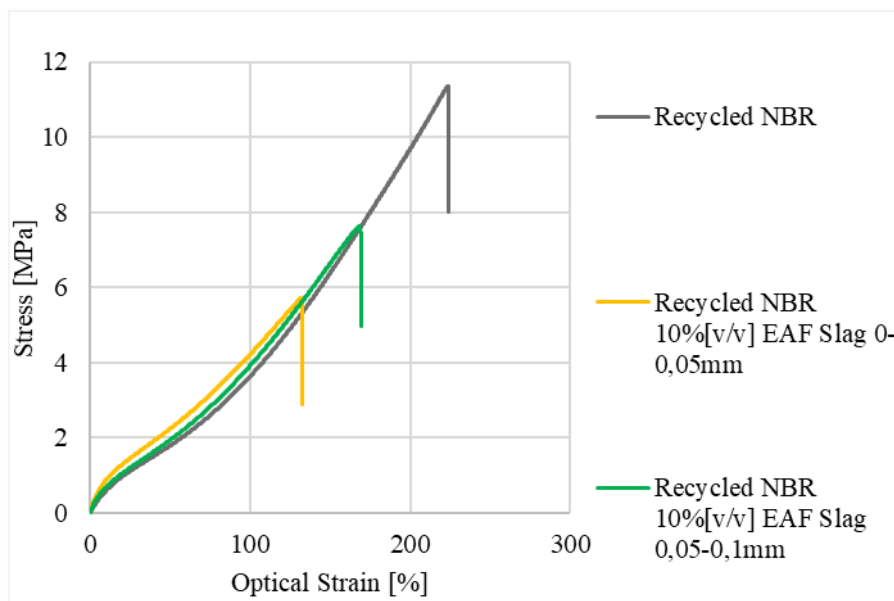


Figure 77 Tensile stress optical strain mean curve for each material (100/mm/min, ISO 37 type 2).

As regard the tensile modulus, the Young's modulus define as the slope of the first linear section of stress-strain curve ( $E$ ), and the secant modulus at 100% strain are shown in Figure 78.

It was found that both moduli are increased by the presence of EAF slag as filler, and in particular the recycled NBR filled with slag grain lower than  $50\mu\text{m}$  shows the highest moduli. This result confirms the hardness and crosslink density findings related to the increases in the rubber-filler surface interaction area which in turn confirms the NBR-slag interaction.

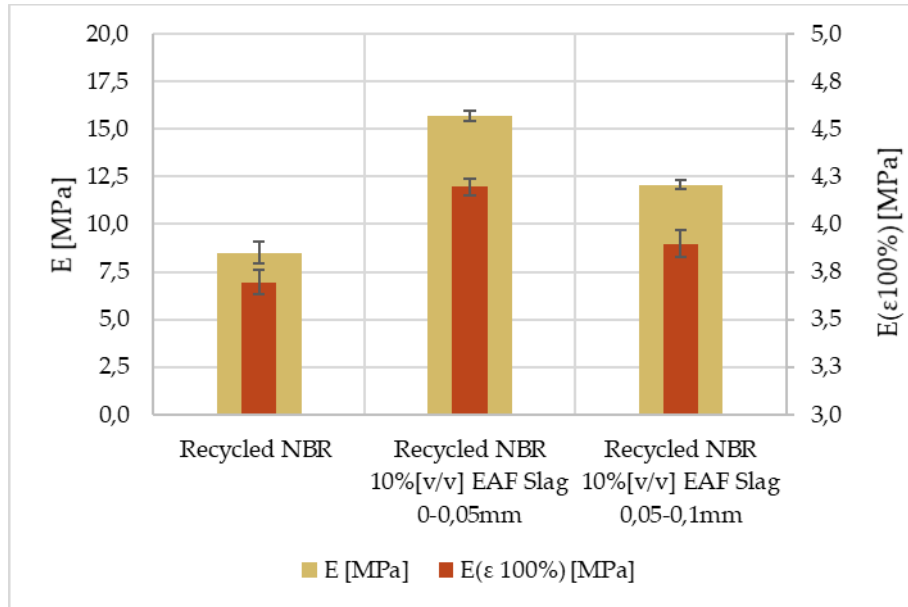


Figure 78 Tensile tangent modulus ( $E$  [MPa]) and tensile secant modulus at 100% optical strain ( $E(100\% \text{ strain})$  [MPa]).

### 3.3.2.7. Dynamic mechanical analysis

In order to further investigate the EAF slag-recycled NBR interaction, the dynamic mechanical analysis was carried out as dynamic moduli as function of tensile strain amplitude. In the range of 0.01 and 50% of strain amplitude it is possible to observe the low strain amplitude storage modulus plateau, a sharp reduction and a high strain amplitude storage modulus plateau for all tested materials. It was found that the low amplitude storage modulus plateau is higher for filled NBR, and in particular, also in this case the material filled with 10%v/v slag lower than  $50\mu\text{m}$  is that showing the highest one. This result is in agreement with hardness crosslink density, and tensile results and analogous considerations can be done. It is interesting to note that at a strain amplitude of about 0.1% the storage modulus decreases until it reaches the high amplitude plateau at about 50% strain. In this plateau the three materials show about the same storage modulus. It is possible to affirm that EAF slag filled NBR shows higher Payne effect than recycled NBR with no added slag. As regard the comparison between the recycled NBR filled with 10% slag in a grain size  $0-50\mu\text{m}$  and that filled with slag grain size  $50-100\mu\text{m}$ , the storage modulus fractional reduction is about the same assessed on about 82% (against the 75% reduction of recycled NBR with no added slag).

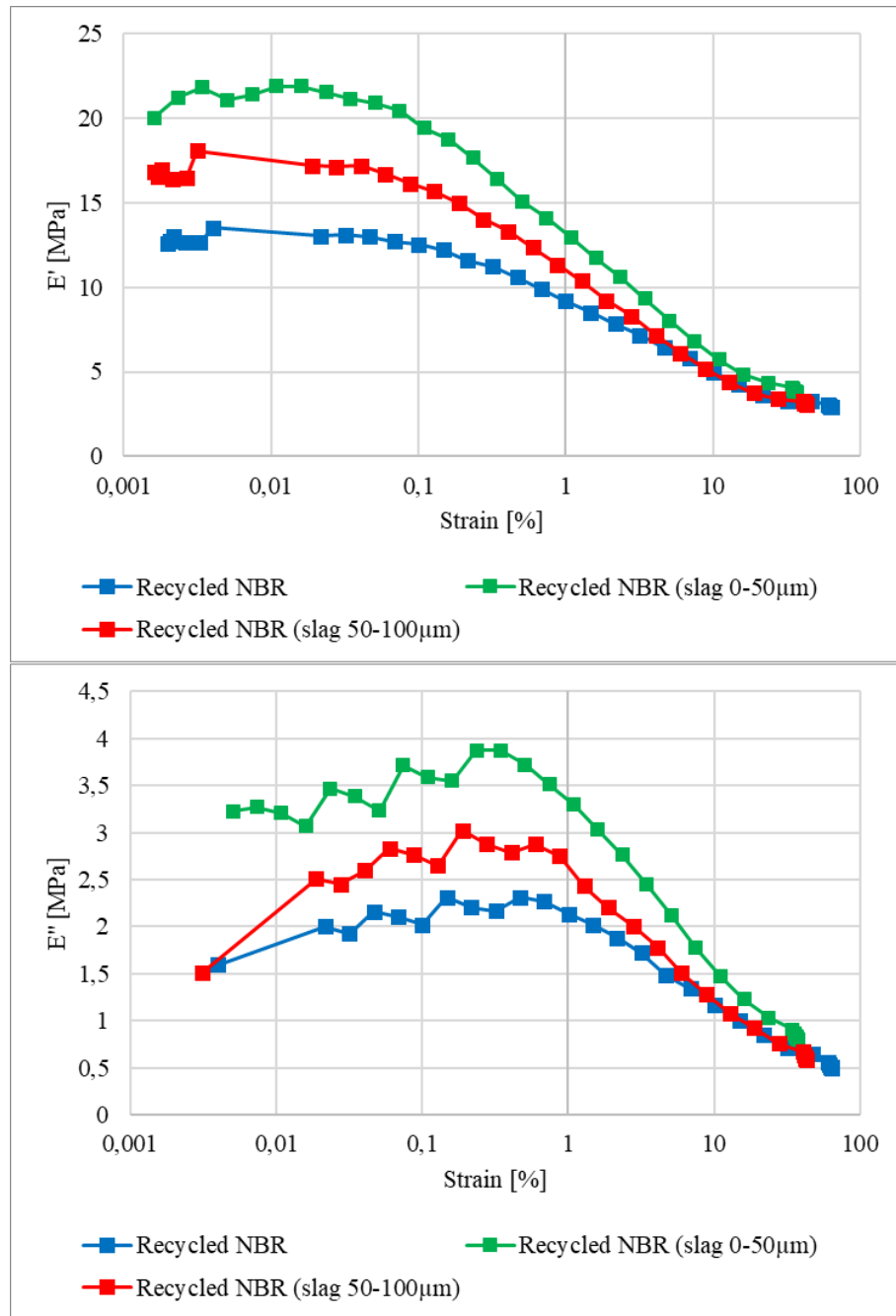


Figure 79 Storage modulus ( $E'$ ) and loss modulus ( $E''$ ) of recycled NBR, and EAF slag filled NBR 10% slag [v/v] in different grain size as function of strain amplitude (1Hz, room temperature).

Experiments of low amplitude storage modulus fractional recovery after the application of a large amplitude dynamic strain were performed for all the material investigated. The results are shown in Figure 80, where the low amplitude storage modulus, measured after the application of the large strain perturbation, is plotted against time. It was found that the presence of EAF slag makes recovery faster even though after a fast recovery the storage modulus settles to a constant value lower than that initially measured. In is interesting to note that the EAF slag filled materials shows a slightly higher and faster fractional recovery, especially that filled with EAF slag grain size lower than 50 $\mu\text{m}$ . This behaviour suggests that the presence of a rigid amorphous rubber layer constrained to the rigid slag particles promotes the elastic recovery after a large strain amplitude perturbation.

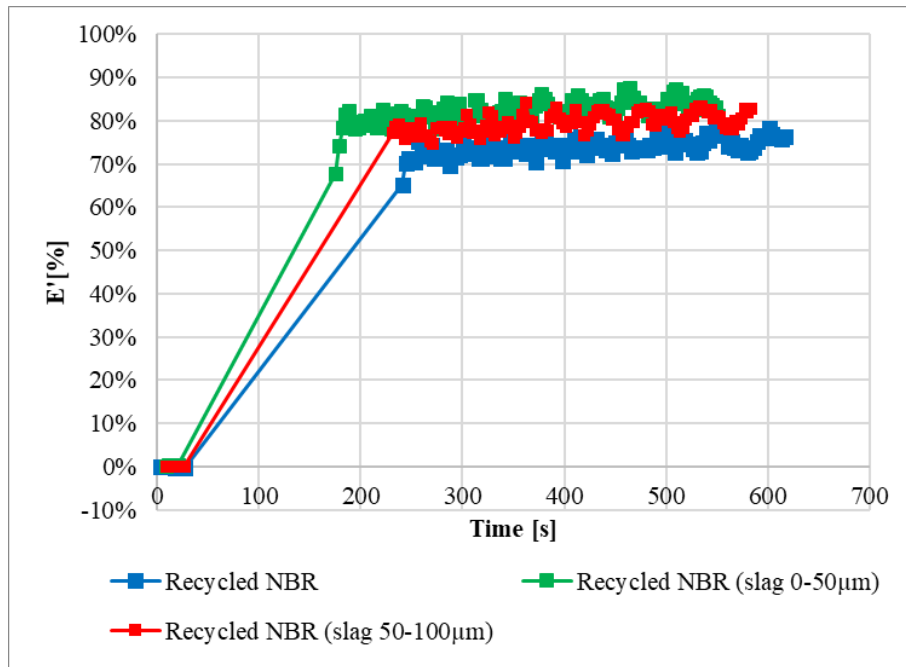


Figure 80 Fractional recovery of low strain amplitude storage modulus after the application of a high amplitude dynamic strain ((1Hz, room temperature) of recycled NBR, and EAF slag filled NBR 10% slag [v/v] in different grain size.

### 3.4. Conclusion

The amount of rubber scraps derived from rubber goods production (gaskets, seals, dumpers etc..) consists of about 20-30% by weight of the processed material, so it is necessary to enhance the potential of this material by developing new recycling techniques as well as new market for recycled rubber products.

This is becoming an increasingly critical problem in the sector as the recycling and reuse of general rubber goods amount to only 1.5% of the total waste generated [130].

The recycling and re-processing of crosslinked elastomers are difficult due to the three-dimensional chemical network. This network makes the material insoluble and non-melting after the vulcanization takes place.

The re-processing of crosslinked elastomers is optimal when the crosslinks formed during the vulcanization (C-S and S-S for sulfur curing) are cleaved without damaging the C-C bonds of the macromolecular chain [130], [132], [133]. Unfortunately, it is very difficult to only cleave crosslinks in the devulcanization process and the damaging of C-C bonds of the principal macromolecular chain usually occurs.

The process of devulcanization and degradation are both interconnected with each other. It is impossible to only cleave crosslinks or to only cleave the main polymer chain during a process. Both the devulcanization and degradation take place during the process. It is important to limit the degradation and increase the devulcanization to enhance the chances of rubber recycling or reusing.

In the present research the NBR scraps are recycled via calendering process at room temperature with no additives. Obviously, as the fraction of recycled rubber increases, the possibility of creating complex geometries decreases due to an ever-greater degree of crosslinking, however for simple geometries and for specific applications it is possible to replace even only partially virgin rubber with recycled industrial waste. This rubber recycling method, according to the best knowledge of the authors, is not reported in any literature work and it doesn't require any specific tool since the calender (or open mixer) is a machine of common use in the rubber industry.

The main findings can be summarized as follow:

- 1) Influence of the recycled rubber fraction at equal process (calendering and compression moulding):
  - The crosslink density determined by the Flory-Rehner equation on swelling data decreases slightly for a 20% recycled NBR before settling on an increasing trend. This behaviour could be attributable on one side to the mechanical devulcanization and on the other side to the increasing amount of material subjected to a double compression moulding process.
  - ATRFT-IR spectra analysis by PLA revealed no changes in NBR chemical structure as a result of oxidation and/or aging.
  - The capability to recover an imposed deformation remains unaffected up to an 80% recycled NBR
  - The elastic modulus slightly increases in tension, while it remains about constant in compression.
  - The hardness measured both ins Shore A and mIRHD remains within the tolerance of 60+/-5 points.
  - The presence of 20% of recycled NBR does not affect significantly the tensile stress and strain at break that are reduced for higher amount of recycled NBR.
- 2) Influence of production methods:
  - Calendering process on uncured virgin NBR improves the mechanical properties due to a better distribution and dispersion of carbon black.
  - Compression moulding does not affect the crosslink density and elastic modulus but makes the material stiffer at high strain both in tensile and compression loading.
- 3) Influence of EAF slag content in different grain size ranges:
  - The crosslink density of recycled NBR is unchanged after the calendering process with respect to the NBR scrap. The compression moulding leads an increase in the crosslink density for each material, but especially in that filled with the finest slag grain size (lower than 50 $\mu$ m).
  - The addition of rigid filler particles increases the composites hardness. In particular, at equal EAF slag content (10%v/v), the filler grain size affects the hardness value. The hardness of the recycled NBR filled with slag grain lower than 50 $\mu$ m is higher than that filled with the same amount of slag in a grain size between 50 and 100  $\mu$ m.
  - The low amplitude storage modulus plateau is higher for filled NBR, and in particular, the material filled with 10%v/v slag lower than 50 $\mu$ m is that showing the highest one.
  - The presence of EAF slag makes recovery faster even though after a fast recovery the storage modulus settles to a constant value lower than that initially measured. The EAF slag filled materials shows a slightly higher and faster fractional recovery, especially that filled with EAF slag grain size lower than 50 $\mu$ m.
  - The obtained results suggest the existence of an interaction between NBR and EAF slag related to filler surface area.

With a view to circular economy, this study shows good results in the valorisation of industrial rubber waste through a simple technology.

#### 4. EAF slag as carbon black replacement for NBR

Carbon black is the most widely used reinforcing filler for rubber. The studies of the reinforcement mechanism of carbon black can be dated back to 1960s. However, the knowledge of its mechanism still remains fragmentary today. While normally the addition of particle charges in polymeric matrices increases the elastic modulus but reduces elongation, in elastomeric matrices the addition of carbon black increases both modulus and elongation at break. With the presence of carbon black, the physical properties of rubber compounds, such as tear and tensile strength, given can be improved. Carbon black increases the hardness and viscosity of rubber-based compounds and it is considered the most efficient additive among all filler materials [324].

Since the carbon black production derived from the partial combustion of heavy hydrocarbons, its carbon footprint is enormous [325]. It has been estimated that the production of 1 ton of carbon black implies the emission of 2.4 tons of carbon dioxide, compared to 0.8 tons of carbon dioxide per ton of cement during production [326]. Carbon black is made up of over 90% pure form of elemental carbon, which is made up of tiny, mostly spherical carbon atoms that fuse together into groups called aggregates. Several aggregates then group together as agglomerates which break down during the mixing period of the rubber. Normally, the diameter of the carbon black particle ranges from 10 nm to 500 nm [325].

Given the increased demand for rubber quality and the rising price of raw rubber and other component ingredients, the rubber industry has made great efforts to limit costs and increase competitiveness. There are several concerns regarding the traditional petroleum-based carbon black filler. On the one hand, the price of hydrocarbons sees a gradual increase every year. The cost of the raw material represents 30-35% of the total selling price of carbon black. On the other side, due to the non-degradability of the petroleum-based carbon black filler, it can cause serious environmental problems. The conservation of the environment is a permanent issue, much research is undertaken with the aim of reducing the dependence of the carbon black raw material on fossil fuels and transforming it into a sustainable material base. For these reasons, sustainable alternatives to carbon black are being studied such as rice husk ash, peanut shell powder etc.

In this study the EAF slag is proposed as substitute, or partial substitute to carbon black. A standard NBR (carbon black filled) has been compared with an NBR filled with EAF slag 100% and an NBR filled with EAF slag 50% and carbon black 50%. First of all for a safe reuse of the slag it is necessary to maintain under control the leaching behaviour, so that the leaching of slag incorporated into the rubber matrix has been measured confirming that NBR shields the slag particles preventing them from leaching. Then the comparison between the tree compounds has been carried out in terms of processability (rheometric curves and complex viscosity), mechanical properties (hardness, tensile test, compression test, stress relaxation and permanent set), swelling behaviour, thermal conductivity and tribological behaviour. The filler-rubber interaction has investigated as bound rubber, immobilized rubber fraction, and non-linear dynamic effect confirming the existence of slag-NBR interaction. From a mechanical point of view, it was found that the EAF slag filled NBR has the same mechanical properties of standard NBR with the same hardness. These preliminary results are promising to continue the research for the best compound formulation according to the final application.

##### 4.1. Materials

This characterization aims to compare the effect of slag as a substitute for carbon black at the same percentage by volume. This choice was made both to be able to investigate some characteristics more in depth, such as the slag-NBR interaction without the interference of the carbon black effects, and because the theory of

composites evaluates the filler effect in percentage by volume as the volume occupied by the two phases and their interaction surface are the determining factors in the characterization of composites. Given the large difference in density between carbon black and slag ( $1.8 \text{ g/cm}^3$  and  $3.7 \text{ g/cm}^3$  respectively), the formulation with the same percentage weight would introduce further variables, in addition to the large difference in particle size (3 orders of magnitude).

Three NBR composites were compounded by the industrial compounder Ligom Spa (Grumello del Monte, BG, Italy):

- Standard NBR 60 ShA
- NBR 100% Slag
- NBR 50% Slag 50% Carbon black

The detailed recipe is given in Table 22.

Table 22 Recipe of standard NBR, NBR 100%slag and NBR 50% slag at equal filler content by volume.

COD AS400	Description	NBR60 STANDARD		NBR 100%	NBR 50%
		phr	%wt	SLAG %wt	SLAG %wt
P.E3330GRN	EUROPRENE 3330 GRN	60,00	31,9%	23,3%	27,0%
P.NDN3350	NIPOL DN 3350	33,90	18,0%	13,2%	15,2%
CA.210	ZINC OXYDE	5,00	2,7%	1,9%	2,2%
CA.106	STEARINA	0,50	0,3%	0,2%	0,2%
PL.219	POLIPLASTOL 15	0,50	0,3%	0,2%	0,2%
AN.110	ANOX HB	1,00	0,5%	0,4%	0,4%
AN.113	MB2	1,00	0,5%	0,4%	0,4%
AN.721	WAX RIOVAX 721	1,80	1,0%	0,7%	0,8%
CA.257	CARBON BLACK SRF 772	60,00	31,9%	-	13,5%
PL.214	MESAMOL	14,00	7,4%	5,4%	6,3%
AC.66	RHENOGRAN S 80	0,40	0,2%	0,2%	0,2%
AC.MMTCS	POLYMER NBR TCS	10,00	5,3%	3,9%	4,5%
	EAF slag	--	-	50,2%	29,0%
	Filler content [%v/v]		21%	21%	21%
	Density [ $\text{g/cm}^3$ ]		1,20	1,63	1,43

In order to compare the mechanical properties of the EAF slag filled rubber compounds, a standard NBR 45 Shore A and a standard NBR 50 Shore A have been also characterized by compression test, tensile test, dynamic mechanical test and wear test.

EAF slag was supplied by the ASONEXT Spa (Ospitaletto BS, Italy) steelmaking plant. Slagging and cooling were performed in a standard way, i.e. without specific procedures aimed at confer specific characteristics to the slag.

EAF slag has been ground by the manual pulverizing mill HSM 100 provided by Herzog (Osnabrück, Germany) for 40 seconds and then sieved to obtain a grain size  $<100 \mu\text{m}$ .

The compounds were then compression moulded at  $160^\circ\text{C}$  to obtain test plates with a dimension of  $200 \times 200 \times 2$  mm from which samples for mechanical tests are obtained by mechanical punching and cylinder samples diameter 12mm thickness 6mm.

It was found that the hardness of the slag filled composites is lower than that carbon black filled. Since the hardness is a property by which the rubber compounds are classified, mechanical tests were also conducted on standard NBR with hardness equal to NBR 100% (named NBR 45,  $45 \pm 5$  SHA) slag and NBR 50% slag (named NBR 50,  $50 \pm 5$  SHA).

## 4.2. Methods

### 4.2.1. EAF slag characterization

#### 4.2.1.1. X-ray fluorescence spectroscopy

EAF slag chemical composition was determined by X-ray fluorescence spectroscopy carried out by the Thermo Scientific™ ARL™ PERFORM'X provided by Thermo Fisher Scientific™ (Waltham, Massachusetts, United States). EAF slag chemical composition is reported in Table 24.

#### 4.2.1.2. SEM-EDXS analysis

The morphological and elemental analysis of the phases is the analysis performed by the Scanning Electron Microscopy (SEM) integrated with Energy Dispersive X-ray Spectrometry (EDXS) [240].

A slag sample polished according to the standard metallographic procedure was analyzed by a SEM-EDXS (SEM Leo Evo 40, Carl Zeiss, Oberkochen, Germany; EDXS microprobe Link Pentafet Oxford mod 7060; Oxford Instruments, Oxfordshire, U.K.). In Figure 81 the SEM-EDXS analysis utilizing back-scattered electron (BSE) mode is reported.

#### 4.2.1.3. Leaching behaviour

The leaching test was conducted both on the composite materials and on the free slag in a grain size lower than  $100 \mu\text{m}$  (as in the composites), and in a grain size lower than 4mm (according to the standard CEN - EN 12457-2 [72]). The results are reported in Figure 83. The composite material plate was cut to a particle size of less than 4 mm and the slag dust lost from the cutting surface was removed to evaluate only the inertizing effect of the polymer matrix (Figure 81). As for the characterization of free slag, the amount of tested composite was calculated to maintain the 90 g of slag in a ratio of 1:10 with the liquid, according to the standard [72].



Figure 81 Samples subjected to the leaching test. a) free EAF slag (grain size lower than 100 $\mu$ m); b) free EAF slag (grain size lower than 4mm); c) NBR filled 100%slag cut in particle size of less than 4 mm; d) NBR filled 50%slag cut in particle size of less than 4 mm; e) standard NBR cut in particle size of less than 4 mm.

## 4.2.2. Compound Characterization

### 4.2.2.1. Thermogravimetric analysis (TGA)

The correctness of the slag and carbon black amount in the different compounds were verified retrospectively by thermogravimetric analysis (TGA). TGA scans are shown in Figure 84.

Samples of about 10mg mass were placed in a platinum crucible and heated in a thermobalance at rate of 10 °C/min from ambient to 560°C in Nitrogen atmosphere. When the sample mass became constant the sample is kept for 2 minutes at 300°C, and in Oxygen atmosphere is heated up to 800°C at 10°C/min in order to facilitate the carbon black and ashes content measurement.

### 4.2.2.2. Rubber process analysis (RPA)

The influence of EAF slag on the processability characteristic is assessed by the parameters extrapolated by the rheometric curves, determined by Rubber Process Analyzer (RPA) D-MDR 3000 (Montech Werkstoffpruefmaschinen GmbH, Germany). The preheating temperature of the rheometer plates is 160°C and an oscillating force is applied to the sample with fixed oscillating amplitude. Testing time is about 20 minutes. Three measurements for each compound were tested.

The rheometric curve gives indications about the vulcanization kinetics, therefore it is possible to evaluate the degree of crosslinking (%) through the normalization of the rheometric curves according to Equation 34.

$$\text{Degree of crosslinking}[\%] = \frac{M_i - M_{min}}{M_{max} - M_{min}}$$

Equation 34

Where  $M_i$  is the measured torque at each time (i), and  $M_{min}$  and  $M_{max}$  are the minimum and the maximum detected torque respectively associated to 0 and 100% degree of crosslinking.

By RPA the flow behaviour of the compounds was investigated in frequency sweep. The viscosity has been determined in oscillating mode ( $\omega = 300 - 6 \text{ rad s}^{-1}$ , frequency (f) = 47.75 - 0.995 Hz), amplitudes sweep 0.1°. The sample is preheated for 4 minutes prior measurement.

Viscosity has been determined in frequency sweep in 2 modes: without preshearing during preheating the amplitude sweep is 0.201°, f = 0.5 Hz; with preshearing during preheating the amplitude sweep is 3°, f = 5 Hz).

### 4.2.2.3. Hardness test

The compounds' hardness was measured according to the Shore A scale. The Shore A measurements were carried out by an automatic hardness tester Shore PC type A provided by Gibitre Instruments (Bergamo, Italy) according to the standard ISO7619-1 [276]. Hardness test results are shown in Figure 89.

### 4.2.2.4. Compression test

Compression tests were performed on three samples for each material by a dynamometer (mod. 3366) provided by Instron (Pianezza, TO, Italy) at room temperature and a strain rate of 10 mm/min on cylindrical specimens with a nominal diameter of 12mm and a height of 6mm. Three loading and unloading cycles at 25% deformation were performed before the compression stress strain curve. The compression test was performed

according to the standard ISO 7743 [121]. Three measurements each compound were performed. Compression test results are shown in Figure 90 and Figure 91.

#### 4.2.2.5. *Stress relaxation*

Stress relaxation is assessed in compression by a dynamometer (mod. 3366) provided by Instron (Pianezza, TO, Italy) at room temperature on cylindrical specimens with a nominal diameter of 12 mm and a height of 6 mm. The stress relaxation is assessed as the stress loss [%] after 600 second at 25% imposed strain.

#### 4.2.2.6. *Permanent set*

The permanent set is determined in compression (compression set). It was determined by imposing a compression deformation of 25% on cylindrical samples (nominal diameter 12 mm and a height of 6 mm) for 24 h at 100°C. The compression set was determined according to the standard ISO 815 (test method A). Compression set was performed on three samples each material, the results are shown in Figure 94.

#### 4.2.2.7. *Tensile test*

Mechanical tensile tests were performed by an Instron dynamometer (mod. 3366) at room temperature and a cross-head rate of 100 mm/min on test pieces of 50 mm length (distance between the grips of about 30 mm) and 4 mm width according to the standard ISO 37:2017 type 2 [197]. The considered strain is the optical one in order to exclude the influence of the sample edges. The measurement is performed three times for each compound. Young's modulus has been determined as the slope of the stress-strain curve in correspondence with the initial linear section. Tensile test results are shown in Figure 95 and Figure 96.

#### 4.2.2.8. *Dynamic mechanical analysis*

Dynamic mechanical analysis performed by a Dynamic Mechanical Thermal Analyser Q800 by TA instruments (New Castle, United States) in the tensile mode at room temperature and a frequency of 1 Hz by varying the applied strain amplitude between 0,01% and 50% to observe the low and high amplitude plateau of the storage modulus. This test was performed twice on specimens of nominal dimension 2x5x30 mm. Storage and loss moduli as function of strain amplitude are shown in Figure 97. The Payne effect, as the storage modulus percentage reduction from the low deformation amplitude plateau to the high deformation amplitude plateau is shown in Figure 98.

#### 4.2.2.9. *Swelling test*

For the swelling test rectangular samples of about 500 mg were cut and immersed in toluene and tetrahydrofuran (THF) in sealed glass tubes for 48 hours at room temperature. The swelling coefficient is determined according to Equation 11.

The equilibrium swelling index is determined by crosslink density and the attractive forces between solvent and polymer. The theoretical extent of swelling is predicted by the Flory–Rehner equation [185], [189], [190] (Equation 12 and Equation 16).

Three samples were tested for each material; the swelling coefficient and the crosslink density of carbon black filled NBR, 100% EAF slag filler NBR and 50% EAF slag filled NBR are shown in

#### 4.2.2.10. *Bound rubber content*

The bound rubber content was determined by extracting the unbound materials such as the compounding ingredients and free rubber in toluene for 7 days (the solvent was renovated after 4 days) at room temperature, followed by drying under suction for 24 h at 40°C.

The uncured samples of about 250mg were wrapped in filter paper of known weight. The samples were weighed before immersion and after drying. Known the filler and rubber fraction (by TGA,) the bound rubber content (BRC %) was determined according Equation 22. The bound rubber content results are shown in Figure 100.

#### 4.2.2.11. Differential scanning calorimetry

The calorimetric glass transition was determined using differential scanning calorimetry (DSC). Measurements were carried out in the temperature range  $-90^{\circ}\text{C}$  to  $80^{\circ}\text{C}$ , in nitrogen atmosphere (purge) using DSC (Model: Q100 provided by TA instruments (New Castle, United States)). The samples were then cooled from room temperature to  $-90^{\circ}\text{C}$  at  $10^{\circ}\text{C}/\text{min}$  and held at this temperature for 60 min at the end of each cooling cycle and the measurement was carried out during subsequent heating at  $10^{\circ}\text{C}/\text{min}$ . The difference of heat flow between the sample pan filled in by sample and the empty reference pan was recorded with increasing temperature at the heating rate of  $10^{\circ}\text{C}/\text{min}$ .

The heat flow [mW] is converted to heat capacity ( $C_p$  [J/(g $^{\circ}\text{C}$ )]). NBR composites samples consist of a weight fraction of filler and a weight fraction of polymer; since only the latter is responsible for the variations associated to the glass transition, the heat capacity has been normalized to the polymer fraction as shown in Equation 23.  $\Delta C_p^*$  is determined in a temperature range of  $\pm 4^{\circ}\text{C}$  with respect to the glass transition temperature ( $T_g$ ).  $\Delta C_p^*$  is determined in a temperature range of  $\pm 4^{\circ}\text{C}$  with respect to the glass transition temperature ( $T_g$ ). DSC scan and  $\Delta C_p^*(T_g)$  values are shown in Figure 101 and Figure 102

#### 4.2.2.12. Thermal conductivity

The guarded heat flow meter DTC-300 (TA Instruments, New Castle, USA) operates at steady-state and employs a heat flux transducer to measure the heat flow through the specimen. A sample with a diameter of  $\varnothing 50$  mm and a maximal thickness of 2 mm is mounted between an upper "hot" and a lower "cold" plate. Considering the low thermal conductivity of rubber compounds, i.e.,  $0.15 - 0.4 \text{ W/mK}$  [327], a sample thickness of 1–4 mm is recommended, as otherwise it can take a long time before thermal equilibrium is reached. In addition, the contact resistance is kept low by applying a pneumatic load of 0.16 MPa and in case of no smooth surface thermal conductivity paste is used. During the measurement, the heat flows from the upper "hot" plate, throughout the specimen, to the lower "cold" plate, establishing a temperature gradient. After reaching thermal equilibrium, the temperature difference across the sample  $\Delta T$  and the resulting heat flow  $\dot{Q}$  are measured. Considering the gathered results, the sample area  $A$  and thickness  $d$ , the thermal conductivity  $\lambda$  is calculated by Fourier's law – see Equation 35.

$$\lambda = \frac{\dot{Q} d}{A \Delta T}$$

Equation 35

The heat flow meter method corresponds to ASTM E1530 [328] with an indicated accuracy of  $\pm 5\%$ . Based on the investigation of the thermal conductivity of seven rubber compounds [327], one sample is sufficient, as the deviation is in general significantly smaller than specified in the ASTM E1530 standard.

Thus, one sample with a diameter of 50 mm (thickness between 1 - 2 mm) was punched out of each crosslinked NBR test plate to measure the thermal conductivity at  $35^{\circ}\text{C}$ .

Thermal conductivity results are shown in Figure 103.

#### 4.2.2.13. Tribological properties

The wear tests were conducted on a CSM Instruments High Temperature In single way and reciprocating configuration. A 5 mm diameter flat pin (100Cr6) was used as a counterpart. A normal load of 5 N, a sliding speed of 80mm/sec, and a total sliding distance of 200m were applied at room temperature. During the test, the friction coefficient as a function of the sliding distance was recorded. After an initial peak the curve settles on a constant value taken as the steady-state coefficient of friction. Known the test parameters and initial and final weight of the sample, the specific wear rate ( $W_s$  [g/(Nm)]) was calculated according to Equation 25. COF and  $W_s$  values are shown in Figure 104.

Finally, the wear mechanisms were studied by SEM LEO EVO 40 VPS equipped by EDS probe. SEM images of wear truck are shown in Figure 105.

#### 4.2.2.14. Injection moulding trials

Thanks to the Italian Gasket Spa company (Paratico, BS, Italy), injection moulding tests were carried out in order to evaluate the processability of the compound not only at the laboratory level but also at the level of the industrial production process. The Process parameters adopted for the injection moulding trials of the compounds are reported in Table 23 and images of the moulded rubber parts are shown in Figure 107.

Table 23 Process parameters adopted for the injection moulding trials of the compounds.

PROCESS PARAMETER		NBR60 0% SLAG	NBR 50% SLAG	NBR 100% SLAG
INJECTION PRESSURE	[bar]	120	125	140
INJECTION SPEED	[%]	80	90	95
SCREW SPEED ROTATION	[%]	20	20	20
BARREL TEMPERATURE	[°C]	65	65	65
INJECTION TIME	[sec]	5	12	30
CURING TIME	[sec]	85	75	75
CURING TEMPERATURE	[°C]	190	180	180
CYCLE TIME	[sec]	114	n/a	n/a

### 4.3. Results and discussion

#### 4.3.1. EAF slag characterization

##### 4.3.1.1. X-ray fluorescence analysis

The chemical composition of the slag is strongly influenced by the production process and the raw materials used during the smelting process. As far as the mineralogy of the slag, its composition is very similar to that of effusive rocks; the microstructure is strongly influenced both by the chemical composition of the slag in the molten state and by the cooling rate [242], [329], [330].

The chemical composition of the EAF slag used as filler in this study is reported in Table 24. The main components of slags are iron oxide ( $Fe_2O_3$ ) and calcium oxide (CaO) and the basicity index  $IB_2 = CaO/SiO_2$  is equal to 3.2. It is important to note that if the basicity factor calculated as  $IB_4 = (CaO + MgO)/(SiO_2 + Al_2O_3)$

+ Al<sub>2</sub>O<sub>3</sub>) is greater than 1 (as in this case), the glass can form. The glass phase shelves the heavy metals and prevent them from leaching [242].

Table 24 EAF slag chemical composition determined by X-ray fluorescence spectroscopy (XRF) and basicity indexes. All amounts are reported in [%wt]

SiO <sub>2</sub>	Al <sub>2</sub> O <sub>3</sub>	Fe <sub>2</sub> O <sub>3</sub>	MnO	CaO	MgO	P <sub>2</sub> O <sub>5</sub>	TiO <sub>2</sub>	Cr <sub>2</sub> O <sub>3</sub>	S	Na <sub>2</sub> O	K <sub>2</sub> O	F
9,4	6,4	33,8	6,9	30,2	5,9	0,5	0,4	6,1	0,1	0,4	0,0	0,1
Basicity [-]		CaO/Al <sub>2</sub> O <sub>3</sub> [-]		Al <sub>2</sub> O <sub>3</sub> /SiO <sub>2</sub> [-]		IB2 CaO/ SiO <sub>2</sub> [-]		IB4 CaO+MgO)/(SiO <sub>2</sub> +Al <sub>2</sub> O <sub>3</sub> ) [-]				
0,7		4,8		0,7		3,2		2,3				

#### 4.3.1.2. SEM/EDS analyses

The literature reports the effects of slagging procedures on the mineralogical and morphological structure of EAF slags [69], [242]. The crystalline phases of EAF-C slag usually identified are larnite (Ca<sub>2</sub>SiO<sub>2</sub>), brownmillerite (Ca<sub>2</sub>(Al, Fe)<sub>2</sub>O<sub>5</sub>), wüstite (FeO), calcium silicate, silicon aluminates, gehlenite (Ca<sub>2</sub>Al (AlSiO<sub>7</sub>)), bredigite (Ca<sub>7</sub>Mg (SiO<sub>4</sub>)<sub>4</sub>), magnetite (Fe<sub>3</sub>O<sub>4</sub>), magnesioferrite (MgFe<sub>2</sub>O<sub>4</sub>) and manganese oxides [331].

The mineralogical phases identification is shown in Figure 82 . At low magnification it is possible to see a homogeneous microstructure with a few drops of steel (brighter); at high magnifications the chemical composition of the various phases was analysed by means of an EDS probe in order to determine their mineralogy. There are 4 phases: 2 mains of larnite and iron oxide; in smaller quantities chromite and very small areas of brownmillerite.

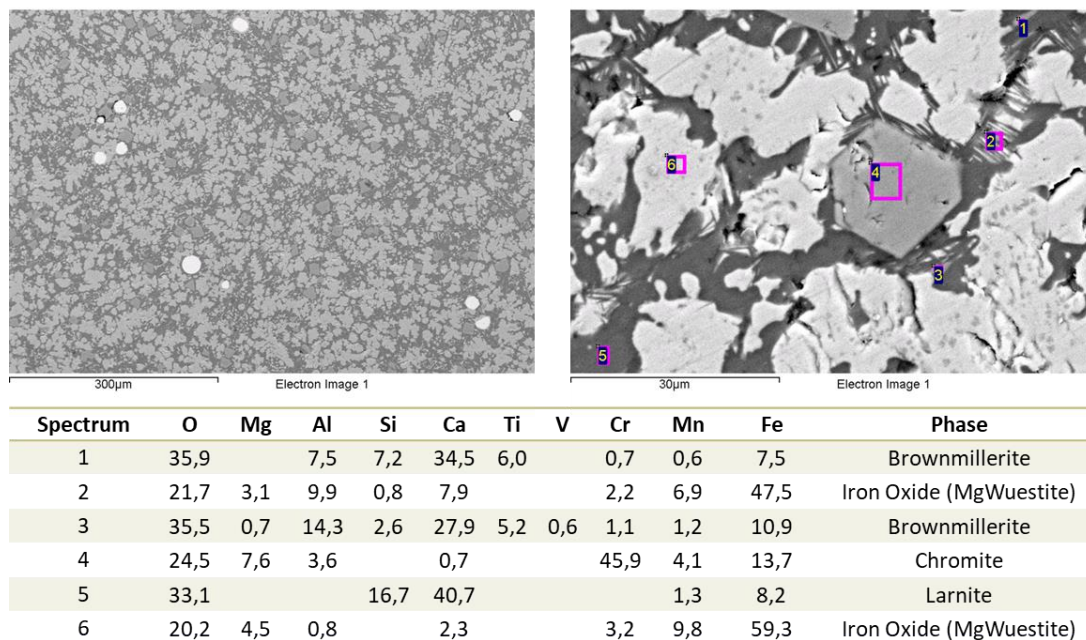


Figure 82 SEM back-scattered electron (BSE) image of slag microstructure [%wt] with its EDXS analysis on metallographically polished sample.

#### 4.3.1.3. Free slag and composite material leaching behaviour

The leaching behaviour of EAF slag both, free and incorporated into the NBR matrix is shown in Figure 83. It was found that, against expectations the, the EAF slag in coarse grain size (lower than 4mm) leaches more

than in fine grain size (lower than 100 $\mu$ m), especially Cr and V. This could be attributable to the high heterogeneity of the slag and to its sampling; nevertheless it is noticeable that the leaching of slag incorporated to NBR is well below the threshold limits imposed by the Italian legislation both as for material reuse (Ministerial Decree 5/4/06 [245]) and for disposal as inert material (Ministerial Decree 30/8/05 [246]). As regard pH and electrical conductivity, it is possible to notice that free slag presents the highest values, in particular the eluate electrical conductivity of fine EAF slag is markedly greater than that of slag in grain size lower than 4mm. As regards the compounds, the electrical conductivity increases proportionally to the EAF slag content.

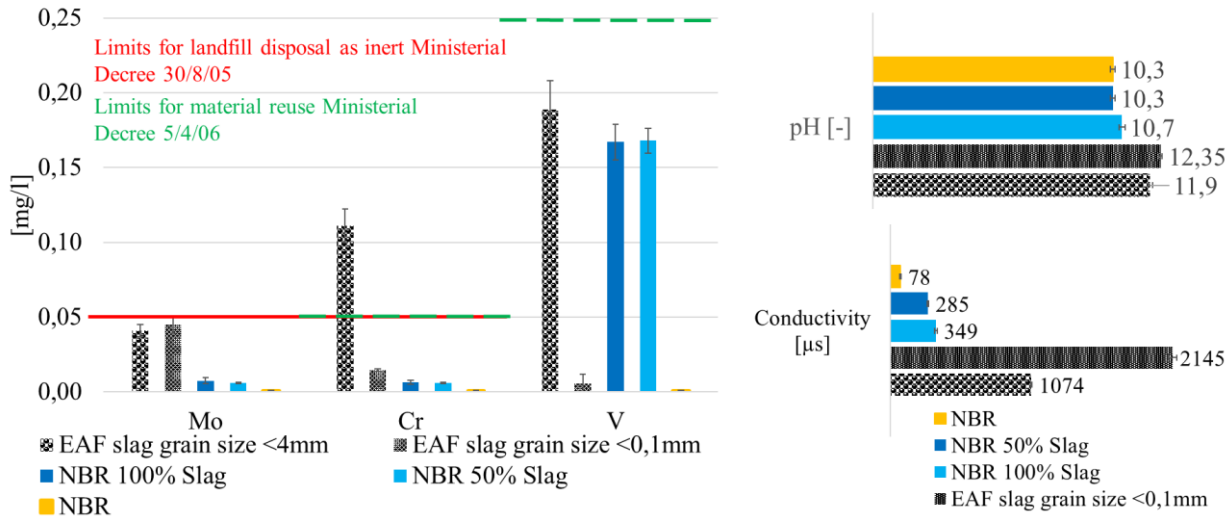


Figure 83 Leaching test CEN EN 12457-2 results of EAF slag (grain size <4mm), free EAF slag ((grain size <0.1mm), NBR filled with EAF slag at 30%v/v (grain size <0.1mm), EAF slag block incorporated into NBR and standard NBR.

### 4.3.2. EAF slag and carbon black filled NBR characterization

#### 4.3.2.1. Thermogravimetric analysis (TGA)

Sometimes the formulation of the analysed materials is not known, for this reason it is necessary to perform measurements to identify the components of the material and the quantities. In this case, the TGA allows to verify ex-post that the formulation of the compounds was consistent with the nominal ones, especially the quantification of carbon black and ash (including slag) is of interest. The percentage weight loss as function of temperature allows the identification of 4 main constituents of the compound: the first weight reduction in the range of about 200-400 $^{\circ}$ C is associated to volatile fraction; the second weight reduction is associated to the polymer fraction (400-550 $^{\circ}$ C); the last reduction is associated to the carbon black content (550-600 $^{\circ}$ C) before the scan assesses at a constant value which is associated to the ash fraction. It was found that NBR consists in about 3% ashes to be subtracted to the ash content of slag filled NBR to obtain the slag content. It was found that the actual carbon black and slag content coincides with the nominal ones (Figure 84).

As regards the standard NBRs at different nominal hardness (45, 50 and 60 SHA), the carbon black content was determined and it was found to be equal to 20%, 23% and 30% by weight respectively at equal ash content (3.5 %wt)

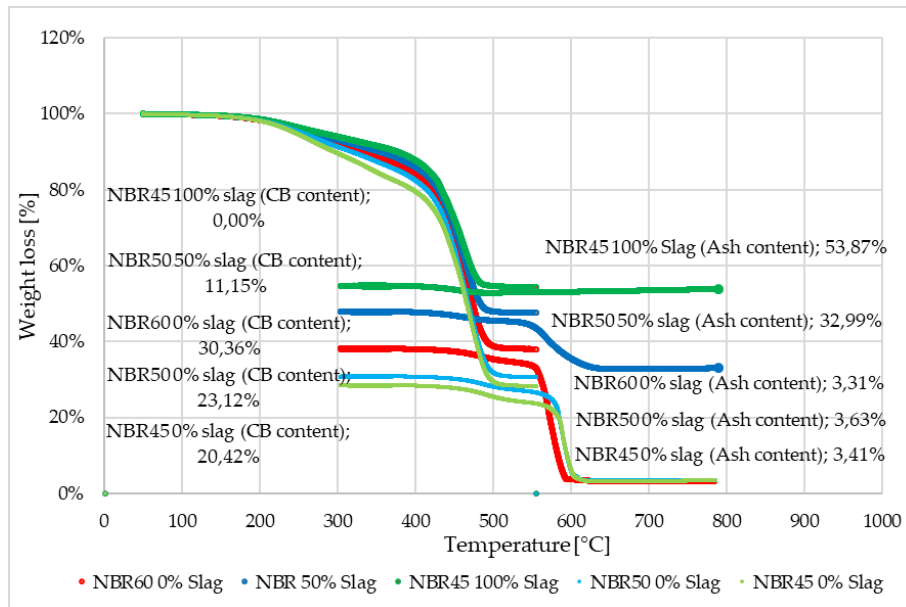


Figure 84 Thermogravimetric scan of carbon black filled NBR SHA60, SHA50, SHA45, 100% EAF slag filled NBR and 50% EAF slag filled NBR ((10 ° C/min, 25-550°C in Nitrogen atmosphere and 550-800° C in Oxygen atmosphere)

#### 4.3.2.2. Rubber process analysis

Figure 85 shows the rheometric curves of carbon black filled NBR, 100% EAF slag filled NBR and 50% EAF slag filled NBR as transmitted torque as function of time at 160°C.

The rheometric curve provides indications regarding the processability characteristics (phase 1), the curing kinetics (phase 2), and the physical properties (phase 3) of the tested materials.

The processability characteristics are related to the compound viscosity, the curing kinetics to the degree of crosslinking and the physical properties to the mechanical behaviour of cured material. From the comparison of the rheometric curves of carbon black filled NBR, 100% EAF slag filled NBR and 50% EAF slag filled NBR, the most evident difference is the reached maximum torque that increases with decreasing the slag content; this suggests that the mechanical performances of the slag filled NBR will be lower than the standard NBR with no added slag (as confirmed by mechanical characterization).

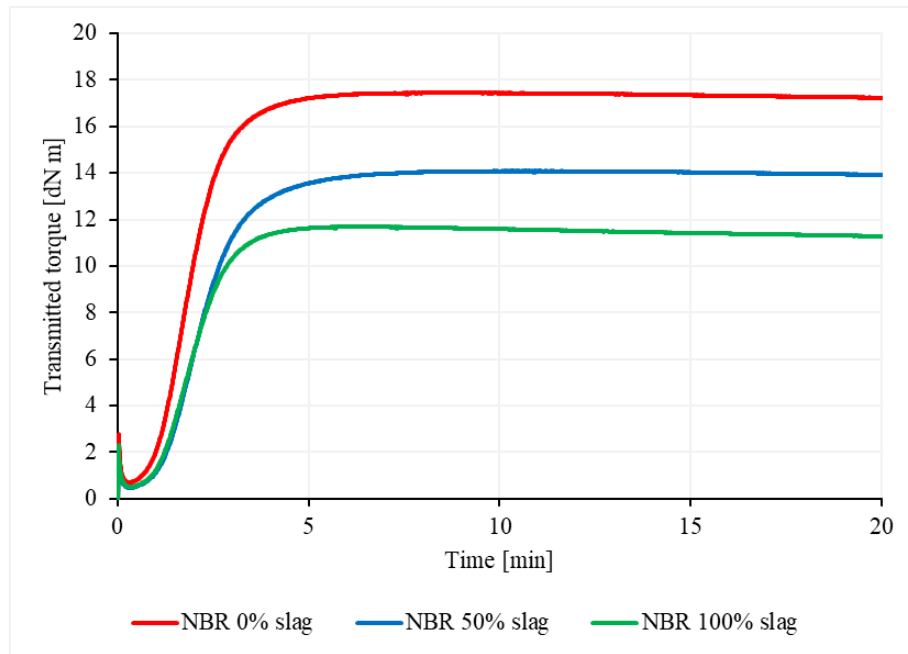


Figure 85 Rheometric curve of carbon black filled NBR, 100% EAF slag filled NBR and 50% EAF slag filled NBR, 160°C.

The assessment of the degree of crosslinking was carried out by normalizing the rheometric curves (in Figure 86) according to Equation 34. It was found that the degree of crosslinking is not affected by the presence of slag as carbon black replacement, as well as the presence of both fillers. This is an encouraging result in a view of slag filled compound's processability.

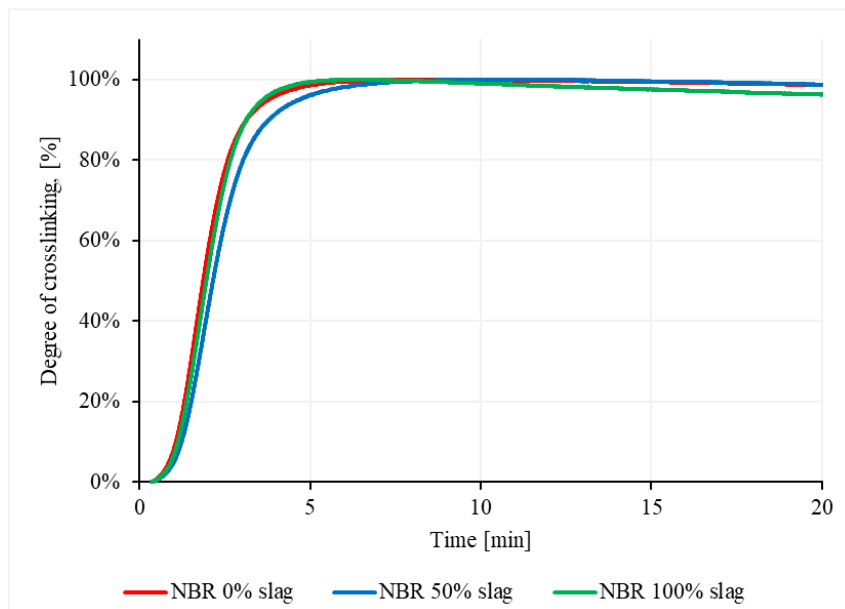


Figure 86 Degree of crosslinking as function of curing time of carbon black filled NBR, 100% EAF slag filled NBR and 50% EAF slag filled NBR, 160°C.

Through RPA, viscosity measurements were made as a function of the stress frequency in order to investigate the influence of slag on viscosity at high shear stress. To do so, the Cox-Merz rule must be considered. The so-called Cox-Merz "rule" is empirical relationship which has been found to be of great use in rheology. It was observed by Cox and Merz [332] that for many polymeric systems correspondence occurred between the

steady state shear viscosity,  $\eta$ , plotted against shear rate,  $\dot{\gamma}$ , and the magnitude of the complex viscosity,  $\eta^*$ , plotted against angular frequency,  $\omega$ .

In injection moulding systems with high shear stress the filler-filler network is broken up reducing the viscosity. This phenomenon does not occur in the case in standard RPA measurements. To break up the filler network in RPA measurements, Fasching [332] studied suitable pre-shear parameters applied during the 4 min heating of the sample prior characterization. He found out for an NBR rubber compound, that an amplitude of  $3^\circ$  and a frequency of 5 Hz destroys the filler network but do not impacting or destroying the macromolecules. Thus, performing viscosity measurements with and without pre-shearing gives us an idea about the filler network, because with a broken filler network the viscosity will be lower.

The complex viscosity as function of angular frequency of carbon black filled NBR, 100% EAF slag filled NBR and 50% EAF slag filled NBR is shown in Figure 87. Solid lines represents the complex viscosity of the three compounds without pre-shearing, dotted lines with pre-shearing. It was found that the NBR 0% slag has a complex viscosity slightly higher than slag filled NBR, while no significant differences were detected between NBR 100%slag and NBR 50% Slag.

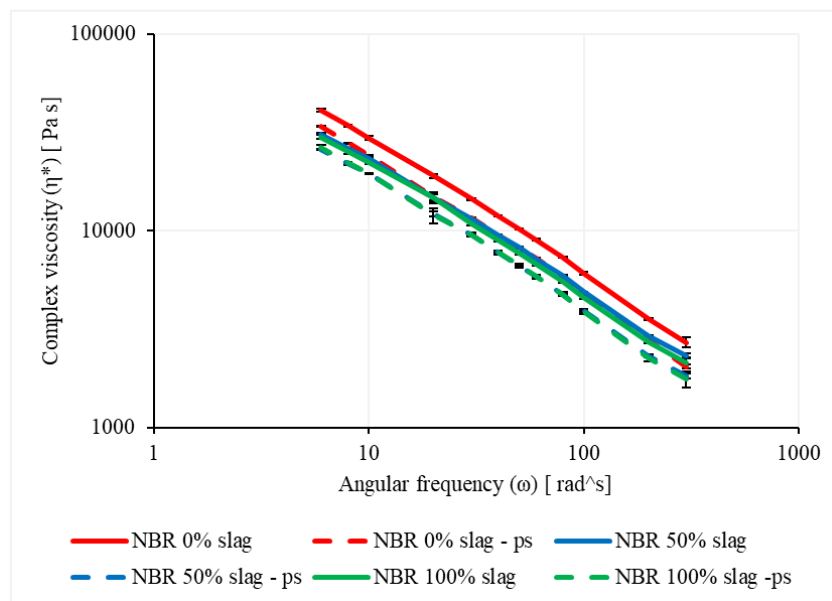


Figure 87 Complex viscosity as function of angular frequency of carbon black filled NBR, 100% EAF slag filled NBR and 50% EAF slag filled NBR.

The difference between viscosity values without and with pre-shearing of carbon black filled NBR, 100% EAF slag filled NBR and 50% EAF slag filled NBR is assessed as function of angular frequency in Figure 88. It was found that NBR 0% Slag shows the highest reinforcement, followed by NBR 50% Slag and NBR 100% Slag. At high frequencies,  $f=47,75$  Hz or  $\omega=300$  rad/s the viscosity is nearly the same. This behaviour can be also compared with the Payne effect (see 4.3.2.8 Dynamic mechanical analysis (DMA)).

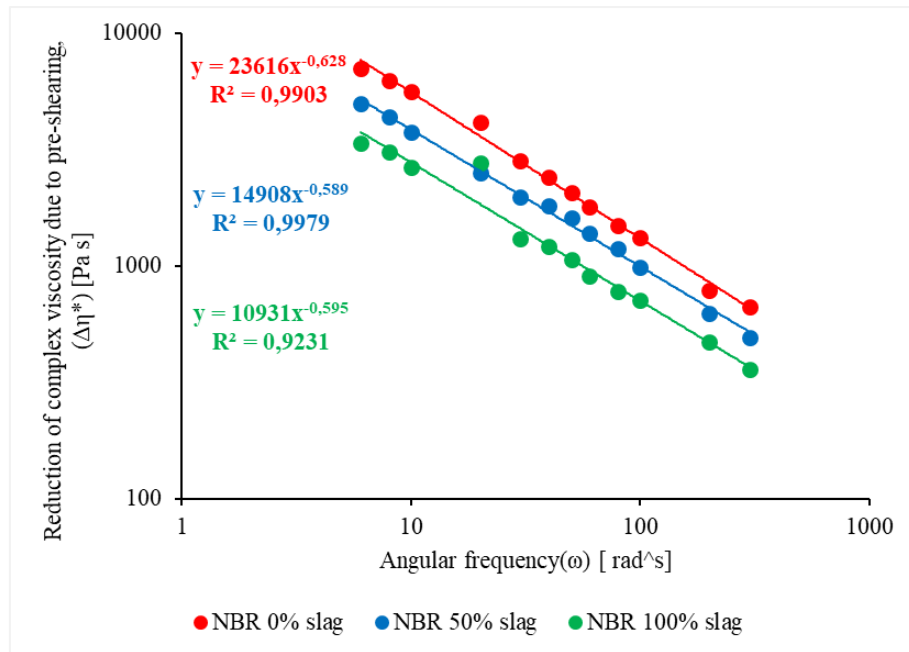


Figure 88 Complex viscosity reduction (without and with pre-shearing) as function of angular frequency of carbon black filled NBR, 100% EAF slag filled NBR and 50% EAF slag filled NBR.

#### 4.3.2.3. Hardness

Figure 89 shows the hardness in Shore A scale of NBR 0% Slag, NBR 50% Slag and NBR 100% Slag. It was found that the hardness decreases with increasing the amount of EAF slag so that the 100% slag filled NBR can be classified as NBR hardness 45 SHA, and 50% slag filled NBR as NBR hardness 50 SHA. This result is compliant with the findings of rheometric curve, in particular the maximum torque value.

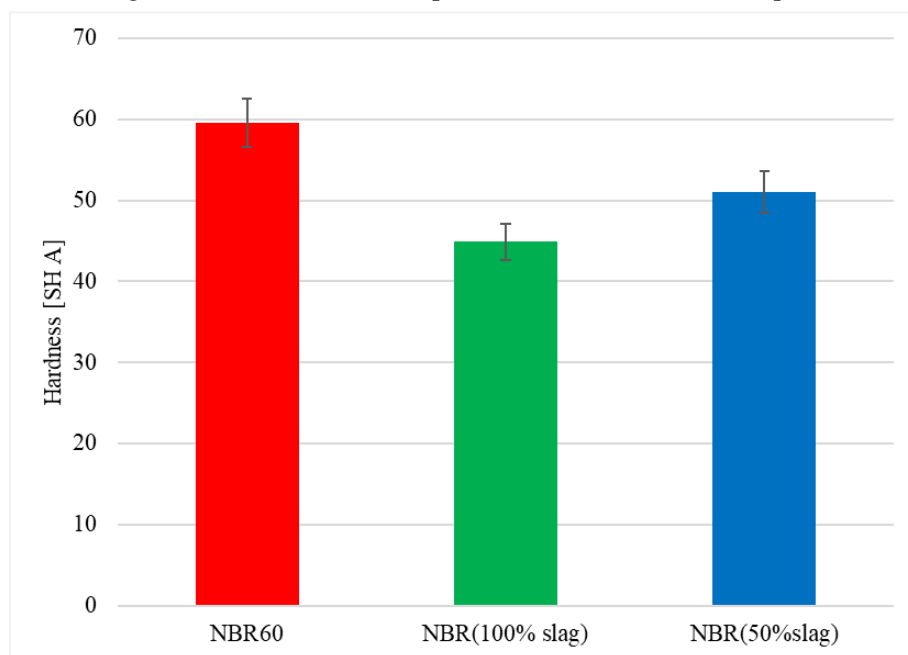


Figure 89 Hardness on Shore A scale of carbon black filled NBR, 100% EAF slag filled NBR and 50% EAF slag filled NBR.

#### 4.3.2.4. Compressive properties

Figure 90 shows the stress compression strain curves of NBR hardness 60 SHA without slag, NBR 100% Slag and NBR 50% Slag as solid lines. To compare the mechanical behaviour of EAF slag filled NBRs to others standard NBR in a view of producing more sustainable materials, as dotted lines Figure 90 shows the stress compression strain curves of a standard NBR of hardness 45 SHA and standard NBR of hardness 50 SHA. It was found that NBR60 0% Slag shows the highest stress strain curve, but it is interesting to note that the NBR 100% Slag shows about the same compressive behaviour of standard NBR50 and higher compressive performances with respect to standard NBR45.

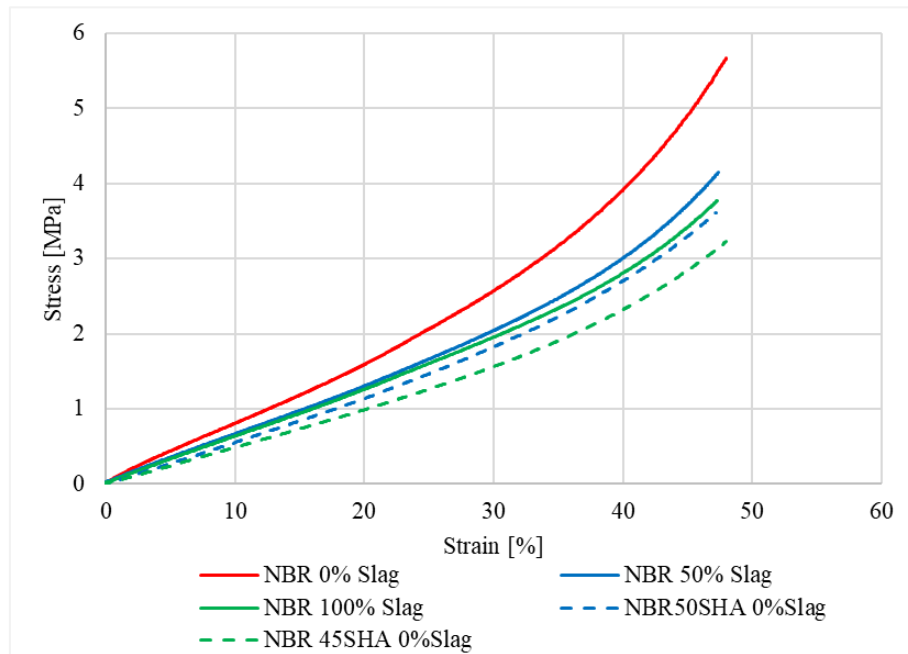


Figure 90 Compression stress strain curve of carbon black filled NBR (60SHA), NBR50 (SHA), NBR45 (45SHA), 100% EAF slag filled NBR and 50% EAF slag filled NBR

Figure 91 shows the compression elastic modulus of the tested materials. The compression elastic modulus was determined as the slope of the first linear section of the stress strain curve. It was found as expected that NBR60 0% Slag shows the highest compressive modulus, but also that the EAF slag filled NBR shows a compressive modulus slightly higher than that of standard NBR at equal hardness.

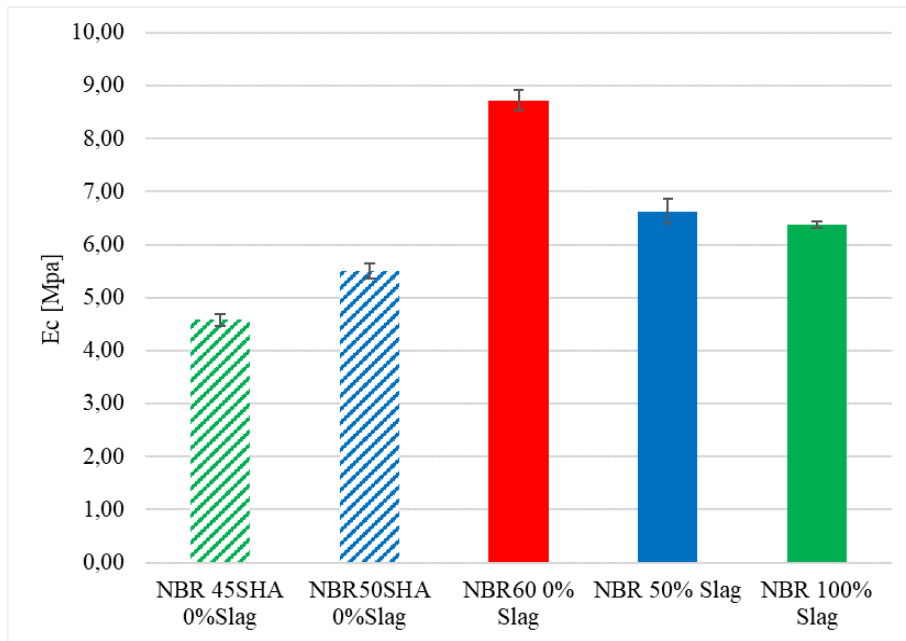


Figure 91 Compression elastic modulus of carbon black filled NBR (60SHA), NBR50 (SHA), NBR45(45SHA), 100% EAF slag filled NBR and 50% EAF slag filled NBR

On the basis of the results obtained from the compression test, it is possible to state that the EAF slag filled NBRs presents the same compression behaviour, if not improved, with respect to standard NBRs at equal hardness, resulting in great economic and environmental benefits.

#### 4.3.2.5. Stress relaxation

Figure 92 shows the stress relaxation curves as function of time at 25% strain of NBR 60 SHA, NBR 50 SHA, NBR 45 SHA, NBR 100% Slag and NBR 50% Slag. It was found that with increasing the compounds hardness the stress reached at 25% strain increases (according to the compression test results), but it is interesting to notice that the stress relaxation curves of slag filled NBR and standard NBR at equal hardness overlap almost perfectly.

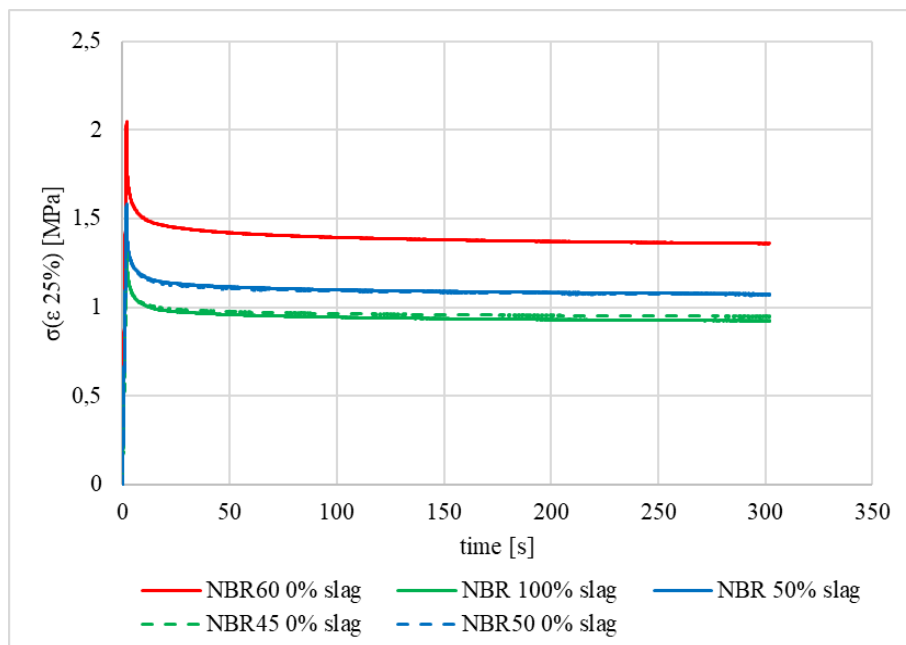


Figure 92 Stress relaxation curves as function of time of carbon black filled NBR(60SHA), NBR50 (SHA), NBR45(45SHA), 100% EAF slag filled NBR and 50% EAF slag filled NBR

The stress relaxation expressed as the percentage stress reduction at 300 seconds of the tested materials is shown in Figure 93. It was found that the stress relaxation of EAF slag filled rubber compounds is about the same as standard NBR 60 SHA, while the standard NBR 45 SHA and 50 SHA shows a minor percentage reduction. This behaviour is likely attributable to the lower rubber fraction in NBR 60 SHA (and also in NBR 100% slag and NBR 50% slag, as they have the same filler volume fraction), that at 25% strain is more stressed than that of NBR 45 and NBR 50, since lower hardness implies lower carbon black content.

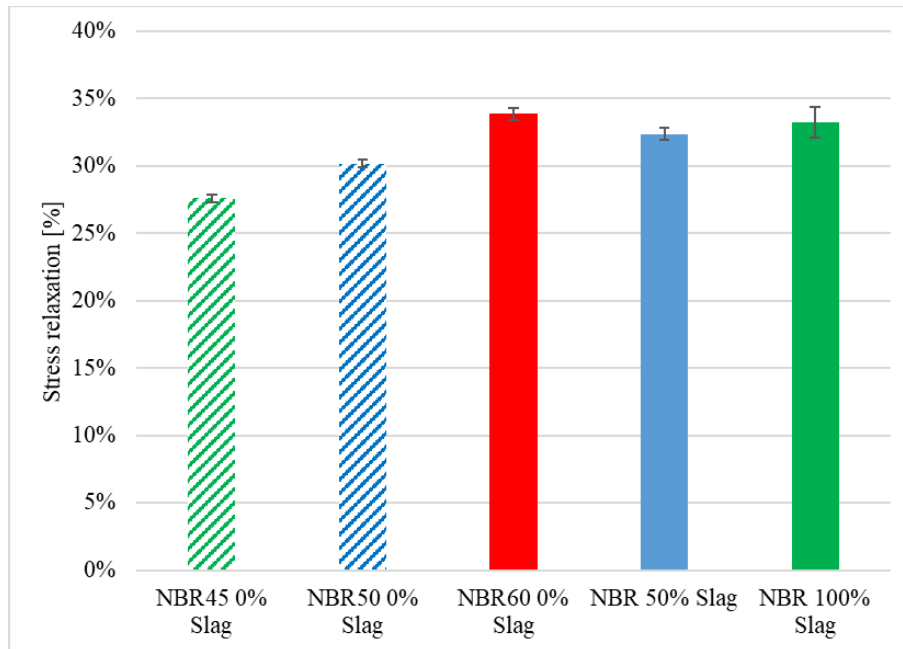


Figure 93 Stress relaxation of carbon black filled NBR(60SHA), NBR50 (SHA), NBR45(45SHA), 100% EAF slag filled NBR and 50% EAF slag filled NBR, after 300s at 25% strain.

#### 4.3.2.6. Permanent set

Permanent set is another method to evaluate the stress relaxation of a rubber material, but it is evaluated as the capability to recover an imposed deformation and not the as the opposing stress.

The permanent set in compression, i.e. the compression set as the permanent deformation of carbon black filled NBR, 100% EAF slag filled NBR and 50% EAF slag filled NBR is shown in Figure 94.

It was found that with increasing of slag content the rubber capability to recover the original dimension is slightly reduced. Nevertheless, it is important to highlight that a compression set (100°C, 24h, 25% strain) lower than 15% it is to be considered a good elastic behaviour.

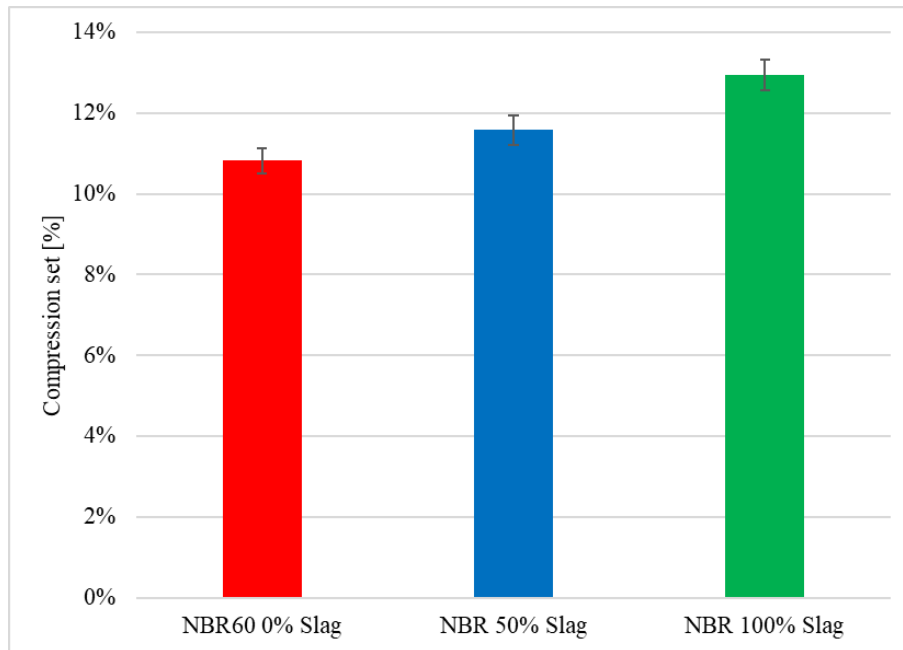


Figure 94 Compression set of carbon black filled NBR, 100% EAF slag filled NBR and 50% EAF slag filled NBR (25% strain, 100°C, 24h).

#### 4.3.2.7. Tensile properties

Figure 95 shows the stress strain curves of NBR hardness 60 SHA without slag, NBR 100% Slag and NBR 50% Slag as solid lines. As dotted lines Figure 95 shows the stress compression strain curves of a standard NBR of hardness 45 SHA and standard NBR of hardness 50 SHA.

As expected, the NBR 60SHA shows the highest tensile strength which is proportionally reduced by increasing the slag content. Analogously it decreases with decreasing the standard NBRs hardness. It is interesting to note that the presence of slag it does not drastically reduce the elongation at break, on the contrary in the case of NBR 50% Slag, it is slightly increased. As regard the comparison between the slag filled NBRs and the standard ones at equal hardness, NBR 50% Slag shows higher elongation at break (about +25%) but lower stress at break (about -15%); NBR 100% Slag shows about equal elongation at break and markedly lower stress at break (about -65%). Nevertheless it is possible to affirm that NBR 50% slag shows better tensile behaviour than standard NBR 45 SHA.

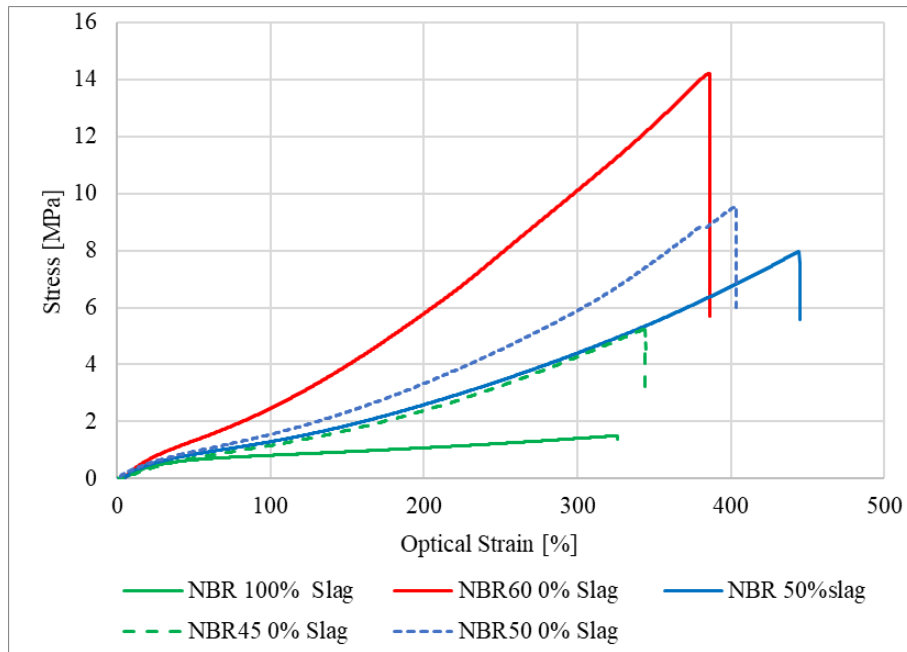


Figure 95 Stress optical strain curves of carbon black filled NBR(60SHA), NBR50 (SHA), NBR45(45SHA), 100% EAF slag filled NBR and 50% EAF slag filled NBR. Displacement rate 100mm/min, room temperature, ISO 37 type 2.

Figure 96 shows the tensile elastic moduli of the tested materials: The Young’s modulus (E) was determined as the slope of the first linear section of the stress strain curve, while E(100%) was determined as the slope of the secant at 100% strain. It was found, as expected, that NBR60 0% Slag shows the highest moduli, but also that the EAF slag filled NBR shows a Young’s modulus slightly higher than that of standard NBR at equal hardness. As regard E(100%), that of slag filled NBR is slightly lower than that of the standard NBR at equal hardness.

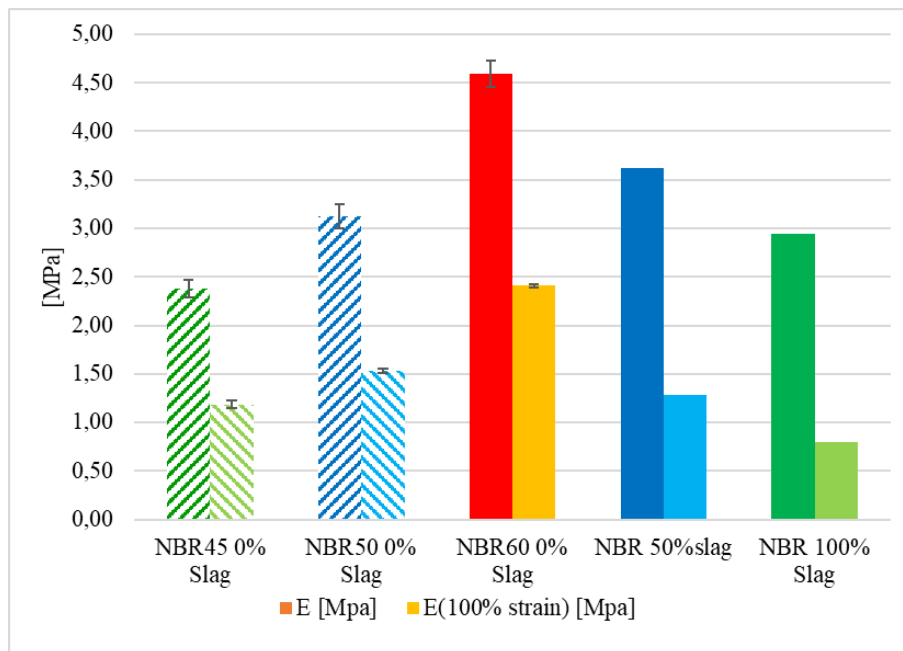


Figure 96 Tensile tangent modulus (E [MPa]) and tensile secant modulus at 100% optical strain (E(100% strain) [MPa]) of carbon black filled NBR(60SHA), NBR50 (SHA), NBR45(45SHA), 100% EAF slag filled NBR and 50% EAF slag filled NBR.

On the basis of the results obtained from the tensile test, it is possible to state that the NBR 50% slag presents improved tensile properties with respect to standard NBR hardness 45 SHA.

#### 4.3.2.8. Dynamic mechanical analysis (DMA)

The dynamic-mechanical behaviour is tested as function of strain amplitude Figure 97. In the range of 0.01 and 50% of strain amplitude it is possible to observe the low strain amplitude storage modulus plateau, a sharp reduction and a high strain amplitude storage modulus plateau for all tested materials. Once again, the NBR softening is appreciable, the storage modulus at low strain amplitude decreases with increasing the slag content (according to the viscosity measurements findings). In agreement with the static tensile Young's modulus standard NBR shows lower storage and loss moduli than that of slag filled ones at equal hardness. It is possible to note that the storage modulus curve of NBR 60 SHA seems rigidly translated upwards with respect to NBR 100% Slag and NBR 50% Slag, while that of NBR 50 SHA and NBR 45 SHA shows a less marked non-linearity. The non-linear effect, i.e. Payne effect expressed as the storage modulus percentage reduction between the storage modulus plateau as low and high strain amplitude, is shown in Figure 98.

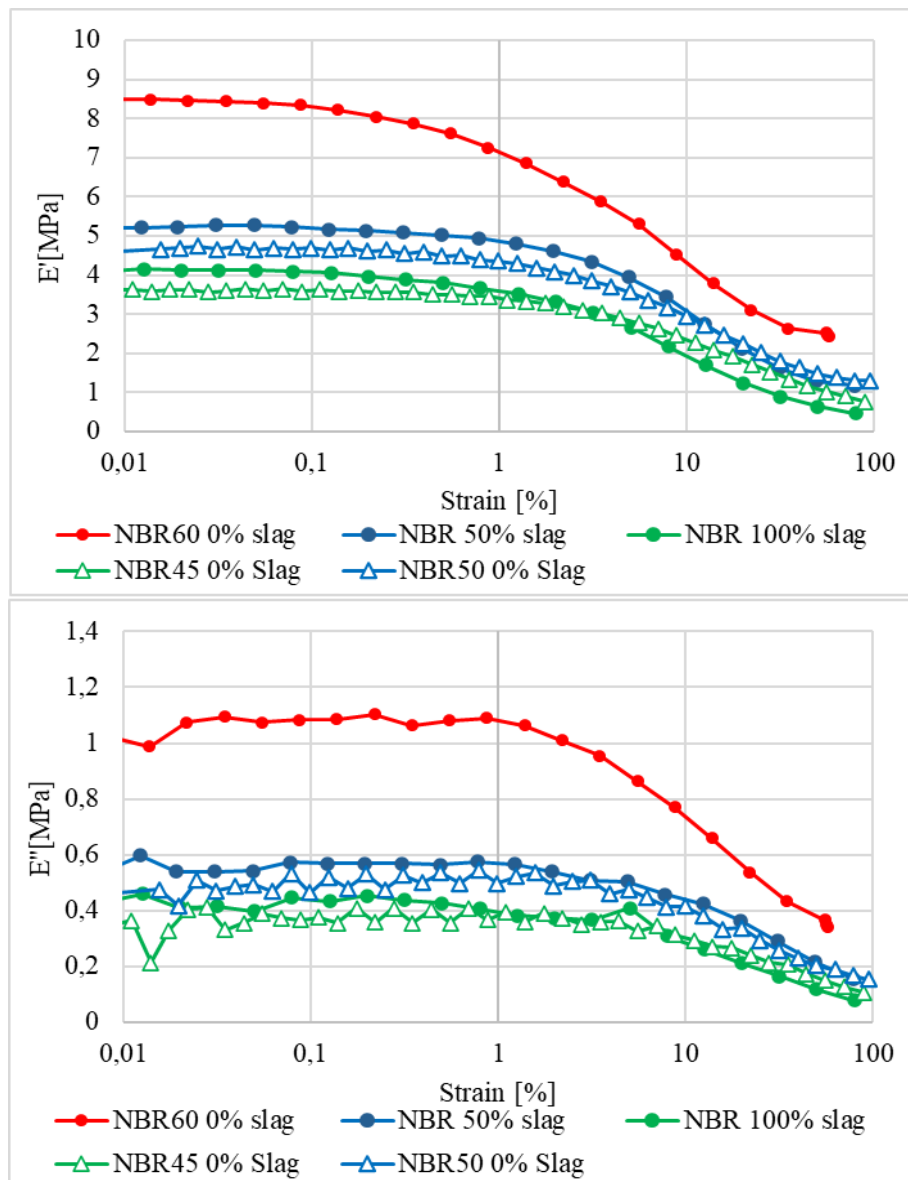


Figure 97 Storage modulus ( $E'$ ) and loss modulus ( $E''$ ) of carbon black filled NBR(60SHA), NBR50 (SHA), NBR45(45SHA), 100% EAF slag filled NBR and 50% EAF slag filled NBR as function of strain amplitude (1Hz, room temperature).

The Payne effect is assumed to be related to the filler-filler interaction and to the rubber-filler interaction, so that as expected it increases with carbon black content in standard NBRs due to the filler-filler network and the greater filler surface area to which rubber can adhere (i.e., bound rubber). It is interesting to note that the 100% slag NBR shows a non-linear effect almost equal to that of NBR 60 SHA, and higher than that of NBR 45 SHA and NBR 50SHA. This behaviour is assumed to be related to the slag-NBR interaction, that seems to be effective also considering the great grain size difference between carbon black and slag, resulting in much lower surface area.

This aspect needs to be further investigated both in terms of characterization of slag compounds with same amount and surface area of filler and in terms of interaction between slag particles.

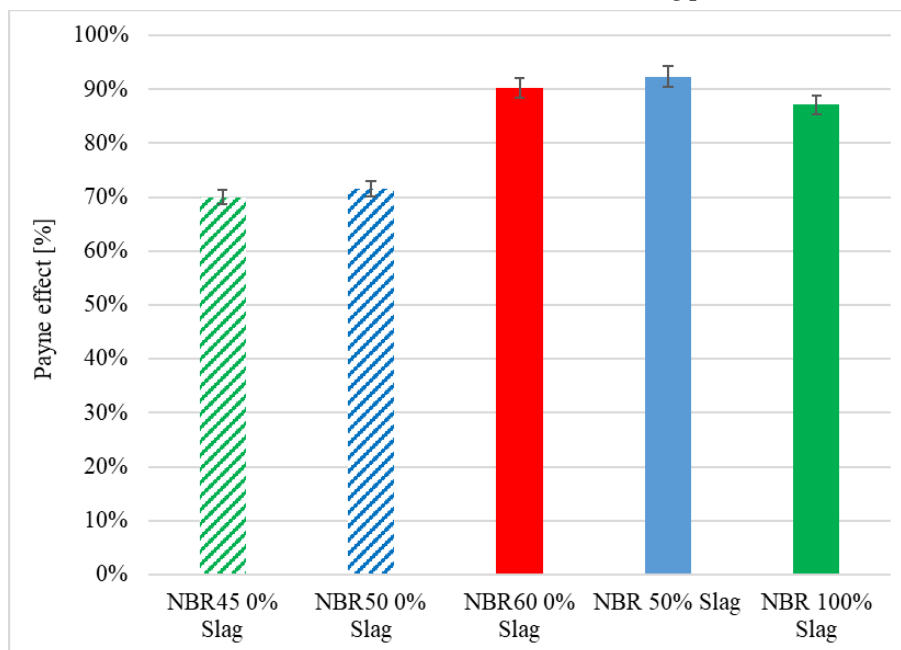


Figure 98 Payne effect as the percentage reduction of the storage modulus from the low deformation amplitude plateau to the high deformation amplitude plateau of carbon black filled NBR(60SHA), NBR50 (50 SHA), NBR45(45SHA), 100% EAF slag filled NBR and 50% EAF slag filled NBR as function of strain amplitude (1Hz, room temperature).

#### 4.3.2.9. Swelling behaviour and crosslink density

Figure 99 shows the swelling index and crosslink density of carbon black filled NBR, 100% EAF slag filled NBR and 50% EAF slag filled NBR determined by swelling test in toluene and THF.

It was found that the slag content does not affect swelling coefficient of the materials, although it is slightly lower for NBR 50% Slag. This small difference results in a higher crosslink density after the conversion of swelling test data in the crosslink density according to the Flory Rehner equation [323]. It is possible to notice that the same trend was found for both solvents, in particular NBR is more permeable to THF than to toluene, and this is evidenced by the higher swelling.

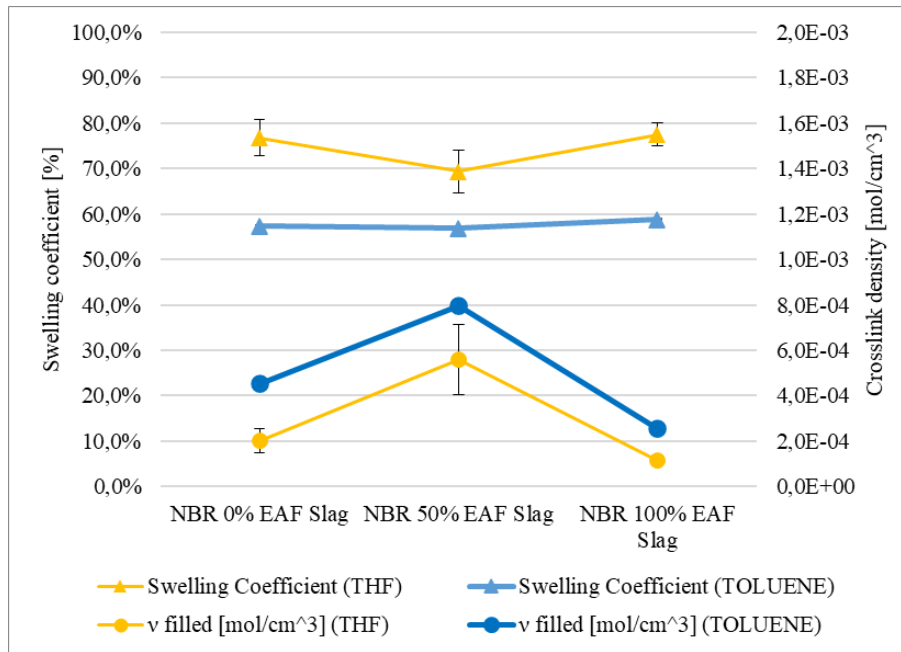


Figure 99 Swelling coefficient and crosslink density of carbon black filled NBR, 100% EAF slag filled NBR and 50% EAF slag filled NBR. Swelling test 48h, Toluene and THF at room temperature.

#### 4.3.2.10. Bound rubber content

To investigate deeply the filler-matrix interaction the bound rubber content is determined (Figure 100). The bound rubber content is a measure of the uncured polymer fraction whose macromolecules are constrained to the filler surface. No significant differences are highlighted between the different fillers; however, it is important to highlight that the slag surface area is significantly lower than that of carbon black so that a NBR-slag interaction is likely.

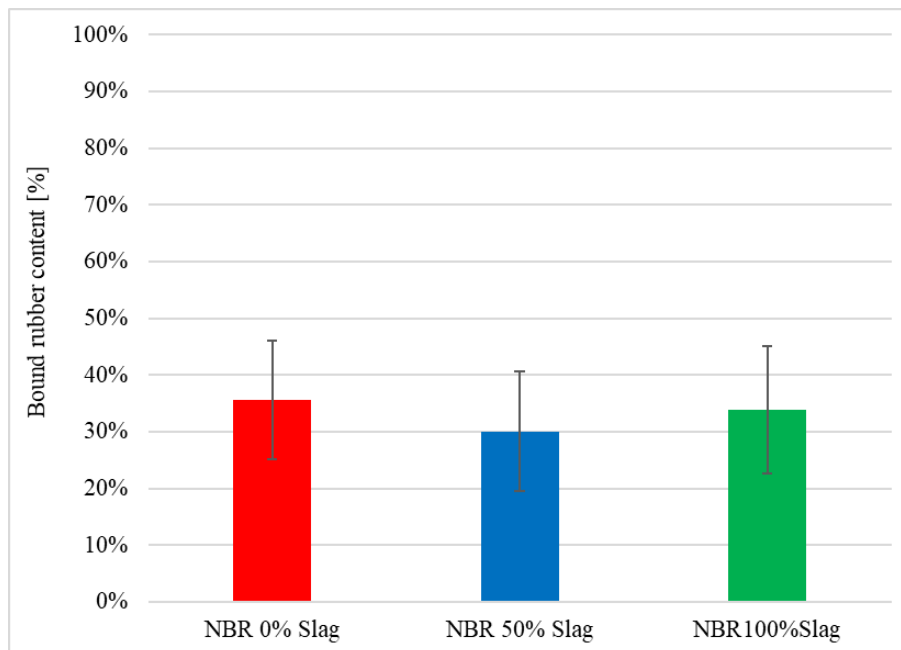


Figure 100 Bound rubber content of carbon black filled NBR, 100% EAF slag filled NBR and 50% EAF slag filled NBR.

#### 4.3.2.11. Differential scanning calorimetry (DSC)

Another method to investigate the rubber-filler interaction is to perform a differential scanning calorimetry analysis on cured rubber and evaluate the variation of heat capacity at neat of filler in correspondence of the glass transition flex ( $\Delta C_p^*(T_g)$ ). The lower this variation, the greater the polymer fraction constrained on the filler particles surface.

Figure 101 shows the DSC scan of carbon black filled NBR, 100% EAF slag filled NBR and 50% EAF slag filled NBR at neat of filler (determined by TGA on the same sample) as solid lines and as rubber composites as dotted lines. It is possible to note that the heat capacity scan of the three materials at neat of filler almost overlap.

The variation of heat capacity at neat of filler in correspondence of the glass transition flex ( $\Delta C_p^*(T_g)$ ) is shown in Figure 102.

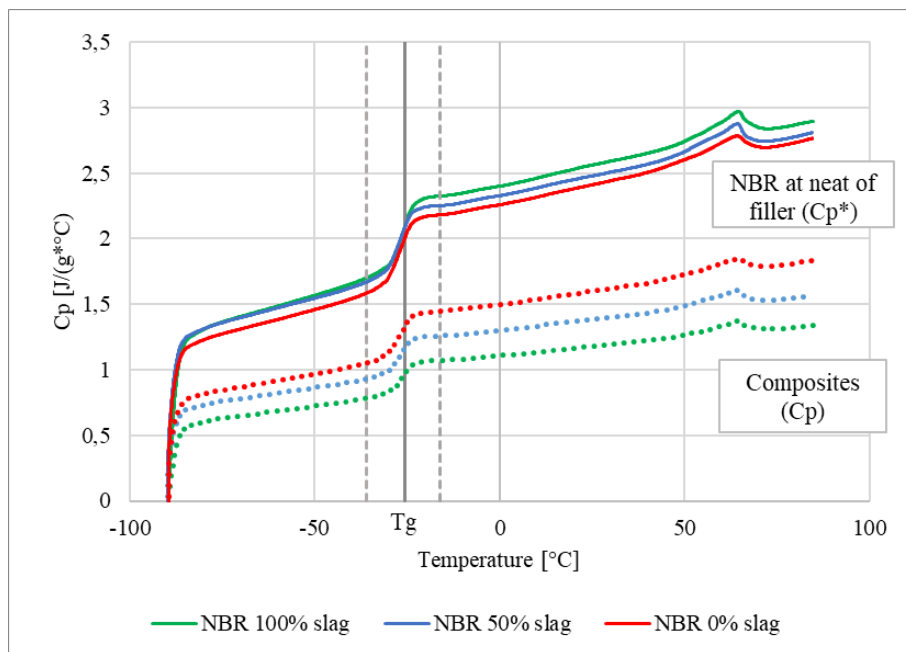


Figure 101 DSC scan of carbon black filled NBR, 100% EAF slag filled NBR and 50% EAF slag filled NBR, 10°C/min nitrogen atmosphere.

The variation of heat capacity at neat of filler in correspondence of the glass transition flex ( $\Delta C_p^*(T_g)$ ) is shown in Figure 102. It was found, according to the bound rubber content, that no significant differences are highlighted between the different fillers.  $\Delta C_p^*(T_g)$  is slightly higher than the others, and this is probably due to the lowest filler surface area to whom the rubber can adhere.

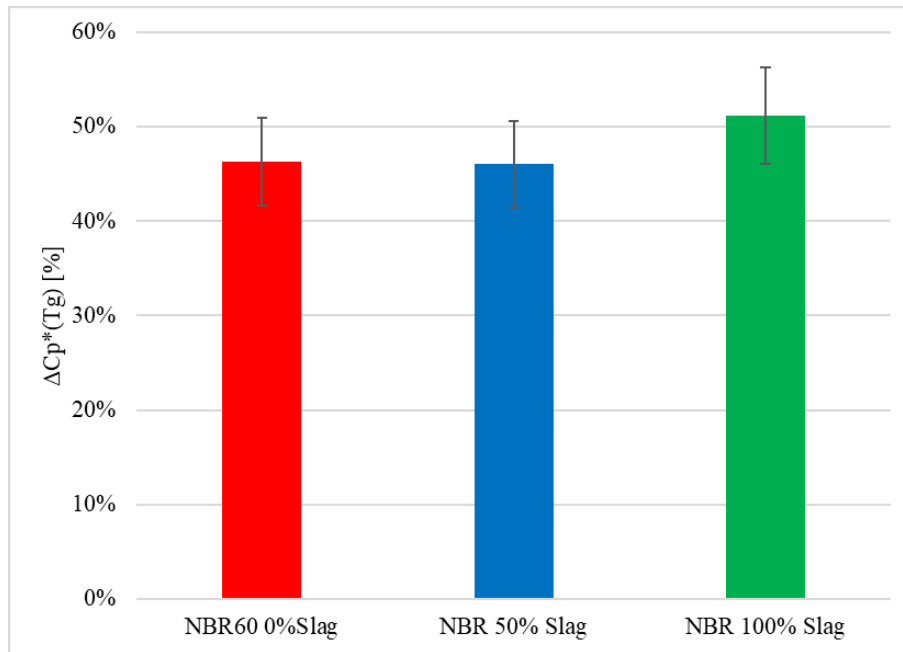


Figure 102 Heat capacity increment of carbon black filled NBR, 100% EAF slag filled NBR and 50% EAF slag filled NBR in correspondence of  $T_g$  at neat of filler.

#### 4.3.2.12. Thermal conductivity

Figure 103 shows the thermal conductivity of carbon black filled NBR, 100% EAF slag filled NBR and 50% EAF slag filled NBR. It was found that the slag has no impact on the thermal conductivity of the compound. The thermal conductivity of the slag has been determined on the basis of the chemical composition determined by XRF and it was found about 146 W/(mK); that of carbon is 140 W/(mK).

Further investigations need to be carried out on the thermal conductivity of bulk slag and carbon black.

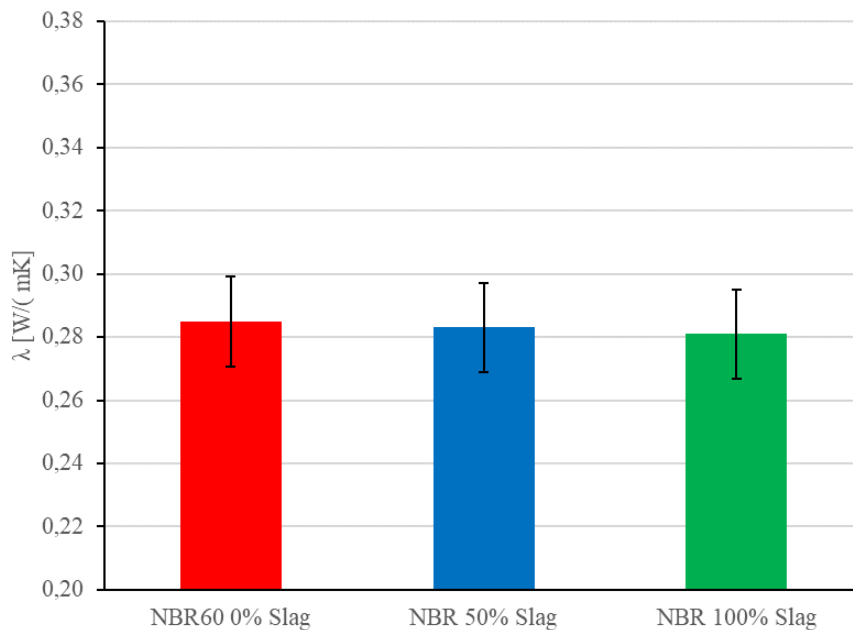


Figure 103 Thermal conductivity ( $\lambda$ ) of carbon black filled NBR, 100% EAF slag filled NBR and 50% EAF slag filled NBR determined according to ASTM E1530 [328]

#### 4.3.2.13. Tribological properties

Figure 104 shows the coefficient of friction (COF) and specific wear rate (Ws) of carbon black filled NBR, 100% EAF slag filled NBR and 50% EAF slag filled NBR in single-way and reciprocating wear configuration. Wear tests show a decreasing of coefficient of friction (COF) with increasing of slag content, however the specific wear rate (Ws) increases in both test configurations (single way and reciprocating).

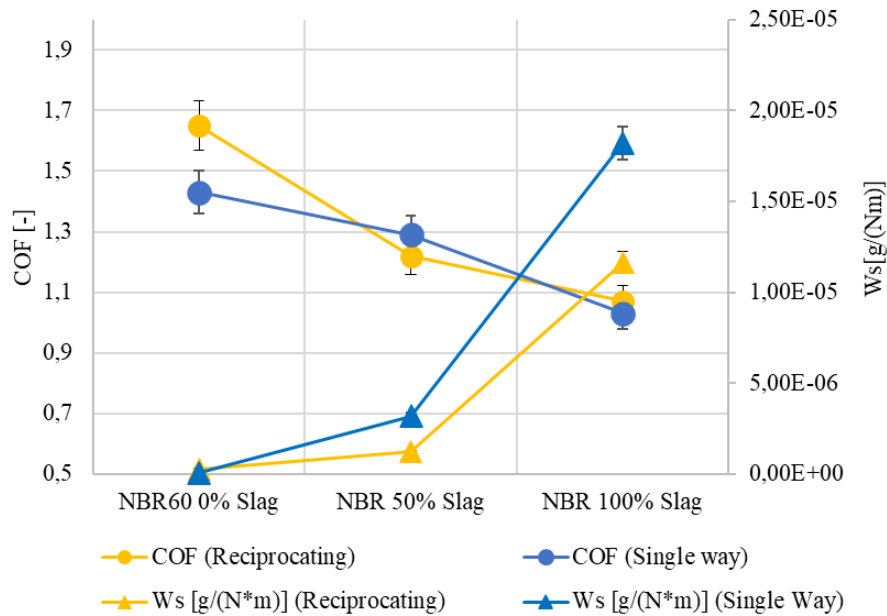


Figure 104 Coefficient of friction (COF) and specific wear rate (Ws) of carbon black filled NBR, 100% EAF slag filled NBR and 50% EAF slag filled NBR in single-way and reciprocating wear configuration (5N, 200m).

SEM analysis of wear traces (Figure 105) suggests the occurrence of 3 different damage mechanism for the 3 materials: NBR0% slag stick slip; NBR 50% slag adhesion; NBR 100% slag abrasion due to slag particles action as third body. The optimum condition is that of 50%slag because the slag particles reduce the COF due to lower adhesion surface, Ws is slightly increased due to the loss of some slag particles characterized by a much higher density with respect to that of rubber matrix.

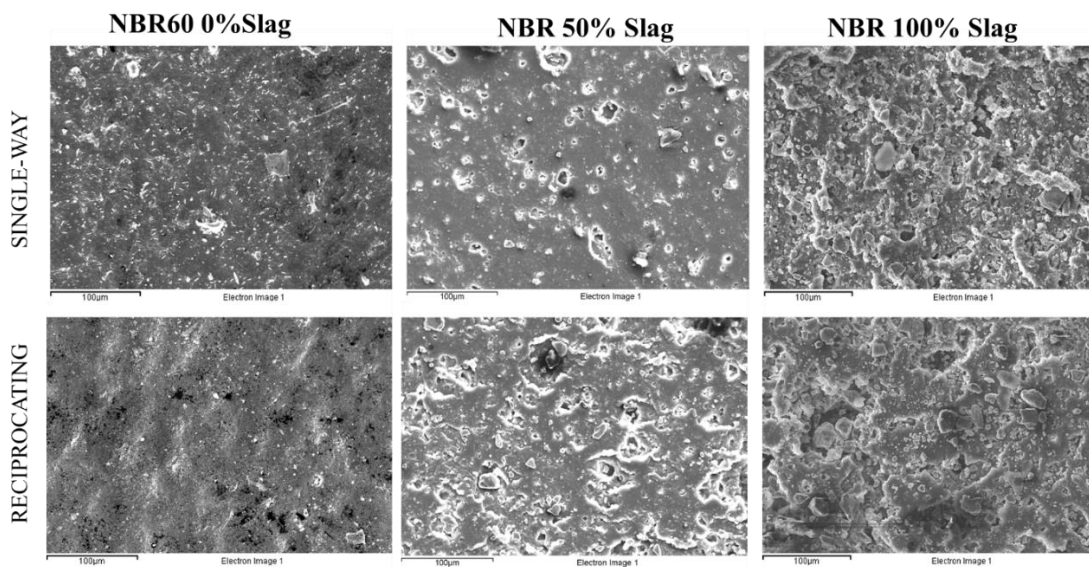


Figure 105 BSE observations of wear track of carbon black filled NBR, 100% EAF slag filled NBR and 50% EAF slag filled NBR in single-way and reciprocating wear configuration (5N, 200m).

It is important to underline that the specific wear rate has been calculated on a mass variation of the sample, but the slag has a density almost 4 times that of the rubber, therefore the removal of a few particles of slag is equivalent to the removal of a large part of the rubber. For this reason it will also be interesting to evaluate the specific wear rate based on the volume variation.

At the same time the hardness affects the rubber tribological behaviour, so that the tribological characterization of NBR 45 SHA and NBR 50 SHA is planned to be carried out.

#### 4.3.2.14. Injection moulding trials

The processability of EAF slag filled NBRs were assessed by injection moulding trials. Figure 106 shows the pictures of moulded rubber parts prior demoulding. Despite the laboratory tests did not show differences in cross-linking kinetics or viscosity, the injection moulding of the compounds highlighted some critical issues. NBR 50% Slag shows an unbalanced moulding shot, while regarding the NBR 100% slag it was difficult to completely fill the mould cavities so that many defective parts were produced. Nevertheless the injection moulding of EAF slag filled NBR can be improved by varying the process parameters such as moulding temperature and pressure.

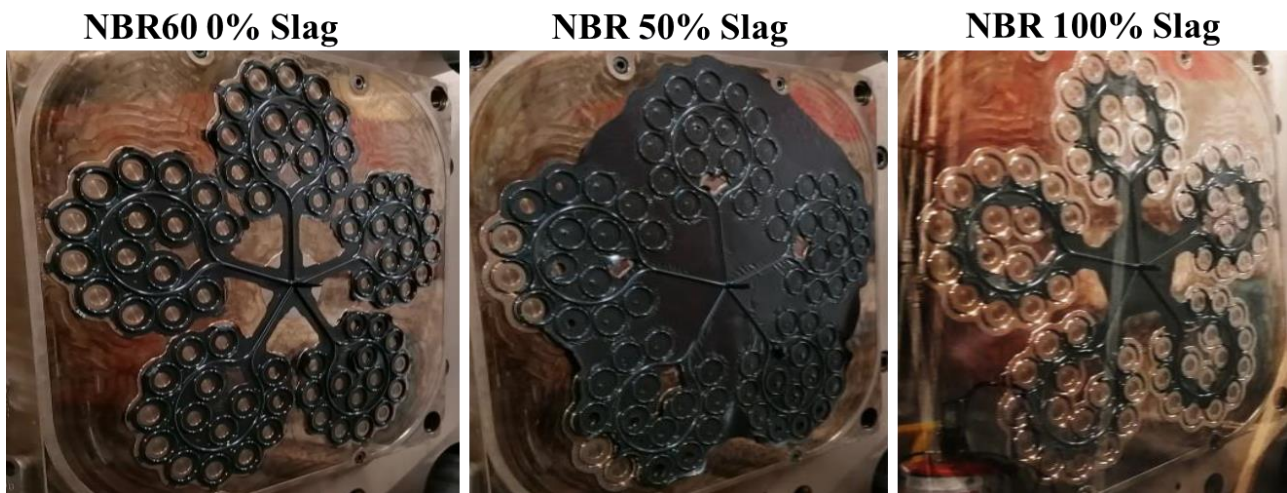


Figure 106 Images of rubber parts produced by injection moulding with carbon black filled NBR, 100% EAF slag filled NBR and 50% EAF slag filled NBR.

## Conclusion

Carbon black is the most widely used reinforcing filler for rubber. Since the carbon black production derived from the partial combustion of heavy hydrocarbons its carbon footprint is enormous [325]. Given the increased demand for rubber quality and the rising price of raw materials, there are several concerns regarding the traditional petroleum-based carbon black filler: on the one hand, the price of hydrocarbons sees a gradual increase every year and on the other side, due to the non-degradability of the petroleum-based carbon black filler, it can cause serious environmental problems. For these reasons, sustainable alternatives to carbon black are being studied. The present study proposed the EAF slag as alternative filler for NBR to compare the effect of slag as a substitute for carbon black at the same percentage by volume. The results can be summarized as follow:

- The slag mineralogical composition consists mainly in 4 phases: 2 mains of larnite and iron oxide; in smaller quantities chromite and very small areas of brownmillerite.
- The incorporation of EAF slag particles as filler into NBR matrix reduces the leaching of Cr, V, and Mo, as well as eluate pH and electrical conductivity making the compounds suitable for reuse (Ministerial Decree 5/4/06 [245]) and for disposal as inert material (Ministerial Decree 30/8/05 [246]).
- Regarding the processability characteristics, the degree of crosslinking is not affected by the presence of slag as carbon black replacement, and complex viscosity of NBR 0% slag is slightly higher than slag filled NBRs; the injection moulding trials demonstrated that the NBR 50% slag is processable, while the process parameters of NBR 100% slag need to be improved.
- The hardness decreases with increasing the amount of EAF slag so that the NBR 100% slag can be classified as NBR hardness 45 SHA, and NBR 50% slag as NBR hardness 50 SHA.
- The EAF slag filled NBRs present the same compression behaviour, if not improved, with respect to standard NBRs at equal hardness (45 and 50 SHA).
- Stress relaxation curves of NBR 50% slag and NBR 100% slag overlap almost perfectly that of NBR 50 SHA and NBR 45SHA respectively.
- With increasing of slag content the rubber capability to recover the original dimension is slightly reduced. Nevertheless it is lower than 15%, i.e. good.
- NBR 50% slag presents improved tensile properties with respect to standard NBR hardness 45 SHA.
- The slag has no impact on the thermal conductivity of the compound.
- The wear optimum behaviour is that of 50% slag because the slag particles reduce the COF due to lower adhesion surface, and  $W_s$  is slightly increased due to the loss of some slag particles characterized by a much higher density with respect to that of rubber matrix.

These preliminary results are promising to continue the research for the best compound formulation according to the final application.

## 5 Influence of EAF slag as filler for recycled end of life tyre (ELT)

The importance of recycling and reusing end-of-life tires has been extensively discussed in paragraph 2.2. End of Life Rubber tyre of the first part of the thesis.

The present study shows the characterization of recycled ELT using a very simple technology, at room temperature and without the addition of additives: calendaring in an open mixer. The recycled rubber thus obtained was mechanically characterized.

In order to enhance some properties, recycled ELT was filled with another waste material such as electric arc furnace slag (EAF) resulting in 100% recycled material combining the waste of two traditionally dissimilar sectors such as that of steel and that of rubber-plastic.

First of all, the leaching behaviour of the slag incorporated in the recycled ELT was evaluated showing a reduction in Cr Mo and V leaching as well as in eluate's pH and electrical conductivity. The leaching of the slag was also studied in terms of mineralogical phases: they were analysed by SEM EDS before and after leaching, highlighting how the larnite is completely dissolved.

As regards the assessment of the composite, a mechanical characterization was carried out in terms of hardness and tensile properties, in addition, the viscoelastic behaviour of the material was also investigated through cyclic (Mullins effect) and dynamic-mechanical analysis and the master curves of the conservative and dissipative modulus as a function of frequency were obtained. It emerged that the end-of-life tire recycled through this simple technology becomes a well-cohesive and compact material so as to present the viscoelastic effects typical of elastomeric materials and that the slag content at small deformations does not significantly affect the properties of the material except for an increase of hardness.

In order to investigate possible applications for this material, tribological tests were also conducted in different configurations. The friction coefficient is reduced by the slag content while the specific wear rate is function of the slag content and the configuration of the test. Finally it was shown how the slag confers the rubber magnetic properties and increases the thermal conductivity making the material interesting for applications where the rubber is required to dissipate heat.

### 5.1 Materials

#### ELT powder

The rubber powder used was supplied by the Ges.Tyre Scrl consortium (Brescia, Italy), a consortium company that provides an efficient service for the collection and recovery of end-of-life tires in strict compliance with the regulations and with the utmost respect for the environment and the health of citizens.

From the industrial bag with an average particle size of 0.5mm, only the particles size less than 0.5mm were sieved in the laboratory. This powder was used to produce ELT specimens filled with EAF slag.

#### EAF slag

The slag was supplied by the company ASONEXT Spa (Ospitaletto BS, Italy). The slag employed in this research has been produced by a specific system named Slag-Rec [333], [334] for dry granulating EAF molten slag. The slag employed as filler in the elastomeric matrix has been grinded by the manual pulverizing mill HSM 100 provided by Herzos for a grinding time of 25 seconds. The pulverized EAF slag has been sieved to obtain a grain size <100  $\mu\text{m}$ .

**Compound ELT filled with EAF slag**

The compounds EAF slag filled ELT has obtained via calendaring process. The compounding process has been carried out as first to transform the ELT powder into a single and workable compound thanks to a partial mechanical devulcanization, and secondly to distribute and disperse the slag particles into this polymeric matrix. The process allow to obtain a rubber sheets of about 1mm as shown in Figure 107 and Figure 108.



Figure 107 During the calendaring process ELT powder (beginning of the process) is transformed into a compound (end of the process).

Known the density of ELT from previous tests equal to 1,13 g/cm<sup>3</sup>, the quantity of rubber powder and EAF slag has been determined. The influence of EAF slag as filler for ELT has been evaluated on different compounds with and increasing amount of filler: 0, 5, 10, 20% by volume.

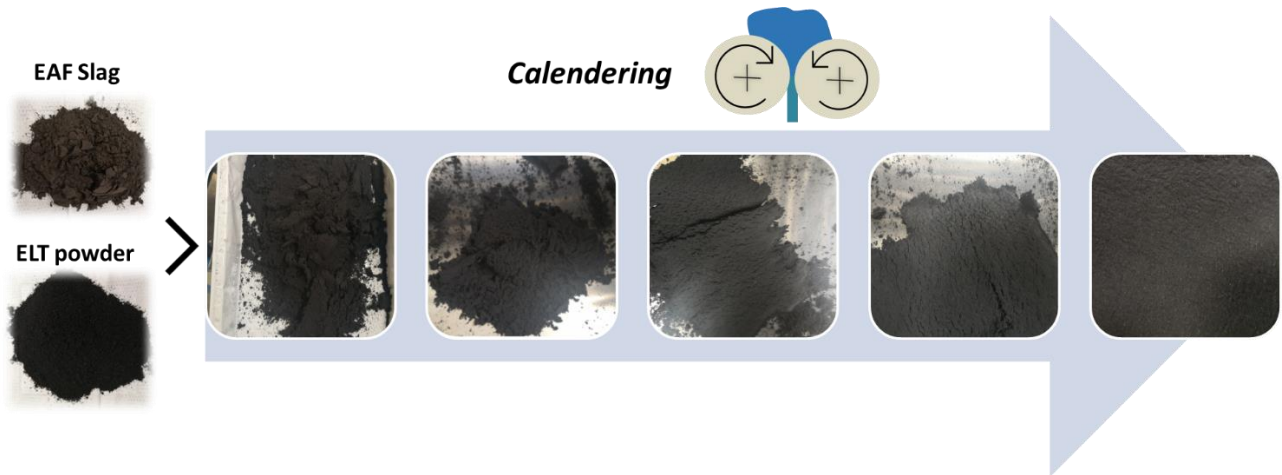


Figure 108 Compounds production steps: EAF slag and ELT powder are compounded via calendaring process in several steps up to obtaining a rubber sheet.

**5.2 Methods**

**5.2.1 EAF Slag Characterization**

**5.2.1.1 X-ray fluorescence spectroscopy (XRF)**

EAF slag chemical composition was determined by X-ray fluorescence spectroscopy carried out by the Thermo Scientific™ ARL™ PERFORM'X provided by Thermo Fisher Scientific™ (Waltham, Massachusetts, United States). EAF slag chemical composition is reported in Table 25.

### **5.2.1.2. Scanning Electron Microscope (SEM-EDXS) analysis**

A Scanning Electron Microscopy (SEM) integrated with Energy Dispersive X-ray Spectrometry (EDXS) for the morphological and elemental analysis of the phases [240] was adopted to characterize the chemical composition and the phases of the slag. For the identification of the phases and structure of the slag with SEM-EDXS (SEM Leo Evo 40, Carl Zeiss, Oberkochen, Germany; EDXS microprobe Link Pentafet Oxford mod 7060; Oxford Instruments, Oxfordshire, U.K.) a standard metallographic polishing procedure was used. In Figure 37 the SEM-EDXS analysis carried out on a metallographically polished sample utilizing back-scattered electron (BSE) mode is reported. The same sample has been analysed after a leaching for 24h in H<sub>2</sub>O to investigate the changes in phases morphology and chemistry.

### **5.2.1.3. Leaching behaviour**

The leaching of heavy metals has been determined following the procedure of the standard CEN - EN 12457-2 [72] and on the EAF slag grain size lower than 100 µm in order to compare the leaching of free slag and slag incorporated into the rubber matrix at equal conditions.

The leachates have been analysed by an Avio 200 ICP Optical Emission Spectrometer Perkin Elmer (Milano, Italy) to measure the concentration in the solution Cr, Mo, and V. Two leachates were prepared and 3 analyses were performed each. The results are given in Figure 38.

## **5.2.2. Compound Characterization**

The composition of the recycled ELT was investigated by thermogravimetric analysis (TGA) performed on thermogravimetric analyser Q500 provided by TA instruments (New Castle, United States). Samples of about 10mg mass were placed in a platinum crucible and heated in a thermobalance at rate of 10 °C/min from ambient to 560°C in Nitrogen atmosphere. When the sample mass became constant the sample is kept for 2 minutes at 300°C, and in Oxygen atmosphere is heated up to 800°C at 10°C/min in order to facilitate the carbon black content measurement. TGA scan is shown in Figure 111.

The accuracy of the slag and rubber amount in the different compounds were verified retrospectively by density measurements and by TGA. TGA were carried out on specimens with a weigh between 7 and 15 mg and heating rate of 10°C/min up to 700°C to determine the complete thermal degradation of the rubber in air.

### **5.2.2.1. Hardness test**

The compounds' hardness was measured according to the micro International Rubber Hardness Grade (mIRHD according to the standard ISO 48 [277]). The mIRHD measurements were carried out by an automatic hardness tester Micro IRHD-PC provided by Gibitre Instruments (Bergamo, Italy).

### **5.2.2.2. Tensile test**

Mechanical tensile tests were performed by an Instron dynamometer (mod. 3366) at room temperature and at a cross-head rate of 100 mm/min on test pieces of 50 mm length (distance between the grips of about 30 mm) and 4 mm width according to the standard ISO 37:2017 type 2 [197]. The considered strain is the optical one in order to exclude the influence of the sample edges. The measurement is performed three times for each compound. The Young's modulus has been determined as the slope of the stress strain curve in correspondence of the initial linear section.

### 5.2.2.3. Scanning Electron Microscope (SEM) analysis

The morphology and distribution of slag particles in the ELT composites were assessed by SEM observations of cross sections of specimens tested in tensile test after coating the surface with sputtered gold.

### 5.2.2.4. Mullins effect

The Mullins effect was evaluated in a cyclic uniaxial tensile configuration. A rectangular specimen of a nominal dimension 50x5x1mm was tested by an Instron dynamometer (mod. 3366).

The maximum strain increased from 10% to 50% by 10% every 4 cycles. The strain rate of the test was 80 mm/min.

### 5.2.2.5. Dynamic mechanical analysis

Dynamic tests were carried out by Dynamic Mechanical Thermal Analyser Q800 by TA instruments (New Castle, United States) by scanning temperature and frequency simultaneously. The specimens consisted of 40x5x1 mm strips, cut from the sheets. The tests were carried out in tensile mode at amplitude strain 15 $\mu$ m at 11 different frequencies, from 1 to 100 Hz by scanning temperature in the range from -90°C to +70°C, at a heating rate of 0.5°C/min.

### 5.2.2.6. Tribological properties

The wear tests were conducted on a CSM Instruments High Temperature In single way and reciprocating configuration. A 5 mm diameter flat pin (100Cr6) was used as a counterpart. A normal load of 5 N, a sliding speed of 80mm/sec, and a total sliding distance of 156 m were applied at room temperature. The diameter of the wear tracks was 5mm in single way configuration and 13mm in reciprocating. During the test, the friction coefficient as a function of the sliding distance was recorded. After an initial peak the curve settles on a constant value taken as the steady-state coefficient of friction. Known the test parameters and initial and final weight of the sample, the specific wear rate ( $W_s$  [g/(Nm)]) was calculated according to Equation 25.

Finally, the wear mechanisms were studied by SEM LEO EVO 40 VPS equipped by EDS probe

### 5.2.2.7. Thermal conductivity

The guarded heat flow meter DTC-300 (TA Instruments, New Castle, USA) operates at steady-state and employs a heat flux transducer to measure the heat flow through the specimen. A sample was mounted between an upper "hot" and a lower "cold" plate. During the measurement, the heat flows from the upper "hot" plate, throughout the specimen, to the lower "cold" plate, establishing a temperature gradient. After reaching thermal equilibrium, the temperature difference across the sample  $\Delta T$  and the resulting heat flow  $\dot{Q}$  are measured. The heat flow meter method corresponds to ASTM E1530 [328]. One sample with a diameter of 50 mm (thickness between 1 - 2 mm) was punched out of each crosslinked ELT test plate to measure the thermal conductivity at 35 °C.

### 5.2.2.8. Magnetic properties

The presence of iron/iron oxides in the slag gives the composite magnetic properties. The magnetic attraction force was evaluated by quantifying the force required to detach a magnet from the ELT filled with different amounts of EAF slag. A magnet was fixed to the beam of the dynamometer in contact with the material, moving the beam at a speed of 10 mm/min a 500N load cell detected the load every 0.01 seconds, the peak of the curve obtained is identified as the detachment load.

### 5.2.2.9. Swelling

For the swelling test rectangular samples of about 500mg were cut and immersed in toluene in sealed glass tubes for 48 hours at room temperature. The swelling coefficient is determined according to Equation 11.

The equilibrium swelling index is determined by crosslink density and the attractive forces between solvent and polymer. The theoretical extent of swelling is predicted by the Flory–Rehner equation [185], [189], [190] (Equation 12 and Equation 16).

The properties of filled elastomers are linked to the interaction between filler and matrix which can be theoretically estimated by Kraus equation [195] (Equation 15).

### Differential scanning calorimetry

The calorimetric glass transition was determined using differential scanning calorimetry (DSC). Measurements were carried out in the temperature range  $-90^{\circ}\text{C}$  to  $80^{\circ}\text{C}$ , in nitrogen atmosphere (purge) using DSC (Model: Q100 provided by TA instruments (New Castle, United States)). The samples were then cooled from room temperature to  $-90^{\circ}\text{C}$  at  $10^{\circ}\text{C}/\text{min}$  and held at this temperature for 60 min at the end of each cooling cycle and the measurement was carried out during subsequent heating at  $10^{\circ}\text{C}/\text{min}$ . The difference of heat flow between the sample pan filled in by sample and the empty reference pan was recorded with increasing temperature at the heating rate of  $10^{\circ}\text{C}/\text{min}$ . DSC analysis is performed twice.

The heat flow [mW] is converted to heat capacity ( $C_p$  [J/(g $^{\circ}\text{C}$ )]). NBR composites samples consist of a weight fraction of filler and a weight fraction of polymer; since only the latter is responsible for the variations associated to the glass transition, the heat capacity has been normalized to the polymer fraction as shown in Equation 23.

$\Delta C_p^*$  is determined in a temperature range of  $\pm 4^{\circ}\text{C}$  with respect to the glass transition temperature ( $T_g$ ). The fraction of immobilized polymer is calculated according to Equation 24, Where  $\Delta C_p^0$  is assumed to be the heat capacity variation of ELT 0% EAF slag.

## 5.3. Results and discussion

### 5.3.1. EAF Slag

#### 5.3.1.1. X-ray fluorescence spectroscopy (XRF)

The chemical composition of the EAF slag used as filler is reported in Table 25.

The ratio between the percentage of basic and acidic components, named basicity index (IB), allows to express and interpret important metal-slag balances, such as the oxidizing power of the slag, the desulphurization balance, and the dephosphorization, metal-slag distribution of manganese.

There are mainly two expressions of IB: the simplest one consists in the CaO and SiO<sub>2</sub> ratio (%wt/wt) and is named IB<sub>2</sub>, in this slag it is equal to 3; the more complete one is IB<sub>4</sub> that considers the presence of other components and it is defined as the ratio between principal basic oxides (CaO+MgO) and main acid oxides (SiO<sub>2</sub>+Al<sub>2</sub>O<sub>3</sub>), here IB<sub>4</sub> is equal to 1.9. The basicity of the slag is required in steelmaking because usually furnace refractories are basic too, and a basic slag can extend their useful life preserving their integrity for longer with consequent economic benefits.

The chemical composition of the slag is important not just because it affects the chemical composition of the liquid steel but also because affects the leaching of heavy metals. The slag leaching behaviour is influenced by the cooling it undergoes: A rapidly cooled slag is inclined to form a glassy phase which shields the heavy

metals and prevents them from leaching [241], [242]. Tossavainen et al. [242] observed that if the basicity factor IB4 is greater than 1 (here IB4 is 1.9) the glassy phase formation occurred so that the slag will have low leaching rate.

Table 25 EAF slag chemical composition determined by X-ray fluorescence spectroscopy and Basicity Indexes.

<b>SiO<sub>2</sub></b>	[% wt]	10
<b>Al<sub>2</sub>O<sub>3</sub></b>	[% wt]	8
<b>Fe<sub>2</sub>O<sub>3</sub></b>	[% wt]	40
<b>MnO</b>	[% wt]	6
<b>CaO</b>	[% wt]	30
<b>MgO</b>	[% wt]	4
<b>P<sub>2</sub>O<sub>5</sub></b>	[% wt]	1
<b>Cr<sub>2</sub>O<sub>3</sub></b>	[% wt]	2
<b>Basicity</b>	[-]	0.6
<b>CaO/Al<sub>2</sub>O<sub>3</sub></b>	[-]	3.7
<b>Al<sub>2</sub>O<sub>3</sub>/SiO<sub>2</sub></b>	[-]	0.8
<b>IB2 CaO/ SiO<sub>2</sub></b>	[-]	3
<b>IB4 (CaO+MgO)/(SiO<sub>2</sub>+Al<sub>2</sub>O<sub>3</sub>)</b>	[-]	1.9

### 5.3.1.2. Scanning Electron Microscope (SEM-EDXS) analysis

Figure 37 shows the micrographs of the same EAF slag sample subjected to phases' chemical and morphological analysis before and after leaching. The morphological structure of the slag phases is strongly affected by the cooling rate it undergoes after the de-slagging phase. In turn the morphological structure and so the chemical composition affect the leaching behaviour: cooling control conditions can represent a strategy to influence the mineral transformation and the solubility of elements such as Cr, which is crucial for problems involving human health and environmental protection [68]. The analyzed slag shows very fine and dendritic phases, a sign of a rapid cooling with some areas characterized by a single larger phase.

It is possible to state that the global morphology of the phases has not been heavily altered by contact with water, but that the most significant change is represented by a large phase (Spectrum Nr 1), identified as larnite, which is completely dissolved leaving a hole such that the analysis in the same area reports the identification of iron oxide on the bottom layer. This result agrees with the research of Gelfi et al. [68].

The phase in correspondence of the spectrum Nr2 is rich in Fe and Mg with other elements in trace. This phase has been identified as Magnesium-Wuestite and it is slightly larger after leaching. Despite this, other areas of the same shade of gray (and therefore presumably characterized by the same chemical composition) are less wide. This could indicate a uniform consumption of a few nanometers in the leaching.

As last, the third identified phase is Brownillerite particularly rich of Ca that maybe attributable to near areas of Larnite that due to the fine phases morphology affect the EDS signal. The zone identified by the spectrum Nr 3 after leaching reduces the amount of Ca and increases that of Fe, while the zone Nr 4 and 5 are slightly richer in Fe.

The chemical and morphological analysis of the slag indicates a low leaching of heavy elements, a result confirmed by the leaching test (Figure 38).

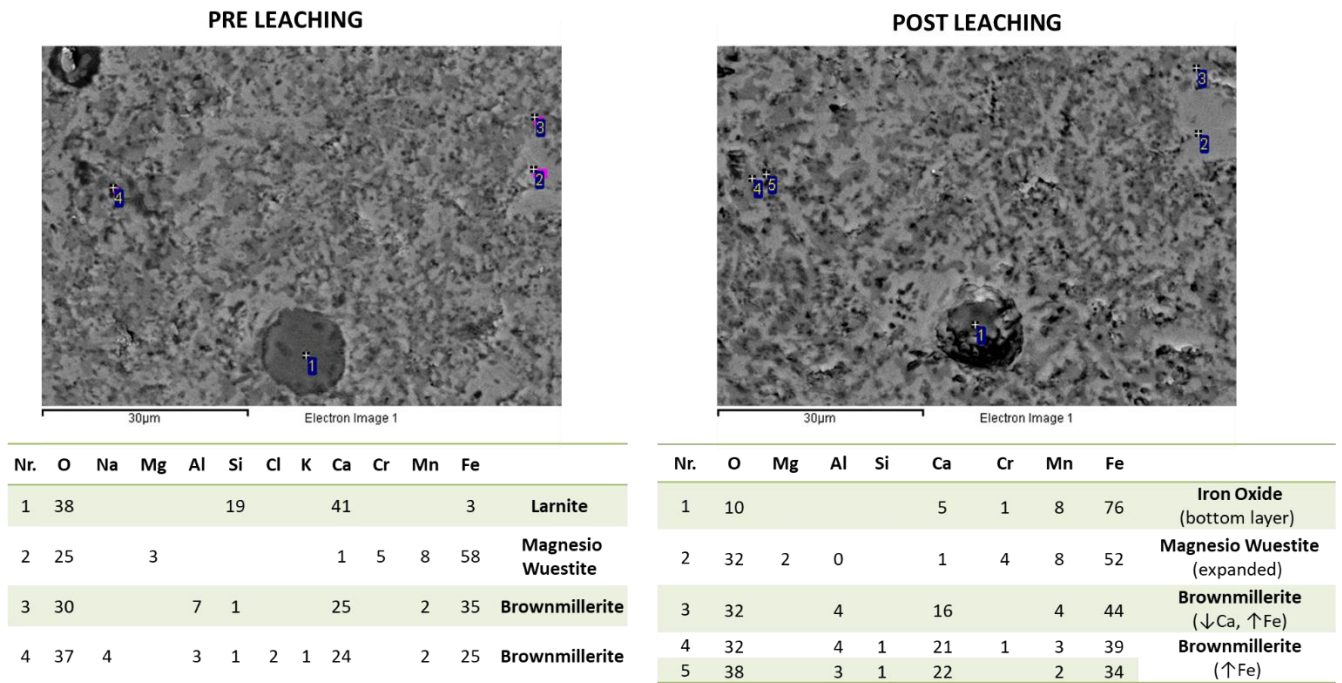


Figure 109 SEM back-scattered electron (BSE) image of slag microstructure with its EDXS analysis on metallographically polished before and after leaching. All results are in weight %.

### 5.3.1.3. Leaching behaviour

Since the EAF slag derives from a melting process of ferrous scrap, it can contain elements that are dangerous for the environment and for humans. These elements deriving from the alloying elements added on purpose in the composition of the original product in order to achieve certain properties.

For this reason, EAF slags which are not classified and commercialized as by-product are classified as waste which CER codes 10 02 02 "Untreated slag", CER 10 09 03 "Fusion slag", and CER 10 02 01 "Wastes from waste treatment". According to the Italian regulation, when the slag is classified as waste it must be compliant to the Ministerial Decree or for material reuse 19/05/06 "Identification of non-hazardous waste subjected to simplified recovery procedures" [245], or for landfill disposal 30/08/2005 "Definition of eligibility criteria for landfill waste" [246]. Both decrees base the slag characterization on leaching behaviour according to the standard CEN-EN 12457-2 [72].

The leaching test was conducted on EAF slag in grain size lower than 4mm according to the standard CEN-EN 12457-2 [72], moreover, since according to literature [247], [335] lower grain size implies higher leaching of heavy metals, the same test was conducted on both free slag in grain size lower than 0.106mm and the same size incorporated into ELT matrix. The results are shown in Figure 38.

It was found that with decreasing the slag grain size the leaching of Mo increases as well as pH and Conductivity. By incorporating the slag particles into the ELT matrix the leaching of Mo, Cr and V is reduced (in particular the Cr leaching falls within the threshold limit for material reuse), and also pH and conductivity are markedly reduced thanks to the shielding ability of the matrix.

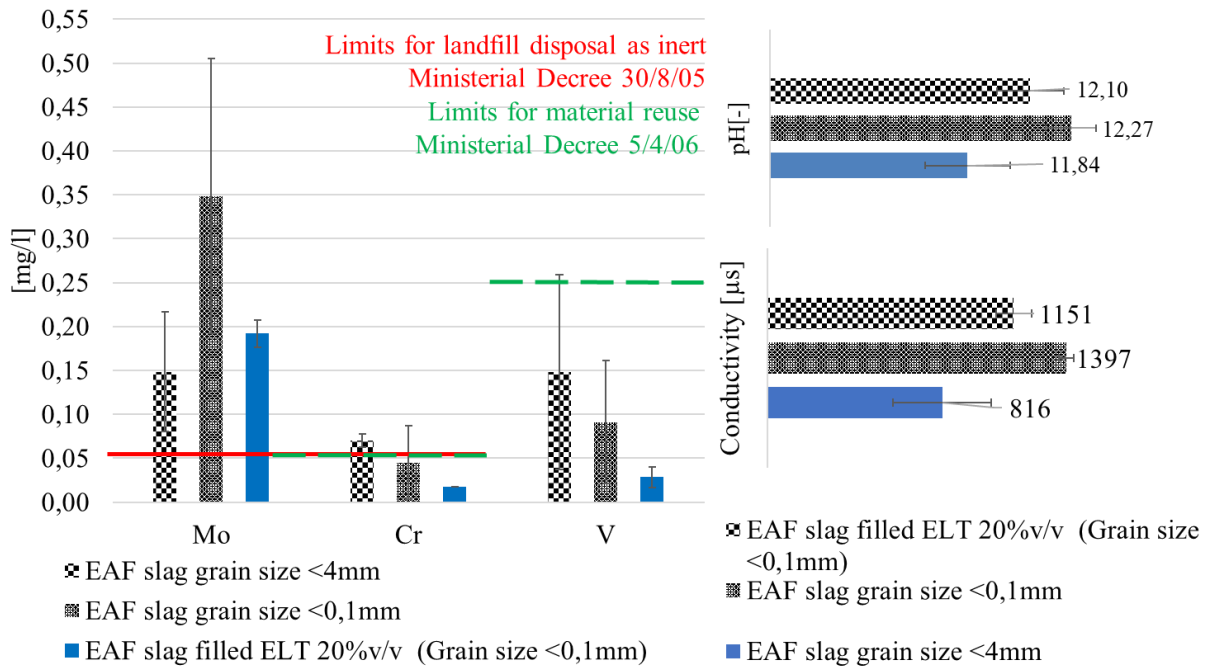


Figure 110 Leaching test results of free EAF slag and EAF slag incorporated into ELT matrix at 20%v/v).

### 5.3.2. Compound characterization

Figure 111 shows the recycled ELT sample decomposition TG and DTG curves. It illustrates the four components of rubber tire that correspond to its decomposition: volatile, rubber, carbon black and ashes weight fraction.

The first weight loss corresponds to the emission of volatile (8%), followed by the decomposition of rubber compounds, natural rubber (with a degradation peak at 375°C [336]) and synthetic rubber with a degradation peak at 430°C for a total of about 56%. Carbon black content is 27.5% and the ashes (antioxidants, dust etc..) content is 7.8%

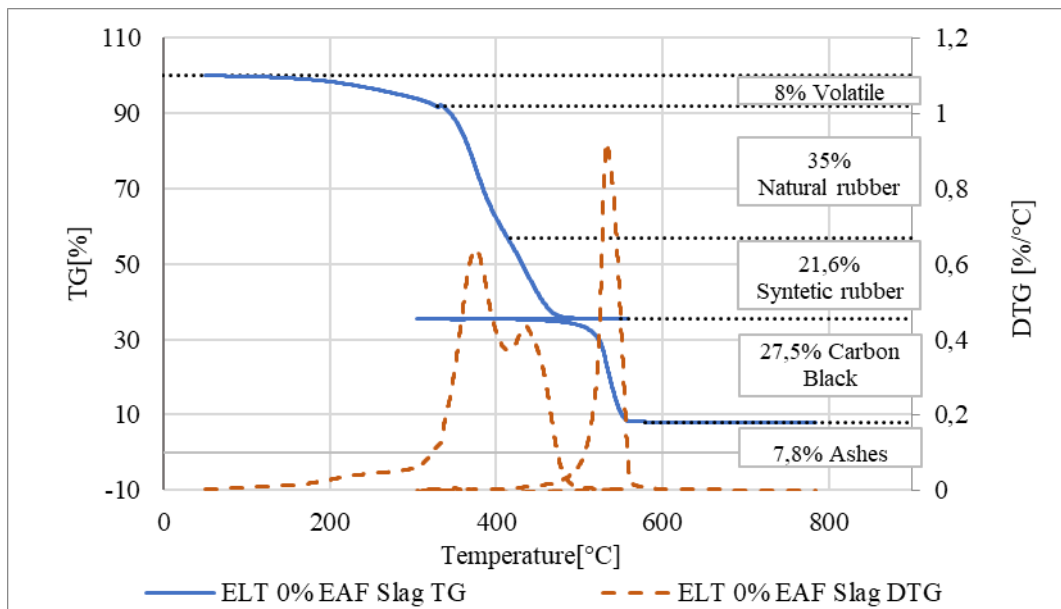


Figure 111 DG and DTG curves of recycled ELT sample and its components decomposition in %wt.

The residue measured by the TGA on ELT compound with no added slag is non-null due to the presence of other filler in the original rubber tyre and the inevitable presence of dirt. By subtracting the unfilled ELT residue, the percentage by weight of EAF slag in the various compounds is lower than the nominal one. This is probably due to the loss of a certain amount of slag dust during the calendaring process. This is also evidenced by the density values: the density measured on the different compounds is slightly lower than the theoretical one, as shown in Table 26.

Table 26 Nominal percentage of EAF slag as filler and real percentage of all fillers measured by TGA. Nominal and measured densities of compounds filled with different amounts of EAF slag.

Nominal EAF slag		TGA residue			Real EAF slag						Nominal Density	Measured Density [g/cm <sup>3</sup> ]			
% [v/v]	% [wt]	% [wt]			% [wt]			% [v/v]			[g/cm <sup>3</sup> ]	[g/cm <sup>3</sup> ]			
0	0	7,8	±	0,2	0	±	0,2	0	±	0,0	1,13	1,17	±	0,003	
5	15	19	±	0,4	12	±	0,4	4	±	0,2	1,27	1,25	±	0,02	
10	28	31	±	0,3	24	±	0,3	8	±	0,2	1,41	1,32	±	0,03	
20	46	47	±	0,9	40	±	0,9	17	±	0,1	1,68	1,53	±	0,002	

### 5.3.2.1. Hardness

Figure 112 shows the hardness value in mIRHD scale for ELT compound filled with different amount of EAF slag. It was found that the hardness value increases with the amount of EAF slag as filler. This behaviour was expected because with increasing the quantity of rigid particles of slag, the compound hardness increases proportionally to the percentage by volume of the rigid filler.

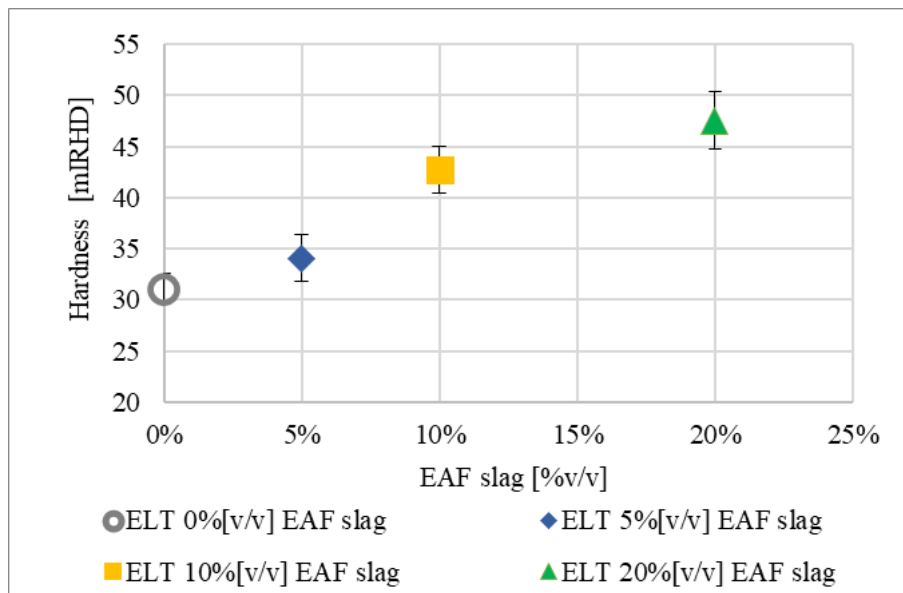


Figure 112 Hardness [mIRHD] of EAF slag filled recycled ELT.

### 5.3.2.2. Tensile properties

Figure 113 shows the stress-optical strain curves for a representative sample for each compound (ELT and ELT filled with 0,5,10,20%v/v of EAF slag). It is possible to notice that with increasing the amount of EAF slag as filler both the stress and the strain at break decrease significantly beyond a slag content equal to 5%v/v .

The presence of rigid filler in the elastomeric matrix limits the polymer mobility resulting in a reduction of the strain at break and in the generation of localized over stresses causing the lower stress at break. The strain hardening occurs only in the recycled ELT with no added slag.

The slag particles act a double role in the material: on one side they promote the mechanical de-vulcanization during the calendaring process by increasing the shear and the macromolecular network breakage; on the other side they act as an obstacle to the mutual adhesion of the rubber particles. According to the tensile test results it is possible to state that the if a polymer fraction is adsorbed by the slag particles, this fraction is not sufficient to make the filler the load bearing fraction of the composite material but on the contrary, it weakens the ultimate tensile properties.

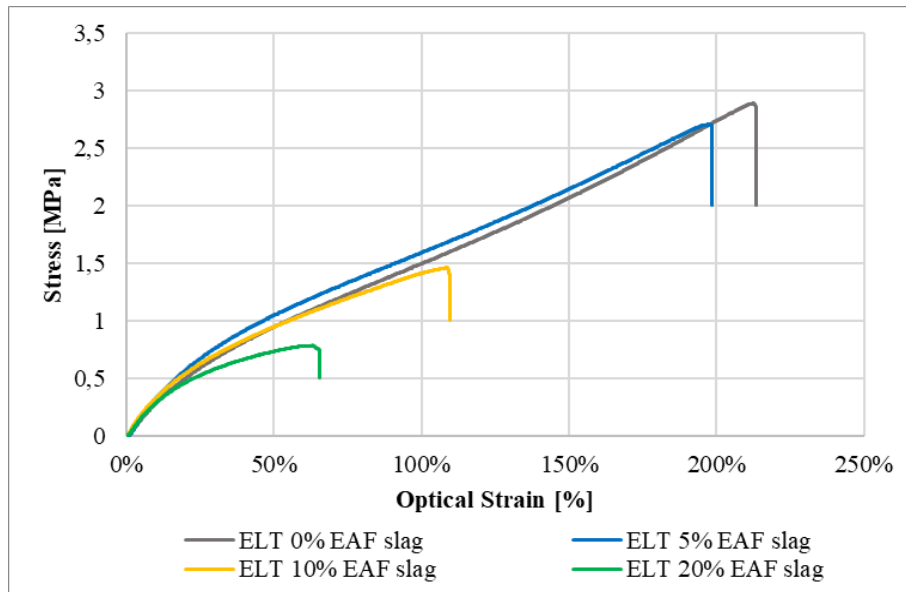


Figure 113 Stress-optical strain curves of EAF slag filled recycled ELT.

Figure 114 shows the elastic modulus calculated as the slope of the first linear section of the stress-optical strain curves. It is possible to observe that the presence of slag as filler slightly increases the composites modulus already for a content of 5%, then it remains about constant. This could be attributable to the double effect of the slag particles which, as aforementioned, promote devulcanization but also constitute the rigid phase of the material resulting in a global stiffening.

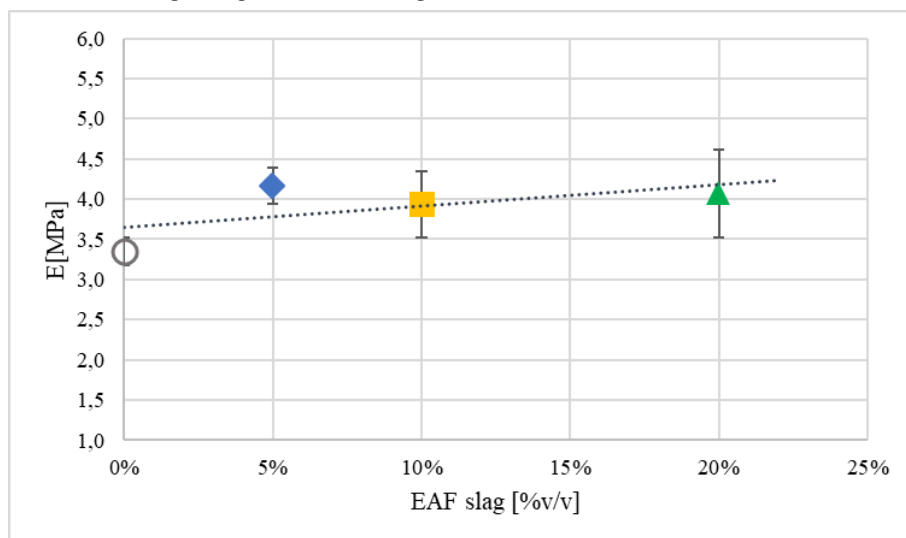


Figure 114 Tensile elastic modulus of recycled ELT filled with EAF slag at 0, 5, 10, 20% v/v.

### 5.3.2.3. Scanning Electron Microscope (SEM) analysis

SEM micrograph and backscattering images of cross sections of specimens tested in tensile test is reported in Figure 115. As first it is possible to notice that the calendaring process allows to obtain a compact and cohesive and compact material; no discontinuities in the elastomeric matrix are visible although the presence of few micro crates. The good distribution of the slag particles can be appreciated from the SEM images in backscattering mode, while the micrographs give information on the fracture topography [337]. Filler particles detachment from the polymer matrix is observed for large particles, while the particles of small dimension seem to be well incorporated in the matrix with good filler-matrix interaction.

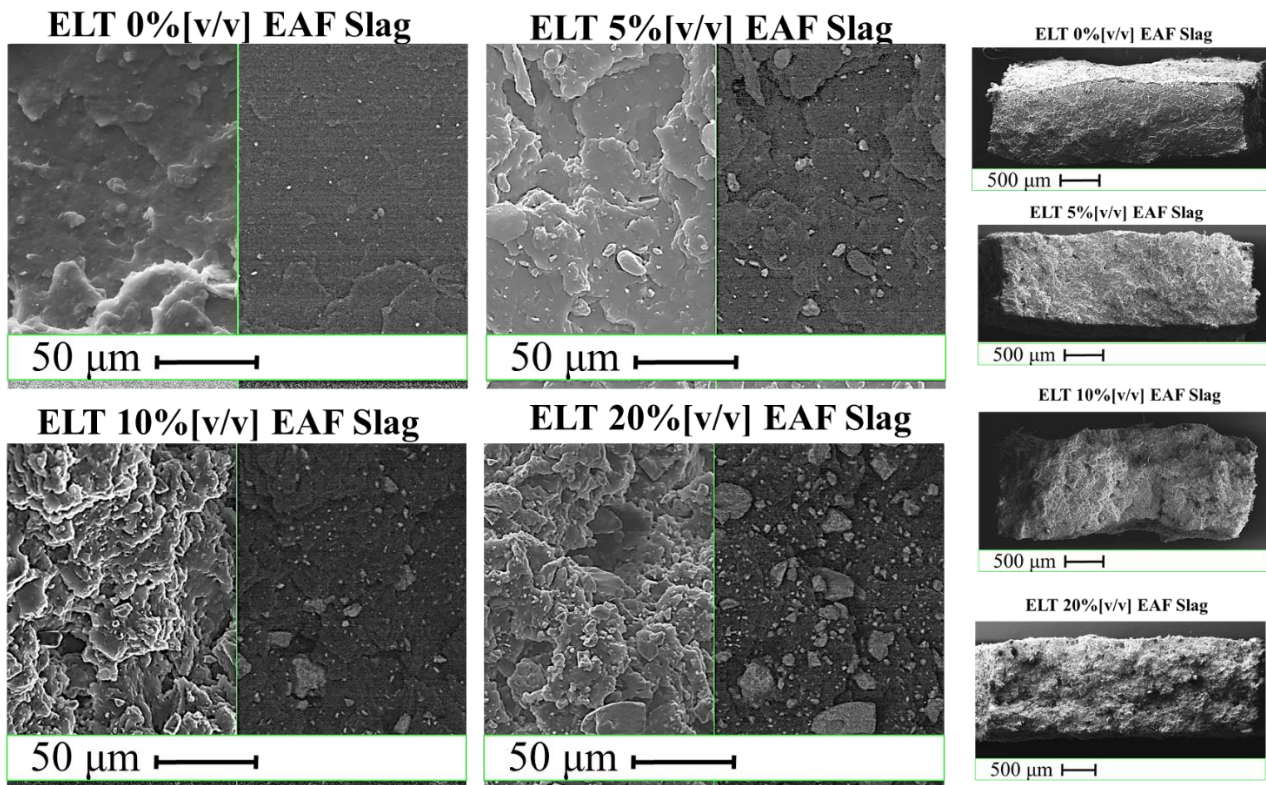


Figure 115 SEM micrograph and backscattering images of cross sections of specimens tested in tensile test at different enlargements.

### 5.3.2.4. Mullins effect

As evidence of the good cohesion and uniformity of the material in Figure 116 the Mullins effect is shown for the different composites. First of all, it is possible to state that the cyclic loading results in hysteresis which is already well visible at the second loading cycled up to reach a stable configuration at the third loading cycle. Moreover, when the applied strain exceeds that of the previous cycle, the stress returns on the same path of the uniaxial stress-strain curve, reported in Figure 116 as dotted line. This behaviour is well known in filled rubber [202].

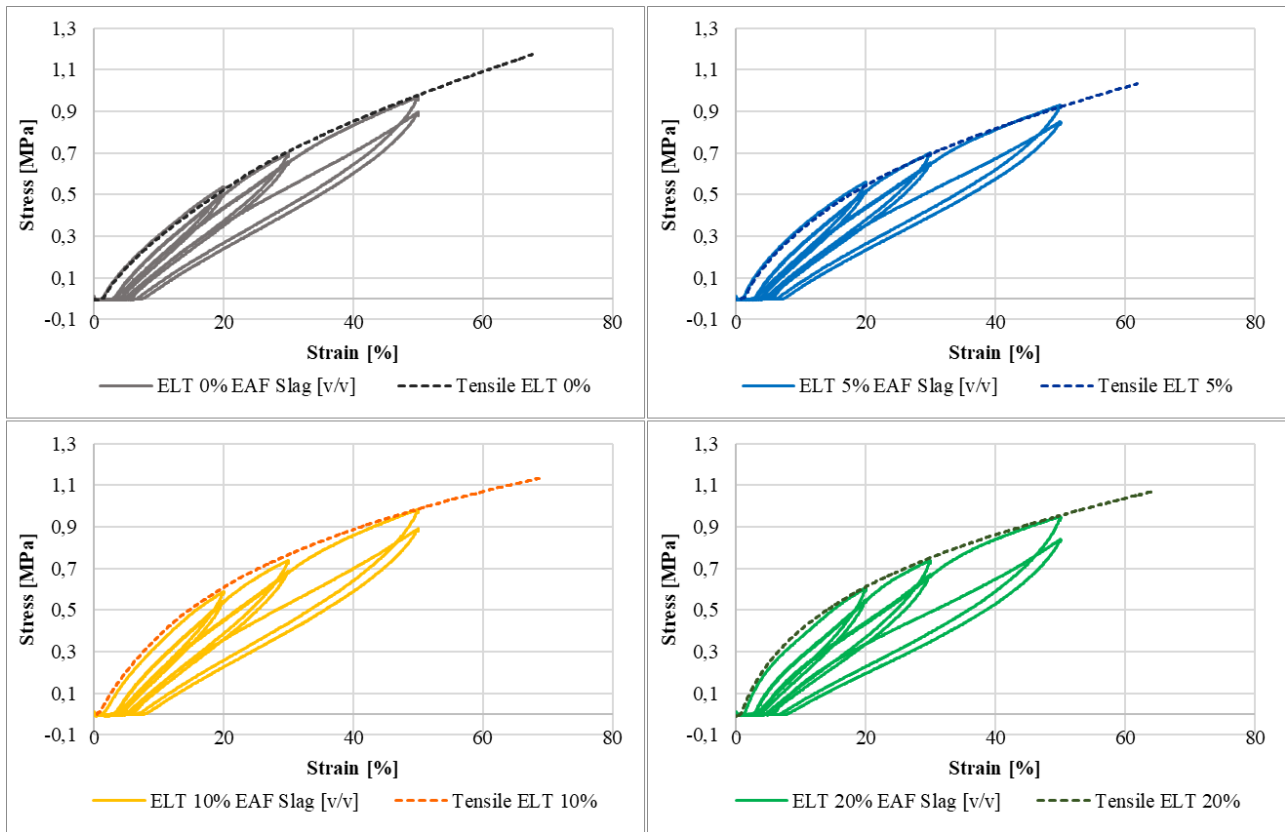
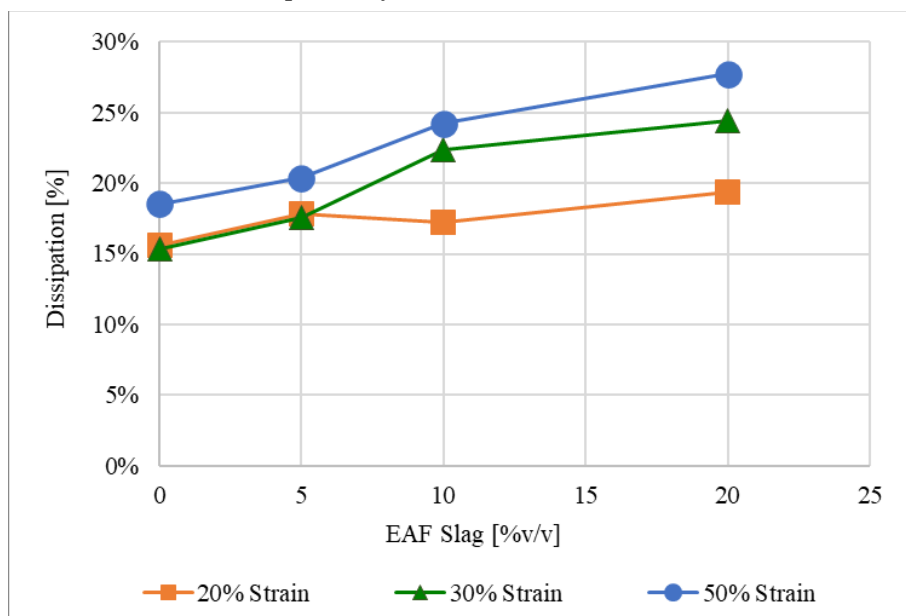


Figure 116 Uniaxial tension stress strain cyclic loading at different strain (20, 30, 50%) of recycled ELT filled with EAF slag at 0, 5, 10, 20% v/v. Uniaxial static stress-strain curve is shown as dotted line.

In the EAF slag filled ELT composites it was found that up to 5% EAF slag content the dissipation is little affected by the imposed deformation (20, 30 and 50%) and remains at 15-18%; for 10% EAF slag the dissipation increases and for 30% and 50% strain it increases up to a value of about 23% while for 20% strain it remains at 18%; as last, for 20% of slag content the dissipation increases with increasing the imposed deformation at 28%, 24% and 19% for 50%, 30% and 20% respectively.



*Figure 117 Mullins effect as energy dissipation [%] between the first and the fourth loading cycle for different imposed strain.*

#### **5.3.2.5. Dynamic mechanical analysis**

Experimental data of the storage modulus ( $E'$ ) and loss modulus ( $E''$ ), were obtained by DMTA by scanning temperature for the different frequencies examined at a strain amplitude of  $15\mu\text{m}$  equal to about 0.03%. The results are shown in Figure 118. Is it possible to observe that, as expected, with increasing the frequency the curves are translated at higher temperatures.

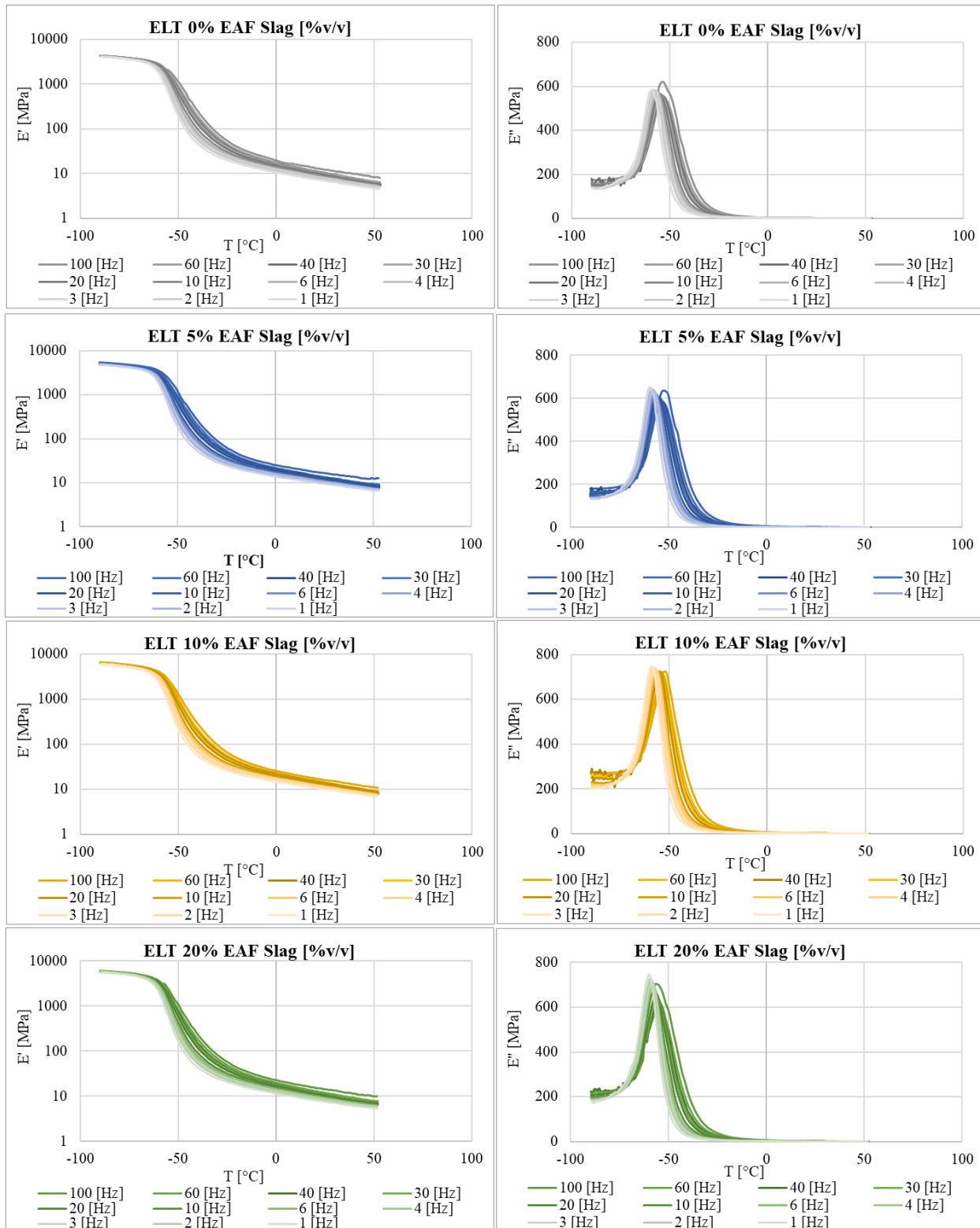


Figure 118 Storage modulus ( $E'$ ) and loss modulus ( $E''$ ) of ELT 0, 5, 10, 20 % EAF slag [v/v] as function of temperature (-90 +70°C) at different frequencies and strain amplitude of  $15\mu\text{m}$ .

The cross-plot of the curves of Figure 118 allowed the construction of a series of isothermal curves at various temperatures (-90 +70°C) as function of frequency (between 1 and 100Hz) as shown in Figure 119.

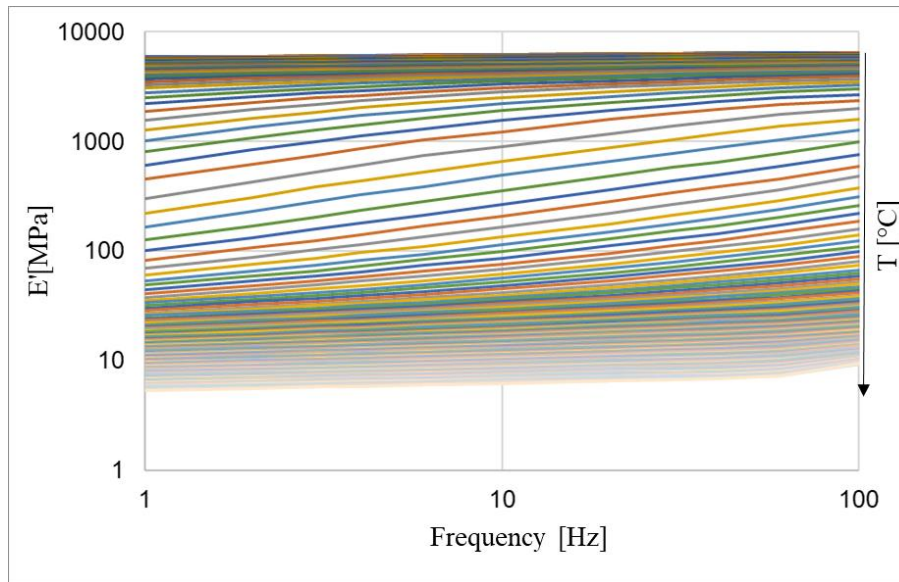


Figure 119 Isothermal storage modulus values for sample ELT 5% EAF Slag [v/v] as function of frequency.

According to the according to a frequency–temperature superposition approach [208] these data were reduced to obtain a the master curve of the dynamic storage and loss moduli as a function of frequency at the reference temperature of 20°C as shown in Figure 120.

From these results is it possible to affirm that the slag content does not affect the dynamic moduli. This result is in agreement with the elastic modulus determined by the tensile test where just a slight increases was found.

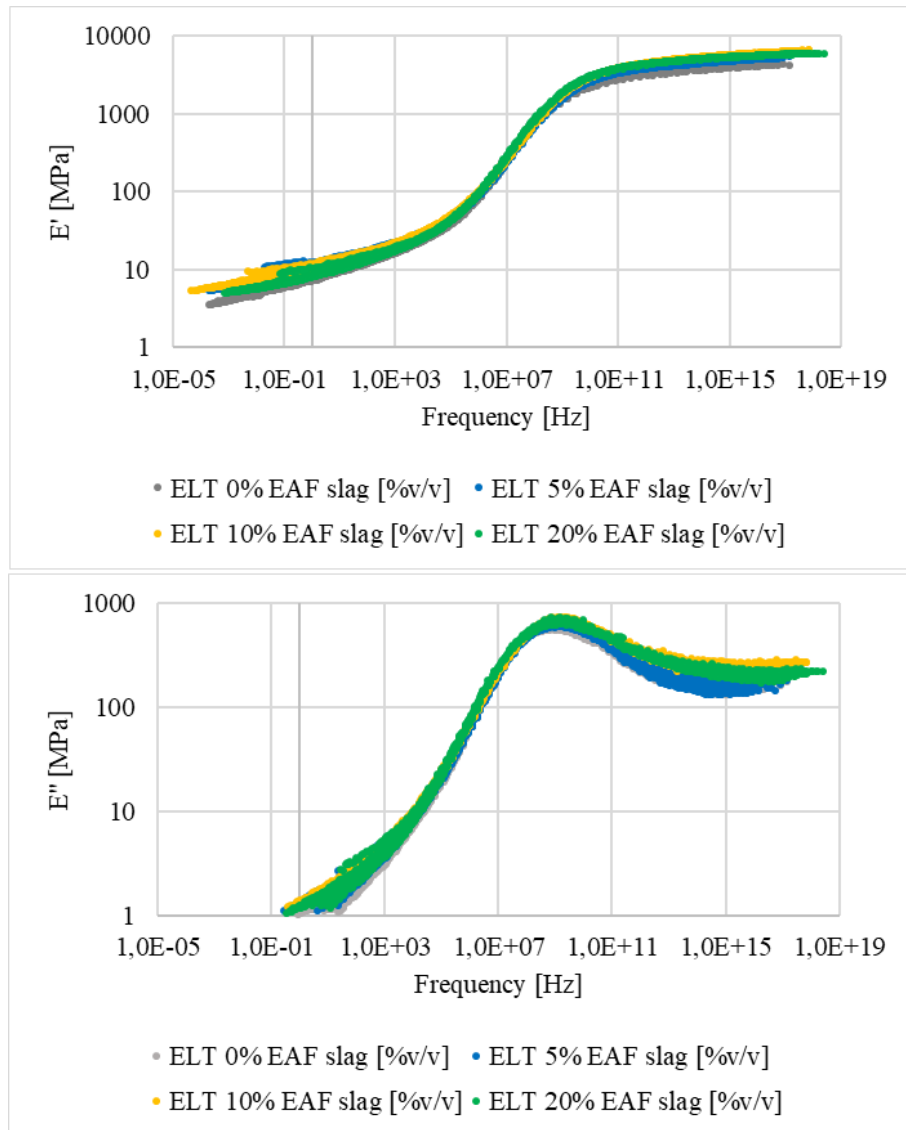


Figure 120 Master curves of storage and loss moduli of ELT 0, 5, 10, 20 % EAF slag [v/v] as function of frequency.

To construct the master curve, the isothermal curves were shifted horizontally to best superposition. The procedure provided an empirical determination of the shift factor  $a(T)$ , that determines the position of the master curve on the frequency axis at any other given reference temperature. The shift factor determined for the recycled ELT with different slag content is shown in Figure 121. Is it possible to observe a change in the slope in correspondence of the glass transition temperature ( $-60^{\circ}\text{C}$ ). The curves of the 4 materials are well overlapped, so that the slag content does not affect  $a(T)$ .

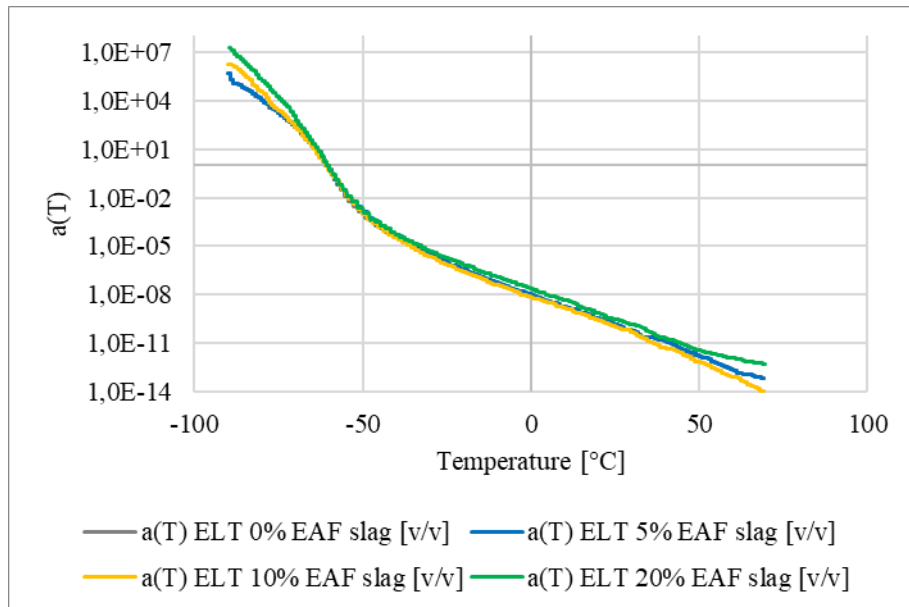


Figure 121 Shift factor of of ELT 0, 5, 10, 20 % EAF slag [v/v] as function of temperature (-90+70 $^{\circ}C$ ).

A series of isothermal master curves of storage and loss moduli referred to different temperatures in the range between -90 and +70 $^{\circ}C$  are reported in Figure 122 for the different tested materials.

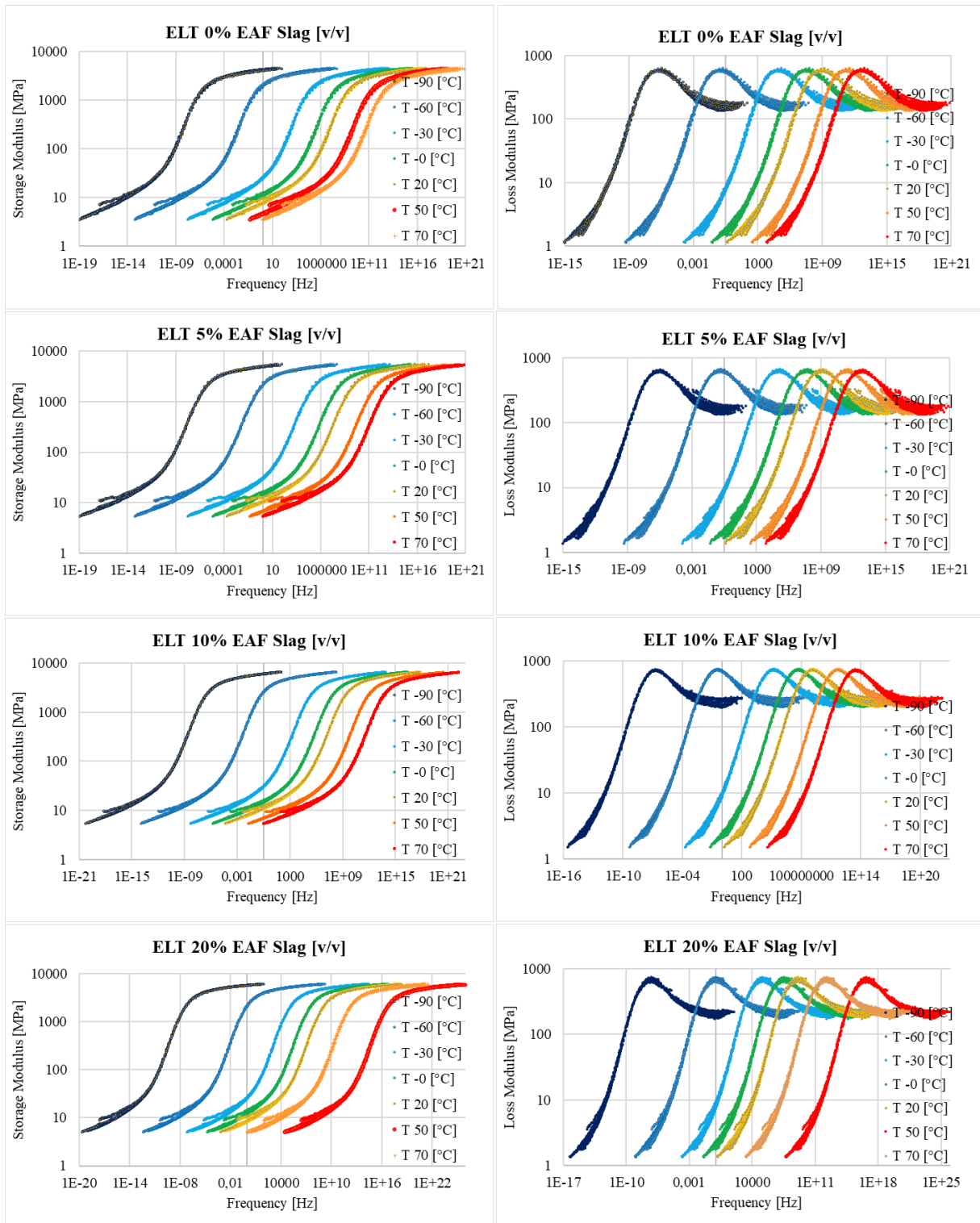


Figure 122 Storage modulus ( $E'$ ) and loss modulus ( $E''$ ) of ELT 0, 5, 10, 20 % EAF slag [v/v] as function of frequencies at different temperatures (-90 +70°C).

**5.3.2.6. Tribological properties**

Figure 123 shows the coefficient of friction (COF) and specific wear rate (Ws) of ELT 0, 5, 10, 20 % EAF slag [v/v] in single-way wear configuration. It is possible to note that the COF decreases with increasing the slag

content, but on the other side the specific wear shows an opposite trend. The tribological mechanism underlying these results can be investigated by observing the wear traces at SEM (Figure 124)

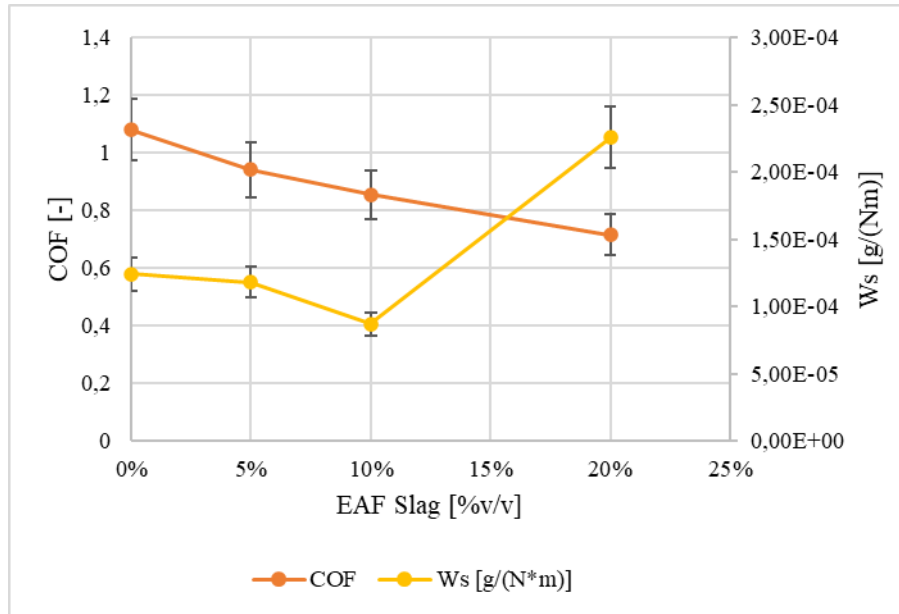


Figure 123 Coefficient of friction (COF) and specific wear rate (Ws) of ELT 0, 5, 10, 20 % EAF slag [v/v] in single-way wear configuration.

The COF decrease can be attributable to a higher compound hardness which reduces both the hysteretic and adhesion effect. This is evidenced by the formation of the Shallamach waves in the ELT 0% EAF slag.

On the other side the specific wear is also reduced up to a slag content of 10% [v/v] and then it dramatically increases for a slag content of 20% [v/v]. The tribological mechanism are investigated by wear traces SEM images (Figure 124). It is interesting to note in the SEM images in ESD at lower magnification the wear trace is clearly visible because inside the trace the slag particles are better visible, probably because the rubber layer that covers them is gradually removed before being able to pullout even the slag particle. Regarding the specific wear rate of materials with a slag content up to 10% [v/v], it is possible to attribute its decrease to the formation of material rolls clearly visible to the SEM that remain on the track and protect the underlying material. This "protective" effect is all the more marked the greater the slag content that hardens the composite. For higher slag contents, we observe the material with 20% slag [v/v] the abrasive effect of the slag particles is preponderant. It is important to underline that the specific wear rate has been calculated on a mass variation of the sample, but the slag has a density almost 4 times higher than that of the rubber, therefore the removal of a few particles of slag is equivalent to the removal of a large part of the rubber. For this reason it will also be interesting to evaluate the specific wear rate based on the volume variation.

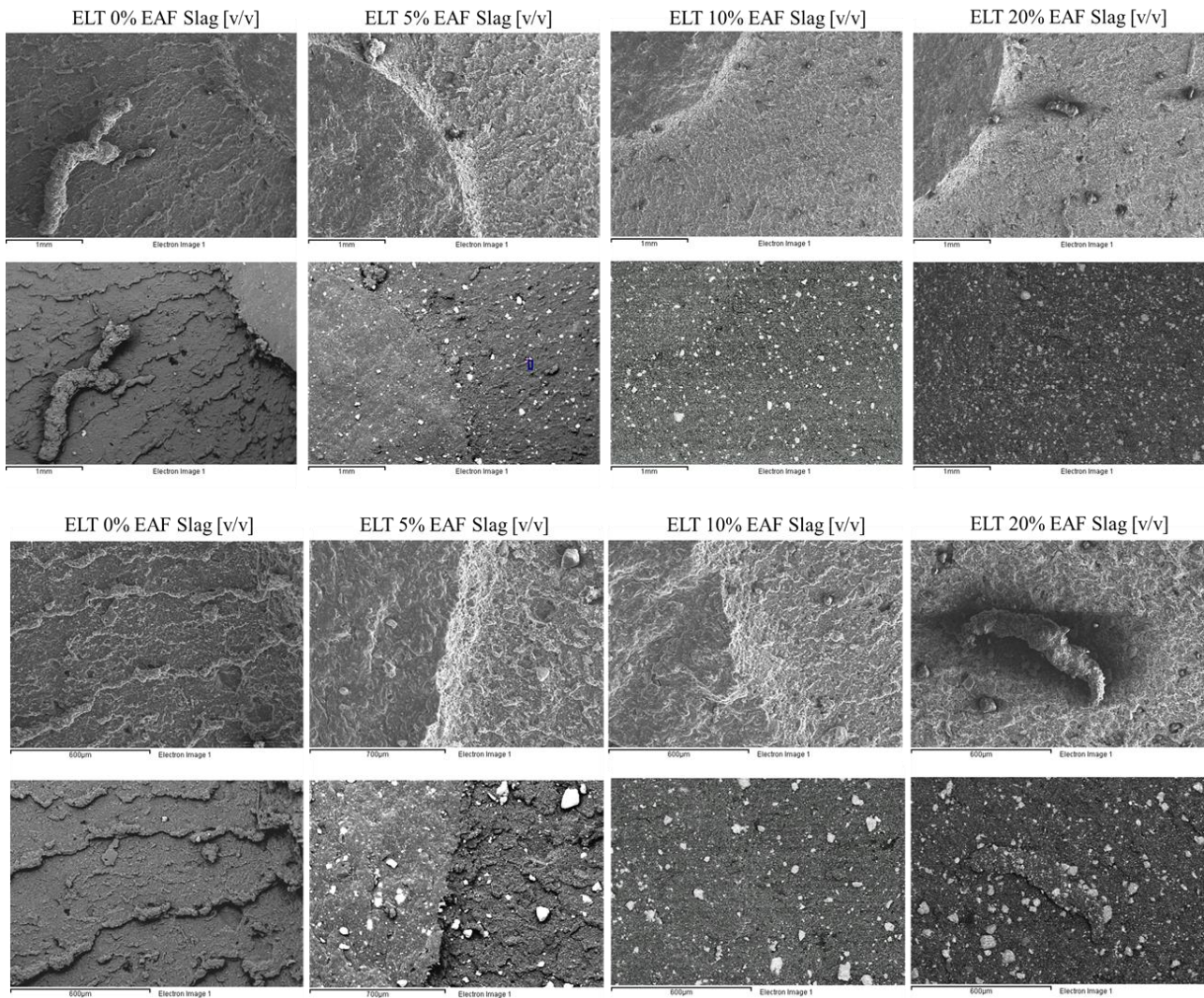


Figure 124 BSE and EDS SEM observations of wear track of ELT 0, 5, 10, 20 % EAF slag [v/v] in single-way wear configuration at different enlargements.

Figure 125 shows the coefficient of friction (COF) and specific wear rate (Ws) of ELT 0, 5, 10, 20 % EAF slag [v/v] in reciprocating wear configuration. It is possible to note that also in this test configuration the COF increases with increasing the slag content. As the slag content increases, the specific wear rate increases up to 10% of added slag, after which it remains constant even for a slag content of 20%. Probably this behaviour is due to the triggering of a phenomenon of abrasive wear due rigid slag particles acting as a third body favoring the material asportation.

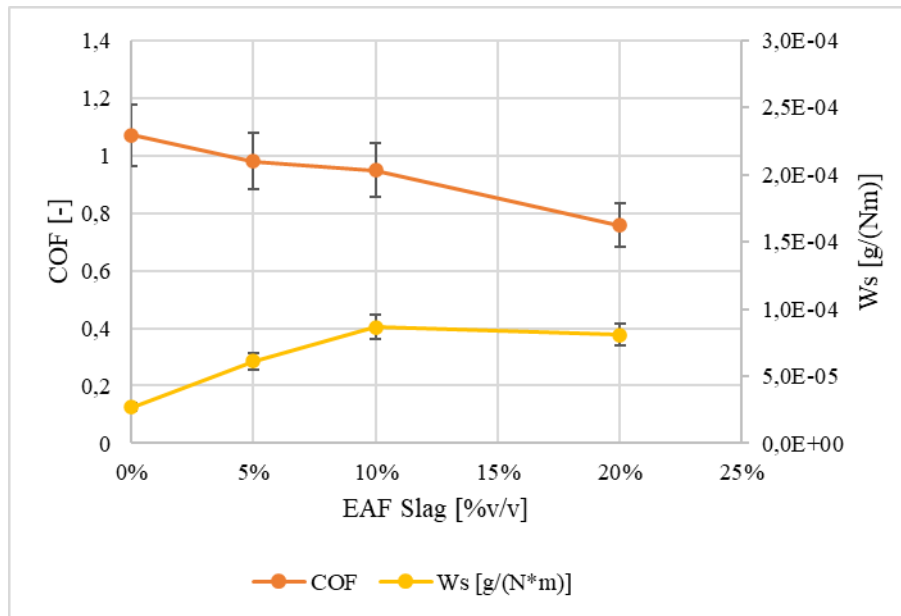


Figure 125 Coefficient of friction (COF) and specific wear rate (Ws) of ELT 0, 5, 10, 20 % EAF slag [v/v] in reciprocating wear configuration.

The COF trend can be explained similarly to the test conducted in single-way configuration. Regarding the specific wear rate, its increase can be attributed to the formation of rolls kept on the track and protecting the underlying material. As the slag content increases, the abrasive phenomenon is a slightly more marked up to the achieving of a balancing of these two phenomena.

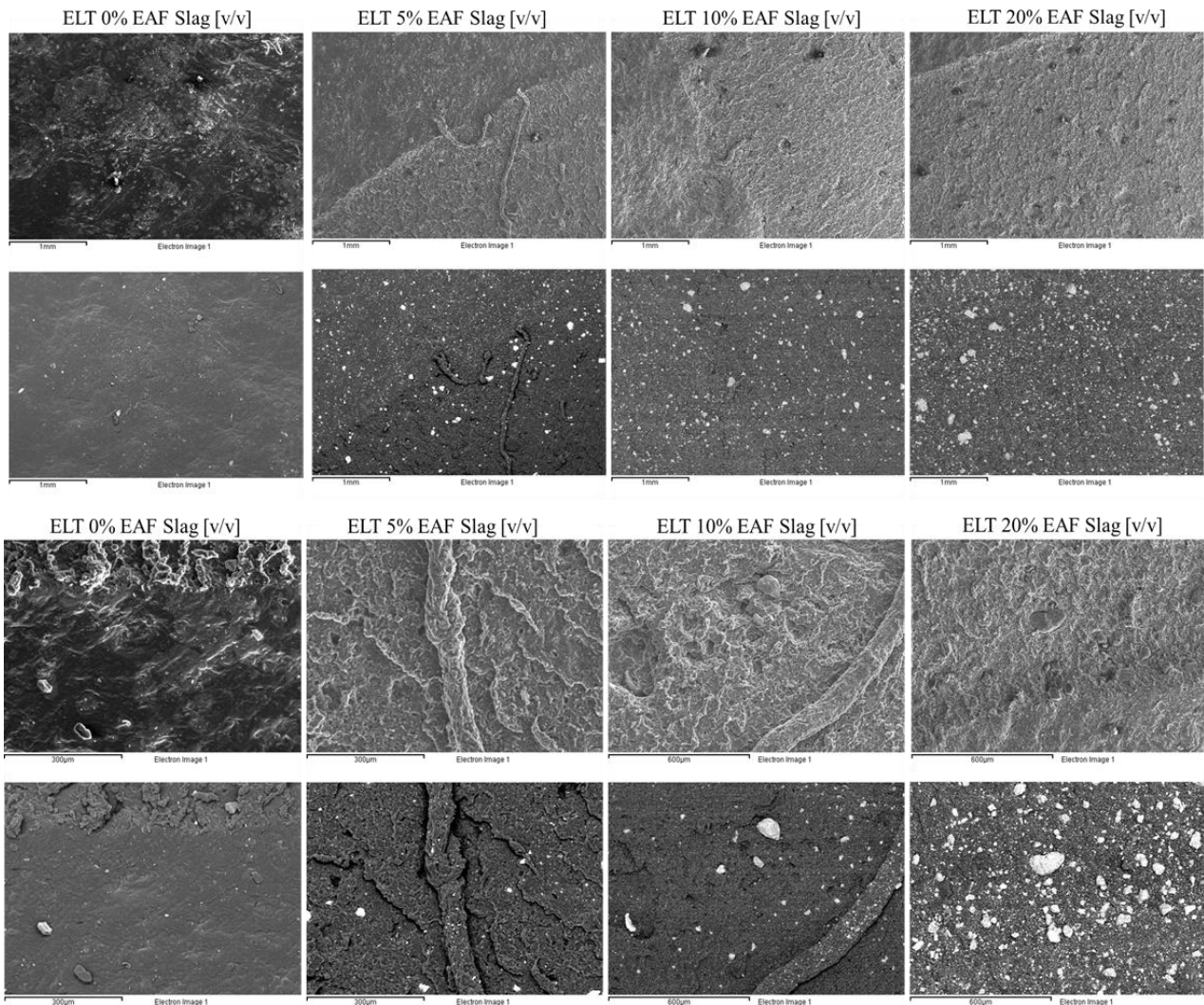


Figure 126 BSE and EDS SEM observations of wear track of ELT 0, 5, 10, 20 % EAF slag [v/v] in reciprocating wear configuration at different enlargements.

### 5.3.2.7. Thermal conductivity

As shown in Figure 127, the thermal conductivity of the ELT samples with 5, 10, and 20% slag follows a linear increase ( $y=0.0043x+0.2505$ ,  $R^2$  of 99.84%). The sample ELT 0% slag deviates from this trend, as in contrast to the expected lowest thermal conductivity, the measurement yielded to 0.284 W/mK. Based on the linear regression,  $\lambda_{ELT0}$  should be 0.250 W/mK. The reason for the difference is that the surface of the ELT 0% slag specimen was very rough compared to the other specimens, which caused the measurement of the specimen thickness to be error-prone in the range of 0.15 mm. If this thickness deviation is inserted in Equation 35, a  $\lambda_{ELT0}$  of 0.261 W/mK would result.

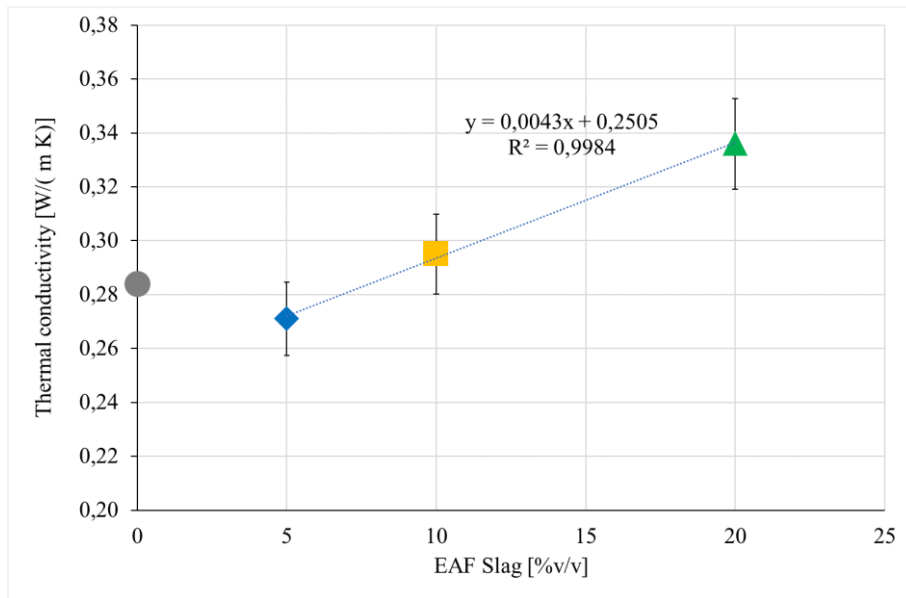


Figure 127 Thermal conductivity ( $\lambda$ ) of ELT 0, 5, 10, 20% EAF slag [v/v] determined according to ASTM E1530 [328].

### 5.3.2.8. Magnetic properties

EAF slag confers the composites magnetic properties due to the presence of both trapped steel drops and iron oxide in the form of magnetite. The load required to detach a magnet from a slag filled ELT sample is shown in Figure 128. It was found that with increasing the slag content the detachment load increases. ELT 0%v/v EAF slag shows a small detachment load probably attributable to some metallic residue in the ELT powder. EAF slag confers to rubber ferromagnetic properties, so it may be used as a shield for magnetic fields. Ferromagnetic materials with greater magnetic permeability than air provide a preferential path to the magnetic field. In this way, they absorb the flux lines of the magnetic field from the area around the source to be shielded. This application requires a specific characterization of the material.

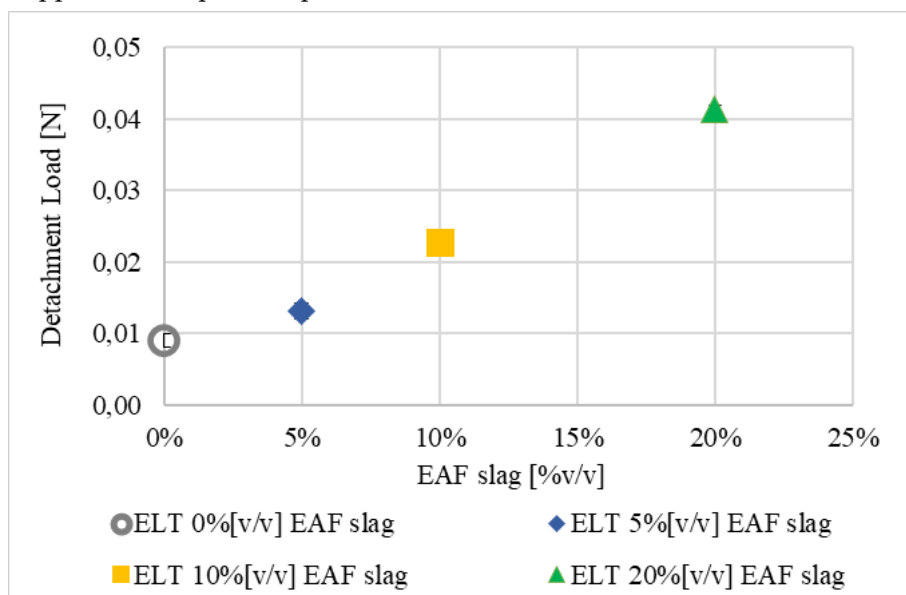


Figure 128 Detachment load between a magnet and the ELT samples filled with 0, 5, 10, 20% v/v EAF slag.

### 5.3.2.9. Swelling

The swelling behaviour of cured rubber indicates the crosslinking density of the material. This property is particularly relevant for rubber recycling, since on the one hand the crosslinking density affects the mechanical properties of the material and on the other hand crosslinks are responsible for the rubber curing, i.e. or the impossibility of further processing it by means of heating the material as thermoplastic polymers.

The crosslink density is an important parameter in the rubber design of virgin cured rubber because the mechanical properties (hardness, tensile strength, elastic modulus) are strongly related to it. These properties strongly depend on the structure of the network, such as its density and the type of crosslinking [302].

The swelling behaviour of the cured rubber indicates the crosslink density of the material. This property is particularly relevant in rubber recycling, since on the one hand the crosslink density affects the mechanical properties of the material and on the other hand the crosslinks are responsible for the curing of the rubber or the inability to process the rubber compound further by heating the material like thermoplastic polymers.

The recycling method adopted in the present study involved the calendaring of rubber powder up to the obtaining of a homogeneous and cohesive material. The rubber powder is mechanically stretched by the application of a shear stress which leads to the occurrence of a mechanical devulcanization. The presence of rigid slag particles can have a double effect: on one side they can promote the mechanical devulcanization because they reduce the space between the rotating cylinder further accentuating the rubber shear stretching; on the other side the rigid slag particles interact with the rubber creating a rigid polymeric layer that reduces the swelling.

Swelling test results are shown in Figure 129. Swelling coefficient is reported as dotted line, while the crosslink density determined by the Flory-Rehner equation is reported as solid line.

It was found that with increasing the EAF slag content the swelling coefficient decreases of about 10%, and the crosslink density slightly increases (Figure 129). These findings show that the presence of EAF slag as particles obstacles the solvent permeation. This could be attributable to the rigid polymeric layer around the slag particles and also to an increase in entanglements density. In the calendaring process the rubber powder became a network which is continuously stretched improving the physical bonds between the macromolecules.

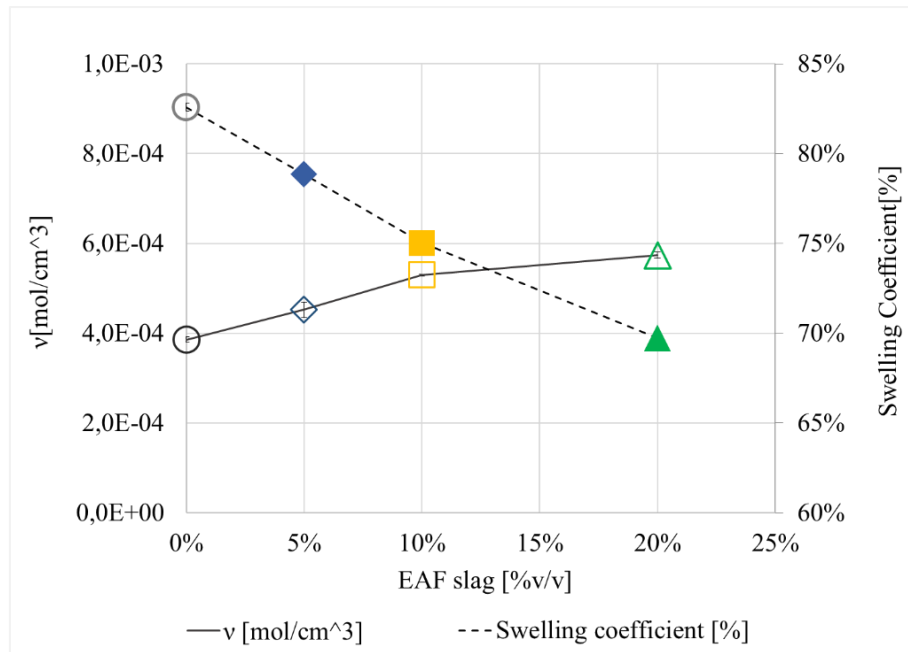


Figure 129 Crosslink density determined by the Flory-Rehmer equation and swelling coefficient on swelling test data (48 h immersion in toluene and 24h drying at 80°C).

Figure 130 shows the Kraus plot of EAF slag filled ELT in order to define the reinforcement (K) versus the filler volume fraction. The slope of the Kraus plot (K) is a measure of the polymer-filler interaction: the higher the negative slope value, the greater is the reinforcement effect.  $V_{r0}$  is assumed equal to  $V_{r0}$  for ELT 0% EAF slag due to the purpose to evaluate the EAF slag influence neglecting that of carbon black which is constant for all the compounds. The negative slope of the Kraus plot denotes a reinforcement effect of EAF slag as filler for ELT.

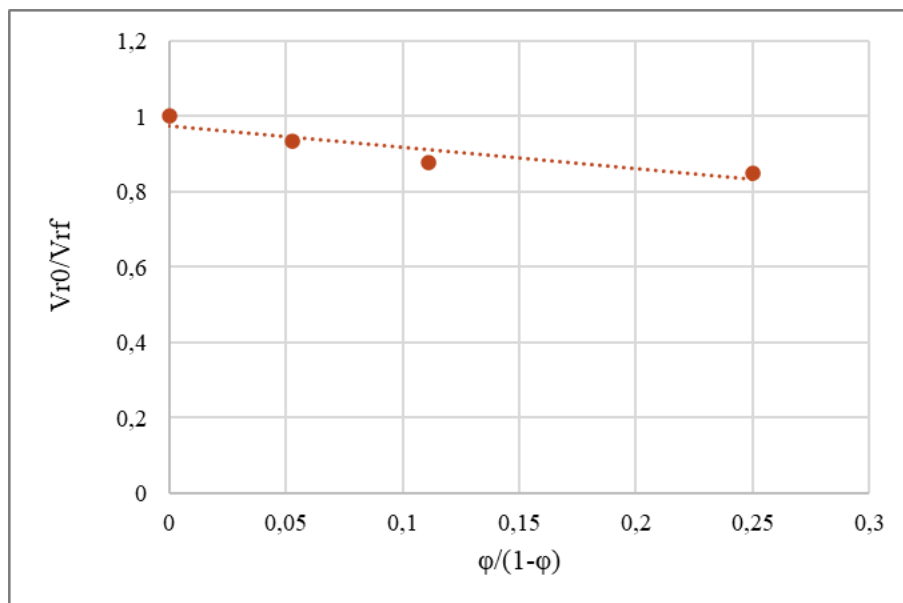


Figure 130 Kraus plot of EAF slag filled ELT.

### 5.3.2.10. Differential scanning calorimetry

The increase in heat capacity net of the filler,  $\Delta C_p^*$  is associated with the quantity of polymer that participates in the glass transition and depends on the polymer-filler interaction. The intermolecular rigidity is correlated to the polymer chains immobilized in the material: the rubber fraction immobilized was calculated according to Equation 24, the results are shown in Figure 131. It is observable that as the EAF slag content increases, the increase in the heat capacity required by the rubber fraction at the glass transition temperature decreases due to the presence of a fraction of rigid rubber which remains in the glass phase even above the  $T_g$ .

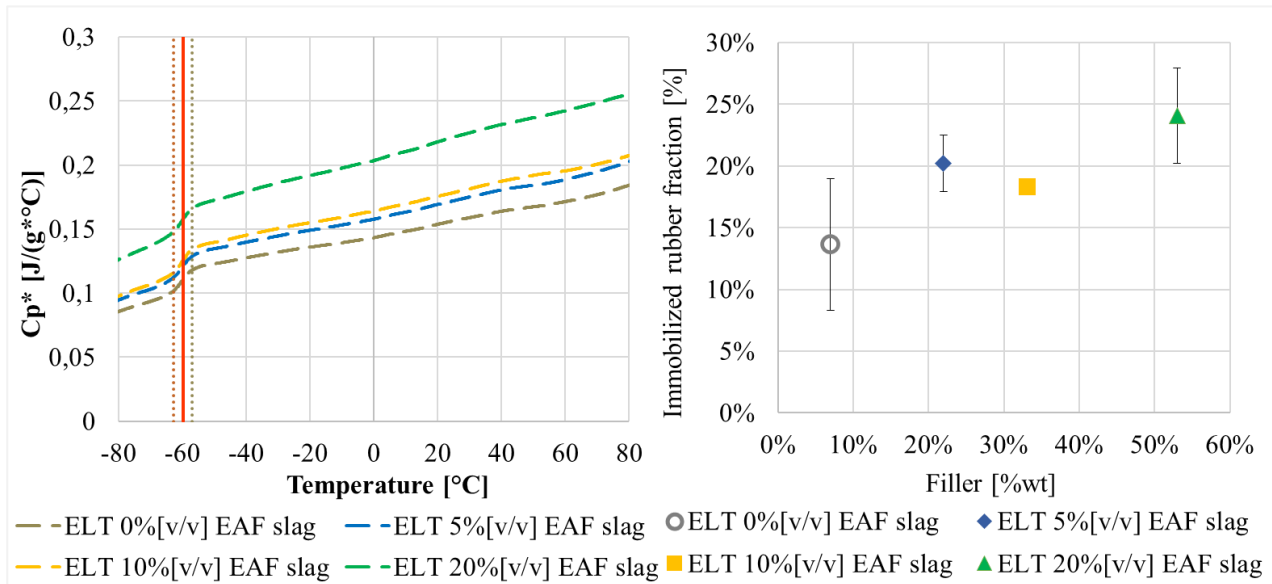


Figure 131a) Heat capacity scan determined by DSC at neat of filler vs temperature for EAF slag filled ELT. b) Immobilized rubber fraction determined as the heat capacity increment at  $T_g \pm 4^\circ\text{C}$ .

It is interesting to highlight that the slag content increases the heat capacity proportionally to the EAF slag content; this result is in agreement with the thermal conductivity test results.

### 5.3. Conclusion

According to the European Directive, 2000/53/EC when a tire is no longer usable, it is important to prefer material recovery over energy recovery. To date, discarded tires are reused in many applications (building materials, structural elements, fillers in plastic compounds, infill or sports flooring, recovery by pyrolysis or gasification, reuses special devulcanized rubber and experimental applications, such as absorbents for the removal of organic pollutants from water or protective layers of guard rails for motorcyclists). However, given the enormous quantity that is decommissioned every year, it is essential to continue researching new recycling methods as well as applications in order to reduce waste and also to preserve new resources.

The present study shows the characterization of recycled ELTs filled with EAF slag from 0 to 20% by volume using a very simple technology, at room temperature and without the addition of additives: calendaring in an open mixer. The obtained results can be summarized as follow:

- The incorporation of the slag into the recycled ELT matrix reduces the leaching of Cr, Mo and V as well as the pH and electrical conductivity of the eluate.
- The mineralogical phase of the slag that is most altered in leaching is larnite as it dissolves.
- The hardness of the composite increases as the presence of slag increases but the static and dynamic modulus of elasticity does not undergo evident variations.

- The recycling process leads to a homogeneous and cohesive material as observed by SEM fracture surfaces. Furthermore, viscoelastic effects such as the Mullins effect are appreciable, in particular the dissipation increases as the slag increases. This can be attributed to the interaction between charge and matrix.
- The interaction between filler and matrix was also highlighted by the DSC data (increase in the fraction of immobilized polymer with increasing filler content) and by the swelling data where the presence of the slag reduces the swelling (indicating an increase in the crosslinking density).
- From the tribological tests it emerged that the COF decreases as the slag increases, while the specific wear rate increases in the single-way wear configuration and decreases (up to 10% of slag) in reciprocating.
- Finally, the slag gives the rubber magnetic properties and increases its thermal conductivity, expanding the possible applications of this 100% recycled material.

In conclusion, experimental results showed how some properties of recycled ELT can be improved without the exploitation of raw materials, enhancing not only the ELT but also the EAF slag in a context of circular economy.

## 6. Potential industrial Symbiosis between Steel and Rubber sector in Lombardy

In the present paragraph possible symbiotic paths between the steel sector and the rubber sector have been identified through the AIDA database and ATECO 2007 codes: 24.1 “Iron and steel industry - Manufacture of iron, steel and ferroalloys” and 22.19.09 “Manufacturing of other rubber parts n.e.c.”. in-depth also at the provincial level. This geographical subdivision was then flanked by the classification by type of enterprise (micro, small, medium and large) in accordance with the European Union Recommendation no. 2003/361/EC. From a regulatory point of view, the application of the by-product regulation articulated in art. 184-bis [338], introduced in Legislative Decree 152/2006 is studied for the case of EAF slag highlighting the critical issues related mainly to the burden of proof [339]. The management of slag as a by-product in a context of industrial symbiosis was deepened, identifying the possible flows, actors and economic advantages.

### 6.1. Waste and by-products

An industrial residue can be managed in a different way by following very different regulatory paths even though it is the same material. When a company has an "output" classified as waste, its management must be entrusted to an environmental manager before it can become a resource to be re-introduced into a system (Figure 132)



Figure 132 Waste Management

When a company has an "output" classified as “by-product”, the environmental manager action is no longer necessary, but the by-product can be managed by any industrial entity (Figure 133).



Figure 133 By-products Management.

From a regulatory point of view, Industrial Symbiosis transfers “by-products” not “waste”.

The by-product is governed by art. 184-bis [338], introduced into Legislative Decree 152/2006 through Legislative Decree 205/2010 which acknowledges the provisions of Directive 2008/98/EC. Any substance or object that meets all the following conditions (paragraph 1) is a by-product and not a waste:

1. The substance or object originates from a production process, of which it forms an integral part, and whose primary purpose is not the production of that substance or object;
2. It is certain that the substance or object will be used, during the same or a subsequent production or use process, by the manufacturer or third parties;
3. The substance or object can be used directly without any further treatment other than normal industrial practice;
4. Further use is legal, i.e. the substance or object meets, for the specific use, all relevant requirements regarding products and the protection of health and the environment and will not lead to overall negative impacts on the environment or human health.

The current legislation requires to assess on a case-by-case basis when a waste can be considered a by-product, or to implement a series of specific controls so that the assessment process allows to prevent any risk, both for

the environment and for the people who will reuse the material in new production processes and for those who will use the resulting product.

### 6.1.1 By-products legislations

The national regulation of the by-product as mentioned in the previous paragraph is articulated in art. 184-bis [338], introduced in Legislative Decree 152/2006 which is divided into paragraph 1 and paragraph 2. Paragraph 1 sets up the conditions that the substance or object must satisfy in order to be considered a by-product and not a waste. Since the regulations relating to by-products are exceptional and derogatory from the ordinary regulations on waste, the burden of proof on the existence of the requirements listed above must be fulfilled by the subjects who produce the residue, use it and manage it as a by-product.

Article 184-bis in paragraph 2 then provides for the possibility, on the basis of the conditions set out in paragraph 1, to take measures to establish qualitative or quantitative criteria to be met so that specific types of substances or objects are considered by-products and not waste. The adoption of these criteria is provided by one or more decrees of the Minister of the Environment.

In order to facilitate and promote the transfer of by-products, Ministerial Decree No. 264 was issued on 13 October 2016 ("Regulation containing indicative criteria to facilitate the demonstration of the existence of the requirements for the qualification of production residues as by-products and not as waste" [340]), provides for the establishment at the Chambers of Commerce of a public list of by-products in which producers and users of by-products can register. It is important to underline that the inclusion in the list of by-products does not constitute an enabling requirement, but it has only the function to ease transfers.

The Italian legal system transfers some competences in the field of waste to the Regions. In this regard In September 2021, the Lombardy region approved the guidelines for the management of black waste not only as a "by-product" but also as an "end of waste" [341].

Although the conditions for the reuse of a production residue as a by-product are established (Article 184-bis paragraph 1 of Legislative Decree 152/06) without the need for explicit authorization from specific entities, entailing undoubted management and economic benefits, the general nature of some of the established conditions does not facilitate the burden of proof, with negative repercussions for both the companies and the supervisory bodies.

In case of failure to prove all the aforementioned conditions, the consequences are of a criminal nature (unauthorized management of waste pursuant to Article 256 of the Consolidated Law on the Environment), which can constitute a disincentive for those who want to operate correctly in the absence of certain indications on the real extent of the conditions listed in art. 184-bis paragraph 1.

In fact, on the one hand, steel mills renounce the advantage deriving from the efficient use of resources, due to the risk of incurring heavy penalties, on the other hand the state cannot loosen controls for the protection of the environment and the health of citizens. It is necessary to think of tools that, in a reasonably short time, lead to a legislative clarification on the criticalities highlighted so that the interested parties know with certainty whether or not a residue can be managed as a by-product.

In order to overcome the difficulties of interpretation and application highlighted above and facilitate the use of production residues as by-products, Claps et al. [339] proposed the following measures:

- Issue of ministerial decrees (pursuant to Article 184-bis paragraph 2 of Legislative Decree 152/2006) for the adoption of qualitative or quantitative criteria to be met so that specific types of substances or objects are considered by-products and not waste;
- promote innovative industrial processes and facilitate production agreements between companies (industrial symbiosis) thanks to which the production residues of one can become production factors for the other;
- set up at a national level a Technical Commission or Technical Roundtable which provides for the involvement of the main stakeholders to better frame the application needs/difficulties of the current legislation and thus provide support to the Central Government and/or the competent Ministries in the adoption of "appropriate measures", starting from the adoption of detailed criteria for the uniform application of the conditions of art. 184-bis paragraph 1 of the Legislative Decree 152/2006 (for specific types of substances or objects) and/or through the modification of the already existing regulatory instrument with the participation of representatives of the supervisory and control authorities;
- favor program agreements on by-products and coordinate State-Regions initiatives, to avoid different situations on the national territory;
- favor the creation and adoption of a national, open-access database, which for each type of residue allows the identification of some of the possible production destinations, taking into account already consolidated paths and experiences of industrial symbiosis for the benefit of their replicability and with an indication, for this purpose, where they exist, of the technical requirements to be satisfied to allow the effective meeting between supply and request for resources;
- based also on the provisions of Ministerial Decree 264/16, art. 6 paragraph 2, on the point of "normal industrial practice", design or re-design the company production process including the activities and operations that are essential so that the production residue, from the origin and according to its specific destination, has the characteristics which allow it to be classified as a by-product;
- implement a technical support system for companies, such as the National Platform for Industrial Symbiosis ENEA, also with regional branches, which makes it possible to identify opportunities for exploiting surplus resources from a technical-scientific point of view and within a regulatory framework outlined, allowing at the same time the intersection of supply and demand on the territory;
- promote training activities for all stakeholders on the discipline of by-products.

### 6.1.2 Waste legislation

The regulatory definition of Waste in Italy is given by art. 183 of the legislative decree 3 April 2006 n. 152, so-called single environmental text: "Any substance or object that the holder discards or intends or has the obligation to discard" where the holder means the person who has it in charge (therefore only a subject who initially produces the good, but also those who have it in charge (for example by having purchased it from third parties) decide to discard it, then start it for disposal or recovery operations.

#### Loading and unloading register

Legislative Decree 152/2006, ART. 190 Waste producers are obliged to keep a loading and unloading register in which they must record information on the qualitative and quantitative characteristics of the waste, to be used for the purposes of annual communication to the Land Registry. The information contained in the register is made available at any time to the supervisory authority upon request.

### Temporary deposit

Temporary deposit is regulated by Legislative Decree 152/2006, ART. 183 and must be carried out for homogeneous categories of waste and in compliance with the relevant technical standards, for hazardous waste in compliance with the rules governing the storage, packaging and labeling of the hazardous substances contained therein; the mixing of different categories of hazardous waste referred to in Annex G to Part IV of Legislative Decree 152/06 DDG Lombardy Region no. 36 of 7/01/1998. The AREAS used for temporary storage must be adequately marked and delimited in order to make known the nature and danger of the waste; The waste containers must be marked with labels showing the main information used to fill in the form (CER code) The times within which they must be started for disposal are regulated by Legislative Decree 152/2006, ART. 183. The accumulation of waste at the place where it is produced is defined by the temporary storage legislation.

option 1. The producer can send the waste for recovery/disposal every 3 months from production regardless of the quantity produced (even greater than 20 cubic meters).

option 2. The producer can send the waste for recovery/disposal within a maximum of one year from production if the quantities are less than 20 cubic meters for non-hazardous waste and 10 cubic meters for hazardous waste, the time limit of 1 year from the date of production (noted on the loading/unloading register) is the absolute maximum allowed even on minimum quantities of waste.

The analysis of the waste is necessary, at least at the time of the first classification, for the purpose of defining the dangerousness of the waste and must be repeated periodically in relation to variations in the composition of the waste or, in the case of no variation, in order to demonstrate the persistence of non-hazardous characteristics.

If changes are made to the production cycle or to the raw materials used, a new analysis will have to be carried out.

### Own-account Transport

Transport on your own account is regulated by ex article 212 paragraph 8 of Legislative Decree 152/2006 and S.M.I. The discipline of registration in the Register for the transport of its self-produced waste is contained in paragraph 8 of Article 212 of Legislative Decree 152/2006.

Companies and entities are needed to register:

- initial producers of non-hazardous waste that collect and transport it.
- initial producers of hazardous waste that collect and transport thirty kilograms or thirty liters per day provided, however, that these operations are an integral and ancillary part of the organization of the manufacturing company.

## **6.2 Case of black slag: management methods**

Blackslag can be considered an emblematic case of co-product as its production is functional to the production of steel itself. Based on the management that the steel producer decides to hire for this material, it can assume the status of "waste" or "by-product". In September 2021, the Lombardy region approved the guidelines for the management of black waste not only as a "by-product" but also as an "end of waste".

### **6.2.1 EAF slag as by-product [341]:**

The producer of the EAF black slag aggregate commercializes a material with CE marking, proving that the characteristics comply with those declared in accordance with the UNI 13242 standard on recycled aggregates. The manufacturer must therefore have a production manual control, or a set of verification and control

procedures that are carried out on the entire process, thus ensuring that it can promptly identify and correct any deviations of the material from the declared characteristics. Based on current legislation, the manufacturer must ensure control of the process through an adequate definition of the criteria to identify, plan and control the work phases into which the process itself can be broken down, both from the point of view of quality and safety.

In this context, to enhance the amount of slag currently disposed of, in this study it is proposed to integrate the current cooperation (building sector) with a new synergy involving the innovative application of slag as filler for rubber matrix in fine grain size.

The flows map sees the crushing of the slag for the recovery of the metal, after which the coarse particle size fraction (by-product) can be destined for the building sector which uses it as a substitute for natural aggregates and the fine fraction (by-product of the by-product) can be used as a filler in polymeric matrices (Figure 134).

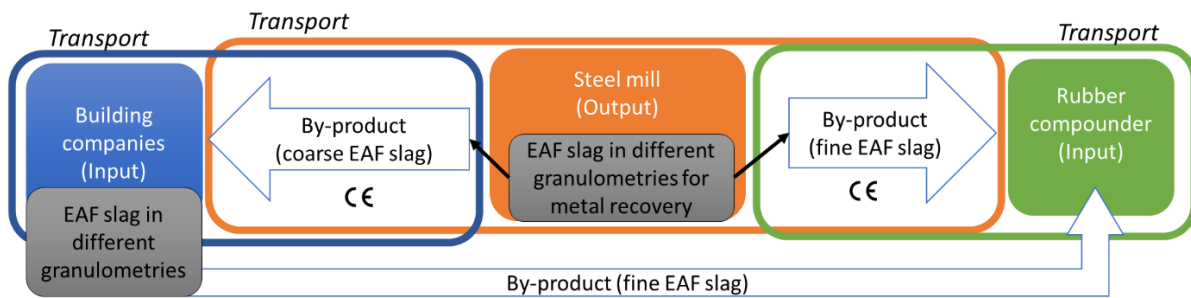


Figure 134 Possible flows of EAF slag as a by-product in a context of Industrial Symbiosis.

In the event that the recovery of the metal fraction is very high, it can be assumed a crushing up to 0.1mm granulometries and then everything goes as a by-product to the rubber sector as a filler (Figure 135).

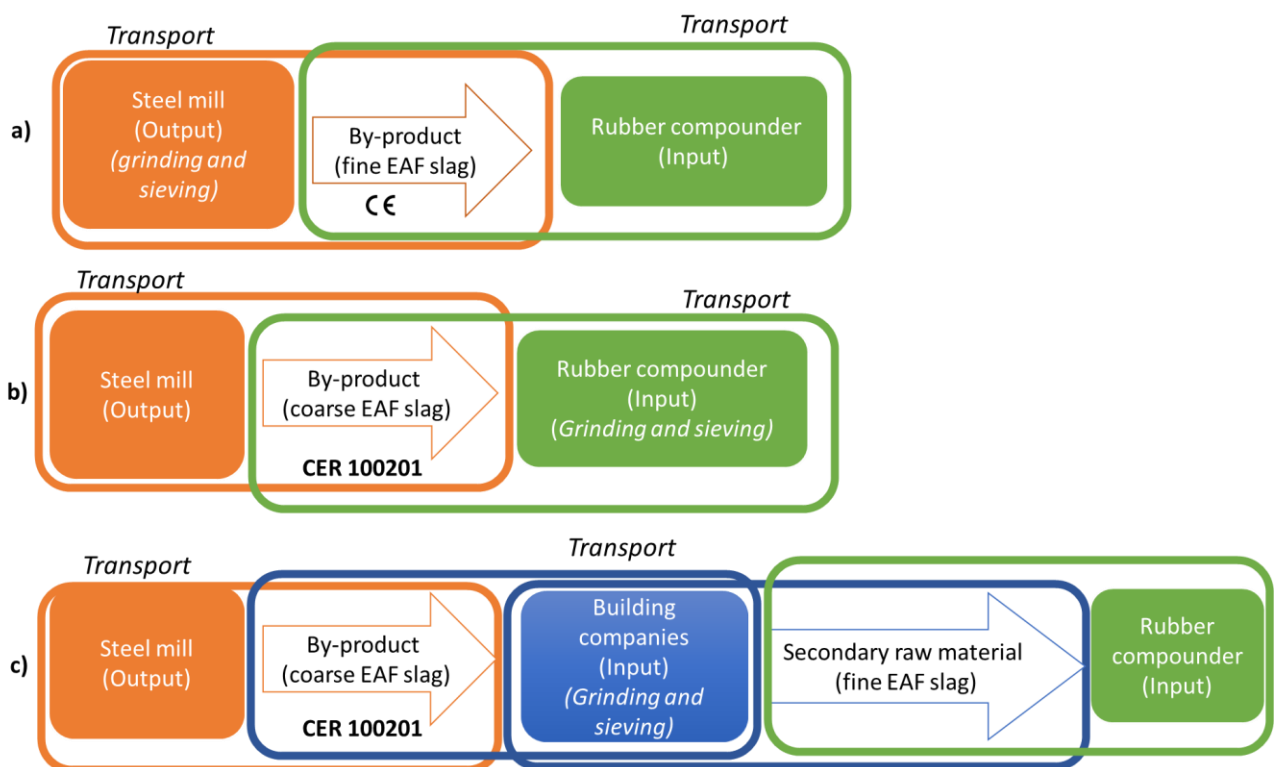


Figure 135 Possible flows of EAF slag as a by-product in a context of Industrial Symbiosis. a) EAF slag is ground and sieved in a suitable grain size to be used as filler by the steel mill and it is transferred to the rubber compounder; b) coarse EAF slag is transferred to the rubber compounder and this latter grinds and sieves it in a suitable grain size to be used as filler; c) coarse EAF slag is transferred to the building company and this latter grinds and sieves it in a suitable grain size to be used as filler and artificial aggregate, than the fine slag fraction is transferred to the rubber compounder to be used as filler.

### 6.2.2 EAF slag as Waste [341]:

Figure 136 illustrates the possible actors and the possible flows related to the transfer of EAF slag in case it is managed as waste.



Figure 136 Flow of EAF slag as waste disposed of in landfill.

In the case that the steel mill attributes the status of waste to the black slag, referring to the European Waste Catalog Decision 2000/532/EEC, it is assigned the CER codes:

- 10 02 02 "Untreated slag".
  - Recovery operations: R4, R5 R10
- 10 09 03 "Fusion slag".
  - Recovery operations: R4, R5 R10
- 10 02 01 "Wastes from waste treatment". This CER code can be attributed to slag-waste deriving from treatment operation.
  - Recovery operations: R4, R5 R10

Black EAF slag are classified by D.M. february5th 1998 [244] at paragraph 4.4.

4.4 Typology: slag from steelworks, slag from smelting in electric furnaces, fuel or converters a oxygen of ferrous metal alloys and their subsequent refining treatments [100202][100903][100201].

4.4.1 Origin: second foundries of iron and steel, production of ferro-alloys, steel industry.

4.4.2 Characteristics of the waste: granulated or block slag more than 80% by weight of SiO<sub>2</sub>, CaO, Al<sub>2</sub>O<sub>3</sub>, MgO, FeO.

4.4.3 Recovery activities:

a) cement factories [R5];

b) production of cement and bituminous conglomerates for building and bricks [R5];

c) glass industry [R5];

d) steel mills and first and second smelting foundries for the recovery of ferrous and non-ferrous materials [R4];

e) formation of embankments, road foundations and railway embankments (recovery is subject to the execution of the transfer on the waste as it is according to the method in annex 3 to this decree) [R5];

f) use for environmental recovery (recovery is subject to the execution of the transfer test on the waste as it is according to the method in annex 3 to this decree) [R10];

g) use to cover landfills for MSW; the percentage of waste that can be used mixed with the raw material is not must be greater than 30% by weight (recovery is subject to the execution of the transfer test on the waste as it is

according to the method in annex 3 to this decree) [R5];

#### 4.4.4 Characteristics of the raw materials and/or products obtained:

- a) cement in the forms usually marketed;
- b) cement and bituminous conglomerates for building and bricks in the forms usually marketed;
- c) glass in the forms usually marketed
- d) ferrous metals and metal alloys in the forms usually marketed.

When the slag is classified as waste it must be compliant to the Ministerial Decree or for material reuse 05/04/06 "Identification of non-hazardous waste subjected to simplified recovery procedures" [245], or for landfill disposal 30/08/2005 "Definition of eligibility criteria for landfill waste" [246].

Both decrees bases the slag characterization on leaching behaviour according to the standard CEN-EN 12457-2 [72].

The recovery operations are regulated by Annex C to part IV of Legislative Decree 3 April 2006, n. 152:

R1 Use primarily as a fuel or other means of producing energy (4)

R2 Regeneration/recovery of solvents

R3 Recycling/recovery of organic substances not used as solvents (including composting operations and other biological transformations) (5)

R4 Recycling/recovery of metals and metal compounds

R5 Recycling/recovery of other inorganic substances (6)

R6 Regeneration of acids or bases

R7 Recovery of products used to reduce pollution

R8 Recovery of products from catalysts

R9 Regeneration or other re-uses of oils

R10 Treatment in a terrestrial environment for the benefit of agriculture or ecology

R11 Use of waste obtained from any of the operations indicated by R1 to R10

R12 Exchange of waste to subject it to one of the operations indicated in R1 to R11 (7)

R13 Storage of waste to be subjected to one of the operations indicated in points R1 to R12 (excluding temporary storage, before collection, in the place where they are produced)

(4) Municipal solid waste incineration plants are included only if their energy efficiency is equal to or greater than: - 0.60 for plants operating and authorized in accordance with Community legislation applicable before 1 January 2009, - 0,65 for plants authorized after 31 December 2008, calculated with the following formula: Energy efficiency =  $[E_p - (E_f + E_i)] / [0.97 \times (E_w + E_f)]$  where:  $E_p$  = annual energy produced under form of thermal or electrical energy is calculated by multiplying the energy in the form of electricity by 2.6 and the thermal energy produced for commercial use by 1.1 (GJ/year)  $E_f$  = annual energy supply in the system with fuels that contribute to the production of steam (GJ/year)  $E_w$  = annual energy contained in the treated waste calculated on the basis of the lower calorific value of the waste (GJ/year)  $E_i$  = annual imported energy, excluding  $E_w$  and  $E_f$  (GJ/year) 0.97 = factor corresponding to energy losses due to bottom ash (slag) and radiation. The formula is applied in accordance with the reference document on best available techniques for waste incineration.

(5) Includes gasification and pyrolysis using components as chemicals.

(6) Includes cleaning resulting in soil recovery and recycling of inorganic building materials.

(7) In the absence of another appropriate R-code, it may include preliminary operations prior to recovery, including pre-treatment such as, inter alia, sorting, fragmentation, compaction, pelletizing, drying, shredding, conditioning, reconditioning, separation, grouping before one of the operations indicated by R 1 to R 11.

Both decrees (MD 05/04/06 “Identification of non-hazardous waste subjected to simplified recovery procedures” [245], and MD 30/08/2005 “Definition of eligibility criteria for landfill waste” [246]) bases the slag characterization on leaching behaviour according to the standard CEN-EN 12457-2 [72]. It is interesting to highlight that different European countries adopt different part of the standard (part 1 to 4) which differ for the test conditions [342] (Figure 137).

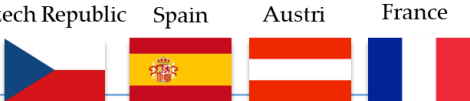
CEN EN 12457 For determining the degree of release of heavy elements				
Standard	Grain Size [mm]	Liquid/Solid Ratio [l/kg]	Agitation Time [h]	EU Country
EN 12457-1	<4	2:1	24	Denmark 
EN 12457-2	<4	10:1	24	Italy, Germany, France 
EN 12457-3	<4	2:1 (phase 1) 8:1 (phase 2)	6(phase 1) 8(phase 2)	Finland 
EN 12457-4	<10m m	10:1	24	Czech Republic, Spain, Austria, France 

Figure 137 Leaching test conditions according to the standard CEN EN 12457 and EU countries adopting different part of the standard [342].

### 6.2.3 EAF slag as End of Waste [341]:

The slag as waste can be sent to an authorized plant for its End of Waste (EoW) recovery, and it will be the task of the EoW recovery plant to comply with the provisions of art. 184-ter of Legislative Decree no. 152/2006, “End of Waste qualification”. It is considered appropriate to emphasize that there may be situations of companies for which the slag produced by the steel mill, despite having all the potential characteristics to be a by-product, is not managed as such. This is the case, for example, of steel mills that enter into commercial agreements with external companies authorized to process aggregates due to economic/operational feasibility assessments that prevent direct processing: for example, the necessary staff and/or adequate space are not available. For storage and in general to be able to carry out crushing and grinding operations suitable for obtaining the granulometric curves described and envisaged by the tender specifications and by the requirements for CE product certification. Or it could be the case of production of insufficient quantities of slag for the economic sustainability of the direct production of the by-product. Or more simply, the steel mill does not want to deal with managing the production of the by-product and instead prefers to entrust the slag as a waste to authorized third parties with the task of recovering it as an End of Waste (please note that the EoW legislation provides simple visual verification and acknowledgment that the refusal has the characteristics of the End of Waste as a processing activity to be authorized). In all these cases, the slag is then

managed inside the steel plant as a waste that can be sold to external companies authorized for its recovery. Furthermore, in these cases it is a question of identifying with respect to the production cycle the moment in which the slag assumes the qualification of waste also in order to comply with the quantities/timing for temporary storage or the quantities for placing in reserve/storage and related authorizations. The border point between the slag "which the producer wants to discard" in the cases illustrated above and therefore susceptible to the classification of waste, and the slag that is still "production residue" for which the normal production process always provides for a separation of the metal fraction to be reintroduced as raw material in the melting furnace, can only be identified downstream of the iron removal operations. Therefore, only at the end of the iron removal will the slag be considered as waste and treated as such (with reference to all the requirements of the case provided for by the current legislation on waste: attribution of the EER code, loading/unloading register, storage, etc.). Obviously, the iron removal operation can take place at different levels, with a partial recovery of the steel through a very coarse crushing or with a much more intense recovery with greater crushing even in several stages. That is, the crushing phase can take place in several steps depending on the intensity (also with reference to the quality of the steel that is produced) with which the metal fraction is to be separated and fed back to the metallurgical process.

The plants authorized for the recovery of EAF-C black slag (slag from low alloy carbon steel) typically operate on the material crushing, grinding and screening operations to obtain the required granulometric curves, possibly deferrization in several phases, and in some cases stabilization/maturation, wetting, washing operations. Lastly, other particular and specific operations, including innovative ones, are not excluded, which in any case must be envisaged and described in the individual authorizations. Even in the case of EoW slag, the recuperator eventually places on the market a CE marked product with the performance characteristics that comply with the technical regulations of the sector for possible uses envisaged in civil engineering works as an alternative to the aggregate of natural origin.

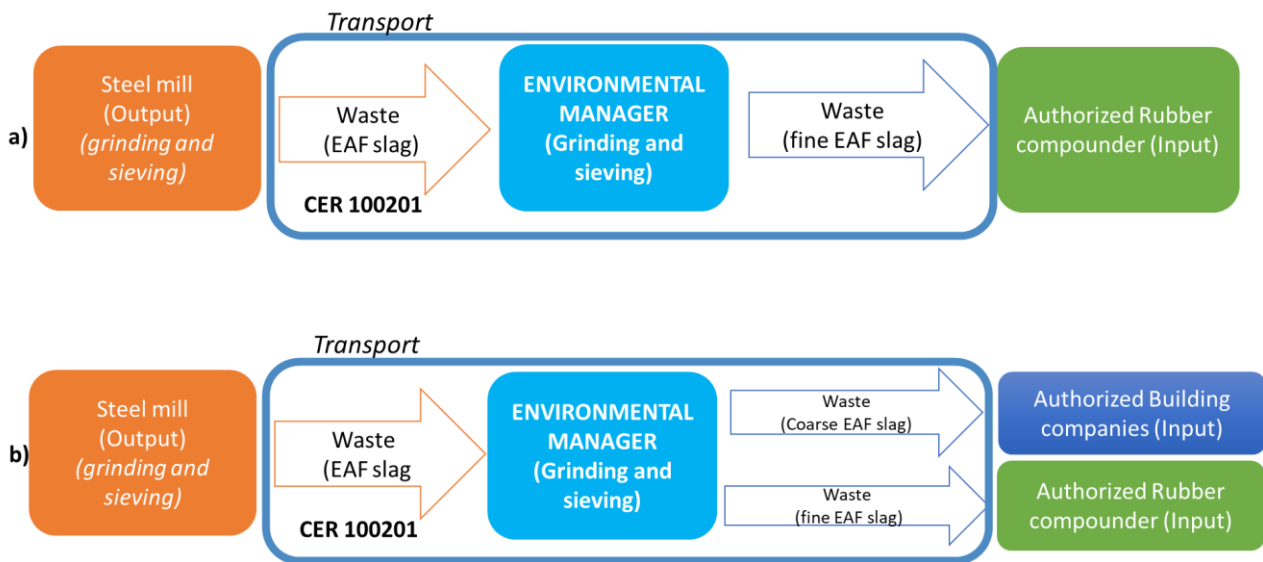


Figure 138 Possible flows of EAF slag as end of waste. a) EAF slag as waste is treated by the environmental manager in fine grain size and it is transferred to the rubber sector to be reused as filler. b) EAF slag as waste is treated by the environmental manager in different granulometries: fine EAF slag is transferred to the rubber sector to be reused as filler, coarse EAF slag is transferred to the building sector to be reused as artificial aggregate.

### 6.3 Advantages arising from the classification of an “output” as a “by-product”

The big advantage of the industrial symbiosis implementation is to eliminate the role of the environmental manager who has a double gain in waste management:

1. It gets paid to withdraw the waste;
2. It gets paid to sell the waste in the form of a resource.

Eliminating the environmental manager:

The **output company** meets the cost of qualification as a by-product (CE marking and procedures) may have (depending on the market):

- Lower disposal cost (in the worst-case scenario the output company pays the input company to collect the material. This cost will be less than that incurred to pay the environmental manager).
- Revenue (the Input company buys the by-product).

The **input company** can (depending on the market):

- Get paid to collect the by-product (from the Output company), process it and/or sell it and/or use it;
- Pay the by-product (to the Output company) less than what a virgin material would pay, process it and sell it;

Further economic advantages derive from the creation of new business networks, new market opportunities, and from the improvement of the relationships of companies with external parties.

From an environmental point of view, an efficient use of resources reduces the demand for ecosystem goods and services (water, coal, oil, fertilizers, etc.) and determines a lower impact of production activities (containment of emissions into water and atmosphere, prevention and waste reduction and consequent disposal in landfills, etc..)[22], [31], [343].

According to a questionnaire made to local steel mills that commercialize slag as a by-product, an environmental benefits derived by the avoided transport of the slag to an external waste treatment plant with related fuel emissions; the economic benefits derived by avoid costs incurred by the waste processing plant that overturns them on the steel mill.

Overall, the valorisation of residues as by-products in paths of industrial symbiosis makes it possible to obtain win-win solutions, in which all the actors involved can benefit from reciprocal interactions. Industrial symbiosis is therefore able to generate a virtuous interaction between companies and the territory through the activation of collaboration processes between the various actors involved. The implementation of this business model creates important advantages for the business system and the community, both in economic and environmental terms [344].

### 6.4 Identification of the subjects that can be involved for the use of black slag as filler in polimer matrix ("by-product")

To date, slag can be classified as a “by-product” or as a “waste”. The third way, that of “cessation of the qualification of waste” (or “end of waste”) is currently being finalized. Therefore, a scenario with the related flows was defined in the case of potential industrial symbiosis, that is, with slag in the form of a by-product. The following are shown with the 2007 ATECO codes of the identified actors.

- **24.10.00 Iron and steel industry - Manufacture of iron, steel and ferroalloys**
- management of blast furnaces, steel converters, rolling mills and finishing workshops

- production of crude and specular cast iron in ingots, blocks or other primary forms
- production of ferroalloys
- production of ferrous products through the direct reduction of iron ore and other spongy products ferrous
- production of iron of exceptional purity obtained by electrolysis or other chemical processes
- production of granular iron and iron powder
- production of semi-finished iron or non-alloy steel products
- production of ingots, other primary forms and semi-finished products in steel
- production of ingots, other primary forms and semi-finished products in stainless steel or other steel tied up
- production of angles and profiles in stainless steel or other alloy steel
- production of hot rolled steel flat products
- production of angles and profiles in iron or non-alloy steel
- production of stainless steel or other alloy steel rods and rods
- production of hot rolled steel bars and rods
- production of sheet piles and welded open sections of steel
- production of materials for steel railway lines (unassembled tracks)
- remelting of iron or steel scrap ingots
- **22.19.09 Manufacture of other rubber products n.e.c.**
- manufacture of other products of natural or synthetic rubber, not vulcanized, vulcanized or hardened: plates, sheets, strips, bars, rubber profiles, rigid and flexible pipes
- manufacture of conveyor belts and rubber transmission belts
- manufacture of rubber hygiene items: condoms, teats, hot water bags, etc.
- manufacture of rubberized textile products (only if sealed, not sewn)
- manufacture of rubber clothing items made by not sewing the various elements together, but by sealing them
- manufacture of rubber boots (only if sealed, not sewn)
- manufacture of rubber ropes and cables
- manufacture of rubber yarns and fabrics
- manufacture of rubber rings, accessories and gaskets
- manufacture of rubber bearing linings
- manufacture of inflatable rubber mattresses
- manufacture of ebonite pipes (pipe straws)
- manufacture of rubber repair materials
- manufacture of fabrics impregnated, coated, coated or laminated with rubber, where this represents the main constituent
- manufacture of rubber water mattresses
- manufacture of rubber bath caps and aprons
- manufacture of rubber diving suits
- manufacture of rubber articles for sex
- manufacture of rubber mats
- manufacture of padding for foam rubber mattresses and similar semi-finished products
- manufacture of rubber expansion joints for the construction sector
- manufacture of foam rubber latex
- manufacture of rubber floor coverings
- **23.51 Concrete Production**

- production of non-pulverized cements called clinkers and hydraulic cements, including Portland cement, aluminous cement, slag cement and superphosphate cements
- production of cementitious agglomerant
  - **42.11 Construction of roads and highways**
- surface work for roads, motorways, bridges or tunnels: asphaltting of roads, stone paving, laying of porphyry, painting of road markings and other signs, installation of
- safety, non-luminous road signs and the like
- construction of runways for airfields
  - **23.61 Manufacture of concrete products for construction**
- Manufacture of concrete products for construction

The possible flows of the EAF slag by-product are illustrated in Figure 134 and Figure 135. The steel mill is the producer of the slag which, as a normal industrial practice, implements a crushing process for the recovery of metals. Different granulometric fractions can be obtained from this ground by-product: a fine one that can be used as a polymer matrix filler and a coarse one suitable for reuse as an artificial aggregate. There is also the possibility that the company purchasing the artificial aggregate needs specific particle sizes, so it is possible that a further crushing may be implemented which once again could generate a fine fraction potentially destined for the rubber sector (Figure 139).

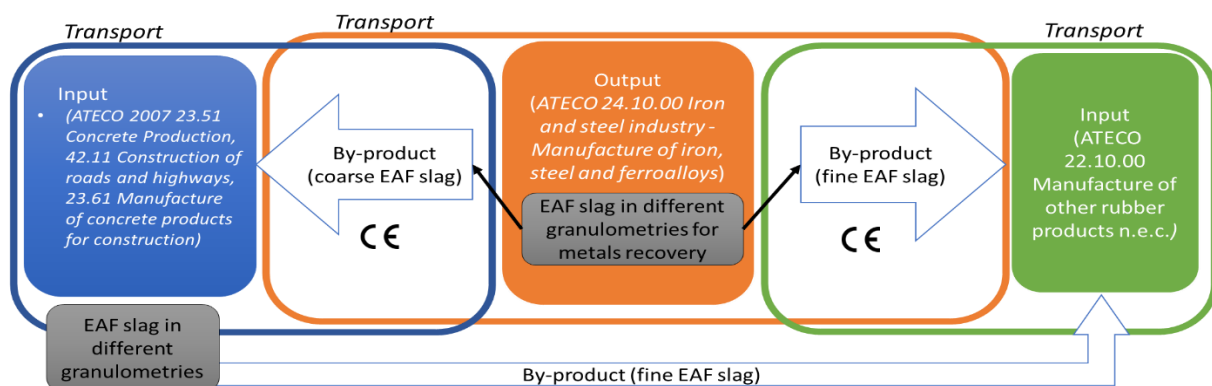


Figure 139 Possible actors involved in the transfer of EAF slag as a by-product in a context of Industrial Symbiosis.

In Italy, economic activities can be classified according to the type of business and ATECO is the classification of economic activities adopted by Istat for statistical purposes, that is, for the production and dissemination of official statistical data. On the basis of ATECO criteria [345], companies operating in the steelmaking belong to number 24.1 “Iron and steel industry - Manufacture of iron, steel and ferroalloys” and that operating in rubber parts production belong to number 22.19.09 “Manufacturing of other rubber parts n.e.c.”. Thanks to AIDA database, the Italian companies belonging to the aforementioned sector, have been geographically subdivided by region. Moreover, thanks to the same database it was possible to define a further classification by size of enterprise: micro, small, medium, and large in accordance with European Union Recommendation no. 2003/361/EC (Table 27).

Table 27 Companies category according to the European Union Recommendation n. 2003/361/EC.

<b>COMPANY CATEGORY</b>	<b>STAFF HEADCOUNT</b>	<b>BALANCE SHEET TOTAL [M€]</b>	<b>TURNOVER [M€]</b>
<b>MICRO ENTERPRISES</b>	<10	<2	<2
<b>SMALL ENTERPRISES</b>	<50	<10	<10
<b>MEDIUM ENTERPRISES</b>	<250	<43	<50
<b>LARGE SIZE ENTERPRISES</b>	>250	>43	>50

Since it was found that more than 40% of Italian companies working in steelmaking industry and in rubber parts production is located in Lombardy, this region was studied also by a provincial subdivision (Table 28, Table 29, Table 30, Table 31). The province of Brescia is particularly rich in companies operating in the steel sector, almost 50% of large size enterprises are located in this area, so that also the adjacent provinces of Trento and Verona were investigated.

<i>ATECO 24.1 Iron and steel industry - Manufacture of iron, steel and ferroalloys</i>			<i>Micro Enterprises</i>		<i>Small Enterprises</i>		<i>Medium Enterprises</i>		<i>Large-Scale Enterprises</i>		<i>Not declared</i>	
<i>Region</i>	<i>nr.</i>	<i>% Italy</i>	<i>nr.</i>	<i>% Region</i>	<i>nr.</i>	<i>% Region</i>	<i>nr.</i>	<i>% Region</i>	<i>nr.</i>	<i>% Region</i>	<i>nr.</i>	<i>% Region</i>
<i>ABRUZZO</i>	6	1%	3	50%	2	33%	1	17%	0	0%	0	0%
<i>BASILICATA</i>	1	0%	1	100%	0	0%	0	0%	0	0%	0	0%
<i>CALABRIA</i>	2	0%	1	50%	1	50%	0	0%	0	0%	0	0%
<i>CAMPANIA</i>	46	11%	30	65%	6	13%	1	2%	0	0%	9	20%
<i>EMILIA-ROMAGNA</i>	21	5%	11	52%	2	10%	5	24%	1	5%	2	10%
<i>FRIULI-VENEZIA GIULIA</i>	15	3%	3	20%	1	7%	5	33%	5	33%	1	7%
<i>LAZIO</i>	31	7%	16	52%	8	26%	3	10%	0	0%	4	13%
<i>LIGURIA</i>	5	1%	2	40%	1	20%	0	0%	2	40%	0	0%
<i>LOMBARDY</i>	189	43%	62	33%	42	22%	49	26%	25	13%	11	6%
<i>MARCHE</i>	5	1%	3	60%	2	40%	0	0%	0	0%	0	0%
<i>MOLISE</i>	1	0%	1	100%	0	0%	0	0%	0	0%	0	0%
<i>PIEDMONT</i>	16	4%	8	50%	3	19%	0	0%	3	19%	2	13%
<i>APULIA</i>	9	2%	4	44%	2	22%	1	11%	1	11%	1	11%
<i>SARDINIA</i>	6	1%	6	100%	0	0%	0	0%	0	0%	0	0%
<i>SICILY</i>	18	4%	9	50%	4	22%	1	6%	0	0%	4	22%
<i>TUSCANY</i>	23	5%	12	52%	4	17%	2	9%	3	13%	2	9%
<i>TRENTINO-ALTO ADIGE</i>	8	2%	2	25%	1	13%	1	13%	4	50%	0	0%
<i>UMBRIA</i>	5	1%	1	20%	2	40%	0	0%	2	40%	0	0%
<i>AOSTA VALLEY</i>	0	0%	0	0%	0	0%	0	0%	0	0%	0	0%
<i>VENETO</i>	30	7%	11	37%	6	20%	7	23%	3	10%	3	10%
<i>Tot</i>	437	-	186	-	87	-	76	-	49	-	39	-

Table 28 Regional subdivision of companies ATECO 2007 24.1 Iron and steel industry - Manufacture of iron, steel and ferro-alloys. For each region, a subdivision by type of company was made in accordance with the European Union Recommendation no. 2003/361/EC. Own data processing on AIDA database.

<i>ATECO 24.1 Iron and steel industry - Manufacture of iron, steel and ferroalloys</i>		<i>Micro Enterprises</i>		<i>Small Enterprises</i>		<i>Medium Enterprises</i>		<i>Large-Scale Enterprises</i>		<i>Not declared</i>		
<i>Region</i>	<i>nr.</i>	<i>% Lombardy</i>	<i>nr.</i>	<i>% Province</i>	<i>nr.</i>	<i>% Province</i>	<i>nr.</i>	<i>% Province</i>	<i>nr.</i>	<i>% Province</i>	<i>nr.</i>	<i>% Province</i>
<i>Bergamo</i>	16	8%	7	44%	5	31%	2	13%	1	6%	1	6%
<i>Brescia</i>	49	26%	12	24%	10	20%	14	29%	12	24%	1	2%
<i>Milan</i>	61	32%	20	33%	14	23%	15	25%	8	13%	4	7%
<i>Pavia</i>	6	3%	4	67%	0	0%	0	0%	0	0%	2	33%
<i>Varese</i>	5	3%	1	20%	1	20%	3	60%	0	0%	0	0%
<i>Lecco</i>	20	11%	7	35%	5	25%	7	35%	0	0%	1	5%
<i>Mantua</i>	5	3%	0	0%	1	20%	0	0%	4	80%	0	0%
<i>Como</i>	6	3%	4	67%	2	33%	0	0%	0	0%	0	0%
<i>Cremona</i>	4	2%	2	50%	2	50%	0	0%	0	0%	0	0%
<i>Monza and Brianza</i>	11	6%	4	36%	1	9%	5	45%	0	0%	1	9%
<i>Sondrio</i>	4	2%	1	25%	0	0%	2	50%	0	0%	1	25%
<i>Lodi</i>	2	1%	0	0%	1	50%	1	50%	0	0%	0	0%
<b>LOMBARDY</b>	189	100%	62	-	42	-	49	-	25	-	11	-
<i>Verona</i>	4	-	0	-	1	-	2	-	1	-	0	-
<i>Trento</i>	7	-	2	-	1	-	1	-	3	-	0	-

Table 29 Provincial subdivision of companies ATECO 2007 24.1 Iron and steel industry - Manufacture of iron, steel and ferro-alloys. For each region, a subdivision by type of company was made in accordance with the European Union Recommendation no. 2003/361/EC. Own data processing on AIDA database.

<i>ATECO 22.19.09 Manufacturing of other rubber parts n.e.c.</i>		<i>Micro Enterprises</i>		<i>Small Enterprises</i>		<i>Medium Enterprises</i>		<i>Large-Scale Enterprises</i>		<i>Not declared</i>		
<i>Region</i>	<i>nr.</i>	<i>% Italy</i>	<i>nr.</i>	<i>% Region</i>	<i>nr.</i>	<i>% Region</i>	<i>nr.</i>	<i>% Region</i>	<i>nr.</i>	<i>% Region</i>	<i>nr.</i>	<i>% Region</i>
<i>ABRUZZO</i>	15	<b>2%</b>	9	<b>60%</b>	1	<b>7%</b>	1	<b>7%</b>	4	<b>27%</b>	0	<b>0%</b>
<i>BASILICATA</i>	7	<b>1%</b>	4	<b>57%</b>	3	<b>43%</b>	0	<b>0%</b>	0	<b>0%</b>	0	<b>0%</b>
<i>CALABRIA</i>	8	<b>1%</b>	5	<b>63%</b>	2	<b>25%</b>	1	<b>13%</b>	0	<b>0%</b>	0	<b>0%</b>
<i>CAMPANIA</i>	41	<b>4%</b>	21	<b>51%</b>	9	<b>22%</b>	1	<b>2%</b>	0	<b>0%</b>	10	<b>24%</b>
<i>EMILIA-ROMAGNA</i>	85	<b>9%</b>	26	<b>31%</b>	31	<b>36%</b>	16	<b>19%</b>	1	<b>1%</b>	11	<b>13%</b>
<i>FRIULI-VENEZIA GIULIA</i>	9	<b>1%</b>	3	<b>33%</b>	4	<b>44%</b>	2	<b>22%</b>	0	<b>0%</b>	0	<b>0%</b>
<i>LAZIO</i>	42	<b>4%</b>	23	<b>55%</b>	12	<b>29%</b>	3	<b>7%</b>	0	<b>0%</b>	4	<b>10%</b>
<i>LIGURIA</i>	12	<b>1%</b>	7	<b>58%</b>	4	<b>33%</b>	0	<b>0%</b>	1	<b>8%</b>	0	<b>0%</b>
<i>LOMBARDY</i>	433	<b>44%</b>	168	<b>39%</b>	152	<b>35%</b>	64	<b>15%</b>	14	<b>3%</b>	35	<b>8%</b>
<i>MARCHE</i>	59	<b>6%</b>	28	<b>47%</b>	21	<b>36%</b>	6	<b>10%</b>	0	<b>0%</b>	4	<b>7%</b>
<i>MOLISE</i>	2	<b>0%</b>	2	<b>100%</b>	0	<b>0%</b>	0	<b>0%</b>	0	<b>0%</b>	0	<b>0%</b>
<i>PIEDMONT</i>	90	<b>9%</b>	41	<b>46%</b>	25	<b>28%</b>	12	<b>13%</b>	5	<b>6%</b>	7	<b>8%</b>
<i>APULIA</i>	23	<b>2%</b>	13	<b>57%</b>	8	<b>35%</b>	2	<b>9%</b>	0	<b>0%</b>	0	<b>0%</b>
<i>SARDINIA</i>	8	<b>1%</b>	6	<b>75%</b>	1	<b>13%</b>	0	<b>0%</b>	1	<b>13%</b>	0	<b>0%</b>
<i>SICILY</i>	12	<b>1%</b>	10	<b>83%</b>	2	<b>17%</b>	0	<b>0%</b>	0	<b>0%</b>	0	<b>0%</b>
<i>TUSCANY</i>	43	<b>4%</b>	21	<b>49%</b>	12	<b>28%</b>	2	<b>5%</b>	0	<b>0%</b>	8	<b>19%</b>
<i>TRENTINO-ALTO ADIGE</i>	7	<b>1%</b>	2	<b>29%</b>	3	<b>43%</b>	2	<b>29%</b>	0	<b>0%</b>	0	<b>0%</b>
<i>UMBRIA</i>	8	<b>1%</b>	3	<b>38%</b>	5	<b>63%</b>	0	<b>0%</b>	0	<b>0%</b>	0	<b>0%</b>
<i>AOSTA VALLEY</i>	0	<b>0%</b>	0	<b>0%</b>	0	<b>0%</b>	0	<b>0%</b>	0	<b>0%</b>	0	<b>0%</b>
<i>VENETO</i>	87	<b>9%</b>	32	<b>37%</b>	38	<b>44%</b>	10	<b>11%</b>	2	<b>2%</b>	5	<b>6%</b>
<i>TOT</i>	991	-	424	-	333	-	122	-	28	-	84	-

Table 30 Regional subdivision of companies ATECO 22.19.09 "Manufacturing of other rubber parts n.e.c.". For each region, a subdivision by type of company was made in accordance with the European Union Recommendation no. 2003/361/EC. Own data processing on AIDA database.

ATECO 22.19.09 Manufacturing of other rubber parts n.e.c.			Micro Enterprises		Small Enterprises		Medium Enterprises		Large-Scale Enterprises		Not declared	
Region	nr.	% Lombardy	nr.	% Province	nr.	% Province	nr.	% Province	nr.	% Province	nr.	% Province
<i>Bergamo</i>	143	33%	54	38%	46	32%	24	17%	8	6%	11	8%
<i>Brescia</i>	62	14%	17	27%	21	34%	11	18%	2	3%	11	18%
<i>Milan</i>	117	27%	48	41%	40	34%	18	15%	3	3%	8	7%
<i>Pavia</i>	27	6%	17	63%	8	30%	1	4%	0	0%	1	4%
<i>Varese</i>	20	5%	6	30%	8	40%	3	15%	1	5%	2	10%
<i>Lecco</i>	7	2%	5	71%	2	29%	0	0%	0	0%	0	0%
<i>Mantua</i>	9	2%	6	67%	3	33%	0	0%	0	0%	0	0%
<i>Como</i>	7	2%	2	29%	2	29%	3	43%	0	0%	0	0%
<i>Cremona</i>	5	1%	2	40%	3	60%	0	0%	0	0%	0	0%
<i>Monza and Brianza</i>	32	7%	10	31%	16	50%	4	13%	0	0%	2	6%
<i>Sondrio</i>	2	0%	1	50%	1	50%	0	0%	0	0%	0	0%
<i>Lodi</i>	2	0%	0	0%	2	100%	0	0%	0	0%	0	0%
<b>LOMBARDY</b>	433	100%	168	-	152	-	64	-	14	-	35	-
<i>Verona</i>	10	-	3	-	6	-	1	-	0	-	0	-
<i>Trento</i>	7	-	2	-	3	-	2	-	0	-	0	-

Table 31 Provincial subdivision of companies ATECO 2007 22.19.09 Manufacturing of other rubber parts n.e.c.. For each region, a subdivision by type of company was made in accordance with the European Union Recommendation no. 2003/361/EC. Own data processing on AIDA database.

<b>ATECO</b> <b>23.51 Concrete Production</b> <b>42.11 Construction of roads and highways</b> <b>23.61 Manufacture of concrete products for construction</b>			<i>Micro Enterprises</i>		<i>Small Enterprises</i>		<i>Medium Enterprises</i>		<i>Large-Scale Enterprises</i>		<i>Not declared</i>	
<i>Region</i>	<i>nr.</i>	<i>% Lombardy</i>	<i>nr.</i>	<i>% Province</i>	<i>nr.</i>	<i>% Province</i>	<i>nr.</i>	<i>% Province</i>	<i>nr.</i>	<i>% Province</i>	<i>nr.</i>	<i>% Province</i>
<b>ABRUZZO</b>	236	<b>3%</b>	149	<b>63%</b>	49	21%	15	<b>6%</b>	1	<b>0%</b>	22	<b>9%</b>
<b>BASILICATA</b>	155	<b>2%</b>	95	<b>61%</b>	32	21%	10	<b>6%</b>	1	<b>1%</b>	17	<b>11%</b>
<b>CALABRIA</b>	258	<b>4%</b>	170	<b>66%</b>	45	17%	12	<b>5%</b>	0	<b>0%</b>	31	<b>12%</b>
<b>CAMPANIA</b>	734	<b>10%</b>	505	<b>69%</b>	126	17%	17	<b>2%</b>	5	<b>1%</b>	81	<b>11%</b>
<b>EMILIA-ROMAGNA</b>	561	<b>8%</b>	326	<b>58%</b>	137	24%	37	<b>7%</b>	16	<b>3%</b>	45	<b>8%</b>
<b>FRIULI-VENEZIA GIULIA</b>	138	<b>2%</b>	68	<b>49%</b>	43	31%	15	<b>11%</b>	2	<b>1%</b>	10	<b>7%</b>
<b>LAZIO</b>	834	<b>11%</b>	518	<b>62%</b>	174	21%	38	<b>5%</b>	21	<b>3%</b>	83	<b>10%</b>
<b>LIGURIA</b>	100	<b>1%</b>	62	<b>62%</b>	24	24%	2	<b>2%</b>	1	<b>1%</b>	11	<b>11%</b>
<b>LOMBARDY</b>	985	<b>13%</b>	499	<b>51%</b>	275	28%	89	<b>9%</b>	24	<b>2%</b>	98	<b>10%</b>
<b>MARCHE</b>	166	<b>2%</b>	103	<b>62%</b>	40	24%	12	<b>7%</b>	1	<b>1%</b>	10	<b>6%</b>
<b>MOLISE</b>	48	<b>1%</b>	25	<b>52%</b>	15	31%	3	<b>6%</b>	0	<b>0%</b>	5	<b>10%</b>
<b>PIEDMONT</b>	431	<b>6%</b>	221	<b>51%</b>	118	27%	30	<b>7%</b>	13	<b>3%</b>	49	<b>11%</b>
<b>APULIA</b>	515	<b>7%</b>	345	<b>67%</b>	80	16%	15	<b>3%</b>	5	<b>1%</b>	70	<b>14%</b>
<b>SARDINIA</b>	238	<b>3%</b>	146	<b>61%</b>	63	26%	10	<b>4%</b>	0	<b>0%</b>	19	<b>8%</b>
<b>SICILY</b>	644	<b>9%</b>	455	<b>71%</b>	89	14%	21	<b>3%</b>	0	<b>0%</b>	79	<b>12%</b>
<b>TUSCANY</b>	339	<b>5%</b>	205	<b>60%</b>	78	23%	24	<b>7%</b>	4	<b>1%</b>	28	<b>8%</b>
<b>TRENTINO-ALTO ADIGE</b>	180	<b>2%</b>	97	<b>54%</b>	49	27%	16	<b>9%</b>	6	<b>3%</b>	12	<b>7%</b>
<b>UMBRIA</b>	141	<b>2%</b>	70	<b>50%</b>	38	27%	11	<b>8%</b>	5	<b>4%</b>	17	<b>12%</b>
<b>AOSTA VALLEY</b>	32	<b>0%</b>	16	<b>50%</b>	11	34%	1	<b>3%</b>	1	<b>3%</b>	3	<b>0%</b>
<b>VENETO</b>	612	<b>8%</b>	330	<b>54%</b>	177	29%	51	<b>8%</b>	9	<b>1%</b>	45	<b>7%</b>
<b>TOT</b>	7347	-	4405	-	1663	-	429	-	115	-	735	-

Table 32 Regional subdivision of companies 23.51 Concrete Production, 42.11 Construction of roads and highways, 23.61 Manufacture of concrete products for construction. For each region, a subdivision by type of company was made in accordance with the European Union Recommendation no. 2003/361/EC. Own data processing on AIDA database.

ATECO 23.51 Concrete Production 42.11 Construction of roads and highways 23.61 Manufacture of concrete products for construction			Micro Enterprises		Small Enterprises		Medium Enterprises		Large-Scale Enterprises		Not declared	
Region	nr.	% Lombardy	nr.	% Province	nr.	% Province	nr.	% Province	nr.	% Province	nr.	% Province
Bergamo	199	20%	80	40%	63	32%	26	13%	8	4%	22	11%
Brescia	168	17%	80	48%	50	30%	22	13%	2	1%	14	8%
Milan	291	30%	166	57%	63	22%	21	7%	11	4%	30	10%
Pavia	39	4%	18	46%	14	36%	2	5%	0	0%	5	13%
Varese	48	5%	25	52%	14	29%	2	4%	1	2%	6	13%
Lecco	18	2%	9	50%	6	33%	0	0%	1	6%	2	11%
Mantua	61	6%	34	56%	21	34%	4	7%	0	0%	2	3%
Como	39	4%	21	54%	12	31%	2	5%	0	0%	4	10%
Cremona	30	3%	15	50%	10	33%	2	7%	0	0%	3	10%
Monza and Brianza	47	5%	23	49%	16	34%	2	4%	0	0%	6	13%
Sondrio	23	2%	15	65%	3	13%	3	13%	1	4%	1	4%
Lodi	22	2%	13	59%	3	14%	3	14%	0	0%	3	14%
LOMBARDY	985	100%	499	-	275	-	89	-	24	-	98	-
Verona	124	-	69	-	36	-	11	-	2	-	6	-
Trento	114	-	60	-	32	-	10	-	3	-	9	-

*Table 33 Provincial subdivision of companies ATECO 2007 23.51 Concrete Production, 42.11 Construction of roads and highways, 23.61 Manufacture of concrete products for construction For each region, a subdivision by type of company was made in accordance with the European Union Recommendation no. 2003/361/EC. Own data processing on AIDA database.*

The data reported in Table 28 and Table 29 are summarized in the map shown in Figure 140. In Italy there are 437 companies operating in this industrial sector and most of them (43%) is in Lombardy. As regard the large size enterprises, 25 on a total of 49 (50%) is located in Lombardy. It was found that the province of Milan, Bergamo and Brescia are the most populated areas of companies operating in this sector.

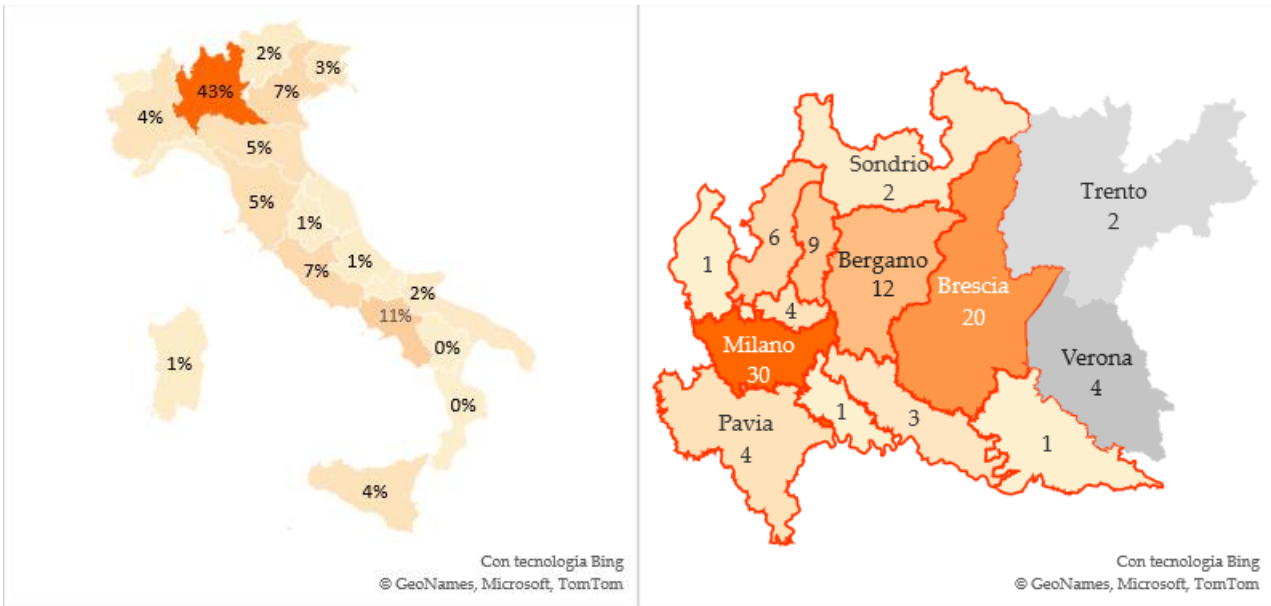


Figure 140 Regional and provincial subdivision of companies ATECO 2007 24.1 Iron and steel industry - Manufacture of iron, steel and ferro-alloys.

The data reported in Table 30 and Table 31 are summarized in the map shown in Figure 141. In Italy there are 991 companies operating in this sector and also in this case, most of them are located in Lombardy: 44% of total and 50% of large size enterprises (14/28). Analogously to the steel sector, the province of Milan, Bergamo and Brescia are the most populated areas of companies operating in the sector of interest.

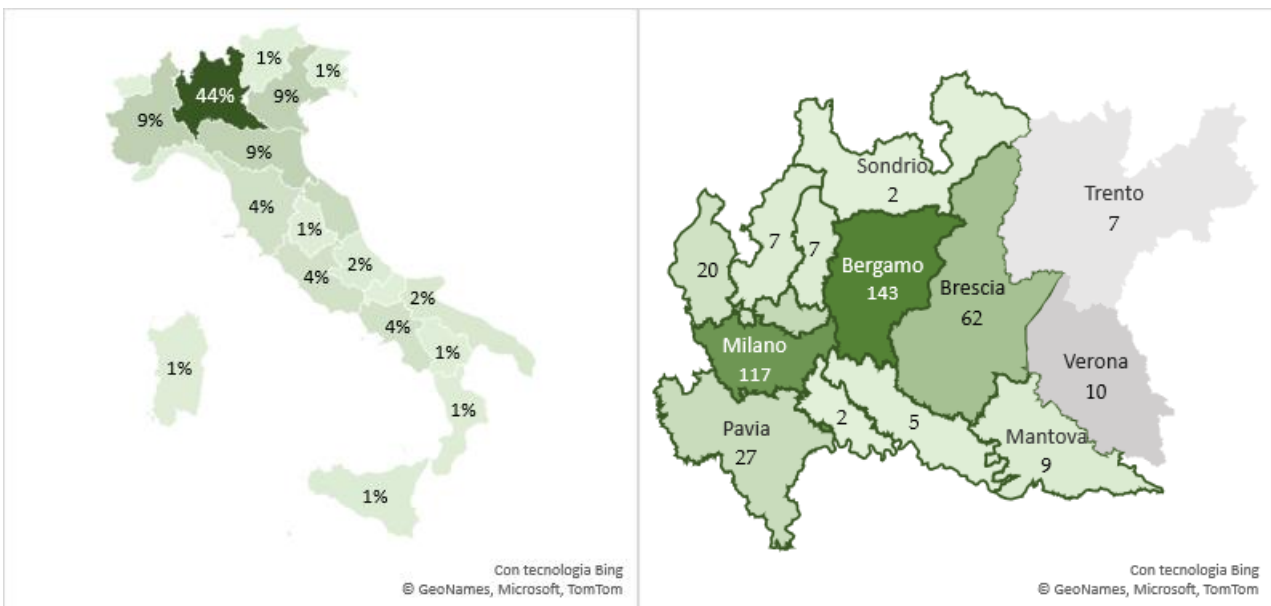


Figure 141 Regional and provincial subdivision of companies ATECO 2007 22.19.09 Manufacturing of other rubber parts n.e.c.

The data reported in Table 32 and Table 33 are summarized in the map shown in Figure 142. Unlike the sectors analyzed above, a region particularly rich in companies in the sectors considered was not found, but the geographical distribution is more homogeneous. In Lombardy there are 13% of the companies, and Brescia and Bergamo are the most populated at the provincial level.

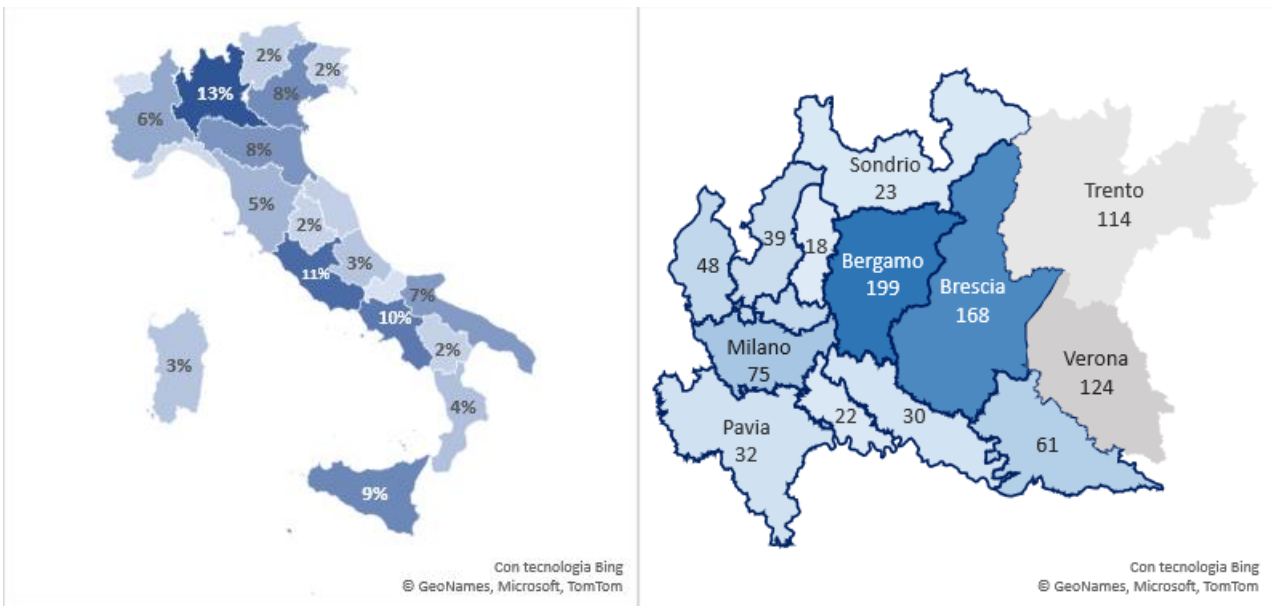


Figure 142 Regional and provincial subdivision of companies ATECO 2007 23.51 Concrete Production, 42.11 Construction of roads and highways, 23.61 Manufacture of concrete products for construction.

**6.5 Scenarios and economic evaluation of EAF slag management through industrial symbiosis**

Based on Federacciai report derived from the Worldsteel data it is estimated that Italy is the European leading producer with a EAF steel production [346] as shown in Figure 143.

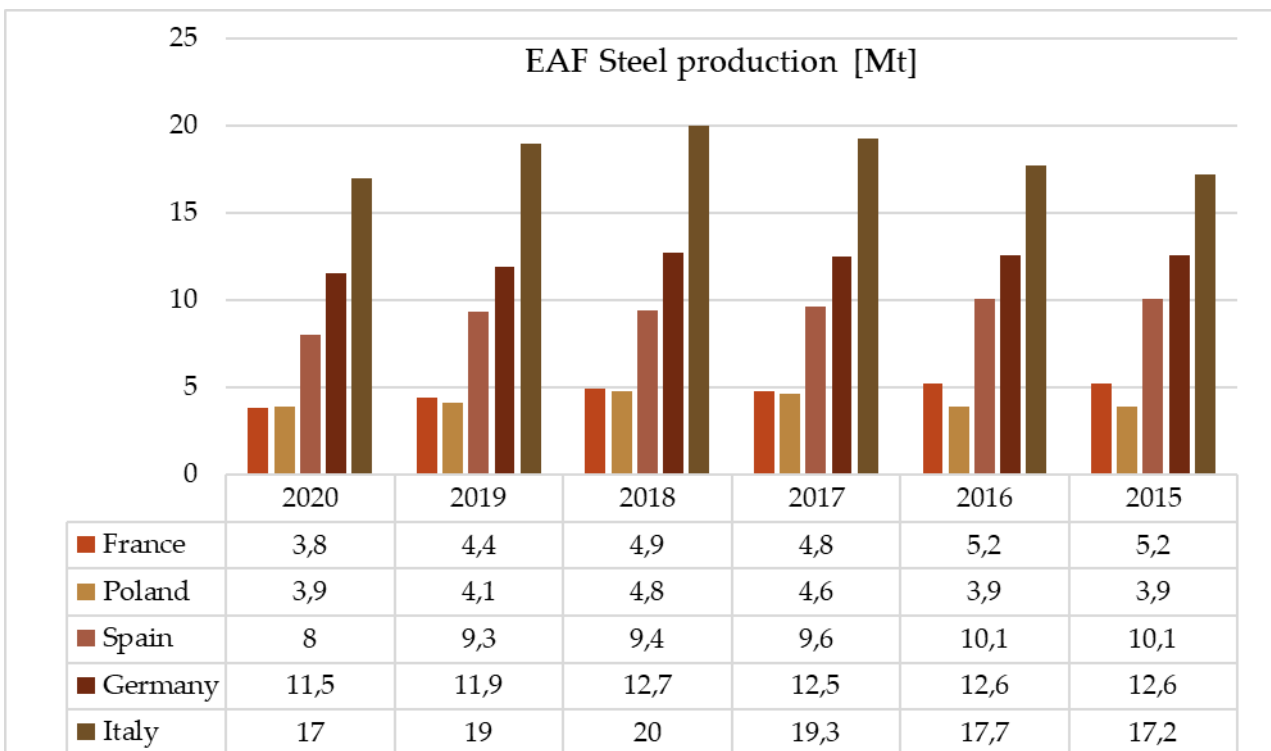


Figure 143 EAF steel production in Europe in 2020. Source Federacciai based on Worldsteel data [60].

Since the EAF black slag consists in about 10-15%wt of the produce steel [347]–[349] it is likely affirm that Italy produces about 2.3Mt of black slag by EAF each year.

According to [350] Lombardy region produces about 12 Mt of steel by EAF resulting in about 1.9Mt of EAF slag.

The Sustainability report drafted by Federacciai [351] affirms that 27% of black slag in Lombardy is not valorized and it is disposed of, for a total of 513.000 tons, 25% equal to 513.000 tons is recovered and 48% equal to 912.000 tons is managed as by-product.

### 6.5.1 Management cost of EAF black slag as waste

When a steel mill decides to manage the slag as waste, it inevitably has to incur disposal costs. The disposal costs can vary between 20 and 80€/ton depending on several factors (first of all the leaching behaviour) but usually for special steel is about 30-60€/tons so that for carbon steel it is lower<sup>1</sup>.

Considering an average disposal cost of 50€/ton, in Lombardy steel mills pay about 49.4M€/year for the black EAF slag withdrawal as waste by the environmental manager (988.000 ton).

### 6.5.2 Profit and loss of the management of EAF black slag as by-product: artificial aggregates

When a steel mill decides to manage the slag as a by-product, as in the case of the slag reuse as artificial aggregate, the slag becomes a commercial product and therefore CE marking is required. According to the data from own interview, the CE marking costs about 2000€/year, which is of little significant compared to the disposal or processing costs.

To reuse the slag as an artificial aggregate it is necessary to process it to obtain a suitable particle size. The processing cost is function of the slag granulometry and it can vary in different range from 0-2mm to 0-6mm for a production cost from 2 to 7€/ton<sup>1</sup>.

The selling price of the artificial aggregate can vary according to the market needs, and it is normally 1-10€/ton<sup>1</sup>.

Figure 144 shows the comparison of the costs incurred by steel mills for slag disposal compared to that incurred in the case of the enhance of slag as artificial aggregate. It is possible to notice that even in the worst-case scenario of low disposal cost (20€/ton) and high processing cost (7€/ton) accompanied by a very low selling price (1€/ton), the steel mill would incur in lower costs for 14€/ton.

---

<sup>1</sup> data from own interview to local companies (second semester 2022).

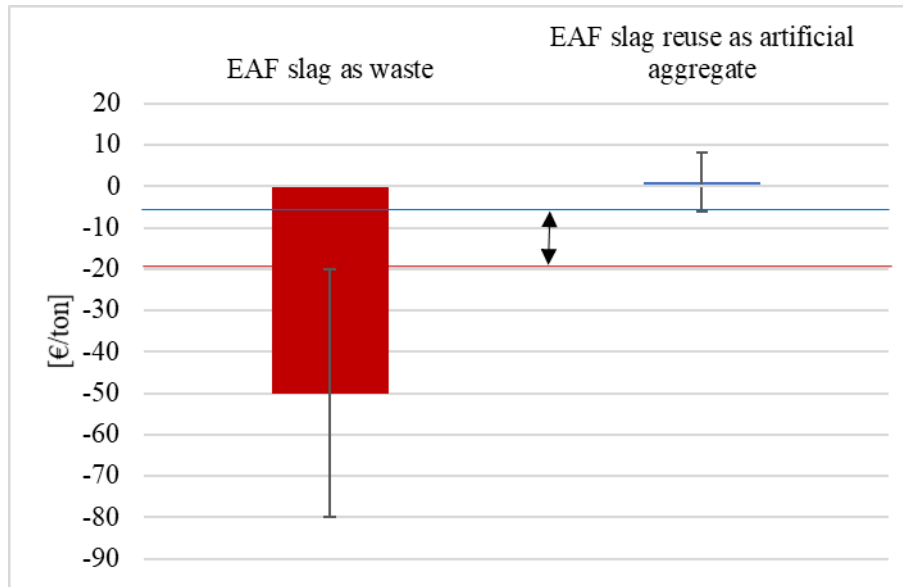


Figure 144 EAF slag costs as waste compared to the cost EAF slag enhance and reuse as artificial aggregate (based on own interview to steel companies).

**6.5.2.1 Economic evaluation of the current management of EAF black slag by Lombard steel mills**

With a view to industrial symbiosis, the costs deriving from the different management of EAF black slag at present have been assessed. Based on the data reported in [350] in Lombardy about 1.9Mt of EAF slag are produced; out of this quantity, according to [351] 27% is disposed of in landfills, 25% is recovered (so that 52% is handled by the environmental manager as waste) and 48% is handled as by-product as artificial aggregate. Based on the waste collection cost (20-80 €/ton)<sup>1</sup> and the by-product processing cost (2-7 €/ton<sup>1</sup>) the total cost incurred by the steel mills in Lombardy has been assessed: the total cost of EAF black slag management (Business As Usual (BAU)) is about 12-85M€ and about 20-79M€ are spent on waste collection by environmental managers (see Table 34).

Table 34 Economic evaluation of the current management (2019) of EAF black slag by Lombard steel mills.

EAF black slag managing in Lombardy		Quantity [ton]	[%] [351]	Waste collection cost / by-product processing cost <sup>1</sup> [€/ton]		Profit <sup>1</sup> [€/ton]		Total cost as waste/ Total cost as by-product <sup>1</sup> [M€]		Profit/Loss [M€]	
				Min	Max	Min	Max	Min	Max	Worst-case scenario	Best-Case scenario
EAF slag as Waste	Landfill	513.000	27%	-20	-80			-41	-10		
	Recovery	475.000	25%	-20	-80			-38	-10		
	TOT	988.000	52%					-79	-20	-79	-20
EAF slag as by-product	Artificial aggregate	912.000	48%	-2	-7	1	10	-6	-2	-5	7
<b>BAU (€)</b>											
<b>EAF black slag in Lombardy [350]</b>		<b>1.900.000</b>	<b>100%</b>							<b>-85</b>	<b>-12</b>

### 6.5.3 Profit and loss of the management of EAF black slag as by-product: filler for polymeric matrix

For the reuse of slag as filler for polymeric matrix it is necessary to reach a fine granulometry, lower than 0.1mm and this implies additional processing costs but also an additional metal recovery of about +5-8%.

The CE marking cost remains unaffected: about 2000€/y<sup>1</sup>.

The grinding cost is estimated to be about 30€/ton plus the energy cost which is assessed to be about 25-35kWh/ton (data based on the own interview to steel companies). Considering the electric energy cost 0.322€/kWh (single national price average from January to September 2022 based on data Luce-Gas.it [352]), the processing energy cost is about 8-11.3€/ton for a total cost of slag production as filler 38.1-41.3€/ton.

Once assessed the processing cost of EAF slag as filler, its selling price can be assessed by considering the market of the receiving sector, i.e., that of rubber. It is considered in a range of 0.06-0.12€/kg, or else considering an assumed rise of +50%/+190% at neat of the assessed processing costs. This estimate was made conservatively with a view to the general economic evaluation: on the one hand, the selling price was calculated with a minimum increase of +50% on production costs to cover other costs not quantified in this valuation; on the other hand, the maximum increase was set at + 190% in order not to exceed the minimum price of other inert fillers (the discussion of which is detailed in the section 6.5.3.1 Rubber Industry perspective).

These data are summarized in Table 35 and Figure 145. For each EAF slag destination (as waste, as artificial aggregate and as filler for polymeric matrix), the costs and any revenues from the sale in the possible aforementioned price ranges have been reported. From these data the earnings derived from worst-case scenario and the best-case scenario were estimated and expressed as average and standard deviation.

Table 35 Cost and profit of different EAF slag management by the steel mill.

EAF slag Management by steel mill	Cost [€/ton]		Profit [€/ton]		Tot [€/ton]		
	Min	Max	Min	Max	Worst case scenario	Best case scenario	Average
EAF slag disposal	-20	-80	0	0	-20	-80	-50 ± 30
EAF slag reuse as artificial aggregate	-2	-7	1	10	-6	8	1 ± 7
EAF slag reuse as filler	-37	-40	60	120	20	82	51 ± 31

It emerged that the EAF slag management as waste implies a cost to be incurred by the steel mills of 80-20€/ton. The management of EAF slag as by-product in the worst-case scenario implies a cost of 6€/ton and in the best case scenario a revenue of 8€/ton if the slag is processed to be suitable as artificial aggregate, while if it is processed to be used as filler the processing costs are well exceeded by the revenues for an average earning of 20-82€/ton.

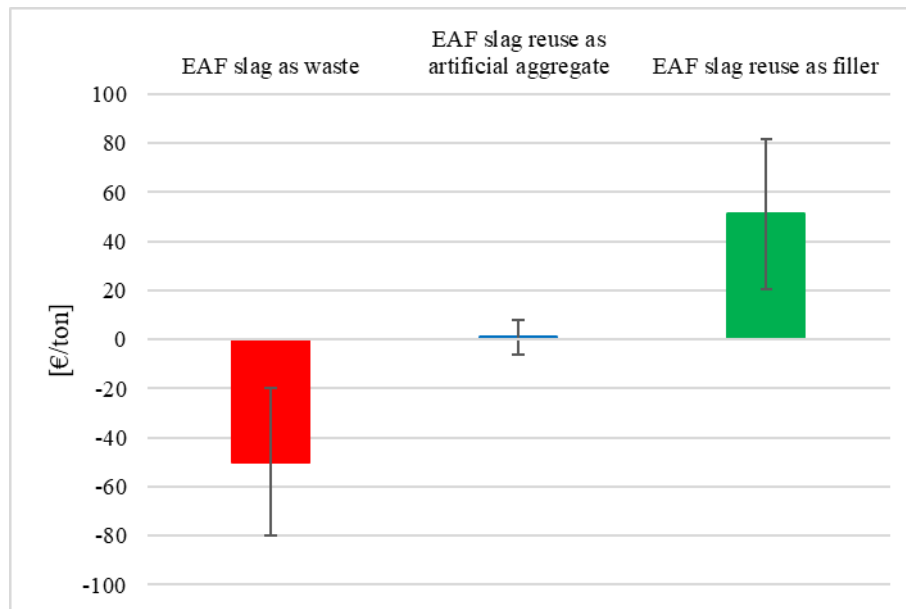


Figure 145 EAF slag disposal costs compared to the cost EAF slag enhance and reuse as artificial aggregate and as filler (based on own interview to steel companies).

Similarly to the assessment made on the money spent on slag management in accordance with current uses and quantities for each use, the savings potentially achievable in 3 different scenarios of 100% reuse of slag as a by-product in a pathway of industrial symbiosis were evaluated in Table 36. Three different scenarios are proposed. Scenario 1 evaluates the reuse of 100% slag as artificial aggregate at, scenario 2 evaluates the reuse of 100% slag as filler, and scenario 3 evaluates the reuse of 27% slag as filler (currently disposed of in landfills) combined to the reuse of slag as artificial aggregate for the remaining quantity (73%). Based on the waste collection cost (20-80 €/ton)<sup>1</sup> and the by-product processing cost (2-7 €/ton)<sup>1</sup> aforementioned, the annual economic advantage of each scenario is assessed with respect to BAU [€] in the worst-case and best-case scenario, as well as the average value. It was found that the reuse of 100% EAF slag as artificial aggregate would incur in revenue of 28-107 [€/year] (scenario 1), the reuse of 100% EAF slag as filler would incur in revenue of 208-384 [€/year] (scenario 2), and the combination of the two, would incur in revenue of 182-129 [€/year] (scenario 3).

Table 36 Assessment of potential economic savings by steel mills in Lombardy using 100% of the slag as a by-product in 3 different scenarios.

Possible Scenarios of Industrial Symbiosis				Processing cost [€/ton] ( <i>Ceteris paribus</i> )		Profit [€/ton]		Profit/Loss [M€]		Annual economic advantage of the scenario compared to BAU [€]		
		Quantity [ton]	%	Min	Max	Min	Max	Worst-case scenario	Best-Case scenario	Worst-case scenario	Best-Case scenario	Average
<b>Scenario 1</b>	Artificial aggregate	1.900.000	100%	-2	-7,0	1	10,0	15	23	28	107	67
<b>Scenario 2</b>	Filler	1.900.000	100%	-38,1	-41,3	62	120	196	300	208	384	296

Scenario 3	Artificial aggregate	1.387.000	73%	-2	-7	1	10	11	17			
	Filler	513000	27%	-38,1	-41,3	62	120	53	81			
	TOT	1.900.000	100%					64	98	76	182	129

### 6.5.3.1 Rubber Industry perspective

Previously, an assessment of the slag process costs to be incurred by the steel mills has been dealt with in order to valorize the EAF slag with evident economic benefits. Obviously, it is necessary to carry out an analogous evaluation also for the "input" sector of this by-product in order to preliminary quantify the possible economic benefits of using slag as a filler on the basis of the experimental results obtained from the characterization of the compounds.

Based on a own interview to a rubber compounds company the considered cost of NBR is 4-6€/kg and that of carbon black is 0.5-0.6 €/kg<sup>1</sup>.

EAF slag can be used as:

EAF slag can be used as:

#### 1) Traditional inert filler replacement

Some inert materials are currently used as low-cost fillers such as calcium carbonate, talc, barite et al. with a commercial price starting from about 150€/ton and function of level of purity, packaging etc.

In the light of these considerations by considering the selling price of EAF slag at filler equal to 60-120€/ton, Figure 146 shows the comparison between EAF slag, carbon black (400-600 €/ton) and a traditional filler (starting from about 150€/ton with 20% uncertainty). In the worst-case scenario, the price of EAF slag is equal to that of traditional fillers but with environmental benefits.

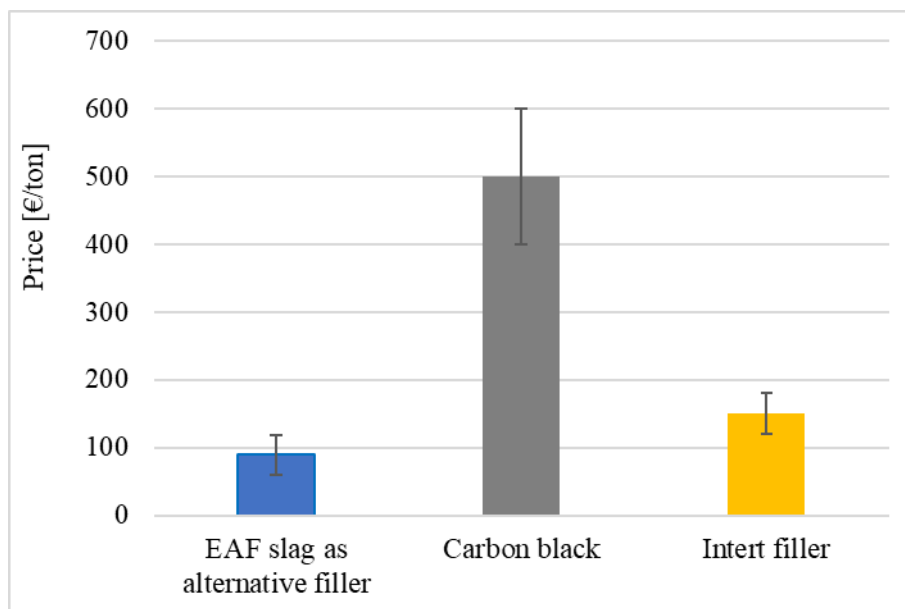


Figure 146 Comparison between the estimated price of EAF slag as a filler (60-120€/ton), carbon black (400-600€/ton) and a traditional filler (starting from 150€/ton). Data based on own interview to rubber and steel companies.

The slag as filler price is here hypothesized, it needs to be defined on the technical performances in relation to the applications purposes.

## 2) Carbon black replacement

In the experimental part of the project, the behavior of the slag as a carbon black replacement was investigated in order to assess even a partial carbon black replacement. Carbon black is a petrochemical product whose production implies a considerable environmental impact. It has been estimated that the production of 1 ton of carbon black implies the emission of 2.4 tons of carbon dioxide, compared to 0.8 tons of carbon dioxide per ton of cement during production [326]. The conservation of the environment is a permanent issue, much research is undertaken with the aim of reducing the dependence of the carbon black raw material on fossil fuels and transforming it into a sustainable material base. For these reasons, sustainable alternatives to carbon black are being studied such as rice husk ash, peanut shell powder etc.

Obviously, it would be misleading to compare the price of carbon black with that of slag, neglecting the performances of the two materials, which are profoundly different. For this reason, the economic evaluation was made by comparing different NBR compounds with similar mechanical properties. Furthermore, given the high specific weight of the slag, it would also be misleading to make an economic evaluation in weight units (biased in favor of the reuse of slag as filler), therefore the comparisons were made in volume units.

Table 37 shows a comparison between the materials cost for the production of 1 cubic meter of different NBR compounds (standard NBR (20% wt carbon black), NBR with partial replacement of carbon black and NBR (13% carbon black and 29% EAF slag) with total replacement of carbon black (50%wt EAF slag)) with comparable mechanical properties and consequent percentage economic savings. It was found that the partial carbon black replacement implies an economic saving of 9%, while a total carbon black replacement implies an economic saving of 11% for the rubber producers (Table 37).

Table 37 Estimation of the material cost for the production of 1 cubic meter of different NBR compounds (standard NBR, NBR with partial replacement of carbon black and NBR with total replacement of carbon black) with comparable mechanical properties and consequent percentage economic savings.

Production cost of 1m <sup>3</sup> of compound	Recipe of materials			Rubber (4.5€/kg)		Carbon black (0.5 €/kg)		EAF Slag (0.09 €/kg)		Average case scenario	
	kg/m <sup>3</sup>	Carbon black [%wt]	EAF slag [%wt]	[kg]	cost [€]	[kg]	cost [€]	[kg]	cost [€]	cost [€]	Saving [%]
Standard NBR	1136	20	0	909	4090	227	113	0	0	4203	
EAF Slag filled NBR (partial carbon black replacement)	1428	13	29	821	3695	193	96	414	37	3828	9%
EAF Slag filled NBR (total carbon black replacement)	1632	0	50	816	3672	0	0	816	73	3744	11%

The percentage economic saving for the use of EAF slag as carbon black replacement at comparable mechanical properties has been assessed in 3 different case scenarios (worst, average and best) with the aforementioned price ranges (Figure 147).

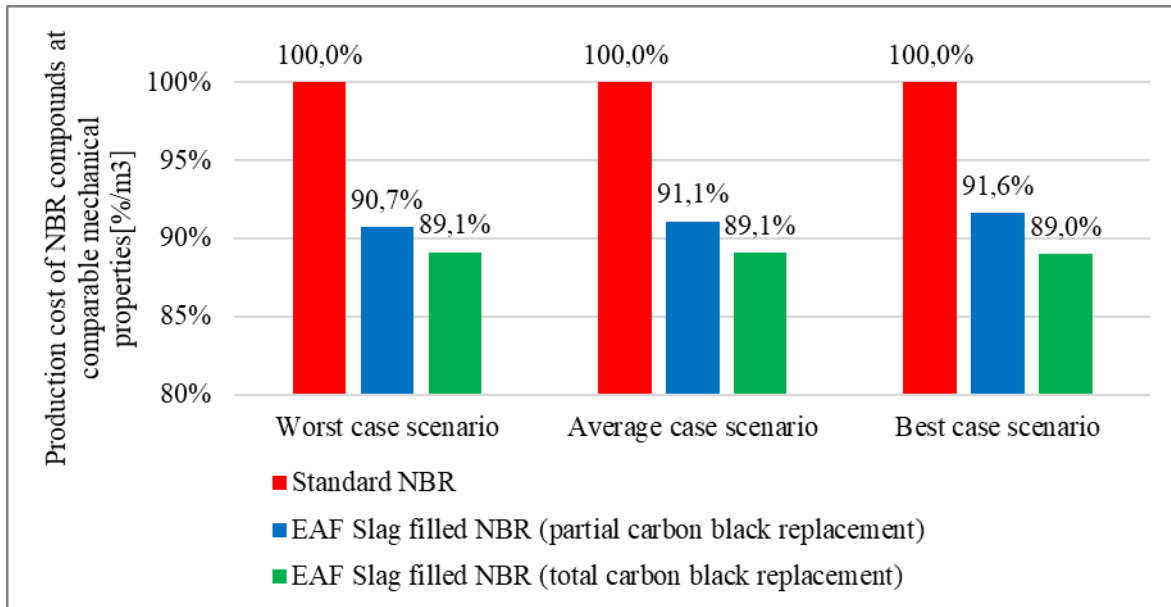


Figure 147 Percentage economic costs for the production of 1 cubic meter of NBR compound by using the EAF slag as carbon black replacement at comparable mechanical properties in 3 different case scenarios (worst, average and best) with the price ranges (NBR 4-7€/kg, carbon black 0.4-0.6 €/kg, EAF slag 0.06-0.12€/kg).

### 3) Filler for standard rubber

Another characterization made within the project was that of adding a standard NBR with different percentages of slag, evaluating its performance in order to reduce the environmental impacts of the new composite which also has a lower price, bringing economic benefits to the rubber sector.

The economic considerations are summarized in Table 38.

Table 38 Estimation of the material cost for the production of 1 cubic meter of NBR compounds (filled with 5, 10, 20 and 30% by volume and consequent percentage economic savings).

Production cost of 1m <sup>3</sup> of compound			NBR (5€/kg)		EAF slag (0.1€/kg)		Average case scenario	
	kg/m <sup>3</sup>	%wt	[kg]	Cost [€]	[kg]	Cost [€]	Cost [€]	Saving [%]
Standard NBR	1240	0	1240	6200	0.00	0	6200	
Standard NBR+5%EAF Slag [v/v]	1365	0.14	1174	5871	191	19	5890	5.0%
Standard NBR+10%EAF Slag [v/v]	1495	0.26	1106	5532	389	39	5571	10.1%

Standard NBR+20%EAF Slag [v/v]	1751	0.44	981	4904	771	77	4981	19.7%
Standard NBR+30%EAF Slag [v/v]	2005	0.57	862	4311	1143	114	4425	28.6%

The percentage economic saving for the use of EAF slag as filler for standard NBR (in different amount) has been assessed in 3 different case scenarios (worst, average and best). Carbon black is here considered included in the cost of NBR. In this case the economic saving is more marked as the amount of EAF slag used is greater, but the mechanical properties can be considered comparable to that of standard NBR up to 10%v/v with an economic saving of about 10%.

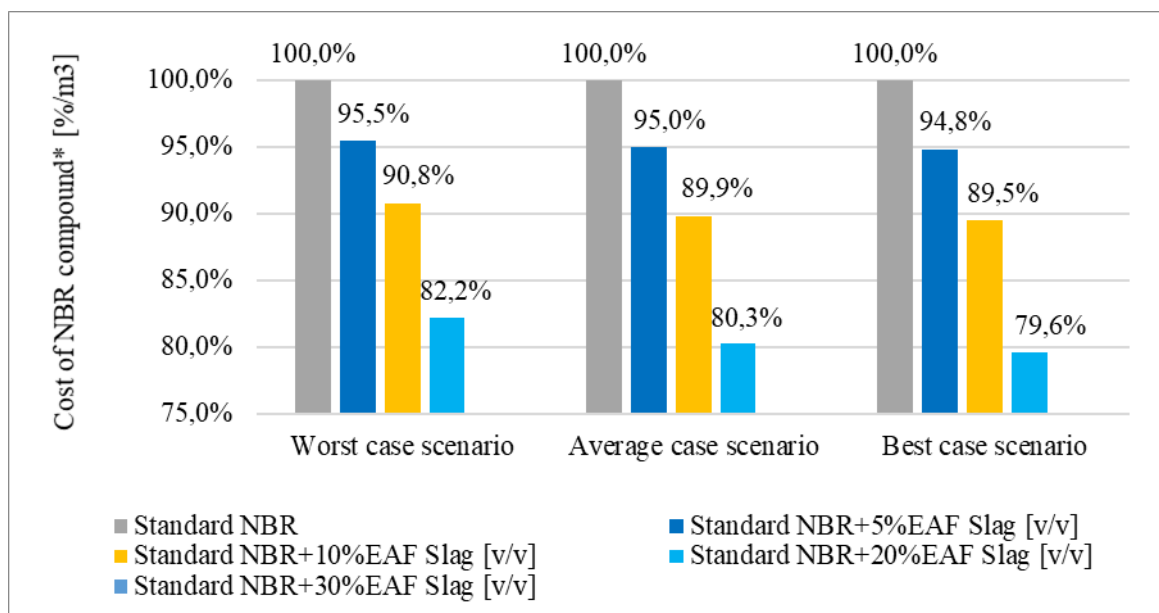


Figure 148 Percentage economic costs for the production of 1 cubic meter of NBR compound by using the EAF slag as filler in 3 different case scenarios (worst, average and best) with price ranges (NBR 4-7€/kg, EAF slag 0.06-0.12€/kg).

Table 39 Summary of the costs assessment of the reuses of EAF slag as by-product.

TYPE OF BY-PRODUCT	APPLICATION	CONSIDERATIONS	OUTPUT (STEEL)	PROCESSING COSTS	PROFIT	TOT	INPUT (RUBBER)	COST FOR MATERIALS PURCHASE
EAF SLAG AS AN ARTIFICIAL AGGREGATE (CURRENTLY USED)	The producer of the EAF black slag aggregate places on the market a material with CE marking [1], demonstrating that the characteristics comply with those declared in accordance with the UNI 13242 standard on recycled aggregates.	1[1] This implies having an ad-hoc quality manual, procedures and operating instructions and dedicated personnel to control the production process and certification/marketing.	2000€/year					
	Processing cost lower than the cost of disposal		Avoid disposal costs (20-80 € ton)	2-7 [€/ton]	1-10 [€/ton]	-6+8 [€/ton]		
EAF SLAG AS INERT FILLER (NEW USE)		More expensive manufacturing process because the smaller the grain size of the filler (<0.1mm) the better the performance of the composite	Economic benefit deriving from a benefit	37-40 [€/ton]	60-120* [€/ton]	20-80* [€/ton]		
	Inert filler alternative to traditional fillers (e.g. calcium carbonate, talc, barite, etc.)						Buy a sustainable paper at a lower price (traditional charge price from about € 150/ton)	0-120*[€/ton]

	Filler for standard rubber						It consumes less standard rubber (NBR ca 4-7 €/kg) as a fraction is occupied by the lower cost filler.	NBR standard: +5%v/v slag: -4,9% [€/kg] +10%v/v slag: -9,8% [€/kg] +20%v/v slag: -19,6% [€/kg]
	Alternative filler to carbon black						Uses a lower quantity of carbon black (polluting oil product 400-600 €/ton and more depending on the characteristics)	Replacement 100% carbon black: -11% [€/kg] Replacement 50% carbon black: -9% [€/kg]
* HYPOTHESIZED SALE PRICE (IT WILL DEPEND ON THE TECHNICAL CHARACTERISTICS AND THE MARKET)								

## 6.6 Conclusion

The present study focuses on the possible benefits derived from the management of EAF black slag as by-product with specific focus on the reuse of it as filler for polymeric matrix in view of industrial symbiosis.

The slag can be considered the main steel mill by-product, as its production is unavoidable and it is functional to the steel production itself. Slag represents more than 90% by mass of all by-products of iron and steel production. Italy is the European leading producer of steel by EAF, so as black slag consists in about 10-15% of the produced steel it is estimated that it produces about 2.3Mt of black slag every year.

In order to implement a new industrial symbiosis based on the EAF black slag transfer it was mandatory to study the geographical distribution of steelmaking industries. This study has been carried out thanks to the AIDA database focusing on ATECO 2007 code 24.1 "Iron and steel industry - Manufacture of iron, steel and ferroalloys". It was found that more than 40% of the companies operating in this sector is located in Lombardy, where more 50% of the Italian large-scale enterprises (according to European Union Recommendation no. 2003/361/EC) are located. Unfortunately, it was estimated by Federacciai in its "Sustainability report 2020" that 27% of black slag in Lombardy it is still disposed of, unlike the European average of 15%.

This could be attributable to the fact that Italy produces a greater quantity of slag and moreover concentrates it in Lombardy, so it is plausible that the construction market that uses it as an artificial aggregate it is not able to absorb more of it.

Because of this, it is necessary to investigate innovative applications of EAF black slag, and that proposed in the project of which this study is part, is that of the reuse as filler for rubber matrix thanks to the geographical proximity of the rubber parts producers with steel mills, requirement for the industrial symbiosis implementation.

The geographical distribution of these last companies has been carried out thanks to AIDA database focusing on ATECO 2007 code 22.19.09 "Manufacturing of other rubber parts n.e.c.". Also in this case more than 50% of the Italian large-scale enterprises are located in Lombardy.

These results suggest that there are prerequisites for the implementation of the industrial symbiosis so that possible scenarios and actors involved are defined.

The management of the slag has been discussed as "waste" and "by-product", with a digression on the "end of waste"; in particular a brief economic assessment of the costs and benefits of the innovative application of slag has been carried out.

It was evidenced that not only does the reuse of slag bring economic benefits to steel mills if it is valued as an artificial aggregate (application currently in use), but the economic benefits could be even greater if it is valued as a filler. In fact, facing a higher processing cost, the reduction in particle size below 0.1mm of the slag would make it a sustainable and cheaper substitute for other inert fillers such as calcium carbonate, talc and barite. Steel mills could even make a profit from selling the slag as a filler, and rubber producers could purchase an inert filler at a lower price by avoiding the production of other fillers with their respective environmental impacts.

## Conclusion

In this research, the new application of slag as a filler in polymeric matrices was investigated, with particular focus on rubber with a view to industrial symbiosis between the steel sector and the rubber sector.

A technical characterization of different compounds filled with electric arc furnace slag was carried out. The main results showed how the slagging processes nowadays, tend to produce increasingly "standard" slag with low leaching rate in order to make this co-product safer and more homogeneous in terms of "sameness" for valorization and reuse. As regards the application of slag as filler, it has been shown how the leaching of Chromium, Vanadium and Molybdenum is further reduced by the incorporation of the slag particles into the polymer matrix, making the composites compliant for reuse in accordance with the Ministerial Decree 5/4/06. From a mechanical performance point of view, it has been found that 100% EAF slag filled compound shows lower hardness than an NBR with carbon black in the same volumetric fraction. This is probably attributable to the lower adsorption of the rubber on the slag and to the different granulometry which implies a different surface area of filler-matrix interaction. Since rubber compounds are usually classified according to their hardness, slag filled compounds were compared with standard NBR of equal hardness, highlighting how the tensile and compressive behavior of slag filled compounds is comparable, if not in some cases better than those of standard NBR with the same hardness. The slag was also evaluated as an additional filler for standard NBR, both virgin and recycled. In general, stiffening was found, probably due to the hydrodynamic effect and the presence of a fraction of rubber well adhered to the filler (bound rubber or immobilized rubber fraction). In this regard, the interaction between slag and rubber has been investigated deeper in detail. In all the elastomeric matrices analyzed, the results indicate the presence of a good interaction since: a) the crosslink density increases as the slag content increases; at equal slag content, it is higher for a greater surface area (i.e. lower granulometry); and in the case of the same volumetric fraction of slag and carbon black, no variations were detected (not even in the bound rubber content test on the uncured compounds); ii) the polymeric fraction that participates in the glass transition decreases as the slag content increases (and remains unchanged in the case of the same volumetric fraction of slag and carbon black); iii) the non-linearity of the dynamic conservative modulus as a function of the strain amplitude (or Payne effect) increases as the slag content increases, it is more marked for finer slag and it is more marked for slag filled compound compared to standard NBR at equal hardness.

The influence of the slag has been assessed also in terms of processability. It was found that adding the slag in a standard rubber leads an increment in viscosity, crosslinking rate and maximum torque; these findings are mainly attributable to the reduction of the polymer fraction. As regard the influence of the slag as carbon black replacement, no relevant changes are detected in viscosity neither crosslinking rate but, on the opposite, the maximum torque is reduced (due to lower adsorption).

The work also highlighted the possibility of recycling vulcanized NBR waste through a very simple technological process without marked deterioration in the properties of the material. As regard the recycled ELT, the addition of the slag increases the thermal conductivity, expanding the spectrum of its possible applications. The use of slag therefore, allows to vary the properties of a recycled material with another waste material, resulting in a 100% recovered material.

The results obtained in this experimental characterization show promising developments for this new application. Similarly, the analysis of the territorial context and its production sectors from an industrial

symbiosis perspective, has shown how not only is there room for new applications of slag but also how they can be advantageous in environmental and economic terms.

### **Future developments**

Although the research developed during these 3 years led to interesting results, further investigations would bring a deeper knowledge of the potential of slag as a filler.

The performances of a slag filled rubber were compared with that of a carbon black filled rubber, i.e. it has been compared with the most reinforcing type of filler. It would be interesting to compare the mechanical behaviour of a rubber filled with slag and an inert filler such as calcium carbonate at equal grain size. This characterization is in progress.

In addition to the mechanical characterization of slag filled compounds, it will also be important to study other technological properties such as sound insulation, flame resistance, EMI shielding capacity, etc. Furthermore, since the slag ground by the technology adopted in this project leads to very angular particles that potentially promote the initiation of cracks, it would be interesting to evaluate other crushing processes aimed at obtaining different geometries. Finally, the slag, as seen, is strongly basic, so this characteristic could be exploited by using it as an acid scavenger.

This research focused on the use of black EAF slag as filler, but in the broader perspective of the valorisation of the slags, also the white slags could be studied for this application.

## References

- [1] P. Ghisellini, C. Cialani, and S. Ulgiati, "A review on circular economy: The expected transition to a balanced interplay of environmental and economic systems," *J. Clean. Prod.*, vol. 114, pp. 11–32, 2016, doi: 10.1016/j.jclepro.2015.09.007.
- [2] Ellen Macarthur Foundation, "Towards the circular economy," 2013. <https://www.ellenmacarthurfoundation.org/news/towards-the-circular-economy>
- [3] World Commission on Environment and Development, "Report of the World Commission on Environment and Development: Our Common Future (The Brundtland Report)," *Med. Confl. Surviv.*, 1987, doi: 10.1080/07488008808408783.
- [4] P. Golinska, M. Kosacka, R. Mierzwiak, and K. Werner-Lewandowska, "Grey Decision Making as a tool for the classification of the sustainability level of remanufacturing companies," *J. Clean. Prod.*, 2015, doi: 10.1016/j.jclepro.2014.11.040.
- [5] HISER, "Approach 'Life Cycle Thinking' apply to the Circular Economy," 2018. [http://hiserproject.eu/index.php/pozycja-1/80-news/166-approach-life-cycle-thinking-apply-to-the-circular-economy#:~:text=Life Cycle Thinking \(LCT\) is,over its entire life cycle.](http://hiserproject.eu/index.php/pozycja-1/80-news/166-approach-life-cycle-thinking-apply-to-the-circular-economy#:~:text=Life Cycle Thinking (LCT) is,over its entire life cycle.)
- [6] P. Schroeder, K. Anggraeni, and U. Weber, "The Relevance of Circular Economy Practices to the Sustainable Development Goals," *J. Ind. Ecol.*, 2019, doi: 10.1111/jiec.12732.
- [7] United Nation, "Sustainable Development Goals. About the sustainable development goals," 2018. <https://www.un.org/sustainabledevelopment/sustainable-development-goals/>.
- [8] European Commission, *Directive 2008/98/EC on waste (Waste Framework Directive)*. 2008. [Online]. Available: <https://ec.europa.eu/environment/waste/framework/>
- [9] Stefan F. Einarsson, "What is the link between Circular Economy (CE) and the Sustainable Development Goals (SDGs)?," 2019, [Online]. Available: <https://www.linkedin.com/pulse/what-link-between-circular-economy-ce-sustainable-goals-einarsson>
- [10] Y. M. B. Saavedra, D. R. Iritani, A. L. R. Pavan, and A. R. Ometto, "Theoretical contribution of industrial ecology to circular economy," *Journal of Cleaner Production*. 2018. doi: 10.1016/j.jclepro.2017.09.260.
- [11] S. Erkman, "Industrial ecology: An historical view," *Journal of Cleaner Production*. 1997. doi: 10.1016/s0959-6526(97)00003-6.
- [12] R. A. Frosch and N. E. Gallopoulos, "Strategies for Manufacturing," *Sci. Am.*, 1989, doi: 10.1038/scientificamerican0989-144.
- [13] R. U. Ayres, "Barriers and breakthroughs: an 'expanding frontiers' model of the technology-industry life cycle," *Technovation*, 1988, doi: 10.1016/0166-4972(88)90041-7.
- [14] S. Anderberg, "Industrial metabolism and the linkages between economics, ethics and the environment," *Ecol. Econ.*, 1998, doi: 10.1016/S0921-8009(97)00151-1.
- [15] M. R. Chertow, "Industrial symbiosis: Literature and taxonomy," *Annu. Rev. Energy Environ.*, vol. 25, p. 113, 2000, doi: 10.1146/annurev.energy.25.1.313.
- [16] E. J. Prosman, B. V. Wæhrens, and G. Liotta, "Closing Global Material Loops: Initial Insights into Firm-Level Challenges," *J. Ind. Ecol.*, 2017, doi: 10.1111/jiec.12535.
- [17] N. Nakajima, "A vision of industrial ecology: State-of-the-art practices for a circular and service-based economy," *Bull. Sci. Technol. Soc.*, 2000, doi: 10.1177/027046760002000107.
- [18] N. Gregson, M. Crang, S. Fuller, and H. Holmes, "Interrogating the circular economy: the moral economy of resource recovery in the EU," *Econ. Soc.*, 2015, doi: 10.1080/03085147.2015.1013353.
- [19] W. Li, "Comprehensive evaluation research on circular economic performance of eco-industrial parks," in *Energy Procedia*, 2011. doi: 10.1016/j.egypro.2011.03.287.
- [20] L. Mortensen and L. Kørnøv, "Critical factors for industrial symbiosis emergence process," *J. Clean. Prod.*, vol. 212, pp. 56–69, 2019, doi: 10.1016/j.jclepro.2018.11.222.
- [21] H. Shi, M. Chertow, and Y. Song, "Developing country experience with eco-industrial parks: a case study of the Tianjin Economic-Technological Development Area in China," *J. Clean. Prod.*, 2010, doi: 10.1016/j.jclepro.2009.10.002.
- [22] L. Cutaia and R. Morabito, "Ruolo della Simbiosi industriale per la green economy," *Energia, Ambient. Innov. - Spec. Green Econ.*, no. 1, pp. 44–49, 2012.
- [23] M. R. Chertow, W. S. Ashton, and J. C. Espinosa, "Industrial symbiosis in Puerto Rico: Environmentally related agglomeration economies," *Reg. Stud.*, vol. 42, no. 10, 2008, doi: 10.1080/00343400701874123.
- [24] F. Boons *et al.*, "Comparing industrial symbiosis in Europe: Towards a conceptual framework and research methodology," in *International Perspectives on Industrial Ecology*, 2015. doi: 10.4337/9781781003572.00013.
- [25] J. S. Mulrow, S. Derrible, W. S. Ashton, and S. S. Chopra, "Industrial Symbiosis at the Facility Scale," *J. Ind. Ecol.*, 2017, doi: 10.1111/jiec.12592.
- [26] L. Sun, W. Spekkink, E. Cuppen, and G. Korevaar, "Coordination of industrial symbiosis through anchoring," *Sustain.*, 2017, doi: 10.3390/su9040549.
- [27] F. Boons, M. Chertow, J. Park, W. Spekkink, and H. Shi, "Industrial Symbiosis Dynamics and the Problem of Equivalence: Proposal for a Comparative Framework," *J. Ind. Ecol.*, 2017, doi: 10.1111/jiec.12468.
- [28] G. T. Renner, "Geography of Industrial Localization," *Econ. Geogr.*, vol. 23, p. 367, 1947, doi: 10.2307/141510.
- [29] E. A. E. A. Lowe and L. K. L. K. Evans, "Industrial ecology and industrial ecosystems," *J. Clean. Prod.*, vol. 3, no. 1–2, pp. 47–53, 1995, doi: 10.1016/0959-6526(95)00045-G.
- [30] J. Ehrenfeld and N. Gertler, "Industrial ecology in practice: The evolution of interdependence at Kalundborg," *J. Ind. Ecol.*, vol. 1, no. 1, pp. 67–79, 1997, doi: 10.1162/jiec.1997.1.1.67.
- [31] M. R. Chertow, "'Uncovering' industrial symbiosis," *Journal of Industrial Ecology*. 2007. doi: 10.1162/jiec.2007.1110.
- [32] N. B. Jacobsen, "Industrial symbiosis in Kalundborg, Denmark: A quantitative assessment of economic and environmental aspects," *J. Ind. Ecol.*, 2006, doi: 10.1162/108819806775545411.
- [33] E. J. Schwarz and K. W. Steininger, "Implementing nature's lesson: The industrial recycling network enhancing regional

- development," *J. Clean. Prod.*, 1997, doi: 10.1016/s0959-6526(97)00009-7.
- [34] C. D. Darlington, "Mendel and the Determinants," in *Genetics in the 20th Century: Essays on the Progress of Genetics During Its First 50 Years*, 1951, pp. 315–332. doi: 10.1038/167407a0.
- [35] M. R. Chertow and D. R. Lombardi, "Quantifying economic and environmental benefits of co-located firms," *Environ. Sci. Technol.*, 2005, doi: 10.1021/es050050+.
- [36] E. M. Harper and T. E. Graedel, "Industrial ecology: A teenager's progress," *Technol. Soc.*, 2004, doi: 10.1016/j.techsoc.2004.01.013.
- [37] S. Yang and N. Feng, "A case study of industrial symbiosis: Nanning Sugar Co., Ltd. in China," *Resour. Conserv. Recycl.*, 2008, doi: 10.1016/j.resconrec.2007.11.008.
- [38] I. Costa and P. Ferrão, "A case study of industrial symbiosis development using a middle-out approach," *J. Clean. Prod.*, 2010, doi: 10.1016/j.jclepro.2010.03.007.
- [39] M. Mirata and T. Emtairah, "Industrial symbiosis networks and the contribution to environmental innovation: The case of the Landskrona industrial symbiosis programme," *J. Clean. Prod.*, 2005, doi: 10.1016/j.jclepro.2004.12.010.
- [40] D. R. Lombardi and P. Laybourn, "Redefining Industrial Symbiosis: Crossing Academic-Practitioner Boundaries," *J. Ind. Ecol.*, 2012, doi: 10.1111/j.1530-9290.2011.00444.x.
- [41] ERVET, "Gestione sostenibile delle aree produttive. Analisi casi studio Internazionali," 2009. [https://ambiente.regione.emilia-romagna.it/it/sviluppo-sostenibile/temi-1/sviluppo-sostenibile/gestione-e-sostenibilita-aree-industriali/materiale-per-approfondire-1/Report\\_casi\\_studio\\_09.pdf](https://ambiente.regione.emilia-romagna.it/it/sviluppo-sostenibile/temi-1/sviluppo-sostenibile/gestione-e-sostenibilita-aree-industriali/materiale-per-approfondire-1/Report_casi_studio_09.pdf)
- [42] Regione Emilia Romagna, "An example of technical assistance provided to companies is the 'Sustainable Prosperity Program for SMEs', aimed at reducing the use of energy, water, chemicals and waste production, with a view to rationalizing operations and reducing costs; the program," 2011.
- [43] . Laura Cutaia, Elisabetta Boncio, Tiziana Beltrani, Grazia Barberio, Erika Mancuso, Andrea Massoli, Susanna Paoni, Silvia Sbaffoni, Marco La Monica, "Implementing circular economy in Umbria through an industrial symbiosis network model," 2018.
- [44] E. M. Laura Cutaia, Marco La Monica, "La simbiosi industriale e territoriale," *Energia, Ambient. e Innov.*, 2019.
- [45] L. Cutaia *et al.*, "The experience of the first industrial symbiosis platform in Italy," *Eng. Manag. J.*, vol. 14 (7), pp. 1521-1533., 2015, doi: 10.30638/eemj.2015.164.
- [46] S. Sbaffoni, "La simbiosi industriale: approccio cooperativo tra le aziende per la valorizzazione delle risorse e per la prevenzione ed il recupero di rifiuti in ottica di economia circolare," 2020. [http://www.unioncamerelombardia.it/images/file/APolAmbGPP/Simbiosi\\_industriale\\_Sbaffoni.pdf](http://www.unioncamerelombardia.it/images/file/APolAmbGPP/Simbiosi_industriale_Sbaffoni.pdf)
- [47] S. Sbaffoni, "Strumenti per favorire la circolarità e nuovi modelli di business nel settore agroindustriale," 2020. [Online]. Available: [https://creiamo-circulareconomy.com/wp-content/uploads/2020/06/Sbaffoni\\_convegno-CREIAMO.pdf](https://creiamo-circulareconomy.com/wp-content/uploads/2020/06/Sbaffoni_convegno-CREIAMO.pdf)
- [48] n. 264. DECRETO 13 ottobre 2016, "Regolamento recante criteri indicativi per agevolare la dimostrazione della sussistenza dei requisiti per la qualifica dei residui di produzione come sottoprodotti e non come rifiuti." [Online]. Available: [https://www.ch.camcom.it/uploaded/DECRETO\\_13\\_ottobre\\_2016\\_n\\_264.pdf](https://www.ch.camcom.it/uploaded/DECRETO_13_ottobre_2016_n_264.pdf)
- [49] F. Boons, W. Spekkink, and W. Jiao, "A Process Perspective on Industrial Symbiosis: Theory, Methodology, and Application Boons *et al.* A Process Perspective on Industrial Symbiosis," *J. Ind. Ecol.*, 2014, doi: 10.1111/jiec.12116.
- [50] N. M. P. Bocken, S. W. Short, P. Rana, and S. Evans, "A literature and practice review to develop sustainable business model archetypes," *Journal of Cleaner Production*. 2014. doi: 10.1016/j.jclepro.2013.11.039.
- [51] N. M. P. Bocken, C. S. C. Schuit, and C. Kraaijenhagen, "Experimenting with a circular business model: Lessons from eight cases," *Environ. Innov. Soc. Transitions*, 2018, doi: 10.1016/j.eist.2018.02.001.
- [52] B. Baldassarre, M. Schepers, N. Bocken, E. Cuppen, G. Korevaar, and G. Calabretta, "Industrial Symbiosis: towards a design process for eco-industrial clusters by integrating Circular Economy and Industrial Ecology perspectives," *J. Clean. Prod.*, 2019, doi: 10.1016/j.jclepro.2019.01.091.
- [53] N. M. P. Bocken, E. A. Olivetti, J. M. Cullen, J. Potting, and R. Lifset, "Taking the Circularity to the Next Level: A Special Issue on the Circular Economy," *Journal of Industrial Ecology*. 2017. doi: 10.1111/jiec.12606.
- [54] G. Massard, O. Jacquat, and D. Zürcher, "International survey on eco-innovation parks," 2014.
- [55] S. W. Short, N. M. P. Bocken, C. Y. Barlow, and M. R. Chertow, "From refining sugar to growing tomatoes: Industrial ecology and business model evolution," *J. Ind. Ecol.*, 2014, doi: 10.1111/jiec.12171.
- [56] L. Fraccascia, M. Magno, and V. Albino, "Business models for industrial symbiosis: A guide for firms," *Procedia Environ. Sci. Eng. Manag.*, 2016.
- [57] European Commission, "Directive 2008/98/EC of the European parliament and of the council," 2008. <https://eur-lex.europa.eu/LexUriServ/LexUriServ.do?uri=OJ:L:2008:312:0003:0030:en:PDF>
- [58] European Commission, "Communication from the Commission - Towards a circular economy: A zero waste programme for Europe," *Eur. Comm.*, 2014.
- [59] I. Netinger Grubeša, I. Barišić, A. Fucic, and S. S. Bansode, "Ferrous slag: Characteristics and properties," *Charact. Uses Steel Slag Build. Constr.*, pp. 15–30, Jan. 2016, doi: 10.1016/B978-0-08-100368-8.00002-6.
- [60] Eurofer, "European Steel in Figures 2021," 2021. Accessed: Mar. 21, 2021. [Online]. Available: <https://www.eurofer.eu/assets/publications/brochures-booklets-and-factsheets/european-steel-in-figures-2021/European-Steel-in-Figures-2021.pdf>
- [61] International Energy Agency, *Energy Technology Perspectives 2010: Scenarios & Strategies to 2050*. 2010.
- [62] T. A. T. A. Branca *et al.*, "Reuse and recycling of by-products in the steel sector: Recent achievements paving the way to circular economy and industrial symbiosis in europe," *Metals (Basel)*, vol. 10, no. 3, 2020, doi: 10.3390/met10030345.
- [63] ASTM, "ASTM C125: Standard Terminology Relating to Concrete and Concrete Aggregates," *Annu. B. ASTM Stand.*, 2011.
- [64] George C. Wang, *The Utilization of Slag in Civil Infrastructure Construction*. 2014.
- [65] W. Gutt and A. D. Russell, "Studies of the system CaO-SiO<sub>2</sub>-Al<sub>2</sub>O<sub>3</sub>-MgO in relation to the stability of blastfurnace slag," *J. Mater.*

- Sci.*, vol. 12, no. 9, 1977, doi: 10.1007/BF00566249.
- [66] I. Z. I. Z. I. Z. Yildirim and M. Prezzi, "Chemical, mineralogical, and morphological properties of steel slag," *Adv. Civ. Eng.*, vol. 2011, 2011, doi: 10.1155/2011/463638.
- [67] I. Netinger Grubeša, I. Barišić, A. Fucic, S. S. Bansode, and Bansode, *Characteristics and uses of steel slag in building construction*. 2016. doi: 10.1016/c2014-0-03994-9.
- [68] R. R. Gelfi M., Cornacchia G., "Investigations on leaching behavior of EAF steel slags," in *Electric Arc Furnace (EAF) slag*, 2010.
- [69] D. Mombelli, C. Mapelli, S. Barella, C. Di Cecca, G. Le Saout, and E. Garcia-Diaz, "The effect of microstructure on the leaching behaviour of electric arc furnace (EAF) carbon steel slag," *Process Saf. Environ. Prot.*, vol. 102, pp. 810–821, 2016, doi: 10.1016/j.psep.2016.05.027.
- [70] P. Lemberge, "Analysis of metallurgical slags with ARL QUANT'X EDXRF Spectrometer (Thermo Fisher Scientific)." <https://assets.thermofisher.com/TFS-Assets/MSD/Application-Notes/XRF-AN41954-edxrf-analysis-metallurgical-slags.pdf> (accessed Jul. 08, 2022).
- [71] L. Miraglia, "Caratteristiche del sistema analitico SEM-EDS: valutazione dell'accuratezza e della precisione delle analisi eseguite su standards internazionali di minerali e vetri." [Online]. Available: [https://istituto.ingv.it/images/collane-editoriali/rappor ti tecnici/rappor ti-tecnici-2012/rappor to233.pdf](https://istituto.ingv.it/images/collane-editoriali/rappor t i tecnici/rappor ti-tecnici-2012/rappor to233.pdf)
- [72] UNI, *EN 12457-2 Characterisation of waste - Leaching - Compliance test for leaching of granular waste materials and sludges - Part 2: One stage batch test at a liquid to solid ratio of 10l/kg for materials with particle size below 4 mm (without or with size r*. 2004.
- [73] I. Matino, V. Colla, and S. Baragiola, "Internal Slags Reuse in an Electric Steelmaking Route and Process Sustainability: Simulation of Different Scenarios Through the EIRES Monitoring Tool," *Waste and Biomass Valorization*, 2018, doi: 10.1007/s12649-018-0264-3.
- [74] European Commission, "EU Action against Climate Change. Leading Global Action to 2020 and beyond, Luxembourg," 2008.
- [75] The European slag association, "Legas Status of Slags, Position Paper on the Status of Ferrous Slag, Duisburg, Germany," 2012.
- [76] R. I. R. I. R. I. Iacobescu, G. N. G. N. Angelopoulos, P. T. Jones, B. Blanpain, and Y. Pontikes, "Ladle metallurgy stainless steel slag as a raw material in Ordinary Portland Cement production: A possibility for industrial symbiosis," *J. Clean. Prod.*, vol. 112, pp. 872–881, 2016, doi: 10.1016/j.jclepro.2015.06.006.
- [77] P. Saranya, P. Nagarajan, and A. P. Shashikala, "Eco-friendly GGBS Concrete: A State-of-The-Art Review," in *IOP Conference Series: Materials Science and Engineering*, 2018. doi: 10.1088/1757-899X/330/1/012057.
- [78] I. Miñano, F. J. Benito, M. Valcuende, C. Rodríguez, and C. J. Parra, "Improvements in aggregate-paste interface by the hydration of steelmaking waste in concretes and mortars," *Materials (Basel)*, 2019, doi: 10.3390/ma12071147.
- [79] Y. Y. Jiang, T.-C. T. C. Ling, C. Shi, and S.-Y. S. Y. S.-Y. Pan, "Characteristics of steel slags and their use in cement and concrete — A review," *Resour. Conserv. Recycl.*, vol. 136, pp. 187–197, 2018, doi: 10.1016/j.resconrec.2018.04.023.
- [80] M. A. Sellitto and F. K. Murakami, "Destination of the waste generated by a steelmaking plant: a case study in Latin America," *Aestimum*, vol. 77, pp. 127–144, 2020, doi: 10.13128/aestim-9025.
- [81] N. Khan, Z.A., Malkawi, R.H., Al-Ofi, K.A., Khan, "Review of Steel Slag Utilization in Saudi Arabia," in *6th Saudi Engineering Conference*, 2002.
- [82] E. A. Oluwasola, M. R. Hainin, and M. M. A. Aziz, "Evaluation of asphalt mixtures incorporating electric arc furnace steel slag and copper mine tailings for road construction," *Transp. Geotech.*, vol. 2, pp. 47–55, 2015, doi: 10.1016/j.trgeo.2014.09.004.
- [83] M. M. A. M. A. Aziz, M. R. R. Hainin, H. Yaacob, Z. Ali, F.-L. L. Chang, and A. M. M. Adnan, "Characterisation and utilisation of steel slag for the construction of roads and highways," *Mater. Res. Innov.*, vol. 18, pp. S6-255-S6-259, 2014, doi: 10.1179/1432891714Z.000000000967.
- [84] T. C. Ling, H. M. Nor, M. R. Hainin, and S. K. Lim, "Long-term strength of rubberised concrete paving blocks," *Proc. Inst. Civ. Eng. - Constr. Mater.*, 2010, doi: 10.1680/coma.2010.163.1.19.
- [85] L. Rohde, W. P. Núñez, and J. A. P. Ceratti, "Electric Arc Furnace Steel Slag: Base Material for Low-Volume Roads," in *Transportation Research Record*, 2003. doi: 10.3141/1819b-26.
- [86] T. A. Branca *et al.*, "Investigation of (BOF) Converter slag use for agriculture in europe," *Metall. Res. Technol.*, 2014, doi: 10.1051/metal/2014022.
- [87] J. W. Lim, L. H. Chew, T. S. Y. Choong, C. Tezara, and M. H. Yazdi, "Overview of Steel Slag Application and Utilization," in *MATEC Web of Conferences*, 2016. doi: 10.1051/mateconf/20167400026.
- [88] A. Drizo, J. Cummings, D. Weber, E. Twohig, G. Druschel, and B. Bourke, "New evidence for rejuvenation of phosphorus retention capacity in EAF steel slag," *Environ. Sci. Technol.*, 2008, doi: 10.1021/es800232r.
- [89] C. Barca *et al.*, "Steel slag filters to upgrade phosphorus removal in small wastewater treatment plants: Removal mechanisms and performance," *Ecol. Eng.*, vol. 68, pp. 224–222, 2014, doi: 10.1016/j.ecoleng.2014.03.065.
- [90] B. De Gennaro, B. Notarnicola, L. Roselli, and G. Tassielli, "Innovative olive-growing models: An environmental and economic assessment," *J. Clean. Prod.*, 2012, doi: 10.1016/j.jclepro.2011.11.004.
- [91] B. Notarnicola, G. Tassielli, and P. A. Renzulli, "Industrial symbiosis in the Taranto industrial district: Current level, constraints and potential new synergies," *J. Clean. Prod.*, vol. 122, pp. 133–143, 2016, doi: 10.1016/j.jclepro.2016.02.056.
- [92] B. Notarnicola, G. Tassielli, and P. A. Renzulli, "Environmental and technical improvement of a grape must concentration system via a life cycle approach," *J. Clean. Prod.*, 2015, doi: 10.1016/j.jclepro.2014.11.020.
- [93] H. Zheng *et al.*, "Exploring Improvement Paths for Eight Industrial Symbiosis Complexes throughout the World," *J. Environ. Account. Manag.*, vol. 1, no. 3, pp. 295–306, 2013, doi: 10.5890/jeam.2013.08.007.
- [94] J. A. Onita, "How does industrial symbiosis influence environmental performance?" p. 61, 2006, [Online]. Available: <https://www.diva-portal.org/smash/get/diva2:22727/FULLTEXT01.pdf>
- [95] R. Van Berkel, T. Fujita, S. Hashimoto, and M. Fujii, "Quantitative assessment of urban and industrial symbiosis in Kawasaki, Japan," *Environ. Sci. Technol.*, 2009, doi: 10.1021/es803319r.

- [96] A. Van Beers, D., A. Bossilkov, and R. van Berkel, "Status report on regional synergies in the Kwinana Industrial Area," Perth, WA, Australia, 2005.
- [97] D. Van Beers, G. Corder, A. Bossilkov, and R. Van Berkel, "Industrial symbiosis in the Australian minerals industry: The cases of Kwinana and Gladstone," *Journal of Industrial Ecology*, 2007. doi: 10.1162/jiec.2007.1161.
- [98] L. Dong *et al.*, "Environmental and economic gains of industrial symbiosis for Chinese iron/steel industry: Kawasaki's experience and practice in Liuzhou and Jinan," *J. Clean. Prod.*, vol. 59, pp. 226–238, 2013, doi: 10.1016/j.jclepro.2013.06.048.
- [99] L. Dong, F. Gu, T. Fujita, Y. Hayashi, and J. Gao, "Uncovering opportunity of low-carbon city promotion with industrial system innovation: Case study on industrial symbiosis projects in China," *Energy Policy*, vol. 65, pp. 388–397, 2014, doi: 10.1016/j.enpol.2013.10.019.
- [100] L. Sun *et al.*, "Eco-benefits assessment on urban industrial symbiosis based on material flows analysis and emergy evaluation approach: A case of Liuzhou city, China," *Resour. Conserv. Recycl.*, vol. 119, pp. 78–88, 2017, doi: 10.1016/j.resconrec.2016.06.007.
- [101] M. T. Brown and S. Ulgiati, "Emergy evaluations and environmental loading of electricity production systems," *J. Clean. Prod.*, vol. 10, no. 4, pp. 321–334, 2002, doi: 10.1016/S0959-6526(01)00043-9.
- [102] Q. Song, J. Li, and X. Zeng, "Minimizing the increasing solid waste through zero waste strategy," *J. Clean. Prod.*, 2015, doi: 10.1016/j.jclepro.2014.08.027.
- [103] J. Li, S. Y. Pan, H. Kim, J. H. Linn, and P. C. Chiang, "Building green supply chains in eco-industrial parks towards a green economy: Barriers and strategies," *J. Environ. Manage.*, 2015, doi: 10.1016/j.jenvman.2015.07.030.
- [104] G. Krese, V. Dodig, B. Lagler, B. Strmčnik, and G. Podbregar, "Global trends in implementing the industrial symbiosis concept in the steel sector," in *International Multidisciplinary Scientific GeoConference Surveying Geology and Mining Ecology Management, SGEM*, 2018, vol. 18, no. 5.2, pp. 485–496. doi: 10.5593/sgem2018/5.2/S20.064.
- [105] S. Ohnishi, H. Dong, Y. Geng, M. Fujii, and T. Fujita, "A comprehensive evaluation on industrial & urban symbiosis by combining MFA, carbon footprint and emergy methods—Case of Kawasaki, Japan," *Ecol. Indic.*, 2017, doi: 10.1016/j.ecolind.2016.10.016.
- [106] J.-H. Park, I.-G. Jung, J.-G. Seo, and S.-H. Kim, "Current Status of By-products Generation and Industrial Symbiosis Network in Pohang, South Korea," *J. Korea Org. Resour. Recycl. Assoc.*, 2015, doi: 10.17137/korrae.2015.23.1.063.
- [107] POSCO, "POSCO Corporate citizenship report 2019 economic, environmental, social & governance performance," 2019. [Online]. Available: [http://corporatetcitizenship.posco.com/citizen/resources/file/report/eng/posco\\_report\\_2019\\_eng.pdf](http://corporatetcitizenship.posco.com/citizen/resources/file/report/eng/posco_report_2019_eng.pdf)
- [108] T. R. Jootae Kim, Yoonki Ahn, "Low-Carbon Management of POSCO in Circular Economy: Current Status and Limitations," in *Towards a Circular Economy: Corporate Management and Policy Pathways*, 2016.
- [109] A. Mangan, "By-Product Synergy: a strategy for sustainable development: a primer." The Business Council for Sustainable Development, Austin (TX), USA, 1998.
- [110] A. Mangan and E. Olivetti, "By-Product Synergy Networks: Driving Innovation through Waste Reduction and Carbon Mitigation," in *Sustainable Development in the Process Industries: Cases and Impact*, 2010. doi: 10.1002/9780470586099.ch6.
- [111] S. Morrison, S. Morrison, E. Fiction, and R. Coover, "Destia annual report 2017," 2018. [Online]. Available: [https://www.destia.fi/media/vuosikertomus-2017/destia\\_annual-report\\_2017.pdf](https://www.destia.fi/media/vuosikertomus-2017/destia_annual-report_2017.pdf)
- [112] M. A. M. A. Sellitto and F. K. F. K. Murakami, "Industrial symbiosis: A case study involving a steelmaking, a cement manufacturing, and a zinc smelting plant," *Chem. Eng. Trans.*, vol. 70, pp. 211–216, 2018, doi: 10.3303/CET1870036.
- [113] L. Bianco, S. Porisiensi, G. Baracchini, L. Battigelli, and C. Ceschia, "Circular Economy in EAF Process: How to Make It Sustainable with Zero Waste Project in Ferriere Nord," *Univers. J. Manag.*, vol. 6, no. 6, pp. 190–197, 2018, doi: 10.13189/ujm.2018.060602.
- [114] Comune di Brescia Settore ambiente ed Ecologia, "Rapporto dell ' Osservatorio Alfa Acciai 2021," Brescia, 2021. [Online]. Available: [https://www.alfaacciai.it/uploads/2021-6-24/Comunicato\\_Stampa\\_Osservatorio.pdf](https://www.alfaacciai.it/uploads/2021-6-24/Comunicato_Stampa_Osservatorio.pdf)
- [115] Expometals.net, "A closer look at ABS departments: Global Blue," *expometals.net*, 2020. <https://www.expometals.net/en-gb/news-page-abs-acciaierie-bertoli-safau/a-closer-look-at-abs-departments-global-blue-id23917> (accessed Sep. 27, 2021).
- [116] Byinnovation.eu, "Ecogravel: dalle scorie siderurgiche prodotti sostenibili per l'edilizia," *Mart Buildings*, 2015. <http://byinnovation.eu/ecogravel-dalle-scorie-siderurgiche-prodotti-sostenibili-per-ledilizia/> (accessed Sep. 27, 2021).
- [117] Arvedi, "Arvedi sostenibilità e responsabilità ambientale." <https://www.arvedi.it/sostenibilita-e-qualita/il-rispetto-ambientale/il-rapporto-con-lambiente/> (accessed Jul. 07, 2022).
- [118] Y. A. Ergün, "Mechanical Properties of Epoxy Composite Materials Produced with Different Ceramic Powders," *J. Mater. Sci. Chem. Eng.*, vol. 07, no. 12, 2019, doi: 10.4236/msce.2019.712001.
- [119] ISO 178:2019, "Plastics - Determination of flexural properties," *Int. Stand.*, 2019.
- [120] ISO 14544:2016, "Fine ceramics (advanced ceramics, advanced technical ceramics) - Mechanical properties of ceramic composites at high temperature - Determination of compression properties (ISO 14544:2013)," *Int. Stand.*, 2016.
- [121] ISO 7743:2011, "Rubber, vulcanized or thermoplastic – Determination of compression stress-strain properties," *Standards*, vol. 3, 2011.
- [122] H. H. Bertram, "Developments in Acrylonitrile–Butadiene Rubber (NBR) and Future Prospects," in *Developments in Rubber Technology*—2, 1981. doi: 10.1007/978-94-009-8108-9\_3.
- [123] I. Tiseo, "Consumption of natural and synthetic rubber worldwide from 1990 to 2020," *statista.com*, 2021. <https://www.statista.com/statistics/275399/world-consumption-of-natural-and-synthetic-caoutchouc/> (accessed Nov. 15, 2021).
- [124] M. Battista, A. Gobetti, S. Agnelli, and G. Ramorino, "Post-consumer tires as a valuable resource : review of different types of material recovery," *Environ. Technol. Rev.*, 2021, doi: 10.1080/21622515.2020.1861109.
- [125] A. Rowhani and T. J. Rainey, "Scrap tyre management pathways and their use as a fuel - A review," *Energies*, vol. 9, no. 11, pp. 1–26, 2016, doi: 10.3390/en9110888.
- [126] V. Torretta, E. Cristina, M. Ragazzi, E. Trulli, I. Aura, and L. Ionel, "Treatment and disposal of tyres : Two EU approaches . A review," *Waste Manag.*, vol. 45, pp. 152–160, 2015, doi: 10.1016/j.wasman.2015.04.018.

- [127] A. Togholi *et al.*, "A review on pavement porous concrete using recycled waste materials," *Smart Struct. Syst.*, vol. 22, no. 4, pp. 433–440, 2018, doi: 10.12989/sss.2018.22.4.433.
- [128] M. Shariati *et al.*, "Application of waste tire rubber aggregate in porous concrete," *Smart Struct. Syst.*, vol. 24, no. 4, pp. 553–566, 2019, doi: 10.12989/sss.2019.24.4.553.
- [129] Ministero dell'ambiente e della tutela del territorio e del mare, *Gazzetta Ufficiale del 31 marzo 2020, n.78*. Italy: Gazzetta Ufficiale, 2020.
- [130] H. Chittella, L. W. Yoon, S. Ramarad, and Z.-W. Lai, "Rubber waste management: A review on methods, mechanism, and prospects," *Polym. Degrad. Stab.*, vol. 194, p. 109761, 2021, doi: 10.1016/j.polymdegradstab.2021.109761.
- [131] H. Liu, X. Wang, and D. Jia, "Recycling of waste rubber powder by mechano-chemical modification," *J. Clean. Prod.*, vol. 245, 2020, doi: 10.1016/j.jclepro.2019.118716.
- [132] L. Asaro, M. Gratton, S. Seghar, and N. Ait Hocine, "Recycling of rubber wastes by devulcanization," *Resour. Conserv. Recycl.*, vol. 133, no. February, pp. 250–262, 2018, doi: 10.1016/j.resconrec.2018.02.016.
- [133] J. Adhikari, A. Das, T. Sinha, P. Saha, and J. K. Kim, "Grinding of Waste Rubber," no. 59, 2019.
- [134] "Divisions and Committees," *J. Soc. Mater. Sci. Japan*, vol. 20, no. 210, pp. 431–443, 1971, doi: 10.2472/jms.20.431.
- [135] M. Abbaspour, E. Aflaki, and F. Moghadas Nejad, "Reuse of waste tire textile fibers as soil reinforcement," *J. Clean. Prod.*, vol. 207, pp. 1059–1071, 2019, doi: 10.1016/j.jclepro.2018.09.253.
- [136] WBCSD, "End of Life Tires - A framework for effective management systems," *World Bus. Counc. Sustain. Dev.*, 2011.
- [137] Technical Committee CEN, "UNI EN 14243-1." CEN, European Standard, 2019.
- [138] S. S. Huang, H. Angelakopoulos, K. Pilakoutas, and I. Burgess, "Reused tyre polymer fibre for fire-spalling mitigation," *Appl. Struct. Fire Eng.*, no. October, pp. 15–16, 2017, doi: 10.14311/asfe.2015.056.
- [139] F. Aslani and J. Kelin, "Assessment and development of high-performance fibre-reinforced lightweight self-compacting concrete including recycled crumb rubber aggregates exposed to elevated temperatures," *J. Clean. Prod.*, vol. 200, pp. 1009–1025, 2018, doi: 10.1016/j.jclepro.2018.07.323.
- [140] M. S. Senin *et al.*, "The durability of concrete containing recycled tyres as a partial replacement of fine aggregate," *IOP Conf. Ser. Mater. Sci. Eng.*, vol. 271, no. 1, pp. 130–137, 2017, doi: 10.1088/1757-899X/271/1/012075.
- [141] A. Wongsu, V. Sata, B. Nematollahi, J. Sanjayan, and P. Chindaprasit, "Mechanical and thermal properties of lightweight geopolymer mortar incorporating crumb rubber," *J. Clean. Prod.*, vol. 195, pp. 1069–1080, 2018, doi: 10.1016/j.jclepro.2018.06.003.
- [142] N. F. Medina, R. Garcia, I. Hajirasouliha, K. Pilakoutas, M. Guadagnini, and S. Raffoul, "Composites with recycled rubber aggregates: Properties and opportunities in construction," *Constr. Build. Mater.*, vol. 188, pp. 884–897, 2018, doi: 10.1016/j.conbuildmat.2018.08.069.
- [143] A. Petrella, R. Di Mundo, S. De Gisi, F. Todaro, C. Labianca, and M. Notarnicola, "Environmentally Sustainable Cement Composites Based on End-of-Life Tyre Rubber and Recycled Waste Porous Glass," pp. 11–17, 2019.
- [144] E. Fraile-Garcia, J. Ferreira-Cabello, M. Mendivil-Giro, and A. S. A. S. Vicente-Navarro, "Thermal behaviour of hollow blocks and bricks made of concrete doped with waste tyre rubber," *Constr. Build. Mater.*, vol. 176, pp. 193–200, 2018, doi: 10.1016/j.conbuildmat.2018.05.015.
- [145] A. Ashori, M. Ghofrani, M. H. Rezvani, and N. Ayrilmis, "Development and material properties of reinforced plywood using carbon fiber and waste rubber powder," *Polym. Compos.*, vol. 39, no. 3, pp. 675–680, 2018, doi: 10.1002/pc.23984.
- [146] C. H. Signes, P. M. Fernández, J. Garzón-Roca, M. E. G. De La Torre, and R. I. Franco, "An Evaluation of the Resilient Modulus and Permanent Deformation of Unbound Mixtures of Granular Materials and Rubber Particles from Scrap Tyres to be Used in Subballast Layers," *Transp. Res. Procedia*, vol. 18, no. June, pp. 384–391, 2016, doi: 10.1016/j.trpro.2016.12.050.
- [147] M. Sol-Sánchez, F. Moreno-Navarro, and M. C. Rubio-Gámez, "The use of deconstructed tires as elastic elements in railway tracks," *Materials (Basel)*, vol. 7, no. 8, pp. 5903–5919, 2014, doi: 10.3390/ma7085903.
- [148] M. A. Al-Neami, "Stabilization of sandy soil using recycle waste tire chips," *Int. J. GEOMATE*, vol. 15, no. 48, pp. 175–180, 2018, doi: 10.21660/2018.48.180228.
- [149] C. Hidalgo-Signes, J. Garzón-Roca, J. M. Grima-Palop, and R. Insa-Franco, "Use of rubber shreds to enhance attenuation of railway sub-ballast layers made of unbound aggregates," *Mater. Constr.*, vol. 67, no. 326, pp. 158–167, 2017, doi: 10.3989/mc.2017.00316.
- [150] Y. Qi, B. Indraratna, A. Heitor, and J. S. Vinod, "Effect of rubber crumbs on the cyclic behavior of steel furnace slag and coal wash mixtures," *J. Geotech. Geoenvironmental Eng.*, vol. 144, no. 2, pp. 270–280, 2018, doi: 10.1061/(ASCE)GT.1943-5606.0001827.
- [151] M. Sol-Sánchez, F. Moreno-Navarro, L. Saiz, and M. C. Rubio-Gámez, "Recycling waste rubber particles for the maintenance of different states of railway tracks through a two-step stoneblowing process," *J. Clean. Prod.*, vol. 244, 2020, doi: 10.1016/j.jclepro.2019.118570.
- [152] F. Belabdelouahab and H. Trouzine, "Research and enhancement of used tyres, such as material innovative in Algeria," *Phys. Procedia*, vol. 55, pp. 68–74, 2014, doi: 10.1016/j.phpro.2014.07.011.
- [153] M. J. Moghadam, A. Zad, N. Mehrannia, and N. Dastaran, "Experimental evaluation of mechanically stabilized earth walls with recycled crumb rubbers," *J. Rock Mech. Geotech. Eng.*, vol. 10, no. 5, pp. 947–957, 2018, doi: 10.1016/j.jrmge.2018.04.012.
- [154] S. B. Reddy, A. M. Krishna, and K. R. Reddy, "Sustainable Utilization of Scrap Tire Derived Geomaterials for Geotechnical Applications," *Indian Geotech. J.*, vol. 48, no. 2, pp. 251–266, 2018, doi: 10.1007/s40098-017-0273-3.
- [155] M. Marconi, D. Landi, I. Meo, and M. Germani, "Reuse of Tires Textile Fibers in Plastic Compounds: Is this Scenario Environmentally Sustainable?," *Procedia CIRP*, vol. 69, no. May, pp. 944–949, 2018, doi: 10.1016/j.procir.2017.11.074.
- [156] U. Kalbe, O. Krüger, V. Wachtendorf, W. Berger, and S. Hally, "Development of leaching procedures for synthetic turf systems containing scrap tyre granules," *Waste and Biomass Valorization*, vol. 4, no. 4, pp. 745–757, 2013, doi: 10.1007/s12649-013-9248-5.
- [157] M. A. Imteaz, A. Arulrajah, S. Horpibulsuk, and A. Ahsan, "Environmental Suitability and Carbon Footprint Savings of Recycled Tyre Crumbs for Road Applications," *Int. J. Environ. Res.*, vol. 12, no. 5, pp. 693–702, 2018, doi: 10.1007/s41742-018-0126-7.

- [158] M. Saberian, L. Shi, A. Sidiq, J. Li, S. Setunge, and C. Q. Li, "Recycled concrete aggregate mixed with crumb rubber under elevated temperature," *Constr. Build. Mater.*, vol. 222, pp. 119–129, 2019, doi: 10.1016/j.conbuildmat.2019.06.133.
- [159] R. Maharaj, C. Maharaj, and M. Mahase, "The performance and durability of polyethylene terephthalate and crumb rubber-modified road pavement surfaces," *Prog. Rubber, Plast. Recycl. Technol.*, vol. 35, no. 1, pp. 3–22, 2019, doi: 10.1177/1477760618798425.
- [160] A. Mohammadinia, M. M. Disfani, G. A. Narsilio, and L. Aye, "Mechanical behaviour and load bearing mechanism of high porosity permeable pavements utilizing recycled tire aggregates," *Constr. Build. Mater.*, vol. 168, pp. 794–804, 2018, doi: 10.1016/j.conbuildmat.2018.02.179.
- [161] D. Li *et al.*, "Application of polymer, silica-fume and crushed rubber in the production of Pervious concrete," *Smart Struct. Syst.*, vol. 23, no. 2, pp. 207–214, 2019, doi: 10.12989/sss.2019.23.2.207.
- [162] D. Abellán-lópez and M. Sánchez-lozano, "NEW MOTORCYCLISTS PROTECTION SYSTEM MADE OF RECYCLED RUBBER," pp. 67–78, 2015.
- [163] K. Banaszkiwicz and M. Badura, "Experimental investigation on the application of recycled tires polymer fibers as a BTEX removal material," *SN Appl. Sci.*, vol. 1, no. 6, pp. 1–10, 2019, doi: 10.1007/s42452-019-0570-9.
- [164] L. Bockstal, T. Berchem, Q. Schmetz, and A. Richel, "Devulcanisation and reclaiming of tires and rubber by physical and chemical processes: A review," *J. Clean. Prod.*, vol. 236, p. 117574, 2019, doi: 10.1016/j.jclepro.2019.07.049.
- [165] Z. Wang, K. G. Burra, T. Lei, and A. K. Gupta, "Co-gasification characteristics of waste tire and pine bark mixtures in CO<sub>2</sub> atmosphere," *Fuel*, vol. 257, no. July, p. 116025, 2019, doi: 10.1016/j.fuel.2019.116025.
- [166] R. Dong and M. Zhao, "Research on the pyrolysis process of crumb tire rubber in waste cooking oil," *Renew. Energy*, vol. 125, pp. 557–567, 2018, doi: 10.1016/j.renene.2018.02.133.
- [167] D. Czajczyńska, R. Krzyżyńska, H. Jouhara, and N. Spencer, "Use of pyrolytic gas from waste tire as a fuel: A review," *Energy*, vol. 134, pp. 1121–1131, 2017, doi: 10.1016/j.energy.2017.05.042.
- [168] X. Zhang, H. Li, Q. Cao, L. Jin, and F. Wang, "Upgrading pyrolytic residue from waste tires to commercial carbon black," *Waste Manag. Res.*, no. 79, pp. 149–157, 2018, doi: 10.1177/0734242X18764292.
- [169] R. Zhong, J. Xu, D. Hui, S. S. Bhosale, and R. Hong, "Pyrolytic preparation and modification of carbon black recovered from waste tyres," *Waste Manag. Res.*, vol. 38, no. 1, pp. 35–43, 2020, doi: 10.1177/0734242X19869987.
- [170] A. D. La Rosa, E. Pergolizzi, D. Maragna, G. Recca, and G. Cicala, "Reuse of carbon black from end-of-life tires in new pneumatic formulations and life-cycle assessment of the thermolysis process," *J. Elastomers Plast.*, vol. 51, no. 7–8, pp. 740–754, 2019, doi: 10.1177/0095244318819242.
- [171] S. A. Y. Shah, M. Zeeshan, M. Z. Farooq, N. Ahmed, and N. Iqbal, "Co-pyrolysis of cotton stalk and waste tire with a focus on liquid yield quantity and quality," *Renew. Energy*, vol. 130, no. x, pp. 238–244, 2019, doi: 10.1016/j.renene.2018.06.045.
- [172] Z. Kerekes, É. Lublóy, and K. Kopecskó, "Behaviour of tyres in fire: Determination of burning characteristics of tyres," *J. Therm. Anal. Calorim.*, vol. 133, no. 1, pp. 279–287, 2018, doi: 10.1007/s10973-018-7001-9.
- [173] O. Sanahuja-Parejo *et al.*, "Catalytic co-pyrolysis of grape seeds and waste tyres for the production of drop-in biofuels," *Energy Convers. Manag.*, vol. 171, no. May, pp. 1202–1212, 2018, doi: 10.1016/j.enconman.2018.06.053.
- [174] N. Ahmed, M. Zeeshan, N. Iqbal, M. Z. Farooq, and S. A. Shah, "Investigation on bio-oil yield and quality with scrap tire addition in sugarcane bagasse pyrolysis," *J. Clean. Prod.*, vol. 196, pp. 927–934, 2018, doi: 10.1016/j.jclepro.2018.06.142.
- [175] R. Rajarao, R. Farzana, R. Khanna, and V. Sahajwalla, "Synthesis of SiC/Si<sub>3</sub>N<sub>4</sub> nanocomposite by using automotive waste tyres as resource," *J. Ind. Eng. Chem.*, vol. 29, pp. 35–38, 2015, doi: 10.1016/j.jiec.2015.04.006.
- [176] G. L. R. Da Silva, R. Dias Silva, L. Cheloni, V. E. De Souza Moreira, N. B. Dias Haneiko, and P. S. Assis, "Characterization of metallurgical coke produced with coal mixtures and waste tires," *Mater. Res.*, vol. 19, no. 3, pp. 728–734, 2016, doi: 10.1590/1980-5373-MR-2015-0741.
- [177] M. T. Islam *et al.*, "Conversion of waste tire rubber into a high-capacity adsorbent for the removal of methylene blue, methyl orange, and tetracycline from water," *J. Environ. Chem. Eng.*, vol. 6, no. 2, pp. 3070–3082, 2018, doi: 10.1016/j.jece.2018.04.058.
- [178] T. A. Saleh and V. K. Gupta, "Processing methods, characteristics and adsorption behavior of tire derived carbons: A review," *Adv. Colloid Interface Sci.*, vol. 211, pp. 93–101, 2014, doi: 10.1016/j.cis.2014.06.006.
- [179] H. Gupta, "Anthracene removal from water onto activated carbon derived from vehicular tyre," *Sep. Sci. Technol.*, vol. 53, no. 4, pp. 613–625, 2018, doi: 10.1080/01496395.2017.1405038.
- [180] M. S. Abdelbassit, S. A. Popoola, T. A. Saleh, H. H. Abdallah, A. A. Al-Saadi, and K. R. Alhooshani, "DFT and Kinetic Evaluation of Chloromethane Removal Using Cost-Effective Activated Carbon," *Arab. J. Sci. Eng.*, vol. 45, no. 6, pp. 4705–4716, 2020, doi: 10.1007/s13369-020-04458-x.
- [181] M. Niksirat, R. Sadeghi, and J. Esmaili, "Removal of Mn from aqueous solutions, by activated carbon obtained from tire residuals," *SN Appl. Sci.*, vol. 1, no. 7, pp. 1–12, 2019, doi: 10.1007/s42452-019-0797-5.
- [182] I. A. H. Al Zubaidi, A. K. Al Tamimi, and H. Ahmed, "Remediation of water from crude oil spill using a fibrous sorbent," *Environ. Technol. Innov.*, vol. 6, pp. 105–114, 2016, doi: 10.1016/j.eti.2016.08.002.
- [183] E. Babiker, M. A. Al-Ghouthi, N. Zouari, and G. McKay, "Removal of boron from water using adsorbents derived from waste tire rubber," *J. Environ. Chem. Eng.*, vol. 7, no. 2, p. 102948, 2019, doi: 10.1016/j.jece.2019.102948.
- [184] M. A. López-Manchado, M. Arroyo, B. Herrero, and J. Biagiotti, "Vulcanization kinetics of natural rubber-organoclay nanocomposites," *J. Appl. Polym. Sci.*, vol. 89, no. 1, 2003, doi: 10.1002/app.12082.
- [185] F. A. Neugebauer, "9.1 Introduction," *Nitrogen Oxyg. Centered Radicals*, pp. 7–9, 2006, doi: 10.1007/10858968\_2.
- [186] L. R. G. Treloar, "Cross-linking and modulus," in *The physics of rubber elasticity*, 1975. doi: 10.1063/1.3060678.
- [187] S. Lee, H. Pawlowski, and A. Y. Coran, "Method for Estimating the Chemical Crosslink Densities of Cured Natural Rubber and Styrene-Butadiene Rubber," *Rubber Chem. Technol.*, 1994, doi: 10.5254/1.3538716.
- [188] A. Yehia and S. El-Sabbagh, "Detection of Crosslink Density by Different Methods for Natural Rubber Blended with SBR and

- NBR," *Egypt J. Solids*, vol. 30, no. 2, pp. 157–173, 2007.
- [189] K. L. Mok and A. H. Eng, "Characterisation of crosslinks in vulcanised rubbers: From simple to advanced techniques," *Malaysian J. Chem.*, vol. 20, no. 1, pp. 118–127, 2018.
- [190] K. Sridharan and K. Elangovan, "Investigation on the swelling characteristics of NR/BR rubber blends," *J. Chem. Pharm. Res.*, vol. 8, no. 1, pp. 553–557, 2016.
- [191] M. Barikani and C. Hepburn, "Determination of crosslink density by swelling in the castable polyurethane elastomer based on 1/4 - cyclohexane diisocyanate and para-phenylene diisocyanate," *Iran. J. Polym. Sci. Technol.*, vol. 1, no. 1, pp. 1–5, 1992.
- [192] G. M. Bristow and W. F. Watson, "Cohesive energy densities of polymers: Part 1. - Cohesive energy densities of rubbers by swelling measurements," *Trans. Faraday Soc.*, 1958, doi: 10.1039/TF9585401731.
- [193] G. M. Bristow and W. F. Watson, "Cohesive energy densities of polymers: Part 2. - Cohesive energy densities from viscosity measurements," *Trans. Faraday Soc.*, 1958, doi: 10.1039/TF9585401742.
- [194] V. P. Swapna, R. Stephen, T. Greeshma, C. Sharan Dev, and M. S. Sreekala, "Mechanical and swelling behavior of green nanocomposites of natural rubber latex and tubular shaped halloysite nano clay," *Polym. Compos.*, vol. 37, no. 2, pp. 602–611, 2016, doi: 10.1002/pc.23217.
- [195] C. Kraus, "Interactions of elastomers and reinforcing fillers," *Rubber Chem. Technol.*, vol. 38, pp. 1070–1114, 1965.
- [196] E. Broitman, "Indentation Hardness Measurements at Macro-, Micro-, and Nanoscale: A Critical Overview," *Tribol. Lett.*, vol. 65, no. 1, pp. 1–18, 2017, doi: 10.1007/s11249-016-0805-5.
- [197] ISO 37, "Rubber, vulcanized or thermoplastic — Determination of tensile stress-strain properties." ISO, 2017.
- [198] S. Das Gupta, R. Mukhopadhyay, K. C. Baranwal, and A. K. Bhowmick, *Reverse Engineering of Rubber Products*. 2013. doi: 10.1201/b15435.
- [199] R. . Datta and A. . Ingham, *Rubber Technologist's Handbook*. 2001.
- [200] L. Dunn, "Introduction to Viscoelasticity in Polymers and its Impact on Rolling Resistance in Pneumatic Tyres," *Int. J. Squiggly Wobbly Mater.*, vol. 23, no. February, 2019.
- [201] J. T. Bauman, "Fatigue, Stress, and Strain of Rubber Components," in *Fatigue, Stress, and Strain of Rubber Components*, 2008. doi: 10.3139/9783446433403.fm.
- [202] J. Diani, B. Fayolle, and P. Gilormini, "A review on the Mullins effect," *Eur. Polym. J.*, vol. 45, no. 3, pp. 601–612, 2009, doi: 10.1016/j.eurpolymj.2008.11.017.
- [203] A. F. Blanchard and D. Parkinson, "Breakage of Carbon-Rubber Networks by Applied Stress," *Ind. Eng. Chem.*, vol. 44, no. 4, 1952, doi: 10.1021/ie50508a034.
- [204] F. Bueche, "Molecular basis for the mullins effect," *J. Appl. Polym. Sci.*, vol. 4, no. 10, 1960, doi: 10.1002/app.1960.070041017.
- [205] R. Houwink, "Slipping of Molecules during the Deformation of Reinforced Rubber," *Rubber Chem. Technol.*, vol. 29, no. 3, 1956, doi: 10.5254/1.3542602.
- [206] G. R. Hamed and S. Hatfield, "On the role of bound rubber in carbon-black reinforcement," *Rubber Chem. Technol.*, vol. 62, no. 1, 1989, doi: 10.5254/1.3536231.
- [207] Y. Fukahori, "New progress in the theory and model of carbon black reinforcement of elastomers," in *Journal of Applied Polymer Science*, 2005, vol. 95, no. 1. doi: 10.1002/app.20802.
- [208] J. D. Ferry, *Viscoelastic properties of polymers*. 1980. doi: 10.1149/1.2428174.
- [209] G. Ramorino, F. Bignotti, L. Conzatti, and T. Ricco, "Dynamic and viscoelastic behavior of natural rubber/layered silicate nanocomposites obtained by melt blending," in *Polymer Engineering and Science*, 2007, vol. 47, no. 10. doi: 10.1002/pen.20849.
- [210] A. R. Payne, "A note on the existence of a yield point in the dynamic modulus of loaded vulcanizates," *J. Appl. Polym. Sci.*, vol. 3, no. 7, pp. 127–127, 1960, doi: 10.1002/app.1960.070030721.
- [211] L. Chazeau, J. D. Brown, L. C. Yanyo, and S. S. Sternstein, "Modulus recovery kinetics and other insights into the Payne effect for filled elastomers," *Polym. Compos.*, vol. 21, no. 2, pp. 202–222, 2000, doi: 10.1002/pc.10178.
- [212] F. Schön, R. Thomann, and W. Gronski, "Shear controlled morphology of rubber/organoclay nanocomposites and dynamic mechanical analysis," *Macromol. Symp.*, vol. 189, pp. 105–110, 2002, doi: 10.1002/masy.200290000.
- [213] J.-T. Kim, T.-S. Oh, and D.-H. Lee, "Preparation and characteristics of nitrile rubber (NBR) nanocomposites based on organophilic layered clay," *Polym. Int.*, vol. 52, no. 7, pp. 1058–1063, 2003, doi: 10.1002/pi.1110.
- [214] S. Varghese, J. Karger-Kocsis, and K. G. Gatos, "Melt compounded epoxidized natural rubber/layered silicate nanocomposites: Structure-properties relationships," *Polymer (Guildf.)*, vol. 44, no. 14, pp. 3977–3983, 2003, doi: 10.1016/S0032-3861(03)00358-6.
- [215] Y. T. Vu, J. E. Mark, L. H. Pham, and M. Engelhardt, "Clay nanolayer reinforcement of cis-1,4-polyisoprene and epoxidized natural rubber," *J. Appl. Polym. Sci.*, vol. 82, no. 6, pp. 1391–1403, 2001, doi: 10.1002/app.1976.
- [216] A. Lion, C. Kardelky, and P. Haupt, "On the frequency and amplitude dependence of the Payne effect: Theory and experiments," *Rubber Chem. Technol.*, vol. 76, no. 2, pp. 533–547, 2003, doi: 10.5254/1.3547759.
- [217] S. Vieweg, R. Unger, K. Schroeter, E. Donth, and G. Heinrich, "Frequency and temperature dependence of the small-strain behavior of carbon-black filled vulcanizates," *Polym. networks & blends*, vol. 5, no. 4, pp. 199–204, 1995.
- [218] S. Vieweg, R. Unger, G. Heinrich, and E. Donth, "Comparison of dynamic shear properties of styrene-butadiene vulcanizates filled with carbon black or polymeric fillers," *J. Appl. Polym. Sci.*, vol. 73, no. 4, pp. 495–503, 1999, doi: 10.1002/(SICI)1097-4628(19990725)73:4<495::AID-APP5>3.0.CO;2-I.
- [219] Z. Xu, Y. Song, and Q. Zheng, "Payne effect of carbon black filled natural rubber compounds and their carbon black gels," *Polymer (Guildf.)*, vol. 185, 2019, doi: 10.1016/j.polymer.2019.121953.
- [220] G. Ramorino, D. Vetturi, D. Cambiaghi, A. Pegoretti, and T. Ricco, "Developments in dynamic testing of rubber compounds: Assessment of non-linear effects," *Polym. Test.*, vol. 22, no. 6, pp. 681–687, 2003, doi: 10.1016/S0142-9418(02)00176-9.
- [221] G. Ramorino, F. Bignotti, S. Pandini, and T. Riccò, "Mechanical reinforcement in natural rubber/organoclay nanocomposites," *Compos. Sci. Technol.*, vol. 69, no. 7–8, pp. 1206–1211, 2009, doi: 10.1016/j.compscitech.2009.02.023.

- [222] M. Rendek and A. Lion, "Amplitude dependence of filler-reinforced rubber: Experiments, constitutive modelling and FEM - Implementation," *Int. J. Solids Struct.*, vol. 47, no. 21, pp. 2918–2936, 2010, doi: 10.1016/j.ijsolstr.2010.06.021.
- [223] S. P. A. Narayan and L. I. Palade, "Modeling Payne effect with a framework of multiple natural configurations," *Int. J. Eng. Sci.*, vol. 157, 2020, doi: 10.1016/j.ijengsci.2020.103396.
- [224] C. Gauthier, E. Reynaud, R. Vassoille, and L. Ladouce-Stelandre, "Analysis of the non-linear viscoelastic behaviour of silica filled styrene butadiene rubber," *Polymer (Guildf.)*, vol. 45, no. 8, pp. 2761–2771, 2004, doi: 10.1016/j.polymer.2003.12.081.
- [225] A. Boonbumrung, P. Sae-Oui, and C. Sirisinha, "Reinforcement of Multiwalled Carbon Nanotube in Nitrile Rubber: In Comparison with Carbon Black, Conductive Carbon Black, and Precipitated Silica," *J. Nanomater.*, vol. 2016, 2016, doi: 10.1155/2016/6391572.
- [226] A. R. Payne, "The dynamic properties of carbon black-loaded natural rubber vulcanizates. Part I," *J. Appl. Polym. Sci.*, vol. 6, no. 19, pp. 57–63, 1962, doi: 10.1002/app.1962.070061906.
- [227] G. Heinrich and M. Klüppel, "Recent advances in the theory of filler networking in elastomers," *Adv. Polym. Sci.*, vol. 160, no. October, pp. 1–44, 2002, doi: 10.1007/3-540-45362-8\_1.
- [228] A. I. Medalia, "Morphology of aggregates. VI. Effective volume of aggregates of carbon black from electron microscopy; Application to vehicle absorption and to die swell of filled rubber," *J. Colloid Interface Sci.*, vol. 32, no. 1, pp. 115–131, 1970, doi: 10.1016/0021-9797(70)90108-6.
- [229] A. I. Medalia, "Elastic modulus of vulcanizates as related to carbon black structure," *Rubber Chem. Technol.*, vol. 46, no. 4, pp. 877–896, 1973, doi: 10.5254/1.3547416.
- [230] M. Gerspacher, C. P. O'Farrell, H. H. Yang, and C. Tricot, "Modeling of the carbon black reinforcement mechanism in elastomers," *Rubber World*, vol. 214, no. 3, pp. 27–49, 1996.
- [231] D. Mondal, S. Ghorai, D. Rana, D. De, and D. Chattopadhyay, "The rubber–filler interaction and reinforcement in styrene butadiene rubber/devulcanize natural rubber composites with silica–graphene oxide," *Polym. Compos.*, vol. 40, no. S2, pp. E1559–E1572, 2019, doi: 10.1002/pc.25076.
- [232] R. Brown, *Physical testing of rubber*. 2006. doi: 10.1007/0-387-29012-5.
- [233] A. Sargsyan, A. Tonoyan, S. Davtyan, and C. Schick, "The amount of immobilized polymer in PMMA SiO<sub>2</sub> nanocomposites determined from calorimetric data," *Eur. Polym. J.*, vol. 43, no. 8, pp. 3113–3127, 2007, doi: 10.1016/j.eurpolymj.2007.05.011.
- [234] B. N. J. Persson and A. I. Volokitin, "Rubber friction on smooth surfaces," *Eur. Phys. J. E*, vol. 21, no. 1, 2006, doi: 10.1140/epje/i2006-10045-9.
- [235] D. F. Moore and W. Geyer, "A review of hysteresis theories for elastomers," *Wear*, vol. 30, no. 1, 1974, doi: 10.1016/0043-1648(74)90055-6.
- [236] L. Mészárosóvá, E. Tűmová, and R. Drochytka, "Epoxy Screed as Possible Protection of Floor Surfaces," *Adv. Mater. Res.*, 2015, doi: 10.4028/www.scientific.net/amr.1100.166.
- [237] J. P. Lu, "Review on application of polymer concrete in Singapore," in *Advanced Materials Research*, 2013. doi: 10.4028/www.scientific.net/AMR.687.416.
- [238] L. Mészárosóvá and R. Drochytka, "Possible substitutes of epoxy screed filler with secondary raw materials," in *Advanced Materials Research*, 2013. doi: 10.4028/www.scientific.net/AMR.645.77.
- [239] R. Roberti, "Impianto per il trattamento delle scorie del forno elettrico ad arco," Impianto per il trattamento delle scorie del forno elettrico ad arco, 2008.
- [240] C. Navarro, M. Díaz, and M. A. Villa-García, "Physico-chemical characterization of steel slag: study of its behavior under simulated environmental conditions," *Environ. Sci. Technol.*, vol. 44, no. 14, 2010, doi: 10.1021/es100690b.
- [241] E. R. Plunkett, *Handbook of Industrial Toxicology*. New York: Chemical Publishing Co., 1976.
- [242] M. Tossavainen, F. Engstrom, Q. Yang, N. Menad, M. Lidstrom Larsson, and B. Bjorkman, "Characteristics of steel slag under different cooling conditions," *Waste Manag.*, vol. 27, no. 10, pp. 1335–1344, 2007, doi: 10.1016/j.wasman.2006.08.002.
- [243] K. E. Daugherty, B. Saad, C. Weirich, and A. Eberendu, "The glass content of slag and hydraulic activity," *Silic. Ind.* 4, vol. 5, pp. 107–110, 1983.
- [244] Supplemento ordinario alla Gazzetta ufficiale 16 aprile 1998 n. 88, *Individuazione dei rifiuti non pericolosi sottoposti alle procedure semplificate di recupero ai sensi degli articoli 31 e 33 del decreto legislativo 5 febbraio 1997, n. 22*. 1998.
- [245] n. 115 Ministero della tutela dell'ambiente e del territorio Gazzetta Ufficiale 19 maggio 2006, *Individuazione dei rifiuti non pericolosi sottoposti alle procedure semplificate di recupero, ai sensi degli articoli 31 e 33 del decreto legislativo 5 febbraio 1997, n. 22*. Italia.
- [246] n. 201 Ministero della tutela dell'ambiente e del territorio Gazzetta Ufficiale del 30 agosto 2005, *Definizione dei criteri di ammissibilità dei rifiuti in discarica*. Italia.
- [247] A. Riboldi *et al.*, "Grain size effect in elution test of electric arc furnace slag," *Appl. Sci.*, vol. 10, no. 2, 2020, doi: 10.3390/app10020477.
- [248] P. L. Teh *et al.*, "The properties of epoxy resin coated silica fillers composites," *Mater. Lett.*, vol. 61, no. 11–12, 2007, doi: 10.1016/j.matlet.2006.08.036.
- [249] A. Assi *et al.*, "A Circular Economy Virtuous Example — Use of a Stabilized Waste Material Instead of Calcite to Produce Sustainable Composites," *Appl. Sci. MDPI*, vol. 10, no. 754, pp. 1–15, 2020, doi: 10.3390/app10030754.
- [250] D. M. Yemam, B. J. Kim, J. Y. Moon, and C. Yi, "Mechanical properties of epoxy resin mortar with sand washing waste as filler," *Materials (Basel)*, vol. 10, no. 3, 2017, doi: 10.3390/ma10030246.
- [251] Y.-J. Wan, L.-X. Gong, L.-C. Tang, L.-B. Wu, and J.-X. Jiang, "Mechanical properties of epoxy composites filled with silane-functionalized graphene oxide," *Compos. Part A Appl. Sci. Manuf.*, vol. 64, pp. 79–89, 2014, doi: 10.1016/j.compositesa.2014.04.023.
- [252] B. Wetzel, P. Rosso, F. Hauptert, and K. Friedrich, "Epoxy nanocomposites - fracture and toughening mechanisms," *Eng. Fract. Mech.*, vol. 73, no. 16, 2006, doi: 10.1016/j.engfracmech.2006.05.018.
- [253] R. Medina, F. Hauptert, and A. K. Schlarb, "Improvement of tensile properties and toughness of an epoxy resin by

- nanozirconium-dioxide reinforcement," *J. Mater. Sci.*, vol. 43, no. 9, 2008, doi: 10.1007/s10853-008-2547-8.
- [254] G. M. Odegard, T. C. Clancy, and T. S. Gates, "Modeling of the mechanical properties of nanoparticle/polymer composites," *Polymer (Guildf.)*, vol. 46, no. 2, 2005, doi: 10.1016/j.polymer.2004.11.022.
- [255] K. J. Wong, B. F. Yousif, K. O. Low, Y. Ng, and S. L. Tan, "Effects of fillers on the fracture behaviour of particulate polyester composites," *J. Strain Anal. Eng. Des.*, vol. 45, no. 1, 2010, doi: 10.1243/03093247JSA553.
- [256] R. V. Silva, D. Spinelli, W. W. Bose Filho, S. Claro Neto, G. O. Chierice, and J. R. Tarpani, "Fracture toughness of natural fibers/castor oil polyurethane composites," *Compos. Sci. Technol.*, vol. 66, no. 10, 2006, doi: 10.1016/j.compscitech.2005.10.012.
- [257] T. Ahmad, O. Mamat, and R. Ahmad, "Studying the Effects of Adding Silica Sand Nanoparticles on Epoxy Based Composites," *J. Nanoparticles*, vol. 2013, 2013, doi: 10.1155/2013/603069.
- [258] G. Li, W. Zhang, P. Zhu, D. Lu, T. Zhao, and R. Sun, "Improvements in thermo-mechanical and rheological properties of SiO<sub>2</sub>/epoxy composites using different types of SiO<sub>2</sub>," *J. Mater. Sci. Mater. Electron.*, vol. 27, no. 1, 2016, doi: 10.1007/s10854-015-3781-x.
- [259] G. H. Rubiolo, J. D. Marconi, and S. N. Goyanes, "Yield stress of epoxy composites filled with quartz powder," *Polym. Int.*, vol. 51, no. 11, 2002, doi: 10.1002/pi.928.
- [260] A. Jumahat, C. Soutis, J. Mahmud, and N. Ahmad, "Compressive properties of nanoclay/epoxy nanocomposites," in *Procedia Engineering*, 2012, vol. 41, doi: 10.1016/j.proeng.2012.07.357.
- [261] J. R. M. D'Almeida and B. H. P. Manfredini, "Hardness evaluation of epoxy resin filled with mineral waste," *J. Appl. Polym. Sci.*, vol. 84, no. 12, pp. 2178–2184, 2002, doi: 10.1002/app.10488.
- [262] J. L. Valentín *et al.*, "Novel experimental approach to evaluate Filler-Elastomer interactions," *Macromolecules*, vol. 43, no. 1, pp. 334–346, 2010, doi: 10.1021/ma901999j.
- [263] S. Thomas, S. C. George, and S. Thomas, "Rigid amorphous phase: Mechanical and transport properties of nitrile rubber/clay nanocomposites," *Prog. Rubber, Plast. Recycl. Technol.*, vol. 33, no. 2, pp. 103–126, 2017, doi: 10.1177/147776061703300204.
- [264] S. Joly, G. Garnaud, R. Ollitraul, L. Bokobza, and J. E. Mark, "Organically modified layered silicates as reinforcing fillers for natural rubber," *Chem. Mater.*, vol. 14, no. 10, pp. 4202–4208, 2002, doi: 10.1021/cm020093e.
- [265] T. Goudarzi, D. W. D. W. Spring, G. H. G. H. Paulino, and O. Lopez-Pamies, "Filled elastomers: A theory of filler reinforcement based on hydrodynamic and interphasial effects," *J. Mech. Phys. Solids*, vol. 80, pp. 37–67, 2015, doi: 10.1016/j.jmps.2015.04.012.
- [266] E. Guth, "Theory of filler reinforcement," *J. Appl. Phys.*, vol. 16, no. 1, pp. 20–25, 1945, doi: 10.1063/1.1707495.
- [267] G. Tsagaropoulos and A. Eisenberg, "Direct Observation of Two Glass Transition in Silica-Filled Polymers. Implications for the Morphology of Random Ionomers," *Macromolecules*, vol. 28, no. 1, pp. 396–398, 1995, doi: 10.1021/ma00105a059.
- [268] G. Tsagaropoulos and A. Eisenberg, "Dynamic Mechanical Study of the Factors Affecting the Two Glass Transition Behavior of Filled Polymers. Similarities and Differences with Random Ionomers," *Macromolecules*, vol. 28, no. 18, pp. 6067–6077, 1995, doi: 10.1021/ma00122a011.
- [269] M.-J. Wang, "Effect of polymer-filler and filler-filler interactions on dynamic properties of filled vulcanizates," *Rubber Chem. Technol.*, vol. 71, no. 3, pp. 520–589, 1998, doi: 10.5254/1.3538492.
- [270] S. Merabia, P. Sotta, and D. R. Long, "A microscopic model for the reinforcement and the nonlinear behavior of filled elastomers and thermoplastic elastomers (Payne and Mullins Effects)," *Macromolecules*, vol. 41, no. 21, pp. 8252–8266, 2008, doi: 10.1021/ma8014728.
- [271] W.-G. Hwang, K.-H. Wei, and C.-M. Wu, "Mechanical, thermal, and barrier properties of NBR/organosilicate nanocomposites," *Polym. Eng. Sci.*, vol. 44, no. 11, pp. 2117–2124, 2004, doi: 10.1002/pen.20217.
- [272] K. Gorna, M. Hund, M. Vučak, F. Gröhn, and G. Wegner, "Amorphous calcium carbonate in form of spherical nanosized particles and its application as fillers for polymers," *Mater. Sci. Eng. A*, vol. 477, no. 1–2, 2008, doi: 10.1016/j.msea.2007.05.045.
- [273] C. M. Roland, "Reinforcement of Elastomers," *Ref. Modul. Mater. Sci. Mater. Eng.*, no. June 2015, 2016, doi: 10.1016/b978-0-12-803581-8.02163-9.
- [274] M. Svanera, S. Panza, F. Uberto, and R. Roberti, "An innovative system for the re-use of slag from the Electric Arc Furnace | Un impianto innovativo nella filiera del recupero della scoria da forno elettrico," *La Metall. Ital.*, vol. 104, no. 2, pp. 37–43, 2012.
- [275] ASTM D5289, "Rubber Property — Vulcanization Using Rotorless Cure," *Astm*, 2015.
- [276] ISO 7619-1, "Rubber, vulcanized or thermoplastic — Determination of indentation hardness — Part 1: Durometer method (Shore hardness)," 2010.
- [277] ISO 48, "Rubber, vulcanized or thermoplastic — Determination of hardness — Part 4: Indentation hardness by durometer method (Shore hardness)," 2018.
- [278] ASTM Standards, "ASTM D395: Standard Test Methods for Rubber Property — Compression Set." 2018.
- [279] S. Çoruh, S. Elevli, O. N. Ergun, and G. Demir, "Assessment of leaching characteristics of heavy metals from industrial leach waste," *Int. J. Miner. Process.*, vol. 123, pp. 165–171, 2013, doi: 10.1016/j.minpro.2013.06.005.
- [280] A. Król and K. Mizerna, "The effect of particle size reduction of waste material on heavy metals release," *Chemik*, vol. 69, no. 10, pp. 670–673, 2015.
- [281] Z. Guo, L. Zhang, Y. Cheng, X. Xiao, F. Pan, and K. Jiang, "Effects of pH, pulp density and particle size on solubilization of metals from a Pb/Zn smelting slag using indigenous moderate thermophilic bacteria," *Hydrometallurgy*, vol. 104, no. 1, pp. 25–31, 2010, doi: 10.1016/j.hydromet.2010.04.006.
- [282] M. N. Satheesh Kumar and Siddaramaiah, "Water absorption behavior of acrylonitrile-butadiene (NBR) latex impregnated jute nonwoven fabric composites," *J. Appl. Polym. Sci.*, vol. 101, no. 3, pp. 2045–2050, 2006, doi: 10.1002/app.23773.
- [283] M. M. Salehi, T. Khalkhali, and A. A. Davoodi, "The physical and mechanical properties and cure characteristics of NBR/silica/MWCNT hybrid composites," *Polym. Sci. - Ser. A*, vol. 58, no. 4, pp. 567–577, 2016, doi: 10.1134/S0965545X16040131.
- [284] F. El-Tantawy and F. S. Deghaidy, "Effect of iron oxide on vulcanization kinetics and electrical conductance of butyl rubber composites," *Polym. Int.*, vol. 49, no. 11, pp. 1371–1376, 2000, doi: 10.1002/1097-0126(200011)49:11<1371::AID-PI496>3.0.CO;2-0.

- [285] K. Roy, M. N. Alam, S. K. Mandal, and S. C. Debnath, "Effect of sol-gel modified nano calcium carbonate (CaCO<sub>3</sub>) on the cure, mechanical and thermal properties of acrylonitrile butadiene rubber (NBR) nanocomposites," *J. Sol-Gel Sci. Technol.*, vol. 73, no. 2, pp. 306–313, 2015, doi: 10.1007/s10971-014-3530-2.
- [286] Q. Wang, F. Yang, Q. Yang, J. Chen, and H. Guan, "Study on mechanical properties of nano-Fe<sub>3</sub>O<sub>4</sub> reinforced nitrile butadiene rubber," *Mater. Des.*, vol. 31, no. 2, pp. 1023–1028, 2010, doi: 10.1016/j.matdes.2009.07.038.
- [287] G. Szabó and K. Váradi, "Large strain viscoelastic material model for deformation, stress and strain analysis of O-rings," *Period. Polytech. Mech. Eng.*, vol. 62, no. 2, pp. 148–157, 2018, doi: 10.3311/PPme.11595.
- [288] A. Wahab and A. S. Farid, "Correlation between compression-set and compression stress-relaxation of epichlorohydrin elastomers," *Polym. Polym. Compos.*, vol. 19, no. 8, pp. 631–638, 2011, doi: 10.1177/096739111101900802.
- [289] P. F. Tuckner, "Compression set vs. compression stress relaxation," *Rubber World*, vol. 234, pp. 38–45, 2006.
- [290] M. Guindani, G. Ramorino, S. Agnelli, L. Conzatti, and I. Schizzi, "Optimization of the sealing performance in transient conditions of rubber based hybrid nanocomposites by carbon nanotubes, as assessed by a tailored recovery test," *Polym. Test.*, vol. 56, pp. 226–236, 2016, doi: 10.1016/j.polymertesting.2016.10.021.
- [291] D. C. Edwards, "Polymer-filler interactions in rubber reinforcement," *Journal of Materials Science*. 1990. doi: 10.1007/BF00581070.
- [292] M. C. H. Lee, "The effects of degree of mixing on the properties of filled elastomers," *J. Appl. Polym. Sci.*, 1984, doi: 10.1002/app.1984.070290205.
- [293] E. Guth and O. Gold, "On the Hydrodynamical Theory of the Viscosity of Suspension," *Phys. Rev.*, vol. 53, 1938.
- [294] L. Petersson and K. Oksman, "Biopolymer based nanocomposites: Comparing layered silicates and microcrystalline cellulose as nanoreinforcement," *Compos. Sci. Technol.*, vol. 66, no. 13, pp. 2187–2196, 2006, doi: 10.1016/j.compscitech.2005.12.010.
- [295] Q. Wang, F. Yang, Q. Yang, H. Guan, J. Chen, and B. Zhao, "Study on magnetic and physical mechanical properties of NBR composites filled with nano-SrO<sub>6</sub>Fe<sub>2</sub>O<sub>3</sub>," *J. Elastomers Plast.*, 2011, doi: 10.1177/0095244310393928.
- [296] PAYNE AR and WHITTAKER RE, "Low strain dynamic properties of filled rubbers," *Rubber Chem. Technol.*, vol. 44, no. 2, pp. 440–478, 1971, doi: 10.5254/1.3547375.
- [297] G. Kraus, "Reinforcement of elastomers by carbon black," *Die Angew. Makromol. Chemie*, vol. 60, no. 1, pp. 215–248, 1977, doi: 10.1002/apmc.1977.050600109.
- [298] F. Clément, L. Bokobza, and L. Monnerie, "Investigation of the Payne effect and its temperature dependence on silica-filled polydimethylsiloxane networks. Part I: Experimental results," *Rubber Chem. Technol.*, vol. 78, no. 2, pp. 211–231, 2005, doi: 10.5254/1.3547879.
- [299] L. Bokobza and O. Rapoport, "Filled elastomers: Mid- and near-IR spectroscopic determination of rubber dimensions in composite in unstretched state and under uniaxial extension," *J. Appl. Polym. Sci.*, vol. 87, no. 8, pp. 1204–1208, 2002, doi: 10.1002/app.11479.
- [300] A. R. Payne, "Dynamic properties of heat-treated butyl vulcanizates," *Journal of Applied Polymer Science*, vol. 7, no. 3, pp. 873–885, 1963. doi: 10.1002/app.1963.070070307.
- [301] A. I. Medalia, "Effect of carbon black on dynamic properties of rubber vulcanizates," *Rubber Chem. Technol.*, vol. 51, no. 3, 1978, doi: 10.5254/1.3535748.
- [302] F. Zhao, W. Bi, and S. Zhao, "Influence of crosslink density on mechanical properties of natural rubber vulcanizates," *J. Macromol. Sci. Part B Phys.*, vol. 50, no. 7, pp. 1460–1469, 2011, doi: 10.1080/00222348.2010.507453.
- [303] J. Berriot, F. Lequeux, L. Monnerie, H. Montes, D. Long, and P. Sotta, "Filler-elastomer interaction in model filled rubbers, a <sup>1</sup>H NMR study," *J. Non. Cryst. Solids*, vol. 307–310, pp. 719–724, 2002, doi: 10.1016/S0022-3093(02)01552-1.
- [304] J. Berriot, H. Montes, F. Lequeux, D. Long, and P. Sotta, "Gradient of glass transition temperature in filled elastomers," *Europhys. Lett.*, vol. 64, no. 1, pp. 50–56, 2003, doi: 10.1209/epl/i2003-00124-7.
- [305] J. Berriot, H. Montes, F. Lequeux, D. Long, and P. Sotta, "Evidence for the shift of the glass transition near the particles in silica-filled elastomers," *Macromolecules*, vol. 35, no. 26, pp. 9756–9762, 2002, doi: 10.1021/ma0212700.
- [306] E. M. Ginting, N. Bukit, Motlan, M. T. Saragih, E. Frida, and B. F. Bukit, "Analysis of natural rubber compounds with filler of Oil Palm Empty Bunches Powder and Carbon Black," *J. Phys. Conf. Ser.*, vol. 1428, no. 1, 2020, doi: 10.1088/1742-6596/1428/1/012024.
- [307] H. W. Siesler, "Vibrational spectroscopy of polymers," *Int. J. Polym. Anal. Charact.*, vol. 16, no. 8, pp. 519–541, 2011, doi: 10.1080/1023666X.2011.620234.
- [308] J. L. Koenig, "Spectroscopy of polymers," p. 491, 1999.
- [309] J. Zhao, R. Yang, R. Iervolino, and S. Barbera, "Changes of chemical structure and mechanical property levels during thermo-oxidative aging of NBR," *Rubber Chem. Technol.*, vol. 86, no. 4, pp. 591–603, 2013, doi: 10.5254/RCT.13.87969.
- [310] J. R. Riba Ruiz, T. Canals, and R. Cantero, "Supervision of Ethylene Propylene Diene M-Class (EPDM) Rubber Vulcanization and Recovery Processes Using Attenuated Total Reflection Fourier Transform Infrared (ATR FT-IR) Spectroscopy and Multivariate Analysis," *Appl. Spectrosc.*, vol. 71, no. 1, pp. 141–151, Jan. 2017, doi: 10.1177/0003702816653131.
- [311] F. Delor-jestin, N. Barrois-oudin, C. Cardinet, J. Lacoste, and J. Lemaire, "Thermal ageing of acrylonitrile-butadiene copolymer Thermal ageing of acrylonitrile-butadiene copolymer," no. May, 2018.
- [312] R. Bro and A. K. Smilde, "Principal component analysis," *Anal. Methods*, vol. 6, no. 9, pp. 2812–2831, 2014, doi: 10.1039/c3ay41907j.
- [313] R. Todeschini, "Introduzione alla chemiometria," *EdiSES, Napoli*, 1998, [Online]. Available: [http://micchem.disat.unimib.it/chm/download/materiale/introduzione\\_alla\\_chemiometria.pdf](http://micchem.disat.unimib.it/chm/download/materiale/introduzione_alla_chemiometria.pdf)
- [314] J. Frigerio *et al.*, "Application of DNA mini-barcoding and infrared spectroscopy for the authentication of the Italian product 'bottarga,'" *Lwt*, vol. 139, no. May, 2021, doi: 10.1016/j.lwt.2020.110603.
- [315] L. Wu, Y. Ding, J. Zhen, Q. Zhang, and S. Chen, "Swelling properties of nitrile-butadiene rubber with different acrylonitrile content in isopropyl nitrate," *Chem. Eng. Trans.*, vol. 59, 2017, doi: 10.3303/CET1759028.
- [316] L. Ślusarski, "Thermal stability of elastomers," *J. Therm. Anal.*, vol. 29, no. 5, pp. 905–912, 1984, doi: 10.1007/BF02188836.
- [317] J. Zhao, R. Yang, R. Iervolino, and S. Barbera, "Changes of chemical structure and mechanical property levels during thermo-

- oxidative aging of NBR," *Rubber Chem. Technol.*, vol. 86, no. 4, 2013, doi: 10.5254/RCT.13.87969.
- [318] J. L. Leblanc, "Rubber-filler interactions and rheological properties in filled compounds," *Progress in Polymer Science (Oxford)*, 2002. doi: 10.1016/S0079-6700(01)00040-5.
- [319] B. B. Boonstra and A. I. Medalia, "Effect of carbon black dispersion on the mechanical properties of rubber vulcanizates," 1963.
- [320] A. Mostafa, A. Abouel-Kasem, M. R. Bayoumi, and M. G. El-Sebaie, "Effect of carbon black loading on the swelling and compression set behavior of SBR and NBR rubber compounds," *Mater. Des.*, vol. 30, no. 5, pp. 1561–1568, 2009, doi: 10.1016/j.matdes.2008.07.043.
- [321] M. Van Der Schuur and R. J. Gaymans, "Influence of chemical crosslinks on the elastic behavior of segmented block copolymers," *Polymer (Guildf.)*, vol. 46, no. 18, pp. 6862–6868, 2005, doi: 10.1016/j.polymer.2005.05.125.
- [322] J. Zhao, R. Yang, R. Iervolino, and S. Barbera, "Investigation of crosslinking in the thermooxidative aging of nitrile-butadiene rubber," *J. Appl. Polym. Sci.*, 2015, doi: 10.1002/app.41319.
- [323] P. J. P. J. Flory, J. Rehner, and J. Rehner Jr., "Statistical mechanics of cross-linked polymer networks II. Swelling," *J. Chem. Phys.*, vol. 11, no. 11, pp. 521–526, 1943, doi: 10.1063/1.1723792.
- [324] S. C. Peterson, S. R. Chandrasekaran, and B. K. Sharma, "Birchwood biochar as partial carbon black replacement in styrene-butadiene rubber composites," *J. Elastomers Plast.*, vol. 48, no. 4, pp. 305–316, 2016, doi: 10.1177/0095244315576241.
- [325] Y. Fan, G. D. Fowler, and M. Zhao, "The past, present and future of carbon black as a rubber reinforcing filler – A review," *Journal of Cleaner Production*, vol. 247, 2020. doi: 10.1016/j.jclepro.2019.119115.
- [326] E. Athanassiades, "Waste tyre pyrolysis: sustainable recovery and reuse of a valuable resource," *PQDT - UK Irel.*, 2013.
- [327] R. C. Kerschbaumer *et al.*, "Comparison of steady-state and transient thermal conductivity testing methods using different industrial rubber compounds," *Polym. Test.*, vol. 80, 2019, doi: 10.1016/j.polymertesting.2019.106121.
- [328] ASTM E1530, "Standard Test Method for Evaluating the Resistance to Thermal Transmission by the Guarded Heat Flow Meter Technique," 2019.
- [329] F. Engström, D. Adolfsson, Q. Yang, C. Samuelsson, and B. Björkman, "Crystallization behaviour of some steelmaking slags," *Steel Res. Int.*, vol. 81, no. 5, pp. 362–31, 2010, doi: 10.1002/srin.200900154.
- [330] D. Mombelli, A. Gruttadauria, S. Barella, and C. Mapelli, "The influence of slag tapping method on the efficiency of stabilization treatment of electric arc furnace carbon steel slag (EAF-C)," *Minerals*, vol. 9, no. 11, p. 706, 2019, doi: 10.3390/min9110706.
- [331] A. Barocci, G. Luzzari, and M. Facchin, "Procedura operativa per la produzione di inerte artificiale in luogo di scoria nera," *Metall. Ital.*, vol. 5, p. 37, 2014.
- [332] W. P. Cox and E. H. Merz, "Correlation of dynamic and steady flow viscosities," *J. Polym. Sci.*, vol. 28, no. 118, 1958, doi: 10.1002/pol.1958.1202811812.
- [333] G. Cornacchia, S. Agnelli, M. Gelfi, G. Ramorino, and R. Roberti, "Reuse of EAF Slag as Reinforcing Filler for Polypropylene Matrix Composites," *Jom*, vol. 67, no. 6, pp. 1370–1378, 2015, doi: 10.1007/s11837-015-1396-6.
- [334] R. Roberti, F. Uberto, M. Svanera, G. Altenburger, and F. Cabra, "The SLAG-REC ® project for an innovative direct dry granulation of EAF slag," 2010.
- [335] A. Gobetti, G. Cornacchia, and G. Ramorino, "Reuse of Electric Arc Furnace Slag as Filler for Nitrile Butadiene Rubber," *JOM*, 2022, doi: <https://doi.org/10.1007/s11837-021-05135-6>.
- [336] K. Formela, M. Cysewska, and J. Haponiuk, "The influence of screw configuration and screw speed of co-rotating twin screw extruder on the properties of products obtained by thermomechanical reclaiming of ground tire rubber," *Polimery/Polymers*, vol. 59, no. 2, pp. 170–177, 2014, doi: 10.14314/polimery.2014.170.
- [337] K. N. Pandey, D. K. Setua, and G. N. Mathur, "Material behaviour: Fracture topography of rubber surfaces: An SEM study," *Polym. Test.*, vol. 22, no. 3, 2003, doi: 10.1016/S0142-9418(02)00112-5.
- [338] Ministero della tutela dell'ambiente e del territorio, *Norme in materia ambientale. (GU Serie Generale n.88 del 14-04-2006 - Suppl. Ordinario n. 96)*. La gazzetta ufficiale della repubblica Italiana, 2006. Accessed: Dec. 13, 2021. [Online]. Available: [https://www.gazzettaufficiale.it/atto/serie\\_generale/caricaArticolo?art.versione=4&art.idGruppo=34&art.flagTipoArticolo=0&art.codiceRedazionale=006G0171&art.idArticolo=184&art.idSottoArticolo=2&art.idSottoArticolo1=10&art.dataPubblicazioneGazzetta=2006-04](https://www.gazzettaufficiale.it/atto/serie_generale/caricaArticolo?art.versione=4&art.idGruppo=34&art.flagTipoArticolo=0&art.codiceRedazionale=006G0171&art.idArticolo=184&art.idSottoArticolo=2&art.idSottoArticolo1=10&art.dataPubblicazioneGazzetta=2006-04)
- [339] D. Claps *et al.*, "L'applicazione della disciplina del sottoprodotto in Italia quale leva strategica per la competitività delle imprese: uno scenario giuridico amministrativo in evoluzione," *Symbiosis Users Netw. – SUN Proc. fourth SUN Conf.*, 2020.
- [340] Ministero dell'ambiente e della tutela del territorio e del mare, *Regolamento recante criteri indicativi per agevolare la dimostrazione della sussistenza dei requisiti per la qualifica dei residui di produzione come sottoprodotti e non come rifiuti. (17G00023) (GU Serie Generale n.38 del 15-02-2017)*. La gazzetta ufficiale della repubblica Italiana, 2016. [Online]. Available: <https://www.gazzettaufficiale.it/eli/id/2017/02/15/17G00023/sg>
- [341] R. Lombardia, *Linee guida per la gestione delle scorie nere di acciaieria a forno elettrico*. 2021. [Online]. Available: [https://anci.lombardia.it/documenti/12691-Linea guida\\_Scoria\\_Nera\\_EAF.pdf](https://anci.lombardia.it/documenti/12691-Linea guida_Scoria_Nera_EAF.pdf)
- [342] K. J. Rodgers, A. Hursthouse, and S. Cuthbert, "The potential of sequential extraction in the characterisation and management of wastes from steel processing: A prospective review," *International Journal of Environmental Research and Public Health*, vol. 12, no. 9, 2015. doi: 10.3390/ijerph120911724.
- [343] M. Mirata, "Experiences from early stages of a national industrial symbiosis programme in the UK: Determinants and coordination challenges," *J. Clean. Prod.*, 2004, doi: 10.1016/j.jclepro.2004.02.031.
- [344] M. La Monica, L. Cutaia, and S. Franco, "La simbiosi industriale come modello per lo sviluppo sostenibile dei sistemi economici territoriali," in *Atti del XXVI Convegno annuale di Sinergie "Manifattura: quale futuro?"*, 2014, pp. 151–164.
- [345] Istituto Nazionale di Statistica, "CLASSIFICAZIONE DELLE ATTIVITÀ ECONOMICHE ATECO," *ISTAT*, 2007. <https://www.istat.it/it/archivio/17888> (accessed Jul. 01, 2022).
- [346] Federacciai, "Relazione Annuale 2021," 2021. [Online]. Available: <https://federacciai.it/pubblicazioni-varie/>

